5-2010

Phyllosilicate mineralogy, 40Ar/39Ar geochronology, and genesis of petrocalcic soils in the Southwest U.S.A.

Colin R. Robins
University of Nevada Las Vegas

Repository Citation

Robins, Colin R., "Phyllosilicate mineralogy, 40Ar/39Ar geochronology, and genesis of petrocalcic soils in the Southwest U.S.A." (2010). *UNLV Theses, Dissertations, Professional Papers, and Capstones*. 230.
https://digitalscholarship.unlv.edu/thesesdissertations/230

PHYLLOSILICATE MINERALOGY, $^{40}Ar/^{39}Ar$ GEOCHRONOLOGY, AND GENESIS OF PETROCALCIC SOILS IN THE SOUTHWEST U.S.A.

by

Colin R. Robins

Bachelor of Arts
Macalester College
2001

Master of Science
Oregon State University
2004

A dissertation submitted in partial fulfillment
of the requirements for the

Doctor of Philosophy in Geoscience
Department of Geoscience
College of Science

Graduate College
University of Nevada, Las Vegas
May 2010

UNLV
UNIVERSITY OF NEVADA LAS VEGAS

THE GRADUATE COLLEGE

We recommend that the dissertation prepared under our supervision by

Colin R. Robins

entitled

Phyllosilicate Mineralogy, ^{40}Ar/^{39}Ar Geochronology, and Genesis of Petrocalcic Soils in the Southwest U.S.A.

be accepted in partial fulfillment of the requirements for the degree of

Doctor of Philosophy
Geoscience

Brenda J. Buck, Committee Chair

Matthew Lachniet, Committee Member

Terry Spell, Committee Member

Spencer Steinberg, Committee Member

Lloyd Stark, Graduate Faculty Representative

Ronald Smith, Ph. D., Vice President for Research and Graduate Studies
and Dean of the Graduate College

May 2010

ABSTRACT

Phyllosilicate Mineralogy, ^{40}Ar/^{39}Ar Geochronology, and Genesis of Petrocalcic Soils in the Southwest U.S.A.

by

Colin R. Robins

Dr. Brenda J. Buck, Examination Committee Chair
Professor of Geoscience
University of Nevada, Las Vegas

Obtaining isotope ages for arid soils and paleosols, including carbonate-cemented (calcic and petrocalcic) horizons, constitutes a significant challenge for soil scientists, geomorphologists, and stratigraphers. Carbonate-cemented soils foster diverse suites of authigenic minerals with exciting potential for geochronology, however, this potential has not been realized. This dissertation describes the timing of pedogenic palygorskite and sepiolite crystallization in extremely old, extant petrocalcic soils of the southwest U.S.A., and assumes that these fibrous, high-magnesium phyllosilicates contain sufficient lattice-bound K to warrant vacuum-encapsulated ^{40}Ar/^{39}Ar geochronology. This three-part study evaluated the (1) selective extraction, (2) ^{40}Ar/^{39}Ar analysis, and (3) pedogenesis of palygorskite and sepiolite.

Effects of selective extraction of the phyllosilicates from carbonate and silica cements using successive buffered sodium acetate and tiron solution treatments, and particle size fractionation via centrifuge, were evaluated using scanning electron microscopy, inductively-coupled plasma spectrometry, and x-ray diffraction analysis. No adverse effects were identified, however, intergrowths and/or inclusions of detrital mineral species persisted in the samples. Moreover, ^{40}Ar/^{39}Ar total gas ages exceeded known relative dates by two orders of magnitude. Gas chromatograph data indicate that hydrocarbon contaminants – derived chiefly from selective dissolution compounds, but also possibly from the natural soil environment – caused these impossible ages. Future work is needed both to constrain argon diffusion parameters for the clays, and also to evaluate methods to remove organic contaminants.

Extensive mineralogical, chemical, and micromorphological analysis of petrocalcic soil samples from Mormon Mesa, NV, permitted conceptual modeling of mineral genesis during pluvial-interpluvial climate oscillations. These models address not only the timing and genetic relationships of palygorskite, sepiolite, calcite, and silica, but also the presence of authigenic barite ($BaSO_4$), in the petrocalcic soil.

Isotopic dates for petrocalcic soils are sorely needed to assess rates at which arid landforms and soils have formed, stabilized, and/or degraded both in the late Holocene, and in the geologic past. Thus, the potential benefit of successful $^{40}Ar/^{39}Ar$ geochronology of pedogenic palygorskite and sepiolite, and other arid soil minerals, strongly merits further experimentation and discussion. Extensive, detailed, and targeted micromorphological analysis is an inescapable prerequisite of any study linking the genesis and geochronology of calcic and petrocalcic soil landscapes.

ACKNOWLEDGEMENTS

I will never be able to sufficiently thank my advisor and committee chair, Brenda Buck, for her unwavering, prompt, and thoughtful critiques, support, encouragement, and time over the years, and for always watching out for my best interests. I am also forever indebted to my hard-working advisory committee, Matthew Lachniet, Terry Spell, and Spencer Steinberg for their suggestions, extensive laboratory work, encouragement, patience, and above all their time. I am also greatly indebted to Lloyd Stark for his time and help in serving as my Graduate College representative.

The original idea for this project was first suggested by H. Curtis Monger, of New Mexico State University, and was very kindly passed along to me as a possible dissertation topic by Brenda Buck.

Generous financial support for research, educational, and living expenses were provided in part by: the UNLV Department of Geoscience, which supported me with experience-building research and teaching assistantships throughout my time at UNLV; the National Science Foundation's Small Grants for Exploratory Research program, without which this project would not have been possible; the Jack and Fay Ross Family Fellowship, awarded through the generosity of the UNLV Geoscience Department, and which afforded me an unparalleled opportunity to focus entirely on my research during the 2008-2009 academic year; the UNLV Bernada E. French scholarship program; the Geological Society of America Graduate Student Research Grants program; the UNLV Graduate College summer stipends program; and last but certainly not least, the UNLV Graduate and Professional Student Association, which partially funded travel, attendance,

and presentation costs associated with international soil science conferences in 2005 and 2006.

Sample collection permits could not have been obtained without the undeterrable and tireless efforts of Cathy Willey and the Public Lands Institute. Access to field sites in New Mexico and Nevada was kindly granted by: H. Curtis Monger and New Mexico State University; the Clark County Bureau of Land Management; and by the Nevada Department of Transportation. Sample collection and other field studies were made easy through the kind, cheerful, and insightful field assistance volunteered by Amy Brock, Jan Brock, Douglas Merkler, Curtis Monger, Caroline Sauvage-Robins, and Amanda Williams.

I was also fortunate to count on the expert analytical guidance and/or kind laboratory assistance from: Kathleen Zanetti, Clay Crow, Deborah Soukup, Spencer Steinberg, Yuanxin Teng, Sean Mulcahy, Haroldo Lledo, Aaron Bell, Amy Brock, Lora Griffin, Mike Howell, and Caroline Sauvage-Robins.

My continued efforts at science writing have (believe it or not) been greatly improved upon through the constructive criticisms offered by Brenda Buck, Wanda Taylor, Kim Johnson, and Robyn Howley. Nevertheless, any typograpical errors or confusing structure sentence are entirely my own fault.

Additional logistical support and services were provided by: many, many, staff (especially the wonderful Maria Figueroa and equally wonderful Liz Smith), faculty, and students from the UNLV Department of Geoscience; UNLV Library Services (especially Document Delivery Services) and by the UNLV Graduate College (especially Eric Lee and Nicholle Booker).

I would also like to thank the following individuals not yet mentioned for their support and kindness over recent years: Lois Alexander, April Azouz, the Brice family, Becky Boulton, Patrick Drohan, Peter Druschke, Jack de Golia, Dirk Goosens, AAron Hirsch, Kim Howell, Joseph Kula, Joshua Boxell, Becki Huntoon, Jan Morton, Jay Noller, Willy Rittase, the Robins family, Alex Roy, the Sauvage family, Nathan Suurmeyer, and Ashley Tibbets. I regret that I cannot name here everyone who has helped me overcome the innumerable challenges that crop up in life from time to time, both as a graduate student and as a human being, but to everyone named here and to anyone I have unintentionally forgotten: Thank you all.

TABLE OF CONTENTS

LIST OF TABLES

CHAPTER 2

CHAPTER 3

CHAPTER 4

LIST OF FIGURES

CHAPTER 2

CHAPTER 3

CHAPTER 4

CHAPTER 1

LINKING COMPLEMENTARY STUDIES OF CALCIC AND PETROCALCIC SOIL GENESIS

Introducing Arid and Calcic Soils Research

Arid regions comprise more than a third of Earth's landscapes and sustain nearly two billion people (UNCCD, 2003), however, the processes and thresholds that shape arid soils and landscapes are not yet fully understood. Especially lacking are numerical ages to assess the rates at which dry land soils and soil minerals have formed, stabilized, and/or degraded both in the late Holocene, and in the geologic past. The need for quantitative measures of soil processes and thresholds has increased in proportion with growing efforts to combat desertification and salinization, and to better manage threatened agricultural resources in arid to semi-arid regions worldwide. Arid soils research may also prove relevant to the study of surficial processes in the extreme environments of other planets, especially Mars.

In comparison to humid soils, which largely reflect the hydrolysis of minerals and the loss of cations from the soil profile, arid landscapes are distinct because their soil profiles typically reflect a net influx of ions to the Earth's surface over time. This influx, combined with alkaline soil solutions and fluctuating moisture conditions, produces a variety of unique authigenic mineral assemblages (Francis et al., 2007) including (but not limited to) carbonates, chlorides, iron and/or manganese oxides, nitrates, and sulfates, as well as unusual, fibrous phyllosilicate species such as palygorskite and sepiolite. Because important geochronologic, pedogenic, and climate change data are coded into the geochemistry of each authigenic species, this range of compositionally diverse minerals raises exciting prospects for the novel application of existing, isotopic analyses to untested pedogenic minerals in arid soil environments.

Calcium-carbonated cemented – "calcic" or "petrocalcic" – soil horizons (also sometimes called "calcretes" or "caliches") are important features that cap extant landforms in arid and semi-arid environments worldwide, and they also occur as paleosols and unconformities in the rock record (e.g. Reeves, 1976; Machette, 1985; Retallack, 2001). Because calcic and petrocalcic horizons form on generally stable surfaces, their morphology – from the macroscale to the microscale – reflects the net product of variable surficial processes acting over hundreds to millions of years. The morphological stage of a calcic soil (from stage I-young, to stage VI-old) generally reflects the relative age of the soil landform, and also the intensity or frequency of climate or surficial-process changes (Gile et al., 1966; Bachman & Machette, 1977; Machette, 1985). By controlling the flow of water into and across land surfaces, and by restricting plant rooting depth (Flach et al., 1969), indurated carbonate horizons can also influence future landscape evolution and ecology.

Like many other types of arid soils, calcic and petrocalcic soils may contain a range of authigenic minerals whose genesis reflects changing soil chemical conditions imparted by fluctuating climate over millions of years. Palygorskite, $Si_8Mg_5O_{20}(OH)_2(OH_2)_4 \cdot 2H_2O$ (Singer, 1984), and sepiolite, $Si_{12}Mg_8O_{30}(OH)_4(OH_2)_4 \cdot 8H_2O$ (Brauner & Preisinger, 1956; Singer, 1984; García-Romero et al., 2007) are fibrous, high-magnesium phyllosilicates that are relatively rare in terrestrial sediments, yet fairly common in calcic and petrocalcic soils (Jones & Galan, 1988). Amorphous silica, pedogenic barite, and other mineral types may also occur in calcic soils. Late stage (III-VI) petrocalcic soils can reach hundreds of thousands to millions of years in age, and as a consequence, they often exhibit polygenetic soil profiles with complex morphological, chemical, and mineralogical properties. Consequently, careful analysis and interpretation of calcic soil morphology, chemistry, and mineralogy can provide important insights into local and regional paleoclimate, paleoecology, and landscape evolution over varying timescales.

Scientific Challenges in Calcic Soil Investigations

The study of calcic and petrocalcic soils encompasses some of the biggest scientific challenges faced by soil scientists, stratigraphers, paleoclimatologists, and geomorphologists today. First, the difficulty of extracting intact, mineralogically pure, pedogenic crystals from cemented soil remains a major obstacle to quantifying the rates and processes of climate and landscape change in arid regions. Without rigorously evaluated methods of extracting or purifying pedogenic minerals from indurated samples, the range of analytical techniques applicable to calcic soils will remain limited. Second, the lack of isotopic age data for authigenic minerals besides carbonate in petrocalcic soils limits our understanding of their genesis. Without absolute age data, the amount of time needed to reach each successive morphological soil carbonate stage within a given region will never be known, and the feasibility of comparing morphologically similar soils between distinct regions will remain limited. Third, it is not known whether or not, nor to what degree calcic and petrocalcic soils (and the authigenic minerals they foster) can act as "closed" isotopic systems. Until this question can be answered, the utility of isotope data for extracted mineral phases will remain uncertain. The following chapters of this dissertation represent, together, an important, if small, step towards resolving each of these challenges.

Linking Complementary Studies

Chapter 2, entitled "Towards $^{40}Ar/^{39}Ar$ geochronology of pedogenic palygorskite and sepiolite, part I: extraction and chemical considerations" (Robins, 2010a) addresses the challenges associated with extracting mineralogically pure, pedogenic palygorskite and/or sepiolite from indurated samples for isotopic analysis. Palygorskite and sepiolite in petrocalcic soils commonly form intergrowths with $CaCO_3$ and amorphous silica. Thus, this study evaluates a method to extract the fibrous, pedogenic clays from calcium carbonate cements using sodium acetate (Jackson, 1965; Kunze & Dixon, 1986), and to remove amorphous silica cements from the phyllosilicates using the tiron method (Biermans & Baert, 1977; Kodama & Ross, 1991). Two late-stage, previously studied petrocalcic soils were sampled on (1) the Mormon Mesa geomorphologic surface in southern Nevada, and (2) the Jornada Experimental Range La Mesa geomorphologic surface near Las Cruces, New Mexico. Scanning electron microscopy (SEM) coupled with energy-dispersive x-ray spectroscopy (EDS), X-ray diffraction (XRD) analysis, and inductively coupled plasma spectrometry (ICP) were employed to evaluate the morphological, mineralogical, and chemical properties of the phyllosilicates before, during, and after treatment.

Chapter 3, entitled " Towards $^{40}Ar/^{39}Ar$ geochronology of pedogenic palygorskite and sepiolite, part II: Lessons and technical implications for dating arid soils" (Robins, 2010b) is the companion study to Chapter 2, and addresses challenges related to the

$^{40}Ar/^{39}Ar$ analysis of the fibrous clays. Geologically impossible $^{40}Ar/^{39}Ar$ ages suggested the presence of unanticipated hydrocarbon contaminants in the extracted clays. The presence of these contaminants was verified using pyrolysis gas chromatograph/mass spectrometry (GC/MS). Although the $^{40}Ar/^{39}Ar$ data produced in this study are inconclusive, the potential benefit of a successful application of $^{40}Ar/^{39}Ar$ geochronology to pedogenic palygorskite and sepiolite makes the topic deserving of further experimentation and could yet produce a viable, exciting new geochronologic method for arid soil geomorphology. Moreover, challenges discussed in this study are immediately relevant to other mineral and isotopic dating systems.

Chapter 4, entitled " Micromorphology, chemistry, and phyllosilicate mineralogy of the Mormon Mesa petrocalcic soil, Nevada, U.S.A.: Genetic implications" (Robins, 2010c), builds upon existing genetic models for the Mormon Mesa petrocalcic soil (Brock, 2007; Brock & Buck, 2009) by focusing on the genesis of key minerals and micromorphological features. XRD, SEM-EDS, and soil chemical analyses including pH, percent carbonate equivalence, soil moisture, electrical conductivity, soluble sulfate content, and soluble chloride content were performed. Models of mineral genesis are presented to explain the formation of the fibrous phyllosilicates and also the genesis of pedogenic barite ($BaSO_4$). In addition, mineral genesis models, in turn, contribute to a non-biogenic model for the formation of ooids in calcic and petrocalcic soil profiles.

Together, these studies address the complex mineralogical, chemical, and micromorphological properties of calcic and petrocalcic soils, as well as the great potential for novel scientific study of arid soil landscapes. Although based in the southwest U.S.A., this study has implications for the analysis of calcic and petrocalcic soils worldwide, and may have implications for study of calcic paleosols, and/or phyllosilicate minerals in non-pedogenic, sedimentary environments.

Appendices referenced within each chapter can be found at the end of this dissertation and are, like the tables and figures, numbered first by chapter, and then in order of occurrence within the chapter. For example, the first appendix referenced within the fourth chapter is Appendix 4.1, the next is Appendix 4.2, etc.

References

Bachman, G.O. and Machette, M.N., 1977. Calcic soils and calcretes in the southwestern United States. U.S. Geological Survey Open File Report 77-794. 163 pages.

Biermans, V. and Baert, L., 1977. Selective extraction of the amorphous Al, Fe and Si oxides using an alkaline Tiron solution. Clay Minerals, 12(127): 127-135.

Brauner, K. and Preisinger, A., 1956. Estruktur und Enstehung des sepiolits. Tschermaks Mineralogische und petrographisches Mitteilungen, 6:120-140.

Brock, A.L., 2007. Characterization of stage VI petrocalcic horizons: S. Nevada and N.W. Arizona. Ph.D. Dissertation. University of Nevada Las Vegas, Department of Geoscience. 148 pages.

Brock, A.L. and Buck, B.J., 2009. Polygenetic development of the Mormon Mesa, NV petrocalcic horizons: Geomorphic and paleoenvironmental interpretations. Catena, 77: 65-75.

Flach, K.W., Nettleton, W.D., Gile, L. H., and Cady, J. G., 1969. Pedocementation: Induration by silica, carbonates, and sesquioxides in the Quaternary. Soil Science, 107(6): 442-453.

Francis, M.L., Fey, M.V., Prinsloo, H.P., Ellis, F., Mills, A.J., and Medinski, T.V., 2007. Soils of Namaqualand: Compensations for aridity. Journal of Arid Environments, 70: 588-603.

García-Romero, E., Suárez, M., Santarén, J., and Alvarez, A., 2007. Crystallochemical characterization of the palygorskite and sepiolite from the Allou Kagne deposit, Senegal. Clays and Clay Minerals, 55 (6): 606-617.

Gile, L.H., Peterson, F.F., and Grossman, R.B., 1966. Morphological and genetic sequences of carbonate accumulation in desert soils. Soil Science, 101(5): 347-360.

Jackson, M.L.,1965. Soil chemical analysis: Advanced Course. Published by the author. Dept. of Soil Science, University of Wisconsin, Madison.

Jones, B.F. and Galan, E., 1988. Sepiolite and palygorskite. Reviews in mineralogy, 19(1): 631-674.

Kodama, H. and Ross, G.J., 1991. Tiron dissolution method used to remove and characterize inorganic components in soils. Soil Science Society of America Journal, 55: 1180-1187.

Kunze, G.W. and Dixon, J.B., 1986. Pretreatment for mineralogical analysis. In: Klute, A., ed. Methods of soil analysis part 1: Physical and mineralogical methods, 2nd edition. Agronomy Monograph 9. Madison, Soil Science Society of America: 91-100

Machette, M.N., 1985. Calcic soils of the southwestern United States. Geologic Society of America Special Paper 203: 1-21.

Reeves, C.C. Jr., 1976. Caliche: Origin, classification, morphology and uses. Lubbock, Estacado Books: 233 pages.

Retallack, G.J., 2001. Soils of the past: An introduction to paleopedology. Blackwell Science, Malden, MA, 404 pp.

Robins, C.R., 2010a. Towards $^{40}Ar/^{39}Ar$ geochronology of pedogenic palygorskite and sepiolite, Part I: extraction and chemical considerations. In: Robins, C.R. Phyllosilicate mineralogy, $^{40}Ar/^{39}Ar$ geochronology, and genesis of petrocalcic soils in the southwest U.S.A. Ph.D. dissertation. UNLV Department of Geoscience, Las Vegas, NV: 1-55.

Robins, C.R., 2010b. Towards $^{40}Ar/^{39}Ar$ geochronology of pedogenic palygorskite and sepiolite, Part II: lessons and technical implications for dating arid soils. In: Robins, C.R. Phyllosilicate mineralogy, $^{40}Ar/^{39}Ar$ geochronology, and genesis of petrocalcic soils in the southwest U.S.A. Ph.D. dissertation. UNLV Department of Geoscience, Las Vegas, NV: 56-94.

Robins, C.R., 2010c. Micromorphology, chemistry and phyllosilicate mineralogy of the Mormon Mesa petrocalcic soil, Nevada, USA: Genetic implications. In: Phyllosilicate mineralogy, $^{40}Ar/^{39}Ar$ geochronology, and genesis of petrocalcic soils in the southwest U.S.A. Ph.D. dissertation. University of Nevada Las Vegas, Department of Geoscience: 95-175.

Singer, A., 1984. The paleoclimatic interpretation of clay minerals in sediments - a review. Earth-Science Reviews, 21: 251-293.

United Nations Commission to Combat Desertification, 1997. Earth Summit +5. Special session of the General Assembly to review and appraise the implementation of Agenda 21. New York, 23-27 June. http://www.un.org/ecosocdev/geninfo/sustdev/desert.htm.

CHAPTER 2

TOWARDS ^{40}Ar/^{39}Ar GEOCHRONOLOGY OF PEDOGENIC PALYGORSKITE AND SEPIOLITE, PART I: EXTRACTION AND CHEMICAL CONSIDERATIONS

Abstract

The difficulty of extracting intact, mineralogically pure, pedogenic crystals from cemented soil remains one of the most significant scientific obstacles to quantifying the rates and processes of climate and landscape change in arid regions. Extant, but geologically old, petrocalcic soils represent one of the best opportunities to obtain a mineralogically "pure" pedogenic clay fraction for vitally important genetic and geochronologic analyses. This study evaluated a procedure to extract palygorskite and sepiolite from indurated soil samples of the Mormon Mesa soil in Nevada, and the JER La Mesa soil in New Mexico, for ^{40}Ar/^{39}Ar geochronology.

Selective dissolution with NaOAc and with Tiron, combined with particle size fractionation, were used to extract pedogenic palygorskite and sepiolite from bulk, indurated petrocalcic soil samples. Scanning electron microscopy, inductively-coupled plasma spectrometry, and x-ray diffraction analytical techniques were employed to search for physical and chemical effects on pedogenic palygorskite and/or sepiolite crystallite extracts, especially with regards to the suitability of the extracted phyllosilicates for ^{40}Ar/^{39}Ar geochronology. Instrument analyses did not detect adverse morphological, geochemical, or mineralogical effects on the clays as a result of the extraction procedures, however, very significant challenges associated with mineralogical heterogeneity and possible particle-size bias of extracted samples were identified.

Specifically, inclusions of clay-sized quartz and non-fibrous phyllosilicates were found in most samples. It is also possible that stirring and centrifugation cycles promoted fracturing and loss of fine fibrous clays, which could affect isotopic measurements. Mineral inclusions or intergrowths must be considered in terms of their contribution to isotopic analyses.

Thus, this study describes an initial attempt to extract pedogenic phyllosilicates from indurated soil samples for $^{40}Ar/^{39}Ar$ geochronology and advances the theoretical potential of a refined method to extract phyllosilicate minerals from ancient petrocalcic soils for dating. This study also holds implications and recommendations for analyses of pedogenic clays using other isotopic systems.

Introduction

Indurated soil horizons are common features of arid regions, which comprise more than a third of Earth's landscapes and sustain two billion people (UNCCD, 1997). Despite the importance of arid soils to population sustainability, the processes which shape them remain only partially understood. Important geochronologic, pedogenic, and climate change data are coded into the geochemistry of each authigenic mineral phase of arid soils. However, the difficulty of extracting intact, mineralogically pure, pedogenic crystals from cemented soil remains one of the biggest scientific obstacles to quantifying the rates and processes of climate and landscape change in arid regions.

Petrocalcic soil horizons containing authigenic clays cap geomorphologic surfaces in many arid and semi-arid regions worldwide, and they also mark unconformities in the rock record (e.g., Reeves, 1976; Machette, 1985; Retallack, 2001). Palygorskite, $Si_8Al_2Mg_2O_{20}(OH)_2(OH_2)_4 \bullet 2H_2O$ (Bradley, 1940), and sepiolite, $Si_{12}Mg_8O_{30}(OH)_4(OH_2)_4 \bullet 8H_2O$ (Brauner & Preisinger, 1956, as cited by García-Romero et al., 2007), are fibrous, high-magnesium phyllosilicates found in arid soils, palustrine sediments, (peri-)marine deposits, alkaline groundwater environments, and possibly some hydrothermal systems (Callen, 1984; Singer ,1989). Pedogenic palygorskite and sepiolite can form in stage II carbonate pendants or nodules (Singer et al., 1995; Brock & Buck, 2005) and in stage III – VI petrocalcic horizons (Vanden Heuvel, 1966; Bachman & Machette, 1977; Watts, 1980; Gile et al., 1981; Monger & Daugherty, 1991a; Brock & Buck, 2009). If successful methods to extract and isotopically date authigenic palygorskite and sepiolite from petrocalcic horizons could be developed, they could be applied to many soils worldwide to help quantify rates of pedogenesis, landscape evolution, and climate change.

The central hypothesis of this study is that existing soil laboratory procedures can be adapted for successful, low-temperature, chemical and physical extraction and purification of authigenic palygorskite and sepiolite from petrocalcic soil samples for isotopic dating purposes. Specifically, this project was designed to determine (1) whether successive chemical and physical treatments cause lattice damage, thereby affecting the mineralogy or geochemistry of pedogenic palygorskite and sepiolite, and (2) whether the methods tested here would yield sufficiently pure and unaltered palygorskite or sepiolite for ^{40}Ar/^{39}Ar geochronology.

Background

Considerations Prior to Extraction

Any study focused on phyllosilicate isolates of arid soils must consider the genesis, micromorphological relationships, composition, and stability of the target clays - in this case, palygorskite and sepiolite. Although generally rare within most geologic deposits, palygorskite and sepiolite are relatively common genetic components of arid soil environments. In fact, palygorskite and sepiolite have been found to progressively dominate the clay mineral fraction of calcic soils over time (Bachman & Machette, 1977; Monger & Daugherty, 1991b; Watts, 1980). In some profiles, pedogenic palygorskite and/or sepiolite comprise nearly 100 percent of the phyllosilicate mineral fraction (Watts, 1980; Jones & Galan, 1988; Francis et al., 2007).

Force of crystallization processes may promote palygorskite and sepiolite authigenesis in some arid soils (Monger & Kelly, 2002; Robins, 2010b). Surface processes (weathering, dust deposition, infiltration, and evapotranspiration) in arid and semi-arid landscapes promote accumulations of cements such as calcium carbonate or amorphous silica (Reeves, 1976; Bachman & Machette, 1977; Machette, 1985; Nettleton, 1991). Progressive induration of soil by calcium carbonate can promote force of crystallization dissolution of engulfed mineral grains (Bachman & Machette, 1977; Hay & Wiggins, 1980; Gile et al., 1981; Monger & Daugherty, 1991b; Brock & Buck, 2005), and subsequent release of Si, Mg, and Al into the alkaline soil solution. Dissolution of non-fibrous, detrital phyllosilicates in the alkaline soil environment can also supply dissolved Si, Al, and other cations. Complexes of these elements (e.g., H_2SiO_4, $Al(OH)_3$, etc.) then react and combine in the alkaline soil solution to form palygorskite, when Al is present, or sepiolite, when Al concentrations are low (Watts, 1980; Galan & Castillo, 1984; Jones & Galan, 1988). Amorphous silica may precipitate after both Al and Mg solution concentrations drop below threshold values for genesis of the fibrous clay and/or when pH thresholds are crossed (Watts, 1980).

Importantly, the high pH of petrocalcic soil environments permits unusually high Si and Al activities compared to other soils, because both Si and Al become much more soluble as soil pH approaches ~9 (Hay & Wiggins, 1980; Drees et al., 1989; Velde, 1992). Fluctuating soil solution chemistry, therefore, is critical to fibrous clay genesis. In soil environments, precipitation of the fibrous clays may be especially favored in zones of textural contrast, whether along soil horizon contacts or within soil microsites, where recurrent but temporarily water-saturated conditions occur (Yaalon & Wieder, 1976;

Bouza et al., 2007). Cyclical variations in soil solution chemistry in response to percolating rainfall, mineral precipitation, and force-of-crystallization dissolution of primary grains can produce correspondingly cyclical or nearly synchronous precipitation of palygorskite and sepiolite (García-Romero et al, 2007).

As a consequence of their precipitation from evaporative soil solutions, palygorskite and sepiolite are closely related, spatially as well as genetically, to carbonate and silica mineral phases in arid soils (Hay & Wiggins, 1980; Jones, 1983; Monger & Daugherty, 1991; Brock & Buck, 2009; Robins, 2010b). Selective chemical extraction is necessary because of the intricate micromorphological relationships of fibrous clays to these cementing agents. Micromorphological studies of calcic and petrocalcic soils indicate that amorphous silica may precipitate as 0.5-1 μm diameter hemispheroids on the tips of ropy aggregates of palygorskite or sepiolite fibers (Weaver & Beck, 1977; Brock, 2007), or as larger, ~ 10 μm hemispheroids intergrown with fibrous clay mats (Brock, 2007). Pedogenic silica can also occur in association with fibrous clay minerals in duripans and/or calcic soils developed on volcanic materials (Blank & Fosberg, 1991; Singer, 2002). Palygorskite and sepiolite fibers also commonly exhibit intergrowths with calcite crystals throughout many petrocalcic soil samples (Robins , 2010b). In calcic to petrocalcic soils, palygorskite and sepiolite commonly occur as apparently delicate, fibrous, skeletal mats diffused throughout the indurated soil matrix or within filled pores (Watts, 1980; Brock, 2007; Robins, 2010b). The fibrous clays can also occur as concentrations within certain morphological soil features, including ~50 μm-diameter porous pellets or masses (Brock, 2007; Robins, 2010b), and 10-200 μm microlaminations within petrocalcic ooids, laminar layers, or other features (Vanden Heuvel 1966; Hay &

Wiggins, 1980; Watts, 1980; Brock, 2007; Robins, 2010b). However, such concentrations are discontinuous, impossible to detect without high-power magnification, and difficult to extract in abundance. Similarly, the hair-like morphology of palygorskite and sepiolite crystallites (< 0.25 μm in diameter, and 1-20 μm in length) complicates their physical separation from cementing agents. Therefore, successive dissolution treatments of bulk soil samples remain, at present, the best means of extracting large (5 to 10 g) amounts of relatively pure pedogenic palygorskite and/or sepiolite from indurated soil horizons in arid landscapes.

Isotopic analyses are increasingly common in studies of pedogenesis and, naturally, the elemental composition of the study mineral, among other factors, dictates its suitability for a given isotopic system. Compositional variability is known to be high within palygorskites and sepiolites alike (Corma et al., 1987; García-Romero et al., 2007), and variability may be as great within each of the clay species as it is between the two (Singer, 2002; García-Romero et al., 2007). Previous researchers have noted that chemical analyses of palygorskite rarely, if ever, yield its ideal chemical formula (Weaver & Beck, 1977). Both clays commonly contain small, variable amounts of other cations, including Ca, Fe, K, Mn, and Na, although some reported instances of such compositions could reflect intergrowths or contamination by other phyllosilicates, or even the presence of exchangeable cations rather than isomorphous substitutes (García-Romero et al., 2004; Weaver & Pollard, 1973). Nevertheless, palygorskite can and often does exhibit notable levels of isomorphous substitution (Paquet et al., 1987; García-Romero et al. 2007), and compositional end members of sepiolite, including Fe-rich xylotile, Ni-rich falcondoite, and Na-rich loughlinite are also well-documented (Jones &

Galan, 1988). Such compositional variability holds implications for clay genesis and soil solution chemistry, but also affects the practical applicability of a given isotopic analysis to extracted palygorskite or sepiolite clays.

There are several critical factors determining the theoretical suitability of pedogenic palygorskite and sepiolite for $^{40}Ar/^{39}Ar$ dating, including intracrystalline K content, crystallization age, and crystal lattice retention or (conversely) diffusion of Ar. Although the mineralogical purity of measured samples is always a concern due to the common inclusion of other phyllosilicate crystallites or intergrowths, the isomorphically substituted (non-exchangeable) K content of the clay fraction in palygorskite- and sepiolite-dominated soils has been reported to range between 0.00 and 3.30 weight percent (Singer et al., 1995), with at least one study reporting very high K_2O values of 5.69 percent (García-Romero et al., 2007). Therefore, palygorskite and sepiolite K contents, though normally low, can reach significant levels (Singer, 1989; García-Romero et al., 2007) and can contain sufficient intracrystalline K to perform $^{40}Ar/^{39}Ar$ dating (Robins, 2010). However, to obtain enough clay for dating, the clays must be chemically extracted from the bulk calcite matrix. To determine the effects of chemical extraction, K content must be measured after each successive selective chemical dissolution procedure.

Elemental composition plays a key role in the chemical and physical behavior of the fibrous clays during extraction and purification procedures. For example, Fe-rich varieties of palygorskite may prove more susceptible than Al-rich palygorskites to acidity (Singer, 1989). It has also been suggested that sepiolite may be less robust than palygorskite to acid solutions (Corma, 1987; Singer, 1989), which poses potential challenges when chemically extracting mixed palygorskite and sepiolite mineral assemblages from petrocalcic soil samples. In addition, differing degrees of isomorphous substitution can affect the cation exchange capacity, adsorption potential, and flocculation behavior of any phyllosilicate. Thus, an extraction procedure that works well for one palygorskite locality may not work as well for a locality having a distinct palygorskite composition.

The uncertain physical stability of these fibrous clays must be considered when selecting a set of extraction procedures, or when evaluating the feasibility of isotopic analyses. Crushing and grinding have been proven to reduce the crystallite size of sepiolite and other clays (Kojdecki et al., 2005; Bastida et al., 2006), which, for this study, is inferred as evidence for the detrimental effect of grinding upon the Ar retention of phyllosilicate lattices. This raises special concern given the already small (~0.25 µm, or less) diameter of observed pedogenic palygorskite and sepiolite fibers. For this reason also, microdrilling zones of concentrated fibrous clay from indurated soil is not an advisable sampling method for geochronologic purposes. Ultrasonic treatments are similarly inadvisable.

Temperature can also adversely affect the stability or isotopic signature of phyllosilicates. Most published research on temperature effects on fibrous clays focuses on the somewhat elevated temperatures at which palygorskite and/or sepiolite begin to dehydrate or to deform structurally. Both palygorskite and sepiolite are known to contain (1) surface-adsorbed water, (2) water molecules in surface channels (zeolitic water), (3) water molecules bound to octahedral sheet edges, and (4) structural hydroxide groups bound within the octahedral sheet (Hayashi et al., 1969; Balci, 1996; and others). Loss of surface-adsorbed or zeolitic water may occur at 70°C, however, loss of structural water and folding of the crystal lattice may not begin below 190°C, and may be reversible up to 350°C (Kuang et al., 2004). Total dehydroxylation has been reported to require temperatures of 860°C (Kuang et al., 2004). At present, there have been no studies to determine the Ar diffusion parameters (E, activation energy, and $D_{0,}$ the frequency factor) from which crystal closure temperatures for palygorskite and sepiolite are derived using the diffusivity equation $D = D_0 \exp(-E/RT)$ (McDougal & Harrison, 1988). However, the extremely fine crystal dimensions of most pedogenic palygorskites and sepiolites, their relatively low potassium contents, and their low crystallization temperature all force assumption of a very low (<<100°C) closure temperature for $^{40}Ar/^{39}Ar$ dating purposes.

Selection of Extraction Methods

For the reasons presented above, selective chemical dissolution of calcium carbonate and amorphous silica cements is an unavoidable procedure for study of pedogenic palygorskite and sepiolite. Existing laboratory methods were considered for this experiment in the light of pH, temperature, and logistical constraints associated with the genesis, micromorphology, geochemistry, and stability of pedogenic palygorskite and sepiolite. There exists no universally accepted nor universally successful procedure to extract or to purify a monomineralic phyllosilicate mineral fraction (Arroyo et al., 2005), let alone one composed chiefly of fibrous clays.

Choices of methods for selective dissolution of pedogenic carbonates are limited; buffered sodium acetate is one of the most commonly cited treatments (Vanden Heuvel, 1966). Hydrochloric acid was rejected as a viable method for carbonate dissolution in this study because existing data suggest that the harshly acidic conditions of HCl treatment can damage the structure of phyllosilicate lattices, especially fibrous clays (Biermans & Baert, 1977; Singer, 1989; Wang et al, 2004). Fibrous clay lattices may be especially affected by strong acids via dilation of structural channels (Alvarez, 1984). Therefore, buffered pH 5 sodium acetate solution (NaOAc) (Jackson, 1965; Kunze and Dixon, 1986) was selected as the most practical alternative. Vanden Heuvel (1966) determined that NaOAc does not affect palygorskite, at least during short-duration treatments, but also demonstrated, based on a broadened 1.23 nm peak in XRD data, that extended NaOAc treatment can damage sepiolite. Importantly, other researchers (Arroyo et al., 2005) have successfully modified the NaOAc carbonate removal method (for extraction of smectite reference clays) to avoid altering clays at high temperatures and low pH, yet to simultaneously ensure that extracted clays are free of carbonates. Thus, a modified version of the NaOAc buffer method (Kunze and Dixon, 1986; Soukup et al., 2008) was chosen as the most practical means of extracting palygorskite and sepiolite.

A second treatment, to remove amorphous silica, is also unavoidable, because of the close association of amorphous silica with pedogenic palygorskite and sepiolite, and because the acetate treatment is only effective at removing carbonates. A wider range of options are available for the selective removal of amorphous silica, iron, and aluminum phases, although each method differs in effectiveness and is tailored to distinct needs. Removal of iron and aluminum oxides is recommended because they are common accessory phases in soil environments, including petrocalcic soils, and can persist as contaminants in extracted phyllosilicate mineral fractions. Tiron treatment was selected as the most practical means to remove not only amorphous silica but also iron and aluminum oxide phases (Biermans & Baert, 1977; Kodama & Ross, 1991) from the clay-sized particle fraction of samples in this study. Tiron (4,5-Dihydroxy-m-benzene disulfonic acid, disodium salt) is reported to be at least as effective at dissolving Fe and Al oxides as hydroxylamine hydrochloride treatment and also the acidified oxalate under darkness method, but more effective at dissolving amorphous silica (Shang & Zelazny, 2008). Moreover, Tiron has been specifically demonstrated not to attack sepiolite (nor illite, kaolinite, halloysite, or montmorillonite) (Biermans & Baert, 1977; Shang & Zelazny, 2008). Alternative treatments, such as citrate-dithionite bicarbonate, and EDTA, either are not specifically designed to dissolve silica, or are more controversial regarding their effect upon the geochemistry or structural integrity of phyllosilicate minerals (Wang et al., 1981; Campbell & Schwertmann, 1985; Shang & Zelazny, 2008).

Treatments for the removal of soil organic matter were not performed because of (1) generally low weight percents of organic matter in late-stage, ancient petrocalcic horizons (Robins, 2010b), and (2) an increased potential for adverse effects with each additional chemical treatment applied to the samples. Common procedures such as H_2O_2 oxidation of soil organic matter have been suggested to damage phyllosilicate crystal integrity (Douglas & Fiessinger, 1971; Soukup et al., 2008), and alternative procedures could have comparably adverse effects (see Campbell & Schwertmann, 1985).

Site Selection

Petrocalcic soil samples were collected from (1) Mormon Mesa, in southern Nevada, and (2) the Jornada Experimental Range (JER) La Mesa geomorphologic surface (also called the La Mesa-Jornada I complex) near Las Cruces, New Mexico (Figures 2.1 and 2.2). In addition, reference standards of palygorskite and sepiolite were purchased from the Clay Minerals Society Source Clays Repository. Mormon Mesa and JER La Mesa represent the best study sites for this project because the genesis, profile morphology, and micromorphology of their petrocalcic horizons are well-studied, and because they are known to contain palygorskite and/or sepiolite clays. These soils are among the best known examples of late-stage petrocalcic soils in the world (Gile et al., 1981; Bachman & Machette, 1977; Brock and Buck, 2009). Moreover, their absolute ages are well-constrained by tephrachronologic and/or magnetostratigraphic markers (Gile et al., 1981; Williams et al., 1997; JER LTER, 2003; House et al., 2005).

Mormon Mesa is an extensive, geologically old (~5 Ma), geomorphologic surface (Figure 2.1) capped by a well-documented stage VI petrocalcic soil containing significant pedogenic palygorskite and sepiolite (Gardner et al., 1972; Brock, 2007; Brock and Buck, 2009). Much of the micromorphological and mineralogical characterization of the Mormon Mesa petrocalcic horizons has already been conducted (e.g., Brock, 2007; Brock & Buck, 2009), thereby laying the groundwork for this study. The present extraction study was also conducted in tandem with new chemical and mineral investigation of the Mormon Mesa petrocalcic soil profile (Robins, 2010b).

Similarly, the JER La Mesa geomorphologic surface is another prime location for this study because it, too, occurs over a broad area (Figure 2.2), is geologically old (~780ka - 2Ma), and exhibits well-documented petrocalcic horizons known to contain pedogenic palygorskite and sepiolite (Bachman & Machette, 1977; Gile et al., 1981; Monger 1991a).

Methods

This experiment was designed to extract the phyllosilicate mineral fraction of the petrocalcic soil in a manner that would preserve clay crystal integrity and chemistry, and which would also yield sufficient mass for comparative instrumental analysis before and after each extraction step. To assess both physical and chemical properties, three types of instrument analysis were employed: (1) scanning electron microscopy coupled with energy dispersive x-ray spectroscopy (SEM-EDS), (2) inductively coupled plasma spectrometry (ICP), and (3) X-ray diffraction (XRD) analysis. Prior to treatment, clays were studied *in situ* via SEM-EDS. Aliquots of extracted clay were studied using all analytical methods following the NaOAc treatment, and again following the subsequent Tiron treatment (Figure 2.3).

Sampling

Intact, oriented blocks of petrocalcic soil approximately 20 x 20 x 20 cm^3 were cut from the massive horizon (*sensu* Brock, 2007; Brock & Buck, 2009) of Mormon Mesa, NV in October, 2006, and from the most indurated horizon (Gile et al., 1981) of the JER La Mesa soil in May, 2007, using a Wacker BTS 1035 diamond-blade concrete-cutting saw. Municipal water was sprayed on the saw blade while sampling these extremely indurated soil horizons to prevent overheating or seizing of the blade. A total of thirteen samples were collected, nine from Mormon Mesa and four from the JER La Mesa soil (Figure 2.4).

Based on existing soil characterization of the Mormon Mesa geomorphologic surface and soil series (Soil Survey Staff, 2006 & 2009; Brock, 2007) and for the JER La Mesa soil geomorphologic surface and soil profiles (Gile et al., 1981), a conservative compositional estimate of five percent clay by mass was assumed for all samples in this study. It was anticipated that 10 g of pedogenic clay would be needed for complete analysis of each sample. Because the goal of this study was to preserve the size and integrity of phyllosilicate crystals as near as possible to their *in situ* condition, samples could not be ground or crushed. Instead, approximately 200 g of petrocalcic soil fragments 1-10 cm^3 in size were hammered and chiseled as lightly and with as few blows as necessary from the primary sample blocks. Care was taken to discard the outermost, one to two centimeter thick erosional rind of the samples (the surface exposed in the soil profile) to prevent contamination by organic matter or recent soil geomorphologic processes. Fragments from the outermost centimeter of the cut surfaces of the samples were also discarded, because these edges were influenced by municipal tap water (normally containing dissolved salts and other compounds) during sampling.

Standards of palygorskite and sepiolite were purchased from the Clay Minerals Society Source Clays Repository and, therefore, arrived already processed (i.e., crushed or mixed). The palygorskite standard, PFl-1 (palygorskite from Gadsden County, Florida) arrived as a finely-ground powder. The sepiolite standard, SEP-Sp1 (a Miocene sepiolite from Valdemore, Spain) arrived as intact, ~8 cm^3 aggregates that were then crushed into a < 2mm powder with a mortar and pestle. No further processing of the standards was done in this study prior to their chemical treatment alongside the petrocalcic samples.

Selective dissolution and fractionation

The first step in the phyllosilicate extraction process was to selectively dissolve soil carbonate, by immersing 200 g of petrocalcic soil from each sample in ~ 1 L pH 5.0 buffered sodium acetate (NaOAc) (Jackson, 1965; Kunze and Dixon, 1986). Because the ultimate goal of this project was to provide material for geochronology, several modifications to the established laboratory methods were necessary. First, 1-8 cm^3 fragments of the intact soil sample blocks had to be used instead of < 2 mm crushed sample, because crushing could potentially cause release of $^{40}Ar^*$ from comminuted clay crystallites (the * indicates accumulated radiogenic argon). Second, phyllosilicates are known to expand, dehydrate, and sometimes undergo changes in crystal geometry upon heating, thus heating of the samples during treatment and to expedite drying was limited to ~ 50°C to prevent $^{40}Ar^*$ diffusion from phyllosilicate lattices. Each sample in solution was heated only one time for one hour, on a hot plate, and was stirred regularly while heating. Third, dissolution procedures were modified to accommodate the large amounts (200 g) of sample needed to obtain the 10 g of clay required by the experimental design.

Daily stirring and regular replacement of neutralized NaOAc with fresh buffer solution (preceded by high-speed centrifugation to retain clay-sized particles) were practiced to expedite dissolution of multiple, large sample masses in one liter beakers at room temperature. Daily stirring was also mandated because CO_2 trapped in settled soil can lower local pH and cause phyllosilicate dissolution (Arroyo et al., 2005). Carbonate dissolution required four to six months on average to produce a minimally sufficient mass of clay for the needs of this study, and the duration of treatment could not be held constant across all samples.

After carbonate dissolution, samples were transferred to 250 mL polycarbonate centrifuge tubes, centrifuged, and rinsed following standard NaOAc procedures. The clay-sized particle fraction of each sample was extracted following the methods of Soukup et al. (2008). Pipetted suspensions of the clay-sized fraction were oven-dried in one liter glass beakers at 50°C to facilitate evaporation. Drying of the samples typically required several days. The phyllosilicate fractions were divided into two aliquots for (1) instrument analysis of acetate-treated phyllosilicate material, and (2) tiron treatment and ^{40}Ar/^{39}Ar geochronology. As much as 13 g of clay were extracted from some samples, however, others produced as little as three grams and additional petrocalcic source material had to be treated with NaOAc to attempt to obtain the necessary mass of clay. Aliquots of three grams, minimum, of the dried clay fraction were taken for instrumental analysis after NaOAc treatment, while four gram aliquots were advanced for Tiron treatment.

Necessary modifications to the Tiron method included reduced heating (~50°C instead of 80°C) of the sample during treatment. In addition, the logistics of treating 14 samples each in excess of four grams precluded use of the prescribed sample-to-solution ratio. Instead, all samples were immersed in one liter of Tiron solution in plastic beakers and heated at 50°C for one hour in a water bath. Following treatment and rinsing, further aliquots were set aside for instrument analysis and for vacuum-encapsulated argon dating. Extensive, repeat rinsing and centrifugation of the samples – eight cycles or more – proved necessary, because a faint green color (indicating Tiron solution) persisted in the supernatant despite the prescribed rinse and centrifugation cycles. Moreover, Tiron appeared to have a deflocculating effect on the fibrous clays, which led to concerns of sample fractionation via loss of the finest clay particles with decanting. Loss of sample was also a concern due to low overall clay yields from some samples. Persistence of Tiron residue despite a colorless supernatant became apparent after drying for some samples, when the residue was visible as a purple stain on dried sample fractions. In such cases, further rinsing was performed. Readers are referred to Appendix 2.1 for further details on extraction procedures employed in this study.

Instrumental Analyses

Instrument analysis of extracted pedogenic clays for this study included SEM-EDS, ICP, and XRD, and was intended to detect any treatment effects, adverse or otherwise, imparted by the extraction procedures.

SEM-EDS analyses were performed on oriented thick sections and billet-mounted extract powders. To characterize the micromorphology and rough elemental composition of pedogenic clays *in situ* within the petrocalcic soil, oriented, glass-mounted one-millimeter thick sections were cut, polished to 1200 grit, etched in 10% HCl for 10 seconds, and sputter-coated with gold for 75 seconds. Analyses of clay aliquots following chemical extraction and fractionation steps were conducted by mounting flakes of dried sample aliquot on aluminum billets capped with two-sided carbon tape. These samples were then sputter-coated with gold for 75 seconds. All samples were analyzed with a JEOL JSM 5600 scanning electron microscope equipped with an Oxford energy dispersive X-ray spectrometer in the UNLV Electron Microanalysis and Imaging Laboratory (EMIL). The EDS data interpretation software was changed during the course of this analysis, therefore some samples were interpreted using ISIS software, while others were interpreted using INCA software.

Aliquots (0.50 g) of extracted palygorskite were taken for inductively-coupled plasma spectrometric (ICP) analysis following the acetate and tiron treatments. ICP analysis was used to determine the content of Al, Ca, Fe, K, Mg, Na and other elements (19 total) in the clay-sized particle fraction of the petrocalcic soils. ICP was chosen in lieu of other geochemical instruments because it seemed best suited to (1) detect trace amounts of intracrystalline K within the clays, (2) assess a wide range of elemental constituents of the clays, and (3) fit the financial and temporal constraints of this study. All ICP aliquots were analyzed by Utah State University Analytical Laboratories (USUAL) staff on a Thermo Electron Iris Advantage inductively coupled plasma photospectrometer, following total digestion of the 0.5 g powdered clay samples via a four-acids treatment. Paired, two-tailed t-tests were performed in GraphPad Prism and Microsoft Excel to assess the statistical significance of changes in elemental concentrations between treatments.

X-ray diffraction analysis of bulk soil mineralogy was conducted on crushed, powdered samples. XRD analysis of the clay-sized particle fraction was performed on aliquots extracted following both the acetate and the tiron treatments. Phyllosilicate aliquots for XRD analysis were further purified using mild sodium hypochlorite and citrate-dithionite buffer treatments following the methods of Soukup et al. (2008). Next, the samples were divided into two further aliquots for saturation with $MgCl_2$ and KCl (standard treatments for differentiation of phyllosilicate minerals in XRD analysis). Following base-line XRD analysis, the Mg-treated samples were saturated with ethylene glycol under vacuum at 50°C overnight, and re-scanned. Similarly, K-saturated slides were scanned, heated to 350°C for two hours and scanned again, and then heated to 550°C for two hours and scanned a third time.

All XRD analyses were conducted on a PANalytical X’pert Pro X-ray diffraction spectrometer at the UNLV XRF/XRD Laboratory. Bulk powder XRD data were obtained using Cu Kα radiation for continuous, 15 minute spinner-plate scans from 4 to 80° 2θ, at

40 kV and 40 mA, and using 1/2° antiscatter and 1/4° divergence slits. All phyllosilicate XRD analyses used Cu Kα radiation for continuous, 10 minute flat-stage scans from 3 to 40° 2θ, at 45 kV and 40 mA, and using 1/4° antiscatter and 1/8° divergence slits. In isolated cases where the 550°C heating caused sample peeling or curling off of the glass slide, the 550°C samples were each re-mounted and scanned as flattened clay flakes on a standard spinner plate. Bulk powder XRD data interpretations were conducted using XPert High Score Plus software. Phyllosilicate interpretations were also made via comparison to published clay mineralogy and x-ray diffraction references (Dixon & Weed, 1989; Moore & Reynolds, 1997; Poppe et al., 2001), as well as to analytical results from the reference standards.

Results

SEM-EDS Data

SEM-EDS analysis of petrocalcic thick-sections revealed the very common occurrence of fibrous clays, inferred to be palygorskite and/or sepiolite, throughout most of the Mormon Mesa samples. Fibrous phyllosilicates were found as skeletal mats around calcite rhombs, as individual fibers radiating from the sides of quartz sand or silt grains, and as concentrically zoned bundles of fibers in pisolites or filled voids (Figure 2.5 A-E). Energy dispersive x-ray spectra reveal elemental compositions dominated by Si, Mg, and variable Al, with occasional, minor peaks of Fe, K, and other cations (Figure 2.5 F), consistent with the known composition of palygorskite and sepiolite. The tiny, nanometer-scale diameter of the fibers relative to the one to two micrometer interaction volume of the EDS beam made it impossible in most cases to obtain a pure spectrum for individual phyllosilicate fibers or aggregates. Influences from surrounding carbonates, carbonate intergrowths, primary grains, or other phases cannot always be eliminated, and it is therefore not possible to confirm mineralogy based solely upon SEM-EDS data (although reasonable inferences can be made). Nevertheless, observations of fibrous clays within the petrocalcic horizon of the study samples match previous observations of palygorskite and sepiolite by other researchers (Brock, 2007; Brock & Buck, 2009).

SEM-EDS analysis of the JER La Mesa thick sections revealed a lesser abundance of the fibrous clays, as well as the common presence of non-fibrous phyllosilicates (Figure 2.6 A&B). Compared to the Mormon Mesa samples, greater amounts and more varied morphologies of amorphous silica were also observed (Figure 2.6 C &D). When present, the fibrous clay species appeared more finely crystalline than the Mormon Mesa samples, with more solitary fibers that proved difficult to image due to charging and which produced only a weak Mg peak (Figure 2.6 E-F). Both fibrous and non-fibrous clays were seen coating primary grains, and fibrous clays were also seen forming porous, skeletal mats within the carbonate-indurated matrix.

SEM-EDS analysis of the extracted phyllosilicate aliquots and reference standards revealed apparently identical crystallite morphologies in both the acetate-treated and the acetate-plus-tiron-treated samples. Palygorskite and/or sepiolite from the post-treatment aliquots retain the fibrous habit and elemental signature exhibited within the *in situ* data, but are concentrated into dense, bladed or matted aggregates (Figure 2.7). In addition, SEM-EDS analysis successfully identified poorly fractionated or incompletely purified samples, i.e., those initially containing silt-sized grains or abundant calcium carbonate of any particle size class. In such cases, the samples were re-fractionated and/or re-treated as needed until extraction was successful. SEM-EDS analysis also failed to detect any obvious morphological or compositional changes to the clays.

ICP Data

Total elemental analysis of all nine Mormon Mesa samples and both reference standards was performed after NaOAc and also after Tiron treatments. Due to limited yield of clay-sized particles, as well as to temporal constraints, it was only possible to obtain ICP aliquots of most JER La Mesa clay samples following the acetate treatment, thus, before-and-after comparisons were possible for only one JER la Mesa sample. Results from ICP analysis of all samples are reported in Tables 2.1 A&B, while standard replicate data are reported in Table 2.2.

ICP data reveal distinct compositional trends between sample groups (see Tables 2.1 A&B). That is, samples from Mormon Mesa were similar to each other, but distinct in composition from the samples from JER La Mesa, the palygorskite standard, and the sepiolite standard. Mormon Mesa samples generally matched the composition of the palygorskite reference standard. For example, the mean Al concentration in the Mormon Mesa acetate-treated aliquots (2.663 %) is similar to the palygorskite acetate value (2.760 %), but distinct from the corresponding JER La Mesa mean (5.330 %) and the sepiolite acetate value (0.651 %). Replicate aliquots of untreated palygorskite and sepiolite standards were used as controls for analytical and background variability (Table 2.2).

Statistically significant treatment effects could only be sought among the Mormon Mesa sample ICP data because there were not enough post-tiron aliquots from the JER La Mesa samples (insufficient mass yields). Paired t-tests between acetate-treated and tiron-treated samples were performed for all elements (Table 2.3) except B, Cd, Mo, and Pb, for which insufficient data pairs were available because elemental concentrations were at or below instrument detection limits. No statistically significant trends between treatments ($p > 0.05$) were found for Fe, Mn, Na, Ni, nor S, however, statistically significant differences ($p < 0.05$) in mean elemental composition between treatments were identified for Al, Ca, Co, Cr, K, Mg, P, Sr, and Zn. Average increases were noted for Al and Mg, as well as Cr, while all other significant differences involved apparent decreases in mean element concentrations.

XRD Data

Bulk soil powder XRD analyses consistently returned compositions of calcite and low magnesian calcite, quartz, and feldspar for both Mormon Mesa and Jornada La Mesa (Figure 2.8). Diffuse, low intensity phyllosilicate peaks, most commonly of palygorskite, were also discernable via bulk powder analysis of some samples. Bulk mineralogy varied little between petrocalcic samples (Appendix 2.2).

Analysis of the clay-sized particle aliquots from the Mormon Mesa samples returned compositions dominated by palygorskite, quartz, minor sepiolite, and trace amounts of chlorite, illite, kaolinite, and/or smectite (Figure 2.9). Insufficient sample yields precluded analysis of all samples in this study, and no XRD data are available for the JER La Mesa samples due to low yields at the time of analysis. Complete XRD data for successfully extracted samples and standards are presented in Appendix 2.3. XRD patterns for Mormon Mesa samples generally approximated the palygorskite reference standard.

Interpretation and Discussion

The two central questions of this study were: (1) whether successive chemical and physical treatments affect the lattices of pedogenic palygorskite and sepiolite, and (2) whether the laboratory procedures tested here affect the geochemistry of the fibrous clays and, therefore, their suitability for isotopic dating. Each of the analytical techniques employed (SEM-EDS, ICP, and XRD) provide a different, but complementary, breadth and depth of information that must be carefully interpreted to answer these questions. Use of the Clay Minerals Society reference standards was the critical factor enabling linkage and interpretation of micromorphological, geochemical, and mineralogical data across the suite of analyses.

No physical extraction effects were detected using SEM-EDS analysis, however, these results must still be interpreted with caution. Transformations or morphological effects may not be truly discernable without nanometer-scale instrument resolution (Krekeler et al., 2005), and EDS data are not sufficient to detect chemical effects. It is acknowledged here that transmission electron microscopy (TEM), impossible in this study due to funding and time constraints, would be better suited than SEM-EDS to resolve nanometer-scale dissolution or pitting of phyllosilicate crystallites. SEM-EDS analysis did successfully facilitate detection of incomplete carbonate dissolution and/or particle size fractionation procedures, which were then rectified with a second round of treatment and particle size fractionation on the problematic sample(s).

Micromorphological observations from SEM-EDS analysis also corroborated the pedogenic origin of the fibrous phyllosilicates in the petrocalcic soil samples. Specifically, the delicate, matted morphology of the phyllosilicate fibers, and their expression and positions relative to other mineral phases within the soil fabric both strongly support a pedogenic origin for the clays and firmly refute a detrital origin (Singer and Norrish, 1974; Watts, 1980; Verrecchia & Le Coustumer, 1996; Robins, 2010b). Further implications of these clays for the pedogenic history of the Mormon Mesa soil profile are discussed elsewhere (Brock, 2007; Robins, 2010b). Micromorphological observations from the JER La Mesa samples, on the other hand, also revealed authigenic, but non-fibrous clays, as well as more clearly detrital phyllosilicate species. Higher concentrations of other cations in the EDS spectra from JER La Mesa samples further suggests the presence of several phyllosilicate species.

ICP analyses are naturally better suited than SEM-EDS techniques to detect chemical changes, but do offer important mineralogical insights as well. For instance, the ICP data favor the conclusion that the Mormon Mesa clays are mostly composed of palygorskite rather than sepiolite, while the JER La Mesa samples match neither palygorskite nor sepiolite compositions and are more likely dominated by another phyllosilicate mineral, such as smectite. Interestingly, Al and Mg weight percents obtained for the palygorskite standard in this study are noticeably less than values reported for palygorskites in previous publications (e.g., Newman & Brown, 1987). In contrast, ICP data for the sepiolite standard match published data well (Newman & Brown, 1987), and the ICP values as a whole seem internally consistent for all sample groups in this study. Contributions from non-palygorskite intergrowths or inclusions could be one explanation for the deviation of the palygorskite standard from externally reported values. Moreover, elemental compositions of both palygorskite and sepiolite can and do often vary widely between, and even within, depositional environments (Corma et al., 1987; Singer, 2002; García-Romero et al., 2007).

Evidence in the ICP data for chemical changes also must be carefully interpreted. Paired elemental data reveal quantitative differences in the composition of clay-sized particle extracts between treatments, but the cause of these differences – whether they indicate desirable purification of sample via successful removal of silica and sesquioxide phases, or whether they instead indicate adverse effects upon the phyllosilicate lattice crystal integrity – remains uncertain. Effects vary from element to element. For example, the paired Fe data are statistically inconclusive, yet do allow tentative interpretations. Variable iron oxide contents (abundant to absent) among the raw Mormon Mesa samples could produce equally variable changes from sample to sample between treatments. Such variability combined with the successful removal of iron oxides by Tiron treatment, would explain the lack of statistical trend in the Fe data. It is also speculated that chelation or partial losses of metals from trace organic compounds might account for some of the decreases in other elements, but additional data are needed to test this possibility.

Aluminum and especially magnesium data may also lend support for successful extraction of silica and sesquioxides. Relative weight percents of Al and Mg increased in the Mormon Mesa samples after treatment, so Tiron may have successfully purified their palygorskite and sepiolite cryptocrystalline impurities (and decreased Si weight percents). Moreover, the overall Mg:Al ratio did not change significantly between the acetate- and tiron-treated aliquots for Mormon Mesa ($p = 0.384$; $t = 0.922$; $df = 8$), implying that the clay crystallites were not damaged. Conversely, Mg and Al percentages did change between treatments for each of the two standards, as well as for the one JER La Mesa sample for which both acetate and tiron aliquots were available. The Mg:Al ratio decreased in the sepiolite standard but increased in the palygorskite standard, possibly confirming distinct behavior of the two clay species in treatment or, alternatively, their distinct amorphous phase contents. Given only one pair of data points for each of the standards, the significance of this observation remains unverified. Moreover, the variability within replicate standard analyses (see Table 2.2) could be suggestive of either compositional heterogeneity or analytical errors.

Although it is difficult to determine from the ICP data alone whether Tiron adversely impacted the crystal integrity and geochemistry of the fibrous clays, the data are interpreted as consistent with effects caused by loss of amorphous silica, iron oxides, and other amorphous phases during Tiron treatment. However, it remains possible that mineralogical impurities within incompletely extracted aliquots, as well as compositional heterogeneity within even mineralogically pure aliquots, have partly masked the full treatment effects. Inseparable mixtures of distinct minerals have previously been found to imply false compositional variability in palygorskite and sepiolite samples (Galan & Carretero, 1999), and could theoretically imply false effects in this study. In this way, ICP data provide (1) suggestive but only partial evidence for the successful extraction of authigenic fibrous clays from amorphous mineral phases, and (2) possible evidence for compositional heterogeneity of the extracted aliquots in the form of natural variability as well as mineralogical intergrowths or inclusions.

Like the ICP data, XRD analyses indicate that the clay-sized particle fraction of the Mormon Mesa samples is predominantly composed of palygorskite. However, XRD data also indicate that the Mormon Mesa samples contain varying amounts of sepiolite and quartz, as well as minor to trace amounts of illite, kaolinite, chlorite, and/or smectite (Figure 2.9). These data are consistent with SEM-EDS observations of isolated smectite clay aggregates in Mormon Mesa by Robins (2010b), as well as previous soil characterization research (Brock, 2007; Brock & Buck, 2009). Quasi-quantitative estimates of one to ten percent non-fibrous clays or clay-sized quartz would certainly explain some of the ICP data variability, and could also indicate inclusions or interlayers of other phyllosilicates within authigenic palygorskite lattices. Although XRD data are not available for the JER La Mesa samples, the SEM data alone are strong enough to confirm the presence of even more abundantly distinct phyllosilicates than were found in Mormon Mesa.

No adverse treatment effects (i.e., no peak broadening or shifting) occurred in the X-ray diffraction spectra of the palygorskite and sepiolite minerals, however, changes are apparent in the relative mineralogical assemblages between treatments. Specifically, relative peak intensities of illite, chlorite, and kaolinite sometimes increased (albeit slightly) after Tiron treatment (see Figure 2.9). Transformation of palygorskite and/or sepiolite to multiple minerals during the one hour, low temperature, alkaline Tiron procedure is clearly not a plausible explanation. Small crystals are more subject to dissolution or alteration during chemical treatments than larger crystals (Shang & Zelazny, 2008), but would be expected to result in some crystallites that were only partially attacked. Such dissolution of the fibrous clays seems unlikely because XRD data do not exhibit the broadened or altered palygorskite and sepiolite peaks that partially dissolved crystallites should produce. Therefore, three plausible explanations remain, including (1) effects from Tiron treatment, removing amorphous phases and enhancing phyllosilicate d spacings, (2) preferential loss of the finest fibrous clays during the sample centrifugation/rinse cycles, and (3) sample heterogeneity. Of these, the first is most likely. The second assumes relatively larger sizes or greater flocculation strength of the non-fibrous clay crystallites, or breaking of fibrous crystallites into smaller fragments upon stirring. Thus, while no evidence was found for damage to palygorskite and sepiolite lattices in the XRD data, it is possible that undesireable crystallite size-biasing may have occurred.

Pretreatment (i.e., sodium hypochlorite, citrate-dithionite buffer, $MgCl_2$, and KCl) of the clay-sized particle extracts for XRD analysis are considered an essential part of phyllosilicate mineral determinations and are needed to produce clear diffraction patterns, and diagnostic peak behaviors. Yet these same pretreatments could also theoretically have damaged palygorskite and sepiolite as described in the introduction, above. Pretreatment could also obscure crystallographic differences between extraction treaments, even though all aliquots (acetate and acetate-plus-Tiron) were treated identically and simultaneously. Fortunately, evidence discounting a "masked" effect is suggested by the aforementioned differences in relative peak intensities in the Tiron samples. Furthermore, geochemical differences indicative of Ar losses would not be expected to appear in the XRD spectra and are only critical for geochronologic analyses. Nevertheless, future geochronologic studies of phyllosilicate extracts should thoroughly explore mineral and geochemical characterization techniques that do not require their own additional suite of chemical treatments.

The combined results of this study indicate that total mineralogical purification of pedogenic clay-sized mineral fractions is extremely challenging, time consuming, and may not be practical, even for petrocalcic soils with phyllosilicate fractions overwhelmingly dominated by palygorskite and sepiolite. Commonly reported accessory minerals in the clay-fraction of palygorskite- and sepiolite-bearing soils include chlorite, illite, smectite, carbonate, and gels of iron and/or silica, as well as clay-sized quartz (Galan & Carretero, 1999). Fine, lamellar intergrowths of smectite with palygorskite and/or sepiolite are not uncommon, and cannot be separated (Starkey & Blackmon, 1984; Abudelgawad et al., 1985; Güven et al., 1992). Even following purification and fractionation, one published analysis of the palygorskite standard used in this study, PFL-1, still resolved peaks representing an estimated 10% smectite, 7% quartz, 2% feldspar, and 1% other minerals – inclusions not greatly reduced from the composition of PFL-1 as shipped from the Source Clays Repository (Chipera & Bish, 2001). It is doubtful that a selective dissolution method for distinct phyllosilicate phases within a single soil sample can be found, given the overlapping or adjacent chemical stability fields of many phyllosilicates. Lattice transformation (dissolution and reprecipitation) during prolonged laboratory treatments can also be difficult to detect visually if the new mineral is morphologically similar to the replaced phase, as has been noted for lath-shaped smectites formed via dissolution of palygorskite and subsequent reprecipitation (Golden & Dixon, 1990).

Obtaining mineralogically and geochemically pure samples is especially challenging for pedogenic palygorskite and sepiolite because of their small size and intimate association with other minerals. Chipera and Bish (2001) note that mineral contaminants may persist even after high-speed centrifugation and particle size fractionation of samples. Even pedogenic carbonates have been reported to persist through treatment and fractionation, contributing to overall sample geochemistry despite their apparent absence in SEM-EDS or XRD data (Arroyo et al., 2005). SEM-EDS data in this study did identify mixed mineralogy as a result of incomplete treatment and fractionation procedures. Following repeat treatments, however, subsequent SEM-EDS data suggested that the clay-sized particle fraction had been successfully purified to solely palygorskite and/or sepiolite. Nevertheless, XRD data conclusively identified the persistence of other mineral phases in the sample, though in minor amounts. If such minerals are present as intergrowths, they may serve as zones of weakness and could behave differently from palygorskite and sepiolite during extended NaOAc buffer treatment, or during Tiron treatment, with uncertain implications for geochronology.

Potassium contents of the extracted clays do suggest theoretical viability for ^{40}Ar/^{39}Ar geochronology as attempted by Robins (2010b), however, several points bear consideration. First, the minimum K weight percent required for dating depends upon the geologic age of the samples. Higher analytical error is anticipated with progressively younger samples, therefore, greater K contents (approaching 1.0 wt % or more) are required in younger clays. Second, K concentrations in this study cannot be irrefutably assigned to either pure, authigenic palygorskite or sepiolite, nor to other phyllosilicates. The possible precipitation of authigenic palygorskite-smectite intergrowths documented in other environments (i.e., Krekeler et al., 2005), though perhaps unlikely in petrocalcic soils due to their soil solution chemistry and clay genesis via force of crystallization processes (Robins, 2010b), cannot be entirely discounted either. Thus, isotopic systems selected for pedogenic clays in petrocalcic soils must either accommodate or be corrected for minor inclusions of different clay species having potentially different stabilities, ages, and genetic histories. Furthermore, even if clay interlayers or inclusions are not present, geochronology studies must take into account that each phyllosilicate crystallite could still incorporate a mixture of distinct crystallization ages.

In summary, and based on all lines of evidence, the procedures performed in this experiment appear to have successfully removed amorphous silica and sesquioxide phases, and successfully isolated the clay-sized particle fraction of petrocalcic soil samples. The mineralogical heterogeneity of samples reflects the phyllosilicate makeup of the bulk soil, and cannot be greatly refined by any method. Because of the experimental design and the lack of better extraction procedures, it cannot be irrefutably determined whether NaOAc influences crystallinity or Ar retention. At a minimum, micromorphological evidence suggests, but cannot prove, that NaOAc has no detectable effect. The buffered NaOAc method is reported not to affect palygorskite (Vanden Heuvel, 1966); and XRD data in this study show strong, persistent peaks in both palygorskite and sepiolite reference standards despite treatment. Adverse chemical effects specifically caused by NaOAc and/or Tiron were not found, and are therefore cautiously refuted.

Physical effects were only tentatively identified in the possible loss of some or all of the smallest palygorskite or sepiolite crystals during extensive centrifugation cycles and incomplete settling of very fine clays. However, this effect could also be due to the successful extraction of amorphous mineral phases from the phyllosilicate fraction. It is also noted here that the use of dilute NaCl solutions during the prescribed rinsing steps required additional rinses in pure, distilled water to prevent interference of Cl^- ions with Ar isotope analysis. This extra rinsing may have exacerbated the size-bias of the phyllosilicate fraction. For the purposes of this study, such bias might prove beneficial by eliminating crystals too small to effectively retain Ar in the soil environment. However, such losses could adversely impact other studies of pedogenic clay genesis or geochemistry, and would certainly bias final determinations of clay-sized mineral percentages. Further work is needed to determine whether size bias indeed occurred, or instead whether sample heterogeneity can account for the mineralogical differences between treatments.

Recommendations for Future Research

Revised instrumental analyses in future attempts to better answer the questions addressed by this study might include TEM rather than SEM analysis to characterize nanometer-scale dissolution or disintegration of phyllosilicate lattices. Even with TEM analysis, however, corroborative datasets would prove necessary to determine with confidence the mineralogy and elemental composition of the extracted clay-sized particle fraction. Moreover, analysis of crystal damage via TEM may not be straightforward given the high susceptibility of palygorskite and sepiolite to electron beam damage (Krekeler & Guggenheim, 2008), and the statistical representivity of small sample aliquots could become an issue. Future studies could also benefit from the application of differential x-ray diffraction techniques, however, additional time, funds, and extraction yields would be requisite.

Modifications to sample processing and treatment temperatures necessary to prevent Ar diffusion out of crystal lattices may create effects that have not yet been quantified.

Results from this experiment can only assess the feasibility of selective chemical extraction at < 50°C. It is possible, if unlikely, that higher or lower temperatures, and shorter or longer sample treatment times could produce different results. Second, very few, if any, fragments of the 200 g petrocalcic samples dissolved completely during prolonged immersion in buffered pH 5 NaOAc solution. Instead, treatment of bulk soil was stopped when it appeared that sufficient clay yield was available, and/or when time constraints prevented further treatment. Future studies may face similar challenges, given the variability of clay and carbonate contents in petrocalcic soil samples. For example, in this study, Mormon Mesa samples were found to be more viable than JER La Mesa samples for geochronology purposes, although both soils present similar challenges.

Investigation of alternative selective dissolution methods for pedogenic carbonate and silica, as well as additional treatments to remove possible organic contaminants (Robins, 2010a) are recommended. Future studies could further quantify the ability of selective extraction procedures to purify phyllosilicates using synthetic solutions and laboratory-grown mineral samples of precisely known compositions. Innovations within isotopic techniques that yield higher detection limits, or which prove capable of additional purification of sample material, may also remedy some of the challenges identified by this study and by Robins (2010a). Last, future studies should also employ a range of geoanalytical techniques, including both micromorphology and geochemistry, to evaluate the quality of extracted pedogenic phyllosilicates.

Conclusions

No adverse chemical or mineralogical effects were identified as a result of NaOAc and Tiron extraction of pedogenic palygorskite and/or sepiolite from petrocalcic soils for isotopic analysis. The clays appear to have been successfully extracted without damage or changes to their crystal lattices nor to their geochemistry. However, theoretical considerations and/or post-analytical corrections must be made to quantitatively account for the phyllosilicate intergrowths or inclusions within the clay-sized particle fraction. Additional extraction treatments or procedures may also prove necessary (see Robins, 2010a). Petrocalcic soils from both Mormon Mesa and JER La Mesa were found to contain variable quantities of detrital phyllosilicates. SEM-EDS data also indicate that JER La Mesa samples especially must be more carefully considered for geochronology purposes, given numerous indications of smectite clay compositions and a reduced abundance of fibrous (authigenic) species as compared to Mormon Mesa.

High-resolution micromorphological and precise geochemical assessment techniques, conducted in tandem, are both essential for evaluations of clay-sized particle fraction extracts, especially from petrocalcic soils. Many chemical analyses of palygorskite and sepiolite published to date remain erroneous because of their inclusion or failure to correct for other mineral phases (Galan & Carretero, 1999; Arroyo et al., 2005), thus important insights to the genetic history of arid soil landscapes and other environments may have been missed. Given the diversification of geochemical toolsets and novel applications of isotopic techniques to pedogenic environments, this study underscores a great need for further research on the extraction and purification of specific mineral species from mineralogically diverse and genetically complex pedogenic samples. As an additional consideration, future efforts must ensure that standard laboratory methods continue to be tailored to and redefined for a given environment of study, and to the mineral phase of study. Publication or other communication of negative as well as positive experimental results are strongly encouraged to expedite the conclusively established success or impossibility of novel laboratory procedures or analytical techniques.

References

Abudelgawad, G., Viani, B.E., and Dixon, J.B., 1985. Palygorskite separation from dodecylammonium-treated clays. Clays and Clay Minerals, 33: 438-442.

Alvarez, A., 1984. Sepiolite: properties and uses. In: Singer, A., & Galan, E., eds. Palygorskite-sepiolite: Occurrences, genesis, and uses. Developments in Sedimentology, 37. New York, El Sevier: 253-287.

Alvarez, A., Santarén, J., Pérez-Castells, R., Casal, B., Ruiz-Hitzky, E., Levitz, P., and Fripiat, J.J., 1987. Surfactant adsorption and rheological behavior of surface-modified sepiolite. Proceedings of the International Clay Conference, Denver, 1985: 370-374.

Arroyo, L. J., H. Li, Teppen, B.J., and Boyd, S.J., 2005. A simple method for partial purification of reference clays. Clays and Clay Minerals, 53(5): 511-519.

Bachman, G.O. and Machette, M.N., 1977. Calcic soils and calcretes in the southwestern United States, U.S. Geological Survey Open File Report 77-794. 163 pages.

Balci, S., 1996. Thermal decomposition of sepiolite and variations in pore structure with and without acid pre-treatment. Journal of Chemical Techniques in Biotechnology, 66: 72-78.

Bastida, J., Kojdecki, M.A., Pardo, P., and Amorós, P., 2006. X-ray diffraction line broadening on vibrating dry-milled Two Crows sepiolite. Clays and Clay Minerals, 54(3): 390-401.

Biermans, V. and Baert, L., 1977. Selective extraction of the amorphous Al, Fe and Si oxides using an alkaline Tiron solution. Clay Minerals, 12(127): 127-135.

Blank, R.R. and Fosberg, M.A., 1991. Duripans of Idaho, U.S.A.: In situ alteration of eolian dust (loess) to an opal-A/X-ray amorphous phase. Geoderma, 48: 131-149.

Bouza, P. J., Simón, M., Aguilar, J., del Valle, H., and Rostagno, M., 2007. Fibrous-clay mineral formation and soil evolution in Aridisols of northeastern Patagonia, Argentina. Geoderma, 139: 38-50.

Bradley, W.F., 1940. The structural scheme of attapulgite. American Mineralogist, 25: 405-411.

Brauner, K. and Preisinger, A., 1956. Estruktur und Enstehung des sepiolits. Tschermaks Mineralogische und petrographisches Mitteilungen, 6:120-140.

Brock, A.L. and Buck, B.J., 2005. A new formation process for calcic pendants from Pahranagat Valley, Nevada: Implication for dating Quaternary landforms. Quaternary Research, 63: 359-367.

Brock, A.L. and Buck, B.J., 2006. Genesis of pisoliths and brecciation features in stage

VI Petrocalcic Horizons, Mormon Mesa, NV, USA. Poster presented at 18th World Congress of Soil Science, Philadelphia, PA, July 9-15 2006.

Brock, A.L., 2007. Characterization of stage VI petrocalcic horizons: S. Nevada and N.W. Arizona. Ph.D. Dissertation. University of Nevada Las Vegas, Department of Geoscience. 148 pages.

Brock, A.L. and Buck, B.J., 2009. Polygenetic development of the Mormon Mesa, NV petrocalcic horizons: Geomorphic and paleoenvironmental interpretations. Catena, 77: 65-75.

Callen, R.A., 1984. Clays of the palygorskite-sepiolite group: Depositional environment, age and distribution. In: Singer, A. and Galan, E., eds. Palygorskite-Sepiolite: Occurrences, genesis, and uses. Developments in Sedimentology, 37. New York, El Sevier: 1-37.

Campbell, A.S. and Schwertmann, U., 1985. Evaluation of selective dissolution extractants in soil chemistry and mineralogy by differential x-ray diffraction. Clay Minerals, 20: 515-519.

Chipera, S. J., and Bish, D.L., 2001. Baseline studies of the Clay Minerals Society source clays: Powder X-ray diffraction analysis. Clays and Clay Minerals, 49(5): 398-409.

Corma, A., Mifsud A., and Sanz, E., 1987. Influence of the chemical composition and textural characteristic of palygorskite on the acid leaching of octahedral cations, Clay Minerals, 22: 225–232.

Dixon, J.B. and Weed, S.B., eds., 1989. Minerals in soil environments, 2nd edition. SSSA Book Series 1. Madison, Soil Science Society of America. 1244 pages.

Douglas, L.A. and Fiessinger, F., 1971. Degradation of clay minerals by H_2O_2 treatments to oxidize organic matter. Clays and Clay Minerals, 19: 67-68.

Francis, M.L., Fey, M.V., Prinsloo, H.P., Ellis, F., Mills, A.J., and Medinski, T.V., 2007. Soils of Namaqualand: Compensations for aridity. Journal of Arid Environments, 70: 588-603.

Galan, E. and Castillo, C., 1984. Sepiolite-palygorskite in Spanish Tertiary basins: genetical patterns in continental environments. p. 87-124 In: Singer, A., & Galan, E., eds. Palygorskite-sepiolite: Occurrences, genesis, and uses. Developments in Sedimentology 37. New York: El Sevier, 352 pages.

Galan, E. and Carretero, M.I., 1999. A new approach to compositional limits for sepiolite and palygorskite. Clays and Clay Minerals, 47(4): 399-409.

García-Romero, E., Suárez Barrios, M., and Bustillo Revuelta, M.A., 2004. Characteristics of a Mg-palygorskite in Miocene rocks, Madrid Basin (Spain). Clays and Clay Minerals, 52(4): 484-494.

García-Romero, E., Suárez, M., Santarén, J., and Alvarez, A., 2007. Crystallochemical characterization of the palygorskite and sepiolite from the Allou Kagne deposit, Senegal. Clays and Clay Minerals, 55 (6): 606-617.

Gardner, L.R., 1972. Origin of the Mormon Mesa Caliche, Clark County, Nevada. Geological Society of America Bulletin, 83: 143-156.

Gile, L.H., Hawley, J.W., and Grossman, R.B., 1981. Soils and geomorphology in the Basin and Range area of Southern New Mexico - Guidebook to the Desert Project. New Mexico Bureau of Mines & Mineral Resources, Memoir 39. University of New Mexico, Socorro, 222 pp.

Golden, D.C. and Dixon, J.B.,1990. Low-temperature alteration of palygorskite to smectite. Clays and Clay Minerals, 38(4): 401-408.

Güven, N., de la Caillerie, J.-B.d'E., and Fripiat, J.J., 1992. The coordination of aluminum ions in the palygorskite structure. Clays and Clay Minerals, 40(4):457-461.

Hay, R.L. and Wiggins, B., 1980. Pellets, ooids, sepiolite and silica in three calcretes of the southwestern United States. Sedimentology, 27: 559-576.

Hayashi, H., Otsuka, R. and Imal, N., 1969. Infrared study of sepiolite and palygorskite on heating. The American Mineralogist, 53: 1613-1624.

House, P.K., Pearthree, P.A., Howard, K.A., Bel, J.W., Perkins, M.E., and Brock, A.L., 2005. Birth of the lower Colorado River – Stratigraphic and geomorphic evidence for its inception near the conjunction of Nevada, Arizona, and California, in: Pederson, J., and Dehler, C.M., eds., Interior Western United States: Boulder Colorado, Geological Society of America Field Guide 6.

Jackson, M.L.,1965. Soil chemical analysis: Advanced Course. Published by the author. Dept. of Soil Science, University of Wisconsin, Madison.

Jones, B.F., 1983. Occurrence of clay minerals in surficial deposits of southwestern Nevada. Sciences Géologiques Mémoires (Strasbourg), 72: 81-92.

Jones, B.F. and Galan, E., 1988. Sepiolite and palygorskite. Reviews in mineralogy, 19(1): 631-674.

Jornada Experimental Range Long Term Ecological Research (LTER) Program, 2003. Chronology of the Desert Project and vicinity, Sheet 2: The Jornada and Mesilla Basins. http://jornada-www.nmsu.edu/galleries/mapgallery.php.

Kodama, H. and Ross, G.J., 1991. Tiron dissolution method used to remove and characterize inorganic components in soils. Soil Science Society of America Journal, 55: 1180-1187.

Kojdecki, M.A., Bastida, J., Pardo, P., and Amorós, P., 2005. Crystalline microstructure of sepiolite influenced by grinding. Journal of Applied Crystallography, 38: 888-899.

Krekeler, M.P.S., Hammerly, E., Rakovan, J., and Guggenheim, S., 2005. Microscopy studies of the palygorskite-to-smectite transformation. Clays and Clay Minerals, 53(1): 92-99.

Krekeler, M.P.S., and Guggenheim, S., 2008. Defects in microstructure in palygorskite-sepiolite minerals: A transmission electron microscopy (TEM) study. Applied Clay Science, 39: 98-105.

Kuang, W., Facey, G.A., and Detellier, C., 2004. Dehydration and rehydration of palygorskite and the influence of water on the nanopores. Clays and Clay Minerals, 52(5): 635-642.

Kunze, G.W. and Dixon, J.B., 1986. Pretreatment for mineralogical analysis. In: Klute, A., ed. Methods of soil analysis part 1: Physical and mineralogical methods, 2nd edition. Agronomy Monograph 9. Madison, Soil Science Society of America: 91-100.

Machette, M.N., 1985. Calcic soils of the southwestern United States. Geologic Society of America Special Paper, 203: 1-21.

Monger, H.C. and Daugherty, L.A., 1991a. Neoformation of palygorskite in a southern New Mexico aridisol. Soil Science Society of America Journal, 55: 1646-1650.

Monger, H.C. and Daugherty, L.A., 1991b. Pressure solution: Possible mechanism for silicate grain dissolution in a petrocalcic horizon. Soil Science Society of America Journal, 55: 1625-1629.

Monger, H.C. and Kelly, E.F., 2002. Silica minerals. In: Dixon, J.B. and Schulze, D.G., eds. Soil mineralogy with environmental applications. SSSA Book Series No.7. Madison, Soil Science Society of America: 611-636.

Moore, D.M. and Reynolds, R.C., 1997. X-ray diffraction and the identification and analysis of clay minerals (2nd edition).New York, Oxford University Press. 378 pages.

Nettleton, W.D., ed., 1991. Occurrence, characteristics, and genesis of carbonate, gypsum and silica accumulations in soils. SSSA Special Publication No. 26. Madison, Soil Science Society of America. 149 pages.

Newman, A.C.D. and Brown, G., 1987. The chemical constitution of clays. In: Newman, A.C.D., ed. Chemistry of clays and clay minerals. Mineralogical Society Monograph No. 6. New York, John Wiley & Sons: 1-128.

Paquet, H., Duplay, J., Valleron-Blanc, M.-M., and Llerena, C.A., 1987. Octahedral compositions of individual particles in smectite-palygorskite and smectite-sepiolite assemblages. Proceedings of the International Clay Conference, Denver, 1985: 73-77.

Poppe, L.J., Paskevich, V.F., Hathaway, J.C. and Blackwood, D.S., 2001. A laboratory manual for X-Ray powder diffraction. U.S. Geological Survey Open-File Report 01-041.

Reeves, C.C. Jr., 1976. Caliche: Origin, classification, morphology and uses. Lubbock, Estacado books. 233 pages.

Retallack, G.J., 2001. Soils of the past: An introduction to paleopedology. Blackwell Science, Malden, MA, 404 pp.

Robins, C.R., 2010a. Towards ^{40}Ar/^{39}Ar geochronology of pedogenic palygorskite and sepiolite, Part II: lessons and technical implications for dating arid soils. In: Robins, C.R. Phyllosilicate mineralogy, ^{40}Ar/^{39}Ar geochronology, and genesis of petrocalcic soils in the southwest U.S.A. Ph.D. dissertation. UNLV Department of Geoscience, Las Vegas, NV: 56-94.

Robins, C.R., 2010b. Micromorphology, chemistry and phyllosilicate mineralogy of the Mormon Mesa petrocalcic soil, Nevada, USA: Genetic implications. In: Robins, C.R. Phyllosilicate mineralogy, ^{40}Ar/^{39}Ar geochronology, and genesis of petrocalcic soils in the southwest U.S.A. Ph.D. dissertation. UNLV Department of Geoscience, Las Vegas, NV: pages 94-174.

Shang, C. and Zelazny, L., 2008. Selective dissolution techniques for mineral analysis of soils and sediments. In: Ulery, A., and Drees, R., eds. Methods of soil analysis, part 5: Mineralogical methods. SSSA Book Series No. 5. Madison, Soil Science Society of America: 33-80.

Singer, A. and Norrish, K., 1974. Pedogenic palygorskite occurrences in Australia. American Mineralogist, 59: 508-517.

Singer, A., 1984. The paleoclimatic interpretation of clay minerals in sediments - a review. Earth-Science Reviews, 21: 251-293.

Singer, A., 1989. Palygorskite and sepiolite group minerals. In: Dixon, J.B. and Weed, S.B., eds. Minerals in Soil Environments (Second Edition). SSSA Book Series. Madison, Soil Science Society of America: 829-872.

Singer, A., Kirsten, W., and Bühman, C., 1995. Fibrous clay minerals in the soils of Namaqualand, South Africa: Characteristics and formation. Geoderma, 66: 43-70.

Singer, A., 2002. Palygorskite and sepiolite. In: Dixon, J.B. and Schulze, D.G., eds. Soil Mineralogy with environmental applications. SSSA Book Series No. 7. Madison, Soil Science Society of America: 555-583.

Soil Survey Staff, 2006. Natural Resources Conservation Service, United States Department of Agriculture. Official Soil Series Descriptions [Online WWW]. Available URL: “http://soils.usda.gov/technical/classification/osd/index.html” [Accessed 1 April 2006]. USDA-NRCS, Lincoln, NE.

Soil Survey Staff, 2009. National Soil Survey Characterization Data. Soil Survey Laboratory. National Soil Survey Center , USDA-NRCS - Lincoln, NE. Accessed Monday, September 14, 2009.

Soukup, D.A., Buck, B.J., and Harris, W., 2008. Preparing soils for mineralogical analysis. In: Ulery, A., and Drees, R., eds. Methods of soil analysis, part 5: Mineralogical methods. SSSA Book Series No. 5. Madison, Science Society of America: 13-31.

Starkey, H.C., and Blackmon, P.D., 1984. Sepiolite in Pleistocene Lake Tecopa, Inyo County, California. In: Singer, A., & Galan, E., eds. Palygorskite-sepiolite: Occurrences, genesis, and uses. Developments in Sedimentology, 37. New York, El Sevier: 137-148.

United Nations Commission to Combat Desertification, 1997. Earth Summit +5. Special Session of the General Assembly to Review and Appraise the Implementation of Agenda 21, New York, 23-27 June. http://www.un.org/ecosocdev/geninfo/ sustdev/desert.htm.

Vanden Heuvel, R.C., 1966. The occurrence of sepiolite and attapulgite in the calcareous zone of a soil near Las Cruces, New Mexico. In: W.F. Bradley and S.W. Bailey, eds. Thirteenth National Conference on Clays and Clay Minerals. Madison, Pergamon Press: 193-207.

Verrecchia, E. P. and Le Coustumer, M.-N., 1996. Occurrence and genesis of palygorskite and associated clay minerals in a Pleistocene calcrete complex, Sde Boqer, Negev Desert, Israel. Clay Minerals, 31: 183-202.

Wang, C., Kodama, H., and Miles, N.M., 1981. Effects of various pretreatments on X-ray diffraction patterns of clay fractions of podzolic B horizons. Canadian Journal of Soil Science, 61(2):311-316.

Wang, J.J., Dodla, S.K., Henderson, R.E., 2004. Soil silicon extractability with seven selected extractants in relation to colorimetric and ICP determination. Soil Science, 169(2): 861-870.

Watts, N.L., 1978. Displacive calcite: Evidence from recent and ancient calcretes. Sedimentology Research Laboratory, 6: 699-703.

Watts, N.L., 1980. Quaternary pedogenic calcretes from the Kalahari (southern Africa): mineralogy, genesis and diagenesis. Sedimentology, 27: 661-686.

Weaver, C.E. and Pollard, L.D., 1973. The chemistry of clay minerals. New York, Elsevier. 213 pages.

Weaver, C.E. and Beck, K.C., 1977. Miocene of the S.E. United States: A model for chemical sedimentation in a peri-marine environment. Sedimentary Geology, 17: 1-234.

Williams, V.S., Bohannon, R.G., and Hoover, D.L., 1997. Geologic map of the Riverside Quadrangle, Clark County, Nevada, Geologic Quadrangle Map GQ-1770.

Yaalon, D.H. and Wieder, M., 1976. Pedogenic palygorskite in some arid brown (calciorthid) soils of Israel. Clay Minerals, 11:73-80.

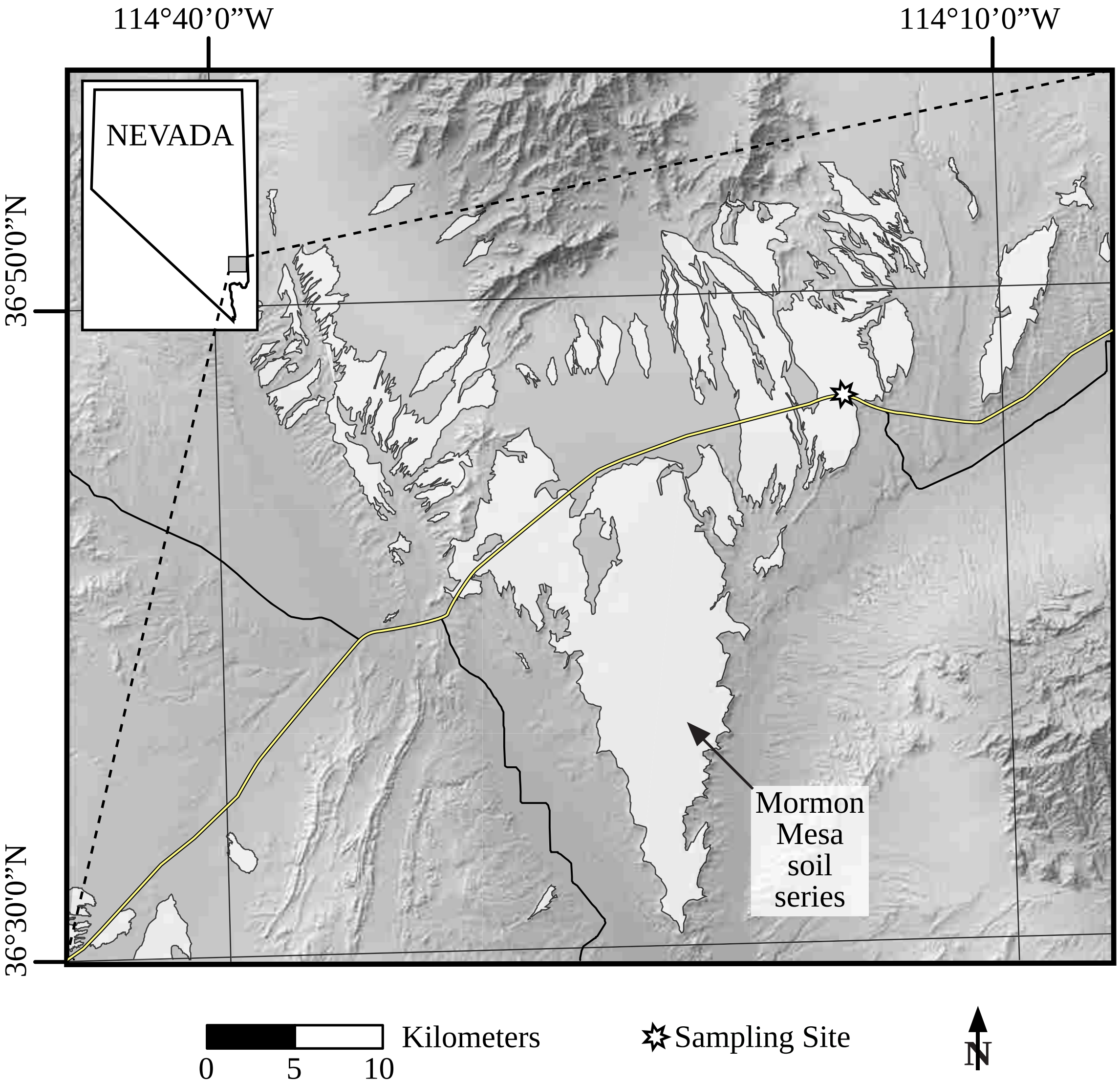

Figure 2.1. Location of the Mormon Mesa soil geomorphologic surface. The approximate extent of the Mormon Mesa soil series is indicated. Soil geormorphological data are modified from Soil Survey Staff (2006); basemap DEM modified from USGS (2005).

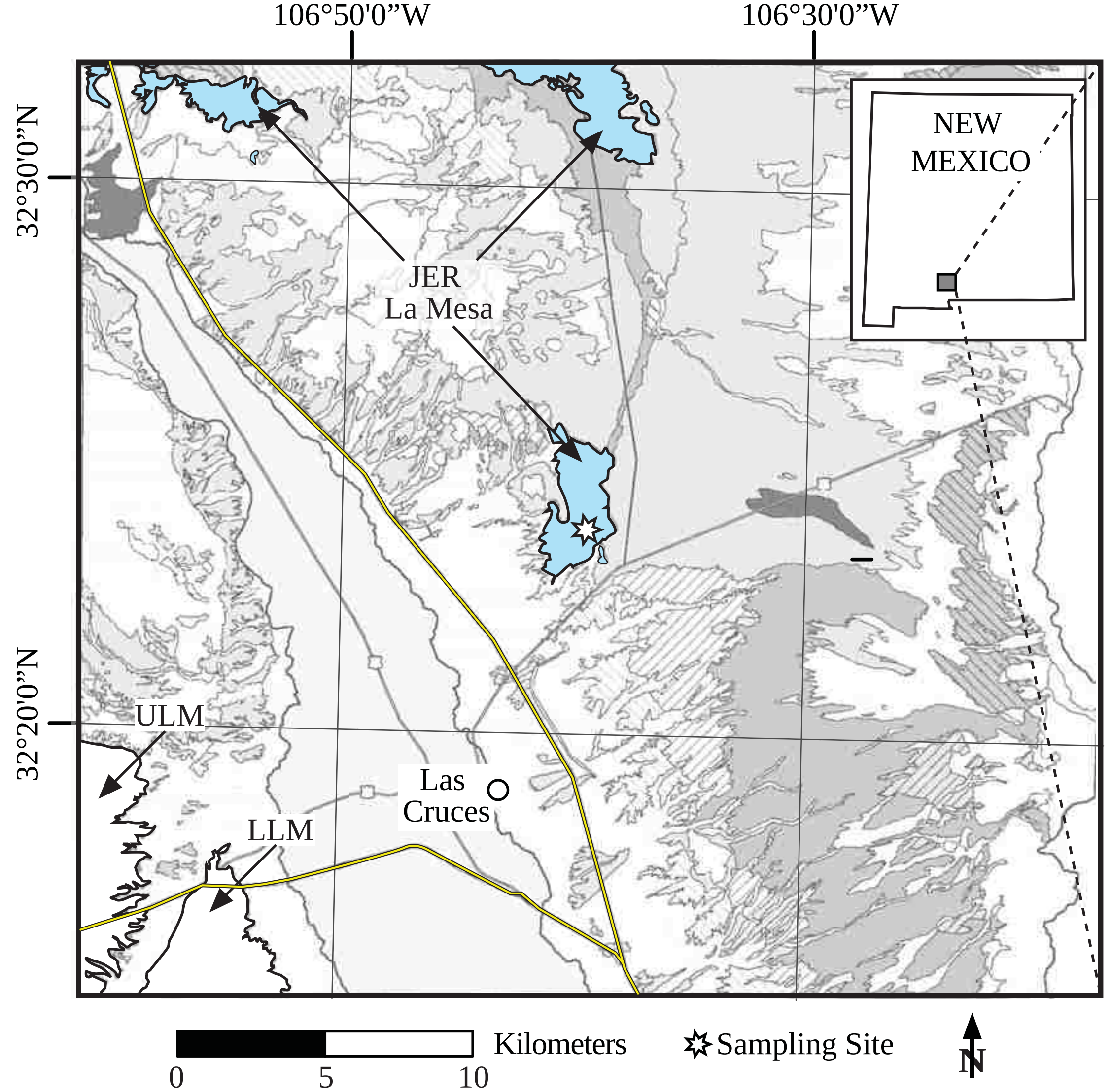

Figure 2.2. Locations of the stage V to VI Jornada Experimental Range La Mesa surface (also called the La Mesa-Jornada I complex), near Las Cruces, New Mexico. Also indicated (to the southwest) are the Upper La Mesa (ULM) and Lower La Mesa (LLM) surfaces, both of which contain stage IV to V petrocalcic soil horizons geomorphologically related to the JER La Mesa surface. Soil geochronologic data and basemap modified from Jornada Basin LTER project (2003).

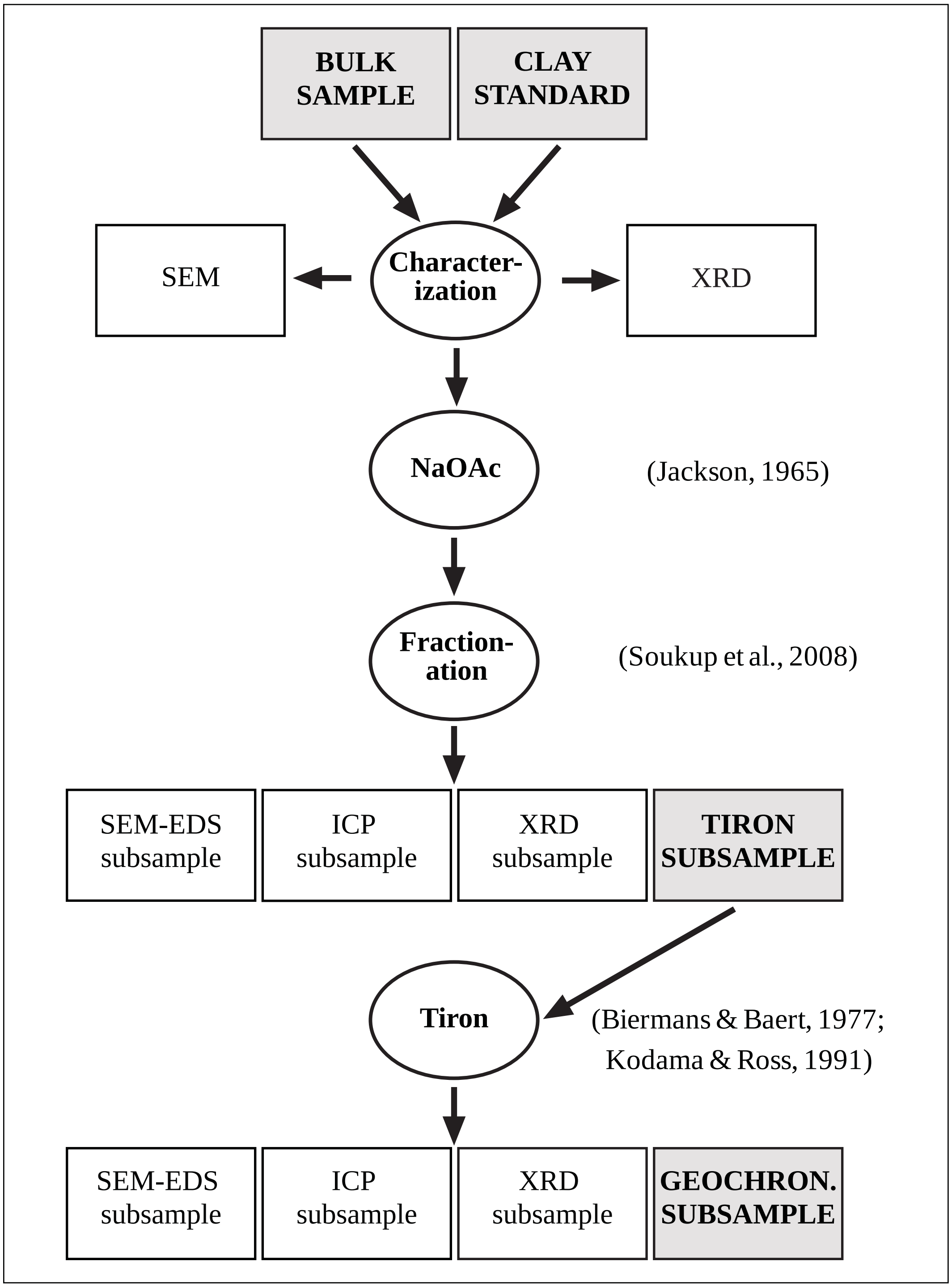

Figure 2.3. Experimental design, showing order of operations. Boxes represent sample aliquots used in treatments and/or taken for instrumental analyses. Ovals indicate chemical or physical laboratory treatments.

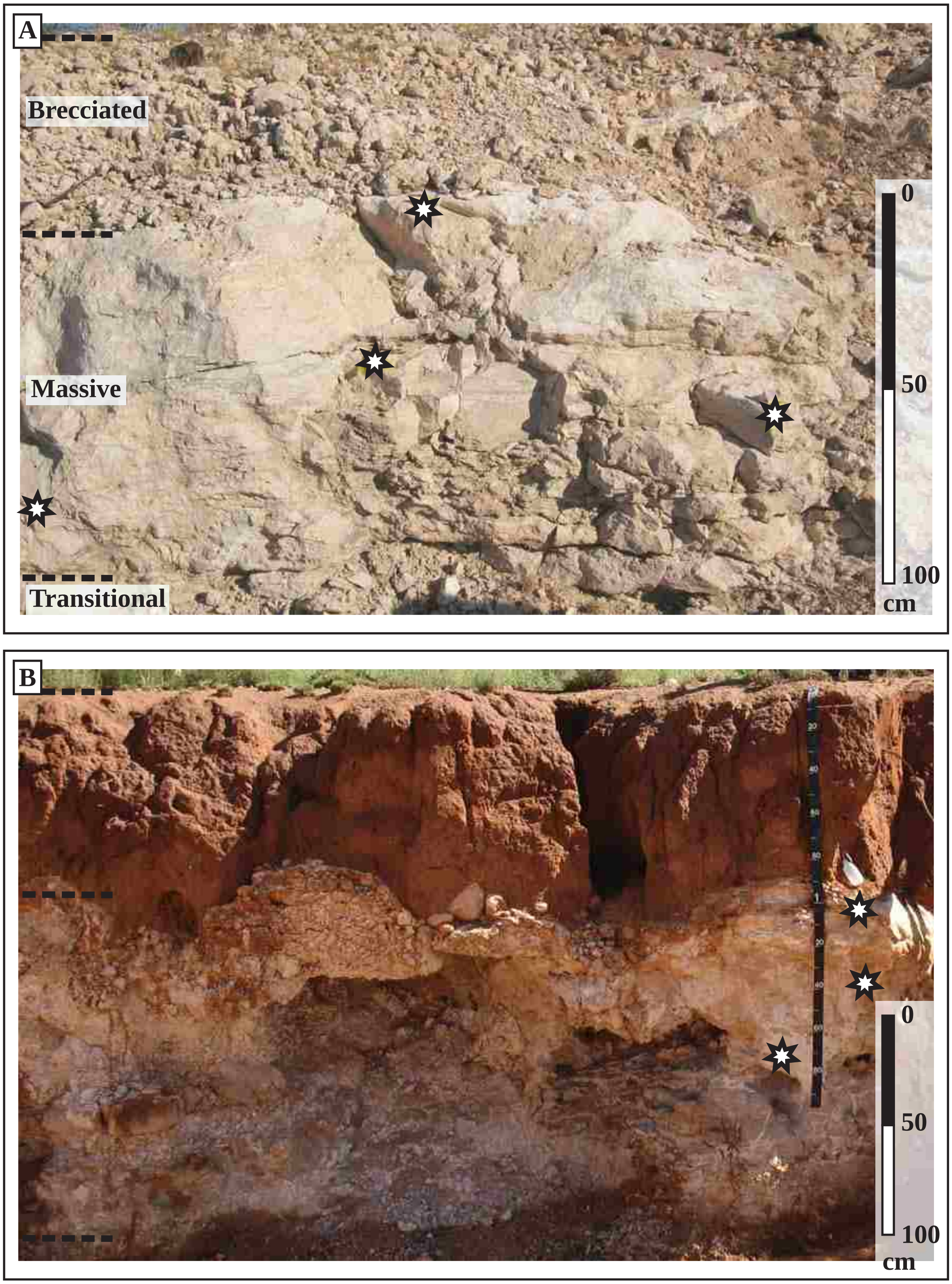

Figure 2.4. Some of the sample locations within laterally extensive, excavated profiles of (A) the Mormon Mesa soil profile (Mormon Mesa soil series), exposed in a road cut; (B) the JER La Mesa soil profile (Hueco soil series), excavated as part of the Desert Project.

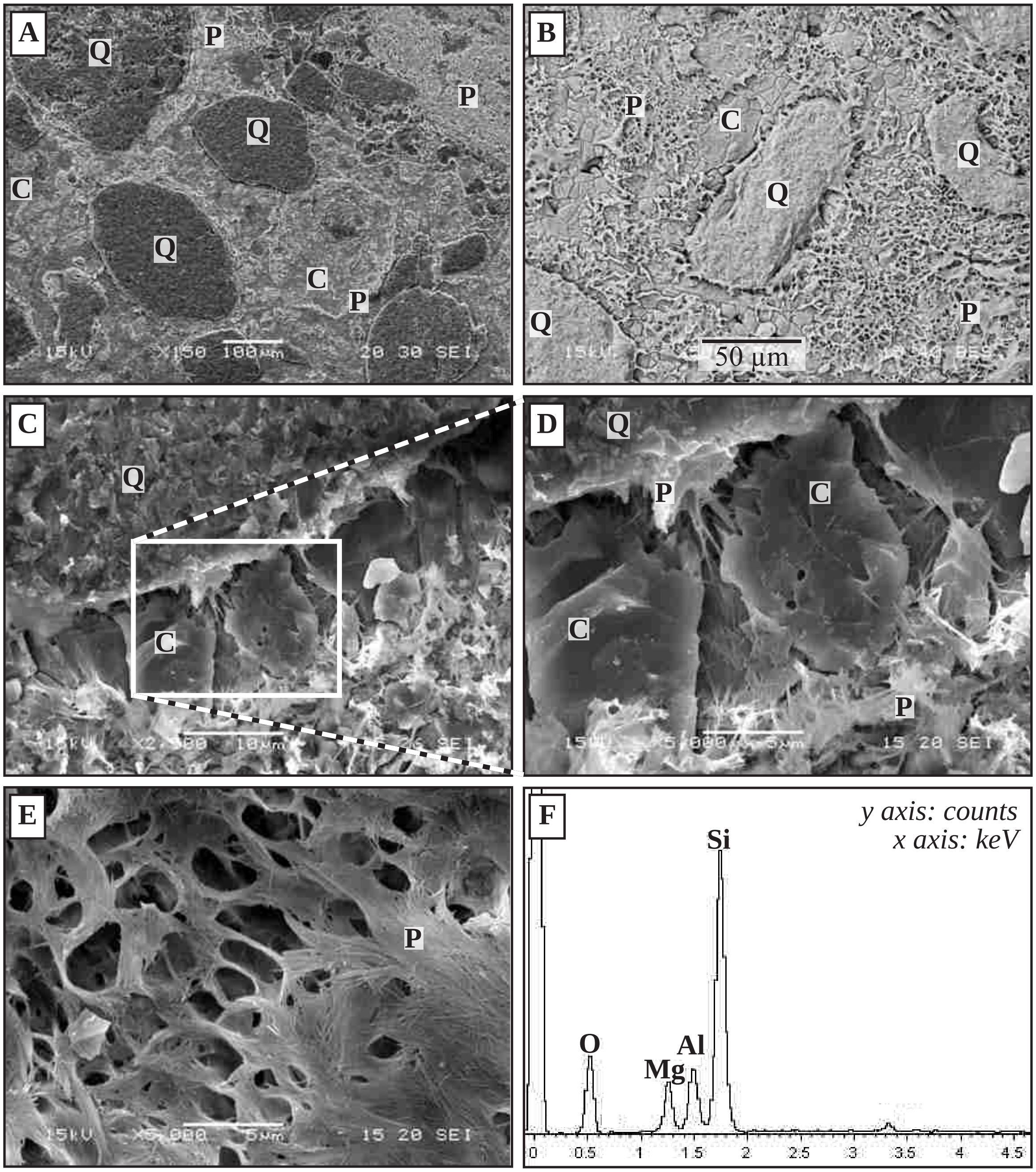

Figure 2.5. Selected SEM-EDS data for Mormon Mesa thick sections. C = calcite; P = fibrous silicate clay (palygorskite and/or sepiolite), Q = quartz. (A) Secondary electron image of fibrous clays coating grains and forming concentric zones within pisolites. (B) Backscatter electron image of fibrous clays coating detrital grains and permeating the soil matrix. (C) & (D) Secondary electron images of palygorskite or sepiolite fibers radiating outwards from quartz grain edges and forming intergrowths with pedogenic carbonate. (E) Porous clay mat, suggesting fibrous clay persistence despite localized carbonate dissolution. (F) Sample EDS spectrum showing typical elemental signature for fibrous clays (Au sputter-coat peak removed by software processing).

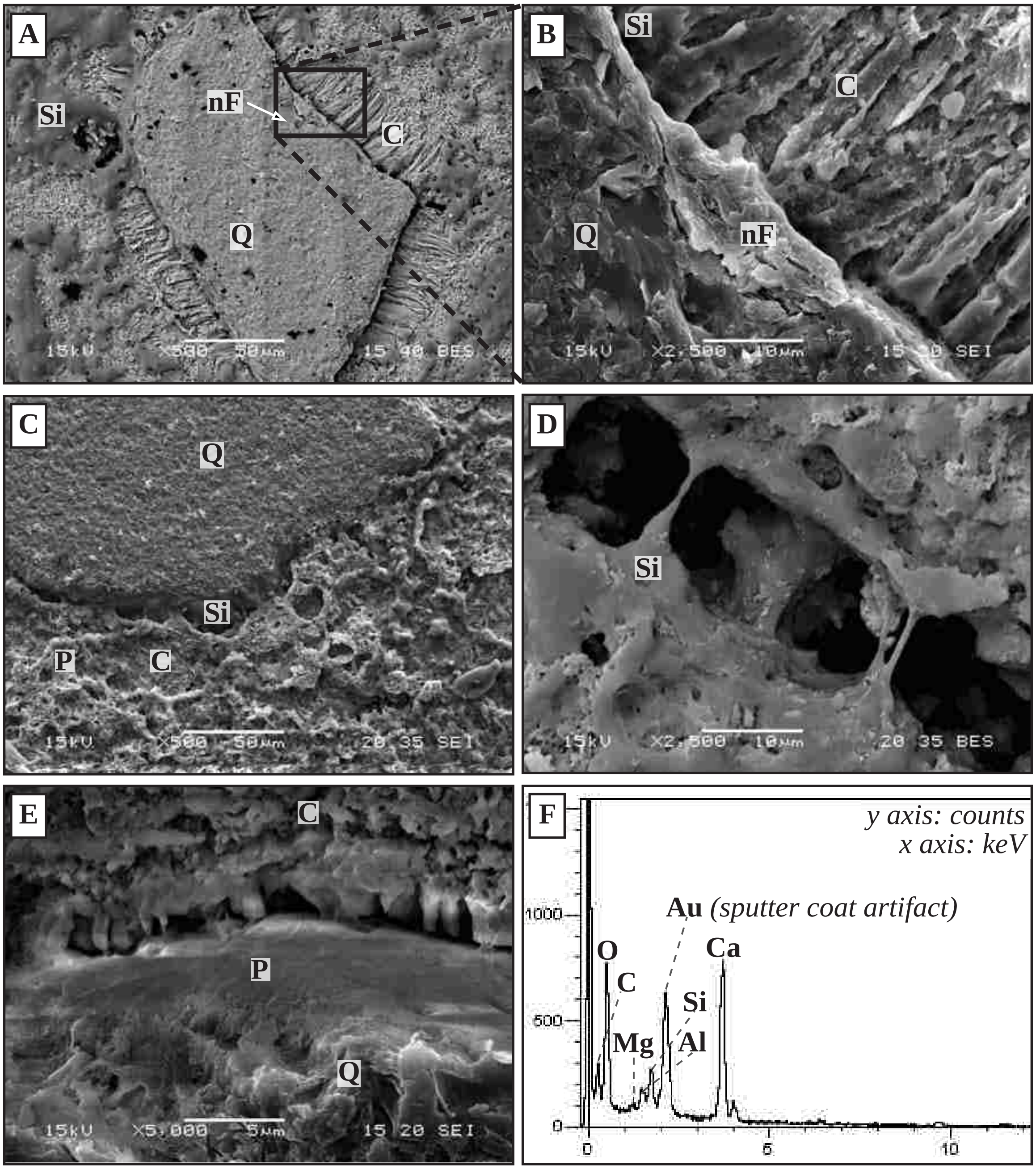

Figure 2.6. Selected SEM-EDS data for JER La Mesa thick sections. C = calcite; nF = non-fibrous phyllosilicate; P = palygorskite or sepiolite; Q = quartz; Si = silica. (A) Quartz grain engulfed by radial calcite, partly replaced by clay. (B) Close-up of (A) showing non-fibrous clay texture. (C) Grain-matrix contact, showing authigenic calcite, silica, and phyllosilicate phases. (D) Amorphous silica bridging pore spaces. (E) Weakly fibrous texture of clays coating a quartz grain; blurring caused by sample charging. (F) Representative JER La Mesa EDS spectrum reflecting mixed mineralogy of phyllosilicate and CaCO3 phases.

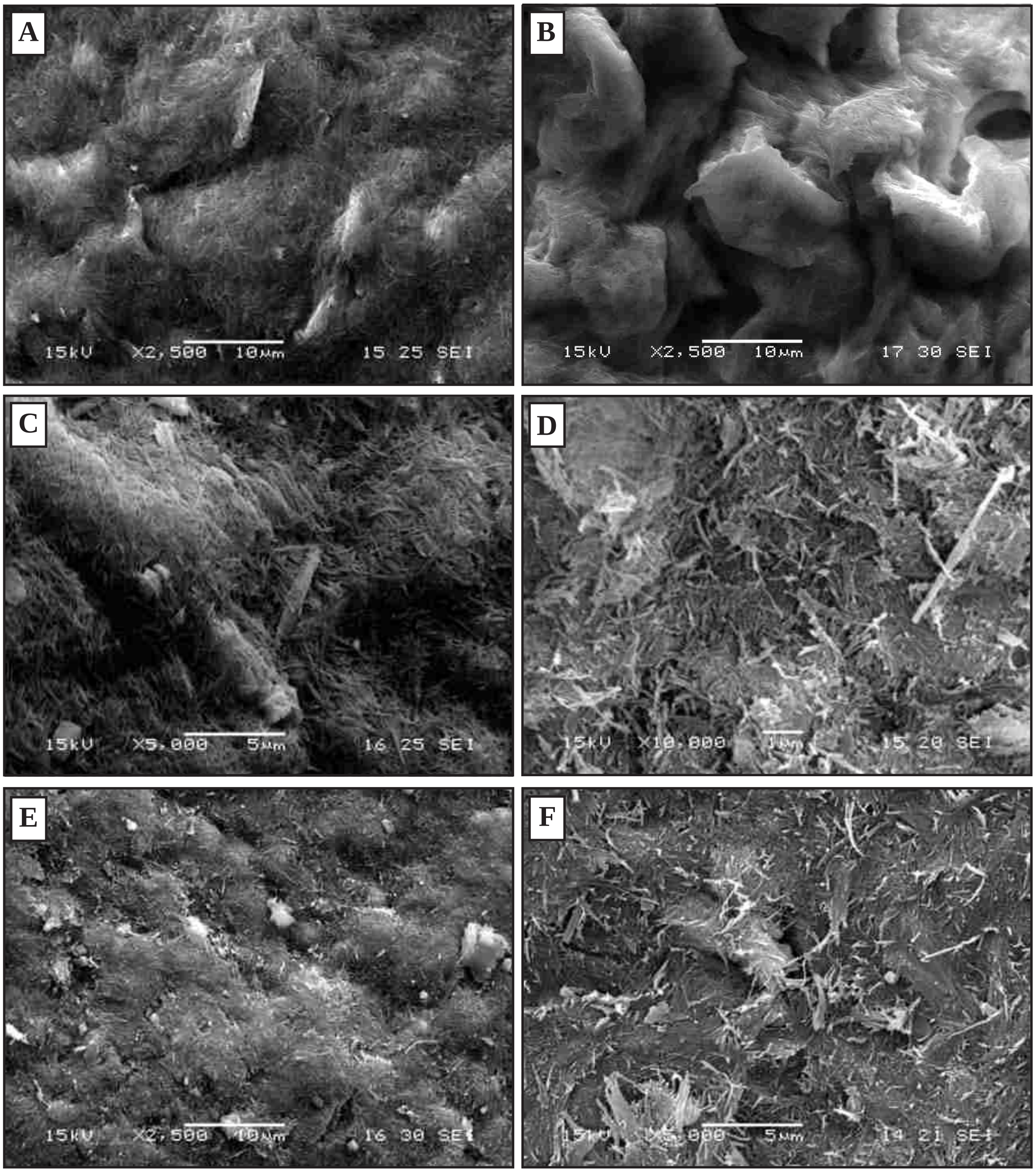

Figure 2.7. Selected SEM images for extracted clay-sized particle fractions. (A) Palygorskite reference standard. (B) Sepiolite reference standard. (C) Sample mB1 following NaOAc treatment and particle size-fractionation, to compare with (D) the same sample after tiron treatment. (E) Sample mB4 following NaOAc treatment and fractionation, and (F) the same sample after tiron treatment. No apparent differences are discernable either in image or EDS data, however, instrument resolution is inadequate to resolve nano-scale changes.

Table 2.1A. ICP data for extracted clay-sized sample aliquots. “-A” indicates NaOAc + particle fractionation; “-T” indicates tiron treatment.

Element-Trtmnt:	**Al-A**	**Al-T**	**B-A**	**B-T**	**Ca-A**	**Ca-T**	**Co-A**	**Co-T**	**Cr-A**	**Cr-T**	**Cu-A**	**Cu-T**	**Fe-A**	**Fe-T**	**K-A**	**K-T**	**Mg-A**	**Mg-T**
Units:	%	%	mg/kg	mg/kg	%	%	mg/kg	mg/kg	mg/kg	mg/kg	mg/kg	mg/kg	%	%	%	%	%	%
Detect. Limit:	0.002	0.002	2.0	2.0	0.002	0.002	5.0	5.0	5.0	5.0	5.0	5.0	0.001	0.001	0.01	0.01	0.002	0.002
mmA1	2.782	2.833	29.7	23.2	0.860	0.238	9.6	6.5	20.8	20.9	17.0	8.52	1.191	1.183	0.38	0.35	3.221	3.310
mmA4	2.905	2.992	25.1	<	0.440	0.064	7.1	5.1	20.7	23.5	19.5	11.1	1.213	1.235	0.43	0.39	3.060	3.277
mmA5	2.524	2.562	45.2	<	1.332	0.233	14.7	16.9	20.7	22.2	26.2	13.6	0.902	0.946	0.25	0.24	4.098	4.107
mmA8	2.412	2.656	91.9	<	2.366	0.041	12.9	8.0	21.7	23.8	41.5	16.9	1.040	1.145	0.31	0.32	2.949	3.154
mmB1	2.552	2.805	28.4	19.6	1.695	0.256	12.0	6.6	19.4	23.0	17.8	9.44	1.011	1.070	0.33	0.32	3.537	4.003
mmB2	2.471	2.539	<	<	0.724	0.016	12.2	6.1	13.1	14.1	7.07	4.98	0.864	0.789	0.21	0.18	3.990	4.169
mmB3	2.792	3.101	36.9	<	1.862	0.138	7.3	<	18.6	19.0	23.4	14.5	1.021	1.104	0.33	0.33	4.519	5.150
mmB4	2.933	2.968	21.8	<	0.487	0.019	5.4	<	15.4	15.2	8.31	5.37	0.938	0.932	0.25	0.23	4.885	5.243
mmB5	2.599	2.741	26.6	<	0.638	0.047	14.8	8.4	24.1	26.7	15.7	9.68	1.696	1.809	0.45	0.40	2.486	2.793
PFL	2.760	2.500	<	<	0.553	0.299	5.2	<	77.2	70.9	<	<	1.317	1.217	0.19	0.16	3.691	3.525
SEP	0.651	0.627	<	<	0.004	0.005	<	<	4.9	<	<	<	0.244	0.156	0.06	0.05	12.899	12.588
JA3	4.887	3.401	30.3	24.5	1.092	1.061	65.5	26.1	24.5	24.5	21.0	10.9	2.367	2.376	0.99	0.67	3.586	2.358

Element-Trtmnt:	**Mn-A**	**Mn-T**	**Na-A**	**Na-T**	**Ni-A**	**Ni-T**	**P-A**	**P-T**	**Pb-A**	**Pb-T**	**S-A**	**S-T**	**Sr-A**	**Sr-T**	**Zn-A**	**Zn-T**
Units:	mg/kg	mg/kg	%	%	mg/kg	mg/kg	%	%	mg/kg	mg/kg	%	%	mg/kg	mg/kg	mg/kg	mg/kg
Detect. Limit:	3.0	3.0	0.002	0.002	15.0	15.0	0.002	0.002	10.0	10.0	0.002	0.002	3.0	3.0	5.0	5.0
mmA1	53.6	56.7	0.372	0.200	22.3	15.2	0.024	0.010	13.3	<	0.009	0.010	15.1	5.1	29.4	26.6
mmA4	60.5	61.2	0.050	0.336	25.3	27.2	0.031	0.017	13.9	<	0.007	0.009	7.2	4.0	37.4	34.1
mmA5	39.8	46.0	0.143	0.082	23.3	25.5	0.013	0.007	10.7	<	0.012	0.009	19.2	4.6	24.4	23.2
mmA8	51.8	51.5	0.087	0.257	36.1	36.0	0.023	0.013	11.7	12.5	0.015	0.013	23.0	4.7	35.7	28.9
mmB1	49.2	50.8	0.141	0.040	21.3	25.2	0.019	0.008	11.3	<	0.009	0.006	23.7	6.5	27.5	26.2
mmB2	57.0	36.5	0.843	0.237	19.1	24.8	0.008	0.004	10.4	<	0.004	0.009	9.3	<	17.2	14.3
mmB3	51.3	50.8	0.050	0.237	32.0	32.0	0.016	0.007	12.5	<	0.025	0.017	36.2	13.3	28.4	25.4
mmB4	39.6	40.0	0.092	0.217	16.4	17.6	0.011	0.004	12.0	<	0.012	0.008	17.4	4.0	20.1	18.8
mmB5	77.2	73.2	0.052	0.271	19.2	17.0	0.026	0.010	16.4	<	0.004	0.007	9.2	3.7	34.1	32.5
PFL	124.9	99.5	0.327	0.404	16.7	14.2	0.208	0.114	<	<	0.048	0.068	22.4	14.2	54.8	50.7
SEP	44.3	25.5	0.130	0.638	<	<	<	<	<	<	<	0.003	<	<	7.7	7.7
JA3	184.5	172.9	0.956	0.258	66.7	49.0	0.029	0.032	22.6	19.4	0.004	0.006	32.1	39.3	61.6	60.5

“<” denotes values below detection limit

Table 2.1B. ICP data for unpaired JER La Mesa samples.

	Al	**B**	**Ca**	**Co**	**Cr**	**Cu**	**Fe**	**K**	**Mg**	**Mn**	**Na**	**Ni**	**P**	**Pb**	**S**	**Sr**	**Zn**
	%	mg/kg	%	mg/kg	mg/kg	mg/kg	%	%	%	mg/kg	%	mg/kg	%	mg/kg	%	mg/kg	mg/kg
JB1-A	5.296	<	0.343	14.9	27.8	15.1	2.720	0.72	2.131	146.1	0.594	42.8	0.041	27.1	0.011	12.0	79.6
JB2-A	5.679	<	0.233	51.9	31.1	22.7	3.051	0.78	1.855	169.9	0.816	42.2	0.048	29.9	0.010	11.4	87.5
JA2-A	5.457	<	0.412	18.2	32.4	15.3	3.021	0.81	1.894	164.8	0.818	48.3	0.046	28.3	0.012	13.8	91.0

“<” denotes values below detection limit

Table 2.2. ICP replicate data for palygorskite and sepiolite reference standards. Note: B,Cd, Co, Cu, Mo, Pb were all below detection limits for the reference clays and are not included.

	Al	**Ca**	**Cr**	**Fe**	**K**	**Mg**	**Mn**	**Na**	**Ni**	**P**	**S**	**Sr**	**Zn**
Units:	wt. %	wt. %	mg/kg	wt. %	wt. %	wt. %	mg/kg	wt. %	mg/kg	wt. %	wt. %	mg/kg	mg/kg
Detection Limit:	0.002	0.002	5.0	0.001	0.01	0.002	3.0	0.002	15.0	0.002	0.002	3.0	5.0
PFL-ST(rep1)	2.798	0.998	75.5	1.313	0.21	3.806	128.1	0.026	15.7	0.265	0.100	37.5	53.5
PFL-ST(rep2)	2.751	0.989	74.7	1.302	0.21	3.786	127.6	0.027	14.0	0.263	0.100	37.0	53.0
PFL-ST(rep3)	2.656	1.027	77.1	1.405	0.23	3.716	128.8	0.024	<	0.276	0.101	40.5	55.0
Mean	2.735	1.005	75.7	1.340	0.214	3.769	128	0.026	14.9	0.268	0.100	38.3	53.8
Stand. Dev.	0.073	0.020	1.24	0.057	0.012	0.048	0.639	0.002	1.15	0.007	0.001	1.918	1.067
SEP ST(rep1)	0.421	0.034	6.5	0.133	0.05	13.090	26.0	0.021	<	0.006	0.008	3.2	5.0
SEP ST(rep2)	0.575	0.047	6.7	0.178	0.06	13.473	24.7	0.022	<	0.010	0.006	3.6	7.2
SEP ST(rep3)	0.783	0.114	15.2	0.286	0.09	12.363	35.6	0.032	<	0.036	0.009	7.5	5.9
SEP ST(rep4)	0.520	0.046	6.4	0.205	0.07	12.380	26.3	0.023	<	0.011	0.006	4.5	<
SEP ST(rep5)	0.357	0.046	4.6	0.141	0.05	11.984	18.6	0.014	<	0.011	0.006	3.2	5.0
Mean	0.531	0.057	7.880	0.189	0.066	12.658	26.243	0.023		0.015	0.007	4.425	5.756
Stand. Dev.	0.164	0.032	4.191	0.062	0.018	0.606	6.097	0.007		0.012	0.001	1.814	1.035

"<" denotes values below detection limit.

The standard deviation of the sepiolite and palygorskite replicates is assumed indicative of analytical variability for all samples (see Table 2.1 A&B).

Table 2.3. Results from paired t-tests of ICP elemental data.

Element	t Statistic	Degrees of freedom	P value	No. of Pairs	Mean Difference	95% Conf. Int.	R^2	Net effect
Al	3.870	8	0.005	9	-0.1363	-0.2176 to -0.05509	0.6518	Increase
Ca	4.689	8	0.002	9	1.039	0.5281 to 1.550	0.7332	Decrease
Co	3.196	6	0.019	7	3.671	0.8602 to 6.483	0.6299	Decrease
Cr	3.507	8	0.008	9	-1.544	-2.560 to -0.5290	0.6059	Increase
Cu	4.149	8	0.003	9	9.154	4.067 to 14.24	0.6827	Decrease
Fe	1.844	8	0.102	9	-0.0374	-0.0843 to 0.00938	0.2983	None
K	3.098	8	0.015	9	0.0200	0.005115 to 0.03489	0.5455	Decrease
Mg	4.280	8	0.003	9	-0.2734	-0.4208 to -0.1261	0.6960	Increase
Mn	0.5795	8	0.578	9	1.478	-4.403 to 7.358	0.0403	None
Na	0.0563	8	0.957	9	-0.0052	-0.2192 to 0.2087	0.0004	None
Ni	0.4956	8	0.634	9	-0.6111	-3.455 to 2.233	0.0298	None
P	7.499	8	< 0.0001	9	0.0101	0.007002 to 0.01322	0.8755	Decrease
S	0.7385	8	0.481	9	0.0010	-0.002122 to 0.004122	0.0638	Decrease
Sr	5.606	7	0.001	8	13.14	7.595 to 18.68	0.8178	Decrease
Zn	4.592	8	0.002	9	2.689	1.339 to 4.039	0.7249	Decrease

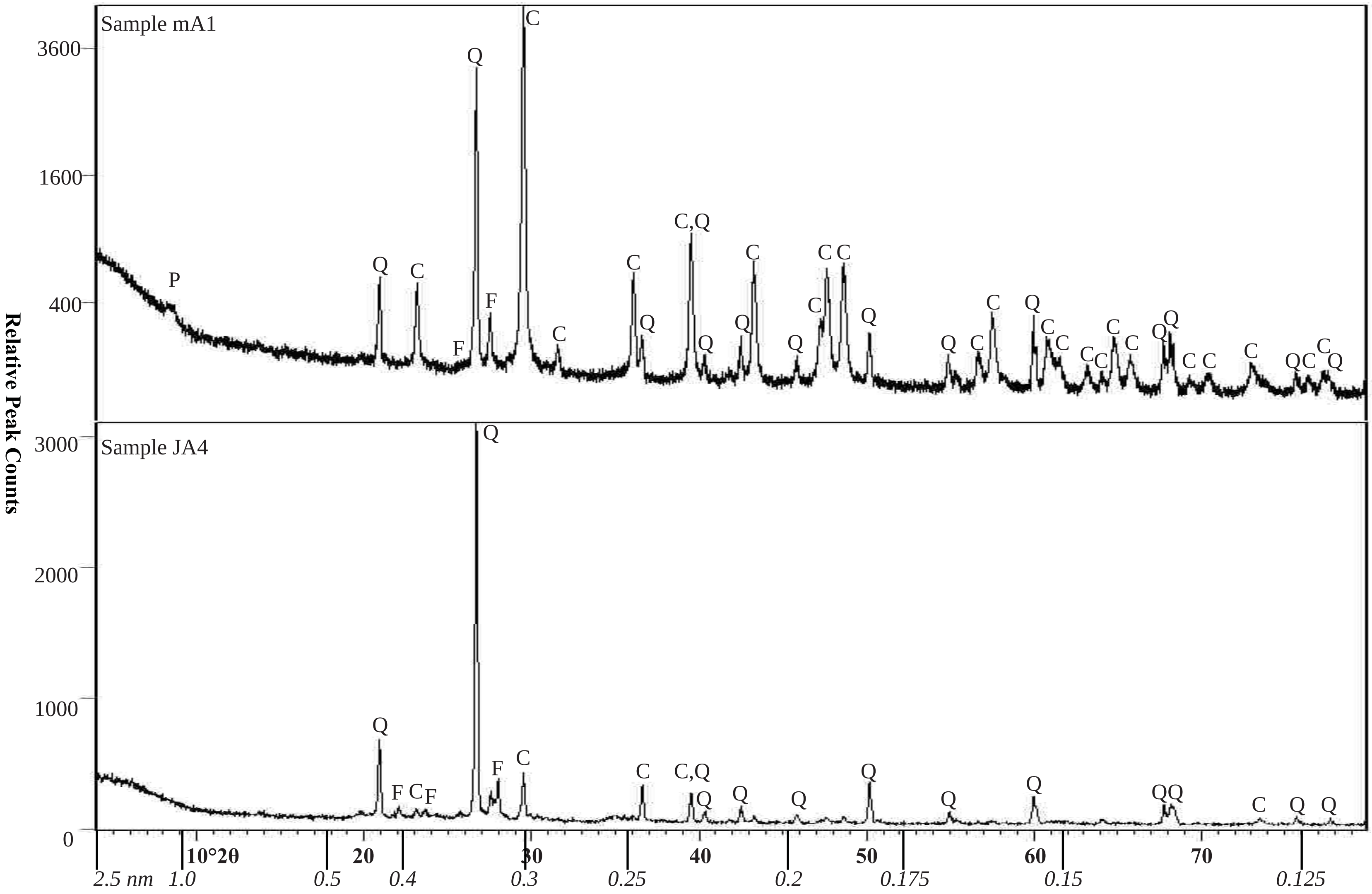

Figure 2.8. Selected XRD data for bulk powder analyses of Mormon Mesa (top) and JER La Mesa (bottom) samples. C = calcite and low-magnesian calcite, F = feldspar, P = palygorskite, Q = quartz.

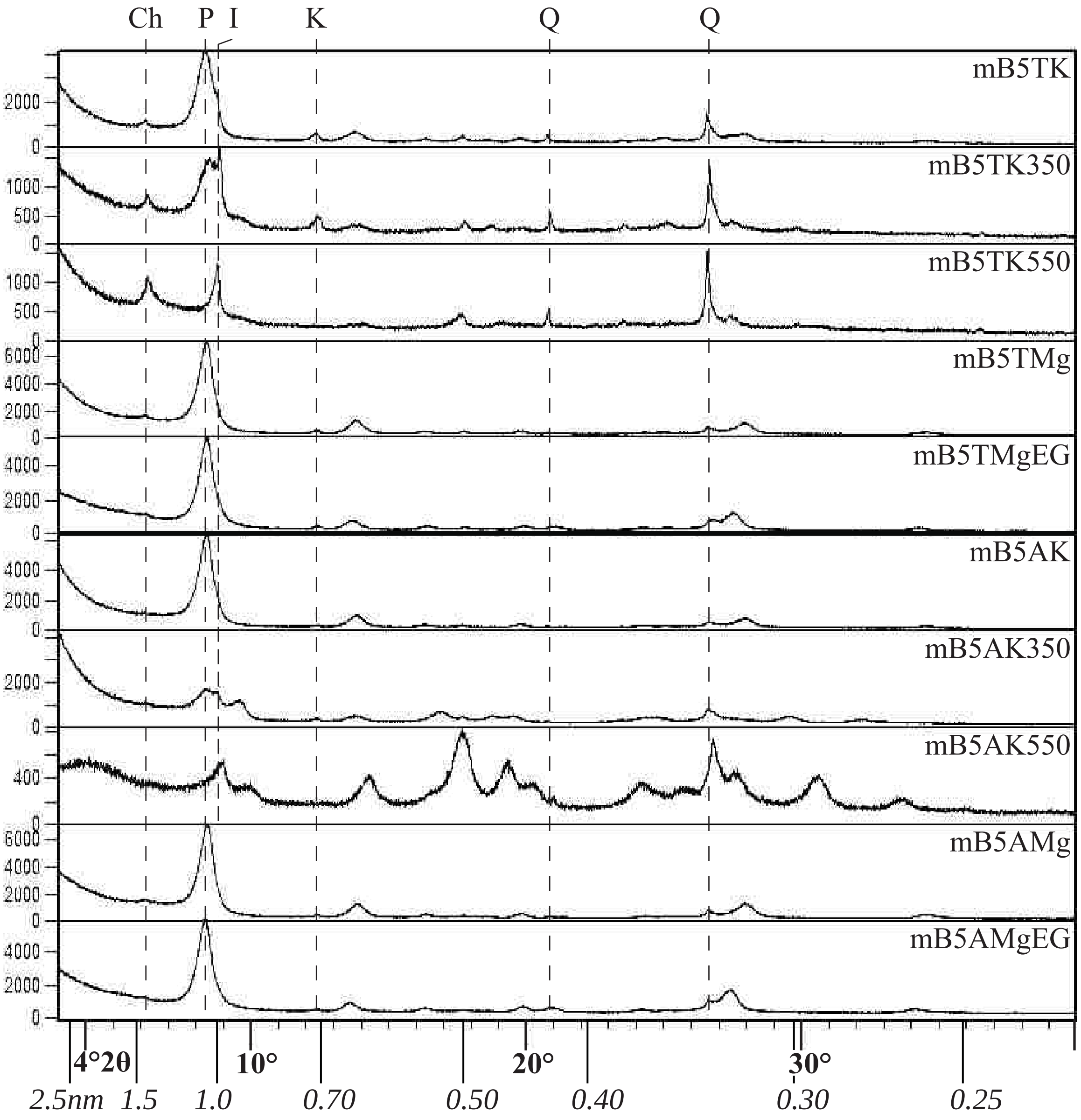

Figure 2.9. Comparison of XRD spectra for aliquots of sample mB5 taken after NaOAc treatment and particle size fractionation (mB5A) and after subsequent tiron treatment (mB5T). Y-axis units are relative peak counts for each spectrum. X-axis indicates scan angle (°2θ) and d-spacing (nm). Treatments are K-saturation (K), K-saturation heated to 350°C (K350) and 550°C (K550), Mg-saturation (Mg), and Mg-saturation with ethylene glycol solvation (MgEG). Note the increased presence of chlorite, illite, and kaolinite peaks in the tiron aliquot data. Ch = chlorite, I = illite, K = kaolinite, P = palygorskite, and Q = quartz.

CHAPTER 3

TOWARDS $^{40}Ar/^{39}Ar$ GEOCHRONOLOGY OF PEDOGENIC PALYGORSKITE AND SEPIOLITE, PART II: LESSONS AND TECHNICAL IMPLICATIONS FOR DATING ARID SOILS

Abstract

The diversity of authigenic minerals found in arid soils, including calcium-carbonate cemented (calcic and petrocalcic) horizons, raises exciting prospects for new applications of isotopic dating techniques to arid landscapes. Nevertheless, obtaining accurate isotopic ages for arid soils, especially geologically old, relict petrocalcic horizons, remains one of the largest scientific hurdles in the fields of geomorphology and sedimentology.

Palygorskite and sepiolite are fibrous, high-magnesium phyllosilicates found to form in many calcic and petrocalcic soils worldwide, and may contain sufficient intra-crystalline K to warrant attempts at vacuum-encapsulated $^{40}Ar/^{39}Ar$ geochronology. Total gas ages for pedogenic palygorskite or sepiolite crystallites could provide ages for modern and relict geomorphologic surfaces, and for paleosols (unconformities) in the stratigraphic record. $^{40}Ar/^{39}Ar$ geochronology of pedogenic phyllosilicates, as described here for palygorskite and sepiolite, has not been investigated previously nor discussed in published scientific literature. The goal of this exploratory research was to evaluate a potential new method of dating calcic and petrocalcic soils using vacuum-encapsulated $^{40}Ar/^{39}Ar$ geochronology of pedogenic palygorskite and sepiolite from (1) the Mormon Mesa soil-geomorphologic surface in Nevada, and (2) the JER La Mesa surface in New Mexico.

$^{40}Ar/^{39}Ar$ analyses in this study returned highly variable crystal ages that were older than the known relative soil geomorphologic ages by two orders of magnitude. These geologically impossible crystal ages were most likely caused by unforeseen contaminants introduced during selective mineral extraction procedures, despite following a prescribed rinsing methodology. Contaminants were partly derived from chemicals used in the mineral extraction procedure, but may also include contributions from the natural soil environment, as well as from plastic laboratory equipment. This study underscores the adverse effect of hydrocarbon contaminants on isotopic measurements of soil samples, and illustrates the difficulty of adapting existing procedures to new soil analyses.

With further experimentation and methodological refinement, vacuum-encapsulated $^{40}Ar/^{39}Ar$ geochronology of pedogenic palygorskite and/or sepiolite could yet prove to be a successful means of dating arid soil landscapes, however, both the theoretical and the practical aspects of the method require further research. It is emphasized that the potential benefit of a successful application of $^{40}Ar/^{39}Ar$ geochronology to pedogenic palygorskite and sepiolite, or to other arid soil minerals, merits further evaluation and discussion.

Introduction

Dating of Arid Soils

The need for quantitative measures of soil formation rates has increased in tandem with efforts to combat desertification and improve agricultural resources in arid regions, which comprise nearly a third of the Earth's land surface and sustain almost two billion people (UNCCD, 1997). However, the processes that shape arid soils and landscapes are not yet fully understood. Especially lacking are numerical ages to assess the rates at which arid soils form, stabilize, and/or degrade both in the present day, and in the geologic past. Accurate soil ages may permit scientists to determine rates of rock weathering and pedogenesis (Vasconcelos & Conroy, 2003; Candy et al., 2004), climate change (Sharp et al., 2003), and landscape evolution. Soil dating techniques can also strengthen interpretations of soil geomorphology (e.g. Ku et al., 1979; Candy et al., 2005; Candy & Black, 2009), terrestrial stratigraphy (e.g. Rasbury et al., 1998), and paleoclimate (Dohrenwend et al., 1986; Candy & Black, 2009). In comparison to humid soils, which largely reflect the hydrolysis of minerals and the loss of cations from the soil profile, arid landscapes are distinct because their soil profiles typically reflect a net influx of ions to the Earth's surface over time. This influx, combined with alkaline soil solutions and fluctuating moisture conditions, produces a variety of unique authigenic mineral assemblages (Francis et al., 2007) including carbonates, sulfates, nitrates, and chlorides (i.e., Buck et al., 2006; Howell, 2009), as well as unusual phyllosilicate species, such as palygorskite and sepiolite. This range of compositionally diverse authigenic minerals raises exciting prospects for the novel application of existing isotopic dating techniques to untested pedogenic minerals in arid soil environments.

Numerical ages and new geochronologic methods are especially needed for calcic and petrocalcic soil horizons (Alonso-Zarza & Arenas, 2004; Brock & Buck, 2009), which are also collectively referred to as "caliches" or "calcretes" in the scientific literature (Machette, 1985). Calcic and petrocalcic horizons occur worldwide as extant and relict soils in arid to semi-arid environments, and also as paleosols in the stratigraphic record (Reeves, 1976; Machette, 1985; Buck and Mack, 1995; Retallack, 2001). Numerical ages for calcic and petrocalcic soil stages are invaluable because they provide minimum surface ages for modern geomorphologic surfaces, and minimum ages for unconformities (paleosols) in the geologic record. A six-stage classification scheme (Gile et al., 1966; Bachman & Machette, 1977; Machette, 1985) describes the progressive morphological development of calcic and petrocalcic soils and, thus, their relative geologic age. However, numerical dates can prove difficult to assign except in isolated cases where stratigraphic relationships with tephrachronologic or magnetostratigraphic markers permit rough estimates of soil ages. Moreover, relative rates and factors of calcic and petrocalcic soil formation are known to vary widely between sites (Bachman & Machette, 1977; Machette, 1985; Mayer et al., 1988). Without absolute age data, the amount of time needed to reach each successive morphological soil carbonate stage within a given region will remain uncertain, and the feasibility of comparing morphologically similar soils between distinct regions will remain limited.

Isotopic dating of arid soils, especially calcic and petrocalcic soil horizons, remains one of the largest scientific hurdles in both geomorphology and sedimentology because of challenges related to: (1) crystal age interpretation, (2) geologically young minerals, (3) complicating soil factors, and (4) the difficulty of selective mineral extraction from arid soil samples.

Numerical ages always require exacting, rigorous interpretation regardless of the mineral or isotopic system used. Ideally, isotopic dates from authigenic soil minerals provide the crystallization age of the mineral, and also the minimum age for the onset of soil formation, however, other factors bear consideration. First, interpretations must employ corroborative micromorphological and/or chemical data to account for or to refute the presence of detrital components with ages older than the soil parent material. For example, phyllosilicate and carbonate minerals in soils may form pedogenically, but they can also be derived in part from diagenically altered bedrock, from weathered rock fragments in alluvium, or from illuviated eolian dust. Second, pedogenic minerals, especially carbonates, can undergo successive, punctuated crystallization events, or episodic, full or partial dissolution and recrystallization during oscillating seasonal, millennial, or longer-scale climate cycles (McDougall & Harrison, 1988; Sharp et al., 2003; Brock & Buck, 2005). These dissolution and recrystallization episodes can violate the closed-system requirements of isotopic dating and they can also produce artificially young, composite dates. These effects can be pronounced even in young, stage II calcic soil pendants (Brock & Buck, 2005), and are especially problematic in stage III-VI petrocalcic soils, which contain horizons that are completely indurated by authigenic carbonate and, often, amorphous silica. In particular, stage VI petrocalcic horizons have, by definition, undergone one or more episodes of brecciation, erosion, and recementation as the result of changing climate over hundreds of thousands to several million years (Gile et al., 1966; Bachman & Machette, 1977; Brock & Buck, 2009). Therefore, the utility of pedogenic mineral ages depends upon careful interpretation of soil mineralogical, chemical, and micromorphological data.

A second challenge associated with dating soil minerals arises from the young geologic age of many soil profiles, especially in arid environments. Geologically young (Holocene-Pleistocene) soils can result in low radiogenic daughter isotope abundances or luminescence activities and prohibitively high measurement uncertainty (McDougall & Harrison, 1988; Sharp et al., 2003; Madsen & Murray, 2009). Conversely, geologically old (Pleistocene-Pliocene) soils, including many late stage (V-VI) petrocalcic horizons, often exceed the maximum applicable age range of commonly used systems, such as ^{14}C (~30 ka) or U-series (~350 ka) isotopes. In the case of ancient, extant petrocalcic horizons, alternative isotopic and/or mineral systems must be tailored to match the anticipated age of the soil-geomorphologic surface.

Tailoring the selection of geochronologic and mineral systems to site characteristics is vital to address complicating soil factors, which comprise a third suite of obstacles in pedogenic mineral dating. Dating techniques can prove difficult to apply and interpret in soil environments because of bioturbation, surface erosion, mineral illuviation, secondary mineral coats, climate fluctuations and other processes (Bull, 1991; Birkeland, 1999; Fuchs & Lang, 2009). These processes must be considered on a site-by-site basis and often require extensive assumptions. Morphological and mineralogical variability between regions also indicates that one dating method may or may not be applicable to all sites, even if the soil taxa are similar (Birkeland, 1999). Given the diversity of pedogenic mineralogy, arid soils may offer several possible means of obtaining isotopic ages, however, care must be taken to study the mode of genesis, stability, diffusion parameters, and compositional variability of any mineral selected for analysis.

Extraction of mineral phases targeted for isotopic dating can prove daunting when the study soils are extremely indurated (Robins, 2010a), as is often the case in arid to semi-arid environments. Physical and chemical procedures must be performed on cemented soil samples to extract the target mineral without compromising its crystal lattice integrity, chemical composition, or isotopic signatures. Therefore, minerals must be selected which are present in abundance within the soil sample, and which are distinct from the indurating or intergrown mineral phase(s) in terms of their stability fields.

Dating of Pedogenic Palygorskite and Sepiolite

Palygorskite, $Si_8Mg_5O_{20}(OH)_2(OH_2)_4 \bullet 2H_2O$ (Singer, 1984), and sepiolite, $Si_{12}Mg_8O_{30}(OH)_4(OH_2)_4 \bullet 8H_2O$ (Brauner & Preisinger, 1956; Singer, 1984; García-Romero et al., 2007) are fibrous, high-magnesium phyllosilicates found in arid soils, palustrine sediments, (peri-)marine deposits, alkaline groundwater environments, and possibly some hydrothermal systems (Callen, 1984; Singer, 1989; and others). Their abundance is generally relatively low within terrestrial deposits (Jones & Galan, 1988), however, they are fairly typical of late-stage petrocalcic soils. Specifically, pedogenic palygorskite and sepiolite have been found in stage II pendants and stage III-VI petrocalcic horizons worldwide (Vanden Heuvel, 1966; Yaalon & Wieder, 1976; Elprince et al., 1979; Hay & Wiggins, 1980; Watts, 1980; Jones, 1983; Monger & Daugherty, 1991a; Botha & Hughes, 1992; Singer et al., 1995; Verrechia & Le Coustumer, 1996; Khadkikar et al., 2000; Achyuthan, 2003; Bouza et al., 2007; Francis et al., 2007; Hillier & Pharande, 2008). These clays form fibrous mineral laths morphogenetically related to stage II to stage VI calcic or petrocalcic horizons (Bachman & Machette, 1977; Watts, 1980; Monger & Daugherty, 1991b; Singer, 2002; Brock and Buck, 2005; Brock & Buck, 2009).

Pedogenesis of the fibrous clays is related to precipitation of soil carbonate, a process which can (1) increase relative Mg activities in the soil solution (Watts, 1980) while also (2) promoting force of crystallization dissolution of engulfed parent minerals and subsequent release of Si and Al (Bachman & Machette, 1977; Hay & Wiggins, 1980; Gile et al., 1981; Monger & Daugherty, 1991b; Brock & Buck, 2005). Alteration of low magnesian calcite to calcite can also contribute Mg for palygorskite and sepiolite formation (Watts, 1980). Progressive domination of petrocalcic soils by the fibrous clays also suggests that they may also eventually replace detrital, precursor phyllosilicates such as illite, kaolinite, or smectite – either following force of crystallization dissolution by carbonate, or following detrital clay dissolution due to chemical instability within the alkaline soil solution (Bachman & Machette, 1977; Monger & Daugherty, 1991b). Thus, a variety of processes and predecessor minerals can supply the Si, Mg, and Al constituents which combine in the alkaline soil environment to form palygorskite and/or sepiolite (Watts, 1978; Watts, 1980; Monger & Daugherty, 1991b). It is generally accepted that palygorskite (the more aluminous species) is favored when reactive Al is available in solution, while sepiolite (the less aluminous species) precipitates when aluminum activities are very low (Watts, 1980; García-Romero et al., 2007).

Thus, palygorskite and sepiolite crystallization ages could date pedogenesis in surficial deposits, and unconformities in sedimentary strata, however, their ages may or may not vary between microsites within even one soil horizon or morphological feature.

On the one hand, adjacent palygorskite and sepiolite crystals could be considered nearly identical in geologic age assuming (1) soil solution chemistry adjusts rapidly to episodic influxes of rainfall in arid environments, (2) phyllosilicate precipitation occurs on a seasonal/annual scale, and (3) once formed, palygorskite and sepiolite do not dissolve in response to climate or other factors. Epitaxial growth of palygorskite and sepiolite has also been suggested for some environments (García-Romero et al., 2007), and supports the near synchronous genesis of the fibrous clays in response to fluctuating soil solution chemistry. Assuming both minerals similarly incorporate intracrystalline (non-exchangeable) K and retain ^{40}Ar* (* denotes radiogenic argon), it could be possible to analyze the two clay species together for ^{40}Ar/^{39}Ar geochronology. On the other hand, there may be no way to constrain the range of time across which successive palygorskite and/or sepiolite growth occurred. Moreover, it is still not certain whether palygorskite and sepiolite experience dissolution-recrystallization cycles along with the calcite matrix during environmental shifts. Similarly, force of crystallization by calcite clearly facilitates authigenesis of the fibrous clays (Bachman & Machette, 1977; Hay & Wiggins, 1980; Watts, 1980; Gile et al., 1981; Monger & Daugherty, 1991b; Brock & Buck, 2005; Robins, 2010b), but it is not clear whether nor to what degree the same process might also contribute to their partial or complete dissolution in extremely indurated soil. Nevertheless, even if crystallization ages for the fibrous clays might not yield the desired ages for the onset of pedogenesis, they could certainly provide an average age of crystallization and, therefore, interesting data about the complex formation history of petrocalcic soils.

Pedogenic palygorskite and sepiolite clays in petrocalcic horizons of the southwestern USA are believed to contain sufficient intra-crystalline potassium to warrant an attempt at ^{40}Ar/^{39}Ar dating (Robins, 2010a). Compositional variability is known to be high within palygorskites (Corma et al., 1987; García-Romero et al., 2007) and sepiolites alike, and variability may be as great among examples of each clay as it is between the two (Singer, 2002; García-Romero et al., 2007). Both clays commonly contain small, variable amounts of other cations, including Ca, Fe, K, Mn, and Na, although some reported instances of such compositions may reflect either intergrowths or contamination by other phyllosilicates, or even exchangeable cations rather than isomorphous substitution (Weaver & Pollard, 1973; García-Romero et al., 2004). Nevertheless, palygorskite can and often does exhibit notable levels of isomorphous substitution (Paquet et al., 1987). Compositional end members of sepiolite, including Fe-rich xylotile, Ni-rich falcondoite, and Na-rich loughlinite are also well-documented (Jones & Galan, 1988). Although the mineralogical purity of measured samples is always a concern due to the common inclusion of other phyllosilicate crystallites or intergrowths (Galan & Carretero, 1999), the K content of the clay fraction in palygorskite- and sepiolite-dominated soils has been reported to range as high as 3.30 weight percent (Singer et al., 1995). Values between 0.00 and 5.69 weight percent K_2O have been reported for epi-marine deposits of palygorskite and/or sepiolite (García-Romero et al., 2007). Thus, the K content of palygorskite, though normally low, can reach significant levels (Singer, 1989; García-Romero et al., 2007).

Other factors or assumptions that must be considered before dating palygorskite and/or sepiolite include: (1) the difficulty of extracting intact, mineralogically pure clay crystals from cemented soil (Robins, 2010a), (2) satisfaction of closed mineral system requirements, (3) small crystal dimensions and radiogenic ^{40}Ar diffusion losses in the natural environment (Clauer & Chaudhuri, 1995; and others), and (4) ^{39}Ar recoil loss during irradiation (McDougall & Harrison, 1988; Lin et al., 1996; and others). Key pitfalls encountered when extracting authigenic palygorskite and sepiolite have been described in the companion project to this study (Robins, 2010a). Assumption of a closed isotopic system for these clay minerals can be tentatively supported by existing SEM data (Robins, 2010a), indicating fibrous, skeletal mats of palygorskite crystals that have persisted despite apparent dissolution of pedogenic calcite rhombs. Such data tentatively support the hypothesis that palygorskite and sepiolite may prove more robust than other petrocalcic mineral phases to dissolution during intervals of changing climate during the Quaternary. However, diffusive 40Ar* losses can occur without any changes in crystal lattice structure or morphology. The assumption of ^{40}Ar* retention in the natural environment and during laboratory extraction can only be evaluated empirically via mass spectrometry of extracted clay phases and comparison with expected stratigraphic ages. As discussed by Dong et al. (1995) for illite and illite-smectite intergrowths, losses of ^{40}Ar* in the natural environment occur especially along pathways created by crystal defects, implying that variable phyllosilicate compositions or intergrowths could impart correspondingly variable ^{40}Ar* losses. Recoil losses are also associated with these same lattice defect sites (Dong et al., 1995) but fortunately, the technique of vacuum encapsulation has been shown to address ^{39}Ar recoil loss during irradiation (Foland et al., 1992; Magloughlin et al., 2001; and others).

$^{40}Ar/^{39}Ar$ geochronology of pedogenic phyllosilicates, as described here for palygorskite and sepiolite, has not been investigated previously. However, researchers have explored the utility of $^{40}Ar/^{39}Ar$ methods in other soil, regolith, sedimentary, and hydrothermal minerals, including many phyllosilicates and other fine-grained authigenic phases. For example, $^{40}Ar/^{39}Ar$ methods have been used to date hypogene jarosite and/or alunite (Vasconcelos et al., 1994; Polyak et al., 1998; Vasconcelos & Conroy, 2003), suggesting that the technique presents many possible applications for surface processes research (Vasconcelos et al., 1994). K/Ar and $^{40}Ar/^{39}Ar$ dating have also been explored for glauconite (Thompson & Hower, 1973; Smith et al., 1993), illite and/or smectite (Aronson & Douthitt, 1986; Clauer et al., 1993; Dong et al., 1997; Onstott et al., 1997; Smith et al., 1998; Wilkinson & Haszeldine, 2002), and authigenic K-feldspar (Sandler et al., 2004) in marine sediments, with mixed success. Importantly, researchers have begun to address dating of fine-grained samples with mixed genetic and geochronologic characteristics, especially in near-surface environments (e.g., van der Pluijm et al., 2001).

Objectives

The goal of this experiment was to test a new method of dating petrocalcic soils using existing vacuum-encapsulated $^{40}Ar/^{39}Ar$ geochronologic methods. In tandem with a companion study designed to evaluate selective chemical and physical extraction of authigenic clays from petrocalcic soils (Robins, 2010a), this experiment was designed to measure, interpret, and evaluate the utility of $^{40}Ar/^{39}Ar$ total gas ages of pedogenic palygorskite and sepiolite. Palygorskite and sepiolite crystallization ages, in conjunction with careful micromorphological characterization and interpretation, offer exciting prospects for numerical age estimates of specific morphogenetic petrocalcic soil stages.

However, no previous attempts to extract and date these clays have been published. Key lessons from this initial attempt are reported here especially to facilitate and to encourage much needed research and discussion on the topic by other scientists.

Site and Sample Selection

Samples for this study were collected from (1) Mormon Mesa, in southern Nevada, and (2) the Jornada Experimental Range (JER) La Mesa geomorphologic surface (also called the La Mesa-Jornada I complex) near Las Cruces, New Mexico. These soils are among the best-known examples of late-stage petrocalcic soils in the world, and are known to contain authigenic palygorskite and sepiolite.

Mormon Mesa is a prime sample location because it is an extensive geomorphologic surface capped by a well-documented stage VI petrocalcic soil containing abundant pedogenic palygorskite and sepiolite (Gardner et al., 1972; Bachman & Machette, 1977; Brock, 2007; Brock & Buck, 2009). Micromorphological characterization and mineral composition of the Mormon Mesa petrocalcic horizon has already been conducted (e.g. Brock, 2007; Brock & Buck, 2009), thereby laying the groundwork for this study. Most importantly, the age of Mormon Mesa has been estimated at 4-5 Ma by correlating stratigraphic and morphostratigraphic units in the region to isotopically-dated tuffs and basalts (Schmidt et al., 1996; Williams et al., 1997). Initiation of pedogenesis on Mormon Mesa could also be considered synchronous with formation of the lower Colorado River drainage system, around 5.4 Ma (House et al., 2005). These values represent maximum ages for the petrocalcic horizon, and are consistent with the strongly-developed morphological stage of the soil. Mormon Mesa exhibits important relationships with the fluvial geomorphology, tectonic evolution, and paleoclimate of the Virgin River and lower Colorado River basins. Therefore, accurate age data for the Mormon Mesa petrocalcic horizon would greatly enhance our understanding of regional soil development rates and landscape evolution.

The JER La Mesa geomorphologic surface (also called the La Mesa-Jornada I complex) is another ideal site location because it, too, is spatially extensive (Gile et al., 1981; Jornada LTER, 2003) and exhibits a well-documented petrocalcic soil containing authigenic palygorskite and sepiolite (Bachman & Machette, 1977; Gile et al., 1981). Age control stems from isotopically-dated ash deposits in strata above and below the petrocalcic soil. Specifically, the JER La Mesa surface is older than the ~780 ka Bishop Ash bed, but younger than a fluvially-reworked pumice estimated at ~2 Ma (Bachman & Machette, 1977; Gile et al., 1981; Jornada LTER, 2003). The geomorphologically related Upper and Lower La Mesa surfaces are estimated at ~780 ka and 400-780 ka, respectively (Gile et al., 1981; Jornada LTER, 2003).

Thus, petrocalcic soils of the Mormon Mesa, NV, and the JER La Mesa, NM, surfaces represent the best sampling sites for this project because the genesis, morphology, and micromorphology of their petrocalcic horizons are well-studied, because they are known to contain palygorskite and sepiolite clays, and because their geomorphologic age has been constrained. If proven successful for these sites, extraction and dating methods described here and in Robins (2010a) may also become applicable to a wider range of calcareous soil stages and paleosols (ex: stage II pendants), as well as other types of palygorskite and sepiolite deposits.

Methods

Phyllosilicates in this study were extracted from indurated, bulk soil samples using pH 5 buffered sodium acetate to dissolve carbonate (Jackson, 1965; Kunze and Dixon, 1986), and then using tiron solution to selectively dissolve amorphous silica and sesquioxide phases (Biermans & Baert, 1977; Kodama & Ross, 1991). Field sampling methods, sample pretreatments, and phyllosilicate extraction methods are presented by Robins (2010a), however, several important notes are repeated here.

Two parameters of the extraction process had to be altered or omitted entirely in response to the very small crystal dimensions of pedogenic palygorskite and sepiolite (~ 0.1 μm in diameter, and 2-10 μm in length). First, samples could not be micro-drilled from bulk soil samples, nor finely ground prior to chemical treatment, because comminution by crushing or grinding of phyllosilicate crystallites could release entrapped argon from their lattices. Instead, indurated petrocalcic samples were simply broken by hammer from bulk sample blocks into ~1-6 cm^3 fragments for chemical dissolution (Robins, 2010a). Second, chemical treatments could not be conducted at their prescribed temperatures of ~80°C. Heating of palygorskite or sepiolite can cause expansion and/or dehydroxylation of the crystal lattice, which could simultaneously promote loss of retained $^{40}Ar^*$. For this reason, all laboratory procedures were operated at or below the conservative temperature limit of ~50°C, an arbitrary point intermediate between plausible peak summertime soil temperatures of 40-45°C (Mojave desert) and higher temperatures at which crystal lattices might expand, dehydrate, and/or undergo diffusive 40Ar* losses.

Extracted aliquots of pedogenic clay were studied using SEM-EDS, ICP, and XRD analysis prior to encapsulation for ^{40}Ar/^{39}Ar dating (Robins, 2010a). Vacuum encapsulation procedures in this study followed the general procedures of Foland et al. (1992). GC/MS analyses were performed as described below.

Sample capsules were prepared at the Nevada Isotope Geochronology Laboratory (NIGL) from 1 mm thick (5 mm outer diameter and 3 mm inner diameter) fused-silica tubing, which was first scored and fractured into segments 8 – 10 cm long, and then fused shut at one end using an oxy-propane torch. Preliminary calculations based on the K content of the extracted clays measured using ICP analysis (Robins, 2010a) suggested that 50 mg samples would prove sufficient for ^{40}Ar/^{39}Ar analysis. Aliquots of thirteen samples were weighed using an analytical balance with a precision of 0.0001 g. Samples were weighed in a funnel of analytical paper, and then gently tapped into the open silica capsule using a 1 mm diameter aluminum rod. Next, a small amount of silica wool was gently pushed into the capsule, to ensure that the entire clay aliquot moved to the bottom of the tube and would not adhere to the upper sides of the capsule, and also to prevent evacuation of sample during vacuum encapsulation.

Four capsules at a time were clamped at their upper, open end into a custom-built vacuum manifold, pumped down overnight (8-12 hours), and sealed by fusing the silica tubing at a point 2-3 cm above the loaded sample with the oxy-propane torch at 10^{-6} torr. The ideal, target vacuum of 10^{-8} torr could not be achieved, perhaps due to the sizeable mass and surface area of the phyllosilicate sample, or to other factors, discussed below. Care was taken to cool the sample-bearing portion of each capsule in a beaker of cold water while operating the torch, and in most instances the torch was applied for less than 30 seconds. The final length of the sealed capsules was ~6-8 cm.

Sample capsules were packed in three separate containers for irradiation at the Oregon State University Radiation Center (OSURC). Neutron fluence monitors (FC-2, Fish Canyon Tuff sanidine) were wrapped in Al foil and placed at regular 5-10 mm intervals within each tube. Synthetic K-glass and optical-grade CaF_2 (to monitor neutron induced argon interferences from K and Ca) were also included in each irradiation package. Sample packages were dosed in the in-core irradiation tube of the 1 MW TRIGA type reactor at OSURC for two hours.

$^{40}Ar/^{39}Ar$ measurements were conducted at the University of Nevada Las Vegas Nevada Isotope Geochronology Laboratory (NIGL), which is equipped with a MAP215-50 mass spectrometer. Correction factors for interfering neutron reactions on K and Ca were developed via repeated analysis of K-glass and CaF_2 fragments using a CO_2 laser, and laser fusion of 4-8 individual neutron fluence monitor crystals was used to determine the irradiation factor, J (see McDougal & Harrison, 1988). Due to the unavoidable packaging of sample capsules in separate containers for irradiation, three distinct correction factors were established for each of the three distinct sample groups (UNLV-62, UNLV-63, and UNLV-64).

Irradiated samples were analyzed in two steps, including (1) measurement of encapsulated (recoil) gases, and (2) total furnace fusion analysis. For the first step, sample capsules were loaded into a custom-built laser chamber equipped with a video camera and a linear motion driver (ramrod). The sample chamber held up to four capsules at a time. Each sample capsule was broken under vacuum by advancing the linear motion driver until it cracked the capsule, and then the sample chamber gas (containing any recoiled ^{39}Ar) was admitted into the mass spectrometer by expansion. Following analysis of the encapsulated gas, the mass spectrometer vacuum line was purged, the sample chamber isolated from the pumps, and the linear motion driver was advanced to the next sample capsule. Following analysis of their encapsulated gases, samples were transferred to tin foil capsules, and loaded into a linear sample dropper for individual furnace heating to 1000°C and measurement of total fusion (crystal-lattice) Ar.

In both steps, reactive gases were removed by three GP-50 SAES getters prior to admission into the mass spectrometer. For this study, an extension cooled by liquid nitrogen was also added to the vacuum line to freeze anticipated, high amounts of water vapor from phyllosilicate sample gas prior to its admission into the spectrometer. Relative volumes of the extraction line and mass spectrometer at NIGL allow up to 80% of sample gas to be admitted to the mass spectrometer by expansion for both vacuum encapsulation analyses and laser-fusion of the fluence monitor and correction standards. For the furnace heating sample analyses, this percentage is 76%. Peak intensities were measured in seven cycles using a Balzers electron multiplier. Initial peak heights were determined by linear regression to the time of gas admission. When peak counts were too high for the detector system, which happened for most of the study samples, sample gases were split into smaller volumes for analysis. The mass spectrometer's discrimination and sensitivity were monitored at regular intervals via repeated analysis of atmospheric argon aliquots admitted through an on-line pipette system, and discrimination corrections were applied to all isotope ratios. Except for movement of the linear motion driver, equipment and analytical operations were performed using LabSPEC software written by B. Idleman (Lehigh University).

Following ^{40}Ar/^{39}Ar analysis and initial data interpretation at NIGL, gas chromatograph/mass spectrometer (GC/MS) analyses were conducted on selected samples (five of the field samples and two reference standards from the Clay Minerals Society). These samples included aliquots from both phyllosilicate extraction procedures: (1) NaOAc and (2) tiron. Two modes of GC/MS analysis, cryo-treatment and tetra-methyl-ammonium hydroxide methods, were employed. GC/MS analyses were conducted at the UNLV Department of Chemistry on a Varian 2200 GC/MS, and were interpreted using both Varian MS Workstation and AMDIS (Automated Mass Spectral Deconvolution and Identification System) software.

Results

Sample Screening

The suitability of selective extraction procedures, and the mineral homogeneity and suitability of samples for ^{40}Ar/^{39}Ar geochronology, were assessed via SEM-EDS, ICP, and XRD analysis (Robins, 2010a). No conclusively adverse effects on the K content or crystallinity (a proxy for Ar retention) were detected using those methods, however, XRD data suggest that 1-5% inclusions of other mineral phases, such as chlorite, illite, smectite, or intergrowths of those phyllosilicates, persist in the Mormon Mesa samples. Similarly, SEM-EDS data indicate even more prevalent inclusions of non-fibrous phyllosilicates in the JER La Mesa samples (Robins, 2010a).

^{40}Ar/^{39}Ar Analysis

Encapsulated and furnace-released gas measurements were combined for the final (total gas) age calculations. ^{40}Ar/^{39}Ar data returned total gas ages that were in excess of anticipated ages by two orders of magnitude on average (Table 3.1). Separate vacuum-encapsulated gas and total fusion gas measurements for each sample are reported in Table 3.2, along with mass spectrometer sensitivity and fluence monitor values.

GC/MS Analysis

Concurrent with initial interpretations of unexpectedly old ^{40}Ar/^{39}Ar ages, gas chromatography/mass spectrometry analysis was employed to search for possible hydrocarbon residues adsorbed to clay surfaces during the selective dissolution procedures. Hydrocarbons and other organic compounds can interfere with ^{40}Ar/^{39}Ar geochronology by breaking into daughter compounds with masses in the same range as argon isotopes (36-40, and baseline at 35.5 amu), and also by contributing to scatter within the vacuum line.

Analysis of aliquots from five samples and the two standards using 600-650°C pyrolysis revealed several important chemical signatures suggestive of hydrocarbon contamination. Broadly, these compounds include a variety of alkanes, alkenes, aromatics, and fatty acids. Compounds which matched the GC/MS peaks especially well include acetic acid or acetic anhydride, benzene, toluene, bisphenol A, and styrene. Selected results are presented in Figures 2.1 and 2.2, and filtered GC/MS spectra for all samples are presented in Appendix 3.1.

Discussion

The ~100+ Ma dates returned by ^{40}Ar/^{39}Ar mass spectrometry are geologically impossible for the two study sites, each of which have an established relative age. Trace amounts of older, detrital clays may occur within the extracted phyllosilicate samples (Robins, 2010a), but none of the non-fibrous clays (such as illite, kaolinite, or smectite) are sufficient to account for the magnitude of error in age. Moreover, the magnitude of diversion from anticipated ages appeared to be comparable for all samples and for both soil profiles. Correction factors and calculations were also checked and found free of error. Although the encapsulated (recoil) gas dates are generally an order of magnitude younger than the total fusion dates, both components of the total gas age are excessively old. Therefore, encapsulated sample contamination by other compounds with masses spanning the argon isotope range is the best explanation for the anomalous ages.

Adsorption of contaminants during treatment is highly plausible. GC/MS data indicate that the palygorskite and sepiolite extracts contain a suite of organic contaminants, many of which were introduced during selective extraction of the clays from indurated petrocalcic soil. The extraction procedures included several carefully followed steps designed to remove the solvents (i.e., NaOAc and Tiron) from the samples following treatment, however, these procedures appear to be insufficiently rigorous for isotope study. These compounds indicate treatment effects and, possibly, natural sample characteristics that must be addressed prior to future attempts at isotopic dating of clays from calcic soil samples. Interestingly, it seems unlikely that the organic compounds identified via GC/MS can account for any of the differences among phyllosilicate ICP data in Robins (2010a). For example, the presence of adsorbed tiron ($C_6H_4Na_2O_8S_2 \cdot H_2O$) (Biermans & Baert, 1977; Kodama & Ross, 1991) molecules might be expected to increase Na and S concentrations between treatments, however, no trend was detected for Na, and statistical analyses suggest that S may have decreased, not increased, following the Tiron treatment (Robins, 2010a). However, failure of ICP analyses to detect the contaminants is plausible given that even very small quantities of contaminants ($<10^{-16}$ moles) can interfere with argon isotope analysis. The presence of adsorbed organic contaminants may also partly account for the failure of encapsulation vacuum pressures to reach the ideal point of 10^{-8} torr.

Adsorption of hydrocarbons and other organic compounds on clay surfaces during selective extraction is highly problematic. As summarized by Yariv & Cross (2002), adsorption of organic matter by clay minerals can occur on: (1) exposed oxygen cleavage planes in 1:1 and 2:1 clays, (2) exposed hydroxide cleavage planes in 2:1 clays, (3) broken bond surfaces or crystal edges in all clays, (4) within interlayer spaces in swelling 2:1 and dioctahedral 1:1 clays, and (5) on the external surfaces, channels, and within the structural tunnels of palygorskite and sepiolite. Crystal lattice defects may serve as additional adsorptive surface area when they occur near crystal surfaces or edges (Alvarez et al., 1987).

Both palygorskite and sepiolite are well known in industry for their ability to adsorb and absorb metal cations, organic molecules, and water (Murray, 2000). For example, Potgeiter et al. (2006) found that palygorskite can readily adsorb metal cations from aqueous solution, while sepiolite can absorb 200% or more of its own weight in water (Pérez-Castells et al., 1987). Naturally occurring palygorskite and sepiolite can also absorb certain types of organic molecules into their surface channels and/or into their structural lattice tunnels (Serna & Vanscoyoc, 1979; Potgeiter et al., 2006; Yildiz & Gür, 2007). The absorption potential for a given compound depends on its polarity and also upon its dimensions relative to the diameter of the structural tunnels. For example, the simple alcohols methanol and ethanol are both known to penetrate the channels of palygorskite and sepiolite (Serna & Vanscoyoc, 1979), and may be difficult to remove. Other compounds may bond (adsorb) only to external clay surfaces, and, depending on the target isotopic system, may not cause any analytical interferences.

Regrettably, data from this experiment indicate that extraction procedures introduce persistent, organic contaminants of equal or greater mass than the isotopes of study (36-40 amu). Other compounds may occur naturally in the soil profile. Each of these contaminants, rarely considered problematic for other soil analytical procedures, can introduce catastrophically large errors into isotopic measurements by breaking into smaller daughter compounds during irradiation, during furnace heating, or by fracturing on the mass spectrometer filament. With this type of contamination, it was not possible in this study to determine the relative contributions of argon and hydrocarbon contaminants to the mass spectrometer data.

Organic contaminants in this study may have originated from multiple, mixed sources, including the soil environment, experimental treatments, and possible wear and tear of laboratory equipment. Acetic acid and benzene identified via GC/MS data are unquestionably the product of the NaOAc and Tiron treatments, and fragments of these compounds could plausibly interfere with geochronologic analyses. Conversely, compounds such as bisphenol A may have been introduced by polycarbonate or similar materials commonly used in laboratory centrifuge tubes, with which the samples in this study were in near constant contact (Robins, 2010a). Fatty acids most likely reflect contributions from soil and/or laboratory bacteria, and may not greatly affect argon isotope mass spectrometry. Due to the sampling design of this study, it is only possible to suggest, not prove, the laboratory or pedogenic origin of each of these classes of compounds. The most problematic source of the contaminants is believed to lie in the selective chemical dissolution treatments.

Consequently, methods must be developed to remove these compounds from the clays before it will be possible to re-evaluate the suitability of ^{40}Ar/^{39}Ar geochronology to arid soil landscapes. Treatment for the removal of organic matter, for example, using sodium hypochlorite (Anderson, 1961; Soukup et al., 2008) is a practical next step for future research on this subject. As cautioned by Robins (2010a), adding further treatments to the extraction methodology cannot be done without cost. Additional time would be required after NaOCl treatment to rinse residual, adsorbed chloride ions from the clays, because chlorine also interferes with argon isotope mass spectrometry. Extensive centrifuge-rinse cycles may also cause losses of the finest clay-sized particle fraction (Robins, 2010a). Moreover, neither the NaOCl nor H_2O_2 methods of organic matter removal commonly practiced in soil laboratories are considered 100% effective, and the persistence of some organic compounds may be impossible to prevent (Shang & Zelazny, 2008). Oxidation of organic compounds using a cupric oxide or other metal catalyst (Sofer, 1980; Vandeputte et al., 1996; Ertl & Spitzy, 2004; Velivetskya et al., 2007) in the furnace step of ^{40}Ar/^{39}Ar mass spectrometry could yield an alternative solution, however, this procedure has not yet been evaluated for the purpose of ^{40}Ar/^{39}Ar geochronology, and adaptation would be required.

Besides removal of organic compounds, there are several other methodological or instrumental refinements that could improve the assessment or development of ^{40}Ar/^{39}Ar geochronology for pedogenic palygorskite and sepiolite. First, use of a quadrapole mass spectrometer coupled with a gas chromatograph would allow real-time analysis of both the sample and potential contaminants. Second, a more extensive and more intimately positioned chilling apparatus could be installed on the mass spectrometer vacuum line to reduce scattering caused by high volumes of structural water or volatile compounds evolved by palygorskite and sepiolite. Third, powdered phyllosilicate samples are highly prone to static electrical charges. Rupturing vacuum capsules can evacuate clay particles into the sample chamber. Custom-built filters, rather than silica wool (which can also escape the sample vial when it breaks, or become entangled with phyllosilicate crystallites), are recommended for the sample capsules as well as the vacuum line in any future studies. Future experiments might also better characterize the effects of variable-term (e.g., 4 mo – 2 yr) immersion of palygorskite and sepiolite in ph 5 NaOAc buffer, Tiron, with or without heating. Arrhenius parameters (E and D_0) also need to be calculated for argon diffusion within palygorskite and sepiolite lattices in order to model the isotopic signatures of the fibrous clays in both the natural environment and the laboratory. In addition, analysis of laboratory-synthesized, "zero-age" phyllosilicate standards alongside extracted pedogenic samples could also help quantify the amount of contamination by adsorbed contaminants in future experiments.

Had geologically acceptable ^{40}Ar/^{39}Ar dates been produced in this study, accurate interpretation of mixed crystallite ages, and definitive proof of closed-system conditions would still have been challenging. This study was conducted on bulk samples of palygorskite and sepiolite, each crystallite of which could have formed at any time across the entire age range of the Mormon Mesa and JER La Mesa soils (Robins 2010b).

Averaged ages from bulk field samples were an anticipated problem in this study, and are a common problem in all geochronologic analyses of pedogenic or groundwater carbonates (e.g., Candy et al., 2004; Brock & Buck, 2005). Suites of ages from distinct horizons or from distinct morphological features, collected in tandem with extensive micromorphological characterization of intact soil samples, are required to model and assess the potential for mixed phyllosilicate ages.

Adequate proof of closed-system behavior (lack of whole-crystal dissolution-reprecipitation events) of pedogenic palygorskite and sepiolite has not yet been established. This is a critical step given the extremely small dimensions (<1 μm diameter) of the fibrous clays. There is some evidence for closed-system behavior of palygorskite and/or sepiolite in micromorphological and chemical data reported in the companion study to this experiment (Robins, 2010a). However, further evidence is needed, especially given the extensive evidence for re-modification of soil mineral fabric in calcic and petrocalcic horizons (Brock & Buck, 2005; Robins, 2010b). Moreover, this assumption may not hold for all petrocalcic soil environments, nor for all micromorphological features or domains within a given calcic horizon. Thus, even geologically plausible dates could reflect artificial isotope ratios influenced by fluctuating temperature, soil solution chemistry, or laboratory procedures. SEM or transmission electron microscopy (TEM) data, corroborative XRD and ICP analyses, and adequate sample replication are all necessary to confirm the statistical validity of any pedogenic palygorskite or sepiolite ^{40}Ar/^{39}Ar ages, and to refute adverse laboratory or sample handling effects.

Even if dating of pedogenic palygorskite and/or sepiolite is not proven a viable geochronologic technique for petrocalcic soil age assessment, the variety of unique authigenic minerals present in arid soils, especially relict landscapes, offers exciting potential for new methods. For example, U-Pb isotopic analysis of pedogenic carbonate may provide useful crystallization ages to help reconstruct the evolution of well-developed (stage VI) petrocalcic soil profiles. Moreover, pedogenic barite has also been identified in the massive horizon of Mormon Mesa (Brock, 2007; Robins, 2010b). As noted by Hanor (2000), the Ca and K concentrations of barite crystals sometimes reach ~1000 ppm or more, but the potential of the mineral for geochronology has not yet been fully explored (Hanor, 2000). Investigation of barite, palygorskite, and other mineral systems employing a diverse range of isotopic analyses is sorely needed for arid soil geochronology.

Conclusions

This experiment represents an important step towards the diversification of geochronologic methods applicable to pedogenic systems. Although the age data produced in this exploratory study are inconclusive, it is emphasized here that the potential benefit of a successful application of ^{40}Ar/^{39}Ar geochronology to pedogenic palygorskite and sepiolite makes the topic deserving of further experimentation and could yet produce a viable, exciting new geochronologic method for arid soil geomorphology. Moreover, challenges discussed in this study are immediately relevant to other mineral and isotopic dating systems. The wide variety of unique authigenic mineral assemblages present in arid soils, especially relict landscapes, offers exciting potential for new applications of existing geochronologic techniques. The most critical challenges to a successful dating method for fine-grained, vacuum-encapsulated clays from 1-5 Ma soil horizons may lie not with the theoretical nor practical analysis, but rather in the physical extraction and chemical purification of the minerals (Robins, 2010a). This may hold true not only for palygorskite and sepiolite, but also for a wealth of other, authigenic arid soil minerals.

With further methodological refinement and experimentation, vacuum-encapsulated $^{40}Ar/^{39}Ar$ geochronology of pedogenic palygorskite and/or sepiolite could yet prove to be a successful way to date arid soil landscapes. Suggested methodological refinements include: (1) revision to sample extraction procedures to address hydrocarbon contamination, (2) use of a mass spectrometer coupled with gas chromatography, and (3) use of a better apparatus to remove evolved sample water from the vacuum line. Side-by-side analysis of extracted phyllosilicate aliquots with XRD, SEM/EDS, TEM and/or electron microprobe analysis are essential to future studies. Also needed are models of K and Ar entrapment, and retention or diffusion within the individual crystallites and aggregates of palygorskite and sepiolite.

Thus, significant work remains to be done before this or other geochronologic methods can be proven suitable for pedogenic environments or untested minerals. Continued effort and publication of even partial results are strongly encouraged, given the great need for accurate numerical dates for petrocalcic soil systems (Alonso-Zarza & Arenas, 2004; Brock & Buck, 2009).

References

Achyuthan, H., 2003. Petrologic analysis and geochemistry of the Late Neogene-Early Quaternary hardpan calcretes of Western Rajasthan, India. Quaternary International, 106-107: 3-10.

Alonso-Zarza, A.M., and Arenas, C., 2004. Cenozoic calcretes from the Teruel Graben, Spain: microstructure, stable isotope geochemistry and environmental significance. Sedimentary Geology 167: 91-108.

Alvarez, A., Santarén, J., Pérez-Castells, R., Casal, B., Ruiz-Hitzky, E., Levitz, P., and Fripiat, J.J., 1987. Surfactant adsorption and rheological behavior of surface-modified sepiolite. Proceedings of the International Clay Conference, Denver, 1985: 370-374.

Anderson, J.U., 1961. An improved pretreatment for mineralogical analysis of samples containing organic matter. In: Swineford, A. and Franks, P.C., eds. Proceedings of the Tenth National Conference on Clays and Clay Minerals. New York, Macmillian: 380-388.

Aronson, J.L. and Douthitt, C.B., 1986. K/Ar systematics of an acid-treated illite/smectite: Implications for evaluating age and crystal structure. Clays and Clay Minerals, 34(4): 473-482.

Bachman, G.O. and Machette, M.N., 1977. Calcic soils and calcretes in the southwestern United States. U.S. Geological Survey Open File Report 77-794. 163 pages.

Biermans, V. and Baert, L., 1977. Selective extraction of the amorphous Al, Fe and Si oxides using an alkaline Tiron solution. Clay Minerals, 12(127): 127-135.

Birkeland, P.W., 1999. Soils and Geomorphology. New York, Oxford University Press, 430 pages.

Botha, G.A. and Hughes, J.C., 1992. Pedogenic palygorskite and dolomite in a late Neogene sedimentary succession, northwestern Transvaal, South Africa. Geoderma, 53: 139-154.

Bouza, P. J., Simón, M., Aguilar, J., del Valle, H., and Rostagno, M., 2007. Fibrous-clay mineral formation and soil evolution in Aridisols of northeastern Patagonia, Argentina. Geoderma, 139: 38-50.

Brock, A.L. and Buck, B.J., 2005. A new formation process for calcic pendants from Pahranagat Valley, Nevada: Implications for dating Quaternary landforms. Quaternary Research.

Brock, A.L., 2007. Characterization of stage VI petrocalcic horizons: S. Nevada and N.W. Arizona. Ph.D. Dissertation. University of Nevada Las Vegas, Department of Geoscience. 148 pages.

Brock, A.L. and Buck, B.J., 2009. Polygenetic development of the Mormon Mesa, NV petrocalcic horizons: Geomorphic and paleoenvironmental interpretations. Catena, 77: 65-75.

Buck, B.J. and Mack, G.H., 1995. Latest Cretaceous (Maastrichtian) aridity indicated by paleosols in the McRae Formation, south-central New Mexico. Cretaceous Research, 16(5): 559-572.

Buck, B.J., Wolff, K., Merkler, D., and McMillan, N., 2006. Salt Mineralogy of Las Vegas Wash, Nevada: Morphology and Subsurface Evaporation. Soil Science Society of America Journal, 70: 1639-1651.

Bull, W.B., 1991. Geomorphic Responses to Climate Change. New York, Oxford University Press. 326 pages.

Callen, R.A., 1984. Clays of the palygorskite-sepiolite group: Depositional environment, age and distribution. In: Singer, A., & Galan, E. eds., 1984. Palygorskite-Sepiolite: Occurrences, genesis, and uses. Developments in Sedimentology, 37. New York: El Sevier, 352 pages.

Candy, I., Black, S., and Sellwood, B.W., 2004. Quantifying time scales of pedogenic calcrete formation using U-series disequilibria. Sedimentary Geology, 170: 177-187.

Candy, I., Black, S., and Sellwood, B.W., 2005. U-series isochron dating of immature and mature calcretes as a basis for constructing Quaternary landform chronologies for the Sorbas basin, southeast Spain. Quaternary Research, 64: 100-111.

Candy, I. and Black, S., 2009. The timing of Quaternary calcrete development in semi-arid southeast Spain: Investigating the role of climate on calcrete genesis. Sedimentary Geology, 218: 6-15.

Clauer, N., Chaudhuri, S., Kralik, M. and Bonnot-Courtois, C., 1993. Effects of experimental leaching on Rb-Sr and K-Ar isotopic systems and REE contents of diagenetic illite. Chemical Geology, 103: 1-16.

Clauer, N. and Chaudhuri, S., 1995. Clays in crustal environments: Isotope dating and tracing. Springer-Verlag, 359 pp.

Corma, A., Mifsud A., and Sanz, E., 1987. Influence of the chemical composition and textural characteristic of palygorskite on the acid leaching of octahedral cations, Clay Minerals, 22: 225–232.

Dohrenwend, J.C., Wells, S.G., and McFadden, L.D., 1986. Geomorphic and stratigraphic indicators of Neogene-Quaternary climatic change in arid and semi-arid environments. Geology, 14: 263-264.

Dong, H., Hall, C.M., Peacor, D.R., and Halliday, A.N., 1995. Mechanisms of argon retention in clays revealed by laser ^{40}Ar-^{39}Ar dating. Science, 267(5196): 355-359.

Dong, H. et al., 1997. ^{40}Ar/^{39}Ar illite dating of Late Caledonian (Acadian) metamorphism and cooling of K-bentonites and slates from the Welsh Basin, U.K. Earth and Planetary Science Letters, 150: 337-351.

Elprince, A. M., Mashhady, A.S., and Aba-Husayn, M.M., 1979. The occurrence of pedogenic palygorskite (attapulgite) in Saudi Arabia. Soil Science, 128(4): 211-218.

Ertl, S. and Spitzy, A., 2004. Low-temperature sealed tube combustion of gaseous, liquid and solid organic compounds for ^{13}C/^{12}C and ^{14}C analysis. Isotopes in Environmental and Health Studies, 20(2): 163-170.

Foland, K.A., Hubacher, F.A., and Arehart, G.B., 1992. ^{40}Ar/^{39}Ar dating of very fine-grained samples: An encapsulated-vial procedure to overcome the problem of ^{39}Ar recoil loss. Chemical Geology (Isotope Geoscience Section) 102: 269-276.

Francis, M.L., Fey, M.V., Prinsloo, H.P., Ellis, F., Mills, A.J., and Medinski, T.V., 2007. Soils of Namaqualand: Compensations for aridity. Journal of Arid Environments, 70: 588-603.

Fuchs, M. and Lang, A., 2009. Luminescence dating of hillslope deposits – A review. Geomorphology, 109: 17-26.

Galan, E. and Carretero, M.I., 1999. A new approach to compositional limits for sepiolite and palygorskite. Clays and Clay Minerals, 47(4): 399-409.

García-Romero, E., Suárez Barrios, M., and Bustillo Revuelta, M.A., 2004. Characteristics of a Mg-palygorskite in Miocene rocks, Madrid Basin (Spain). Clays and Clay Minerals, 52(4): 484-494.

García-Romero, E., Suárez, M., Santarén, J., and Alvarez, A., 2007. Crystallochemical characterization of the palygorskite and sepiolite from the Allou Kagne deposit, Senegal. Clays and Clay Minerals, 55 (6): 606-617.

Gardner, L.R., 1972. Origin of the Mormon Mesa Caliche, Clark County, Nevada. Geological Society of America Bulletin, 83: 143-156.

Gile, L.H., Peterson, F.F., and Grossman, R.B., 1966. Morphological and genetic sequences of carbonate accumulation in desert soils. Soil Science, 101(5): 347-360.

Gile, L.H., Hawley, J.W., and Grossman, R.B., 1981. Soils and geomorphology in the Basin and Range area of Southern New Mexico - Guidebook to the Desert Project. New Mexico Bureau of Mines & Mineral Resources, Memoir 39. University of New Mexico, Socorro, 222 pp.

Hanor, J.S., 2000. Barite-celestine geochemistry and environments of formation. In: Alpers, C.N., Jambor J.L., and Nordstrom, D.K., eds. Sulfate minerals: Cyrstallography, geochemistry, and environmental significance. Reviews in Mineralogy and Geochemistry, 40. Washington, The Mineralogical Society of

America**:** 192-275.

Hay, R.L. and Wiggins, B., 1980. Pellets, ooids, sepiolite and silica in three calcretes of the southwestern United States. Sedimentology, 27: 559-576.

Hillier, S. and Pharande A.L., 2008. Contemporary pedogenic formation of palygorskite in irrigation-induced, saline-sodic, shrink-swell soils of Maharashtra, India. Clays and Clay Minerals, 56(5): 531-548.

Howell, M.S., 2009. Mineralogy and micromorphology of an Atacama Desert soil, Chile: A model for hyperarid soil genesis. M.S. Thesis. University of Nevada Las Vegas, Department of Geoscience.

House, P.K., Pearthree, P.A., Howard, K.A., Bel, J.W., Perkins, M.E., and Brock, A.L., 2005. Birth of the lower Colorado River – Stratigraphic and geomorphic evidence for its inception near the conjunction of Nevada, Arizona, and California. In: Pederson, J., and Dehler, C.M., eds. Interior Western United States. Geological Society of America Field Guide 6. Boulder, Geological Society of America.

Jackson, M.L.,1965. Soil chemical analysis: Advanced Course. Published by the author. Dept. of Soil Science, University of Wisconsin, Madison.

Jones, B.F., 1983. Occurrence of clay minerals in surficial deposits of southwestern Nevada. Sciences Géologiques Mémoires (Strasbourg), 72: 81-92.

Jones, B.F. and Galan, E., 1988. Sepiolite and palygorskite. Reviews in Mineralogy, 19(1): 631-674.

Jornada Basin Long-Term Ecological Research (LTER) project, 2003. Geochronology of the Desert Project and vicinity: The Jornada and Mesilla Basins, chronology of La Mesa surfaces, and time of entrenchment of the Rio Grande Valley. Spatial Data Laboratory, USDA, ARS, Jornada Experimental Range. http://jornada-www.nmsu.edu.

Khadkikar, A.S., Chamyal, L.S., and Ramesh, R., 2000. The character and genesis of calcrete in Late Quaternary alluvial deposits, Gujarat, western India, and its bearing on the interpretation of ancient climates. Palaeogeography, Palaeoclimatology, Palaeoecology, 162: 239-261.

Kodama, H. and Ross, G.J., 1991. Tiron dissolution method used to remove and characterize inorganic components in soils. Soil Science Society of America Journal, 55: 1180-1187.

Ku, T.-L., Bull, W.B., Freeman, S.T. and Knauss, K.G., 1979. Th^{230}-U^{234} dating of pedogenic carbonates in gravelly desert soils of Vidal Valley, southeastern California. Geologic Society of America Bulletin, 90(1): 1063-1073.

Kunze, G.W. and Dixon, J.B., 1986. Pretreatment for mineralogical analysis. In: Klute, A., ed. Methods of soil analysis part 1: Physical and mineralogical methods, 2nd edition. Agronomy Monograph 9. Madison, Soil Science Society of America: 91-100.

Lin, L.-H., Onstott, T.C., and Dong, H., 1996. Backscattered ^{39}Ar loss in fine-grained minerals: Implications for ^{40}Ar/^{39}Ar geochronology of clay. Geochimica et Cosmochimica Acta, 64(23): 3965-3974.

Machette, M.N., 1985. Calcic soils of the southwestern United States. Geologic society of America Special Paper, 203: 1-21.

Madsen, A.T. and Murray, A.S., 2009. Optically stimulated luminescence dating of young sediments: A review. Geomorphology, 109: 3-16.

Magloughlin, J.F., Hall, C.M., and van der Pluijm, B.A., 2001. ^{40}Ar/^{39}Ar geochronometry of pseudotachylytes by vacuum encapsulation: North Cascade Mountains, Washington, USA. Geology, 29(1): 51-54.

Mayer, L, McFadden, L.D., and Harden, J.W., 1988. Distribution of calcium carbonate in desert soils: A model. Geology, 16: 303-306.

McDougall, I. and Harrison, T.M., 1988. Geochronology and thermochronology by the ^{40}Ar/^{39}Ar method. Oxford University Press, New York, 212 pp.

Monger, H.C. and Daugherty, L.A., 1991a. Neoformation of palygorskite in a southern New Mexico aridisol. Soil Science Society of America Journal, 55: 1646-1650.

Monger, H.C. and Daugherty, L.A., 1991b. Pressure solution: Possible mechanism for silicate grain dissolution in a petrocalcic horizon. Soil Science Society of America Journal, 55: 1625-1629.

Murray, H.H., 2000. Traditional and new applications for kaolin, smectite, and palygorskite: a general overview. Applied Clay Science, 17: 207-221.

Onstott, T.C., Mueller, C., Vrolijk, P.J., and Pevear, D.R., 1997. Laser ^{40}Ar/^{39}Ar microprobe analyses of fine-grained illite. Geochimica et Cosmochimica Acta, 61(18): 3851-3861.

Paquet, H., Duplay, J., Valleron-Blanc, M.-M., and Llerena, C.A., 1987. Octahedral compositions of individual particles in smectite-palygorskite and smectite-sepiolite assemblages. Proceedings of the International Clay Conference, Denver, 1985: 73-77.

Pérez-Castells, R., Alvarez, A., Gavilanes, J., Lizarbe, M.A., Martínez del Pozo, A., Olmo, N., and Santarén, J., 1987. Adsorption of collagen by sepiolite. Proceedings of the International Clay Conference, Denver, 1985: 359-362.

Polyak, V.J., McIntosh, W.C., Güven, N. and Provencio, P., 1998. Age and origin of Carlsbad Cavern and related caves from ^{40}Ar/^{39}Ar of Alunite. Science, 279: 1919-1922.

Potgieter, J. H., Potgieter-Vermaak, S. S., and Kalibantonga, P.D., 2006. Heavy metals removal from solution by palygorskite clay. Minerals Engineering, 19: 463-470.

Rasbury, E.T. et al., 1998. U-Pb dates of paleosols: Constraints on late Paleozoic cycle durations and boundary ages. Geology, 26(5): 403-406.

Reeves, C.C. Jr., 1976. Caliche: Origin, classification, morphology and uses. Lubbock, Estacado books. 233 pages.

Retallack, G.J., 2001. Soils of the past: An introduction to paleopedology. Blackwell Science, Malden, MA, 404 pp.

Robins, C.R., 2010a. Towards ^{40}Ar/^{39}Ar geochronology of pedogenic palygorskite and sepiolite, Part I: extraction and chemical considerations. IN: Robins, C.R. Phyllosilicate mineralogy, ^{40}Ar/^{39}Ar geochronology, and genesis of petrocalcic soils in the southwest U.S.A. Ph.D. dissertation. University of Nevada Las Vegas, Department of Geoscience: 1-55.

Robins, C.R., 2010b. Micromorphology, chemistry and phyllosilicate mineralogy of the Mormon Mesa petrocalcic soil, Nevada, USA: Genetic implications. In: Phyllosilicate mineralogy, ^{40}Ar/^{39}Ar geochronology, and genesis of petrocalcic soils in the southwest U.S.A. Ph.D. dissertation. University of Nevada Las Vegas, Department of Geoscience: 94-174.

Sandler, A., Harlavan, Y. and Steinitz, G., 2004. Early formation of K-feldspar in shallow-marine sediments at near-surface temperatures (southern Israel): evidence from K-Ar dating. Sedimentology, 51: 323-338.

Schmidt, D.L., Page, W.R. and Workman, J.B., 1996. Preliminary geologic map of the Moapa West Quadrangle, Clark County, Nevada. U.S. Department of the Interior, U.S. Geological Survey Open-File Report 96-521. 1:24,000.

Serna, C.J., and VanScoyoc, G.E., 1979. Infrared study of sepiolite and palygorskite surfaces. In: Mortland, M.M., and Farmer. V.C., eds. International Clay Conference 1978. Amsterdam, El Sevier Scientific Publishing Company**:** 197-207.

Shang, C. & Zelazny, L., 2008. Selective dissolution techniques for mineral analysis of soils and sediments. In: Ulery, A. and Drees, R., eds. Methods of Soil Analysis part 5: Mineralogical Methods. SSSA Book Series No. 5. Madison, Soil Science Society of America: 33-80.

Sharp, W.D., Ludwig, K.R., Chadwick, O.A., Amundson, R. and Glaser, L.L., 2003. Dating fluvial terraces by 230Th/U on pedogenic carbonate, Wind River Basin, Wyoming. Quaternary Research, 59: 139-150.

Singer, A., 1989. Palygorskite and sepiolite group minerals. In: Dixon, J.B. and Weed, S.B., eds., Minerals in soil environments, 2nd edition. SSSA Book Series 1. Madison, Soil Science Society of America: 829-872.

Singer, A., Kirsten, W., and Bühman, C., 1995. Fibrous clay minerals in the soils of Namaqualand, South Africa: Characteristics and formation. Geoderma, 66: 43-70.

Singer, A., 2002. Palygorskite and sepiolite. In: Dixon, J.B. and Schulze, D.G., eds. Soil mineralogy with environmental applications. SSSA Book Series No. 7. Madison, Soil Science Society of America: 555-583.

Smith, P.E., Evensen, N.M., and York, D., 1993. First successful $^{40}Ar/^{39}Ar$ dating of glauconies: Argon recoil in single grains of cryptocrystalline material. Geology 21: 41-44.

Smith, P.E., Evensen, N.M., York, D., and Odin, G.S., 1998; Single grain$^{40}Ar/^{39}Ar$ ages of glauconies: Implications for the geologic time scale and global sea level variations. Science, 279: 1517-1519.

Sofer, Z., 1980. Preparation of carbon dioxide for stable carbon isotope analysis of petroleum fractions. Analytical Chemistry, 52(8): 1389-1391.

Soukup, D.A., Buck, B.J., and Harris,W., 2008. Preparing soils for mineralogical analysis. In: Ulery, A. and Drees, R., eds. Methods of soil analysis, part 5: Mineralogical methods. SSSA Book Series No. 5. Madison, Science Society of America, p. 13-31.

Thompson, G.R. and Hower, J., 1973. An explanation for low radiometric ages from glauconite. Geochimica et Cosmochimica Acta, 37: 1473-1491.

United Nations Commission to Combat Desertification, 1997. Earth Summit +5. Special session of the General Assembly to review and appraise the implementation of Agenda 21. New York, 23-27 June. http://www.un.org/ecosocdev/geninfo/sustdev/desert.htm.

Vanden Heuvel, R.C., 1966. The occurrence of sepiolite and attapulgite in the calcareous zone of a soil near Las Cruces, New Mexico. In: W.F. Bradley and S.W. Bailey, eds. Thirteenth National Conference on Clays and Clay Minerals. Madison, Pergamon Press: 193-207.

Vandeputte, K., Moens, L., and Dams, R., 1996. Improved sealed-tube combustion of organic samples to CO_2 for stable carbon isotope analysis, radiocarbon dating and percent carbon determinations. Analytical Letters, 29(15):2761-2773.

van der Pluijm, B.A., Hall, C.M., Vrolijk, P.J., Pevear, D.R., and Covey, M.C., 2001. The dating of shallow faults in the Earth's crust. Nature, 412: 172-175.

Vasconcelos, P.M., Brimhall, G.H., Becker, T.A. and Renne, P.R., 1994. $^{40}Ar/^{39}Ar$ analysis of supergene jarosite and alunite: Implications to the paleoweathering history of the western USA and West Africa. Geochimica et Cosmochimica Acta, 58: 401-420.

Vasconcelos, P.M. and Conroy, M., 2003. Geochronology of weathering and landscape evolution, Dugald River valley, NW Queensland, Australia. Geochimica et Cosmochimica Acta, 67(16): 2913-2930.

Velivetskaya, T.A., Ignatyev, A.V., Reize, M.V., and Kiyasho, S.I., 2007. Open tube combustion method of organic samples for stable carbon isotope analysis. Rapid Communications in Mass Spectrometry, 21: 2451-2455.

Verrecchia, E. P. and Le Coustumer, M.-N., 1996. Occurrence and genesis of palygorskite and associated clay minerals in a Pleistocene calcrete complex, Sde Boqer, Negev Desert, Israel. Clay Minerals, 31: 183-202.

Watts, N.L., 1978. Displacive calcite: Evidence from recent and ancient calcretes. Sedimentology Research Laboratory, 6: 699-703.

Watts, N.L., 1980. Quaternary pedogenic calcretes from the Kalahari (southern Africa): mineralogy, genesis and diagenesis. Sedimentology, 27: 661-686.

Weaver, C.E., and Pollard, L.D., 1973. The chemistry of clay minerals. New York, Elsevier. 213 pages.

Wilkinson, M. and Haszeldine, R.S., 2002. Problems with argon: K-Ar ages in Gulf Coast shales. Chemical Geology, 191: 277-283.

Williams, V.S., Bohannon, R.G. and Hoover, D.L., 1997. Geologic map of the Riverside Quadrangle, Clark County, Nevada, Geologic Quadrangle Map GQ-1770.

Yaalon, D.H. and Wieder, M., 1976. Pedogenic palygorskite in some arid brown (calciorthid) soils of Israel. Clay Minerals, 11:73-80.

Yariv, S. and H. Cross, eds., 2002. Organo-clay complexes and interactions. New York, Marcel Dekker, Inc., 688 pages.

Yildiz, A., and Gür, A., 2007. Adsorption of phenol and chlorophenols on pure and modified sepiolite. Journal of the Serbian Chemical Society, 72(5): 467-474.

Table 3.1. Calculated ages for the pedogenic phyllosilicates

Mormon Mesa	**NIGL ID**	**Total Gas Age**			
mA1	UNLV 64-1-1	96.56	±	10.67	Ma
mA4	UNLV 62-1-1	261.05	±	5.76	Ma
mA5	UNLV 62-1-2	100.49	±	12.86	Ma
mA8	UNLV 62-1-3	99.36	±	26.11	Ma
mB1	UNLV 62-1-4	261.84	±	8.95	Ma
mB2	UNLV 62-1-5	200.90	±	6.97	Ma
mB3	UNLV 63-1-5	200.10	±	8.14	Ma
mB4	UNLV 62-1-6	222.26	±	9.10	Ma
mB5	UNLV 63-1-4	208.65	±	2.21	Ma
JER La Mesa	**NIGL ID**	**Total Gas Age**			
jA2	UNLV 63-1-2	178.35	±	0.69	Ma
jA3	UNLV 63-1-1	557.06	±	2.48	Ma
jB1	UNLV 63-1-6	254.91	±	0.94	Ma

Table 3.2A. Argon isotope analysis of Mormon Mesa Sample mA1.

Method	**T (°C)**	**t (min.)**	**^{36}Ar**	**^{37}Ar**	**^{38}Ar**	**^{39}Ar**	**^{40}Ar**	**%^{40}Ar***	**%^{39}Ar rlsd**	**Ca/K**	**^{40}Ar*/^{39}ArK**
encap	Vial	6	207.33	2.93	41.25	125.61	59509.06	1.9	125.61	0.62	89.57
furnace	1000	12	144.01	17.09	33.59	41.1	48588.81	17.4	41.1	12.46	2078.13

Method	**Age (Ma)**	**1s.d.**	**Analyt. Err**	**37/39c**	**%^{39}ArK**	**Total^{39}Ar**	**mol ^{39}Ar**	**Wmdata**	**WMs**	**wfactor**	**WxX**
encap	9.389	5.766	5.766	0.27	99.98	333.42	7.54E-15	9.39	5.77	0.03	0.28
furnace	206.24	14.092	14.083	5.40	99.64		2.47E-15	206.24	14.08	0.01	1.04

Method	**37d**	**method**	**39/40c**	**39/40err**	**36/40c**	**36/40err**	**R^2**	**T°(C)**	**36c**	**39c**	**40c**
encap	11.79	encap	0.0020852	1.170588	0.001623	1.846651	0.447514	Vial	101.32074	125.587	59493.19364
furnace	13.37	furnace	0.0008319	1.085049	0.002795	1.331678	0.773547	1000	143.61901	40.9654	48533.09342

Method	**%36err**	**%39err**	**%40err**	**36err**	**40err**	**%36err**	**%40err**	**WtdAge39Ar**
encap	0.8	0.8	0.72	1.658643	428.4652	1.637022	0.720192	11.7935229
furnace	0.77	0.01	0.94	1.10888	456.735	0.772098	0.94108	84.76464

TOTAL GAS AGE: 96.558 ± 10.67 Ma

4 amu discrimination = 1.04940 ± 0.46%, 40/39K = 0.0678 ± 98.08%, 36/37Ca = 0.000268 ± 24.66%, 39/37Ca = 0.000668 ± 14.10%

4 amu discrimination = 1.05877 ± 0.54% for furnace run

Note: Isotope values are reported in mV, as measured beam intensity at t_0 from regressions.

Table 3.2B. Argon isotope analysis of Mormon Mesa Sample mA4.

Method	**T (°C)**	**t (min.)**	**^{36}Ar**	**^{37}Ar**	**^{38}Ar**	**^{39}Ar**	**^{40}Ar**	**%^{40}Ar***	**%^{39}Ar rlsd**	**Ca/K**	**40Ar*/39ArK**
encap	Vial	6	146.33	1.88	31.63	118.81	41230.3	1.3	118.81	0.42	43.67
furnace	1000	12	100.78	1.72	20.45	77.21	56028.8	49.9	77.21	0.59	3635.08

Method	**Age (Ma)**	**1s.d.**	**Analyt. Err**	**37/39c**	**%^{39}ArK**	**Total^{39}Ar**	**mol ^{39}Ar**	**Wmdata**	**WMs**	**wfactor**	**WxX**
encap	4.362	3.948	3.948	0.18	99.99	392.04	7.13E-15	4.36	3.95	0.06	0.28
furnace	331.387	4.273	4.192	0.26	99.98		4.63E-15	331.39	4.19	0.06	18.86

Method	**37d**	**method**	**39/40c**	**39/40err**	**36/40c**	**36/40err**	**R^2**	**T°(C)**	**36c**	**39c**	**40c**
encap	11.79	encap	0.0028562	1.270404	0.003342	1.141177	0.61641	Vial	145.05281	118.796	40989.44575
furnace	12.80	furnace	0.0013589	0.725352	0.001697	0.682782	0.445517	1000	100.56826	77.197	55986.50375

Method	**%36err**	**%39err**	**%40err**	**36err**	**40err**	**%36err**	**%40err**	**WtdAge39Ar**
encap	0.54	0.78	0.84	0.790182	346.3371	0.544755	0.844942	5.1824922
furnace	0.29	0.38	0.3	0.292264	168.0866	0.290612	0.300227	255.8639027

TOTAL GAS AGE: 261.05 ± 5.762 Ma

4 amu discrimination = 1.05877 ± 0.54%, 40/39K = 0.125 ± 36.95%, 36/37Ca = 0.000234 ± 23.01%, 39/37Ca = 0.000642 ± 5.1%

Note: Isotope values are reported in mV, as measured beam intensity at t_0 from regressions.

Table 3.2C. Argon isotope analysis of Mormon Mesa Sample mA5.

Method	**T (°C)**	**t (min.)**	**^{36}Ar**	**^{37}Ar**	**^{38}Ar**	**^{39}Ar**	**^{40}Ar**	**%^{40}Ar***	**%^{39}Ar rlsd**	**Ca/K**	**40Ar*/39ArK**
encap	Vial	6	106.85	1.89	21.75	36.11	30030.47	0.7	36.11	1.38	61.45
furnace	1000	12	292.49	5.48	57.29	23.04	92596.86	11.9	23.04	6.28	4807.42

Method	**Age (Ma)**	**1s.d.**	**Analyt. Err**	**37/39c**	**%^{39}ArK**	**Total^{39}Ar**	**mol ^{39}Ar**	**Wmdata**	**WMs**	**wfactor**	**WxX**
encap	6.135	6.783	6.783	0.60	99.96	118.3	2.17E-15	6.14	6.78	0.02	0.13
furnace	426.553	20.153	20.125	2.72	99.83		1.38E-15	426.55	20.12	0.00	1.05

Method	**37d**	**method**	**39/40c**	**39/40err**	**36/40c**	**36/40err**	**R^2**	**T°(C)**	**36c**	**39c**	**40c**
encap	11.79	encap	0.001185	1.217225	0.003359	0.815604	0.48751	Vial	106.76879	36.0957	30019.54025
furnace	12.77	furnace	0.0002448	0.731856	0.002983	0.643507	0.187482	1000	292.34788	22.9985	92578.31

Method	**%36err**	**%39err**	**%40err**	**36err**	**40err**	**%36err**	**%40err**	**WtdAge39Ar**
encap	0.22	0.93	0.57	0.235071	171.1737	0.220168	0.570208	2.2153485
furnace	0.3	0.46	0.18	0.877471	166.6743	0.300146	0.180036	98.2778112

TOTAL GAS AGE: 100.49 ± 12.86 Ma

4 amu discrimination = 1.05877 ± 0.54%, 40/39K = 0.125 ± 36.95%, 36/37Ca = 0.000234 ± 23.01%, 39/37Ca = 0.000642 ± 5.1%

Note: Isotope values are reported in mV, as measured beam intensity at t_0 from regressions.

Table 3.2D. Argon isotope analysis of Mormon Mesa Sample mA8.

Method	**T (°C)**	**t (min.)**	**^{36}Ar**	**^{37}Ar**	**^{38}Ar**	**^{39}Ar**	**^{40}Ar**	**%^{40}Ar***	**%^{39}Ar rlsd**	**Ca/K**	**40Ar*/39ArK**
encap	Vial	6	95	3.16	24.08	27.81	26451.67	-1	27.81	2.74	-99.04
furnace	1000	12	158.58	2.64	30.95	17.34	51984.56	14.33	17.34	3.65	6954.74

Method	**Age (Ma)**	**1s.d.**	**Analyt. Err**	**37/39c**	**%^{39}ArK**	**Total^{39}Ar**	**mol ^{39}Ar**	**Wmdata**	**WMs**	**wfactor**	**WxX**
encap	-9.931	-14.758	14.758	1.19	99.92	90.3	1.67E-15	-9.93	14.76	0.00	-0.05
furnace	588.911	28.041	28.002	1.59	99.90		1.04E-15	588.91	28.00	0.00	0.75

Method	**37d**	**method**	**39/40c**	**39/40err**	**36/40c**	**36/40err**	**R^2**	**T°(C)**	**36c**	**39c**	**40c**
encap	10.72	encap	0.0010385	1.965965	0.003418	1.530066	0.403485	Vial	94.802071	27.7882	26431.45375
furnace	12.09	furnace	0.0003348	1.097821	0.002901	0.810628	0.181334	1000	156.64838	17.3218	50996.0825

Method	**%36err**	**%39err**	**%40err**	**36err**	**40err**	**%36err**	**%40err**	**WtdAge39Ar**
encap	1	1.59	1.06	0.950001	280.3877	1.002089	1.060811	-2.7618111
furnace	0.502	0.898	0.321	0.796155	166.9739	0.508243	0.327425	102.1171674

TOTAL GAS AGE: 99.355 ± 26.11 Ma

4 amu discrimination = 1.04940 ± 0.46%, 40/39K = 0.125 ± 36.95%, 36/37Ca = 0.000234 ± 23.01%, 39/37Ca = 0.000642 ± 5.1%

4 amu discrimination = 1.05877 ± 0.54% for furnace run

Note: Isotope values are reported in mV, as measured beam intensity at t_0 from regressions.

Table 3.2E. Argon isotope analysis of Mormon Mesa Sample mB1.

Method	**T (°C)**	**t (min.)**	**^{36}Ar**	**^{37}Ar**	**^{38}Ar**	**^{39}Ar**	**^{40}Ar**	**%^{40}Ar***	**%^{39}Ar rlsd**	**Ca/K**	**40Ar*/39ArK**
encap	Vial	6	161.02	2.85	34.03	70.14	47236.58	4.2	70.14	0.94	284.44
furnace	1000	12	71.85	1.76	14.77	69.2	46783.1	56.9	69.2	0.60	3856.80

Method	**Age (Ma)**	**1s.d.**	**Analyt. Err**	**37/39c**	**%^{39}ArK**	**Total^{39}Ar**	**mol ^{39}Ar**	**Wmdata**	**WMs**	**wfactor**	**WxX**
encap	28.224	13.565	13.565	0.41	99.97	278.68	4.21E-15	28.22	13.56	0.01	0.15
furnace	349.771	4.798	4.718	0.26	99.98		4.15E-15	349.77	4.72	0.04	15.72

Method	**37d**	**method**	**39/40c**	**39/40err**	**36/40c**	**36/40err**	**R^2**	**T°(C)**	**36c**	**39c**	**40c**
encap	10.29	encap	0.0014703	2.013036	0.003242	2.306951	0.452519	Vial	160.17914	70.1212	47117.5415
furnace	10.55	furnace	0.0014624	0.891856	0.00146	0.970931	0.447767	1000	71.579763	69.1884	46734.53

Method	**%36err**	**%39err**	**%40err**	**36err**	**40err**	**%36err**	**%40err**	**WtdAge39Ar**
encap	1.78	1.39	1.44	2.866183	680.2102	1.789361	1.443645	19.7963136
furnace	0.66	0.54	0.54	0.474213	252.6292	0.662495	0.540562	242.041532

TOTAL GAS AGE: 261.84 ± 8.946 Ma

4 amu discrimination = 1.04870 ± 0.19%, 40/39K = 0.125 ± 36.95%, 36/37Ca = 0.000234 ± 23.01%, 39/37Ca = 0.000642 ± 5.1%

4 amu discrimination = 1.04940 ± 0.46% for furnace run

Note: Isotope values are reported in mV, as measured beam intensity at t_0 from regressions.

Table 3.2F. Argon isotope analysis of Mormon Mesa Sample mB2.

Method	**T (°C)**	**t (min.)**	**^{36}Ar**	**^{37}Ar**	**^{38}Ar**	**^{39}Ar**	**^{40}Ar**	**%^{40}Ar***	**%^{39}Ar rlsd**	**Ca/K**	**40Ar*/39ArK**
encap	Vial	6	172.19	2.62	36.44	78.77	49607.47	2.2	78.77	0.77	141.17
furnace	1000	12	41.13	1.21	9.05	53.76	353.099	64.4	53.76	0.53	3897.17

Method	**Age (Ma)**	**1s.d.**	**Analyt. Err**	**37/39c**	**%^{39}ArK**	**Total^{39}Ar**	**mol ^{39}Ar**	**Wmdata**	**WMs**	**wfactor**	**WxX**
encap	14.062	3.539	3.539	0.33	99.98	265.06	4.73E-15	14.06	3.54	0.08	1.12
furnace	353.099	20.073	20.054	0.23	99.99		3.23E-15	353.10	20.05	0.00	0.88

Method	**37d**	**method**	**39/40c**	**39/40err**	**36/40c**	**36/40err**	**R^2**	**T°(C)**	**36c**	**39c**	**40c**
encap	10.27	encap	0.0015689	0.693893	0.003309	0.571672	0.384768	Vial	172.11271	78.7527	49591.76275
furnace	10.49	furnace	0.1732574	1.054235	0.127056	1.01504	0.424744	1000	40.861094	53.752	306.459

Method	**%36err**	**%39err**	**%40err**	**36err**	**40err**	**%36err**	**%40err**	**WtdAge39Ar**
encap	0.39	0.554	0.372	0.671541	184.5398	0.390175	0.372118	11.0766374
furnace	0.62	0.686	0.561	0.255011	2.00775	0.624092	0.655145	189.8260224

TOTAL GAS AGE: 200.90 ± 6.970 Ma

4 amu discrimination = 1.04870 ± 0.19%, 40/39K = 0.125 ± 36.95%, 36/37Ca = 0.000234 ± 23.01%, 39/37Ca = 0.000642 ± 5.1%

4 amu discrimination = 1.04940 ± 0.46% for furnace run

Note: Isotope values are reported in mV, as measured beam intensity at t_0 from regressions.

Table 3.2G. Argon isotope analysis of Mormon Mesa Sample mB3.

Method	T (°C)	t (min.)	^{36}Ar	^{37}Ar	^{38}Ar	^{39}Ar	^{40}Ar	%^{40}Ar*	%^{39}Ar rlsd	Ca/K	40Ar*/39ArK
encap	Vial	6	122.97	2.77	27.78	37.44	34217.03	-0.4	37.4	1.74	-34.58
furnace	1000	12	99.62	0.97	20.25	58.3	49986.6	43.9	58.3	0.40	3804.54

Method	Age (Ma)	1s.d.	Analyt. Err	37/39c	%^{39}ArK	Total^{39}Ar	mol ^{39}Ar	Wmdata	WMs	wfactor	WxX
encap	-3.46	-13.37	13.373	0.76	99.95	191.48	2.25E-15	-3.46	13.37	0.01	-0.02
furnace	345.46	4.34	4.251	0.17	99.99		3.5E-15	345.46	4.25	0.06	19.12

Method	37d	method	39/40c	39/40err	36/40c	36/40err	R^2	T°(C)	36c	39c	40c
encap	10.50	encap	0.0010832	1.629125	0.003398	1.429151	0.49394	Vial	121.60609	37.4189	34129.50104
furnace	10.74	furnace	0.0011526	0.719814	0.001897	0.594376	0.123057	1000	99.426167	58.2924	49955.8483

Method	%36err	%39err	%40err	36err	40err	%36err	%40err	WtdAge39Ar
encap	0.926	1.22	1.06	1.138705	362.7291	0.936388	1.062802	-1.2957984
furnace	0.34	0.53	0.16	0.338708	79.97892	0.340663	0.160099	201.400265

TOTAL GAS AGE: 200.10 ± 8.141 Ma

4 amu discrimination = 1.04870 ± 0.19%, 40/39K = 0.109 ± 12.16%, 36/37Ca = 0.000272 ± 14.63%, 39/37Ca = 0.000725 ± 8.32%

4 amu discrimination = 1.04940 ± 0.46% for furnace run

Note: Isotope values are reported in mV, as measured beam intensity at t_0 from regressions.

Table 3.2H. Argon isotope analysis of Mormon Mesa Sample mB4.

Method	T (°C)	t (min.)	^{36}Ar	^{37}Ar	^{38}Ar	^{39}Ar	^{40}Ar	%^{40}Ar*	%^{39}Ar rlsd	Ca/K	40Ar*/39ArK
encap	Vial	6	166.36	1.46	35.13	59.18	48305.56	3.4	59.2	0.57	280.76
furnace	1000	12	81.3	0.73	16.22	56.02	45600.51	49.9	56.0	0.31	4070.51

Method	Age (Ma)	1s.d.	Analyt. Err	37/39c	%^{39}ArK	Total^{39}Ar	mol ^{39}Ar	Wmdata	WMs	wfactor	WxX
encap	27.86	13.76	13.760	0.25	99.98	230.40	3.55E-15	27.86	13.76	0.01	0.15
furnace	367.32	4.89	4.800	0.13	99.99		3.36E-15	367.32	4.80	0.04	15.94

Method	37d	method	39/40c	39/40err	36/40c	36/40err	R^2	T°(C)	36c	39c	40c
encap	10.28	encap	0.0012132	1.936731	0.003273	1.726529	0.513527	Vial	165.41049	59.1704	48186.3325
furnace	10.53	furnace	0.0012147	0.797017	0.001695	0.701205	0.615581	1000	81.032244	56.0152	45553.5875

Method	%36err	%39err	%40err	36err	40err	%36err	%40err	WtdAge39Ar
encap	1.11	1.42	1.3	1.846664	627.9818	1.116413	1.303236	16.4881398
furnace	0.26	0.46	0.46	0.211386	209.7626	0.260866	0.460474	205.7709834

TOTAL GAS AGE: 222.26 ± 9.102 Ma

4 amu discrimination = 1.04870 ± 0.19%, 40/39K = 0.125 ± 36.95%, 36/37Ca = 0.000234 ± 23.01%, 39/37Ca = 0.000642 ± 5.1%

4 amu discrimination = 1.04940 ± 0.46% for furnace run

Note: Isotope values are reported in mV, as measured beam intensity at t_0 from regressions.

Table 3.2I. Argon isotope analysis of Mormon Mesa Sample mB5.

Method	T (°C)	t (min.)	^{36}Ar	^{37}Ar	^{38}Ar	^{39}Ar	^{40}Ar	%^{40}Ar*	%^{39}Ar rlsd	Ca/K	40Ar*/39ArK
encap	-	6	116	2.82	31.37	143.84	36225.53	8.5	143.84	0.38	215.82
furnace	1000	12	45.84	0.6	9.96	46.29	32510.39	60.3	46.29	0.28	4283.16

Method	Age (Ma)	1s.d.	Analyt. Err	37/39c	%^{39}ArK	Total^{39}Ar	mol ^{39}Ar	Wmdata	WMs	wfactor	WxX
encap	21.442	1.711	1.710	0.17	99.99	190.13	8.63E-15	21.44	1.71	0.34	7.33
furnace	384.126	1.748	1.314	0.12	99.99		2.78E-15	384.13	1.31	0.58	222.36

Method	37d	method	39/40c	39/40err	36/40c	36/40err	R^2	T°(C)	36c	39c	40c
encap	8.64	encap	0.0039394	0.639949	0.003097	0.699274	0.51461	-	115.90537	143.822	36204.46644
furnace	9.71	furnace	0.0014072	0.226744	0.001342	0.226757	0.941176	1000	45.742416	46.2858	32496.17539

Method	%36err	%39err	%40err	36err	40err	%36err	%40err	WtdAge39Ar
encap	0.39	0.27	0.34	0.452401	123.1668	0.39032	0.340198	30.8421728
furnace	0.03	0.03	0.12	0.013767	39.01251	0.030098	0.120053	177.8119254

TOTAL GAS AGE: 208.65 ± 2.21 Ma

4 amu discrimination = 1.03362 ± 0.47%, 40/39K = 0.109 ± 12.16%, 36/37Ca = 0.000272 ± 14.63%, 39/37Ca = 0.000725 ± 8.32%

4 amu discrimination = 1.04870 ± 0.19% for furnace run

Note: Isotope values are reported in mV, as measured beam intensity at t_0 from regressions.

Table 3.2J. Argon isotope analysis of JER La Mesa Sample jA2.

Method	T (°C)	t (min.)	^{36}Ar	^{37}Ar	^{38}Ar	^{39}Ar	^{40}Ar	%^{40}Ar*	%^{39}Ar rlsd	Ca/K	40Ar*/39ArK
encap	Vial	6	56.68	1.63	12.79	125.84	15854.13	-0.7	125.84	0.27	-8.52
furnace	1000	12	14.26	1.27	3.84	104.68	22703.52	82.1	104.68	0.27	1799.04

Method	Age (Ma)	1s.d.	Analyt. Err	37/39c	%^{39}ArK	Total^{39}Ar	mol ^{39}Ar	Wmdata	WMs	wfactor	WxX
encap	-0.852	-0.357	0.357	0.12	99.99	230.52	7.55E-15	-0.85	0.36	7.85	-6.69
furnace	171.4	1.517	1.427	0.12	99.99		6.28E-15	171.40	1.43	0.49	84.15

Method	37d	method	39/40c	39/40err	36/40c	36/40err	R^2	T°(C)	36c	39c	40c
encap	9.32	encap	0.0078504	17.64088	0.003408	17.64151	0.675461	Vial	56.591867	125.829	15835.54744
furnace	9.75	furnace	0.0045648	0.854358	0.000589	0.557662	0.011428	1000	13.998633	104.671	22654.33388

Method	%36err	%39err	%40err	36err	40err	%36err	%40err	WtdAge39Ar
encap	0.15	0.02	0.14	0.085024	22.19604	0.150241	17.63984	-1.0721568
furnace	0.51	0.83	0.07	0.072734	15.90164	0.519577	0.070192	179.42152

TOTAL GAS AGE: 178.35 ± 0.6932 Ma

4 amu discrimination = 1.04870 ± 0.19%, 40/39K = 0.109 ± 12.16%, 36/37Ca = 0.000272 ± 14.63%, 39/37Ca = 0.000725 ± 8.32%

Note: Isotope values are reported in mV, as measured beam intensity at t_0 from regressions.

Table 3.2K. Argon isotope analysis of JER La Mesa Sample jA3.

Method	T (°C)	t (min.)	^{36}Ar	^{37}Ar	^{38}Ar	^{39}Ar	^{40}Ar	%^{40}Ar*	%^{39}Ar rlsd	Ca/K	40Ar*/39ArK
encap	Vial	6	38.64	2.02	8.12	48.42	10829.99	-0.4	48.4	0.87	-8.97
furnace	1000	12	48.05	9.26	12.17	245.11	72330.65	81.3	245.1	0.83	2425.36

Method	Age (Ma)	1s.d.	Analyt. Err	37/39c	%^{39}ArK	Total^{39}Ar	mol ^{39}Ar	Wmdata	WMs	wfactor	WxX
encap	-0.897	-1.29	1.293	0.38	99.97	293.53	2.91E-15	-0.90	1.29	0.60	-0.54
furnace	227.45	4.48	4.428	0.36	99.97		1.47E-14	227.45	4.43	0.05	11.60

Method	37d	method	39/40c	39/40err	36/40c	36/40err	R^2	T°(C)	36c	39c	40c
encap	9.32	encap	0.00442	0.631002	0.003398	0.571501	0.598077	Vial	38.55088	48.4063	10819.84622
furnace	9.73	furnace	0.0033538	0.577366	0.000632	0.568375	0.894114	1000	47.8645	245.045	72184.94001

Method	%36err	%39err	%40err	36err	40err	%36err	%40err	WtdAge39Ar
encap	0.31	0.41	0.44	0.119787	47.65207	0.310724	0.440414	-0.4343274
furnace	0.16	0.19	0.51	0.07688	368.8863	0.160621	0.511029	557.4904395

TOTAL GAS AGE: 557.06 ± 2.483 Ma

4 amu discrimination = 1.04870 ± 0.19%, 40/39K = 0.109 ± 12.16%, 36/37Ca = 0.000272 ± 14.63%, 39/37Ca = 0.000725 ± 8.32%

Note: Isotope values are reported in mV, as measured beam intensity at t_0 from regressions.

Table 3.2L. Argon isotope analysis of JER La Mesa Sample jB1.

Method	**T (°C)**	**t (min.)**	**^{36}Ar**	**^{37}Ar**	**^{38}Ar**	**^{39}Ar**	**^{40}Ar**	**%^{40}Ar***	**%^{39}Ar rlsd**	**Ca/K**	**40Ar*/39ArK**
encap	Vial	6	94.32	2.05	22.26	254.48	5948.572	0.8	254.5	0.18	8.99
furnace	1000	12	79.07	10.72	20.9	139.59	48254.43	54.4	139.6	2.12	1904.70

Method	**Age (Ma)**	**1s.d.**	**Analyt. Err**	**37/39c**	**%^{39}ArK**	**Total^{39}Ar**	**mol ^{39}Ar**	**Wmdata**	**WMs**	**wfactor**	**WxX**
encap	0.898	0.48	0.479	0.08	99.99	394.07	1.53E-14	0.90	0.48	4.36	3.91
furnace	180.98	2.35	2.285	0.92	99.93		8.38E-15	180.98	2.29	0.19	34.65

Method	**37d**	**method**	**39/40c**	**39/40err**	**36/40c**	**36/40err**	**R^2**	**T°(C)**	**36c**	**39c**	**40c**
encap	9.91	encap	0.0424953	0.421741	0.01519	0.453334	0.508967	Vial	94.243473	254.465	5916.02968
furnace	12.32	furnace	0.0028516	0.691424	0.001544	0.697068	0.906673	1000	78.833074	139.494	48209.89169

Method	**%36err**	**%39err**	**%40err**	**36err**	**40err**	**%36err**	**%40err**	**WtdAge39Ar**
encap	0.3	0.25	0.28	0.28296	16.65605	0.300244	0.281541	2.2852304
furnace	0.147	0.118	0.415	0.116291	200.2559	0.147516	0.415383	252.6271902

TOTAL GAS AGE: 254.9124 ± 0.9380 Ma

4 amu discrimination = 1.04870 ± 0.19%, 40/39K = 0.109 ± 12.16%, 36/37Ca = 0.000272 ± 14.63%, 39/37Ca = 0.000725 ± 8.32%

4 amu discrimination = 1.05877 ± 0.54% for furnace run

Note: Isotope values are reported in mV, as measured beam intensity at t_0 from regressions.

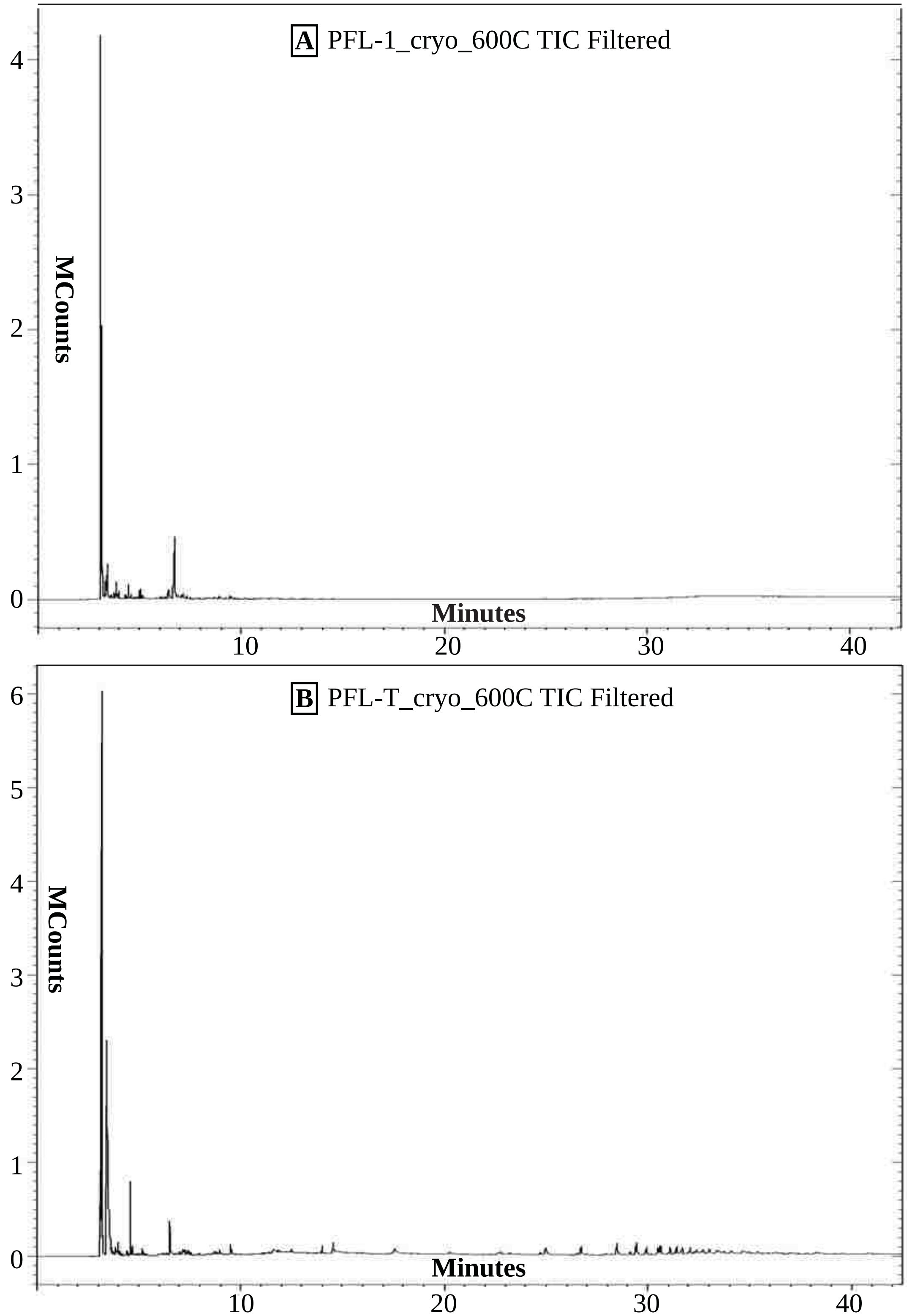

Figure 3.1. Bulk GC/MS chromatographs for the palygorskite reference standard (A) as received from the Source Clays Repository, and (B) following both NaOAc and Tiron treatments. Hydrocarbon signatures are present in both samples, but signatures differ and the relative peak counts are higher in the chemically-treated clays.

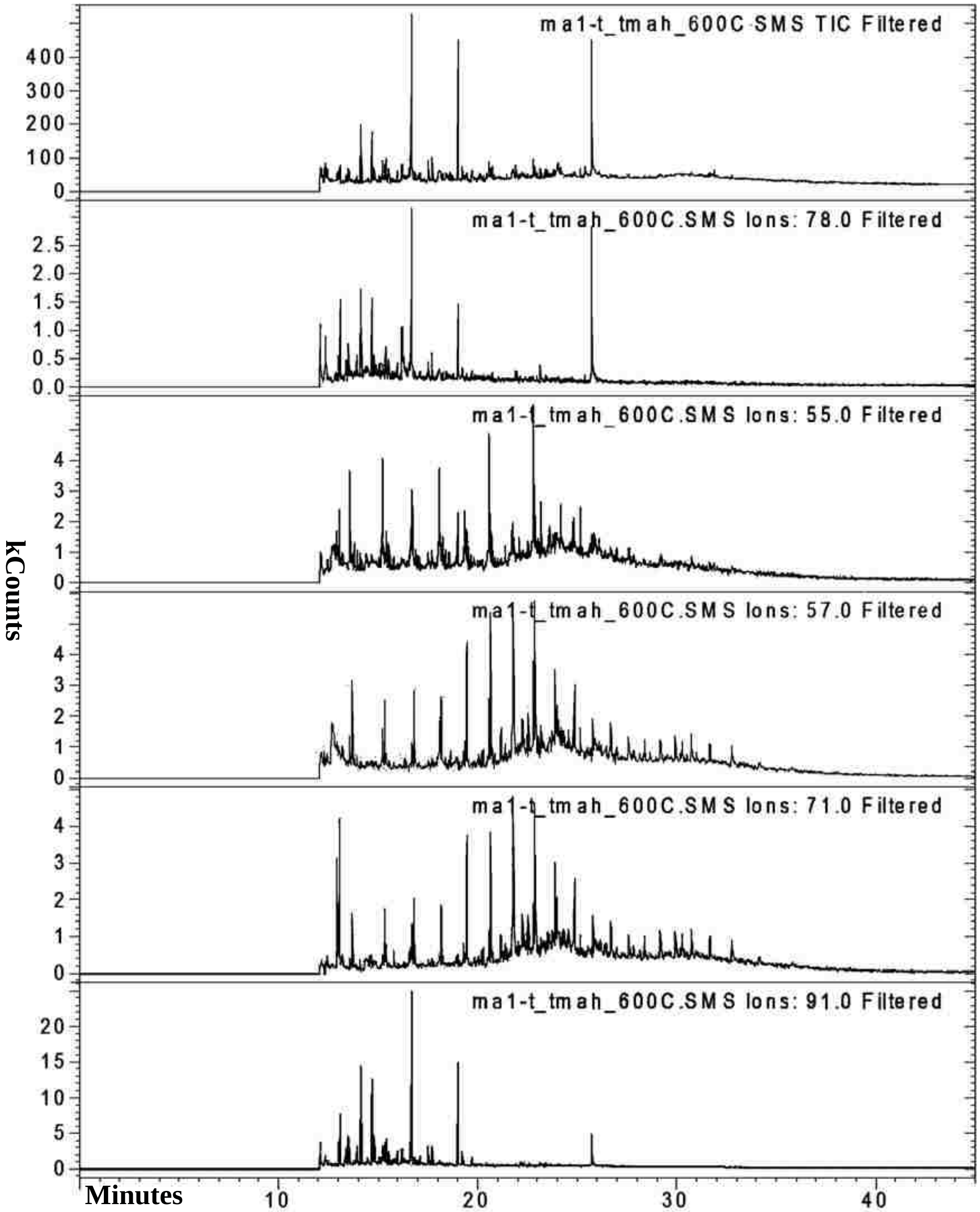

Figure 3.2. GC/MS spectra from Mormon Mesa geochronology sample mA1 (analyzed using tetra-methyl ammonium hydroxide). The plots reveal relative contributions to the bulk chromatograph (top) from ion masses 78, 55, 57, 71, and 91. These ranges are especially typical for GC/MS products of alkanes, alkenes, and some aromatic compounds. Strong peak intensities confirm the presence of organic contaminants, possibly including NaOAc and tiron, in the geochronology samples dated in this study.

CHAPTER 4

MICROMORPHOLOGY, CHEMISTRY AND PHYLLOSILICATE MINERALOGY OF THE MORMON MESA PETROCALCIC SOIL, NEVADA, USA: GENETIC IMPLICATIONS

Abstract

Study of calcic and petrocalcic soils can help constrain rates of soil development, climate change, and landscape evolution in arid regions, however, the dynamics of calcic soil genesis are not fully understood. For example, the relative crystallization timing of carbonates, phyllosilicates, and other pedogenic minerals has not been well constrained. Moreover, it is not known whether or to what extent individual mineral phases or morphological features within petrocalcic soils can act as closed systems during 10^2 to 10^6 years of fluctuating soil, climate, and landscape processes.

This study was designed: (1) to refine and to test conceptual models of pedogenic mineral crystallization throughout the evolution of the 4-5 Ma Mormon Mesa petrocalcic soil in southern Nevada, USA, and (2) to identify key implications of distinct soil mineralogical, chemical, and micromorphological characteristics for future isotopic dating of this ancient soil landform. X-ray diffraction (XRD) and scanning electron microscope (SEM) analyses were performed alongside bulk chemical analyses including soil pH, percent carbonate equivalence, gravimetric moisture content, EC, soluble sulfate content, and soluble chloride content. Contributions of eolian dust to the soil surface were expressed in the presence of detrital clays and distinct chemical properties in the surface soil horizon. No trends in the relative dominance of palygorskite or sepiolite were seen

with depth. However, soil chemical properties do reveal increasing chloride and EC values with depth, and highlight discontinuities above and below the massive horizon.

Results from this study suggest that fluctuations in soil solution chemistry have controlled the complex genetic relationships between pedogenic carbonate, palygorskite, sepiolite, amorphous silica, and barite in this petrocalcic soil. Conceptual models of sequential mineral crystallization cycles were developed to address both pluvial and interpluvial climates. These models help explain the development of key differences between horizons and also within specific micromorphological features such as pisolites or ooids. It is also suggested here that pisolites form from evaporating soil solutions held to soil microsites by surface tension, and not as a result of biological processes. Pedons, horizons, and individual crystals largely act as open systems, however, isolated micromorphological features or minerals may still exist. An important implication for isotopic dating is that pedogenic barite may have crystallized only during distinct climate episodes and in late-stage (stage IV-VI) petrocalcic horizons of Mormon Mesa, while palygorskite and sepiolite may have precipitated nearly continuously and in all horizons beginning as soon as stage II calcic horizon morphology was attained.

Introduction

Calcic and petrocalcic soil profiles are the product of intricately related processes operating on late Cenozoic landscapes at regional to microscopic scales. Especially key processes include: (1) atmospheric deposition of ions at the soil surface as eolian dust or dissolved in rainfall, (2) infiltration of dissolved ions in soil solution during and following precipitation events, (3) soil-sediment modification through force of crystallization dissolution of primary grains by the growth of pedogenic minerals, and (4) chemical feedbacks between mineral precipitation, soil solution chemistry, and evaporation. The relative importance of these processes may increase dramatically with time – for example, force of crystallization dissolution may be restricted to specific soil micro-environments or may not happen at all in young, calcic horizons. Perturbations which modify the rates, depths, thresholds, or occurrences of these calcic-soil forming processes include climate change, geological events (e.g., baselevel change), surficial processes (e.g., sedimentation, quiescence, or erosion), and biological activity (e.g., bioturbation, mineral fixation, evapotranspiration). Each of these processes should be considered across landform, pedon, horizon, and mineral (microscopic) scales.

Ultimately, the goal of most petrocalcic soil studies is to model the timing and rates of pedogenesis, climate change, and geomorphologic processes in arid environments. Such models can improve understanding of modern landscapes and lead to better land management. Research efforts can also employ calcic paleosols to partially reconstruct landscapes of the geologic past. Thus, pedogenic models for calcic and petrocalcic soils can be beneficial to soil scientists, geologists, geomorphologists, and paleoclimatologists. General concepts of calcic and petrocalcic soil formation, such as the four- or six-stage models of progressive morphogenesis (Gile et al., 1966; Bachman & Machette, 1977; Machette, 1985) have been developed for general application, and can yield crude, relative pedogenic age assessments. Such models must be modified to address specific formative events or factors on a case-by-case basis for individual calcic and petrocalcic soil localities (e.g., Alonso-Zarza et al., 1998; Brock & Buck, 2009) because different landscapes experience distinct pedogenic and geomorphologic histories. Pedogenic models must be rigorously tested against soil profile micromorphology, chemistry, and mineralogy, as well as to regional geologic and climate records (when available).

Arid soils, and especially petrocalcic profiles, are complex systems that fundamentally reflect the changing interaction of water and dissolved ions with the land surface over long time spans. Soil horizon components can either be isolated from or re-opened to soil solution flow by successive climate change, geomorphologic change, or pedogenesis. When modeling pedogenesis, it is important to account for even low permeability in late-stage petrocalcic horizons or other hardpans, because any influx of solute-rich pore water has the potential to refresh soil microsites with calcium and other dissolved ions, and to maintain portions of the soil as open, dynamic systems. Moreover, published research demonstrates that even highly indurated petrocalcic soil horizons can absorb and retain water in greater amounts than is generally recognized (Hennessy et al., 1983; Duniway et al., 2007), an especially important characteristic when considering soil-water interactions over 10^3 to 10^6 years.

Moisture transmissivity within calcic and petrocalcic soil horizons depends upon yet also influences horizon morphology and mineralogy. For example, massive petrocalcic horizons can transmit solution more readily than very thin laminar horizons (Duniway et al., 2007). This could be due to the presence of porosity-enhancing, authigenic hydrous phyllosilicates in the soil matrix (Brock, 2007), versus their absence in the nearly-pure silica or micritic calcite composition of laminar horizons (Duniway et al., 2007). Concentrations of authigenic phyllosilicates may be especially important sources of plant-available moisture (Francis, 2007) as well as solution mobility in calcic and petrocalcic horizons. Persistent zones of even limited moisture retention could lead to enhancement of soil solution networks over time, through preferential rooting or solution flow. Furthermore, structural fractures, root cracks, or bioturbation features in late-stage petrocalcic soils can quickly transmit soil moisture between horizons and across zones of distinct morphology (Hennessy et al., 1983; Duniway et al., 2007). At the profile scale, the geometry of these hydrological networks can change over 10^2 to 10^6 years in response to intrinsic (e.g., degree of induration) and extrinsic factors (e.g., climate). Long-standing fractures or permeable matrix zones may become completely filled by pedogenic carbonate or silica, restricting or otherwise redirecting soil solution flow. Alternatively, plugged horizons may episodically develop new dissolution features or fractures, as is likely for brecciated, stage VI petrocalcic horizons (Bachman & Machette, 1977; Brock & Buck, 2009).

Infiltration, retention, and diffusion of soil solutions through all morphological stages (I-VI) of calcic soils enables transmission of atmospherically deposited ions into the soil profile. Atmospheric deposition has been extensively cited as the dominant source of key elemental constituents of many soils worldwide, but especially in arid environments (Junge & Werby, 1958; Bachman & Machette, 1977; Hay & Wiggins, 1980; Watts, 1980; Gile et al., 1981; Reheis et al., 1989; Reheis & Kihl, 1995; Capo & Chadwick, 1999;

Chiquet et al., 1999; Naiman et al., 2000; Van der Hoven & Quade, 2002; Lintern et al., 2006; Graham et al., 2008). Ions deposited in eolian sediment or in rainfall include Ca^{2+}, Ba^{2+}, Mn^{4+}, Na^{+}, SO_4^{2-} and many other species. This influx fuels the crystallization and accumulation of pedogenic carbonate and other salts in the soil profile. Detrital, parent grains or rock fragments engulfed by pedogenic carbonate may eventually become altered or entirely replaced by calcite growth fueled largely by atmospheric inputs (Bachman & Machette, 1977; Brock, 2007). This degradation of parent grains is caused in part by the force of crystallization of pedogenic carbonate.

Force of crystallization (Weyl, 1959) acting in tandem with fluctuating soil solution chemistry describes a process which partially or entirely fractures, dissolves, and replaces engulfed primary grains and rock fragments in stage II carbonate pendants, stage III-VI petrocalcic soils, and some near-surface, alkaline diagenetic environments. Sometimes called pressure solution in soil science literature, this process has been previously described for calcic and petrocalcic environments (Bachman & Machette, 1977; Watts, 1978; Hay & Wiggins 1980; Watts 1980; Reheis, 1988; Monger & Daugherty, 1991a; Monger & Kelly, 2002; Brock & Buck, 2005) notably including Mormon Mesa, Nevada (Brock, 2007; Brock & Buck, 2009). Force of crystallization dissolution of primary grains occurs especially in microsites or already plugged horizons in which grain displacement is impossible. Dissolution is enabled during the (temporary) presence of a thin solution film, perhaps with very unique chemical characteristics, between the impinging calcite crystals and the primary grain or rock fragment (e.g., Steiger, 2005). Eventual evaporation of this film halts both calcite precipitation and dissolution of the primary grain until the next solution influx.

Dissolution of silicate grains during the force of crystallization process releases complexes of Si^{4+} (e.g. H_2SiO_4), Al^{3+} (e.g., Al_2OH_3), and other ions into the soil solution, moreover, the high pH of petrocalcic soil environments permits unusually high Si and Al activities as compared to other soils. Amorphous silica phases are especially soluble above pH 9 (Drees et al., 1989), however, some researchers report that silanol groups start to ionize at or above pH 7 (Yariv & Cross, 2002). Aluminum solubility is comparable to that of Si under highly alkaline conditions (Velde, 1992), and may especially increase above pH 8.5 (Hay & Wiggins, 1980). Other soil environmental factors, including common ion effects and the presence of organic matter, can also catalyze grain dissolution (Drees et al., 1989). Once released to solution, Si^{4+} and Al^{3+} complexes can directly fuel the precipitation of pedogenic palygorskite and sepiolite clays (Weaver & Beck, 1977; Watts, 1980; Verrecchia & Le Coustumer, 1996; Singer, 1989; Monger & Daugherty, 1991a&b; Singer et al., 1995).

Palygorskite, $Si_8Mg_5O_{20}(OH)_2(OH_2)_4{\bullet}2H_2O$ (Singer, 1984), and sepiolite, $Si_{12}Mg_8O_{30}(OH)_4(OH_2)_4{\bullet}8H_2O$ (Brauner & Preisinger, 1956; Singer, 1984; García-Romero et al., 2007) are fibrous, high-magnesium phyllosilicates that are relatively rare in terrestrial sediments, yet fairly typical of late-stage petrocalcic soils (Jones & Galan, 1988). In fact, both palygorskite and sepiolite can each comprise nearly 100 % of the non-carbonate clay-sized particle fraction of certain petrocalcic profiles (Watts, 1980; Jones & Galan, 1988; Francis et al., 2007). The predominance of these clays in calcic soils may also indicate that they eventually replace other, detrital phyllosilicate species such as smectite or illite. Precipitation of palygorskite and sepiolite may be especially favored in zones of textural contrast, whether along soil horizon contacts or within soil micropores (Yaalon & Wieder, 1976; Bouza et al., 2007). Fluctuating soil solution chemistry is vital for the genesis of palygorskite and sepiolite, as well as for the morphological development of petrocalcic soils.

Mineral genesis in calcic to petrocalcic horizons is the product of chemical feedbacks and thresholds operating across geological timescales and multiple climates. The cycle of multi-phase mineral genesis begins with the crystallization of pedogenic carbonate upon soil solution evaporation and/or Ca saturation. Eventually, calcite authigenesis leads to dissolution of primary silicate grains via the force of crystallization process. Calcite crystallization also changes the partial pressure of CO_2 and increases the activity of Mg^{2+} relative to Ca^{2+} (Watts, 1980; Reheis 1988; Deocampo, 2005). As stated above, the Si and Al ion complexes produced by silicate dissolution may combine with Mg^{2+}, OH^-, and other ions to generate fibrous phyllosilicates or, in Mg-poor solutions, amorphous silica (Weaver & Beck, 1977; Watts, 1980; Reheis, 1988; Singer, 1989; Monger & Daugherty, 1991a; Singer et al., 1995; Verrecchia & Le Coustumer, 1996). It is generally accepted that palygorskite forms at higher Al^{3+} activities, whereas sepiolite precipitates instead during low Al^{3+} conditions (Hay & Wiggins, 1980; Jones, 1983; Jones & Galan, 1988; Singer, 1989). However, intergrowths of the two clays may be possible and would reflect oscillating soil solution chemistry.

Similarly, amorphous silica may precipitate when there is insufficient Mg for sepiolite growth, when soil chemical thresholds (e.g., pH) are crossed, and/or when localized soil solutions have been reduced to a gel-like state by progressive evaporation and mineral growth (Hay & Wiggins, 1980). Silica spheroids have been found crystallized upon the tips of palygorskite and sepiolite fibers in petrocalcic soils (Brock,

2007) and in some alkaline diagenetic environments (Weaver & Beck, 1977). Thus, within each crystallization episode, amorphous silica commonly precipitates just before total solution evaporation, but after calcite and/or magnesian clay. Saline conditions or high contents of dissolved CO_2 may also influence silica and phyllosilicate precipitation (Watts, 1980; Jones & Galan, 1988; Deocampo, 2005). Completing the feedback cycle, crystallization of magnesian phyllosilicates decreases Mg^{2+} soil solution activity relative to Ca^{2+} (Weaver & Beck, 1977; Watts, 1980) and creates an environment conducive to renewed calcite growth and primary grain dissolution, given continued influx or reserves of soil solution, Ca^{2+}, and dissolved CO_2. It has also been suggested that palygorskite may adsorb Mg^{2+} preferentially over Ca^{2+}, further forcing conditions favorable to calcite crystallization (Weaver & Beck, 1977).

Naturally, ions of many other elements – including chloride, barium, iron, manganese, nitrate, potassium, sodium, and organic compounds – play crucial roles in soil solution chemistry and add additional complexity to the mineralogical evolution of arid soils. Climate changes and other external forces lead to distinct soil formative events and conditions between regions. Thus, mineralogical, chemical, and micromorphological properties must be evaluated as a whole before modeling pedogenesis for any given calcic soil locality. Important considerations include trends within individual horizons as well as trends with depth (i.e., between horizons). Mineralogical, chemical, and/or micromorphological characteristics can help identify external factors pivotal to both petrocalcic soil development as well as to broader landscape processes.

This study was designed to advance existing pedogenic models of horizon and profile development for the ~ 4-5 Ma petrocalcic soil of Mormon Mesa, Nevada (Brock, 2007;

Brock & Buck, 2009), and to facilitate interpretation of isotopic ages for distinct pedogenic mineral species forming within the profile. The chief objectives of this study were: (1) to refine and to test conceptual pedogenic models of sequential mineral crystallization at Mormon Mesa, and (2) to identify key implications of distinct soil mineralogical, chemical, and micromorphological characteristics for future isotopic dating of this ancient petrocalcic soil landform.

Site Selection

The ~ 4-5 Ma stage VI petrocalcic soil profile of Mormon Mesa, Nevada, is one of the oldest and best expressed, extant petrocalcic soil landscapes in the world. Petrocalcic horizons within the Mormon Mesa soil series have been described and studied previously by Gardner (1972), Soil Survey Staff (2006a), Brock (2007), and by Brock & Buck (2009), however, the extreme complexity of these profiles warrants further research. Mormon Mesa is also important because of its close links to the fluvial geomorphology, tectonic evolution, and paleoclimate of the Virgin River and, most significantly, the lower Colorado River basin. Initiation of pedogenesis on Mormon Mesa is considered synchronous with formation of the lower Colorado River system (House et al., 2005). The age of Mormon Mesa and, therefore, the maximum age of the petrocalcic horizon, has been bracketed to a date between 4.1 and 5.4 Ma by correlating regional stratigraphic and morphostratigraphic units to isotopically dated tuffs and basalts (Schmidt et al., 1996; Williams et al., 1997). This advanced age is consistent with the strongly-developed morphological stage of the soil. Profiles in this study were chosen to facilitate comparison of data from x-ray diffraction (XRD), soil chemical, and scanning electron microscopy with energy dispersive x-ray spectroscopy (SEM-EDS) analyses to previous studies of the genesis of the Mormon Mesa petrocalcic soil (Brock, 2007; Brock & Buck, 2009). Profiles were also selected to complement concurrent attempts to evaluate the viability of ^{40}Ar/^{39}Ar geochronology of pedogenic fibrous phyllosilicates in petrocalcic horizons (Robins, 2010 a&b).

Methods

Sampling

Four profiles were sampled at two roadside exposures of the Mormon Mesa petrocalcic soil near Mesquite, NV (Figure 4.1), in February, 2008. Three profiles spaced approximately five meters apart were chosen at the southernmost site, MM1, and one profile was sampled at the northernmost site, MM2 (Figure 4.2). Intact, oriented samples approximately 20 x 20 x 20 cm were collected from stage IV and higher petrocalcic horizons using a Wacker BTS 1035 diamond-bladed concrete-cutting saw. To minimize alteration of pedogenic salts, no water was applied to the saw blade during sampling. Unoriented samples of the less indurated, stage III calcic horizons were collected with a sedimentary rock hammer and stored in plastic bags. Because the surficial rubble horizon was roughly bimodal – containing one part eolian silts or sands, and another part large petrocalcic rock fragments – samples from the shallow, eolian-influenced surface horizon were collected with a shovel and then sieved into < 2 mm (fine) and > 2 mm (coarse) size fractions. The coarse fractions were then crushed to pass the 2 mm sieve, and were processed as separate samples from the fine fraction of the surface horizon. Portions of the soil surface immediately adjacent to all profiles at both sites showed signs of past disturbance by heavy construction equipment. While attempts were made to avoid the most disrupted areas, physical effects of machinery on the soil surface and surface samples (erosion, artificial brecciation, compaction, or mixing of surface and near-surface horizons, etc.) bear consideration in this study.

When permitted by the depth of profile exposures and by local horizon thicknesses, three samples spaced at 25-75 cm intervals were collected from each soil horizon. Samples were extensively processed for laboratory chemical and physical analysis. Samples were first fractured with a hammer as needed, then comminuted to 1-3 cm diameter fragments using a mechanical rock chipper, and then crushed to < 2 mm using a mechanical disk mill. Further grinding was conducted with a diamondite mortar and pestle as noted below for analyses requiring sample materials significantly finer than 2 mm.

XRD Analysis

Crushed samples were immersed in pH 5 sodium acetate buffer solution (NaOAc) for several months to digest carbonates (Jackson, 1965; Kunze & Dixon, 1986) and were then treated once with sodium hypochlorite to remove organic matter (Soukup et al., 2008). Next, the clay-sized particle fraction of the purified silicate sample was fractionated by centrifugation and pipetting (Soukup et al., 2008). Samples were then treated with citrate-dithionite buffer solution (Soukup et al., 2008) to remove any amorphous iron and aluminum oxides. After oven-drying, each sample was divided into separate aliquots for $MgCl_2$ and KCl saturation (Soukup et al., 2008). Mg- and K-saturated samples were then smeared onto standard glass thin-section slides that had been frosted by coarse-grit polishing for 30 seconds.

Following base-line XRD analysis of the samples at room-temperature, Mg-treated sample slides were saturated with ethylene glycol under vacuum at 50°C overnight. K-treated slides were heated to 350°C for two hours and then analyzed. After analysis, the K-treated slides were heated again for two hours at 550°C and re-scanned. All slides were analyzed within 1-8 hours of heating and/or ethylene glycol saturation. Reference clays from the Clay Minerals Society Source Clays Repository were also treated and analyzed alongside the clay-sized particle fractions from Mormon Mesa soil horizons. Reference clays analyzed included kaolinite KGa-1, montmorillonite Sca-2, palygorskite PFL-1, and sepiolite SEP-Sp1. All clay mineralogical analyses were conducted on a PANalytical X'pert Pro X-ray diffraction spectrometer at the UNLV XRF/XRD Laboratory. XRD analyses used Cu Kα radiation for continuous, 10 minute flat-stage scans from 3 to 40° 2θ, at 45 kV and 40 mA, and using 1/4° antiscatter and 1/8° divergence slits. In isolated cases where the 550°C heat treatment caused peeling or curling off of the glass slide, the 550°C samples were each re-mounted and scanned as flattened clay flakes on a standard spinner plate. XRD data were interpreted using XPert High Score Plus software. Detailed interpretations were also made by comparing data to published clay mineralogy and x-ray diffraction references (Dixon & Weed, 1989; Moore & Reynolds, 1997; Poppe et al., 2001), as well as to analytical results from the reference standards (see Appendix 4.1).

Chemical Analyses

Chemical analyses were conducted on bulk, crushed (< 2 mm) samples at the UNLV Environmental Soil Analytical Laboratory, except as noted. Measurements included soil pH, electrical conductivity, percent carbonate equivalence, soil moisture content, available sulfur content, and water-soluble chloride content. Sample pH was determined via the 1:1 water pH method (4C1a2a1) of Burt (2004) using a Thermo Electron Corporation Orion 720A+ Advanced ISE/pH/mV/ORP meter and an Orion Ross Ultra combination pH electrode (Appendix 4.2). Electrical conductivity was determined following method 4F1 of Burt (2004) on a Fisher Scientific Accumet BASIC AB30 conductivity meter. Soil carbonate percent equivalence was determined using a titration method on finely ground sample material (Pansu & Gautheyrou, 2006), and air-dry/oven-dry water retention (soil moisture) was determined gravimetrically following method 3D1 of Burt (2004). Sulfate-S (available sulfur) and water-soluble chloride were analyzed by Utah State University Analytical Laboratories in Logan, Utah.

Micromorphological Analysis

Thick sections for SEM-EDS analyses were made from intact, oriented samples of the massive horizon and the transitional horizon, to characterize soil micromorphology and to assist interpretation of mineralogical and chemical data. Sixteen glass-mounted thick-sections were polished to 1200 grit, etched with 10% hydrochloric acid for 10 seconds, air-dried, and sputter coated with gold for 75 seconds. All samples were analyzed in the UNLV Electron Microanalysis and Imaging Laboratory (EMIL) with a JEOL JSM 5600 scanning electron microscope equipped with an Oxford electron dispersive X-ray spectrometer (EDS). EDS data processing software was upgraded midway through this project. Consequently, some samples were processed with ISIS software, whereas others were processed using INCA software.

Results

Profile Morphology

Within all four profiles studied, five horizons were distinguished based on their carbonate morphology, structure, and other characteristics (Figures 4.2 & 4.3). Profiles at both sites sampled in this study closely matched descriptions by Brock (2007) and Brock & Buck (2009) (Figure 4.3), and site MM1 profiles are located at or adjacent to the Riverside profile of Brock (2007), along the eastern edge of Mormon Mesa (Figure 4.1). The five horizons identified in this study are, from top to bottom: (1) a partly eroded, surface horizon of eolian sediments and petrocalcic rubble, (2) a brecciated stage VI petrocalcic horizon, (3) a stage VI massive petrocalcic horizon, (4) a stage III transitional calcic-to-petrocalcic horizon, and (5) a stage II-III calcic paleosol in the upper Muddy Creek sediments (Brock, 2007). The informal horizon nomenclature of previous studies (e.g., Brock, 2007; Brock & Buck, 2009) is used in lieu of traditional USDA soil taxonomic horizon nomenclature (Soil Survey Staff, 2006b), because in the USDA system, all sampled horizons classify as either a "Bk" (stage II-III calcic horizons) or "Bkm" (stage III-VI, indurated, petrocalcic horizons).

Surface horizons described elsewhere on Mormon Mesa by Soil Survey Staff (2006a) have, at both site MM1 and site MM2, been partly mixed and/or removed by heavy machinery, resulting in the anthropogenic "rubble" horizon described above. However, the soil geomorphologic surface ~5 m beyond the disturbed areas at MM1 consists of a gravelly silty sand "A" horizon composed chiefly of red, eolian sediment and 10-20% petrocalcic rock fragments (gravel, cobbles, and stones) (Figure 4.2 C), much as described by Soil Survey Staff (2006a) for the rest of Mormon Mesa. At the study profiles, however, there is no "A" horizon; the surface "rubble" (Figure 4.2 A) was 10-40 cm thick and graded downward across a diffuse smooth contact into the brecciated, stage VI petrocalcic ("Bkm") horizon comprised entirely of carbonate-cemented, very coarse angular to very thick platy soil blocks. Based on visual estimates, the < 2 mm (fine) particle size content of the surface horizon was 20-50 %, however, in the brecciated horizon this < 2 mm fraction dropped well below 20 %.

Below a clear, wavy contact with the brecciated horizon, the stage VI, massive ("Bkm") horizon consists of extremely large (10-100 cm diameter) subangular, massively indurated petrocalcic blocks. These blocks often exhibit 1-3 cm thick laminar layers, both internally, and also along their vertical and horizontal surfaces. The massive horizon also contains variable amounts of pisoliths (carbonate clast pendants which have been engulfed by younger, matrix carbonate) and pisolites (concentric pedogenic concretions, or large ooids), with some blocks consisting almost entirely of cemented pisolith structures (Figure 4.2 D), and other blocks lacking them entirely. Below a clear, wavy contact with the massive horizon, the stage III "transitional" horizon of Brock (2007) and Brock & Buck (2009) was present in all MM1 profiles, but was mostly covered at profile MM2. This friable horizon of medium to coarse subangular blocky aggregates is underlain by a clear wavy contact with a stage II, buried soil horizon in the upper Muddy Creek formation. This buried horizon, referred to here as the paleosol in the upper Muddy Creek sediments, contains common carbonate nodules and carbonate-filled root traces and constitutes the basal horizon in this study. Exposure of the paleosol occurred only in profiles MM1-A and MM1-B.

Phyllosilicate Mineralogy

Results from XRD analysis of the clay-sized particle fraction from the Mormon Mesa soil samples reveal variable phyllosilicate compositions both with depth below the soil surface (i.e., between horizons) and also between profiles (Figures 4.4 -4.7). In general, the fine (< 2 mm) fraction of the surface soil horizon was found to contain varying amounts of palygorskite, sepiolite, kaolinite, illite, smectite and/or smectite-chlorite, and quartz. Variable low-magnesium calcite and/or calcite persisted in most samples despite the NaOAc pre-treatment. Barite was also identified as a match for peaks in five samples (6, 20, 21, 32, and 34) from the upper massive horizon in all three MM1 profiles (Appendix 4.1). Palygorskite and/or sepiolite were found to dominate the phyllosilicate mineral fraction of all subsurface horizons and also the indurated fraction of the surface rubble, however, variable amounts of illite were also identified in some samples from the brecciated horizon.

Reference standards of palygorskite (Figure 4.8), sepiolite (Figure 4.9), kaolinite (Appendix 4.1), and montmorillonite (Appendix 4.1) were analyzed to assist with the identification of the Mormon Mesa phyllosilicates, and also to confirm the effects of saturation and heat treatments on mineral diffraction peaks. Mineralogical constituents of each sample and standard were determined by carefully comparing effects among all treatments (e.g., Figures 4.10 & 4.11). XRD spectra of Mormon Mesa samples dominated by palygorskite and/or sepiolite were found to closely resemble the Clay Minerals Society palygorskite and sepiolite patterns. However, none of the samples exhibited a monomineralic phyllosilicate composition, and no clear trends could be identified to describe nor to predict the relative predominance of palygorskite versus sepiolite with depth (by horizon). Data for all samples and standards are presented in Appendix 4.1.

Soil Chemistry & Statistics

Soil chemical properties of the Mormon Mesa petrocalcic profiles are summarized by genetic horizon in Table 3.1, and complete chemical data are reported in Appendix 4.3. Key observations from each analysis, including soil pH, percent carbonate equivalence, air-dry moisture content, electrical conductivity, available sulfur content, and chloride content, are plotted as averaged values for each genetic horizon (Figures 4.12 & 4.13) and also as individual profiles (Figures 4.14 - 4.21). Soil pH was found to range between 8.28 and 9.40 with an average value of 8.90 (n = 47 samples). Soil pH was relatively variable within each horizon and between profiles, but was generally lowest for the < 2 mm fraction of the surface horizon and for the paleosol in the upper Muddy Creek sediments. Percent carbonate equivalence, a proxy for the degree of soil induration by pedogenic carbonate, was relatively similar across all horizons and between all profiles except for the uncemented surface horizon and the stage II paleosol in the upper Muddy Creek sediments (Figure 4.12). The mean carbonate value for all samples (n = 47) was 68.25%, with a minimum of 14.53% in the < 2 mm surface material, and a maximum of 87.25 % in the massive horizon. The air-dry moisture content of the samples paralleled their relative degree of induration, with an average value of 1.08%, a minimum value of 0.29% in the massive horizon, and a maximum value of 3.69% in the uncemented < 2 mm surface material. Electrical conductivity ranged between 66.70 μS and 4,145 μS, with an average value of 463.5 μS for all samples. Conductivity values for all profiles generally increased with depth below the soil surface, reaching a noticeably higher average in the transitional horizon (Table 4.1; Figure 4.13). Sulfate and water soluble chloride contents were variable within each horizon, but increased overall with depth below the soil surface. Maximum sulfate contents were noted for the paleosol in the upper Muddy Creek sediments, but were also high in the massive horizon. Chloride values peaked near the lower contact of the transitional horizon. Sulfate values ranged between 2.83 and 259.31 mg/kg, with an overall average (n = 45) of 60.34 mg/kg. Chloride values ranged between 2.14 and 12,469.51 mg/kg, with an average (n = 45) of 896.79 mg/kg.

Correlations tested via linear and non-linear regression models were sought between data sets (i.e., $CaCO_3$ versus Cl^-), however, the results were generally variable between profiles and frequently produced very low regression coefficients ($R^2 < 0.1$) whether within each individual profile's data, or between two or more profiles. Better correlations ($R^2 = 0.7$ or higher) were noted between moisture content and carbonate content, because both of these variables reflect the degree of soil cementation. Qualitative trends may be interpreted from plots of each soil chemical property with depth below the soil surface, either by plotting mean horizon values for all profiles combined (Figures 4.12 & 4.13), or by plotting and comparing data between individual profiles (Figures 4.14 - 4.21).

Soil Micromorphology

Image and elemental composition data from SEM-EDS analyses reveal complex and diverse relationships between several distinct mineralogical and morphological constituents in the massive and transitional horizons. Mineralogical constituents include detrital quartz grains and pedogenic carbonate, clay minerals, silica, and barite. Morphological features include varying amounts and arrangements of these minerals in pisolites, laminae, pore fillings, *Microcodium*, and mineral dissolution/replacement features. Key aspects of these mineralogical and morphological elements are described here.

Detrital, primary minerals seen in the SEM images consist predominantly of subrounded to subangular, equant to oblate (100 - 500 μm diameter) silt- to fine sand-sized quartz grains that float in a groundmass of calcium carbonate or calcium carbonate and fibrous silicate clay. This well-documented morphology has been called "K-fabric" by other researchers (Gile et al., 1965; Reheis, 1988). Due to their clear edges and morphological relationships to other mineral phases, these grains are among the most immediately obvious features visible in the SEM at low magnification despite their low color contrast in backscatter mode (Figure 4.22 A). All of the grains seen have clear, well-defined edges, however, many of the grains are embayed, pitted, and/or fractured (Figure 4.22 B-F). Although most of the detrital grains are quartz, fragments of granite, limestone, and other rock types occur in many samples. These rock types supply occasional feldspar and iron-oxide mineral grains to the soil matrix. These minerals can be differentiated from quartz grains in SEM images based on their cleavage planes or crystal habit, color contrast in backscatter mode, and EDS spectra. Iron oxide grains especially are visible at low magnification as stark white, smooth grains with sharp edges in backscattered electron images (Figure 4.23 A). Limestone fragments or detrital calcite crystals differ morphologically only in terms of their extensive, internal expression of calcite cleavage and far more diffuse grain boundaries with pedogenic carbonate and fibrous silicate clay (Figure 4.23 B). Finally, floating grains within the petrocalcic groundmass may also consist of detrital phyllosilicates: one very fine sand-sized grain consisting of a well-rounded, smectite-textured phyllosilicate aggregate with smooth, sharp edges was also identified in one sample (Figure 4.23 C). Rarely, weathered grains with partial phyllosilicate replacement rinds or cores were also seen. Aggregates of non-authigenic minerals can also be found as clay-sized to fine-sand sized silicates filling pore spaces in some samples (Figure 4.23 D). More common accessory mineral phases with significantly smaller dimensions than the quartz silt grains are pedogenic in origin and include fibrous phyllosilicates, amorphous silica, and barite.

Fibrous phyllosilicates inferred to be palygorskite and/or sepiolite are a prominent mineral constituent in most of the petrocalcic thick sections studied. The mineralogy of these magnesian clays is inferred based on XRD analyses, their morphology in SEM images, and their previous identification in petrocalcic soils. However, it is not possible to differentiate the two minerals using SEM-EDS data alone. In secondary electron images at low to intermediate magnification, both palygorskite and sepiolite fibers stand out as a jagged, pale, high relief texture among the groundmass of grey, finely subhedral calcium carbonate and floating, primary mineral grains (Figure 4.23 E). Individual fibers are typically 2 to 10 μm in length and < 0.25 μm in diameter, and are usually not discernable at less than 5,000 to 10,000 times magnification (Figure 4.23 F). Although their small crystal dimensions normally preclude EDS spectra free from contribution by surrounding minerals, palygorskite and sepiolite are characterized by distinct elemental peaks of Si, Mg, O, variable Al (Figure 4.24 A), and occasionally minor Fe, K, or other elements.

Although the morphology of individual palygorskite and sepiolite crystallites is relatively constant, their aggregate morphology was found to vary in relation to the other mineral phases. Fibrous phyllosilicates were found as (1) intricately interwoven skeletal mats throughout the carbonate-impregnated soil matrix (Figure 4.24 B), (2) delicate, individual fibers or bundles of fibers radiating outwards from the edges of quartz grains (Figure 4.24 C), (3) well-defined rings or halos (crusts, in 3D) surrounding and closely paralleling detrital grain edges or carbonate-filled pore boundaries (Figure 4.24 D), (4) porous and apparently sub-spherical aggregates intergrown with calcium carbonate (Figure 4.24 E), and (5) individual whiskers or small bundles of fibers welded to or growing outwards from the surfaces of pedogenic carbonate crystallites (Figure 4.24 F). Palygorskite and sepiolite are almost ubiquitous in the studied samples; they can be identified at high magnification within almost any morphological expression of pedogenic carbonate.

Besides the fibrous clays, pedogenic silica and barite also occur within the Mormon Mesa petrocalcic horizon, however, in lesser quantities. In the petrocalcic samples studied here, amorphous silica occurs exclusively as common, extremely thin (< 2 μm), smooth coats (silans) on silicate grain or rock fragment surfaces (Figure 4.25 A&B). Barite occurs as subhedral to anhedral masses filling pore spaces among fibrous phyllosilicates and calcite, and stands out in bright contrast from these and other mineral phases in backscattered electron images at intermediate to high magnification. EDS spectra collected on these crystals (Figure 4.25 C) exhibit clear peaks of Ba, S, and O, and serve to differentiate barite from other minerals in SEM. Most barite masses seen in the petrocalcic horizon are oblong and 10 to 40 μm in diameter, consisting of aggregates of subhedral, disoriented crystallites each approximately 2 μm by 5 μm in size (Figure

4.25 D). However, barite masses of up to 200 µm in length also occur along porous, subhorizontal carbonate laminae in the massive horizon.

Unsurprisingly, pedogenic carbonate comprises the most abundant mineral constituent of the samples and occurs in a wide variety of crystal habits and morphological features. EDS spectra consistently revealed strong peaks of Ca, C, and O. Instances of low-magnesium calcite are also likely, but Mg peaks could not be definitively ascribed to carbonate phases due to the close physical association of calcite with palygorskite and sepiolite, which impart their own Mg peaks to the EDS data. No Mg was detected in the absence of Si in any EDS analyses. Crystallite shapes of pedogenic carbonate include rhombohedra, blades, prisms, needles, and also irregular habits. Individual carbonate crystallites vary in their angularity and degree of crystallinity. In the soil matrix and laminae, pedogenic carbonate is mostly angular to subangular, with smooth edges and irregular shapes that vary from equant to triaxial. This overall morphology does not differ in the presence of fibrous clays or barite. Carbonate crystal diameters are most commonly 2-10 µm, especially within the indurated matrix, however, morphologies in some of the most indurated samples reached 100 µm or more across their longest axis.

Morphological expressions of pedogenic carbonate vary widely within the Mormon Mesa petrocalcic horizons. Apart from the relatively small, irregular carbonate crystals found throughout the soil matrix and laminae, large, concentrically zoned, subhedral to anhedral growth features were also seen in the most extremely indurated samples (Figure 4.25 E&F). These features typically contain ~0.5 to 5.0 µm pores throughout, with each growth ring ranging between 5 and 20 µm in width, and each crystal impinging tightly upon similarly zoned crystals in the surrounding groundmass. These carbonate features can also include internal rings of relatively pure palygorskite or sepiolite. Zoned calcite in Mormon Mesa can be found adjacent to radiating, prismatic calcite crystals more than 250 µm in length. Additional crystal morphologies expressed in the massive and transitional horizons include the ~50 to 100 µm euhedral carbonate rhombohedra in soil pore spaces (Figure 4.26 A), and numerous features of possible biological origin. The latter include rod-shaped casts of roots or fungal filaments (Figure 4.26 B), and bladed, platy, or prismatic crystals in *Microcodium* (Figure 4.26 C&D). Pedogenic carbonate was also found as a completely impregnated matrix consisting of interlocking, 100-µm-diameter nuclei of radiating, subangular blades or lobes (Figure 4.26 E&F). In three dimensions, these features might resemble starbursts in form.

Importantly, prominent micro- to macro-morphological features are identified that incorporate most, if not all, of the above mineral phases in the petrocalcic horizons. These features include clast pendants, pisolites/ooids, laminae, and filled fractures. Pendants may occur on all mineral grains or rock fragments from the micro- to the macro-scale, and are also found on indurated petrocalcic soil matrix or carbonate laminae fragments within the sample. Multiple generations of pendants are present, each having a different vertical orientation. Pisoliths (stalactitic successions of stacked pendants) are prominent in the soil profile and in the bulk soil samples, but are not apparent in any of the prepared thick sections in this study. Concentrically zoned, apparently spherical features are prominent in almost all samples, range in diameter from a few millimeters to a centimeter or more, and are called pisolites (Hay & Wiggins, 1980). Pellets and ooids, as defined by previous researchers, are similar to pisolites but are less than 2 mm in diameter (Bachman & Machette, 1977; Hay and Wiggins, 1980). Pedogenic ooids consist of concentric, circular coatings of calcium carbonate around a detrital grain nucleus, while pellets are similar but entirely lack detrital grains within their nuclei (Hay & Wiggins, 1980). All three features have been identified in this study (Figure 4.27 A&B), and are especially prevalent within, underlying, and overlying zones of laminar calcite.

Laminar features and fractures are present in most of the thick sections (Figure 4.27 C-F) and are also visible within or coating 10- to 100-cm diameter blocks of petrocalcic soil. Calcite laminae vary in thickness from a few millimeters to more than a centimeter. These undulatory features are mostly subhorizontal in orientation, however, some laminae were found oriented up to 90° from horizontal. Some of these laminae may have been rotated away from horizontal during erosion-recementation cycles, but others have formed vertically. Similarly, some horizontal laminae may have been completely overturned (rotated 180°), however, it was not possible to distinguish *in situ* from overturned laminae in thick section analyses. Fragments of laminae were also found serving as the host clasts for rotated carbonate pendants (Figure 4.27 E&F). All samples exhibit fractures to varying degrees, and at all orientations. Fractures range in width from several micrometers to several centimeters, and their length also varies. Thus, both microscopic and macroscopic fractures cross-cut indurated matrix sections, carbonate laminae, and other features, and many fractures have been filled by calcium carbonate.

Interpretation and Discussion

Four major processes, namely: (1) illuviation of dust and ions with infiltrating rainfall, (2) force of crystallization dissolution by carbonate, (3) mineral precipitation in response to dynamic chemical thresholds and feedbacks, and (4) episodic modification of soil solution networks, have driven the mineral genesis and morphological development of the Mormon Mesa petrocalcic soil. These processes have fluctuated in response to millions of years of climate oscillations. Each distinct pedogenic mineral phase thus represents a subset of brief, but recurring chemical conditions crucial to soil profile development. Similarly, each distinct class or suite of morphological features is a product of a specific suite of processes driving broad-scale pedogenesis at Mormon Mesa.

By conceptually linking the four processes described above to one another, and by placing them within the context of climate change and landscape evolution, generalized models of mineral genesis can be developed for the Mormon Mesa petrocalcic soil profile. These models identify genetic relationships between pedogenic carbonate, phyllosilicates, silica, and barite, and supplement the landscape model of Brock & Buck (2009). Based on data from this study, it is also possible to construct a non-biogenic origin for pisolites and pedogenic ooids in calcic to petrocalcic soils.

Mineral Genesis Models

The first, generalized model of mineral genesis in the petrocalcic horizons of Mormon Mesa is presented in Figure 4.28, and is a compilation of previous solution chemistry, mineral genesis, and calcic soil research outlined in the introduction of this paper (Gile et al., 1965; Gile et al., 1966; Bachman & Machette, 1977; Weaver & Beck, 1977; Watts, 1978; Watts, 1980; Hay & Wiggins, 1980; Gile et al., 1981; Jones, 1983; Jones & Galan, 1988; Reheis, 1988; Drees et al., 1989; Singer, 1989; Monger & Daugherty, 1991a&b; Velde, 1992; Singer et al., 1995; Verrecchia & Le Coustumer, 1996; Monger & Kelly, 2002; Yariv & Cross, 2002; Brock & Buck, 2005; Deocampo, 2005), as well as corroborative data from this study. In this model, atmospheric deposition at the soil surface, infiltration of groundwater to the soil profile, force of crystallization by carbonate, and chemical feedbacks (especially related to Ca^{2+} and Mg^{2+}), all play critical roles in the mineralogy and morphology of calcic and petrocalcic soils.

A second, extended model of mineral genesis is presented in Figure 4.29. This model extends the explanation of mineral genesis to not only address the precipitation of pedogenic barite in the Mormon Mesa soil, but also to illustrate probable differences in soil processes between pluvial and interpluvial climates. In particular, soluble salts are likely to have played an important role in soil solution chemistry especially during the drier, more arid interpluvial episodes, when deposition on Mormon Mesa of dust eroded from upwind playas was likely to have been significant (Reheis, 1995). During wetter climate episodes, or more deeply infiltrating rain events, these salts could have been flushed from the upper petrocalcic horizons and into the less-indurated transitional horizon or Muddy Creek sediments. Together, these two models depict some of the most critical processes of pedogenesis in the Mormon Mesa petrocalcic soil, and can add further detail to existing models of soil profile development at Mormon Mesa (e.g., Brock & Buck 2009).

Support for the Generalized Model

Evidence for the generalized mineral genesis model in Figure 4.28 comes from (1) morphological observations, (2) phyllosilicate XRD data, and (3) soil chemical data. Micromorphological data in this study indicate that the occurrences of authigenic minerals in Mormon Mesa closely reflect the distribution, movement, evaporation, and changing chemical composition of soil solutions. In turn, soil solution chemistry fluctuates in response to influxes of dissolved ions from rainfall, and to the growth of pedogenic carbonate and concurrent force-of-crystallization dissolution of primary grains. Micromorphological evidence for the dissolution of quartz grains includes embayed grain edges, fractured grains, and partial replacement features, however, not all grain alteration is pedogenic in origin. Pitting of quartz grains can occur as a result of grain-to-grain impact during eolian or fluvial transport, or may result from lattice defects during crystal growth. Nevertheless, SEM data reveal that even pits that might have formed non-pedogenically (Figure 4.22D) do become impregnated by pedogenic minerals, and may become weak points that permit cracking or dissolution by force of crystallization, chemical attack, or other soil processes.

Important phyllosilicate XRD data observations that support the general model of mineral genesis include high variability of palygorskite and sepiolite predominance from sample to sample, and mineralogical distinctions between the surface rubble horizon and the rest of the profile. Bulk powder XRD analyses of Mormon Mesa soil samples, including identification of calcite and low-magnesium calcite have been conducted by Brock (2007) and more tentatively by Robins (2010a). These data are important to the genetic interpretations made in this study, because the occurrence of low-magnesium calcite indicates high Mg^{2+} activities in the soil solution. Conversely, clay-sized quartz and carbonate signatures in XRD analyses of the clay-sized particle fraction do not greatly contribute to interpretations in this study, for the following reasons. Clay-sized quartz is a near-ubiquitous soil constituent, and in Mormon Mesa profiles may result from grain-to-grain collisions during eolian and fluvial transport, as well as from chemical and physical weathering of sediments within the soil profile (see Figure 4.22 E-F). Clay-sized quartz contributions to the samples could also have been artificially increased by frequent stirring of samples during laboratory pre-treatments. Similarly, clay-sized calcite and (in lesser quantities) low-magnesium calcite comprise such a large percentage of the total mineral composition of petrocalcic soil that their persistence through lengthy, bulk sample NaOAC treatment is unsurprising, but also not representative of the original carbonate content of the samples. Clay-sized carbonate peaks were especially noted in the highly-indurated samples, when NaOAc pretreatments were run for as long as time constraints permitted (~4-6 months), but not to completion. Minor contributions from limestone rock fragments are also possible.

Phyllosilicate XRD data from the surface horizon provide critical insights into the genesis of the Mormon Mesa soil. Results indicate that the fine fraction of the surface horizon contains variable proportions of palygorskite and/or sepiolite, kaolinite, illite, quartz, and minor smectite. This assemblage is interpreted as a mixture of detrital (quartz, kaolinite, illite, and smectite) and authigenic (palygorskite and sepiolite) minerals. The detrital assemblage is consistent with episodic aeolian deposition on Mormon Mesa. The presence of palygorskite and sepiolite is interpreted as a contribution of eroded petrocalcic horizon fragments to the loose, sieved, < 2 mm particle size fraction of the surface horizon. Some fibrous clays could have been deposited in eolian dust, however, this origin seems less probable than a petrocalcic fragment source for several reasons. First, the extremely delicate, finely-crystalline, fibrous crystallites of palygorskite and sepiolite might not physically survive transport as well as illite, kaolinite, or smectite. Although wind abrasion could produce small fragments of the fibrous clays which could travel large distances, XRD patterns of these more randomly oriented crystallite fragments in oriented slides might produce broader, more diffuse peaks as compared to the more uniform diffraction spacings of long, undamaged, and better-aligned fibrous crystallites. Moreover, the coarse fraction of the surface rubble (fragments or clasts > 2mm in diameter) are dominated by palygorskite and/or sepiolite. Sand-sized or smaller fragments of indurated carbonate are visible in hand sample and may act as a source of fibrous clays to the unconsolidated, fine (< 2mm) fraction of the surface horizon.

Phyllosilicates from the brecciated horizon downwards consisted almost entirely of palygorskite and/or sepiolite, with occasional barite, and trace amounts of chlorite or illite group minerals. Brock (2007) suggested that sepiolite dominates in the deepest portion of the Mormon Mesa soil profile, especially within the transitional horizon and the paleosol in the upper Muddy Creek sediments. Such a trend would raise interesting questions regarding either (1) illuviation of soil solutions into the transitional zone, or (2) greater physical and genetic discontinuity between the upper and lower portions of the Mormon Mesa soil profile. However, this study demonstrates that palygorskite was present, even dominant, in many transitional horizon samples. In fact, the chief conclusion to draw from XRD data profiles (Figures 4.4-4.7) in this study is that palygorskite and sepiolite in bulk samples do not vary predictably with depth, neither between horizons nor between profiles. Thus, it can be inferred from XRD data that the two clays form in relatively close physical proximity in response to localized changes in soil solution chemistry. This interpretation lends support to the chemical-feedback model of mineral genesis in Figure 4.28.

Zones characterized by episodic hydrologic saturation and rapid evaporation, such as grain-to-matrix contacts, horizon boundaries, and soil pore spaces, are thought to be especially favorable for the genesis of palygorskite and sepiolite (Yaalon & Wieder, 1976; Singer, 1989; Verrecchia & Le Coustumer, 1996). Mats of palygorskite or sepiolite fibers were seen closely paralleling silicate grain boundaries, even at right angles (Figure 4.24 D). SEM images also reveal individual phyllosilicate fibers radiating outwards from grain edges, which might lend support to models of crystal growth from thin, evaporating solution films that can favor fibrous or acicular crystals (Zehnder & Arnold, 1989). More broadly, skeletal matrices of palygorskite and/or sepiolite in Mormon Mesa are especially dense above carbonate laminae (Figure 4.27 C), which may function as aquitards or aquicludes in the petrocalcic soil (Duniway et al., 2007).

The presence of kaolinite, illite, and smectite-group minerals in the surficial sediments, and their near absence from the indurated and subsurface soil samples, is an important topic for discussion. The simplest explanation is that most of the non-fibrous, detrital phyllosilicates dissolved in the highly alkaline petrocalcic soil environment, and that their constituents either recrystallized as palygorskite or leached out of the soil profile. Alteration of precursor phyllosilicates – especially smectite – to palygorskite, and vice versa, has been discussed at length in the scientific literature (Weaver & Beck,1977; Jones, 1983; Jones & Galan, 1988; Singer, 1989; and others). Although no consensus exists as to the precise chemical conditions required for this conversion, published evidence for dissolution-recrystallization transformations is strong. Hillier & Pharande (2008) offer convincing TEM and XRD evidence for the alteration of smectite to Fe-rich palygorskite in response to soil chemical changes induced by irrigation practices in saline-sodic soils. As mentioned above, saline conditions and soil microenvironments prone to episodic saturation are conducive to palygorskite genesis (Watts, 1980; Jones & Galan, 1988). Interestingly, Hillier & Pharande (2008) cautiously suggest that the process can happen rapidly, within 40-50 years of a change in environmental regime. Given the repeated episodes of climate change, erosion, and partial burial by eolian sediments experienced by Mormon Mesa over the last four to five million years, it is probable that detrital phyllosilicates were unstable at the high pH values, dissolved into their elemental constituents, and then re-precipitated as palygorskite or sepiolite, depending on solution chemistry. Krekeler et al. (2005) also note that palygorskite-smectite intergrowths can form as original solution precipitates. These alteration episodes likely occurred frequently or near-continuously, over the extensive geological history of Mormon Mesa, and are reflected in the general crystallization mechanisms postulated in Figure 4.28.

At least one aggregate of smectitic clay was found persisting within the massive horizon of Mormon Mesa (Figure 4.23 C), and trace amounts of illite, smectite, or smectite-chlorite do appear in the XRD data for some subsurface samples (Appendix 4.1). Along with other surficial sediments or unconsolidated soil particles, detrital clays may have been introduced into vertical fractures which periodically formed in the petrocalcic horizons, and could then have been incorporated into the horizon by carbonate induration. Additional clays may have persisted within rare, embayed, diagenetically-weathered silicates seen via SEM-EDS (Appendix 4.1). Therefore, not all detrital clays have dissolved. The smectite aggregate may indicate stability of non-fibrous phyllosilicates within certain microenvironments or when having a certain morphology. For example, its abrupt edges may indicate that the aggregate was prone to expansion during influxes of soil moisture, exerting an opposing force to impinging pedogenic calcite crystals within the soil matrix. Highly adsorbent clays may also retain moisture longer than the soil matrix. Upon desiccation, the aggregate would contract, leaving a thin, circumferential pore space. This model raises interesting possibilities for a second commonly cited question in petrocalcic soil environments: How do authigenic clays resist the force of crystallization exerted by calcite precipitation?

Authigenic clays (palygorskite and sepiolite) occurring either in pisolites, ooids, or around primary grains within the undifferentiated matrix do not contain features suggestive of dissolution or replacement whereas primary silicates and soil carbonates do (Reheis, 1988; and this study). Apart from making an assumption about the reduced chemical stability of primary minerals in near-surface environments (Reheis, 1988), it is speculated here that the role of hydrous and expansive crystal lattices in phyllosilicates and other minerals plays an important role in their stability. Palygorskite and sepiolite are well known for their absorbency (Murray, 2000), retaining up to 200% and 250% of their own mass in water, respectively (Jones & Galan, 1988). Thus, these clays may create and maintain important microporosity networks within the petrocalcic soil matrix (Brock, 2007), while also exchanging solution cations and simultaneously expanding and resisting crystallization forces from surrounding minerals.

It is not possible to conclusively determine from the data in this study whether or not palygorskite and sepiolite clays have dissolved and re-precipitated. Micromorphological data – including the presence of skeletal mats with rhomb-shaped pore spaces (Figure 4.24B), rings of fibrous clay around replaced silicate grains (Figure 4.27B), and the occurrence of pisolitic aggregates of fibrous clay engulfed by pedogenic carbonate

(Figure 4.24E) – strongly suggest that palygorskite and sepiolite, and perhaps other phyllosilicates, can indeed persist during dissolution of primary silicates and/or pedogenic calcite, however, further work is needed to support this hypothesis.

Soil chemical data from this study largely reflect the influx of water and dissolved ions, especially Ca^{2+}, SO_4^{2-}, and Cl^-, to the subsoil, and corroborate previous studies of the Mormon Mesa soil profile (Brock, 2007). Loss of structural water from hydrous minerals including palygorskite and sepiolite can produce positive error in soil moisture measurements (Burt, 2004), but given an arid soil consisting of only ~5 % phyllosilicates, this error is presumably minor. Air-dry/oven-dry moisture contents correspond well to the degree of induration by calcium carbonate. Similarly, pH values roughly match changes in carbonate content. The normal pH for bicarbonate-dominated soil solutions at equilibrium with atmospheric CO_2 is ~8.3 (Brady & Weil, 1999). Conversely, Mormon Mesa soil pH values in this study and in Brock (2007) often exceed 9.0, indicating influence by excessive carbonate ions and the probable presence of Na_2CO_3 (Brady & Weil, 1999). Electrical conductivity, sulfate, and chloride values generally increase with depth below the soil surface, however, average conductivity values decrease below the transitional horizon. Profiles could not be sampled to uniform depth due to limited exposures, however, horizon thicknesses and depths are unlikely to have been uniform across the mesa due to spatial and temporal variations in surface (aeolian) sediment thickness or ephemeral channel locations.

Chemical trends, especially the conductivity, sulfate, and chloride data, do raise implications for the genesis of the Mormon Mesa petrocalcic horizons, and corroborate the general model presented in Figure 4.28. The first observation is that of a clear difference between the chemical composition of the uncemented, fine (eolian) surface material and the composition of the indurated samples. Especially important are the low conductivity, sulfate, and chloride values, which indicate that recent sediment additions are most likely being leached of ions by percolating rain water (Brock, 2007).

The second key observation is that of a clear change below the contact of the stage VI massive horizon with the stage III-IV transitional horizon. Below this point, carbonate percentages decrease while other soluble ion contents rise sharply. This trend supports the presence of a discontinuity at the massive-transitional horizon boundary (e.g., Brock, 2007; Brock & Buck, 2009). Influence by groundwater is not likely given the high relative elevation of Mormon Mesa above the Virgin River Valley beginning around 4-5 Ma (Williams, 1996). This relative elevation difference is preserved today with approximately 200 m of vertical relief between the southern tip of the Mormon Mesa surface (~570 m amsl) and the surface of Lake Mead (~370 m amsl). Therefore, soluble ion and carbonate trends in the Mormon Mesa soil profile must result from evaporation of infiltrating soil solutions. Excluding the more variable sulfate values (which are discussed below as evidence supporting the model in Figure 4.29), the relative homogeneity of bulk soil chemistry above the massive-transitional boundary implies that either: (1) infiltrating moisture is largely bypassing the upper profile and infiltrating directly to the more permeable transitional horizon through subvertical networks of fractures or pipes in the upper, stage-VI petrocalcic horizons, (2) that the transitional horizon is a relict, buried soil horizon formed in a more saline paleoenvironment, and which has been largely sealed off from subsequent solution inputs, or (3) some combination of these possibilities has occurred.

Given the extensive, polygenetic history of the Mormon Mesa surface and the petrocalcic soil profile (Brock, 2007; Brock & Buck, 2009), the third scenario is most likely. Long-term, uninterrupted isolation of the transitional horizon is highly improbable. Bioturbation by roots or fungi is apparent from micromorphological data in this study, and burrowing has been suggested in previous work (Brock, 2007). Climate oscillations during the Quaternary are likely to have repeatedly affected the intensity and seasonality of storm events and, consequently, the depth of wetting in soil profiles. Pluvial climates and/or intense storms could have episodically flushed salts out of the upper soil profile and into the transitional horizon at any time during Mormon Mesa's history. Thus, the most likely scenario is that the transitional horizon developed according to the model of Brock & Buck (2009), and has been successively receiving newly-leached ions from the upper soil profile. Chemical data from this study, therefore, also support the extended mineral genesis model in Figure 4.29.

Support for the Extended Model

Soil chemical data, particularly sulfate concentrations, indicate that moisture is not entirely bypassing the upper soil profile horizon, neither in the present day, nor in the past. Sulfate concentrations are elevated near the brecciated-massive horizons contact in all of the MM1 profiles. This data fits well with micromorphological evidence of barite ($BaSO_4$) authigenesis within the upper massive horizon (Brock, 2007; and this study), and confirms that moisture may percolate through the surface and brecciated horizons before pooling or flowing laterally along this zone of textural and structural contrast. At the same time, it is likely that some moisture continues to percolate into the lower soil profile through fractures, pipes, and other hydrological conduits. With sustained pluvial climate or even successive severe storms, soluble salts such as gypsum and halite could be flushed out of the upper soil horizons and into the transitional horizon or even the upper Muddy Creek sediments.

Barium is an important but rare indicator of soil chemical processes. The common occurrence of pedogenic barite in the massive horizon of Mormon Mesa, as well as the sheer volume of pedogenic calcium carbonate present, both argue for sizeable inputs of atmospherically deposited ions over geologic time. It is especially unlikely that dissolution of primary grains alone could provide sufficient Ba^{2+} to account for the amount of pedogenic barite in Mormon Mesa (see also Brock, 2007). Thus, contributions to soil profiles of Ba^{2+} and other ions from eolian processes are likely.

Barium is likely delivered to the soil profile as barite ($BaSO_4$) dust, but it is also possible that hollandite, $Ba(Mn^{II\text{-}IIII+})_8O_{16}$, may play a role in the supply of Ba^{2+} ions to Mormon Mesa soil solutions. Hollandite, along with other manganese oxides, is a common constituent of desert varnish (Turner & Buseck, 1979; Kabata-Pendias, 2000; Garvie et al., 2008). Barium-manganese oxides may either form on coarse fragments at the soil surface, or be abraded, eroded, and transported to Mormon Mesa from varnished bedrock exposures upwind. Mn-oxides can also form along solution cavities, infiltrate into the profile as dust, and persist in the soil at depth (e.g., Dragovich, 1984). Hollandite contains variable amounts of both Mn^{2+} and Mn^{4+} (Turner & Buseck, 1979; McKenzie, 1989), thus, oxidation or mineral dissolution caused by fluctuations in surface or soil solution chemistry could release Ba^{2+} (Hem, 1972; McKenzie, 1989; Garvie et al., 2008). Possible hollandite peak matches were suggested by XRD analysis of the clay sized particle fraction in many samples in this study, however, the matches are uncertain at best, and if correct would indicate only trace amounts of the mineral. Thus, the role of hollandite in the genesis of pedogenic barite at depth within the Mormon Mesa soil profile, as well as its place in the extended model in Figure 4.29, remain uncertain.

Although barite has traditionally been considered insoluble (Lynn et al., 1971; Kabata-Pendias, 2000), it is widely accepted that the halite in solute-rich solutions can measurably increase barite solubility and mobility (e.g., Stoops & Zavaleta, 1978; Blount, 1977; Sullivan & Koppi, 1993; Deutsche, 1997; Hanor, 2000). In particular, Ba^{2+} solubility nearly doubles with each tenfold increase in ionic strength from Na^{+} and Cl^{-} (Deutsche, 1997; Hanor, 2000). It has also been demonstrated that Mg^{2+} also increases Ba^{2+} solubility in alkaline pH conditions (Deutsche, 1997) – an especially relevant point for mineral genesis in the Mormon Mesa petrocalcic soil. Thus, soil solution conditions during the dynamic evolution of the ~4-5 Ma Mormon Mesa soil, especially during warmer, more arid interpluvial episodes, could produce episodic increases in atmospherically-sourced, dissolved Ba^{2+} inputs to the soil (Brock, 2007) as depicted in Figure 4.29.

The presence of barite along the base of the massive horizon is also important because it reflects soil hydrological dynamics. Soil chemical data suggest that the Mormon Mesa soil profile is most likely the product of both recent and relict infiltration dynamics, and reflects multiple episodes of brecciation, erosion, re-cementation, fracturing, and cryptocrystalline reorganization within extensive portions of each soil horizon (Brock, 2007; Brock & Buck, 2009; and this study). Textural and hydrological discontinuity between the massive and transitional horizons has likely been maintained and augmented since the onset of Pleistocene pluvial-interpluvial climate oscillations

(Brock & Buck, 2009). Barite would have precipitated along with soluble salts when ion-saturated solutions pooled at this boundary during drier climates. During wetter climate episodes, more voluminous solutions of reduced ionic strength might have been sufficient to transport soluble salts laterally, and to leach them out of the profile through vertical fractures or pipes. During these episodes, barite would have remained essentially insoluble and would not have been mobilized into the lower horizons.

Episodic saturation and evaporation of micropores by solutions of variable Ca^{2+} and Mg^{2+} content, driven by climate change, could also promote the zoned calcite growth structures seen in the massive horizon (Figure 4.25 E-F). Episodic growth of calcite crystals from evaporating soil solutions could create the concentrically zoned crystals that include layers of Mg- and Si-rich phyllosilicates. Elemental mapping of these features confirmed distinct zones of calcite and magnesium-rich clay, however, no compositional zoning of calcite was found (all calcite zones were compositionally similar in terms of Mg, Fe, Al, Si, K, etc.). This could mean either that solution chemistry is always similar between growth episodes, or that any compositional variation is homogenized by subsequent solution saturation and cryptocrystalline modification. Larger, radiating calcite structures (see the right-hand side of Figure 4.25 E) most likely reflect fractures or void spaces that have been filled with calcium carbonate. In some cases these radiating structures can be further modified by subsequent mineral growth. Although clearly pedogenic in origin in this study, their overall morphology is similar to structures reported elsewhere for groundwater-diagenetic calcite (e.g., Chafetz & Butler, 1980).

Micromorphology and Pisolite Genesis

Pedogenic concretions or pisolites – rounded, concentric growth structures – occur within many Mormon Mesa samples (see Figure 4.27 A-C). These features have also been photomicrographed and described in calcic soil localities around the world (Vanden Heuvel, 1966; Reeves, 1976; Bachman & Machette, 1977; Hay & Wiggins, 1980; Calvet & Juliá, 1983; Reheis, 1988; Alonzo-Zarza et al., 1998; and others), and comparable features of reported biological origin were sketched by Alonso-Zarza (1999). Different authors have employed terms such as "concretion", "pellet", "pelletoid", "pisolite", "pisolith", "pisoid," "ooid", "oolith", and "spherulite" to distinguish between features with or without a nucleus, or to discern features greater or less than a certain diameter (Bachman & Machette, 1977; Hay & Wiggins, 1980). Many of these terms have been imported from geological rather than pedological references, and have had their meanings changed or lost as a consequence of their adaptation to soil environments. Firm terminology for these features was found challenging and disadvantageous to assign in this study because of the high variability between neighboring features in terms of their size, morphology, and mineralogical composition of concentric layers and/or nuclei. Confusion also arises because of differences in continued applications of the terms between published studies, and between pedogenic, lacustrine, and other geologic settings. In this study, "pisolites" are defined as spherical, concentrically-zoned pedogenic concretions of carbonate, phyllosilicates, and amorphous silica > 2 mm in diameter, with or without a grain nucleus. "Pedogenic ooids" are similar but < 2 mm in diameter.

Previous researchers have attempted to ascribe distinct modes of genesis to each different pisolite morphology (see below). However, the fact that great morphological variability exists among immediately adjacent pisolites seen in both this study and others (e.g., Calvet & Juliá, 1983; Hay & Wiggins, 1980) suggests that one sole mode of genesis can, in fact, be responsible for the entire suite of morphologies.

Both biogenic and non-biogenic modes of genesis have been proposed for pisolites. Biogenic models emphasize the relationship between pisolites and laminar horizons or rooting-zones in petrocalcic soils, and note the close morphological similarities to calcified root cross-sections with fungal filaments in both pedogenic and groundwater-influenced carbonate horizons (Calvet & Juliá, 1983; Alonso-Zarza et al., 1998; Alonzo-Zarza, 1999). In contrast, non-biogenic models better explain nuclei of detrital grain fragments or pelletal, porous clay-carbonate aggregates (e.g., Hay & Wiggins, 1980). Furthermore, laboratory experiments by Bosak et al. (2004) demonstrate that pisolite structures can form inorganically, and that their morphology is dictated by variations in solution chemistry. Thus, non-biogenic models of pisolite genesis emphasize the role of solution chemistry and the behavior of evaporative solution films, which may persist preferentially around primary grains due to surface tension and matric suction (Hay & Wiggins, 1980; Reheis, 1988; Mees, 1999). Such models, combined with subsequent cryptocrystalline modification or the force of crystallization process, might also explain how smaller pisolites can coalescence into larger ones (Bachman & Machette, 1977). SEM data from this study offer only limited evidence for the possible coalescence of small pisolites at Mormon Mesa (Appendix 4.4).

The potential for confusion between pisolites and pisoliths also bears mention. Pisoliths (sensu Brock & Buck, 2009) are stalactitic soil pendants, formed as successive carbonate coats on the underside of clasts in loose, young soil (Brock, 2007). Pisoliths result from the competing forces of surface tension and gravity on evaporating soil solutions and are then engulfed by pedogenic carbonate as the horizon reaches stage III. They can be preserved even in stage VI horizons. In perfect cross-section, pisoliths would appear as concentrically coated circular blocks or rock fragments (i.e., pisolites), especially if rotated away from their original vertical orientation due to progressive soil genesis, erosion, and/or reburial and re-cementation (Brock & Buck, 2009). Nevertheless, the spherical or pendant nature of the feature should be verifiable through field profile description, careful review of bulk sample blocks, and also based on the number and characteristics of the suspect pisolites. Oblong pisolites were not seen in thick sections in this study, indicating that the pisolites studied here lack preferred orientations, are spherical, and did not form like pendants. Moreover, pisoliths are less likely to be found as small (< 5mm) features, nor (especially) within laminar layers.

Data from this study suggest that the concentric, spherical growth of pisolites and pedogenic ooids, with and without nuclei, is a consequence of surface tension as thin soil solution films evaporate within tiny pore spaces and around detrital grains. Proposed here for Mormon Mesa, this mechanism builds upon an earlier model offered by Mees (1999) to refute subaerial exposure as a prerequisite for calcite spherulite genesis in laminar, palustrine calcretes. Surface tension, rather than gravity, would dominate soil microenvironments and thin solution films. These sites might especially occur within indurated and laminar features, perhaps even including zones within carbonate pendant laminae. In this model, fluctuating soil solution chemistry, particularly the activity of Ca, Mg, Al, and Si ions or complexes determines the mineralogy of each successive growth layer. Nuclei could be rock fragments, petrocalcic soil fragments, single mineral grains, or even empty micropores – anywhere moisture is held prior to desiccation. Furthermore, the outermost pisolite mineral coats could be modified, rounded, or dissolved by successive solutions. Fibrous clay coats paralleling right-angles along grain boundaries (Figure 4.24 D) are strong evidence for the precipitation of authigenic crystals from solution envelopes held to grains by surface-tension. Similarly, the presence of angular quartz grains within some spherical (circular in 2-D SEM images) carbonate and fibrous clay pisolites (Figure 4.27), constitute strong support for episodic cryptocrystalline remodeling during successive solution inflows.

Although this non-biogenic model of pisolite genesis suits well the Mormon Mesa pisolites studied here, microbial activity, bioturbation, and other biogenic processes do play important roles in the overall morphogenesis of petrocalcic horizons. Moreover, pisolites or pedogenic ooids in other sites, particularly those with septal features or clear, radial fibrous structures, likely do in fact have fungal or root origins (Alonso-Zarza, 1999; Phillips & Self, 1987). In Mormon Mesa, biological activity is very likely an important factor in the reorganization and re-opening of soil mineral systems to surface processes. Root and fungal networks serve as conduits for ion-rich soil solutions, and decaying organic matter or associated microbial activity could provide nucleation sites for further mineral precipitation. Microbial activity has also been reported to influence chemical conditions needed for carbonate precipitation (Checkroun et al., 2004; Lian et al., 2006). In particular, metabolic activity almost certainly supplies the CO_2 needed for calcite precipitation at depth (Monger et al., 1991; Monger & Gallegos, 2000). Biogenic features including *Microcodium*, branching structures, lobed structures, and calcified roots or hyphae occur throughout most samples in this study and are also important sinks or catalysts of calcite precipitation. Similarly, the formation and degradation of opal phytoliths could represent another compartment in the silicon-cycle of petrocalcic soils.

Linking Mineral Genesis to the Landscape Scale

All of the models presented above fit within the soil genesis sequence presented by Brock & Buck (2009). The models would be especially relevant after the massive horizon had begun to form, following erosion and reburial of the transitional horizon circa 2.8-2.0 Ma (Brock & Buck, 2009). Similarly, genesis of barite along the infiltration-restrictive base of the massive horizon would be especially important beginning with the onset of Pleistocene pluvial-interpluvial climate fluctuations (Brock & Buck, 2009). The timing of crystallization of distinct minerals have important implications for isotopic dating of pedogenic minerals in the Mormon Mesa profile. Palygorskite and sepiolite, along with calcite and amorphous silica, have likely crystallized continuously across all climates, even if the quantity, micromorphology, and location of the crystals may have varied. Barite, on the other hand, is far more likely to have crystallized chiefly or even exclusively during interpluvial climates along textural contrasts within late stage profile.

Unfortunately, isotopic age data for each distinct mineral phase are needed to accurately and precisely place this study's models of mineral and pisolite genesis within the context of climate change and soil system dynamics, and to confirm the soil genesis sequence proposed by Brock & Buck (2009). Isotope data are also needed to determine whether individual minerals have acted as closed systems, or whether they have indeed been subject to dissolution and recrystallization. Robins (2010b) presents an initial attempt to date pedogenic palygorskite and sepiolite extracted from petrocalcic soil horizons, and also suggests the potential viability of pedogenic barite for dating. The geochemical association of Ba^{2+} with K^{+} due to their similar ionic radii (Kabata-Pendias, 2000), and the potential of dating distinct pedogenic mineral phases make an accurate soil geochronology for Mormon Mesa an exciting goal in great need of further research.

Additional Considerations

The difficulty of mining sufficient volumes of specific morphological features forced this study to employ bulk soil samples in chemical analysis. The bulk nature of sample analyses, and the avoidance of exposed or fractured soil material during sampling, partially explains chemical variability between profiles, horizons, and samples of the same horizon in the Mormon Mesa petrocalcic soil. High chemical variability is not surprising for natural soil systems, especially petrocalcic profiles – each part of a calcrete complex can exhibit distinct chemical and mineralogical characteristics (Verrecchia & Le Coustumer, 1996). Indeed, horizon thickness, depth, and chemical properties were all variable between profiles in this study. Therefore, further chemical analysis of the Mormon Mesa petrocalcic soil is warranted, especially for additional profiles, and for specific morphological features. Targeted study of soil chemistry along fracture networks and within 'pipe' pedons could also provide important data.

Two considerations must also be made regarding micromorphological interpretations in this study. First, although care was taken to preserve the natural condition of the soil samples, slide preparation for SEM analysis in this study could easily have destroyed any soluble salts. Therefore, the chemical data is needed to consider the possible presence and significance of more soluble mineral phases in the soil. Secondly, rare, extremely fine needle-like or fibrous crystals with Si and Al EDS peaks were identified in SEM images of one limestone clast collected from a gravel deposit in Muddy Creek sediments a few meters below the Mormon Mesa petrocalcic soil. Therefore, rare palygorskite or sepiolite crystals can and do sometimes occur in engulfed limestone rock fragments (having formed either contemporaneously with the marine limestone, or diagenetically at any time after burial and lithification). These clay crystallites could theoretically contribute to the mineralogy of the Mormon Mesa petrocalcic soil. Such contributions, however, are considered minimal given the extremely fine, individual nature of the crystals (see Appendix 4.4), their rarity, and above all the clear genetic relationships between the fibrous phyllosilicates and all other definitively pedogenic mineral phases identified in the studied samples. Fibrous carbonate crystals are also common in limestones and other deposits (Folk, 1974), therefore EDS or other chemical data showing Si and Al, at a minimum, are needed to prove the phyllosilicate nature of the minerals.

Mineralogical interpretations of pedogenic palygorskite and sepiolite are also limited by instrument resolution and capabilities. Palygorskite and sepiolite cannot be differentiated from one another during SEM-EDS analysis. Therefore it is not possible to determine whether distinct chemical or physical microenvironments (i.e., grain-to-matrix contacts, pore spaces, pisolites) preferentially foster one of the fibrous clays over the other. Further electron microscope work, coupled with targeted XRD analysis of individual (micro)morphological features is needed to quantify and to better constrain the genesis of the magnesian clays. Data is especially needed regarding the relative abundance of palygorskite versus sepiolite in different morphological features, including massive matrix, laminar horizons, pisolites, and pendants.

In addition, small (<<1 μm), bright, angular masses of unknown origin were found to be scattered evenly across some samples in this study (Appendix 4.4). Unfortunately, their small size relative to the ~2.5 μm interaction diameter of the EDS beam made compositional data unobtainable. These features are too large to be a product of normal gold-coating processes, but appear to be smaller than the silica hemispheroids imaged by Brock (2007). Thus, they are tentatively interpreted as an undetermined artifact of acid-etching prior to SEM-EDS analysis.

Summary and Conclusions

Mineralogical, chemical, and micromorphological data from this study support the sequence of horizon and profile development proposed by Brock and Buck (2009) for the 4-5 Ma Mormon Mesa petrocalcic soil in southern Nevada, U.S.A. Furthermore, data from this study yield refined conceptual models of the genesis of distinct soil minerals in the Mormon Mesa soil. The first model describes general soil solution and mineral precipitation dynamics for calcium carbonate, palygorskite, sepiolite, and amorphous silica. The second model differentiates these dynamics to reflect the effects of climate change, and also to address the presence of pedogenic barite in the Mormon Mesa soil profile. These models advance understanding of regional petrocalcic soil genesis by highlighting process-feedbacks caused by Quaternary climate oscillation. Thus, pedogenesis on the Mormon Mesa surface has been especially driven by: (1) illuviation of dust and ions with infiltrating rainfall, (2) force of crystallization dissolution by pedogenic carbonate, (3) barite, magnesian-phyllosilicate, and silica precipitation in response to dynamic soil solution chemistry, and (4) frequent, punctuated modification of soil solution networks.

Specifically, it is suggested here that pedogenic barite precipitated along zones of restricted vertical solution flow (laminar caps and horizon contacts) during drier, interpluvial climates, and was then preserved in these locations during the wetter, pluvial periods. Barite authigenesis and preservation are considered to have become especially significant after the Mormon Mesa soil profile developed stage IV petrocalcic horizon morphology. Conversely, pedogenic carbonate, palygorskite and/or sepiolite, and amorphous silica genesis may have been especially pronounced during interpluvials, yet likely continued across all climate phases and could have begun as soon as the Mormon Mesa soil expressed stage II morphology (i.e., carbonate nodules).

This paper not only presents viable mineral models which dovetail with previous research on both Mormon Mesa, but also provides a non-biological formation mechanism for pedogenic pisolites or ooids with varying morphologies. Microporosity, surface tension, and soil solution chemical feedbacks during evaporation are considered critical factors not only for driving (1) carbonate precipitation, (2) force of crystallization dissolution of primary silicate grains or rock fragments, and (3) authigenesis of palygorskite and sepiolite, but also for development of pisolites and other micromorphological features.

As suggested by Brock (2007), crystallization of fibrous phyllosilicates within solution conduits in Mormon Mesa may play a critical role in the preservation of those same conduits and, in consequence, the continued, future influx of solutions to soil microsites. It is also tentatively concluded in this paper that expansion of phyllosilicate lattices through soil solution influx and evaporation cycles may be the mechanism protecting fibrous or expansive clays against force of crystallization dissolution by impinging carbonate.

Snapshot mineralogical, chemical, and micromorphological data cannot always determine whether a soil system is experiencing change today, however, data from this study certainly add further evidence that portions of the Mormon Mesa petrocalcic soil have in the past and will certainly in the future experience open-system dynamics. Soils in general evolve as open systems, however, in some cases individual horizons can mimic chemically and mineralogically closed systems when local equilibrium is achieved – if only temporarily on soil geomorphologic timescales (Jones & Galan, 1988). Therefore, it remains possible that isolated, closed-system peds or minerals can and do exist somewhere within the 4-5Ma Mormon Mesa soil profile. The persistence of even trace amounts of detrital phyllosilicates in highly-indurated soil experiencing force of crystallization dissolution of silicate grains may support this claim. Moreover, crystals of pedogenic barite also may be examples of closed-system minerals. The clear implication of this study for genetic interpretations and isotopic dating of petrocalcic soil systems is that extensive, detailed, and targeted micromorphological analysis is an inescapable prerequisite of any study on calcic and petrocalcic soil landscapes.

Unless strong evidence exists for the coeval genesis of one specific mineral phase within a given horizon or micromorphological feature, isotopic dating studies must also adapt to the need for targeted mining of distinct mineral phases from soil samples. Bulk sample extractions at the scale conducted by Robins (2010a&b) are not likely to generate meaningful age data unless the sample is comprised, by luck, of a rare, closed-system ped. Although arid soils including calcic horizons contain a many unique minerals that could be suitable for diverse isotopic dating techniques (Robins, 2010b), the low abundance of these minerals and their genetic restriction to tiny morphological features pose significant challenges. Moreover, as demonstrated by Brock & Buck (2005) for carbonate laminae within stage II pendants, and as suggested in this study for pisolites and zones of textural contrast along horizon and grain boundaries, individual micromorphological features can grow in pulses over a wide range of geological ages, and growth structures can always be partially dissolved and re-crystallized at any site within the feature.

The Mormon Mesa petrocalcic soil is demonstrated to contain diverse and unique microenvironments warranting considerable future study. Mineralogical, chemical, and isotopic data on transects of individual micromorphological features are greatly needed to constrain the timing of distinct pedogenic episodes. New isotopic dating methods, and further analysis of phyllosilicate mineral trends and geochemical properties of distinct pedological zones are greatly needed for these unique and ancient systems.

References

Alonzo-Zarza, A.M., Silva, P.G., Goy, J.L., and Zazo, C., 1998. Fan-surface dynamics and biogenic calcrete development: Interactions during ultimate phases of fan evolution in the semiarid SE Spain (Murcia). Geomorphology, 24: 147-167.

Alonso-Zarza, A.M., 1999. Initial stages of laminar calcrete formation by roots: examples from the Neogene of central Spain. Sedimentary Geology, 126: 177-191.

Bachman, G.O. and Machette, M.N., 1977. Calcic soils and calcretes in the southwestern United States. U.S. Geological Survey Open File Report 77-794. 163 pages.

Blount, C.W., 1977. Barite solubilities and thermodynamic quantities up to 300°C and 1400 bars. American Mineralogist, 62: 942-957.

Brauner, K. and Preisinger, A., 1956. Estruktur und Enstehung des sepiolits. Tschermaks Mineralogische und petrographisches Mitteilungen, 6:120-140.

Bosak, T., Souza-Egipsy, V., and Newman, D.K., 2004. A laboratory model of abiotic peloid formation. Geobiology, 2: 189-198.

Bouza, P.J., Simón, M., Aguilar, J., del Valle, H., and Rostagno, M., 2007. Fibrous-clay mineral formation and soil evolution in Aridisols of northeastern Patagonia, Argentina. Geoderma, 139: 38-50.

Brady, N.C. and Weil, R.R., 1999. The nature and properties of soils, twelfth edition. New Jersey: Prentice Hall. 881 pages.

Brock, A.L. and Buck, B.J., 2005. A new formation process for calcic pendants from Pahranagat Valley, Nevada: Implication for dating Quaternary landforms. Quaternary Research, 63: 359-367.

Brock, A.L., 2007. Characterization of stage VI petrocalcic horizons: S. Nevada and N.W. Arizona. Ph.D. Dissertation. University of Nevada Las Vegas, Department of Geoscience. 148 pages.

Brock, A.L. and Buck, B.J., 2009. Polygenetic development of the Mormon Mesa, NV petrocalcic horizons: Geomorphic and paleoenvironmental interpretations. Catena, 77: 65-75.

Burt, R., ed., 2004. Soil Survey Laboratory methods manual. Soil Survey Investigations Report No. 42, Version 4.0. United States Department of Agriculture Natural Resources Conservation Service. 700 pages.

Calvet, F. and Juliá, R., 1983. Pisoids in the caliche profiles of Tarragona (N.E. Spain). In: Peryt, T.M., ed. Coated grains. Berlin, Springer-Verlag: 456-473.

Capo, R. and Chadwick, O., 1999. Sources of strontium and calcium in desert soil and calcrete. Earth and Planetary Science Letters, 170: 61-72.

Chafetz, H.S. and Butler, J.C., 1980. Petrology of recent caliche pisolites, spherulites, and speleothem deposits from central Texas. Sedimentology, 27: 497-518.

Chekroun, K.B., Rodríguez-Navarro, C., González-Muñoz, M.T., Arias, J.M., Cultrone, G., and Rodríguez-Gallego, M., 2004. Precipitation and growth morphology of calcium carbonate induced by *Myxococcus xanthus*: Implications for recognition of bacterial carbonates. Journal of Sedimentary Research, 74(6): 868-876.

Chiquet, A., Michard, A., Nahon, D., and Hamelin, B., 1999. Atmospheric input vs. in situ weathering in the genesis of calcretes: An Sr isotope study at Gálvez (central Spain). Geochimica et Cosmochimica Acta, 63(3/4): 311-323.

Deocampo, D., 2005. Evaporative evolution of surface waters and the role of aqueous CO_2 in magnesium silicate precipitation: Lake Eyasi and Ngorongoro Crater, northern Tanzania. South African Journal of Geology, 108: 493-504.

Deutsche, W.J., 1997. Groundwater geochemistry: Fundamentals and applications to contamination. Boca Raton: Lewis Publishers. 221 pages.

Dixon, J.B. and Weed, S.B., eds., 1989. Minerals in soil environments, 2nd edition. SSSA Book Series 1. Madison, Soil Science Society of America. 1244 pages.

Dragovich, D., 1984. The survival of desert varnish in subsurface positions, western New South Wales, Australia. Earth Surface Processes and Landforms, 9: 425-434.

Drees, L.R., Wilding, L.P., Smeck, N.E. and Senkayi, A.L., 1989. Silica in soils: Quartz and disordered silica polymorphs. In: Dixon, J.B. and Weed, S.B., eds., Minerals in soil environments, 2nd edition. SSSA Book Series 1. Madison, Soil Science Society of America: 913-974.

Duniway, M.C., Herrick, J.E. and Monger, H.C., 2007. The high water-holding capacity of petrocalcic horizons. Soil Science Society of America Journal, 71(3): 812-819.

Folk, R.L., 1974. The natural history of crystalline calcium carbonate: Effect of magnesium content and salinity. Journal of Sedimentary Petrology, 44(1): 40-53.

Francis, M.L., Fey, M.V., Prinsloo, H.P., Ellis, F., Mills, A.J., and Medinski, T.V., 2007. Soils of Namaqualand: Compensations for aridity. Journal of Arid Environments, 70: 588-603.

García-Romero, E., Suárez, M., Santarén, J., and Alvarez, A., 2007. Crystallochemical characterization of the palygorskite and sepiolite from the Allou Kagne deposit, Senegal. Clays and Clay Minerals, 55 (6): 606-617.

Gardner, L.R., 1972. Origin of the Mormon Mesa Caliche, Clark County, Nevada. Geological Society of America Bulletin, 83: 143-156.

Garvie, L.A.J., Burt, D.M., and Buseck, P.M., 2008. Nanometer-scale complexity, growth, and diagenesis in desert varnish. Geology, 36(3): 215-218.

Gile, L.H., Peterson, F.F., and Grossman, R.B., 1965. The K horizon – A master soil horizon of carbonate accumulation. Soil Science, 99: 74-82.

Gile, L.H., Peterson, F.F., and Grossman, R.B., 1966. Morphological and genetic sequences of carbonate accumulation in desert soils. Soil Science, 101(5): 347-360.

Gile, L.H., Hawley, J.W., and Grossman, R.B., 1981. Soils and geomorphology in the Basin and Range area of Southern New Mexico - Guidebook to the Desert Project. Socorro, University of New Mexico. 222 pages.

Graham, R.C., Hirmas, D.R., Wood, Y.A., and Amrhein, C., 2008. Large near-surface nitrate pools in soils capped by desert pavement in the Mojave Desert, California. Geology, 36(3): 259-262.

Hanor, J.S., 2000. Barite-celestine geochemistry and environments of formation. In: Alpers, C.N., Jambor, J.L., and Nordstrom, D.K., eds. Sulfate minerals: Crystallography, geochemistry and environmental significance. Reviews in Mineralogy and Geochemistry, 40. Washington, D.C., The Mineralogical Society of America: 193-275.

Hay, R.L. and Wiggins, B., 1980. Pellets, ooids, sepiolite and silica in three calcretes of the southwestern United States. Sedimentology, 27: 559-576.

Hem, J.D., 1972. Chemical factors that influence the availability of iron and manganese in aqueous systems. Geological Society of America Bulletin, 83: 443-450.

Hennessy, J.T., Gibbens, R.P., Tromble, J.M., and Cardenas, M., 1983. Water properties of caliche. Journal of Range Management, 36(6): 723-726.

Hillier, S. and Pharande, A.L., 2008. Contemporary pedogenic formation of palygorskite in irrigation-induced, saline-sodic, shrink-swell soils of Maharashtra, India. Clays and Clay Minerals, 56 (5): 531-548.

House, P.K., Pearthree, P.A., Howard, K.A., Bel, J.W., Perkins, M.E., and Brock, A.L., 2005. Birth of the lower Colorado River – Stratigraphic and geomorphic evidence for its inception near the conjunction of Nevada, Arizona, and California. In: Pederson, J., and Dehler, C.M., eds., Interior Western United States: Boulder Colorado, Geological Society of America Field Guide 6.

Jackson, M.L., 1965. Soil chemical analysis: Advanced Course. Published by the author. Dept. of Soil Science, University of Wisconsin, Madison.

Jones, B.F., 1983. Occurrence of clay minerals in surficial deposits of southwestern Nevada. Sciences Géologiques Mémoires (Strasbourg), 72: 81-92.

Jones, B.F. and Galan, E., 1988. Sepiolite and palygorskite. Reviews in Mineralogy, 19(1): 631-674.

Junge, C.E. and Werby, R.T., 1958. The concentration of chloride, sodium, potassium, calcium, and sulfate in rain water over the United States. Journal of Meteorology, 15 (5): 417-425.

Kabata-Pendias, A., 2000. Trace elements in soils and plants, 3rd edition. New York: CRC Press. 413 pages.

Krekeler, M.P.S., Hammerly, E., Rakovan, J., and Guggenheim, S., 2005. Microscopy studies of the palygorskite-to-smectite transformation. Clays and Clay Minerals, 53(1): 92-99.

Kunze, G.W. and Dixon, J.B., 1986. Pretreatment for mineralogical analysis. In: Klute, A., ed. Methods of soil analysis part 1: Physical and mineralogical methods, 2nd edition. Agronomy Monograph 9. Madison, Soil Science Society of America: 91-100.

Lian, B., Hu, Q., Chen, J., Ji, J., and Teng, H.H., 2006. Carbonate biomineralization induced by soil bacterium *Bacillus megaterium*. Geochimica et Cosmochimica Acta, 70: 5522-5535.

Lintern, M.J., Sheard, M.J., and Chivas, A.R., 2006. The source of pedogenic carbonate associated with gold-calcrete anomalies in the western Gawler Craton, South Australia. Chemical Geology 235: 299-324.

Lynn, W.C., Tu, H.Y., and Franzmeier, D.P., 1971. Authigenic barite in soils. Soil Science Society of America Proceedings, 35: 160-161.

Machette, M.N., 1985. Calcic soils of the southwestern United States. Geologic Society of America Special Paper 203: 1-21.

McKenzie, R.M., 1989. Manganese oxides and hydroxides. In: Dixon, J.B. and Weed, S.B., eds. Minerals in soil environments, 2nd edition. SSSA Book Series 1. Madison, Soil Science Society of America: 439-465.

Mees, F., 1999. The unsuitability of calcite spherulites as indicators of subaerial exposure. Journal of Arid Environments, 42: 149-154.

Monger, H.C. and Daugherty, L.A., 1991a. Pressure solution: Possible mechanism for silicate grain dissolution in a petrocalcic horizon. Soil Science Society of America Journal, 55: 1625-1629.

Monger, H.C. and Daugherty, L.A., 1991b. Neoformation of palygorskite in a southern New Mexico aridisol. Soil Science Society of America Journal, 55: 1646-1650.

Monger, H.C., Daugherty, L.A., Lindemann, W.C., and Liddell, C.M., 1991. Microbial precipitation of pedogenic calcite. Geology, 19: 997-1000.

Monger, H.C. and Gallegos, R.A., 2000. Biotic and abiotic processes and rates of pedogenic carbonate accumulation in the Southwestern United States – Relationship to atmospheric CO_2 sequestration. In: Lal, R., Kimble, J., Eswaran, H., and Stewart, B.A., eds. Global climate change and pedogenic carbonates. Washington, D.C., Lewis Publications: 273-289.

Monger, H.C. and Kelly, E.F., 2002. Silica minerals. In: Dixon, J.B. and Schulze, D.G., eds. Soil mineralogy with environmental applications. SSSA Book Series No.7. Madison, Soil Science Society of America: 611-636.

Moore, D.M. and Reynolds, R.C., 1997. X-ray diffraction and the identification and analysis of clay minerals (2nd edition).New York, Oxford University Press. 378 pages.

Murray, H.H., 2000. Traditional and new applications for kaolin, smectite, and palygorskite: a general overview. Applied Clay Science, 17: 207-221.

Naiman, Z., Quade, J., and Patchett, P.J., 2000. Isotopic evidence for eolian recycling of pedogenic carbonate and variations in carbonate dust sources throughout the southwest United States. Geochimica et Cosmochimica Acta, 64(18): 3099-3109.

Pansu, M. and Gautheyrou, J., 2006. Handbook of soil analysis: Mineralogical, organic, and inorganic methods. Germany: Springer. 993 pages.

Phillips, S.E. and Self, P.G., 1987. Morphology, crystallography and origin of needle-fibre calcite in Quaternary pedogenic calcretes of South Australia. Australian Journal of Soil Research, 25: 429-444.

Poppe, L.J., Paskevich, V.F., Hathaway, J.C., and Blackwood, D.S., 2001. A laboratory manual for X-Ray powder diffraction. U.S. Geological Survey Open-File Report 01-041.

Reeves, C.C., Jr., 1976. Caliche: Origin, classification, morphology and uses. Lubbock, Estacado Books: 233 pages.

Reheis, M., 1988. Pedogenic replacement of aluminosilicate grains by $CaCO_3$ in Ustollic Haplargids, south-central Montana, U.S.A. Geoderma, 41: 243-261.

Reheis, M.C., Harden, J.W., McFadden, L.D., and Shroba, R.R., 1989. Development rates of Late Quaternary soils, Silver Lake Playa, California. Soil Science Society of America Journal, 53: 1127-1140.

Reheis, M.C. and Kihl, R.,1995. Dust deposition in southern Nevada and California, 1984-1989: Relations to climate, source area, and source lithology. Journal of Geophysical Research, 10 (D5): 8893-8918.

Robins, C.R., 2010a. Towards $^{40}Ar/^{39}Ar$ geochronology of pedogenic palygorskite and sepiolite, Part I: extraction and chemical considerations. In: Robins, C.R. Phyllosilicate mineralogy, $^{40}Ar/^{39}Ar$ geochronology, and genesis of petrocalcic soils in the southwest U.S.A. Ph.D. dissertation. UNLV Department of Geoscience, Las Vegas, NV: 1-55.

Robins, C.R., 2010b. Towards $^{40}Ar/^{39}Ar$ geochronology of pedogenic palygorskite and sepiolite, Part II: lessons and technical implications for dating arid soils. In: Robins, C.R. Phyllosilicate mineralogy, $^{40}Ar/^{39}Ar$ geochronology, and genesis of petrocalcic soils in the southwest U.S.A. Ph.D. dissertation. UNLV Department of Geoscience, Las Vegas, NV: 56-94.

Schmidt, D.L., Page, W.R., and Workman, J.B., 1996. Preliminary geologic map of the Moapa West Quadrangle, Clark County, Nevada. U.S. Department of the Interior, U.S. Geological Survey Open-File Report 96-521. 1:24,000.

Singer, A., 1984. The paleoclimatic interpretation of clay minerals in sediments - a review. Earth-Science Reviews, 21: 251-293.

Singer, A., 1989. Palygorskite and sepiolite group minerals. In: Dixon, J.B. and Weed, S.B., eds., Minerals in soil environments, 2nd edition. SSSA Book Series No. 1. Madison, Soil Science Society of America: 829-872.

Singer, A., Kirsten, W., and Bühman, C., 1995. Fibrous clay minerals in the soils of Namaqualand, South Africa: Characteristics and formation. Geoderma, 66: 43-70.

Soil Survey Staff, 2006a. Official Soil Series Descriptions [Online WWW]. Available URL: “http://soils.usda.gov/technical/classification/osd/index.html” [Accessed 1 April 2006]. Lincoln, United States Department of Agriculture Natural Resources Conservation Service.

Soil Survey Staff, 2006b. Keys to soil taxonomy, tenth edition. Washington, D.C., United States Department of Agriculture National Resources Conservation Service. 332 pages.

Soukup, D.A., Buck, B.J., and Harris, W., 2008. Preparing soils for mineralogical analysis. In: Ulery, A. and Drees, R., eds. Methods of soil analysis, Part 5: Mineralogical methods. SSSA Book Series No. 5. Madison, Science Society of America: 13-31.

Steiger, M., 2005. Crystal growth in porous materials - I: The crystallization pressure of large crystals. Journal of Crystal Growth, 282: 455-469.

Stoops, G.J. and Zavaleta, A., 1978. Micromorphological evidence of barite neoformation in soils. Geoderma, 20: 63-70.

Sullivan, L.A. and Koppi, A.J., 1993. Barite pseudomorphs after lenticular gypsum in a buried soil from central Australia. Australian Journal of Soil Research, 31: 393-396.

Turner, S. and Buseck, P.R., 1978. Manganese oxide tunnel structures and their intergrowths. Science, 203: 456-458.

United States Geological Survey (USGS), 2005. Seamless Data Distribution Digital Elevation Models. United States Department of the Interior: http://seamless.usgs.gov/.

Vanden Heuvel, R.C., 1966. The occurrence of sepiolite and attapulgite in the calcareous zone of a soil near Las Cruces, New Mexico. In: W.F. Bradley and S.W. Bailey, eds. Thirteenth National Conference on Clays and Clay Minerals. Madison, Pergamon Press: 193-207.

Van der Hoven, S.J. and Quade, J., 2002. Tracing spatial and temporal variations in the sources of calcium in pedogenic carbonates in a semiarid environment. Geoderma, 108: 259-276.

Velde, B., 1992. Introduction to clay minerals: Chemistry, origins, uses and environmental significance. New York, Chapman & Hall. 198 pages.

Verrecchia, E.P. and Le Coustumer, M.-N., 1996. Occurrence and genesis of palygorskite and associated clay minerals in a Pleistocene calcrete complex, Sde Boqer, Negev Desert, Israel. Clay Minerals, 31: 183-202.

Watts, N.L., 1978. Displacive calcite: Evidence from recent and ancient calcretes. Sedimentology Research Laboratory, 6: 699-703.

Watts, N.L., 1980. Quaternary pedogenic calcretes from the Kalahari (southern Africa): mineralogy, genesis and diagenesis. Sedimentology, 27: 661-686.

Weaver, C.E. and Beck, K.C., 1977. Miocene of the S.E. United States: A model for chemical sedimentation in a peri-marine environment. Sedimentary Geology, 17: 1-234.

Weyl, P.K., 1959. Pressure solution and the force of crystallization - A phenomenological theory. Journal of Geophysical Research, 64(1): 2001-2025.

Williams, V.A., 1996. Preliminary Geologic Map of the Mesquite Quadrangle, Clark and Lincoln Counties, Nevada and Mohave Counties, Arizona. USGS Open File Report 96-0676. http://pubs.usgs.gov/of/1996/ofr-96-0676/.

Williams, V.S., Bohannon, R.G. and Hoover, D.L., 1997. Geologic map of the Riverside Quadrangle, Clark County, Nevada, Geologic Quadrangle Map GQ-1770.

Yaalon, D.H. and Wieder, M., 1976. Pedogenic palygorskite in some arid brown (calciorthid) soils of Israel. Clay Minerals, 11 (1): 73-80.

Yariv, S. and Cross, H., eds., 2002. Organo-clay complexes and interactions. New York, Marcel Dekker, Inc.

Zehnder, K. and Arnold A., 1989. Crystal growth in salt efflorescence. Journal of Crystal Growth, 97: 513-521.

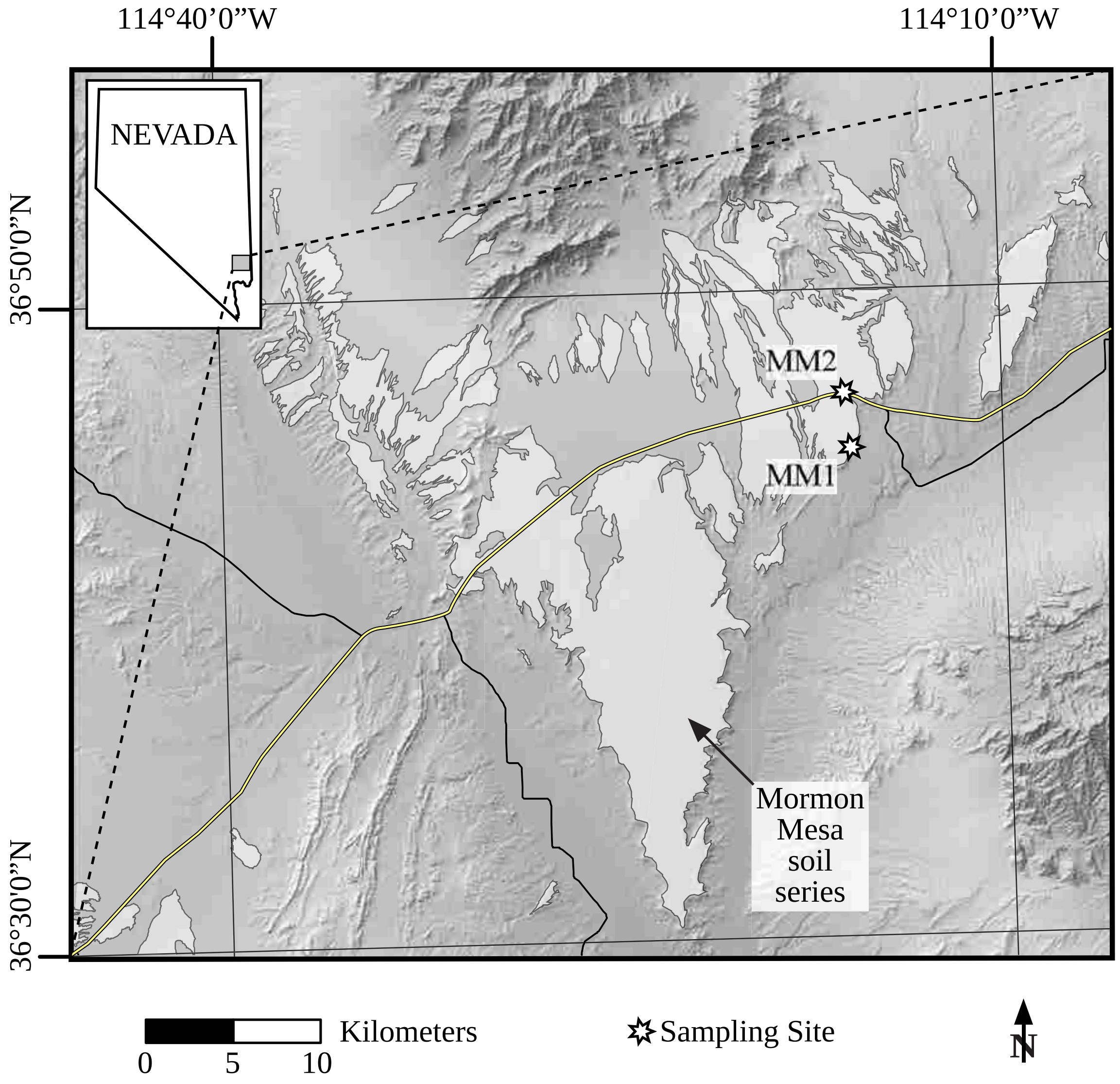

Figure 4.1. Location of sampled profiles on the Mormon Mesa geomorphologic surface, and approximate extent of the Mormon Mesa soil series. Soil-geomorphologic spatial data are modified from Soil Survey Staff (2006); basemap digital elevation data are modified from USGS (2005).

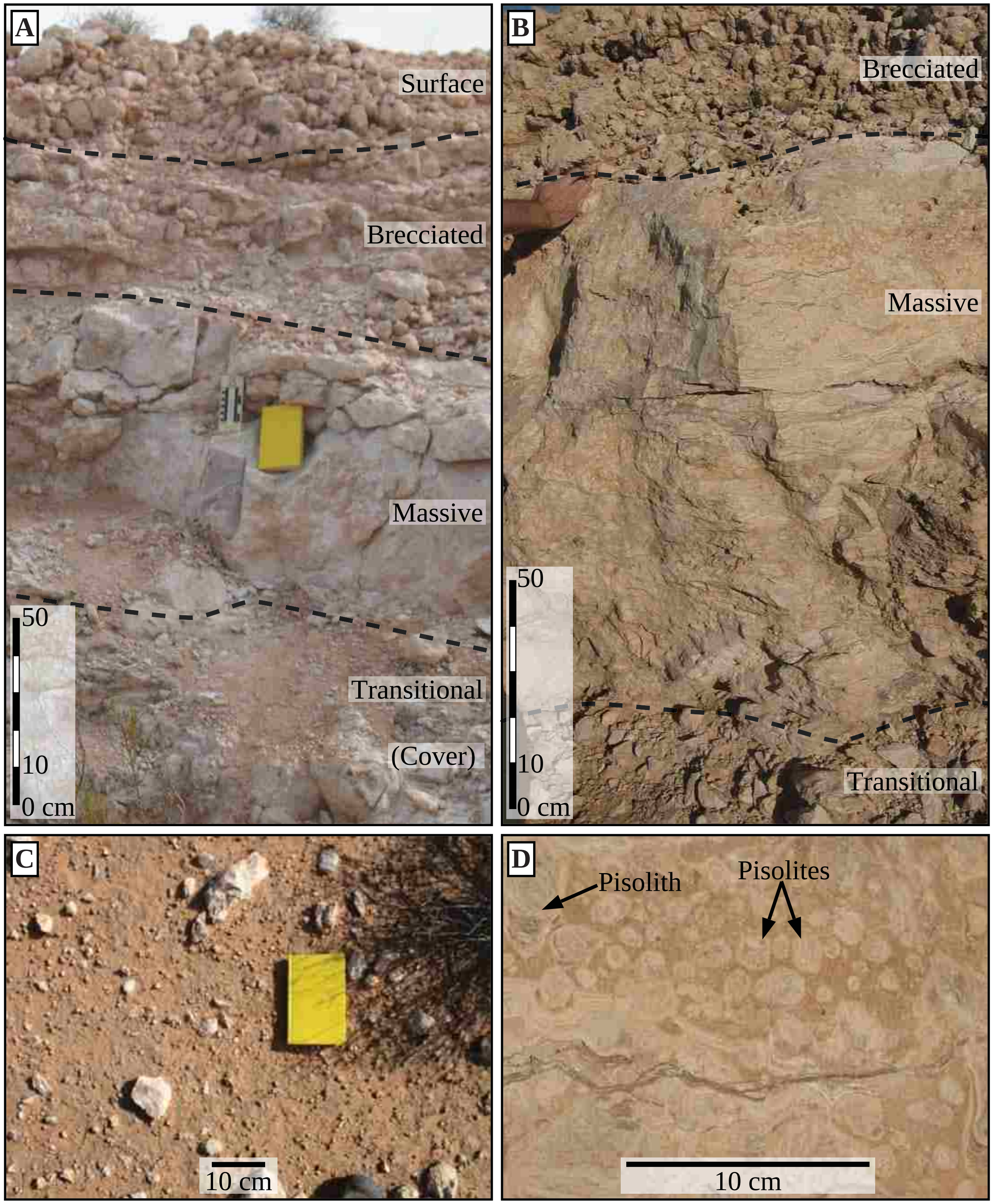

Figure 4.2. Photographs of profiles (A) MM1-C and (B) MM2, showing approximate horizon contacts. (C) Undisturbed surfaces of the Mormon Mesa A horizon reveal common petrocalcic soil fragments dispersed within a groundmass of red, eolian silts and fine sands. Microbiotic crusts are also common on the soil surface. (D) Centimeter-scale pisolites and pisoliths are common features in the stage VI petrocalcic horizons. Millimeter-scale pisolites (= pedogenic ooids) are also seen in microscope samples. Note prominent subhorizontal fracture partially filled by calcium carbonate.

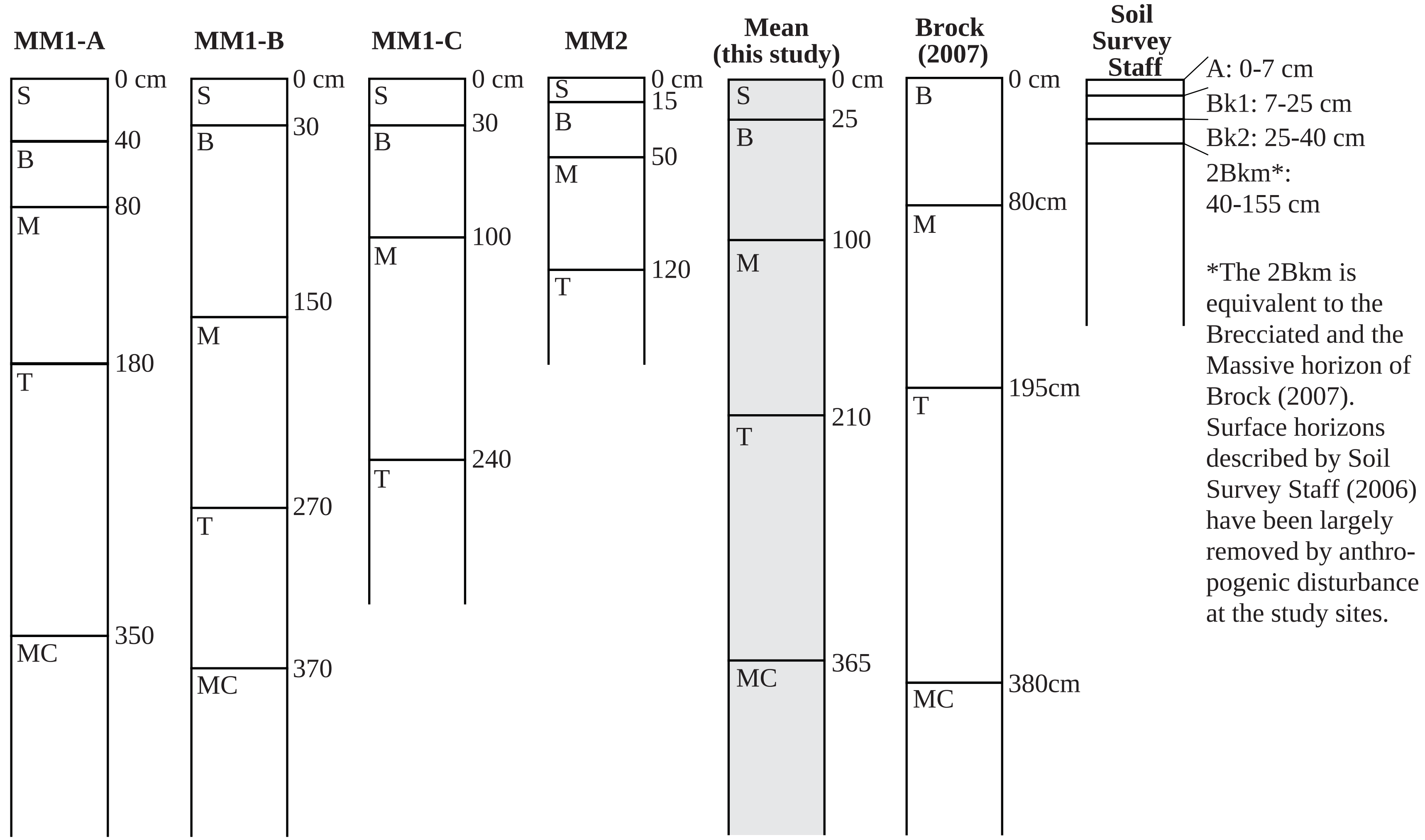

Figure 4.3. Comparison of soil horizon thicknesses between this study, the Riverside profile of Brock (2007), and the Mormon Mesa Soil Series type pedon (Soil Survey Staff, 2006). S = Surface horizon, B = brecciated horizon, M = massive horizon, T = transitional horizon, MC = upper Muddy Creek formation sediments and stage II calcic paleosol. Horizon nomenclature after Brock (2007).

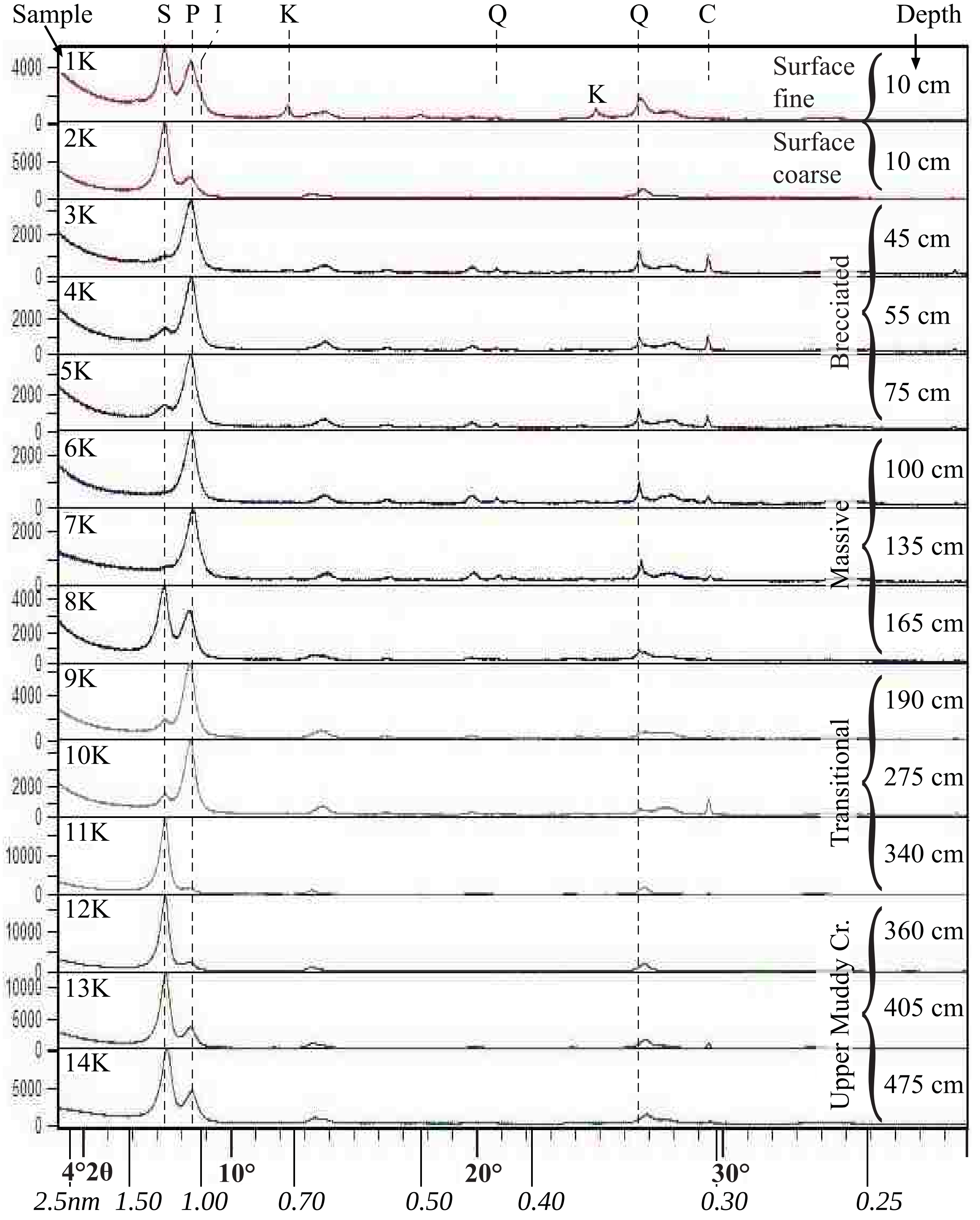

Figure 4.4. XRD spectra for baseline K-saturated Profile MM1-A samples, showing variable mineralogy with depth. Y-axis values are peak counts for each spectrum. X-axis indicates scan angle (°2θ) and d-spacing (nm). Approximate sample depths below the soil surface are indicated to the right of each spectrum. Important mineral peak locations are labeled as C = calcite, I = illite, K = kaolinite, P = palygorskite, Q = quartz, and S = sepiolite.

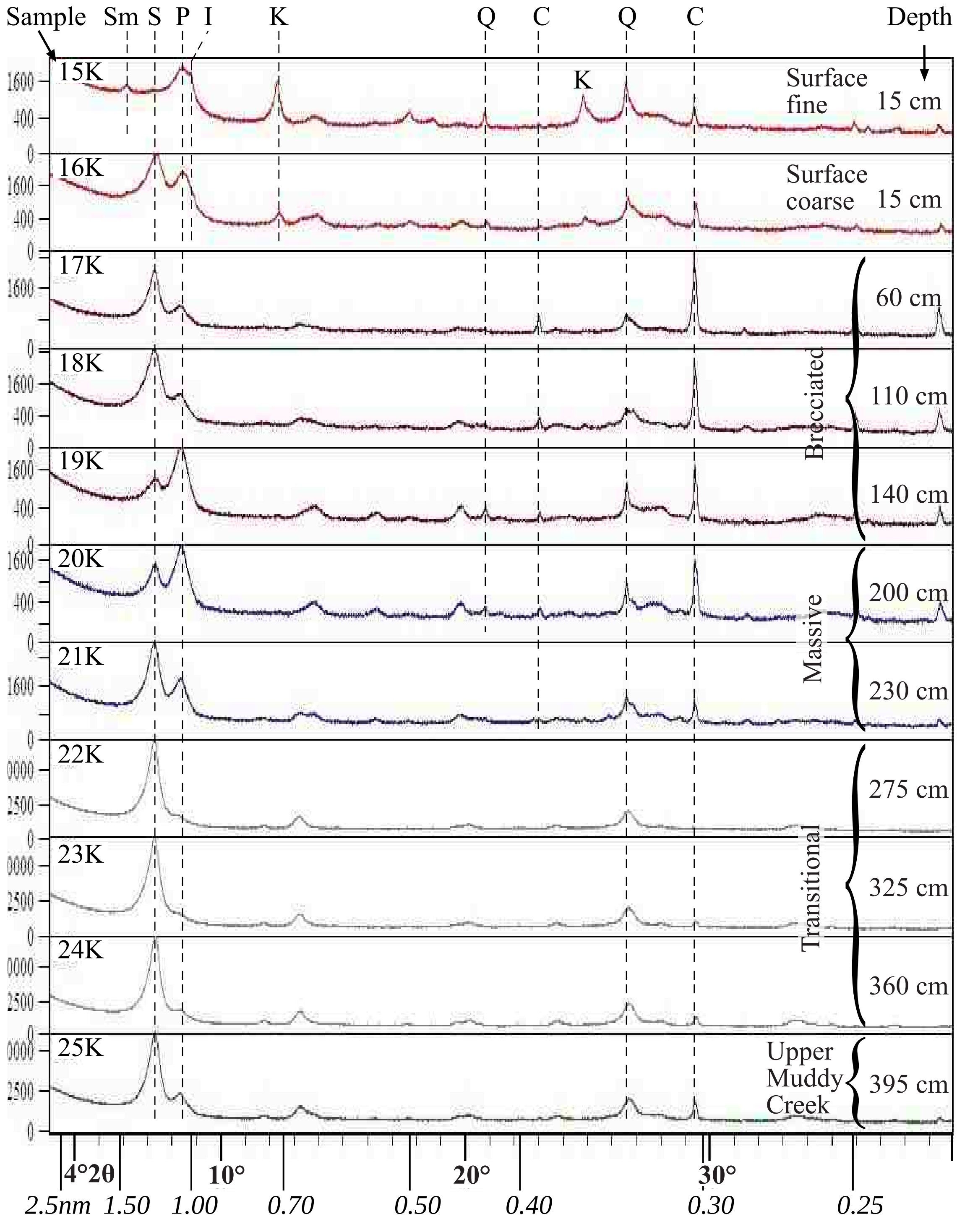

Figure 4.5. XRD spectra for baseline K-saturated Profile MM1-B samples, showing variable mineralogy with depth. Y-axis values are peak counts for each spectrum. X-axis indicates scan angle (°2θ) and d-spacing (nm). Approximate sample depths below the soil surface are indicated to the right of each spectrum. Important mineral peak locations are labeled as C = calcite, I = illite, K = kaolinite, P = palygorskite, Q = quartz, S = sepiolite, and Sm = smectite.

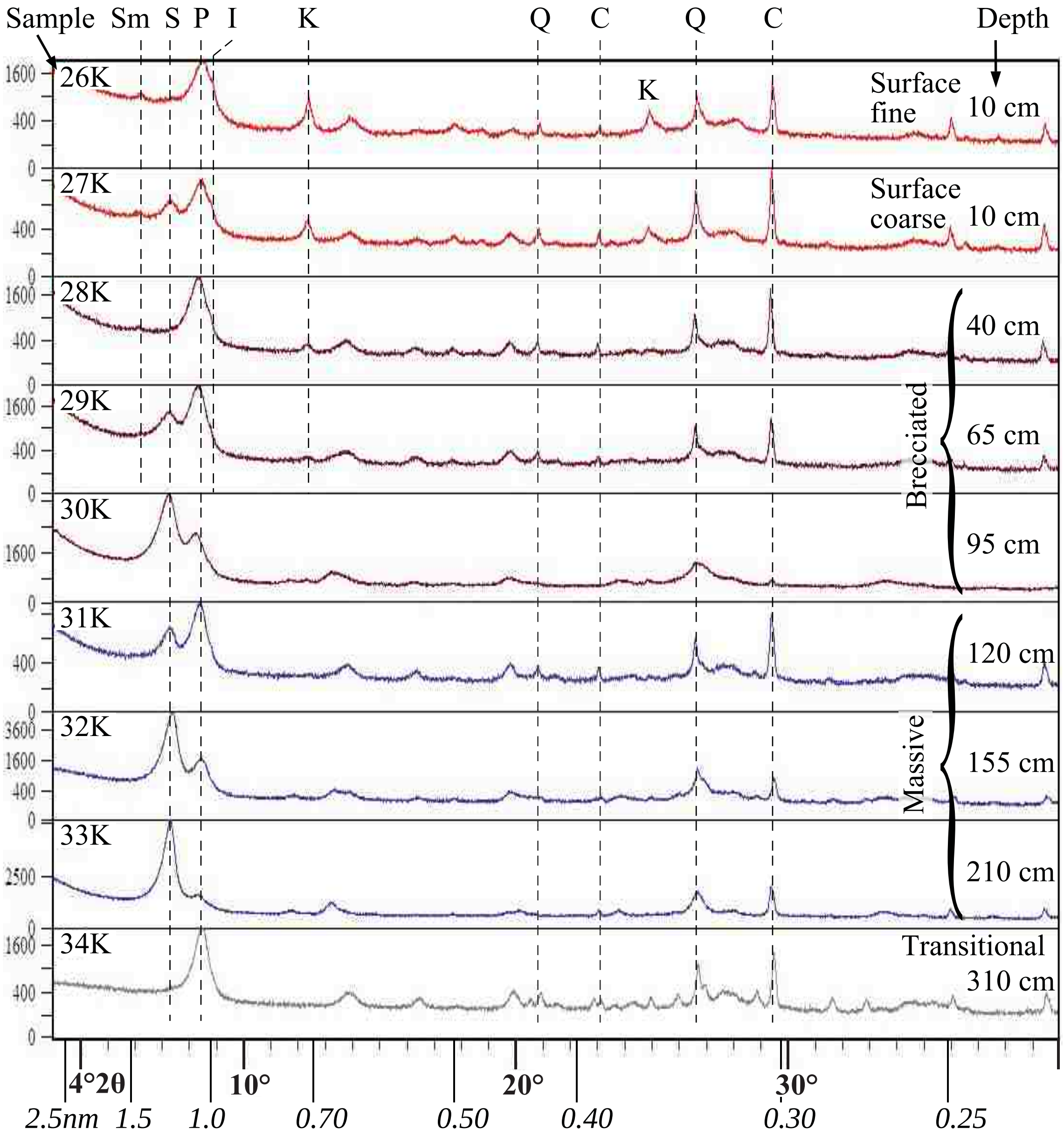

Figure 4.6. XRD spectra for baseline K-saturated Profile MM1-C samples, showing variable mineralogy with depth. Y-axis values are peak counts for each spectrum. X-axis indicates scan angle (°2θ) and d-spacing (nm). Approximate sample depths below the soil surface are indicated to the right of each spectrum. Important mineral peak locations are labeled as C = calcite, I = illite, K = kaolinite, P = palygorskite, Q = quartz, S = sepiolite, and Sm = smectite.

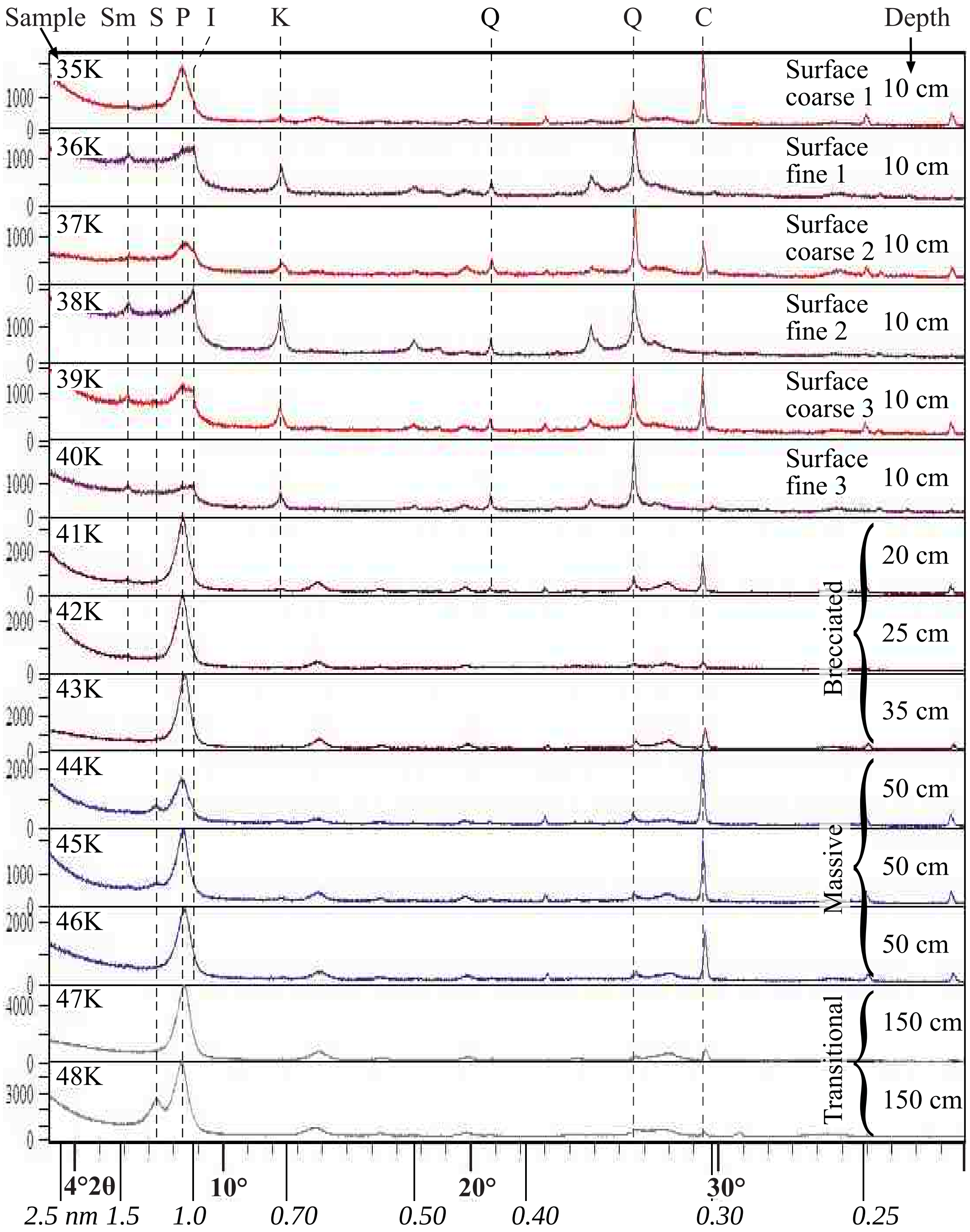

Figure 4.7. XRD spectra for baseline K-saturated Profile MM2 samples. Samples within each horizon are replicates. Y-axis values are peak counts for each spectrum. X-axis indicates scan angle (°2θ) and d-spacing (nm). Approximate sample depths below the soil surface are indicated to the right of each spectrum. Important mineral peak locations are labeled as C = calcite, I = illite, K = kaolinite, P = palygorskite, Q = quartz, S = sepiolite, and Sm = smectite.

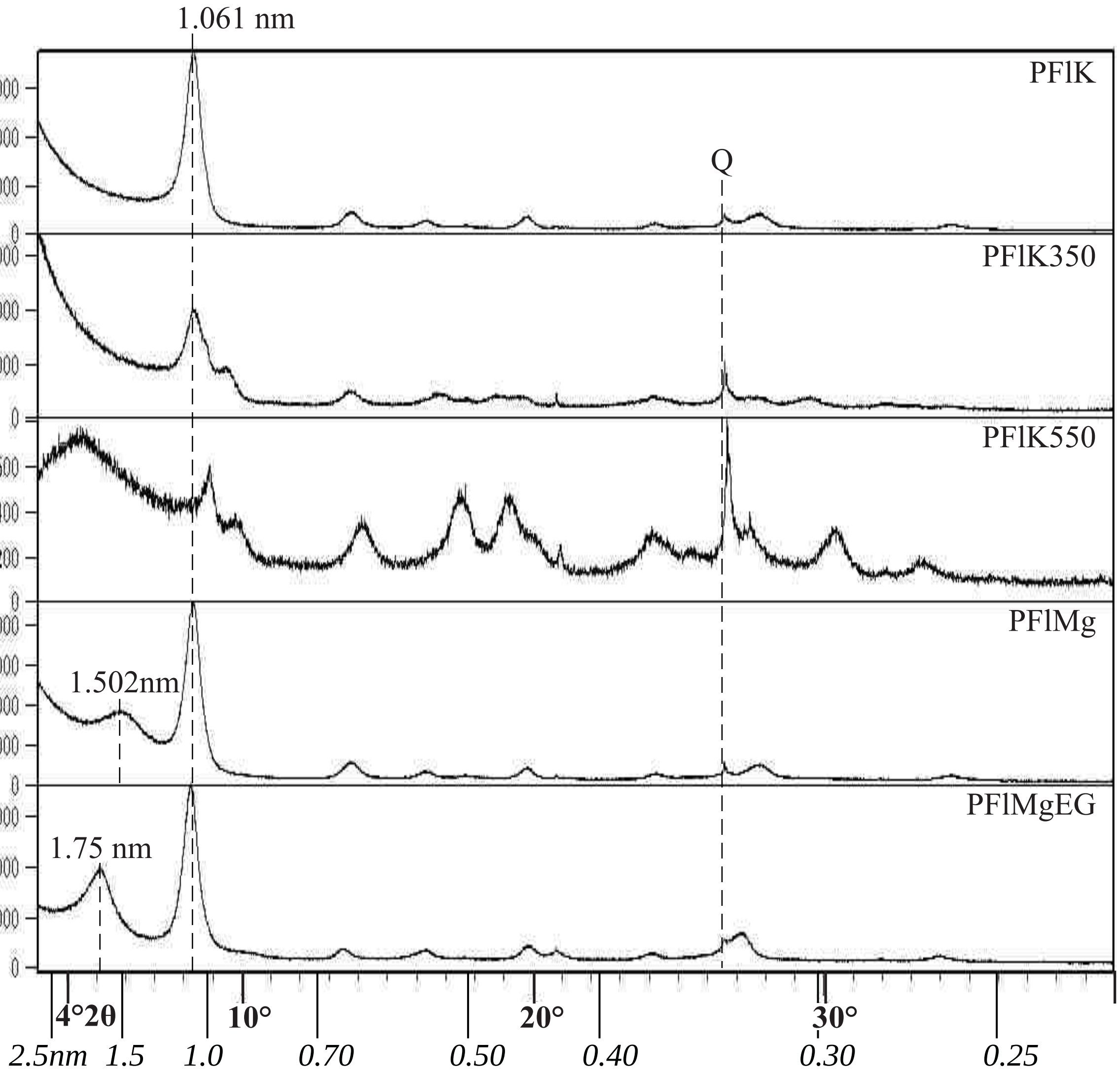

Figure 4.8. XRD spectra for Source Clays Repository palygorskite standard PFl-1 from Gadsden County, Florida. Y-axis units are relative peak counts for each spectrum. X-axis indicates scan angle (°2θ) and d-spacing (nm). Treatments are K-saturation (K), K-saturation heated to 350°C (K350) and 550°C (K550), Mg-saturation (Mg), and Mg-saturation with ethylene glycol solvation (MgEG). Collapse of the 1.061 nm peak with associated development of a small 0.930 nm peak occurs upon heating. Weak expansion of this peak to 1.070 nm occurs after ethylene glycol solvation. Note emergence of a 1.502 nm peak after Mg treatment, and a 1.750 nm peak after ethylene glycol solvation, both of which suggest smectite content. Minor quartz (Q) is also indicated at 0.335 nm in all treatments.

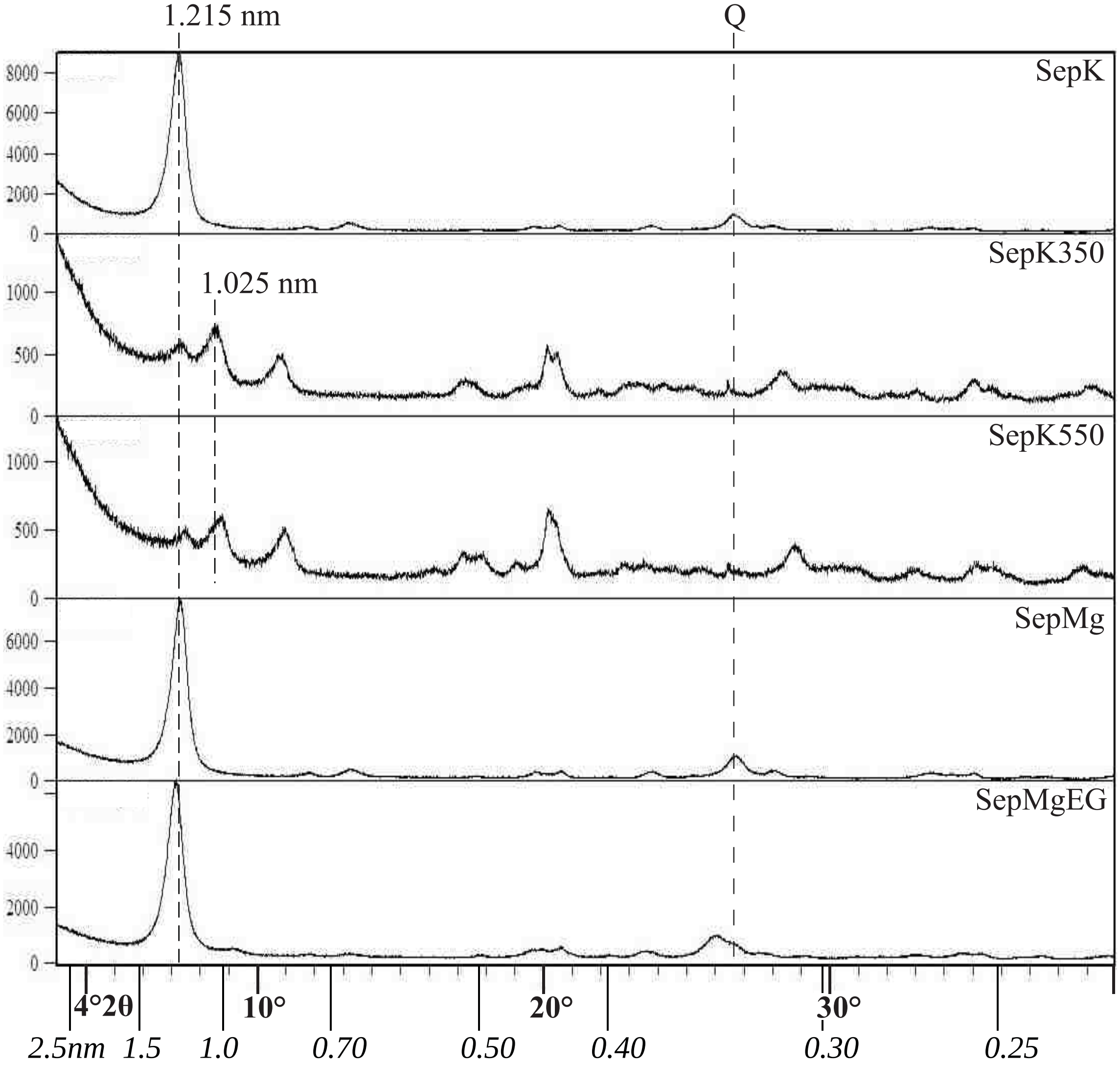

Figure 4.9. XRD spectra for Source Clays Repository sepiolite standard Sep-1 from Valdemore, Spain. Y-axis units are relative peak counts for each spectrum. X-axis indicates scan angle (°2θ) and d-spacing (nm). Treatments are K-saturation (K), K-saturation heated to 350°C (K350) and 550°C (K550), Mg-saturation (Mg), and Mg-saturation with ethylene glycol solvation (MgEG). Note minor expansion of the 1.22 nm peak (to 1.25 nm) after ethylene glycol treatment, and collapse of the same peak with associated development of a small 1.03 nm peak upon heating. Trace quartz (Q) is also detected at 0.34 nm.

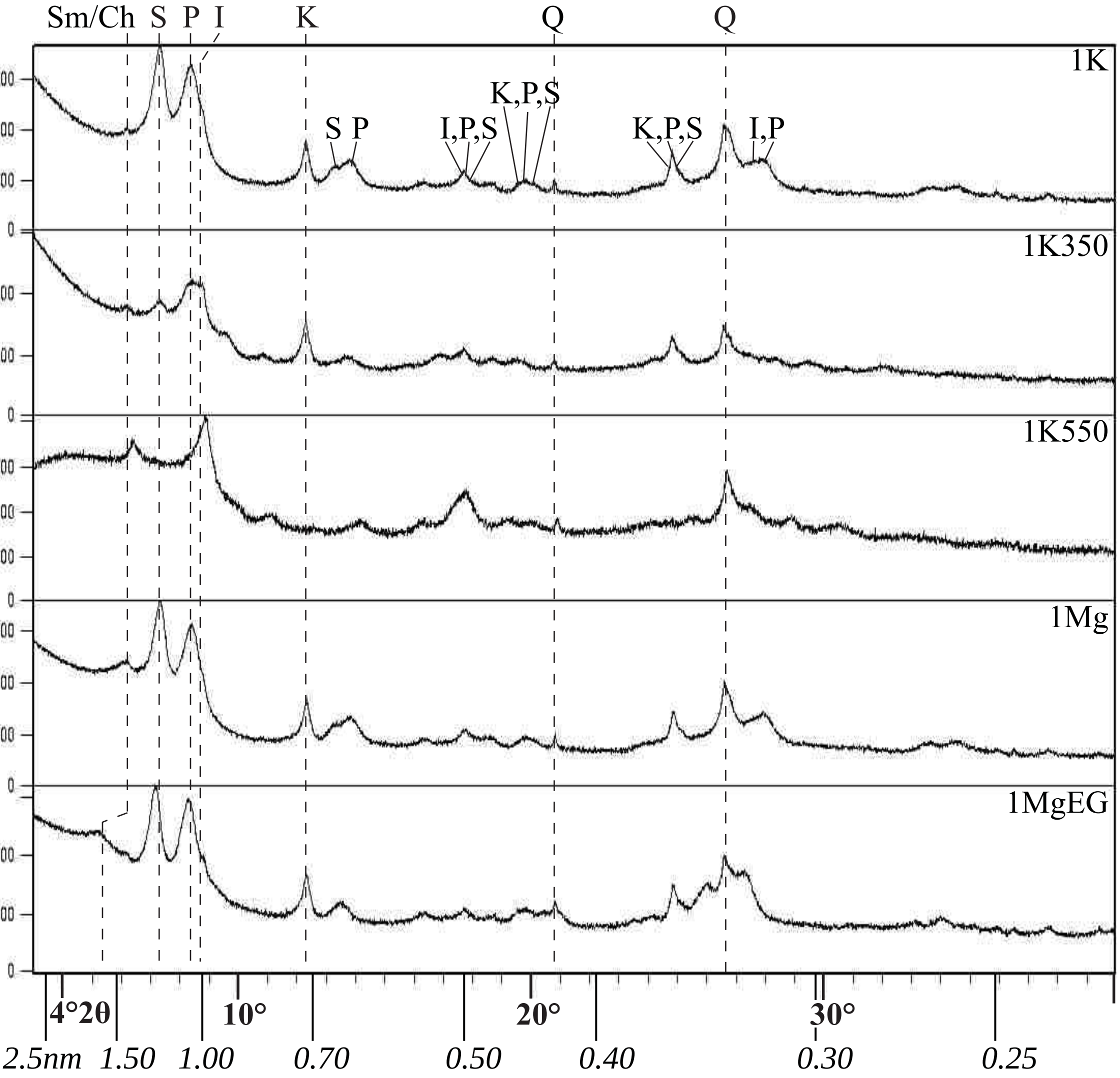

Figure 4.10. XRD spectra for Sample #1 (clay-sized mineralogy of the < 2mm fraction of the surficial rubble horizon of profile MM1-A). Y-axis units are relative peak counts for each spectrum. X-axis indicates scan angle (°2θ) and d-spacing (nm). Treatments are K-saturation (K), K-saturation heated to 350°C (K350) and 550°C (K550), Mg-saturation (Mg), and Mg-saturation with ethylene glycol solvation (MgEG). The sample contains, in order of decreasing relative abundance: sepiolite, palygorskite, kaolinite, quartz, illite, and minor amounts of chlorite/smectite. Diagnostic peaks are indicated as S = sepiolite, P = palygorskite, k = kaolinite, q = quartz, I = illite, Sm/Ch = smectite-chorite.

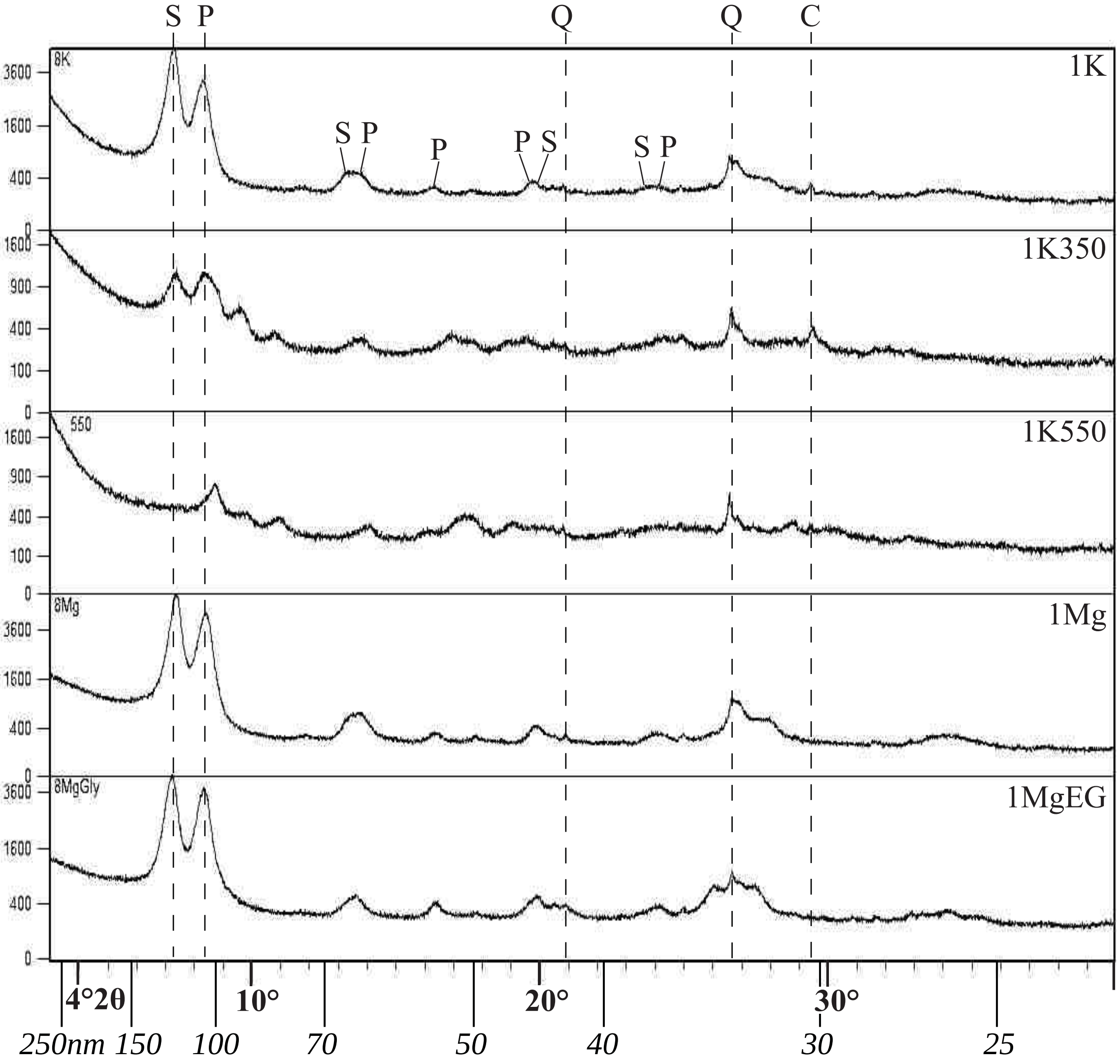

Figure 4.11. XRD spectra for Sample #8 (clay-sized mineralogy at the base of the massive horizon of profile MM1-A). Y-axis units are relative peak counts for each spectrum. X-axis indicates scan angle (°2θ) and d-spacing (nm). Treatments are K-saturation (K), K-saturation heated to 350°C (K350) and 550°C (K550), Mg-saturation (Mg), and Mg-saturation with ethylene glycol solvation (MgEG). The sample contains, in order of decreasing relative abundance: sepiolite, palygorskite, quartz, and minor amounts of calcite. Diagnostic peaks are indicated as S = sepiolite, P = palygorskite, Q = quartz, C = calcite.

Table 4.1. Summary of soil chemical data by genetic horizon.

Horizon	**Statistic**	**pH**	**EC (uS)**	**$CaCO_3$%**	**Moisture (%)**	**SO_4^{2-}(mg/kg)**	**Cl^-(mg/kg)**
Surface, fine (< 2 mm) fraction only	Mean	8.78	88.70	23.93	2.19	4.65	10.88
	Stand. Dev	0.23	11.91	12.33	0.91	1.23	15.00
	Minimum	8.43	69.36	14.53	1.43	2.83	2.14
	Maximum	9.03	103.40	46.78	3.69	5.90	41.06
	n	6	6	6	6	6	6
Surface, coarse (>2 mm) fraction only	Mean	9.01	92.44	75.55	0.69	6.62	13.82
	Stand. Dev	0.18	5.12	4.24	0.30	1.84	7.37
	Minimum	8.80	86.59	70.81	0.29	4.49	7.60
	Maximum	9.20	97.79	82.35	1.12	8.97	23.24
	n	6	6	6	6	4	4
Brecciated	Mean	8.92	360.17	77.49	0.68	44.85	79.41
	Stand. Dev	0.11	397.38	5.62	0.30	38.54	116.03
	Minimum	8.72	81.95	67.22	0.38	13.03	4.56
	Maximum	9.10	1460.00	86.33	1.38	153.27	404.35
	n	12	12	12	12	12	12
Massive	Mean	9.03	258.68	76.79	0.53	76.91	14.93
	Stand. Dev	0.20	148.38	3.44	0.16	68.62	12.53
	Minimum	8.70	69.76	72.09	0.24	20.73	4.95
	Maximum	9.30	581.70	84.55	0.78	259.31	48.50
	n	11	11	11	11	11	11
Transitional	Mean	8.88	1383.80	75.30	1.41	87.23	3145.73
	Stand. Dev	0.42	1461.24	7.60	1.11	82.39	4532.15
	Minimum	8.28	66.70	62.49	0.25	5.48	4.22
	Maximum	9.40	4145.00	87.25	3.49	225.91	12469.51
	n	13	13	13	13	13	13
Muddy Creek	Mean	8.57	384.65	56.64	2.00	137.92	2925.78
	Stand. Dev	0.08	289.07	12.83	0.52	76.95	2865.15
	Minimum	8.47	187.00	46.00	1.56	65.49	60.59
	Maximum	8.63	806.90	74.35	2.59	212.26	6015.65
	n	4	4	4	4	4	4

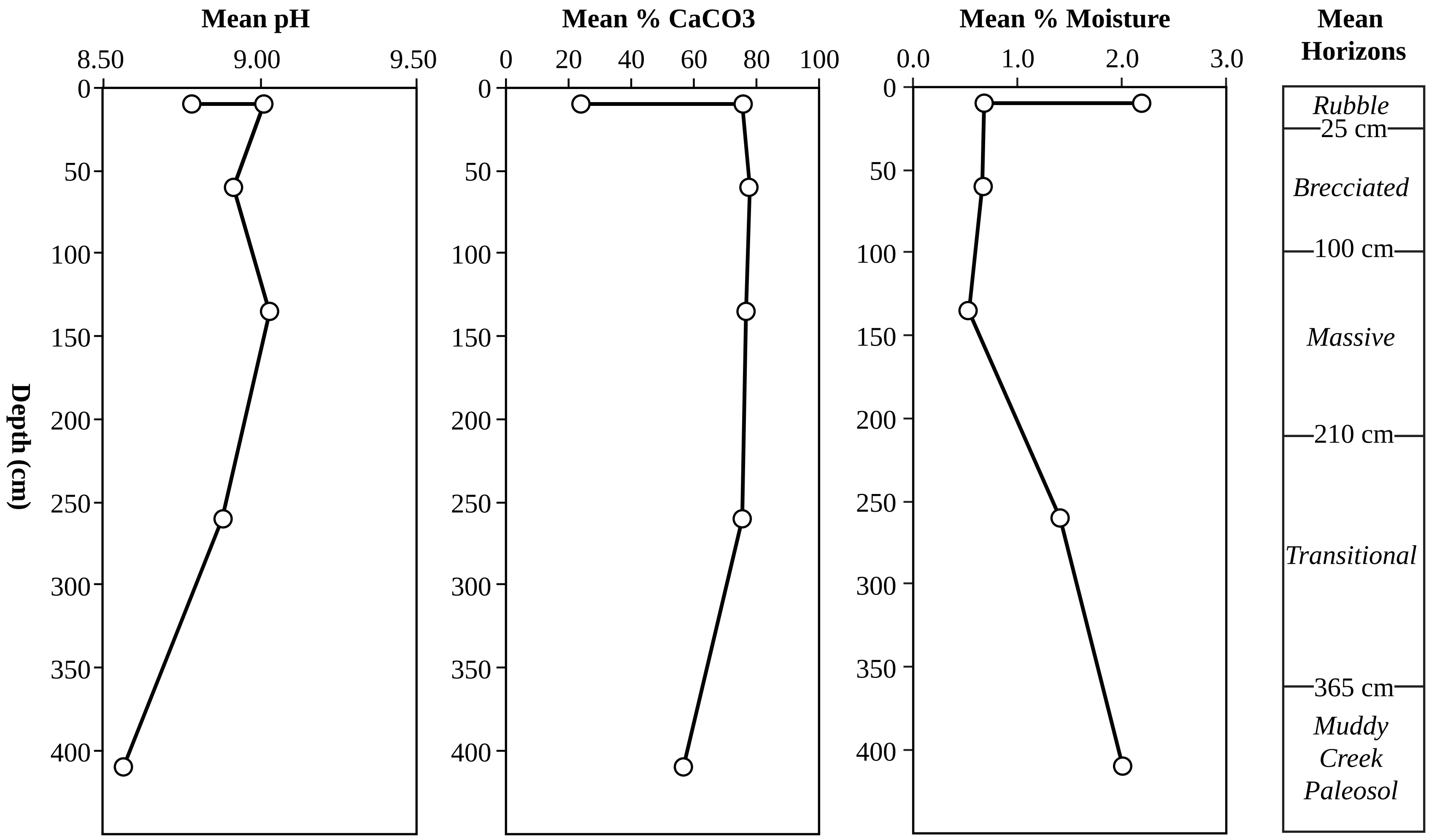

Figure 4.12. Plots of soil pH, percent carbonate equivalence, and percent air-dry soil moisture content with depth below the soil surface. These chemical data represent average values per horizon for all four profiles sampled. Depths are approximate horizon centroid averages for all four profiles, and average horizon contact depths are illustrated in the right-side column.

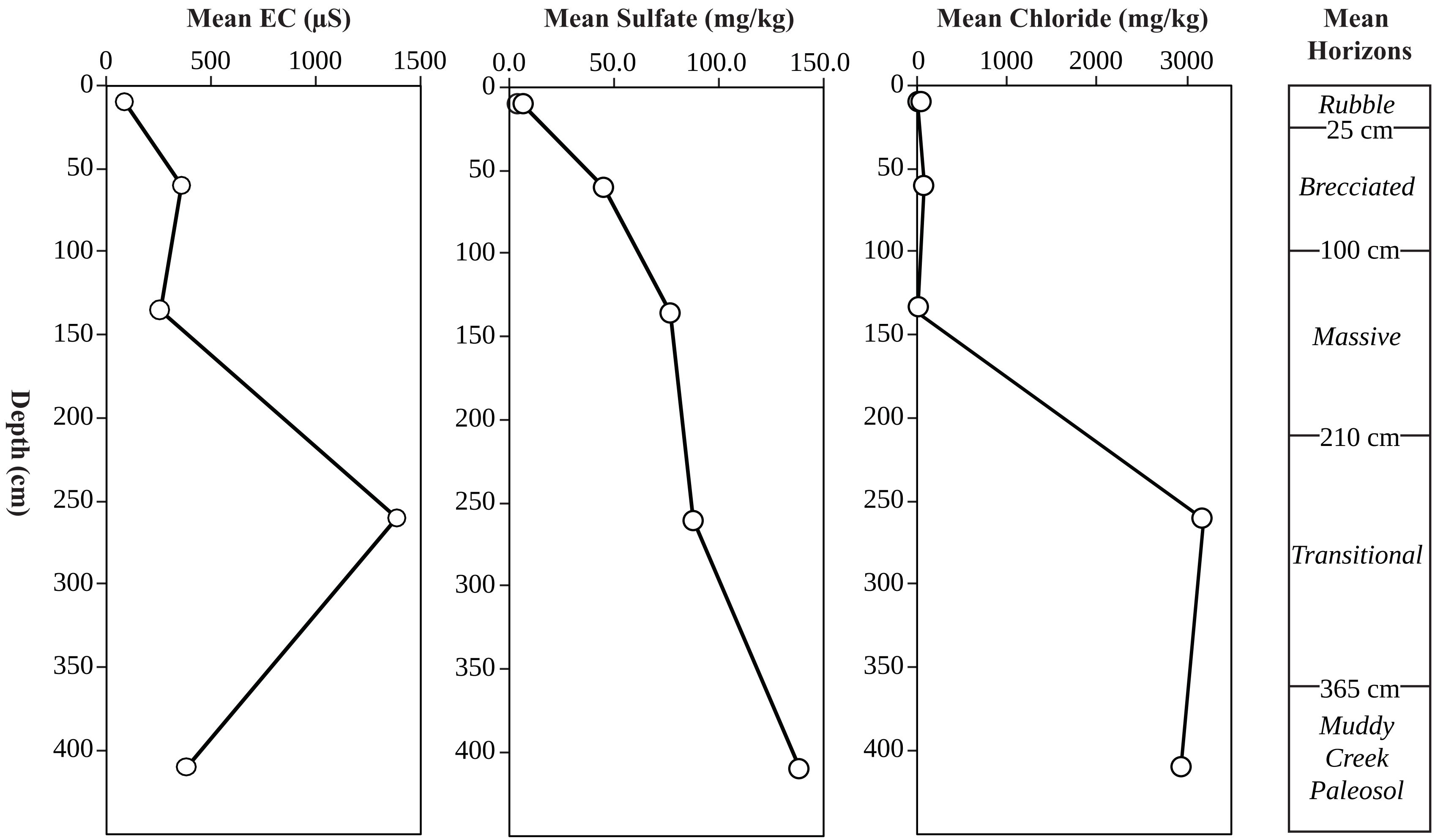

Figure 4.13. Plots of electrical conductivity, available sulfur content, and water soluble chloride content with depth below the soil surface. These chemical data represent average values per horizon for all four profiles sampled. Depths are approximate horizon centroid averages for all four profiles, and average horizon contact depths are illustrated in the right-side column.

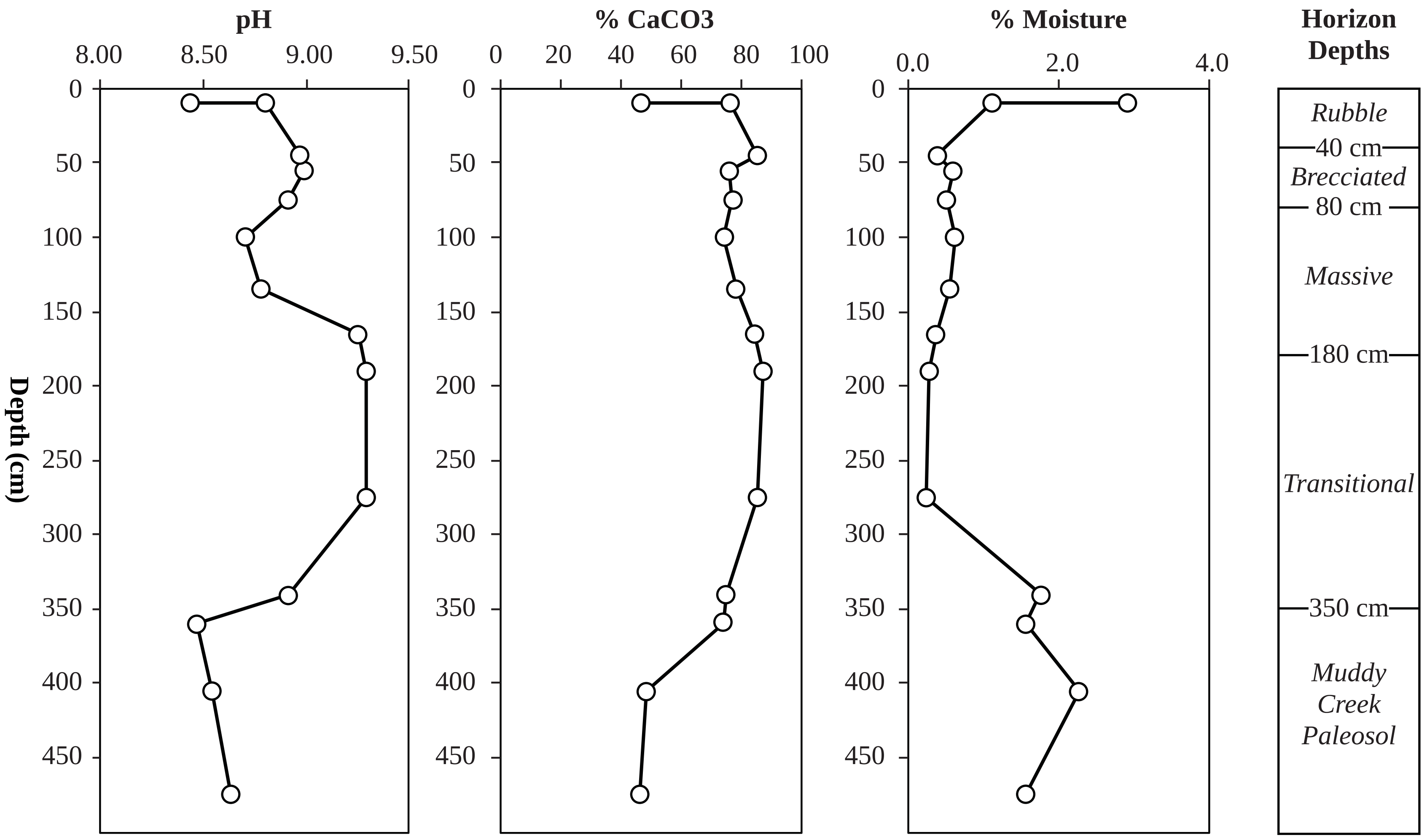

Figure 4.14. Plots of soil pH, percent calcium carbonate equivalence, and percent air-dry soil moisture content with depth below the soil surface for Profile MM1-A. Horizon contacts are also indicated.

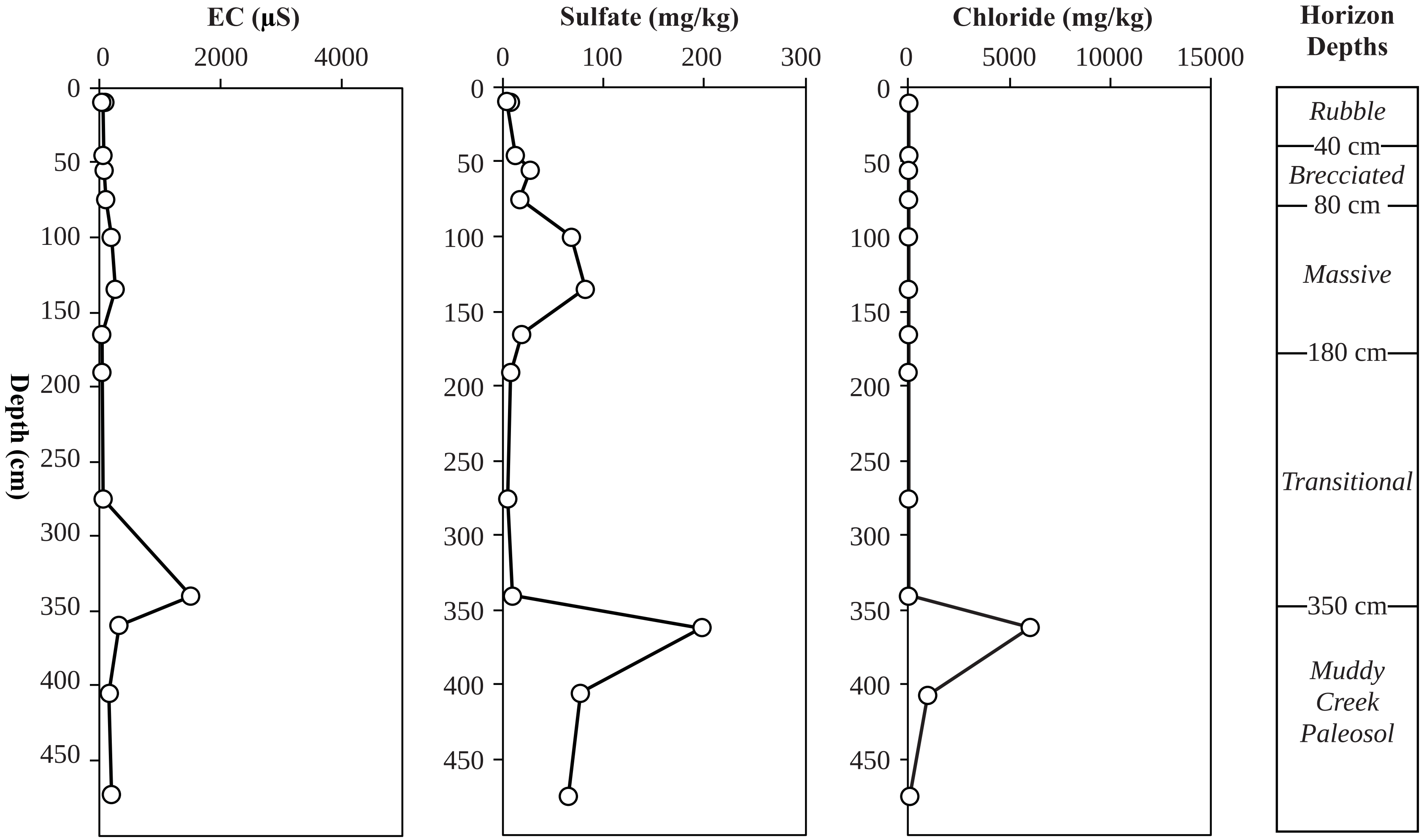

Figure 4.15. Plots of electrical conductivity, available sulfur content, and water soluble chloride content with depth below the soil surface for Profile MM1-A. Horizon contacts are also indicated.

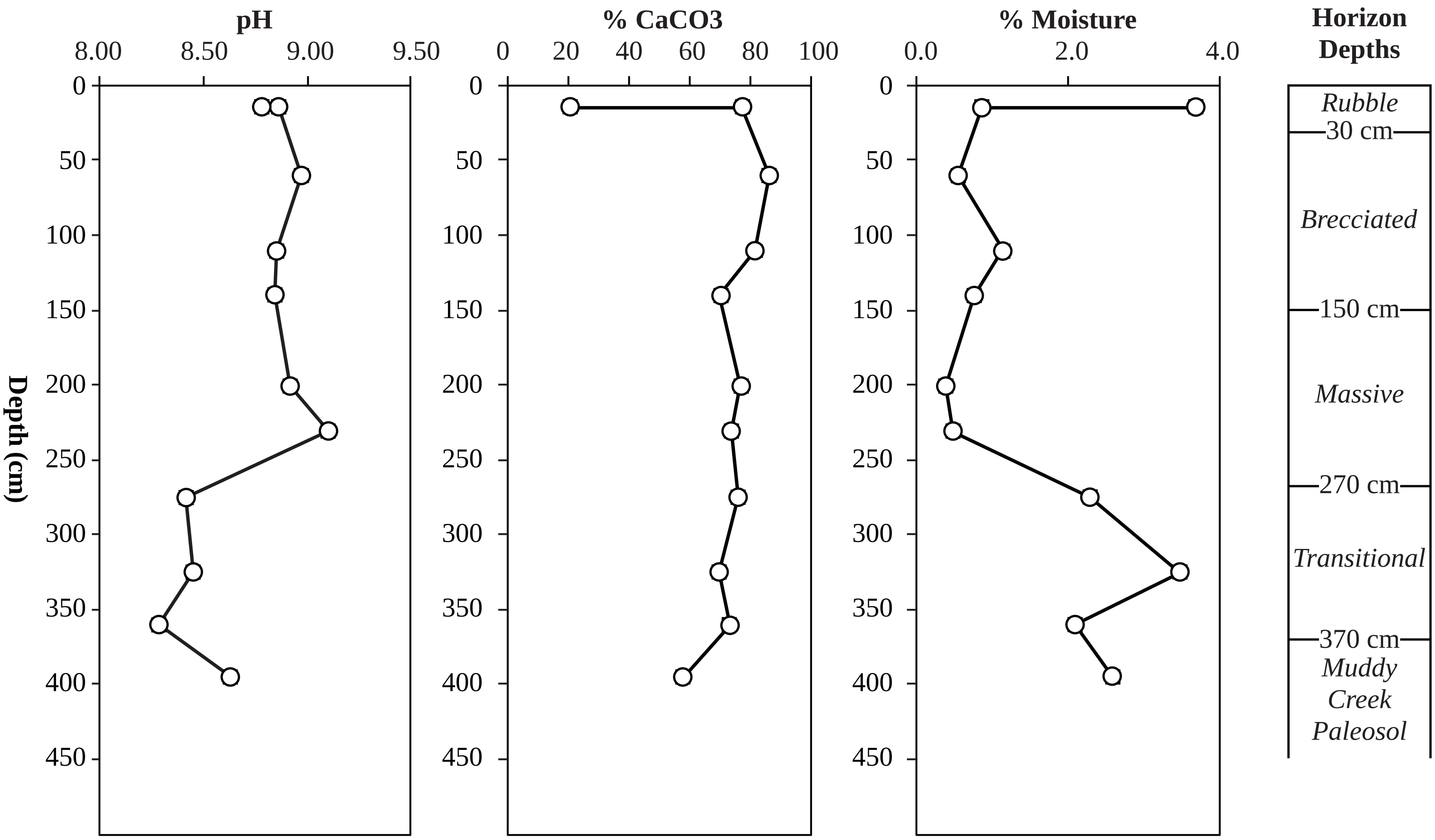

Figure 4.16. Plots of soil pH, percent calcium carbonate equivalence, and percent air-dry soil moisture content with depth below the soil surface for Profile MM1-B. Horizon contacts are also indicated.

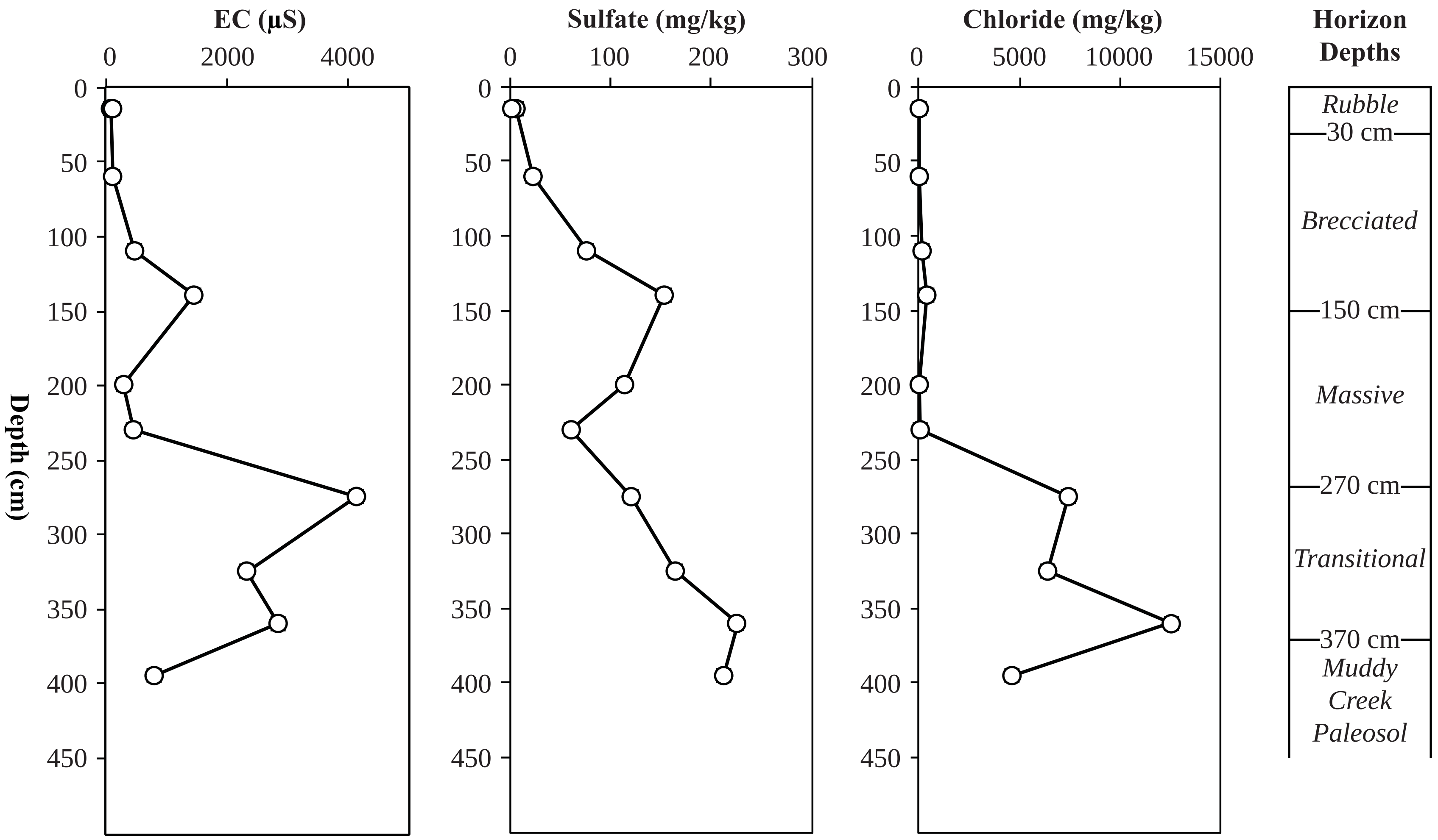

Figure 4.17. Plots of electrical conductivity, available sulfur content, and water soluble chloride content with depth below the soil surface for Profile MM1-B. Horizon contacts are also indicated.

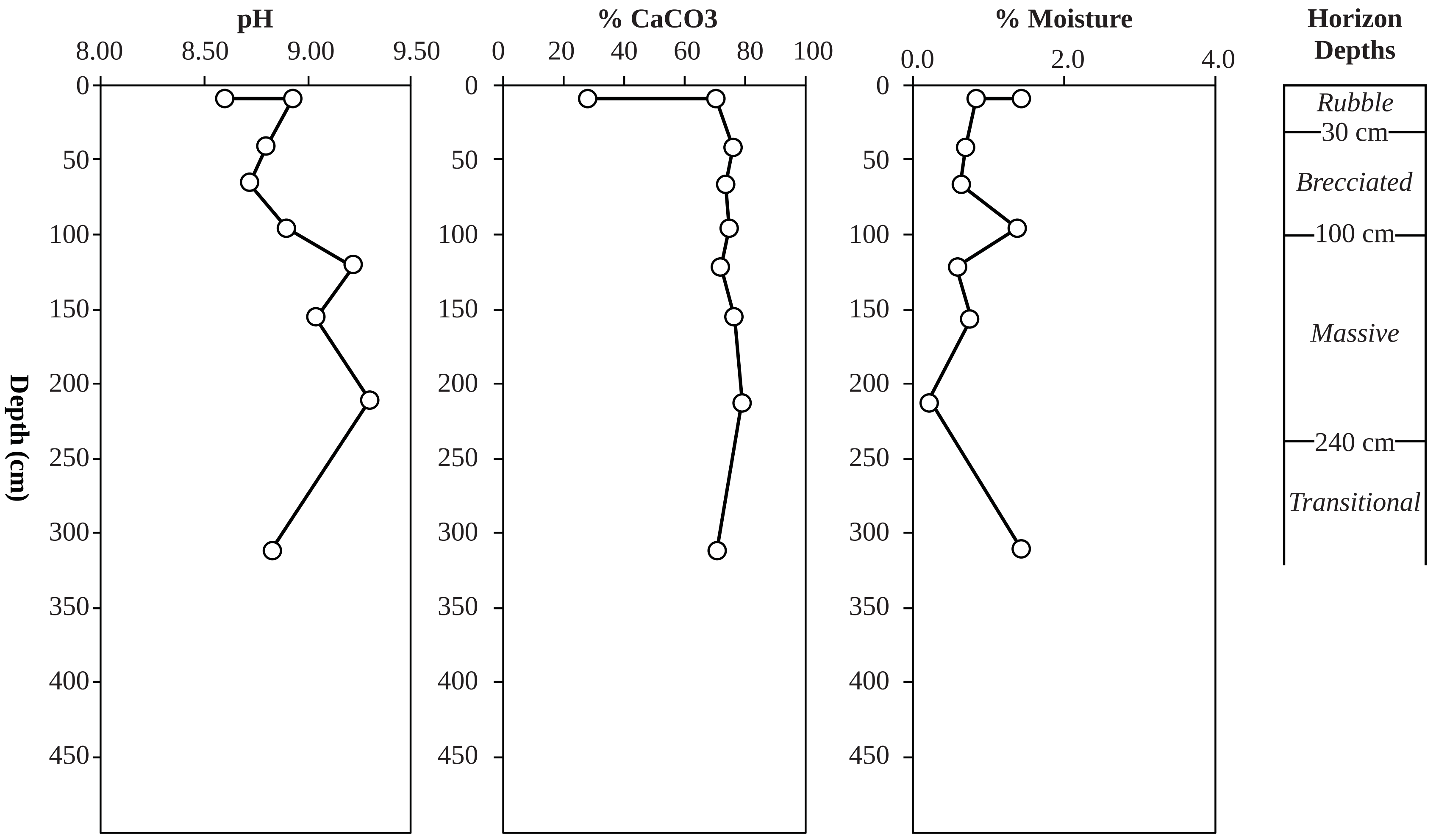

Figure 4.18. Plots of soil pH, percent calcium carbonate equivalence, and percent air-dry soil moisture content with depth below the soil surface for Profile MM1-C.

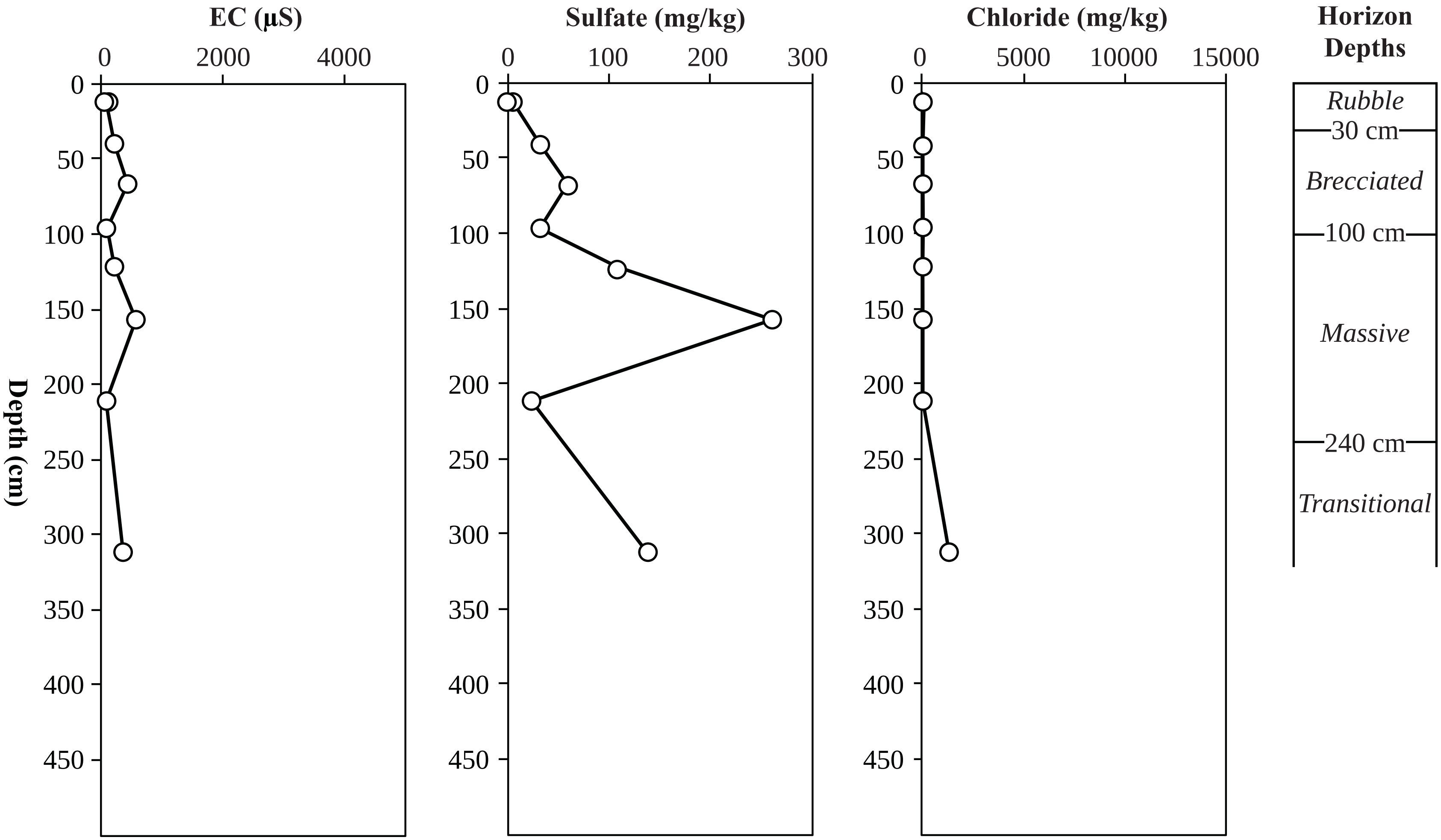

Figure 4.19. Plots of electrical conductivity, available sulfur content, and water soluble chloride content with depth below the soil surface for Profile MM1-C.

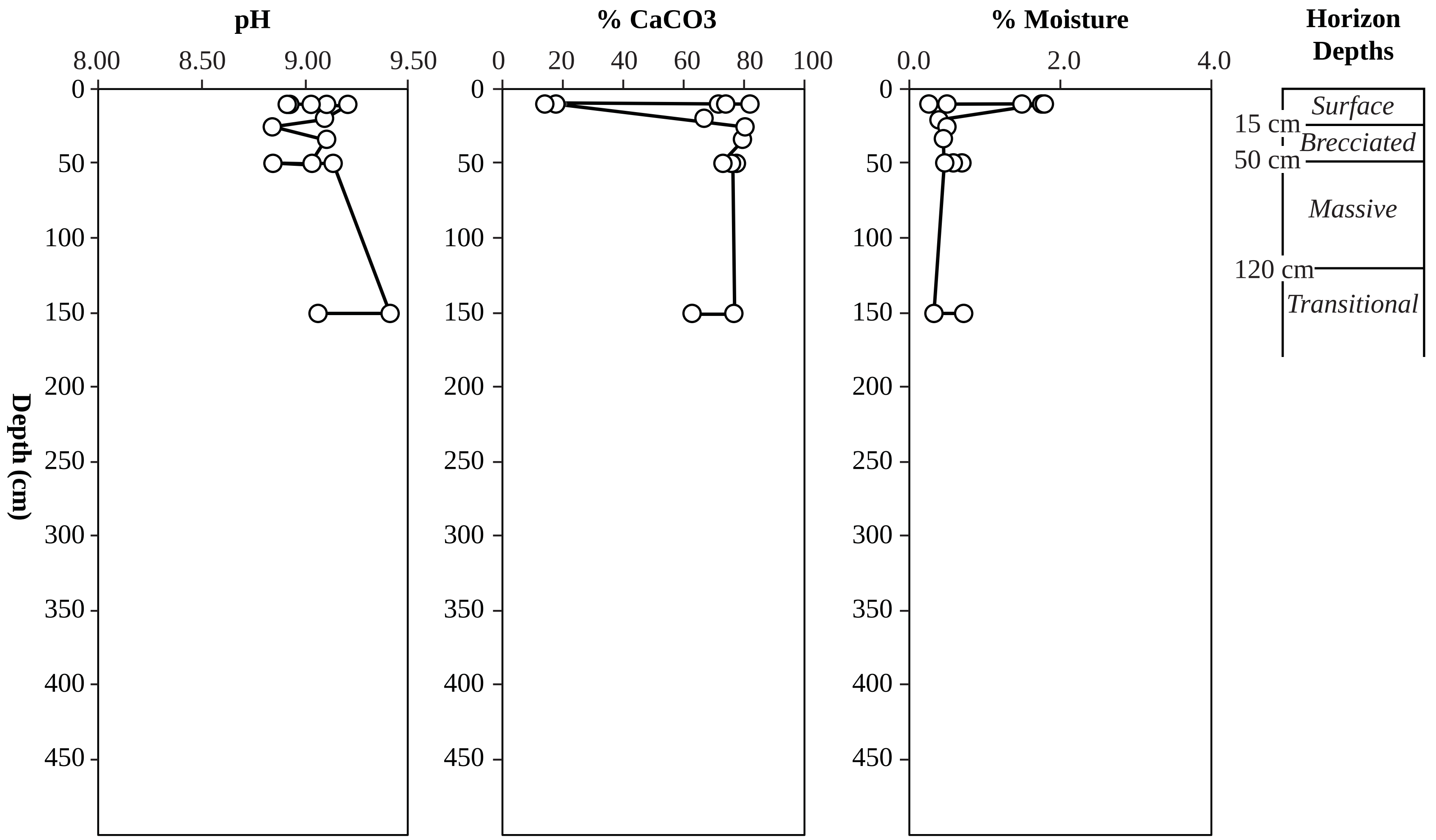

Figure 4.20. Plots of soil pH, percent calcium carbonate equivalence, and percent air-dry soil moisture content with depth below the soil surface for Profile MM2.

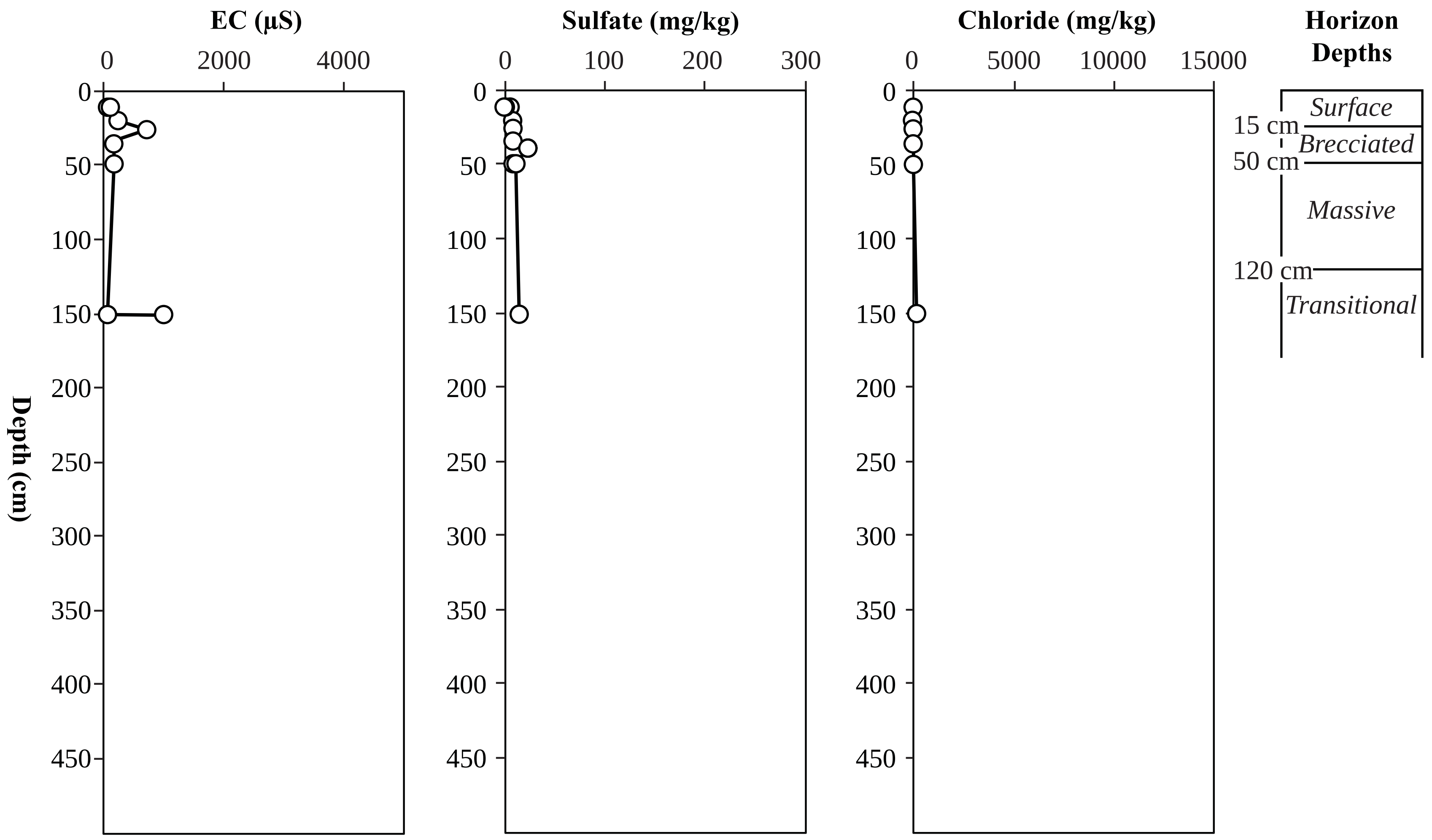

Figure 4.21. Plots of electrical conductivity, available sulfur content, and water soluble chloride content with depth below the soil surface for Profile MM2.

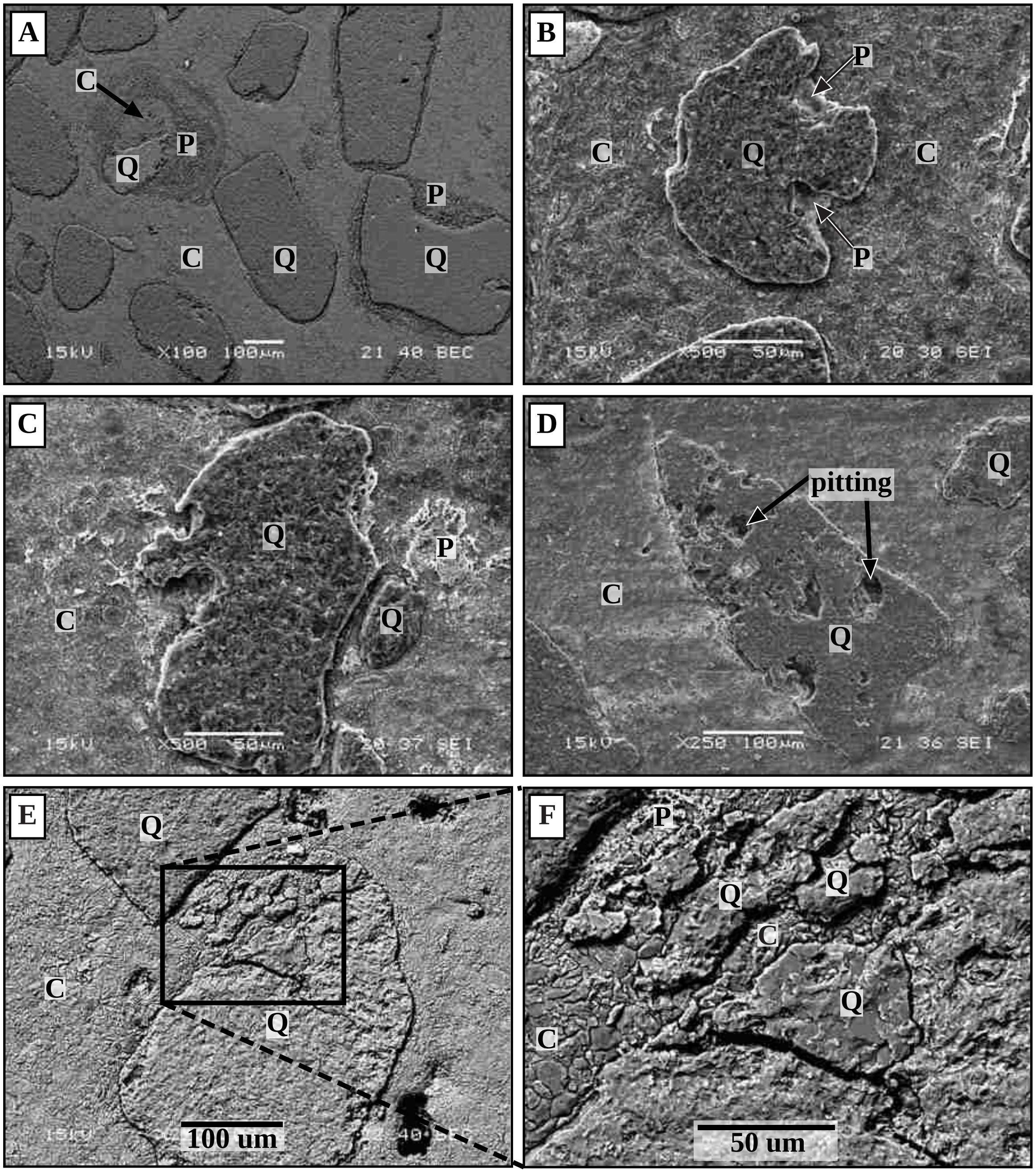

Figure 4.22. SEM-EDS data. (A) Quartz grains ‘floating’ in a matrix of pedogenic carbonate and fibrous silicate clay. Coats of concentrated fibrous clay are common around most grains, including features with mixed quartz and calcite cores. (B) Embayed quartz grain, showing fibrous clay growth concentrating within the embayments. (C) Embayed quartz grain, showing calcite filling the embayments. (D) Pitted quartz grain, with some carbonate and minor fibrous clay growth within the pits. (E) Backscatter image of a fractured quartz grain. Pedogenic carbonate entirely fills zones between the quartz fragments. (F) Contrast-adjusted close-up of grain fragments within the black rectangle in image (E). Note: Up is to the right in all images. C = carbonate, P = fibrous silicate clay (palygorskite and/or sepiolite), Q = quartz.

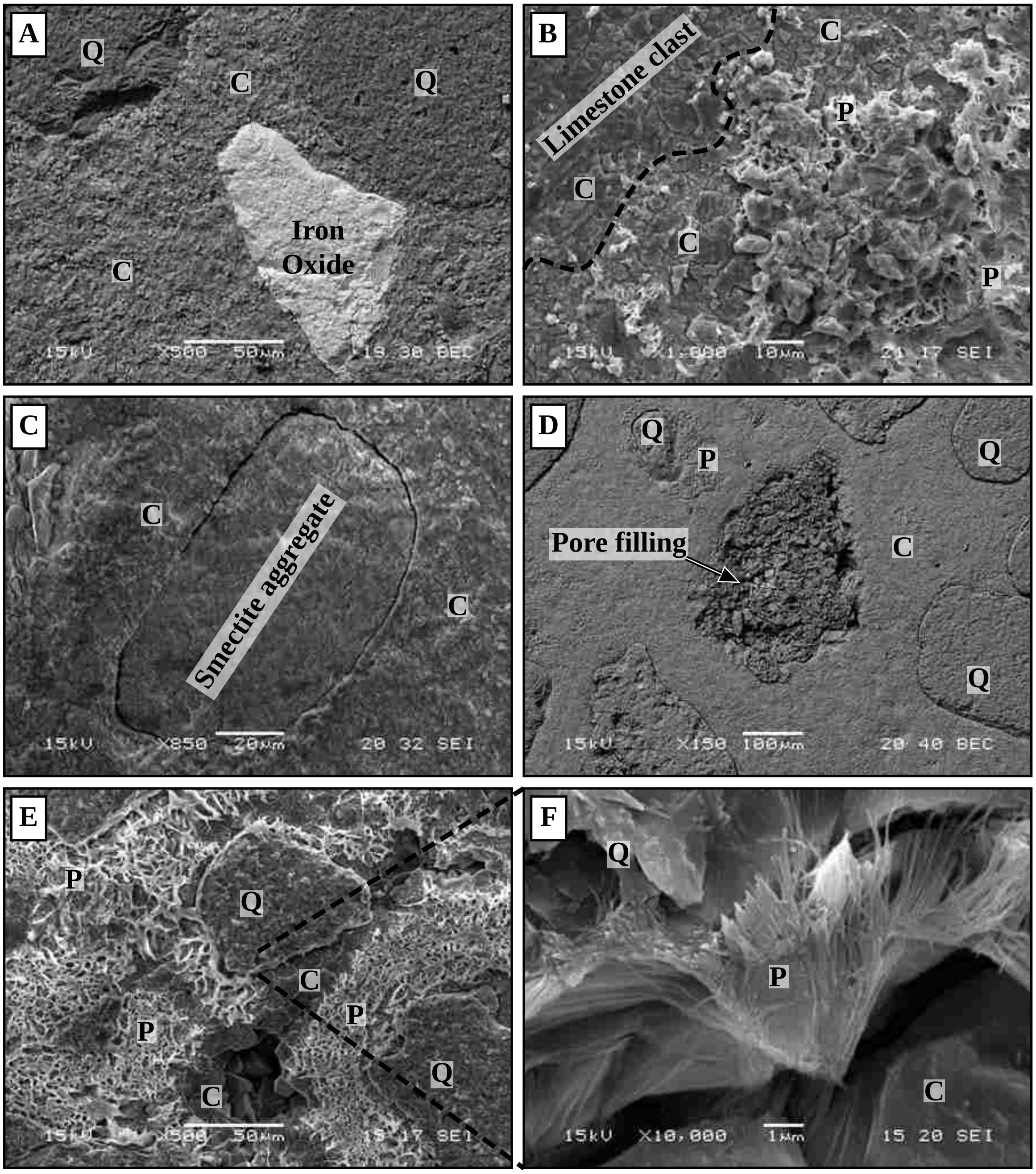

Figure 4.23. SEM-EDS data. (A) Typical backscatter image of a detrital iron-oxide grain. (B) Indistinct contact (dashed line) between a limestone pebble and the indurated petrocalcic soil matrix. (C) Detrital phyllosilicate aggregate with sharp edges. (D) Infilled soil pore containing a mixture of clay- to fine sand-sized silicates. (E) Typical fabric of carbonate and fibrous phyllosilicate matrix. Fibrous clays stand out as a high relief, pale mesh in secondary electron images. (F) close-up of delicate palygorskite or sepiolite fibers within the black rectangle in (E). Note: up is to the right in all images. C = carbonate, P = fibrous silicate clay (palygorskite and/or sepiolite), Q = quartz.

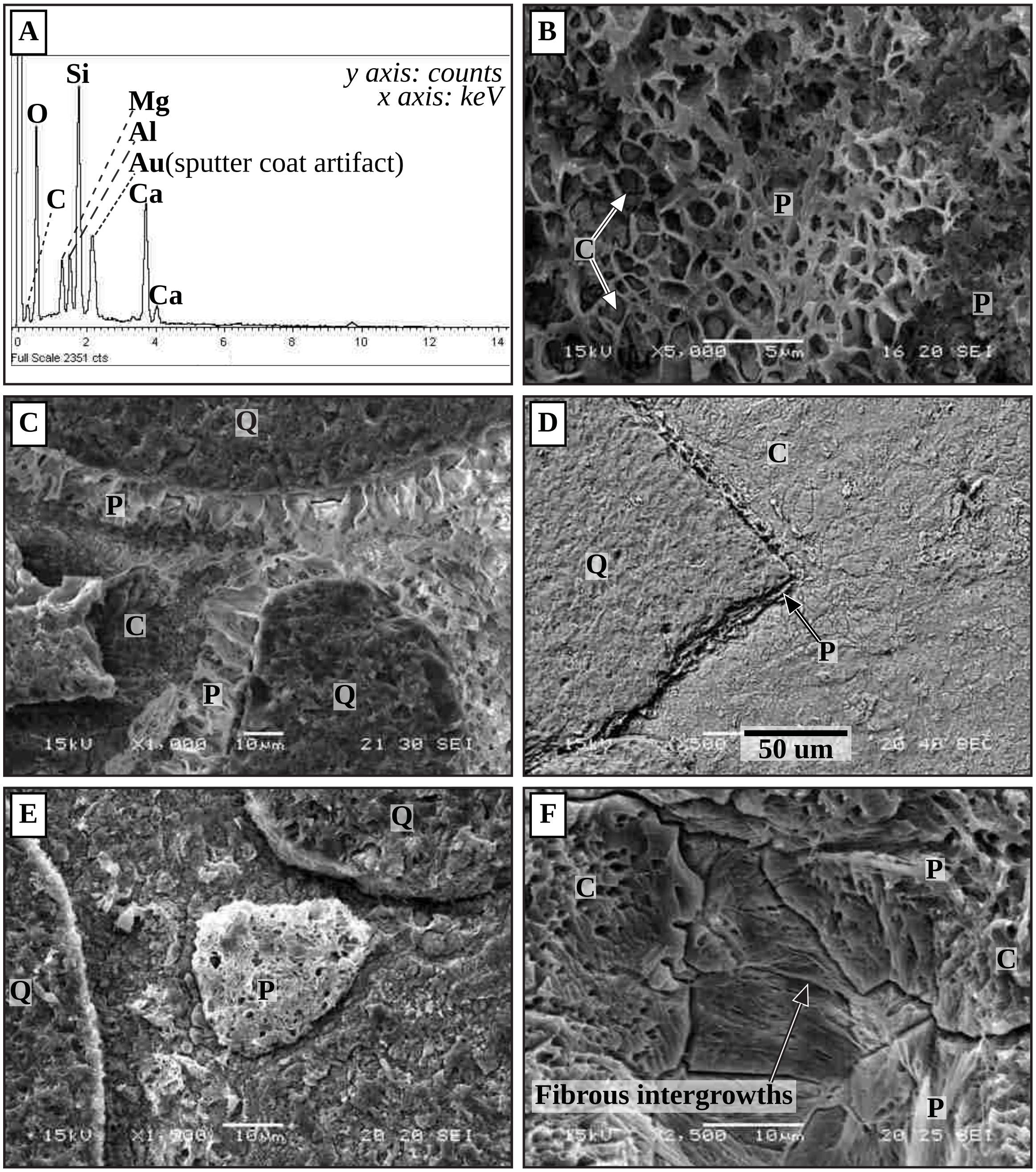

Figure 4.24. SEM-EDS data. (A) Typical EDS spectrum of fibrous palygorskite/sepiolite clay with unavoidable calcite peaks. (B) Skeletal mat of fibrous Mg-phyllosilicates interwoven with pedogenic carbonate. Rhombohedral or prismatic pores closely resemble pedogenic carbonate crystal shapes. (C) Fibrous clays coating and radiating outwards from quartz grains. These coats closely parallel grain surfaces, as can be seen by the acute angles in (D). (E) Porous mass of fibrous clay. (F) Intergrowths of fibrous clays and calcite enhanced by etching with HCl. Note: Up is to the right in all SEM images. C = carbonate, P = fibrous silicate clay (palygorskite and/or sepiolite), Q = Quartz.

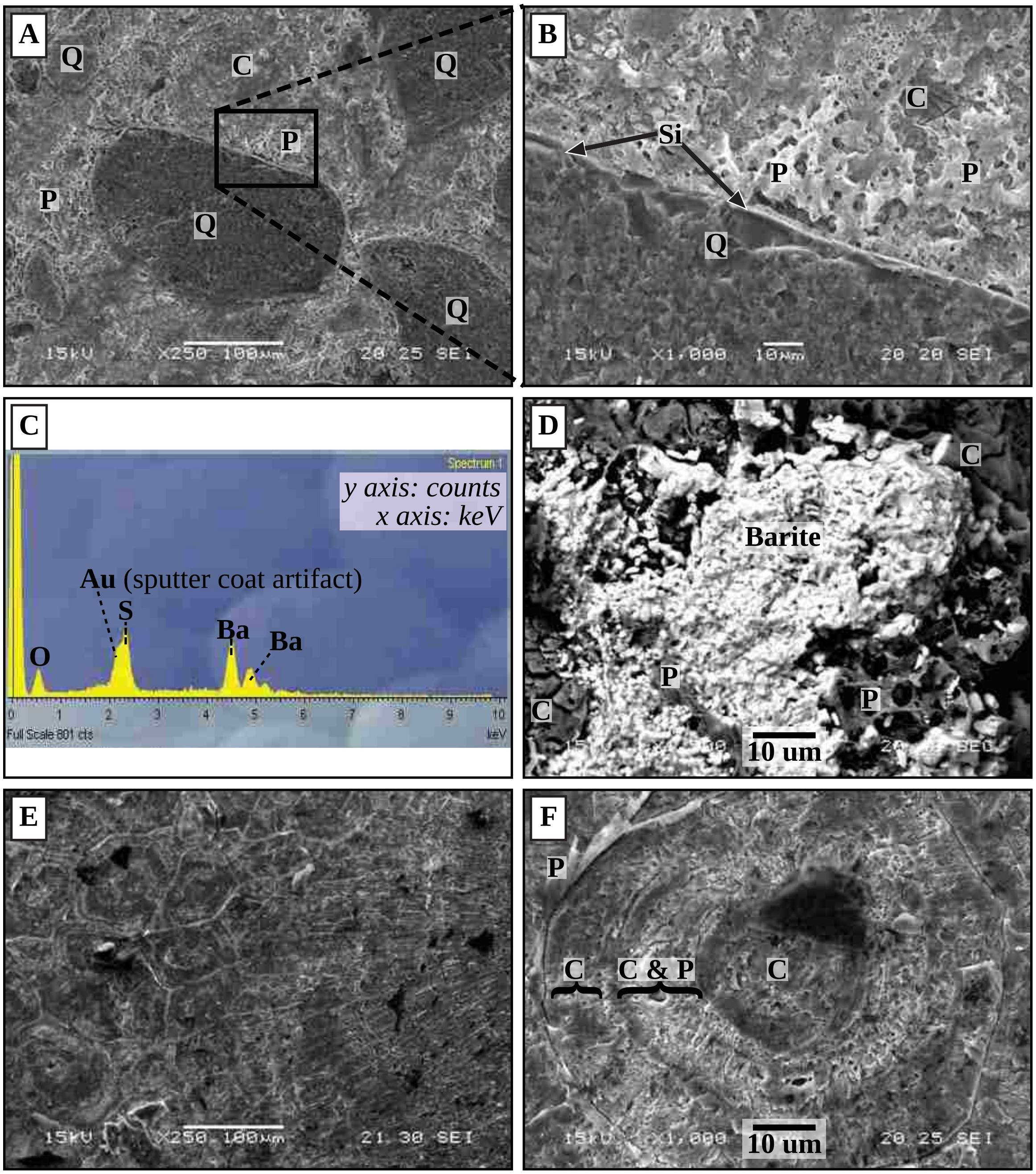

Figure 4.25. SEM-EDS data. (A) Quartz grain with a silan (amorphous silica coating). (B) Close-up image of the silan in (A). (C) Typical EDS spectrum for pedogenic barite in this study. (D) Concentration of subhedral barite (BaSO4) crystals found in association with calcite and fibrous Mg-phyllosilicates. Backscatter image. (E) Concentrically zoned pedogenic carbonate abutting a zone of radial, prismatic calcite. (F) Close-up of concentric growth zones comprised of pedogenic carbonate, or pedogenic carbonate and clay. Dark grain is a dust particle. Note: Up is to the right in all images. C = carbonate, P = fibrous silicate clay (palygorskite and/or sepiolite), Q = Quartz, Si = amorphous silica.

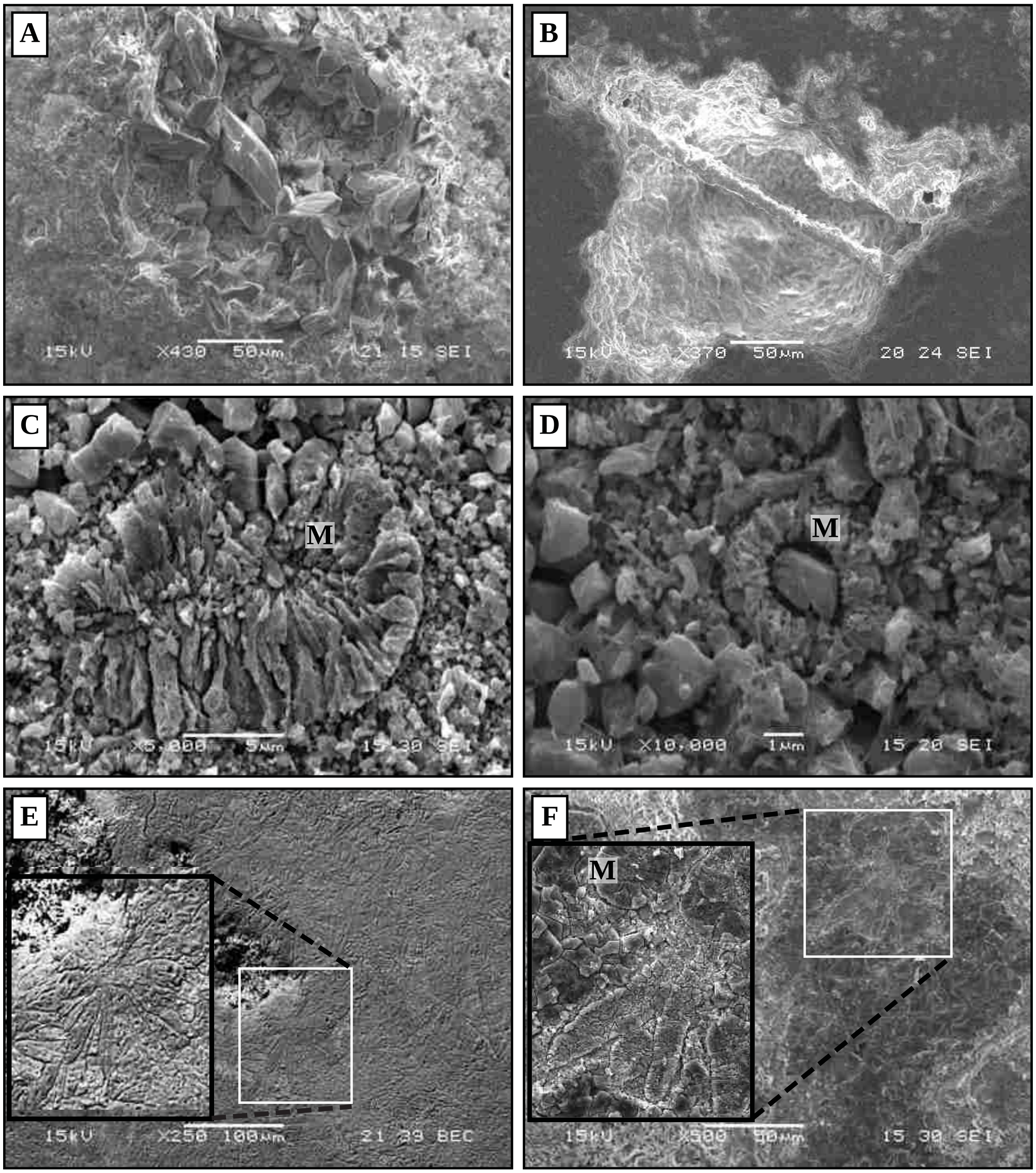

Figure 4.26. SEM-EDS data. (A) Calcite rhombohedra in a pore space. (B) A common example of a calcified root or fungal filament. (C) and (D) The two common morphological features identified as *Microcodium*. Both morphologies are composed of bladed to prismatic calcite and fibers of palygorskite or sepiolite. (E) Radial calcite "starbursts" of possible biogenic origin. The inset is a contrast-enhanced close-up of the white rectangle. (F) Lobate, radial features of probable biogenic origin, possibly related to *Microcodium*, also present here. The inset image is a contrast-enhanced close-up of the white rectangle. Note: Up is to the right in all images. M = *Microcodium.*

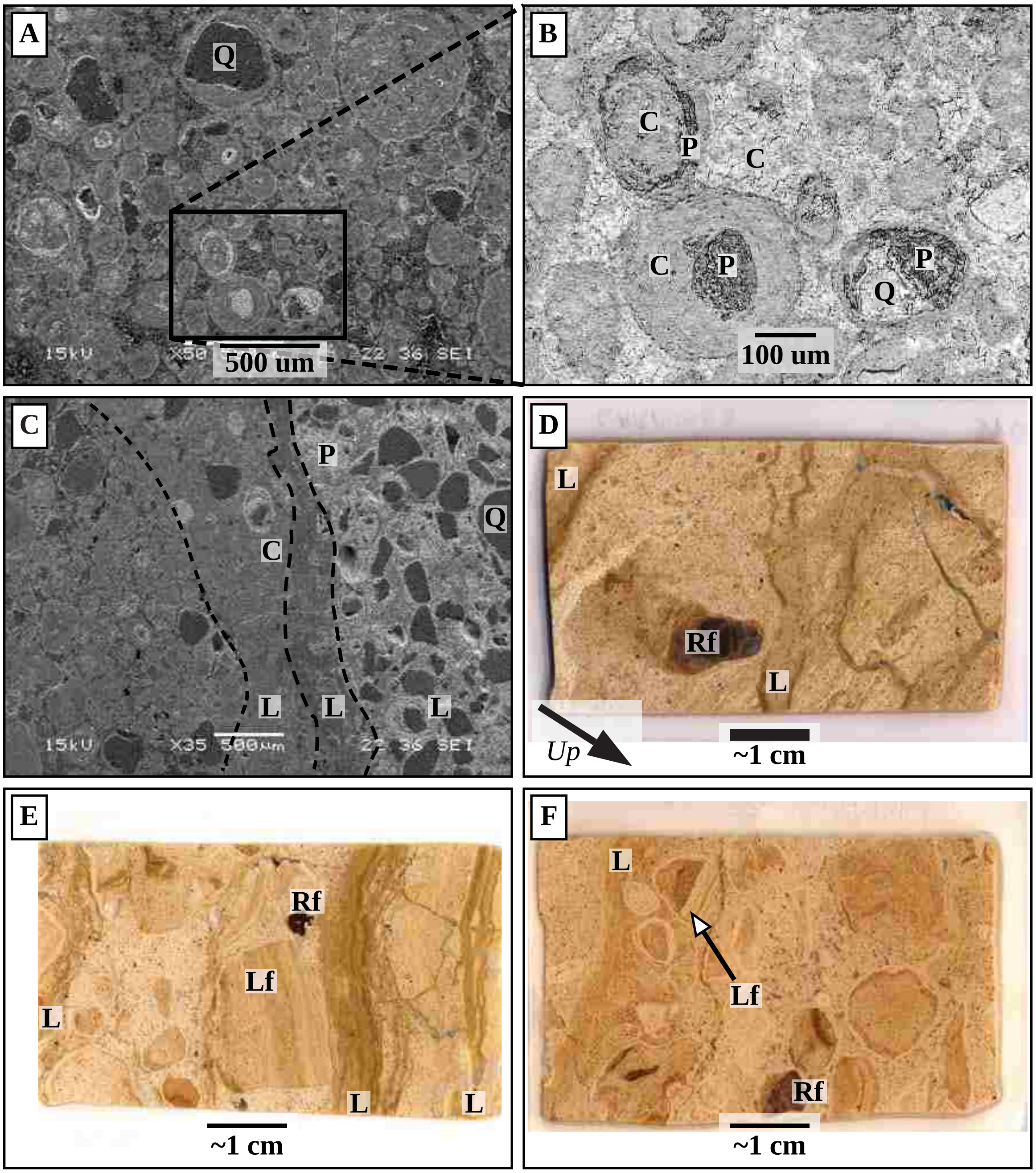

Figure 4.27. SEM-EDS data and thick section photographs. (A): Pisolites and ooids, with varying cores of quartz, carbonate, and palygorskite and/or sepiolite. Rings of fibrous clay within the structures are not uncommon. (B) Enlarged portion of (A), showing concentric, alternating mineralogy. (C) Laminar zones, indicated by dashed lines, including laminae dominated by fibrous clay and floating quartz grains (right), calcium carbonate (middle), and pisolitic textured soil (left). (D-F) Three thick sections studied in SEM, prior to sputter coating (color/contrast enhanced scans). Note laminae, laminar fragments, pendants, and fractures. Up is to the right in all images except where indicated. C = carbonate, L = laminar layer, Lf = laminar fragment, P = fibrous silicate clay (palygorskite and sepiolite), Q = Quartz, Rf = rock fragment.

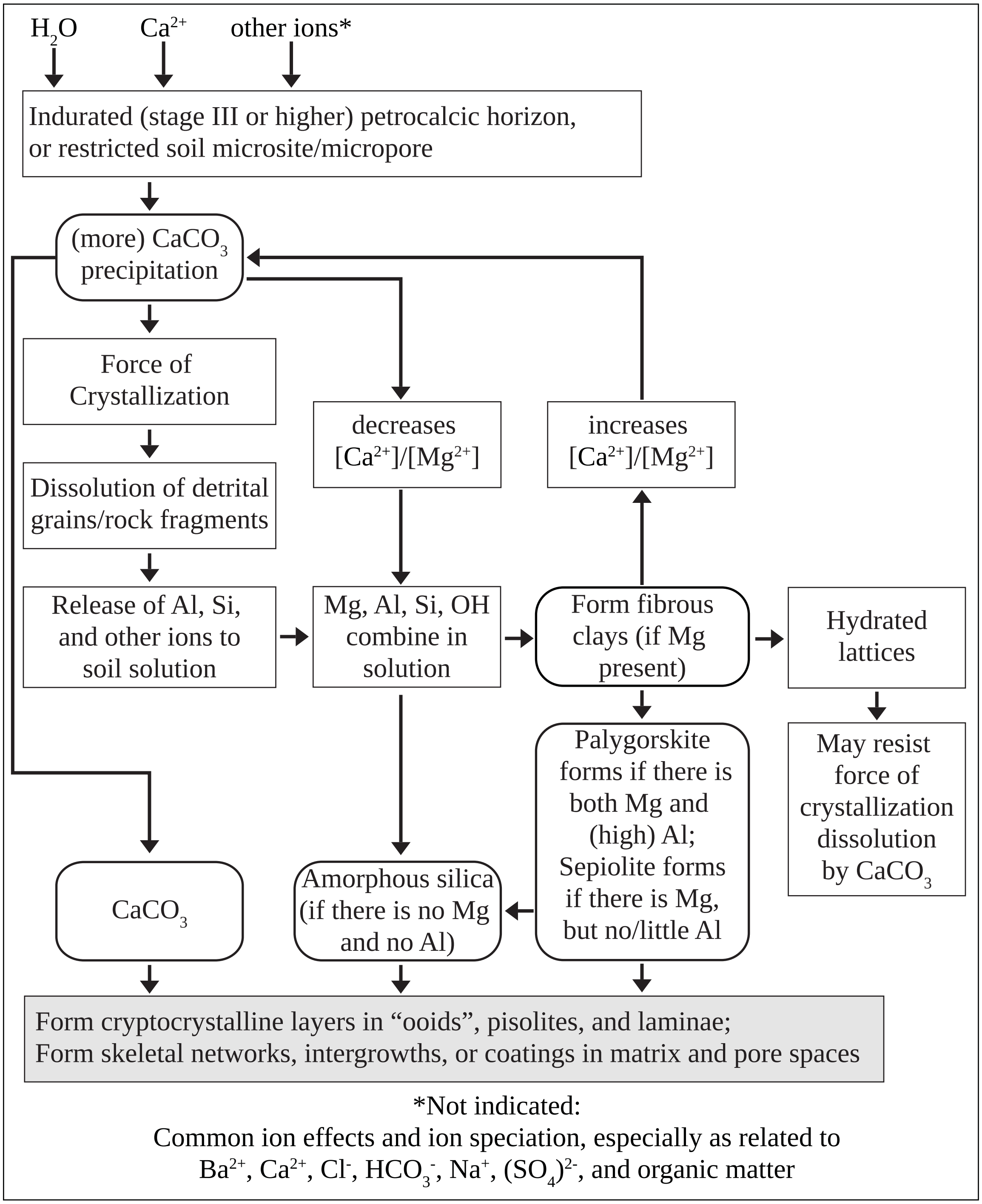

Figure 4.28. Generalized mineral genesis model for calcite, palygorskite and/or sepiolite, and silica in calcic and petrocalcic soil horizons. This model starts with a plugged (stage III or higher) calcic horizon, but also applies to any microsite (e.g., in pendants or laminae) indurated with carbonate and in which displacive crystal growth cannot occur. Solutions may migrate within or out of the horizon or microsite. Final mineral locations and morphologies depend on: ion concentrations, solution flux rates, ion solubility/ mobility, solution evaporation rate (both across the horizon and within micropores), and many other factors.

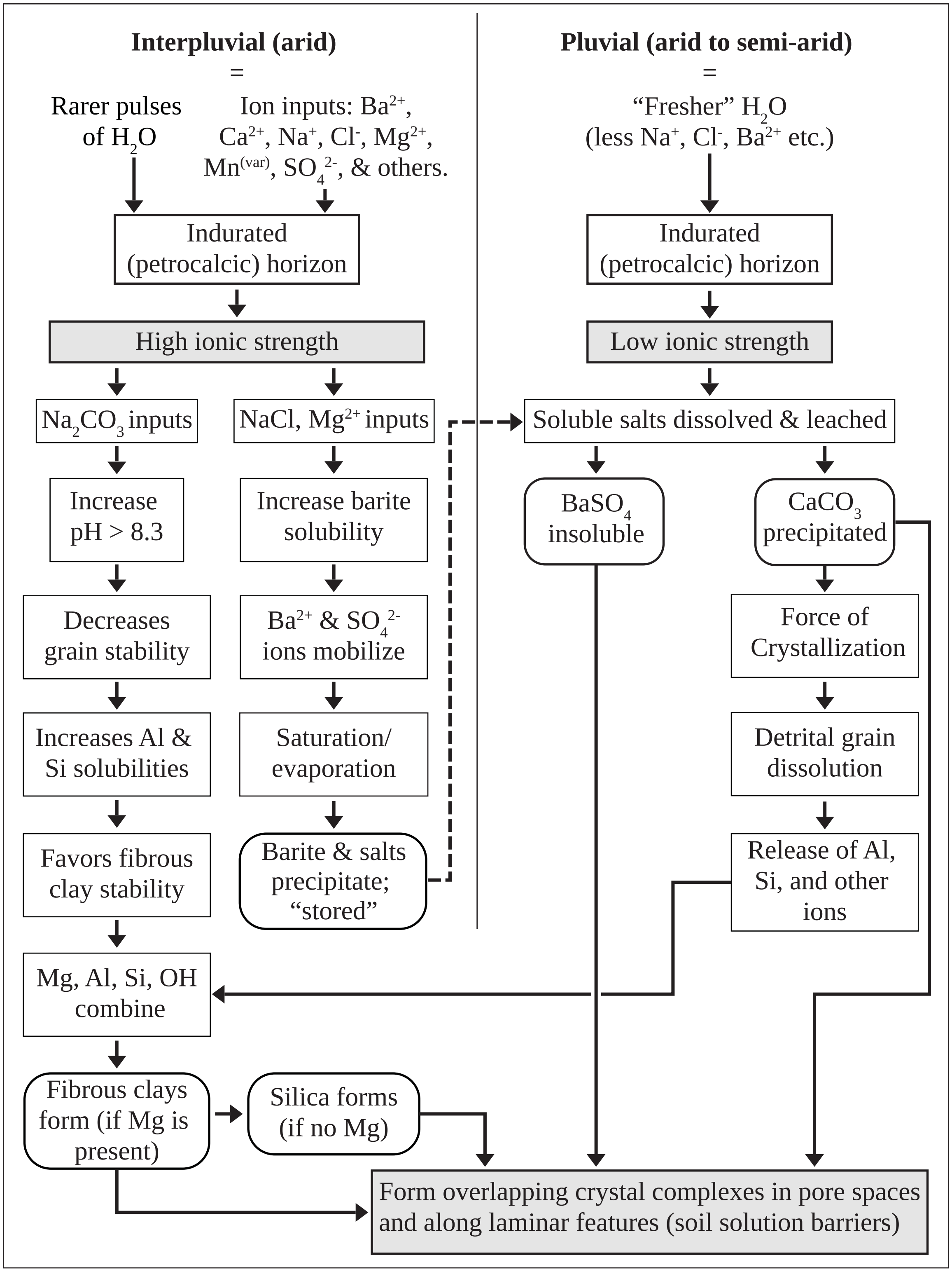

Figure 4.29. Generalized model for barite authigenesis in calcic and petrocalcic horizons in response to pluvial and interpluvial climate changes. This model supplements the model of calcite, fibrous clay, and silica genesis in Figure 4.28.

APPENDIX 2.1

DETAILED EXTRACTION METHODOLOGY

The following appendix outlines procedures performed for: (1) dissolution of bulk carbonate samples in pH 5 buffered sodium acetate solution (NaOAc) (Jackson, 1965; Kunze & Dixon, 1986; Soukup et al., 2008), (2) separation of the clay-sized particle fraction from the NaOAc-treated residue (Soukup et al., 2008), (3) treatment of the clay-sized particle fraction with Tiron to remove amorphous silica and Fe_2O_3 and Al_2O_3 phases (Biermans & Baert, 1977; Kodama & Ross, 1991).

Dissolution of Carbonate

Large volumes of 1$\underline{N}$ NaOAc were prepared by combining 82.00 g of anhydrous NaOAc powder and 27.0 mL of acetic acid (glacial) per liter of solution with reverse-osmosis H_2O in one- to two-liter beakers (see Jackson, 1965; Kunze & Dixon, 1986; Soukup et al., 2008) . Occasionally, additional acetic acid was needed to bring the pH of the solution to 5.0. Generally, five or more liters of pH 5 1$\underline{N}$ NaOAc stock solution were prepared at a time from one liter increments and stored at room temperature in 2.5 L glass jugs (acid bottles).

Bulk soil samples were fractured into fragments approximately 2.5 cm diameter or less using as few light blows of a 3-lb rock hammer and steel chisel as necessary. Approximately 200 g of each soil sample (the estimated sample mass required to produce ~10g of phyllosilicate clays) was transferred to labeled, 1-L glass beakers (2 L beakers can also be used).

NaOAc solution was added to the samples in ~100 mL increments to avoid loss of sample with overflow of the initially vigorously-fizzing solutions. All treatments were conducted in a fume hood. Excessive bubbling was also reduced by short jets of RO water from a plastic laboratory squeeze bottle. Sample solutions were gently stirred with a glass stir rod. Once the most vigorous fizzing had subsided, each beaker was either covered with a large watch glass or sealed with Parafilm "M"^{TM}.

The samples were allowed to soak in solution overnight in the fume hood. The next day, each sample was heated to 50°C on a hot plate for one hour with near-constant stirring, and then allowed to cool and to sit overnight again. 50°C was arbitrarily chosen as the maximum safe temperature to which the soil samples and phyllosilicates might be subjected, based on the assumption that peak summertime soil temperatures in the Mojave Desert could theoretically reach 40-45°C. Further research is needed to constrain the diffusion parameters for Ar in palygorskite and sepiolite lattices, and to determine accurate safe temperatures for the isotopic signature of pedogenic clays. Heating of the samples to 80°C or 100°C as prescribed in many dissolution procedures was deemed almost certain to cause Ar losses.

Subsequently, the samples were stirred and re-covered daily. When the samples no longer produced bubbles, or when pH checks revealed a pH of 6 or higher after addition of ~ 2mL acetic acid glacial, the NaOAc solution was changed. Generally, solutions were changed after approximately one month.

Refreshing the NaOAc solution involved decanting each solution into centrifuge tubes, and centrifuging the solutions at 1500-2000 RPM for 20-25 minutes to settle suspended clays before decanting the clear NaOAc solution. Generally, two 250-mL polycarbonate centrifuge tubes were used for each sample (two different samples were centrifuged at a time) and three cycles were needed to fully remove and rinse all of the solution from each sample beaker. RO water was used to rinse residual solution from samples into the centrifuge tubes for the final run. Upon completion, the settled sediments were rinsed with jets of RO water or scooped with a steel stirring rod back into the beaker, and then the beaker was refilled with 1N NaOAc solution and adjusted to pH 5 with acetic acid as before. No further heating was conducted for fear of enhanced Ar diffusion from phyllosilicate lattices with greater, cumulative heating time (further steps in the clay extraction, as described below, also required heating). Samples were stirred daily, and their solutions changed as needed.

Dissolution of the samples for geochronology purposes ran continuously from July 2007 through October 2007, yet the carbonates never fully digested – perhaps 30% to 50% of the original soil carbonates remained after dissolution. Use of finely ground sample material, and greater heating of solutions, would both expedite carbonate dissolution, but were not performed in this study due to the risk of Ar isotope losses.

Isolation of the clay-sized particle fraction

This procedure, adapted from Soukup et al. (2008), is based on the differential settling rates of particles in suspension following Stoke's Law, and relies upon centrifugation to expedite the settling process. Dilute NaCl solutions, commonly used to flocculate clays, were avoided whenever possible in this study due to the risk of chlorine interference with $^{40}Ar/^{39}Ar$ analysis. It is noted here that the speed and amount of time needed to centrifuge clays out of suspension vary according to the physical parameters of the centrifuge used (Soukup et al., 2008). Readers are referred to Soukup et al. (2008) for details.

Phyllosilicates released by selective dissolution of pedogenic carbonate were visible as a low-density colloidal gel or solution hovering above the settled coarse sample residue. When it appeared that enough of the original soil carbonates had dissolved to release the desired mass of phyllosilicates, the samples were stirred vigorously, allowed to settle for 10-30 seconds, and then decanted into centrifuge tubes. Particles were settled by centrifugation (Soukup et al., 2008) and the NaOAc decanted as before. When all but trace amounts of the NaOAc had been removed from the beaker, sample residues were rinsed with several hundred mL of RO H2O, stirred, and again decanted into the centrifuge tubes. At this point, it was assumed that most of the phyllosilicate fraction had been transferred to the centrifuge tubes, and that the sediment in the centrifuge tubes was nearly free of clay sized carbonates. Additional treatment of this fraction in NaOAc was performed later if carbonate contamination of the centrifuge sediments was detected or suspected.

Separation of the <2 mm (clay) sized particle fraction was performed according to Soukup et al. (2008) using 250-mL centrifuge bottles and no more than 1.5 cm of sediment per bottle. First, the centrifuge bottles were marked at 9 and 3 cm from the bottom of the bottle and RO water was added up to the 9-cm mark (Soukup et al., 2008). The sample was shaken well and then centrifuged at 500 RPM for 6 min. Next, the cloudy, dispersed <2-mm fraction in suspension was siphoned into a 1 L glass beaker from 3 cm above the bottom of the centrifuge bottle (Soukup et al., 2008). Care was taken to ensure that no portion of the sediment below the 3-cm mark, was siphoned

(Soukup et al., 2008). These steps were repeated until the suspension was consistently clear or only slightly cloudy after centrifugation (Soukup et al., 2008). On average, six to eight repetitions were generally performed to ensure successful fractionation, as recommended by Soukup et al. (2008).

The siphoned sediment solution was set to dry in an oven at 50°C until dry, with occasional rinsing of the sides of the beaker with RO to prevent excessive adhesion of clays to the sides of the beaker. Generally, this step was performed after three to four of the centrifugation-siphoning step repetitions mentioned above, thus, several days were needed to fully fractionate and to dry the sample.

After fractionation, the dried clay-sized particle fractions were divided into separate aliquots for instrument analysis and subsequent tiron treatment (and eventual isotopic analysis). On occasion, SEM-EDS analyses revealed incomplete carbonate dissolution or inadequate particle-size fractionation (see Chapter 2), and those procedures were repeated as needed.

Tiron Treatment

To make the 0.09 M tiron solution used in this study, 31.42 g of anhydrous tiron powder (from Acros Organics) were added to 800 mL of RO H_2O and stirred. Next, 5.30 g of Na_2CO_3 were added to 100 mL of RO H_2O in a separate beaker and stirred. These two solutions were then combined. 23.5 mL of 4 M NaOH were added to this solution, and RO H_2O was added to bring the final volume up to 1 L.

The clay sized particle fractions were each weighed in a pre-tared, plastic, 1 L beaker, immersed in ~1 L of tiron solution, and stirred with plastic stir rods. The beakers were placed in a water bath and heated to 50°C for one hour, with frequent stirring. After one hour, samples were removed from the water bath, decanted into 250 mL centrifuge tubes, and centrifuged at high RPM for 25 to 30 minutes. Following centrifugation and settling of the clay, the clear, green tiron supernatant was decanted. Extensive, repeat rinsing in RO H_2O and centrifugation of the samples – eight cycles or more – proved necessary, because a faint green color (indicating Tiron solution) persisted in the supernatant. Tiron appeared to have a deflocculating effect on the fibrous clays, which led to concerns of sample fractionation via loss of the finest clay particles with decanting. Loss of sample was also a concern due to low overall clay yields from some samples. Persistence of tiron residue despite a colorless supernatant became apparent after drying (overnight in small 250 mL glass beakers in a 50°C oven, as above) for some samples, when the residue was visible as a purple stain on dried sample fractions. In such cases, further rinsing was performed.

Following this procedure, further aliquots of each sample were taken for instrument analysis (SEM, ICP, and XRD), and the remaining sample was retained for $^{40}Ar/^{39}Ar$ isotopic analysis.

References

Biermans, V. and Baert, L., 1977. Selective extraction of the amorphous Al, Fe and Si oxides using an alkaline Tiron solution. Clay Minerals, 12(127): 127-135.

Jackson, M.L.,1965. Soil chemical analysis: Advanced Course. Published by the author. Dept. of Soil Science, University of Wisconsin, Madison.

Kodama, H. and Ross, G.J., 1991. Tiron dissolution method used to remove and characterize inorganic components in soils. Soil Science Society of America Journal, 55: 1180-1187.

Kunze, G.W. and Dixon, J.B., 1986. Pretreatment for mineralogical analysis. In: Klute, A., ed. Methods of soil analysis part 1: Physical and mineralogical methods, 2nd edition. Agronomy Monograph 9. Madison, Soil Science Society of America: 91-100.

Soukup, D.A., Buck, B.J., and Harris, W., 2008. Preparing soils for mineralogical analysis. In: Ulery, A., and Drees, R., eds. Methods of soil analysis, part 5: Mineralogical methods. SSSA Book Series No. 5. Madison, Science Society of America: 13-31.

APPENDIX 2.2

BULK POWDER XRD DATA FOR MORMON MESA AND JER LA MESA SAMPLES

The following pages display the results of x-ray diffraction (XRD) analysis of bulk powder samples from the Mormon Mesa and JER La Mesa petrocalcic soils. Sample compositions are chiefly calcite, low-magnesium calcite, quartz, and minor amounts of feldspars or other silicates.

Calcite and low-magnesium calcite have not been differentiated in the following data, because it is assumed, based on the detection of d-spacings that are intermediate between the two minerals, that most if not all of the calcium carbonate in these samples contains some substituted Mg. The 100% relative intensity peak at 0.3025 nm (in most samples) supports the argument for Mg content in the carbonate. However, slightly higher d-spacings (nearer to 0.3030 nm) in many bulk powder reference diffraction patterns for both (low-)magnesium calcite and calcite suggest that the 0.3025 nm peak is not by itself diagnostic for the samples in this study. Nevertheless, two ~20% relative intensity peaks at 0.190 and 0.187 nm, as well as several lower intensity peaks, in the petrocalcic samples are also intermediate between most of the calcite and low-magnesium calcite reference patterns. Therefore, there exists strong evidence for the occurrence of both calcite and low-magnesium calcite in the Mormon Mesa and JER La Mesa samples.

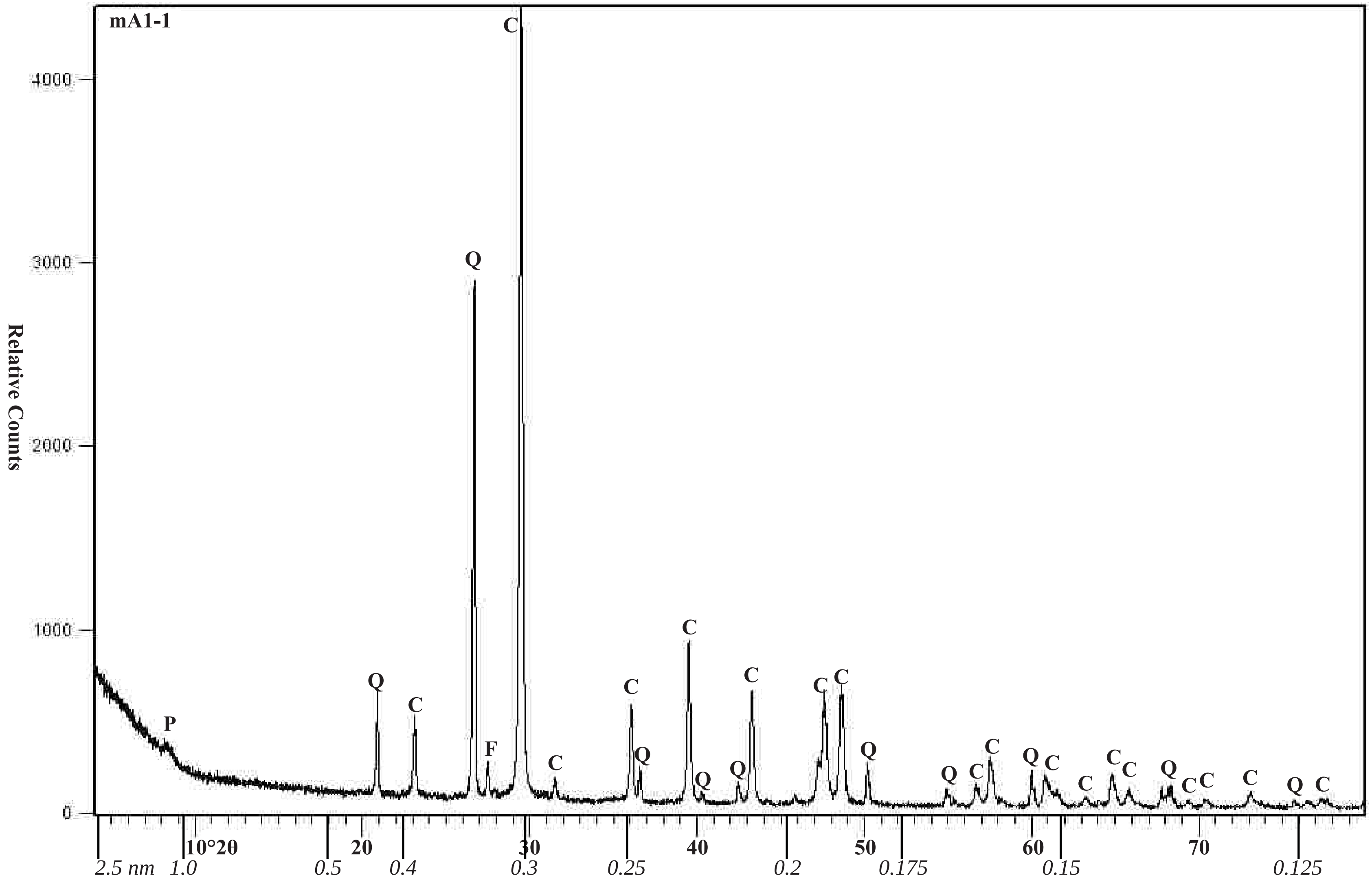

Bulk powder XRD data for Sample mA1-1. C = calcite/low-magnesian calcite, F = feldspar, P = palygorskite, Q = quartz.

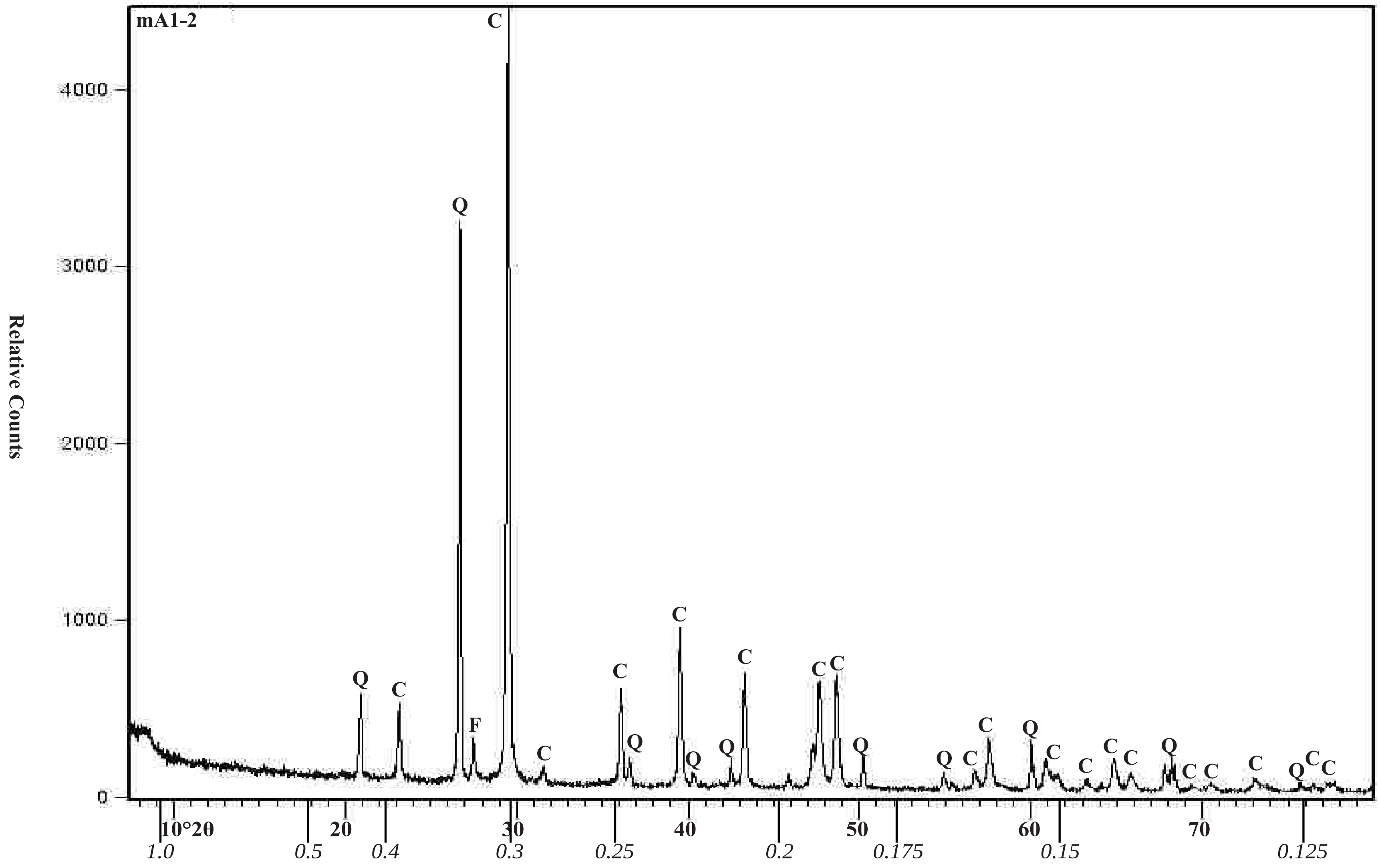

Bulk powder XRD data for Sample mA1-2. C = calcite and/or low-magnesian calcite, F = feldspar, Q = quartz.

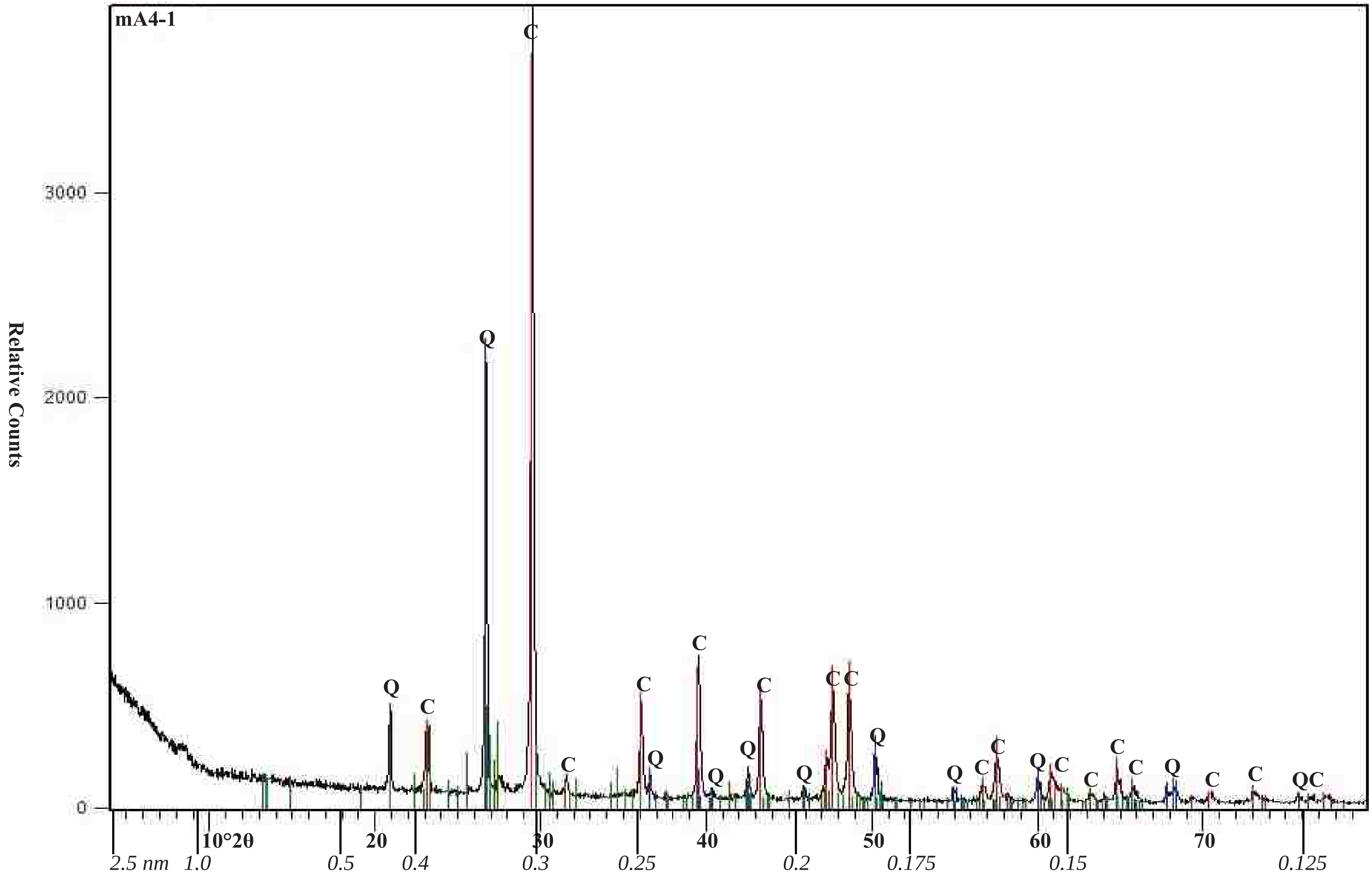

Bulk powder XRD data for Sample mA4-1. C = calcite and/or low-magnesian calcite, F = feldspar, Q = quartz.

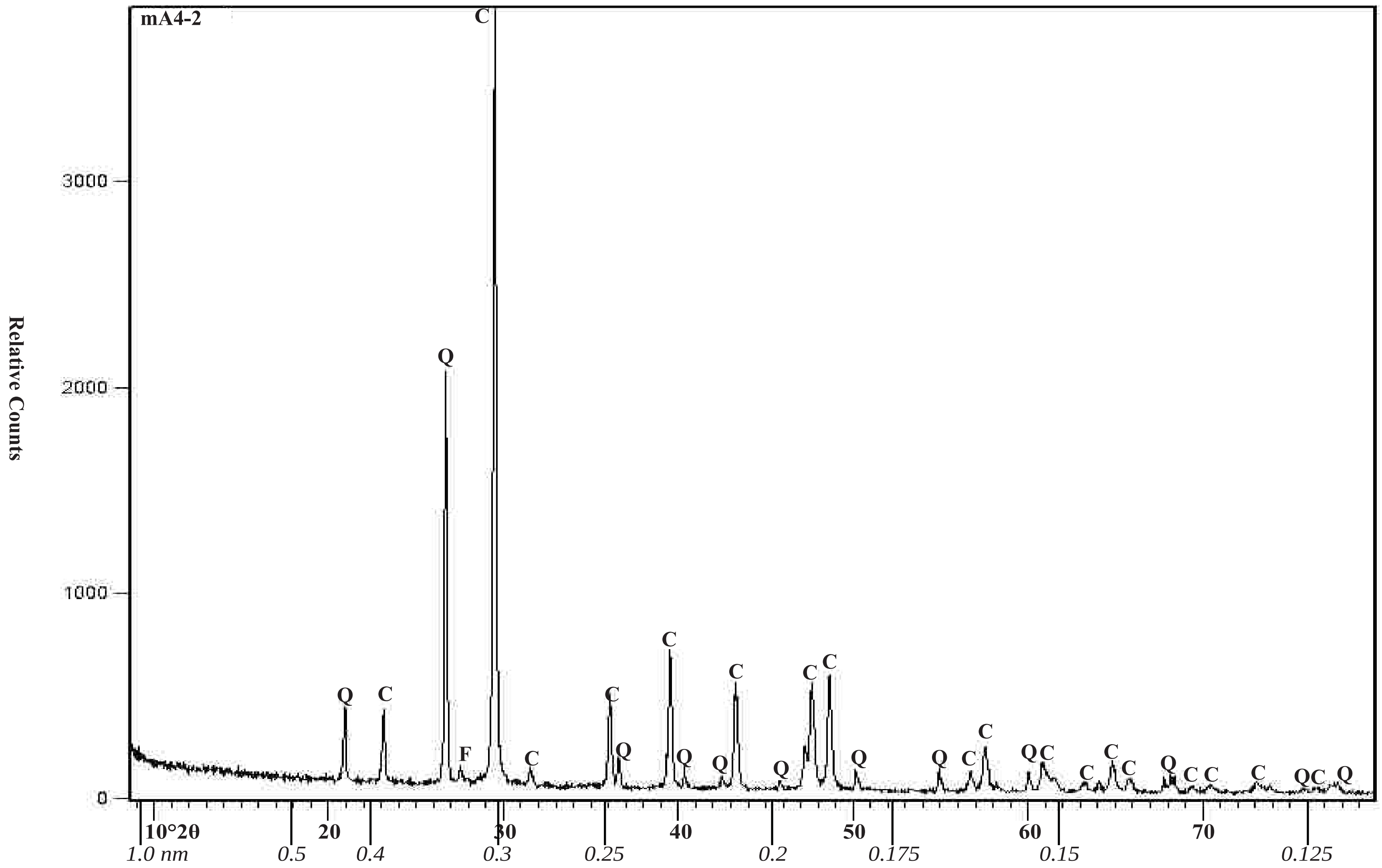

Bulk powder XRD data for Sample mA4-2. C = calcite and/or low-magnesian calcite, F = feldspar, Q = quartz.

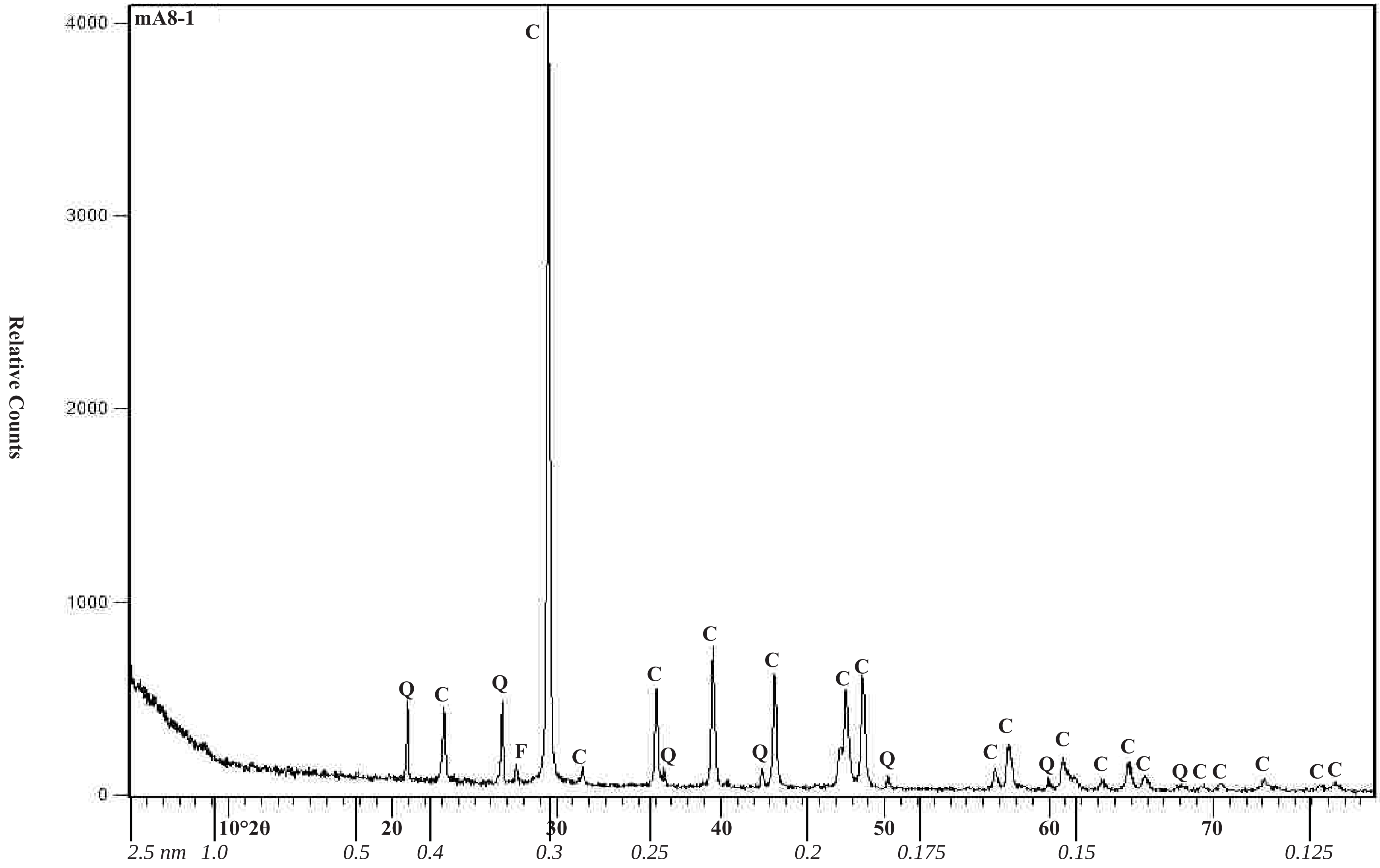

Bulk powder XRD data for Sample mA8-1. C = calcite and/or low-magnesian calcite, Q = quartz.

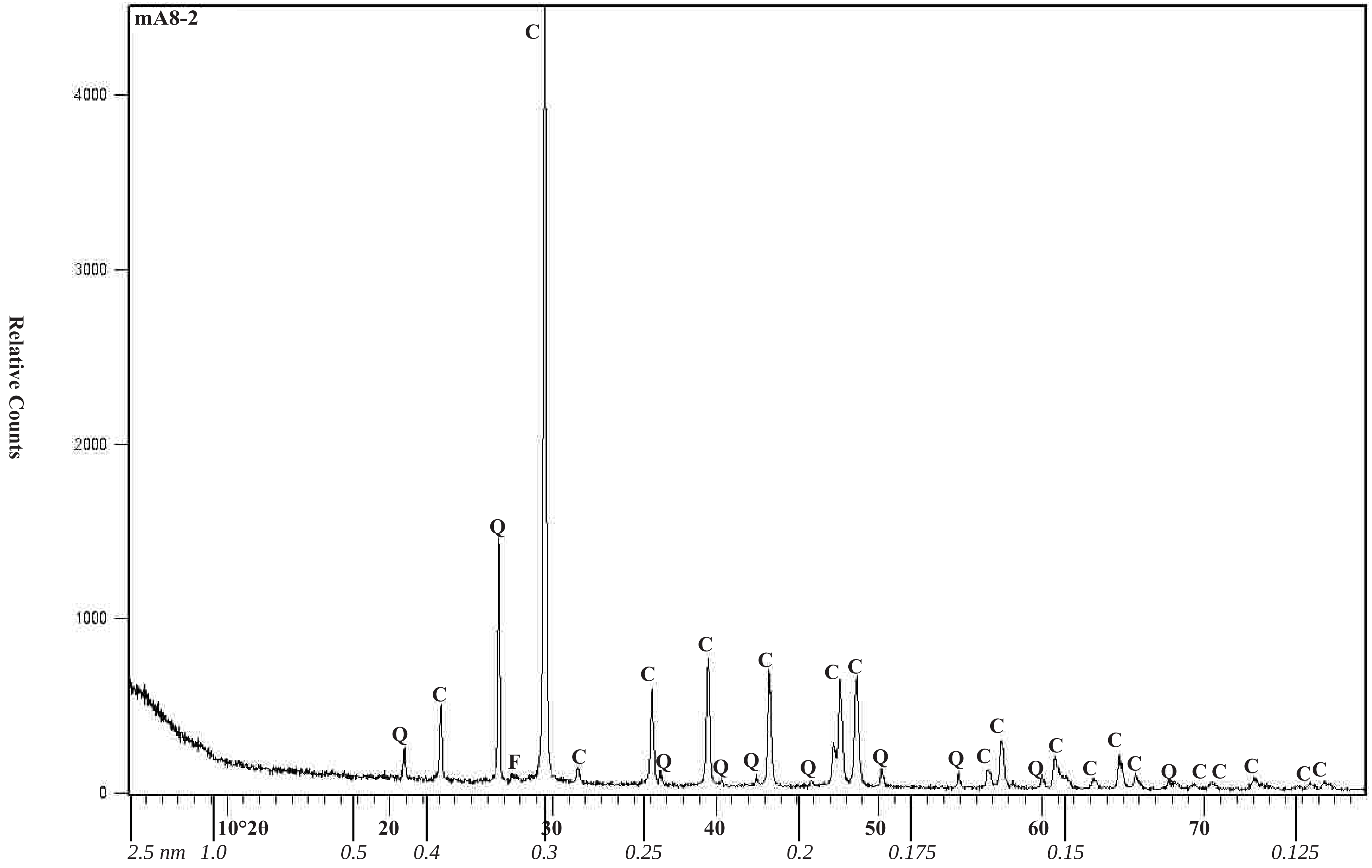

Bulk powder XRD data for Sample mA8-2. C = calcite and/or low-magnesian calcite, Q = quartz.

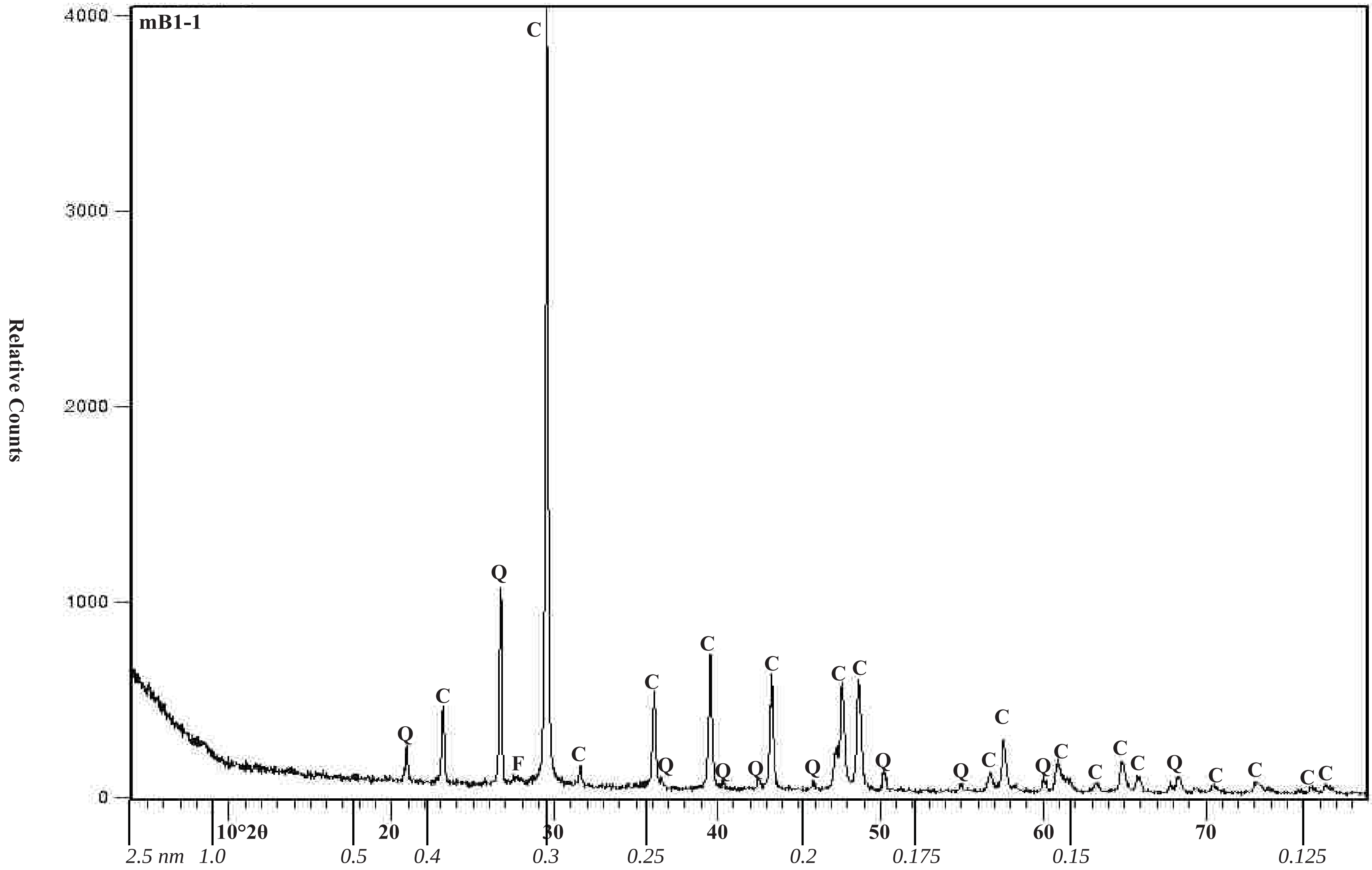

Bulk powder XRD data for Sample mB1-1. C = calcite and/or low-magnesian calcite, F=feldspar, Q = quartz.

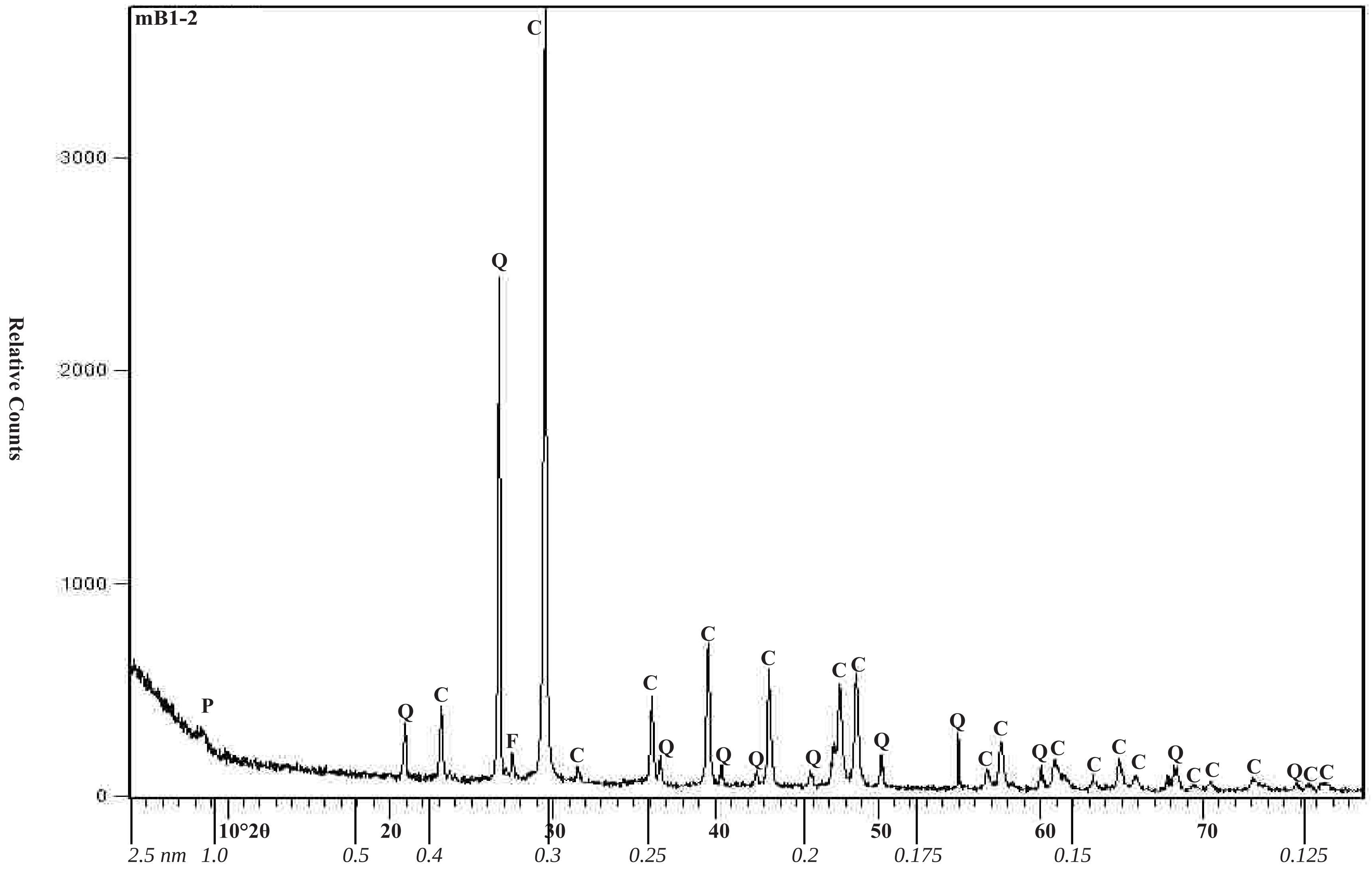

Bulk powder XRD data for Sample mB1-2. C = calcite/low-magnesian calcite, F = feldspar, P = palygorskite, Q = quartz.

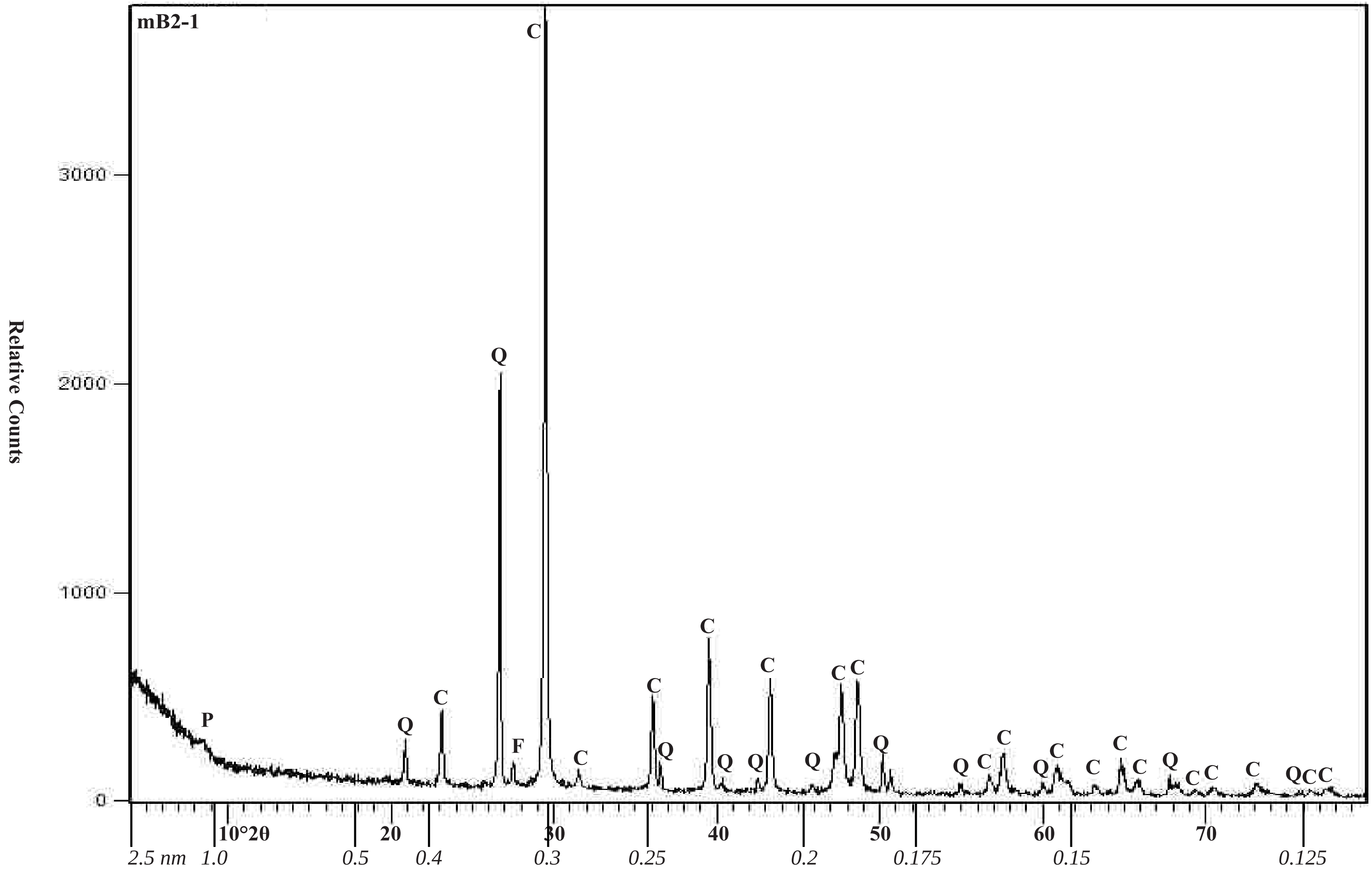

Bulk powder XRD data for Sample mB2-1. C = calcite/low-magnesian calcite, F=feldspar, P = palygorskite, Q = quartz.

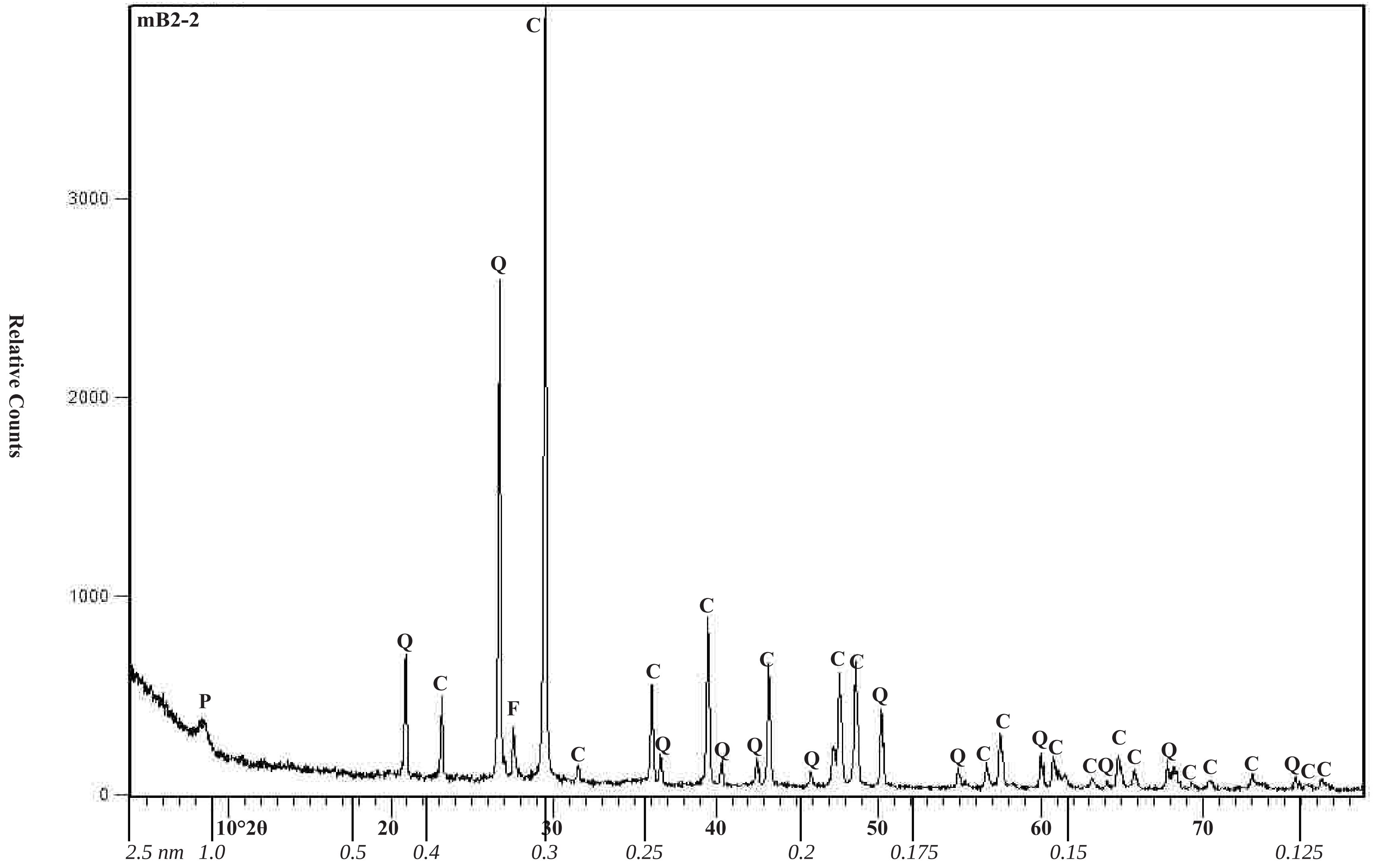

Bulk powder XRD data for Sample mB2-2. C = calcite/low-magnesian calcite, F=feldspar, P = palygorskite, Q = quartz.

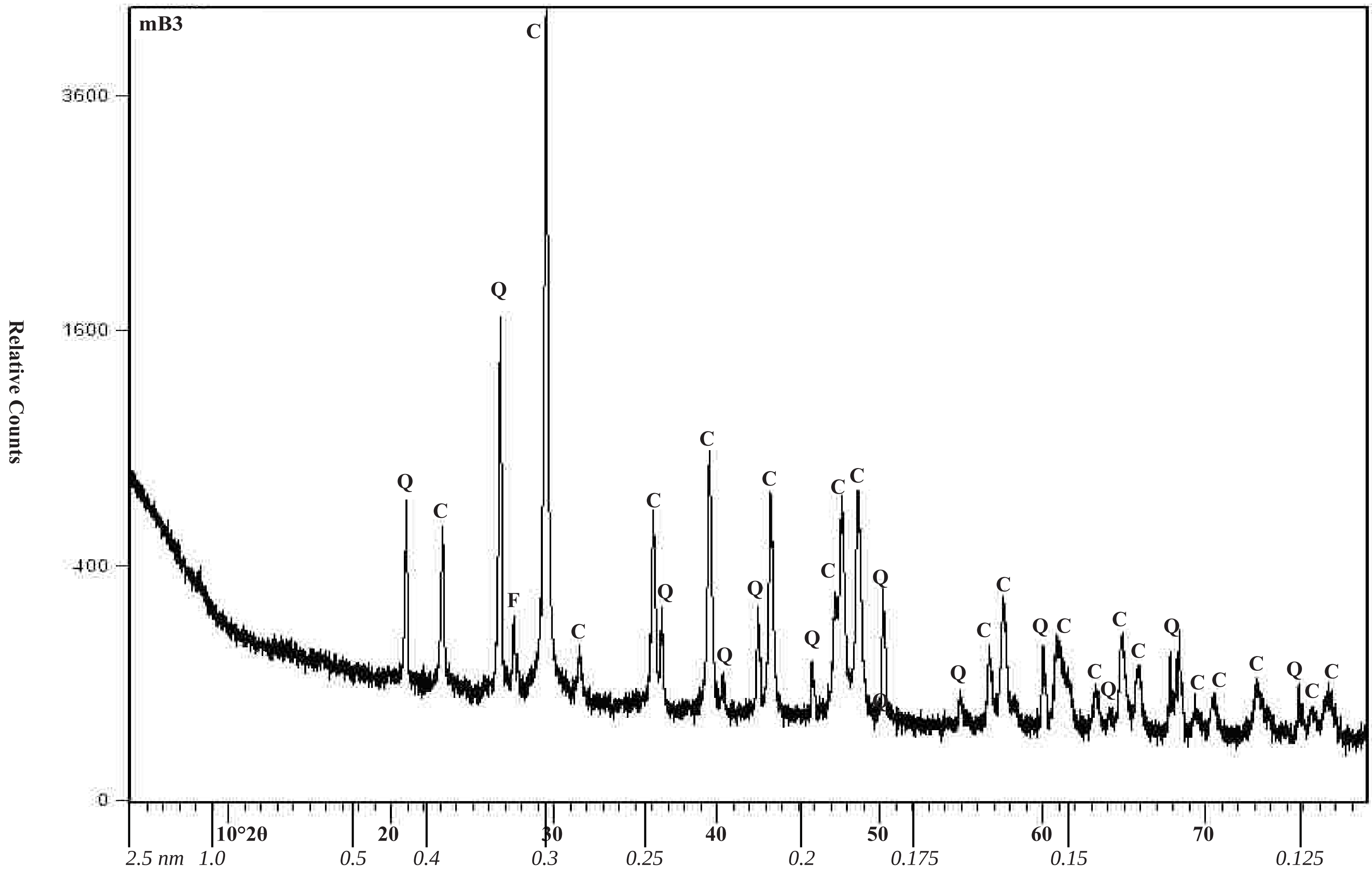

Bulk powder XRD data for Sample mB3. C = calcite/low-magnesian calcite, F=feldspar, Q = quartz.

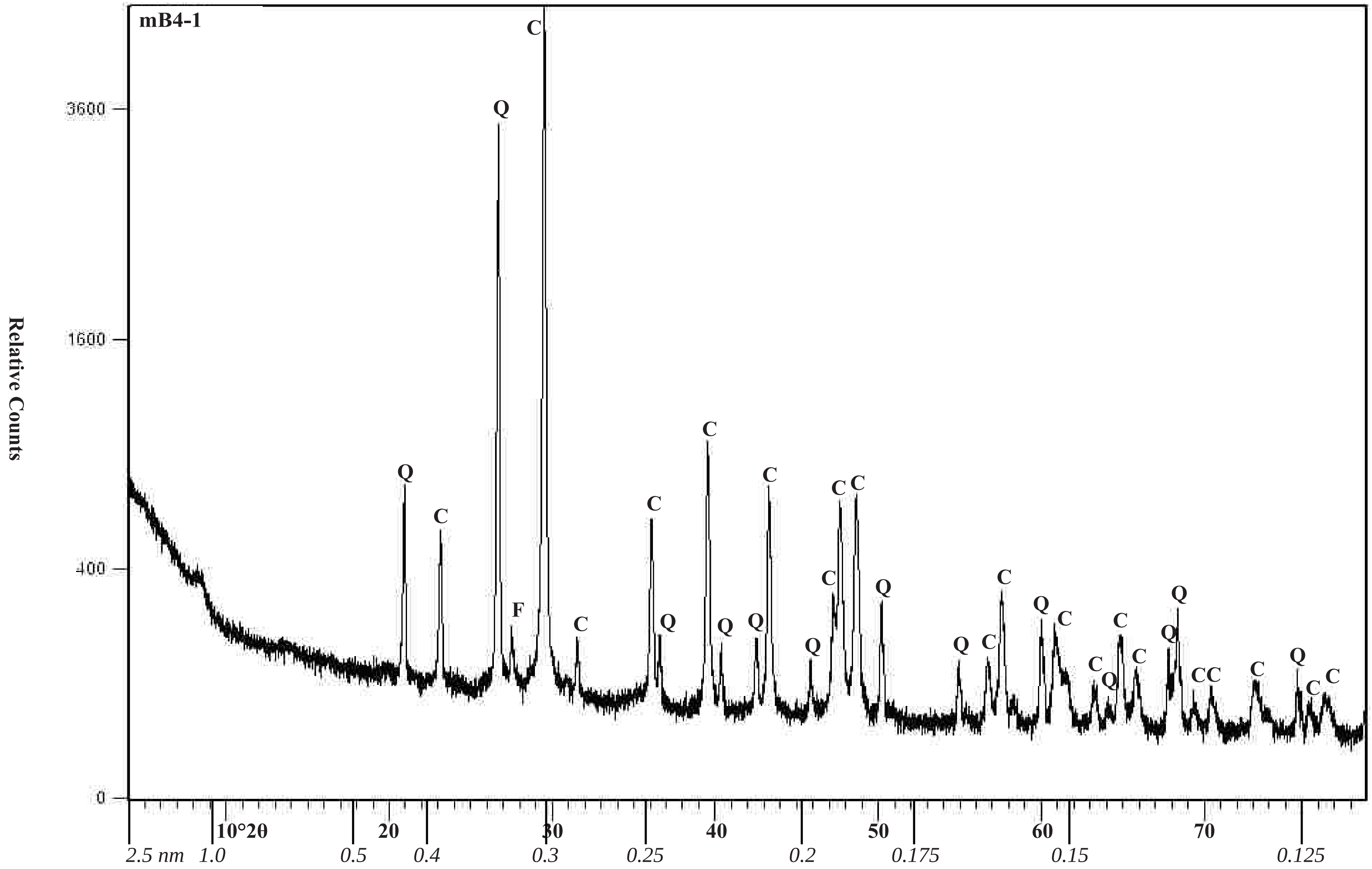

Bulk powder XRD data for Sample mB4-1. C = calcite/low-magnesian calcite, F=feldspar, Q = quartz.

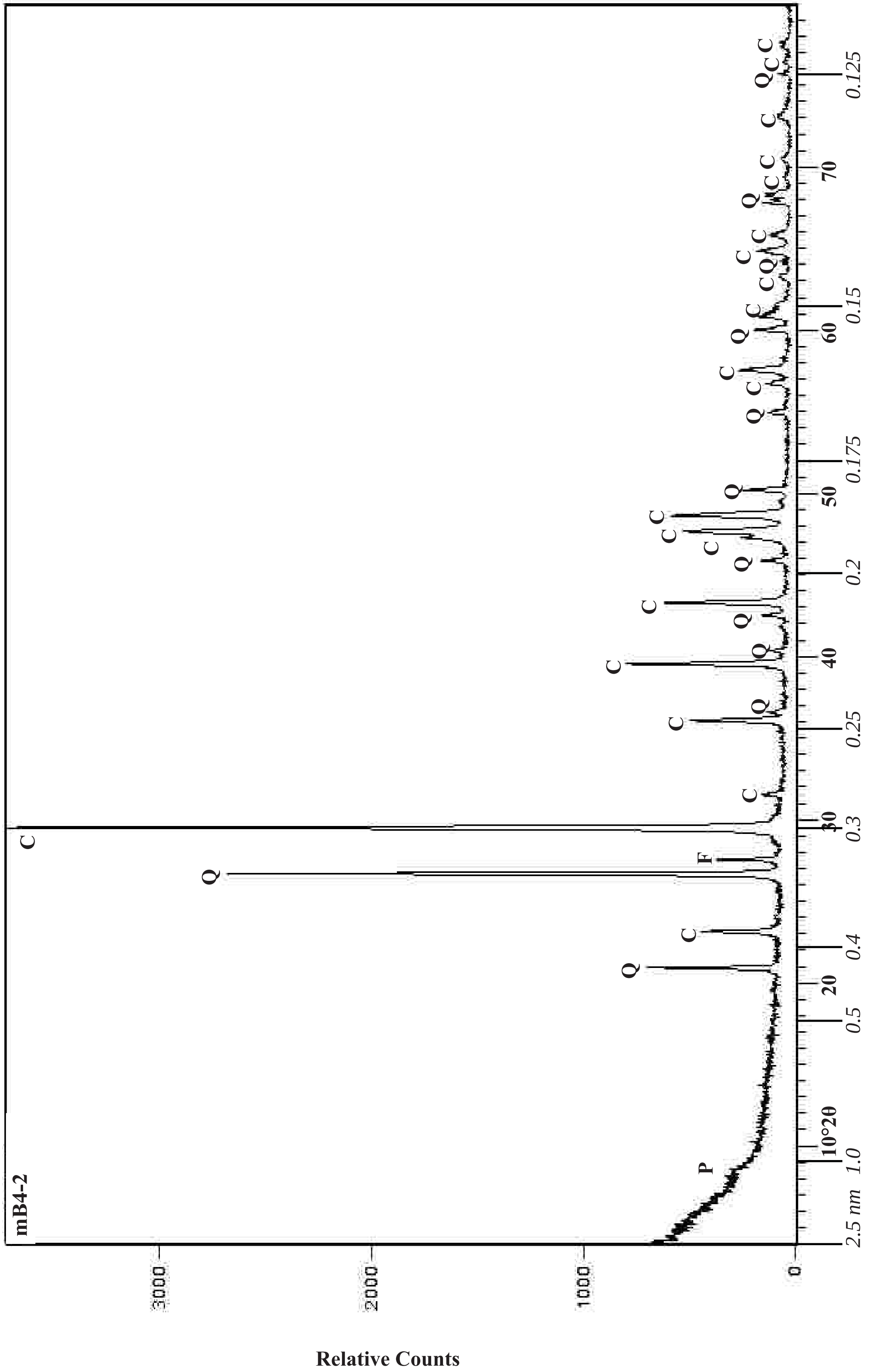

Bulk powder XRD data for Sample mB4-2. C = calcite/low-magnesian calcite, F=feldspar, P = palygorskite, Q = quartz.

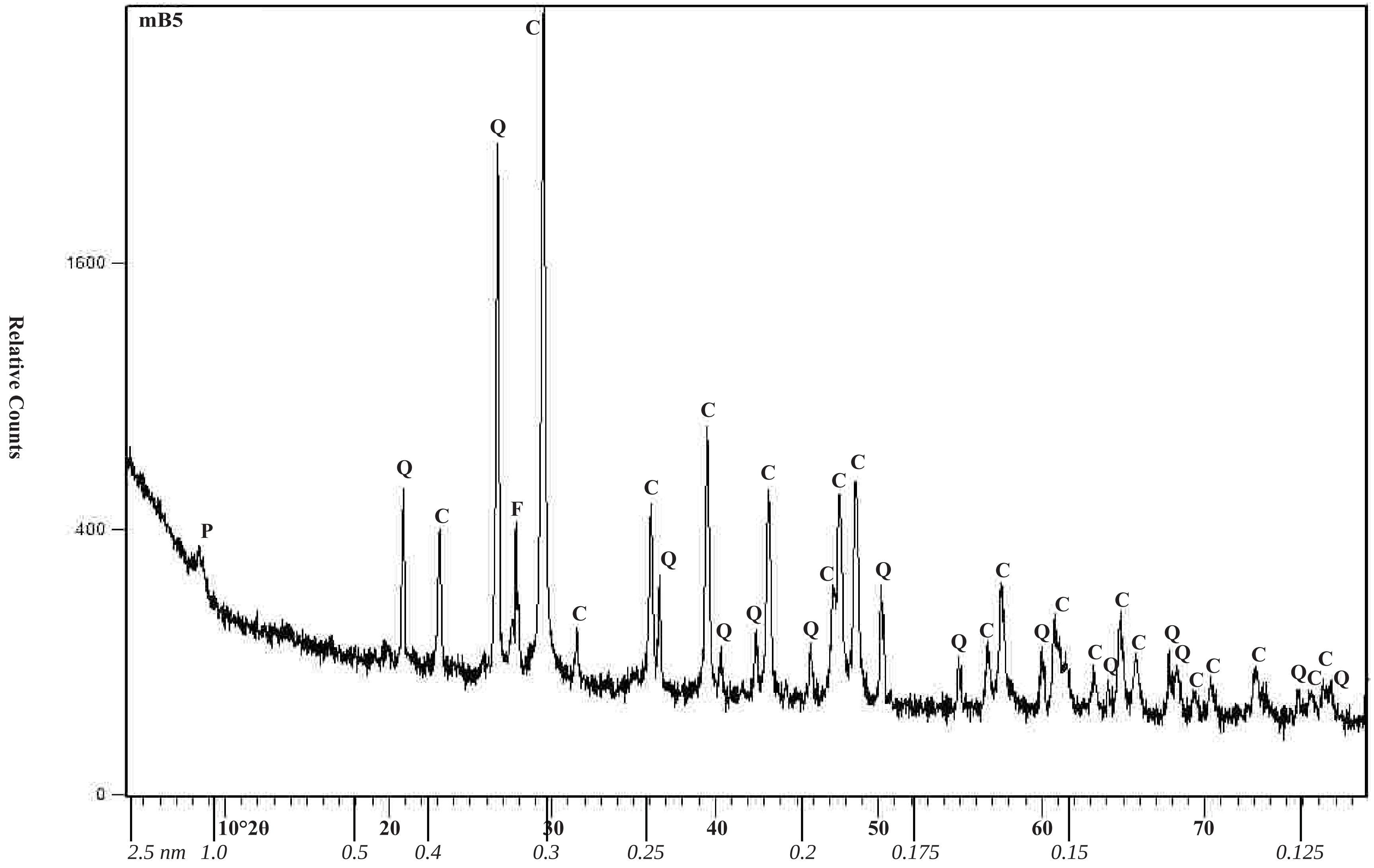

Bulk powder XRD data for Sample mB5. C = calcite/low-magnesian calcite, F = feldspar, P = palygorskite, Q = quartz.

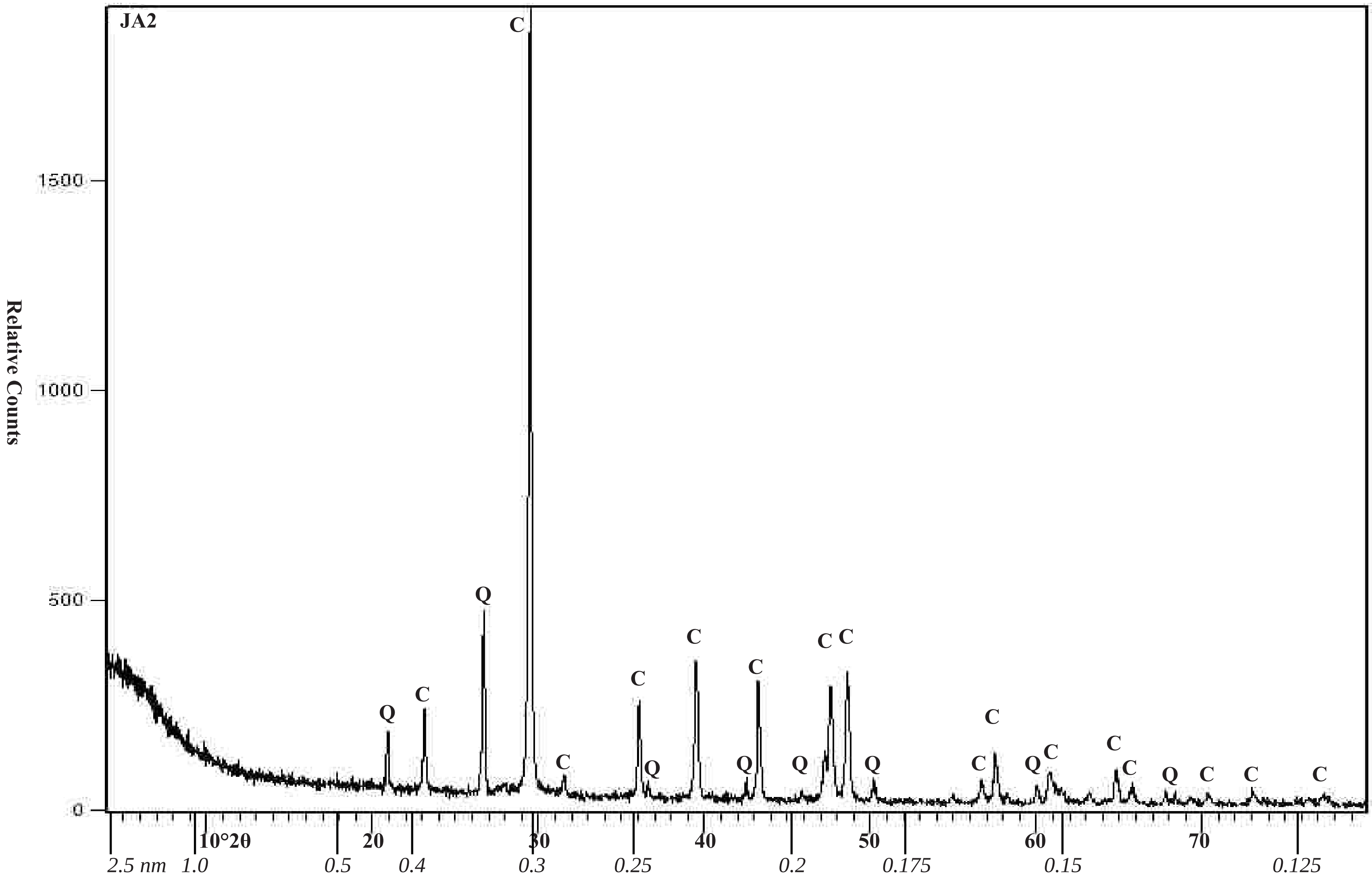

Bulk powder XRD data for Sample JA2. C = calcite and/or low-magnesian calcite, Q = quartz.

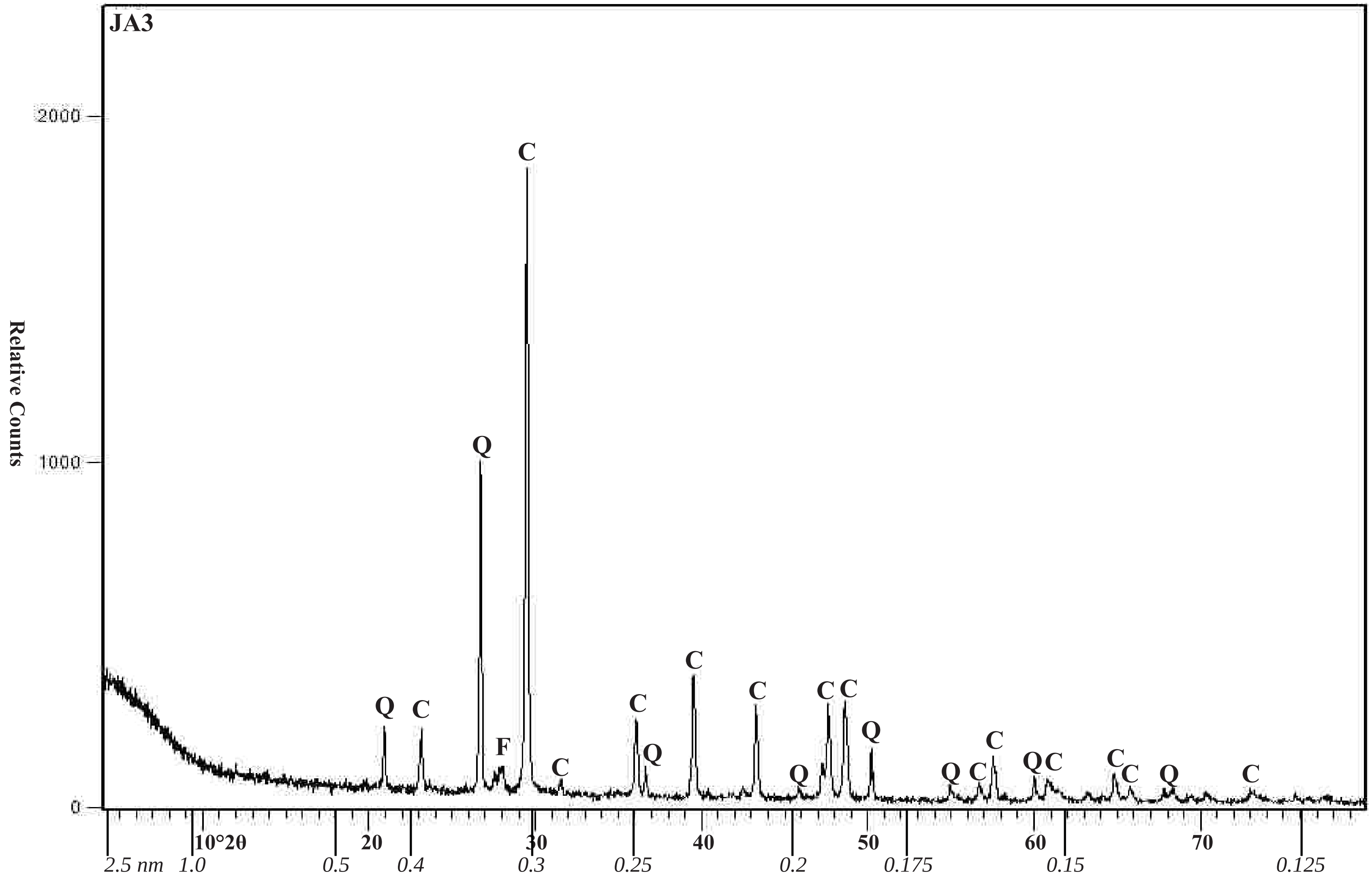

Bulk powder XRD data for Sample JA3. C = calcite and/or low-magnesian calcite, F = Feldspar, Q = quartz.

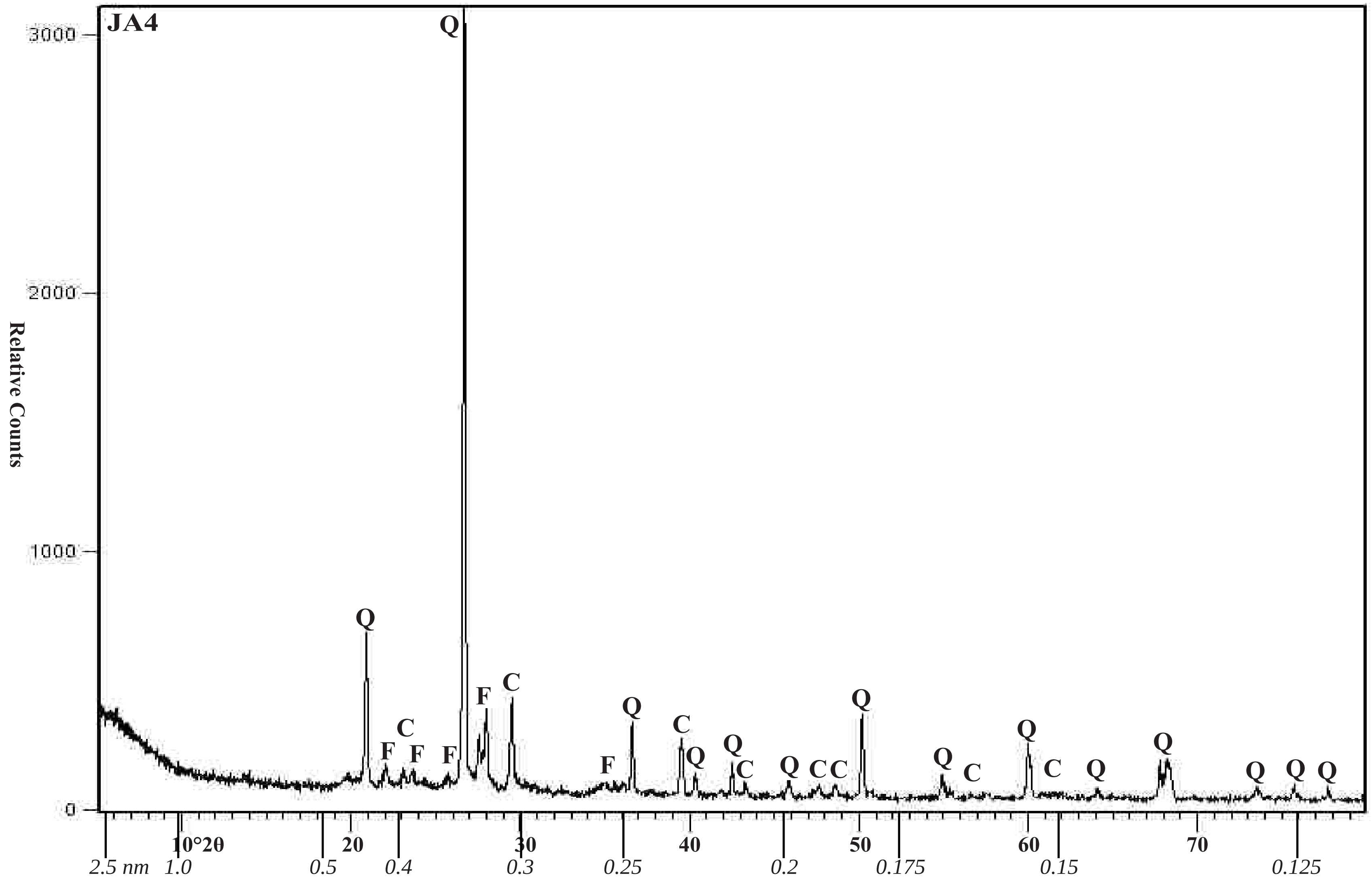

Bulk powder XRD data for Sample JA4. C = calcite and/or low-magnesian calcite, F = Feldspar, Q = quartz.

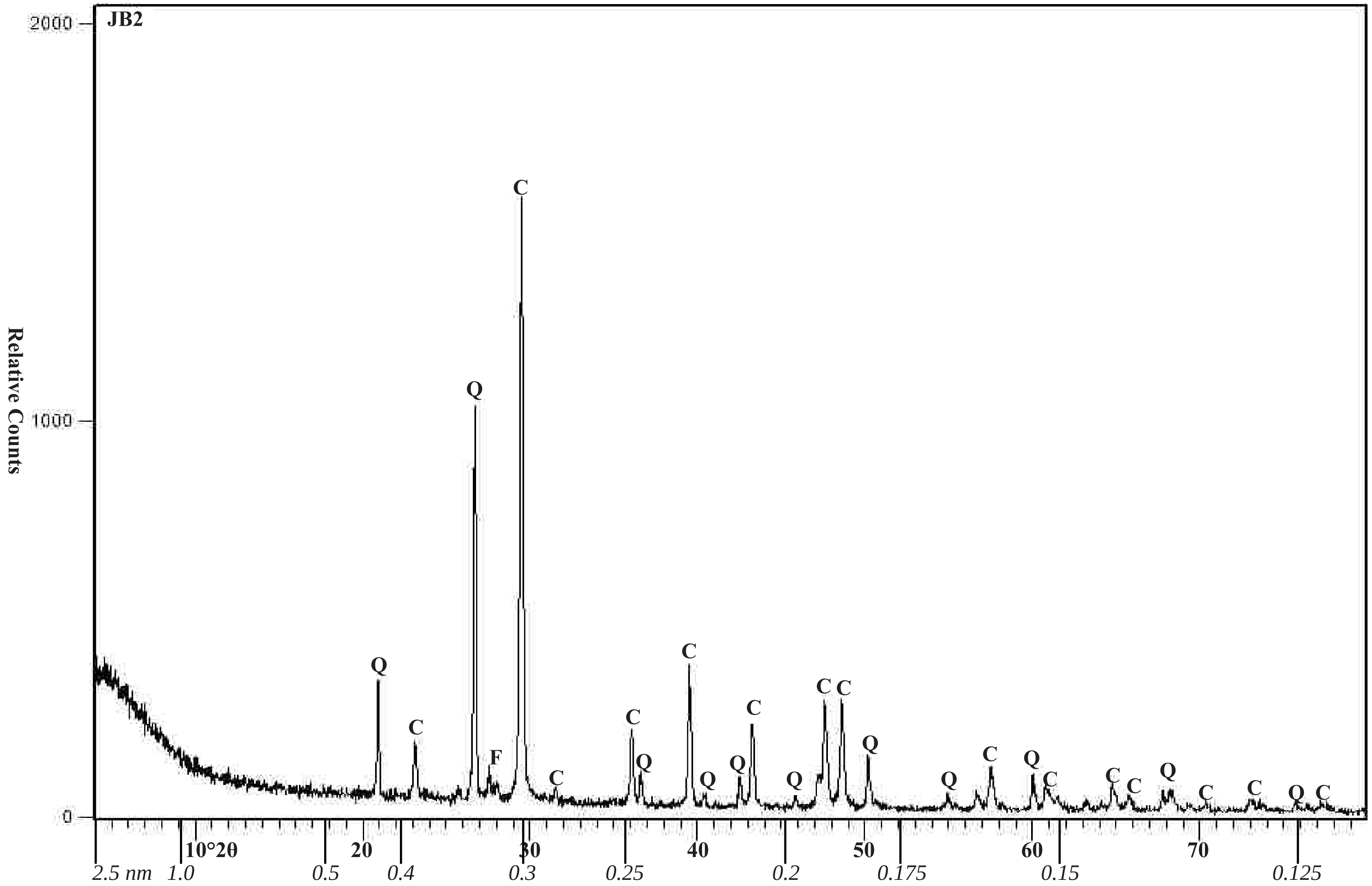

Bulk powder XRD data for Sample JB2. C = calcite and/or low-magnesian calcite, F = feldspar, Q = quartz.

APPENDIX 2.3

PHYLLOSILICATE FRACTION XRD DATA

The following data consist of XRD spectra for the clay-sized particle fraction of Mormon Mesa geochronology samples and Source Clays Repository reference standards. Data could not be obtained for all geochronology samples because of insufficient sample yields and also because of time constraints.

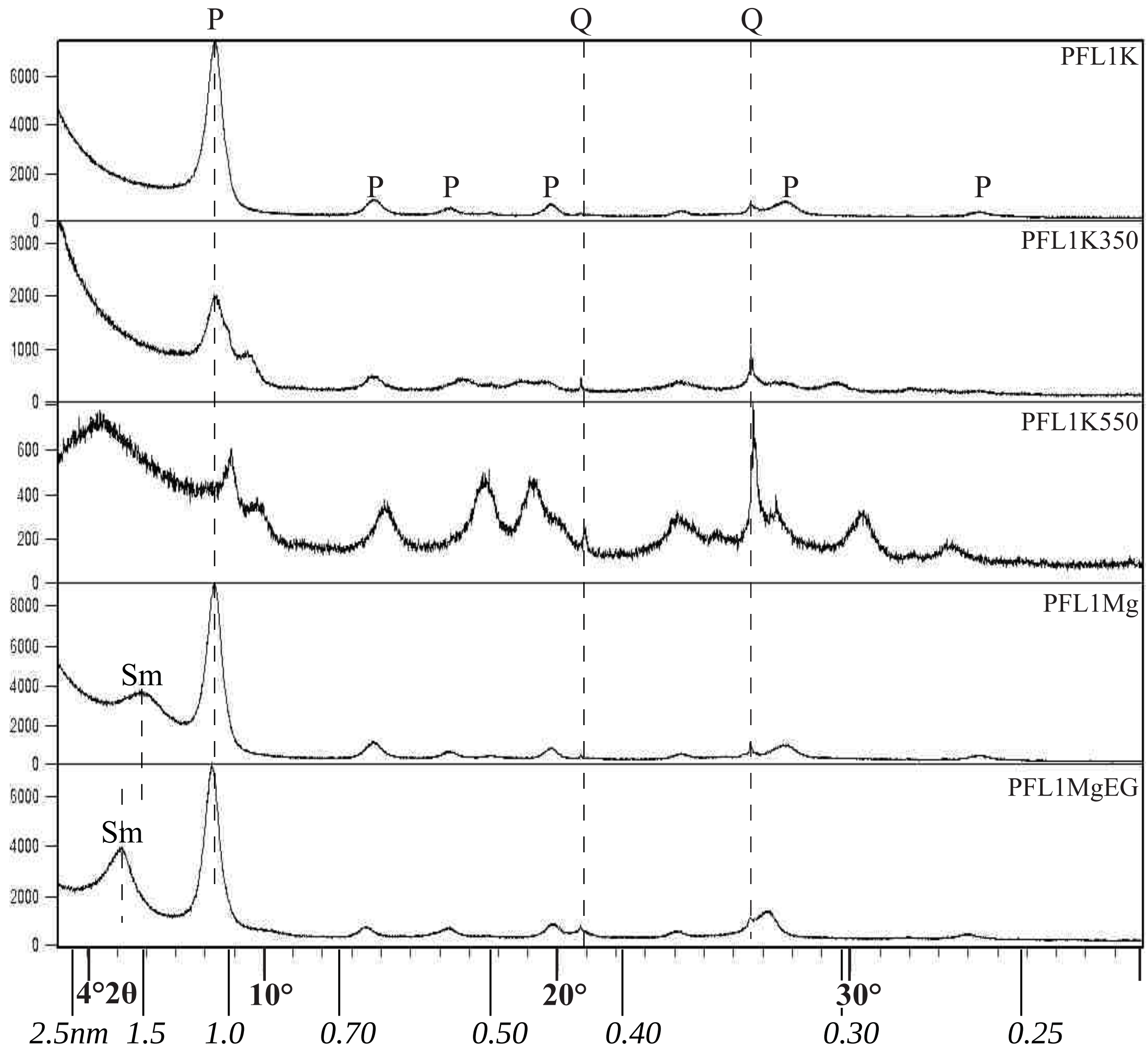

Clay-sized particle fraction XRD spectra for the Source Clays Repository palygorskite reference standard PFL-1. Y-axis units are relative peak counts for each spectrum. X-axis indicates scan angle (°2θ) and d-spacing (nm). Treatments are K-saturation (K), K-saturation heated to 350°C (K350) and 550°C (K550), Mg-saturation (Mg), and Mg-saturation with ethylene glycol solvation (MgEG). P = palygorskite, Q = quartz, Sm = smectite. Collapse of the 1.061 nm peak with associated development of a small 0.930 nm peak occurs upon heating. Weak expansion of this peak to 1.070 nm occurs after ethylene glycol solvation. These effects are normal. Note emergence of a 1.502 nm peak after Mg treatment, and a 1.750 nm peak after ethylene glycol solvation, both of which suggest smectite content. Minor quartz is also indicated at ~0.335 nm in all treatments.

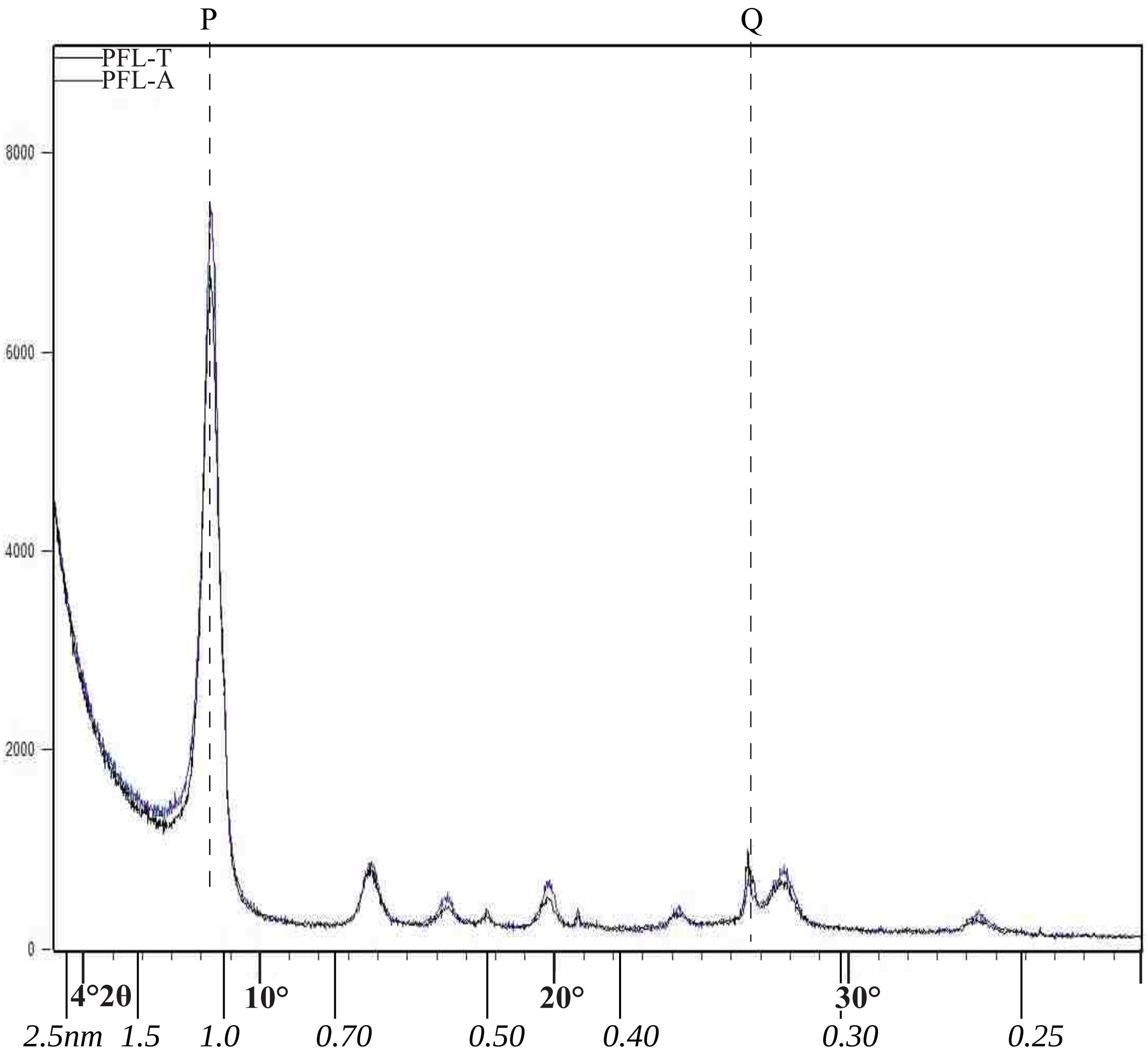

XRD spectra for aliquots of the Source Clays Repository palygorskite reference standard PFL-1. Aliqouts are “-A” after acetate treatment, and “-T” after acetate and tiron treatments. Y-axis units are relative peak counts for each spectrum. X-axis indicates scan angle (°2θ) and d-spacing (nm). Only the base-line K-treatment scans are shown. P = palygorskite, Q = quartz. Note general similarity of the two aliquots.

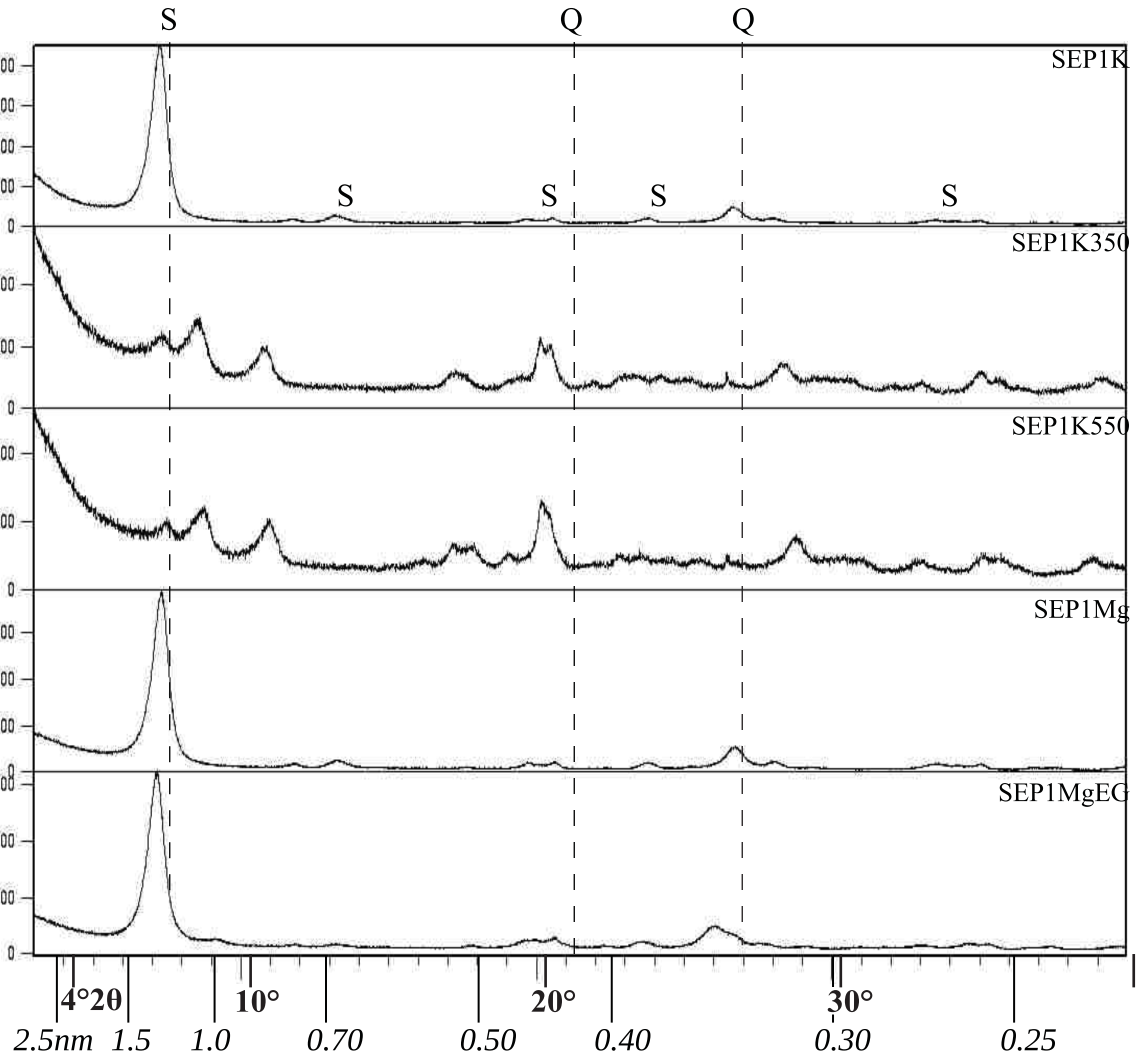

Clay-sized particle fraction XRD spectra for the Source Clays Repository sepiolite reference standard SEP-1. Y-axis units are relative peak counts for each spectrum. X-axis indicates scan angle (°2θ) and d-spacing (nm). Treatments are K-saturation (K), K-saturation heated to 350°C (K350) and 550°C (K550), Mg-saturation (Mg), and Mg-saturation with ethylene glycol solvation (MgEG). Q = quartz, S = sepiolite. Note slight expansion of the 1.22 nm peak in the Mg spectrum to 1.25 nm after ethylene glycol treatment, and collapse of the 1.22 nm peak upon heating with associated development of a small 1.03 nm peak.

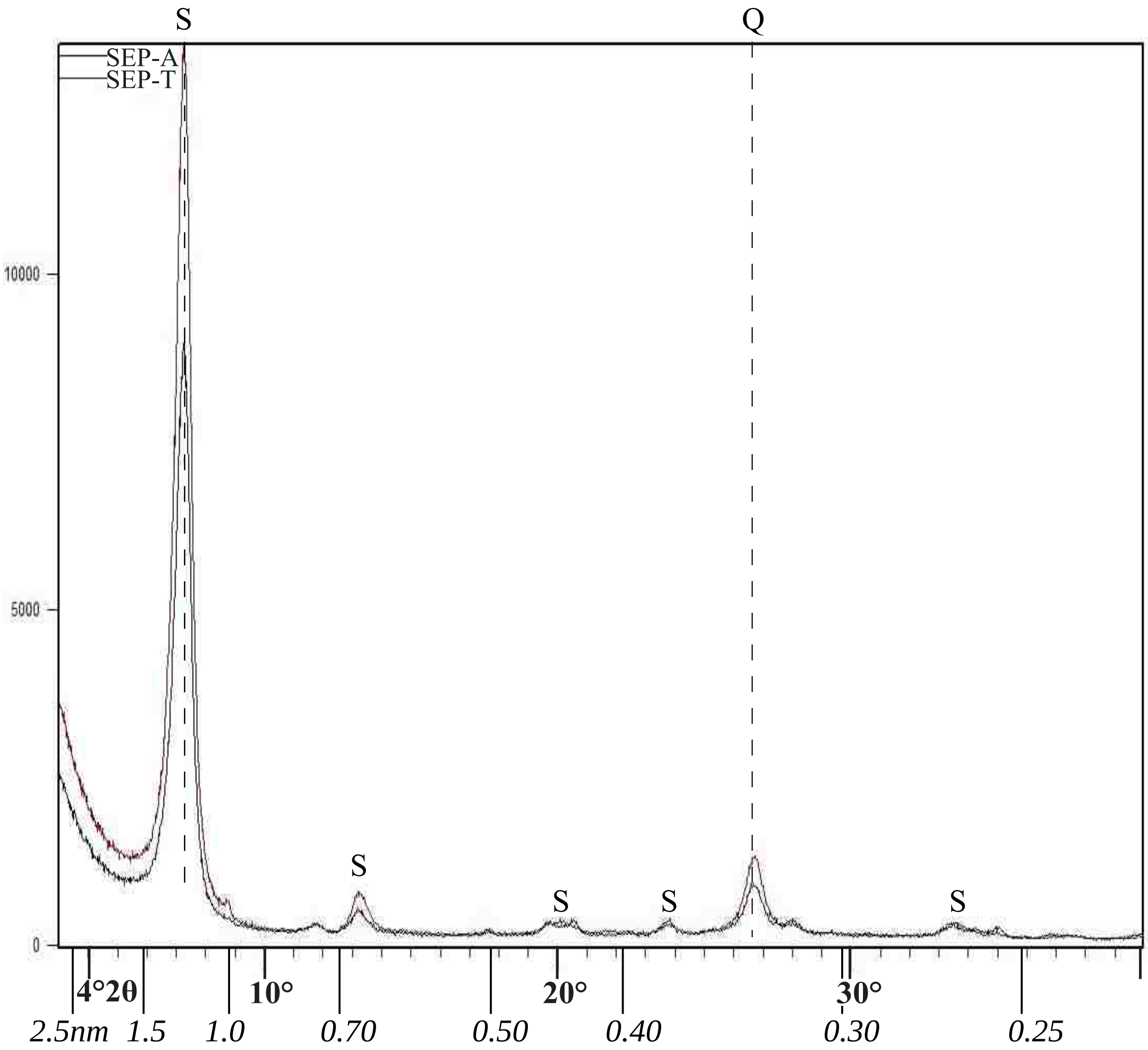

XRD spectra for aliquots of the Source Clays Repository sepiolite reference standard SEP-1. Aliqouts are "-A" after acetate treatment, and "-T" after acetate and tiron treatments. Y-axis units are relative peak counts for each spectrum. X-axis indicates scan angle (°2θ) and d-spacing (nm). Only the base-line K-treatment scans are shown. Q = quartz, S = sepiolite. Note general similarity of the two aliquots.

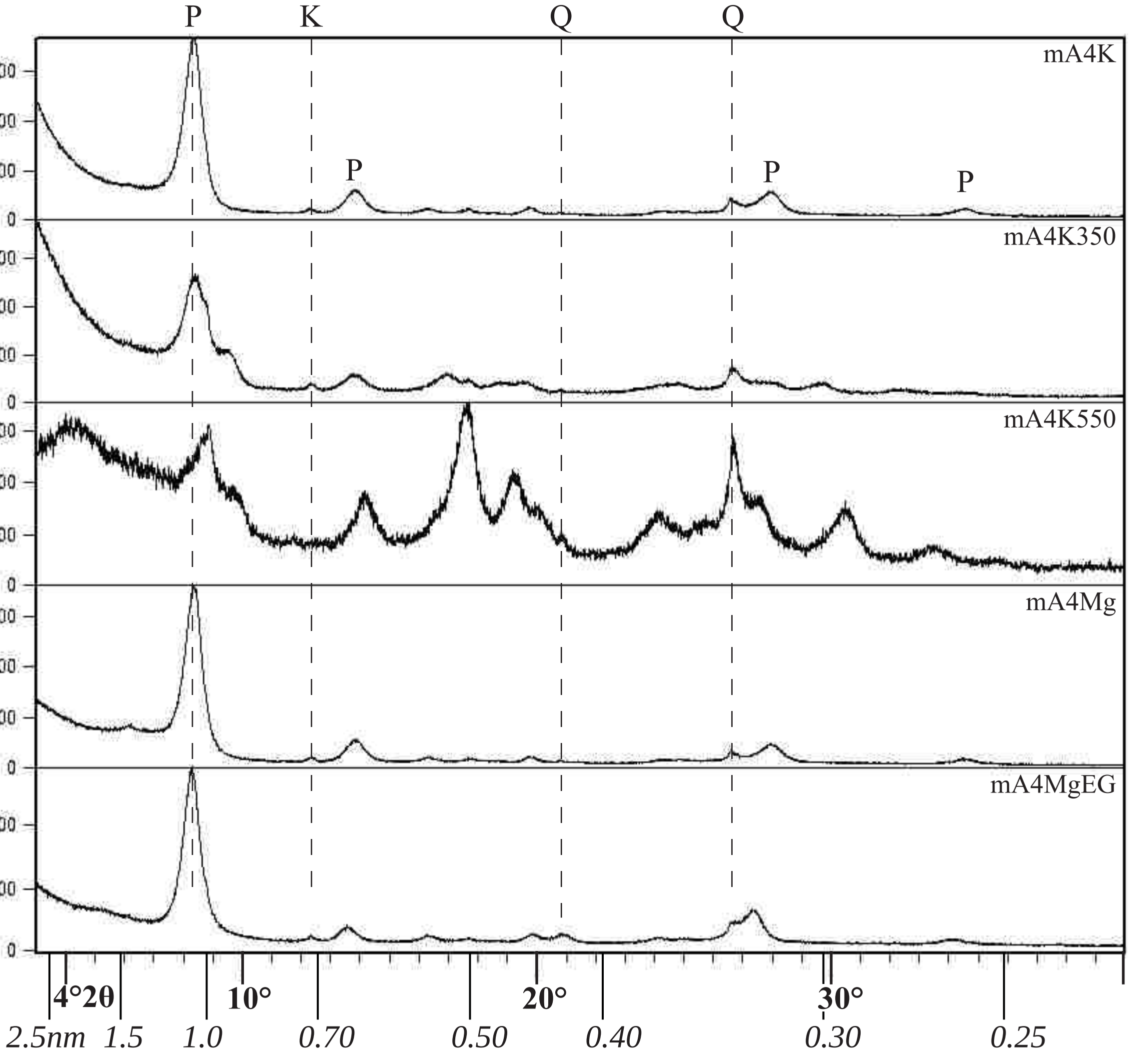

Clay-sized particle fraction XRD spectra for sample mA4. Y-axis units are relative peak counts for each spectrum. X-axis indicates scan angle (°2θ) and d-spacing (nm). Treatments are K-saturation (K), K-saturation heated to 350°C (K350) and 550°C (K550), Mg-saturation (Mg), and Mg-saturation with ethylene glycol solvation (MgEG). Ch = chlorite, I = illite, K = kaolinite, P = palygorskite, and Q = quartz.

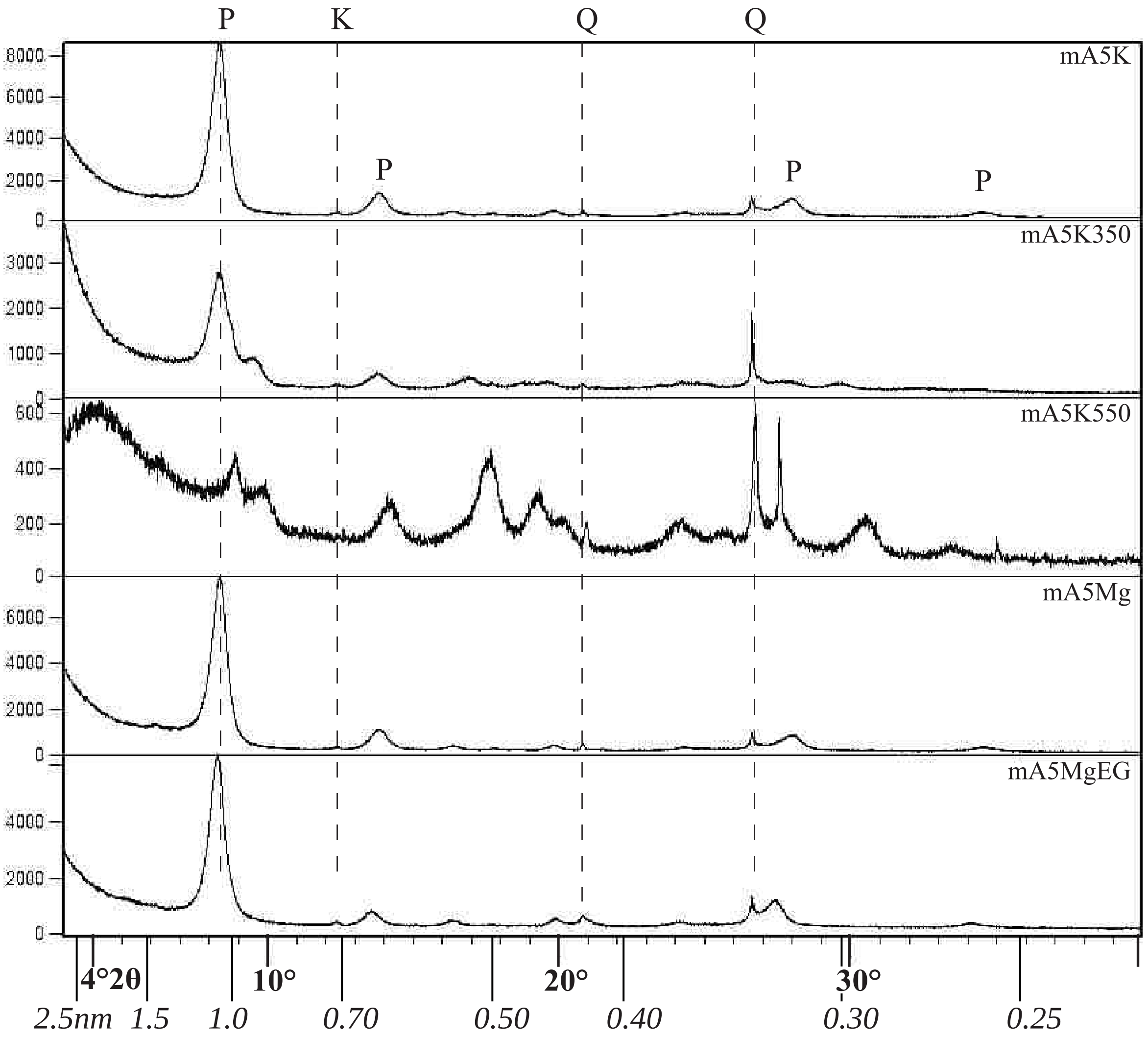

Clay-sized particle fraction XRD spectra for sample mA5. Y-axis units are relative peak counts for each spectrum. X-axis indicates scan angle (°2θ) and d-spacing (nm). Treatments are K-saturation (K), K-saturation heated to 350°C (K350) and 550°C (K550), Mg-saturation (Mg), and Mg-saturation with ethylene glycol solvation (MgEG). Ch = chlorite, I = illite, K = kaolinite, P = palygorskite, and Q = quartz.

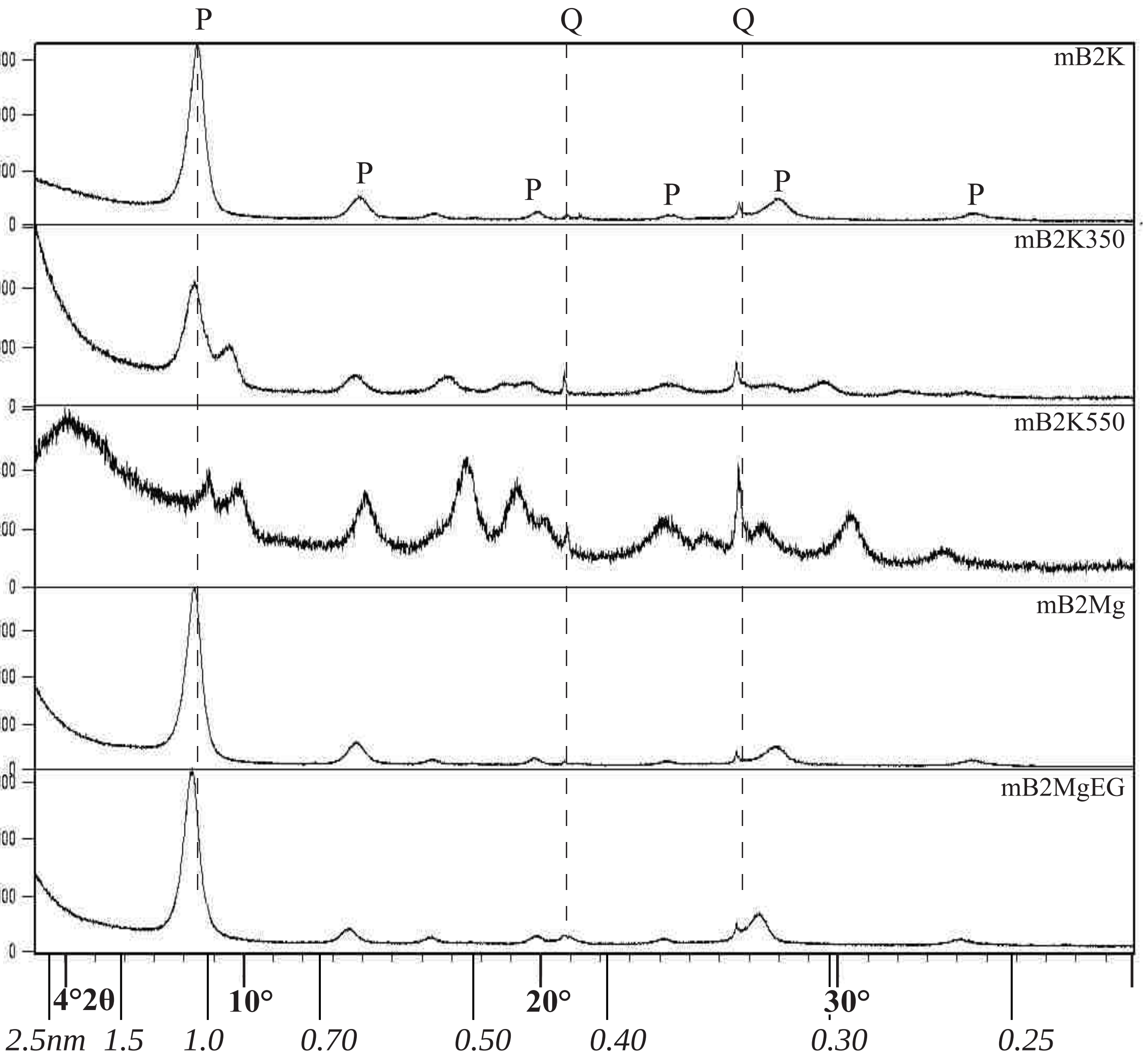

Clay-sized particle fraction XRD spectra for sample mB2. Y-axis units are relative peak counts for each spectrum. X-axis indicates scan angle (°2θ) and d-spacing (nm). Treatments are K-saturation (K), K-saturation heated to 350°C (K350) and 550°C (K550), Mg-saturation (Mg), and Mg-saturation with ethylene glycol solvation (MgEG). P = palygorskite, and Q = quartz.

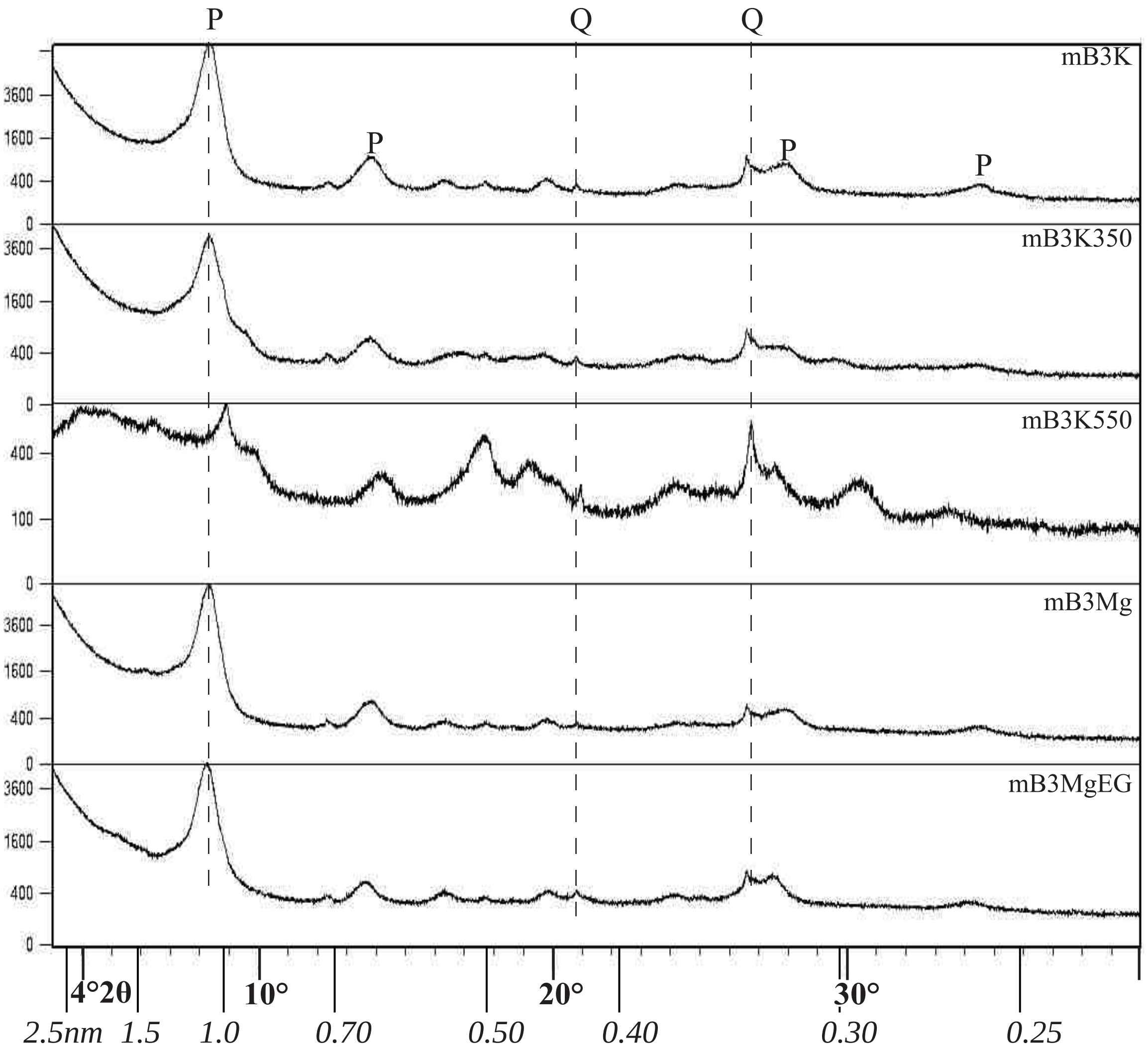

Clay-sized particle fraction XRD spectra for sample mB3. Y-axis units are relative peak counts for each spectrum. X-axis indicates scan angle (°2θ) and d-spacing (nm). Treatments are K-saturation (K), K-saturation heated to 350°C (K350) and 550°C (K550), Mg-saturation (Mg), and Mg-saturation with ethylene glycol solvation (MgEG). Ch = chlorite, I = illite, K = kaolinite, P = palygorskite, and Q = quartz.

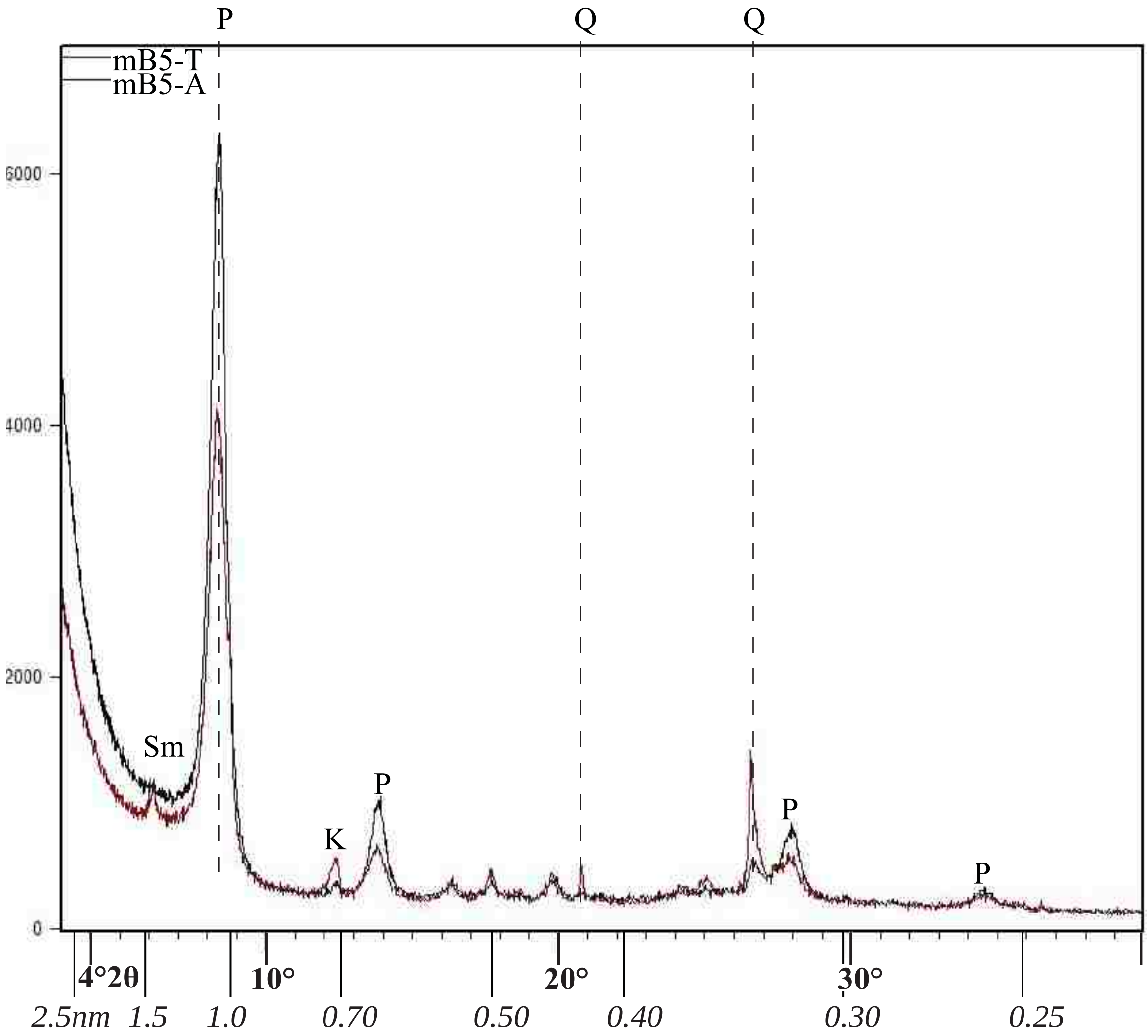

XRD spectra for aliquots of Sample mB5. Y-axis units are relative peak counts for each spectrum. Aliqouts are “-A” after acetate treatment, and “-T” after acetate and tiron treatments. Y-axis units are relative peak counts for each spectrum. X-axis indicates scan angle (°2θ) and d-spacing (nm). Only the base-line K-treatment scans are shown.K = kaolinite, P = palygorskite, Q = quartz., Sm = smectite. Note apparent increases in smectite and kaolinite signatures between acetate and tiron treatments, suggesting possible loss of the finest, palygorskite clay-sized particle fraction.

APPENDIX 3.1

SELECTED GC/MS DATA

Five geochronology samples from Mormon Mesa, and two reference standards from the Clay Minerals Society Source Clays repository were analyzed using GC/MS. Mormon Mesa samples include samples mA1, mA4, and mB4 from the massive horizon, and samples mB1 and mB2 from the uppermost transitional horizon. Reference standards include PFL-1 (palygorskite) and SEP-1 (sepiolite).

Both acetate-treated and tiron-treated aliquots of the Mormon Mesa samples were studied. Both palygorskite and sepiolite were analyzed as received from the Source Clays Repository (the sepiolite sample arrived in aggregate and was crushed to << 2 mm, otherwise, no additional processing was performed). Acetate- and tiron-treated aliquots of the palygorskite reference standard were also studied. No samples from the Jornada (JER) La Mesa soil were analyzed.

The following data includes bulk GC/MS chromatographs obtained using cryo- and tetra-methyl ammonium hydroxide (TMAH) GC/MS procedures, as well as selected mass-filtered chromatographs juxtaposed to differentiate broad groups of compounds, and to compare relative compositions of each sample.

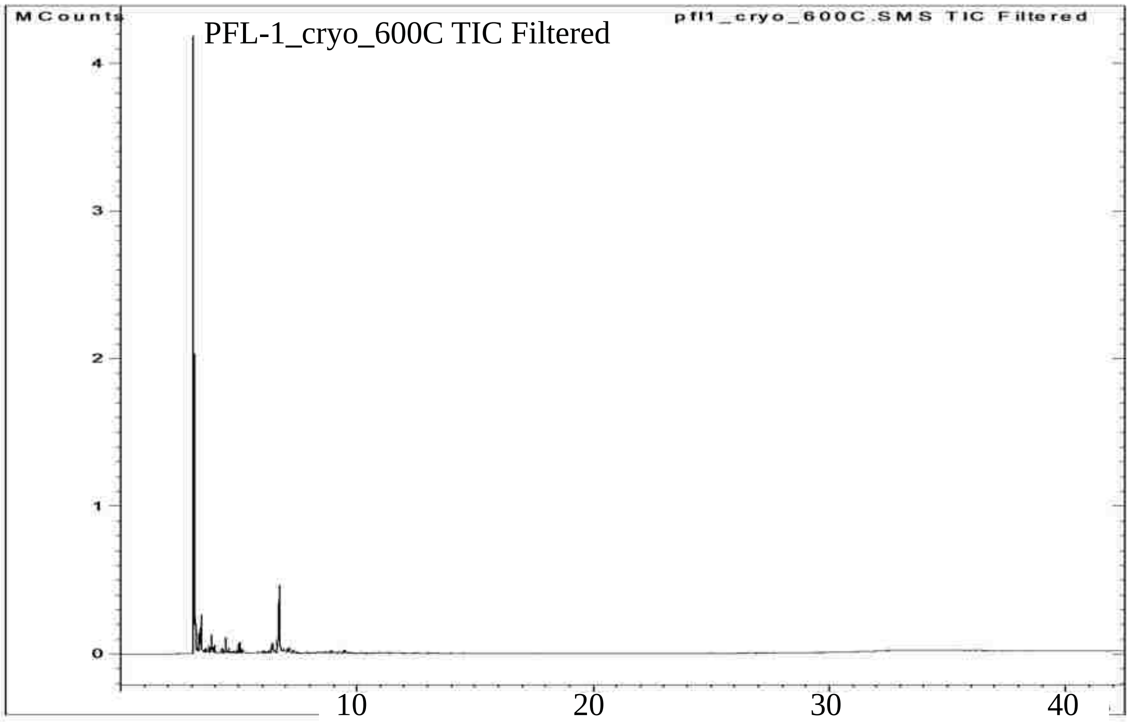

Bulk GC/MS chromatograph (cryo treatment) of palygorskite reference standard PFL-1 as received from the Source Clays Repository. Y-axis units are MCounts. X-axis units are minutes.

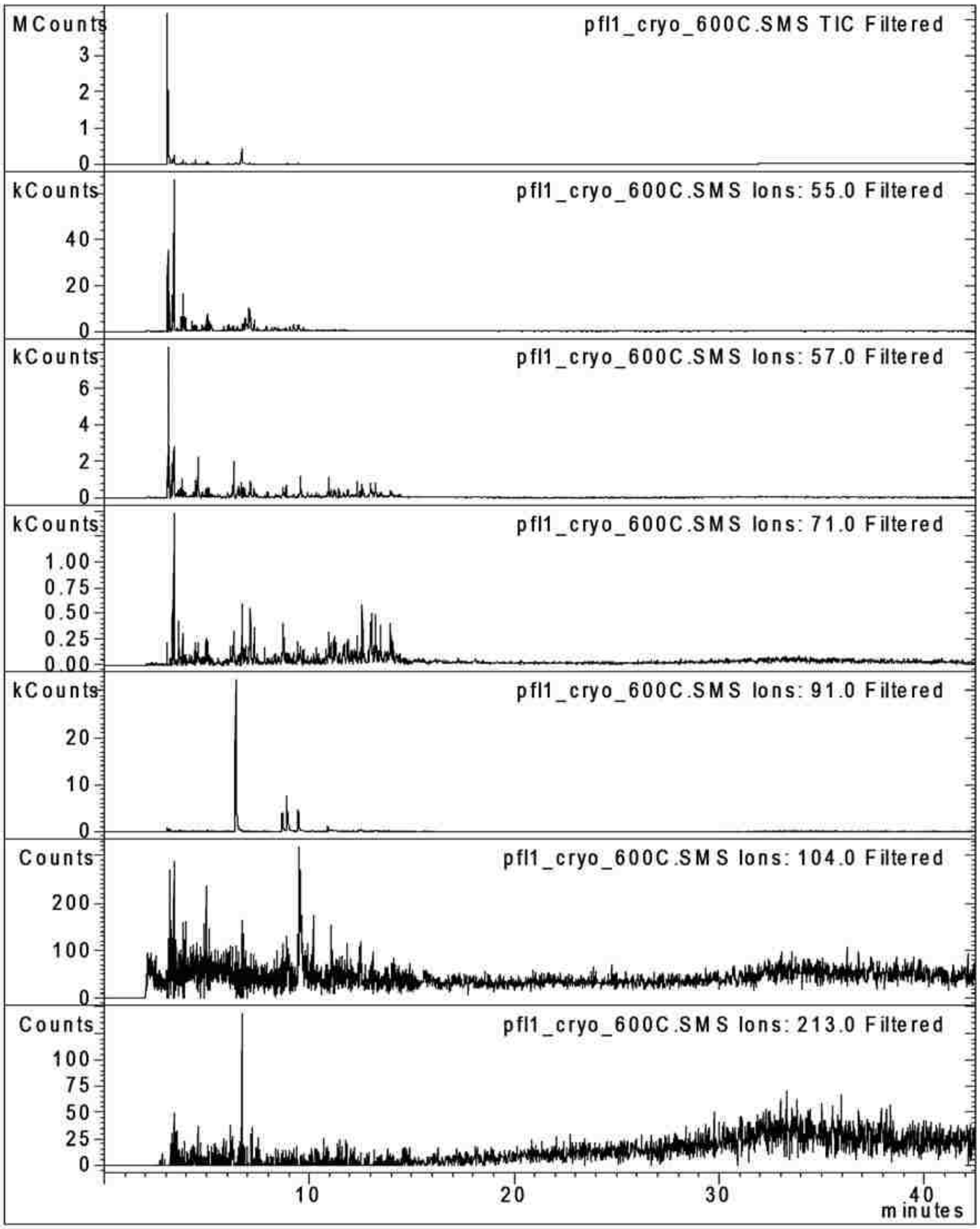

GC/MS spectra from the untreated (as received from the Source Clays Repository) Palygorskite reference standard (cryo analysis). The plots reveal relative contributions to the bulk chromatograph (top) from ion masses 55, 57, 71, 78, 91, 104, and 213.

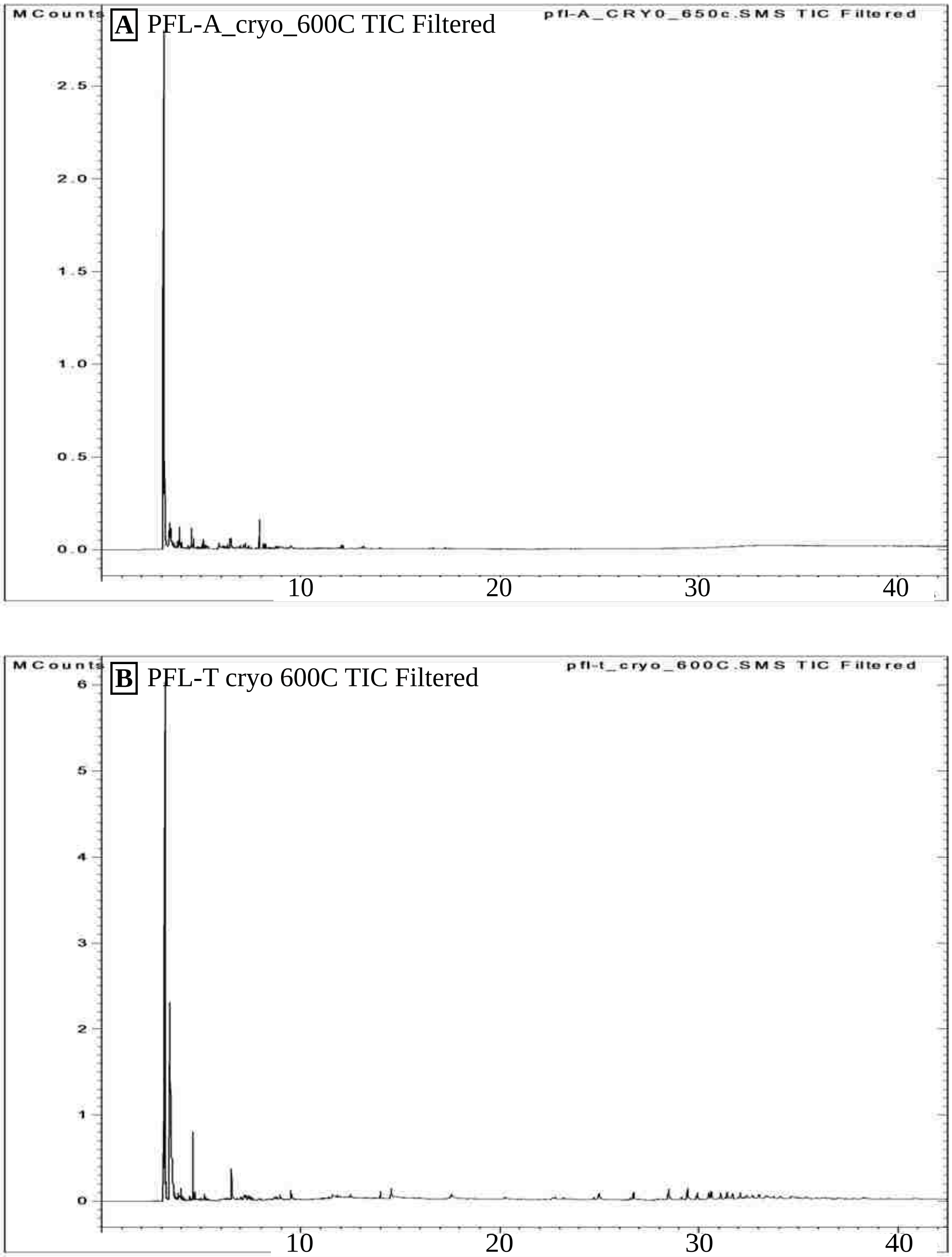

Palygorskite reference standard PFL-1 - Acetate and Tiron aliquots. Bulk GC/MS chromatographs from (A) acetate aliquot and (B) tiron aliquot cryo analyses. No tmah analyses were conducted on this standard. Y-axis units are MCounts. X-axis units are minutes.

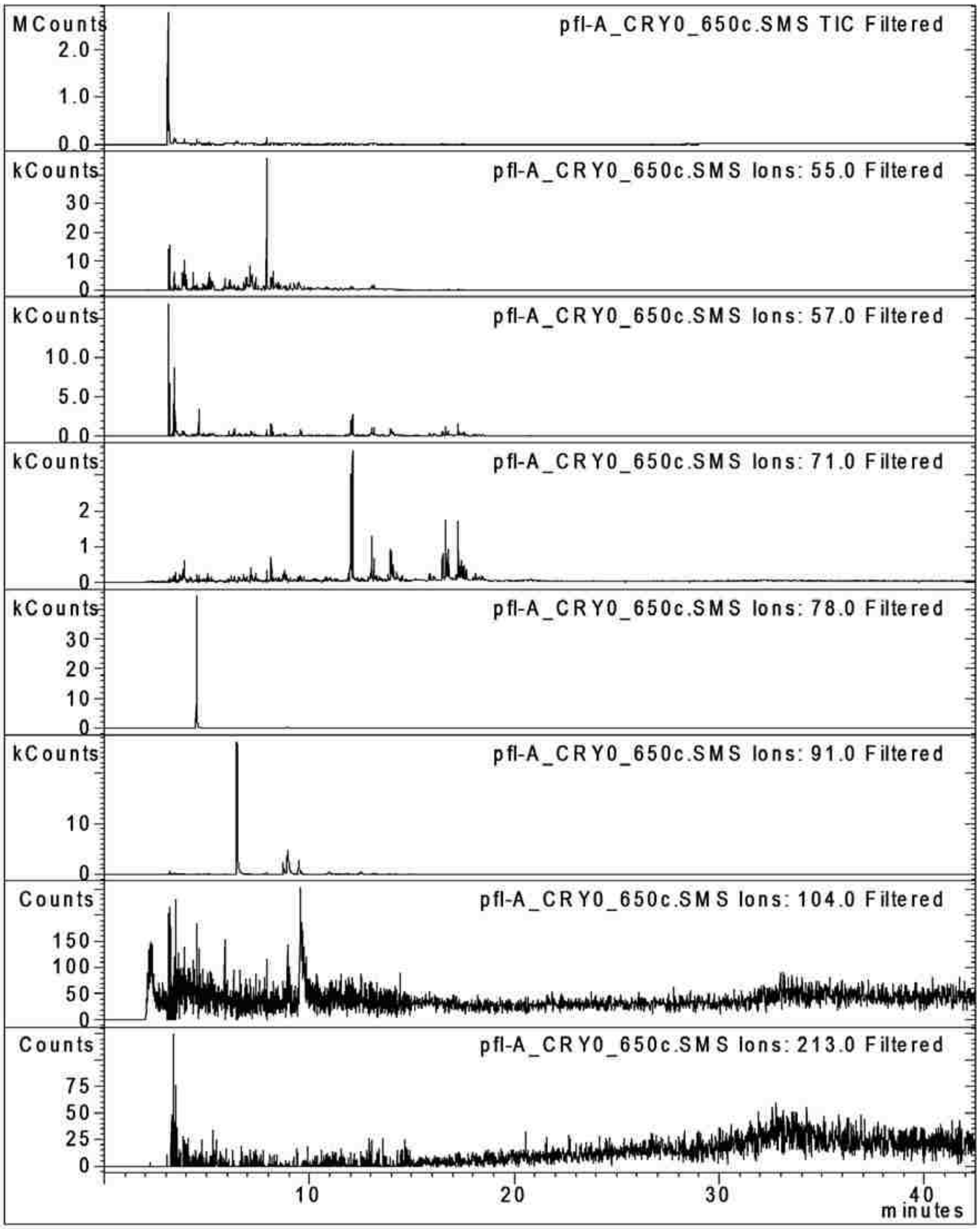

GC/MS spectra from the acetate-treated palygorskite reference standard (cryo analysis). The plots reveal relative contributions to the bulk chromatograph (top) from ion masses 55, 57, 71, 78, 91, 104, and 213.

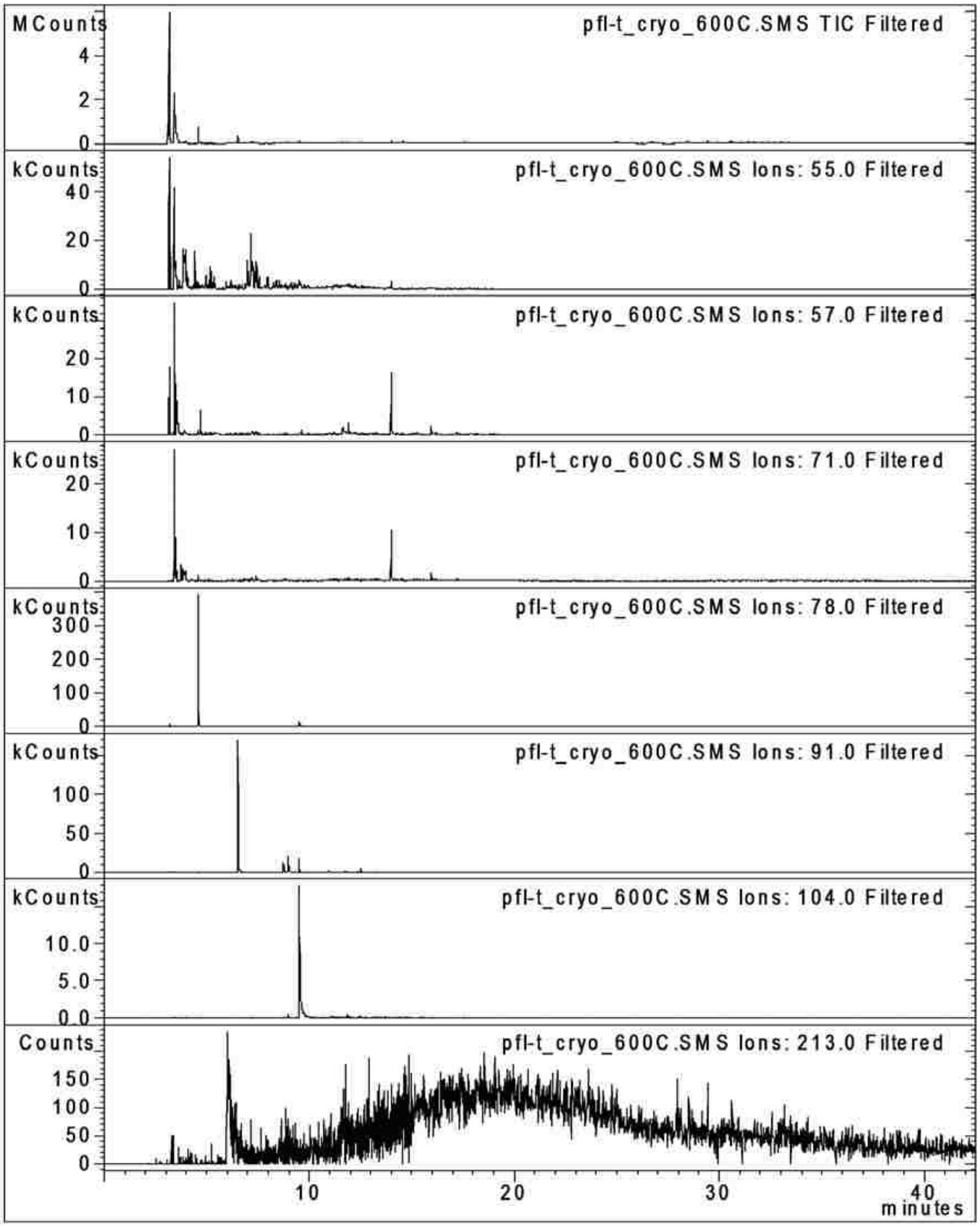

GC/MS spectra from the tiron-treated palygorskite reference standard (cryo analysis). The plots reveal relative contributions to the bulk chromatograph (top) from ion masses 55, 57, 71, 78, 91, 104, and 213.

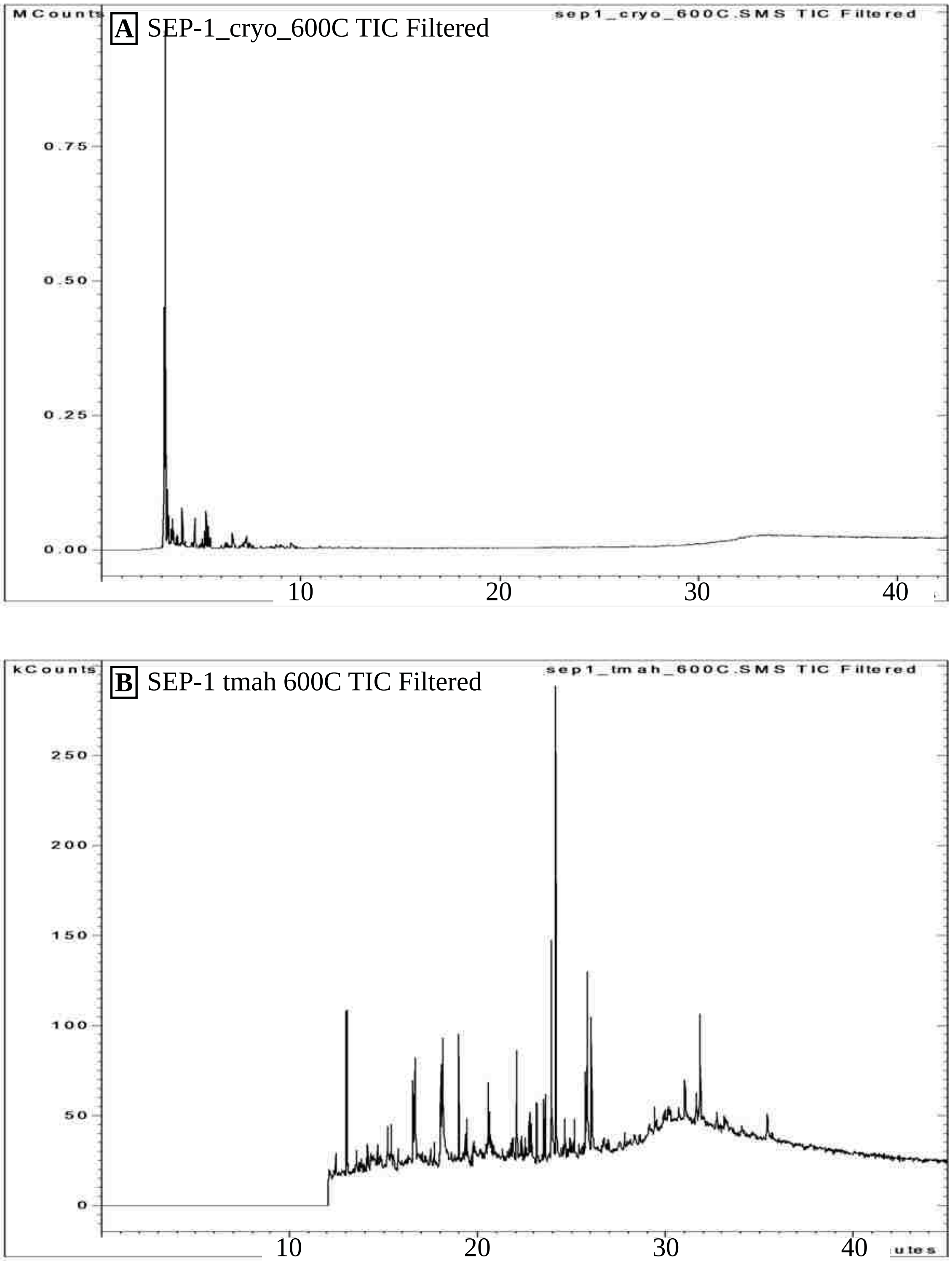

Sepiolite reference standard Sep-1 as received from the Source Clays Repository. Bulk GC/MS chromatographs from (A) cryo and (B) TMAH analyses. Y-axis units are MCounts in (A), kCounts in (B). X-axis units are minutes.

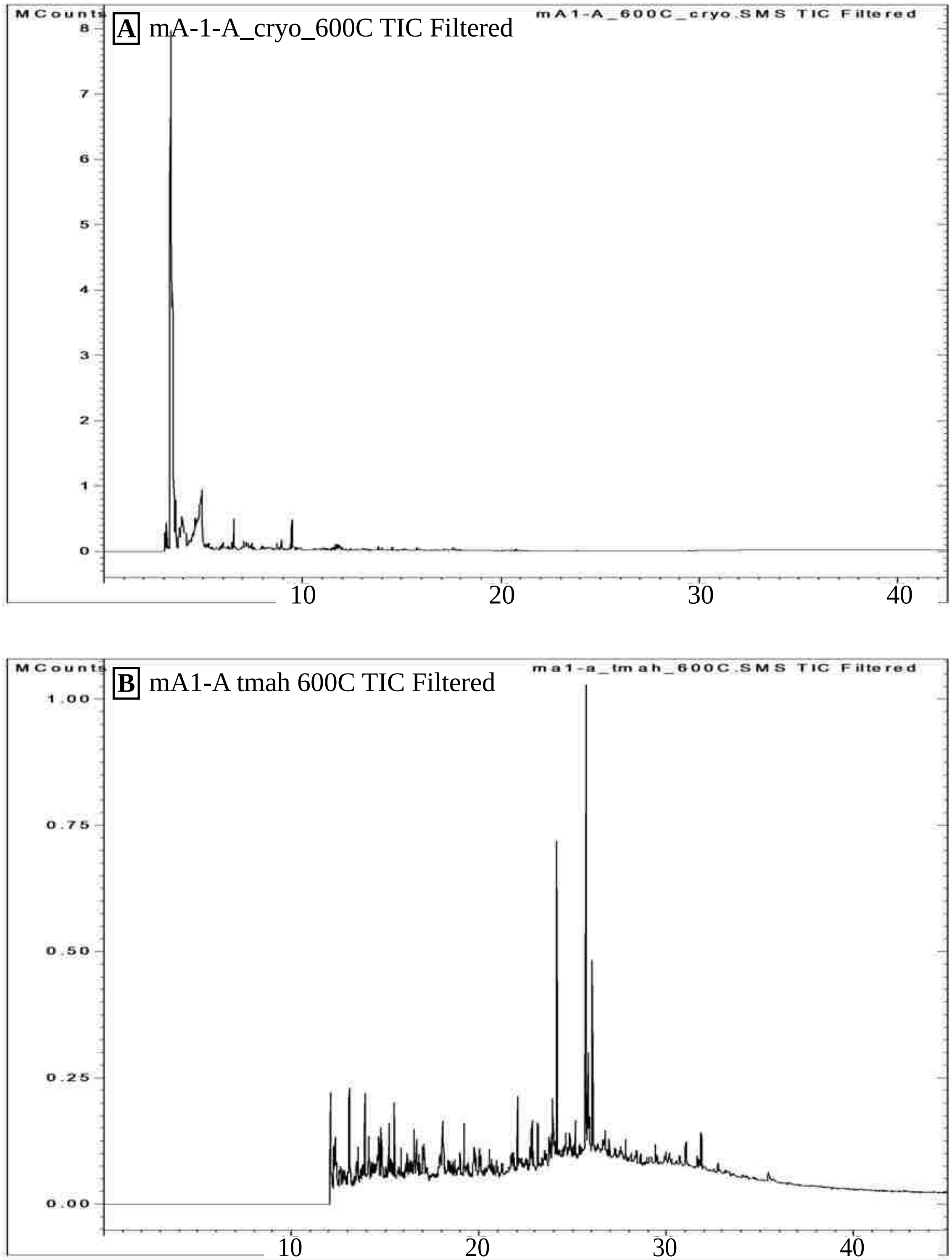

Sample mA1 - Acetate aliquot. Bulk GC/MS chromatographs from (A) cryo and (B) tmah analyses. Y-axis units are MCounts, X-axis units are minutes.

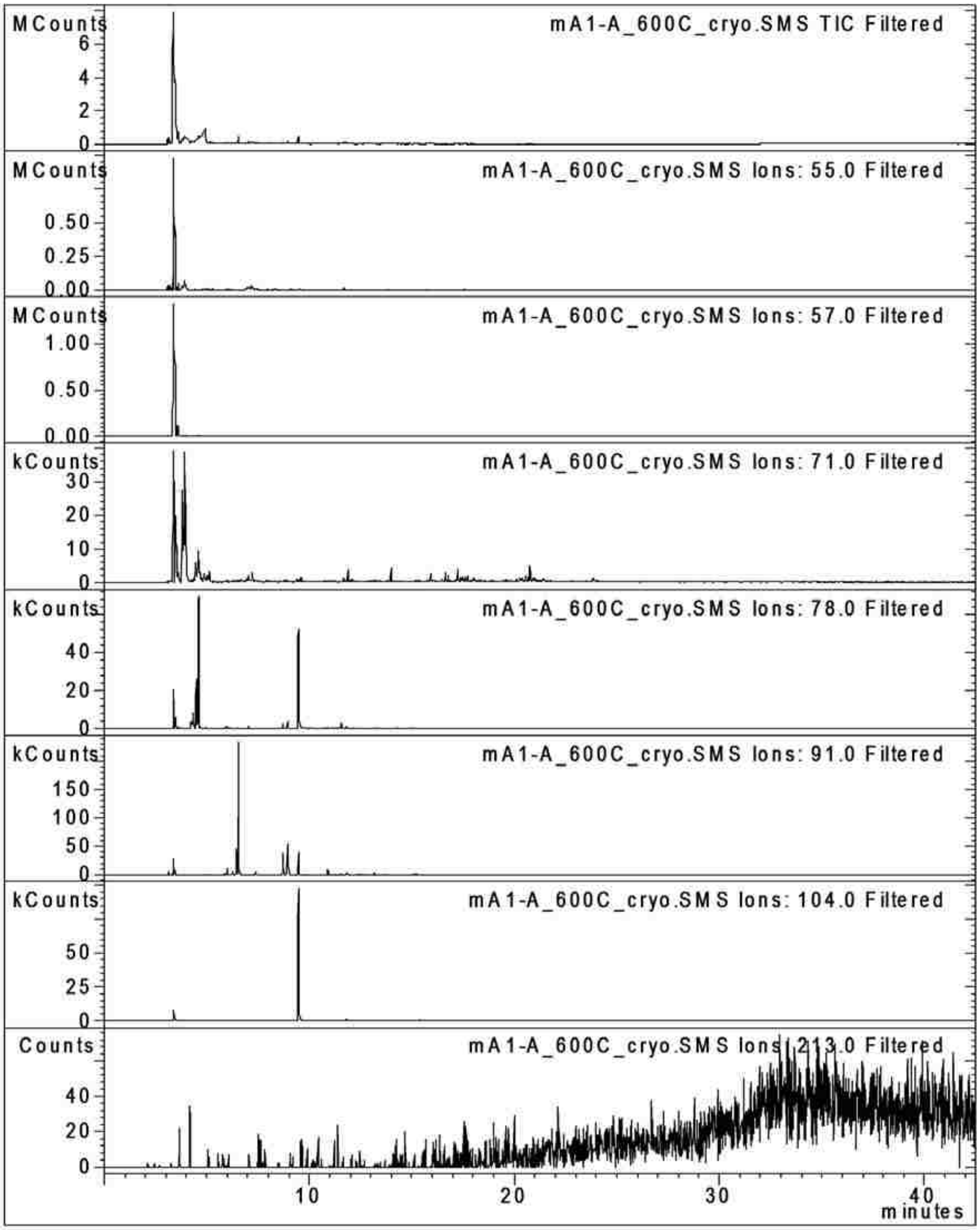

Sample mA1-Acetate aliquot. GC/MS spectra from Mormon Mesa geochronology sample mA1 (cryo analysis). The plots reveal relative contributions to the bulk chromatograph (top) from ion masses 55, 57, 71, 78, 91, 104, and 213.

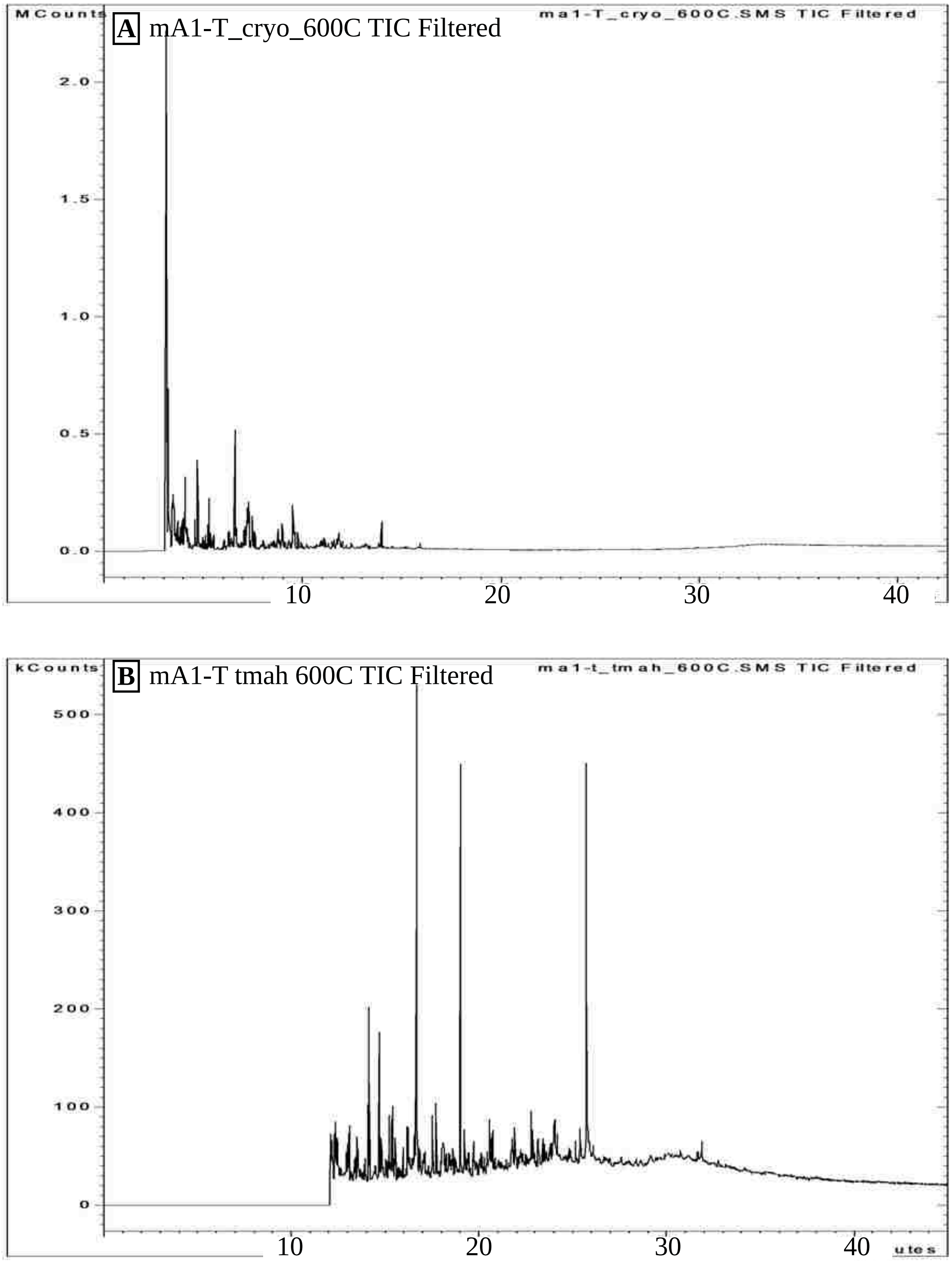

Sample mA1 - Tiron aliquot. Bulk GC/MS chromatographs from (A) cryo and (B) tmah analyses. Y-axis units are MCounts in (A), KCounts in (B). X-axis units are minutes.

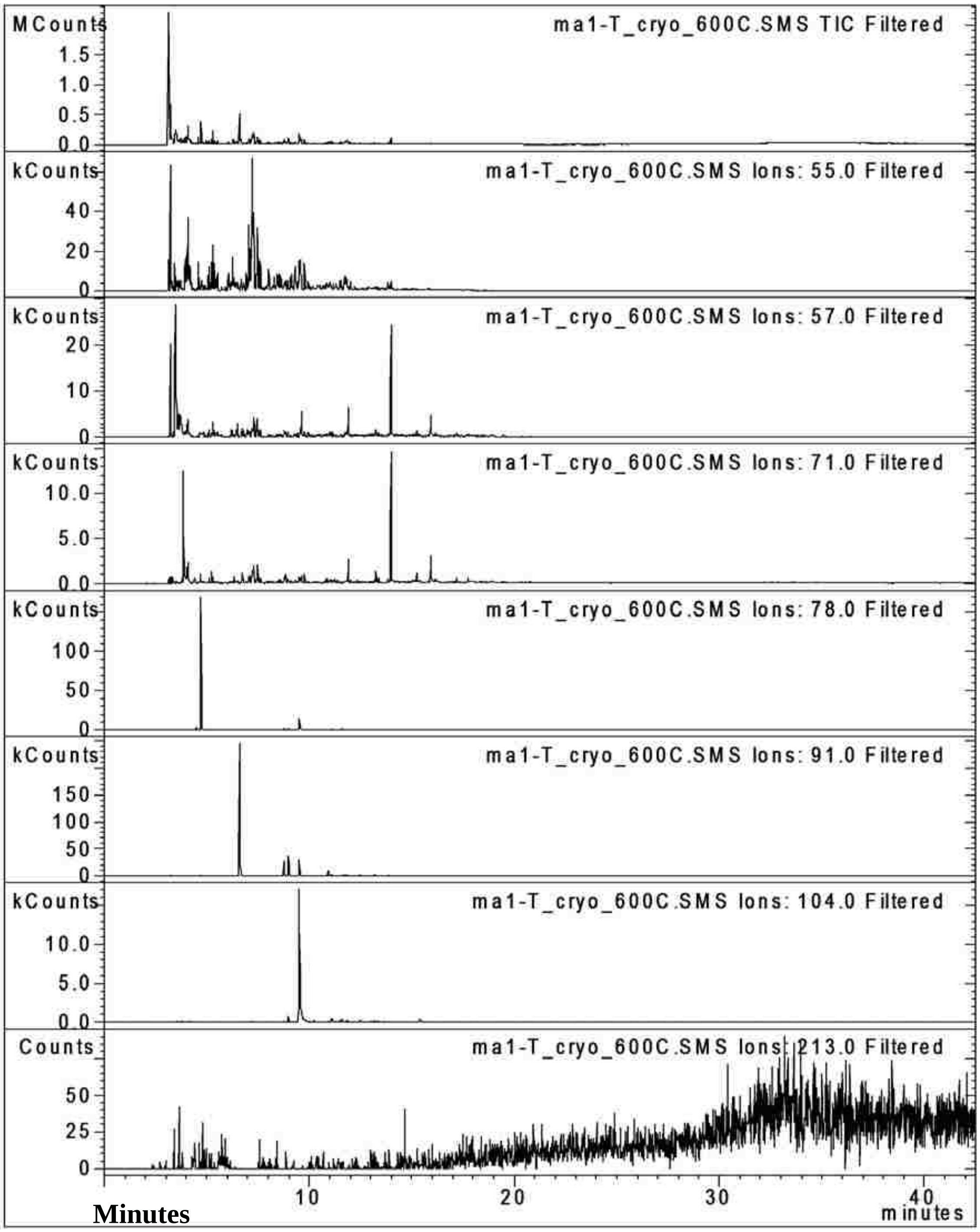

Sample mA1-Tiron aliquot. GC/MS spectra from Mormon Mesa geochronology sample mA1 (cryo analysis). The plots reveal relative contributions to the bulk chromatograph (top) from ion masses 78, 55, 57, 71, and 91.

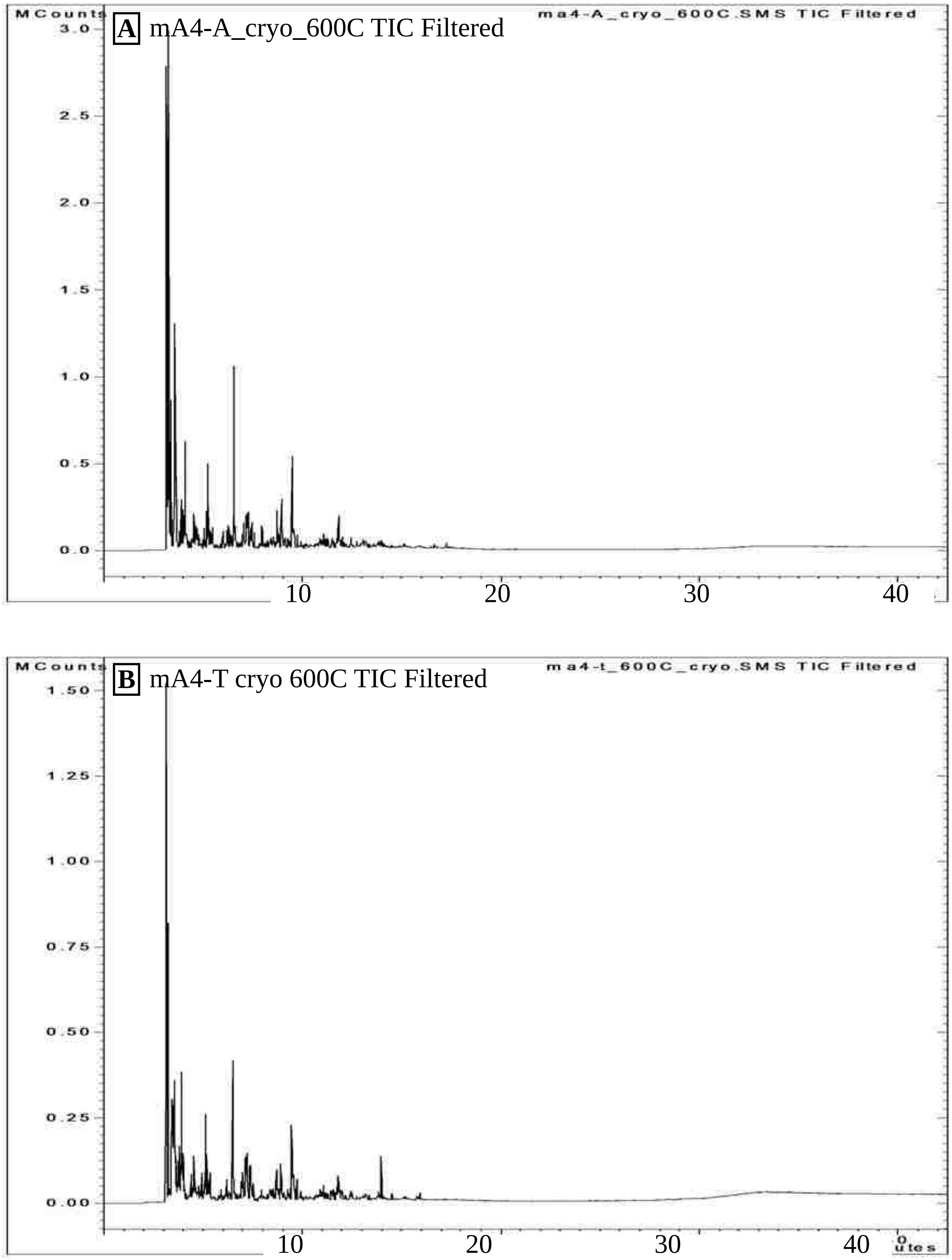

Sample mA4 - Acetate and Tiron aliquots. Bulk GC/MS chromatographs from (A) acetate aliquot and (B) tiron aliquot cryo analyses. No tmah analyses were conducted on this sample. Y-axis units are MCounts. X-axis units are minutes.

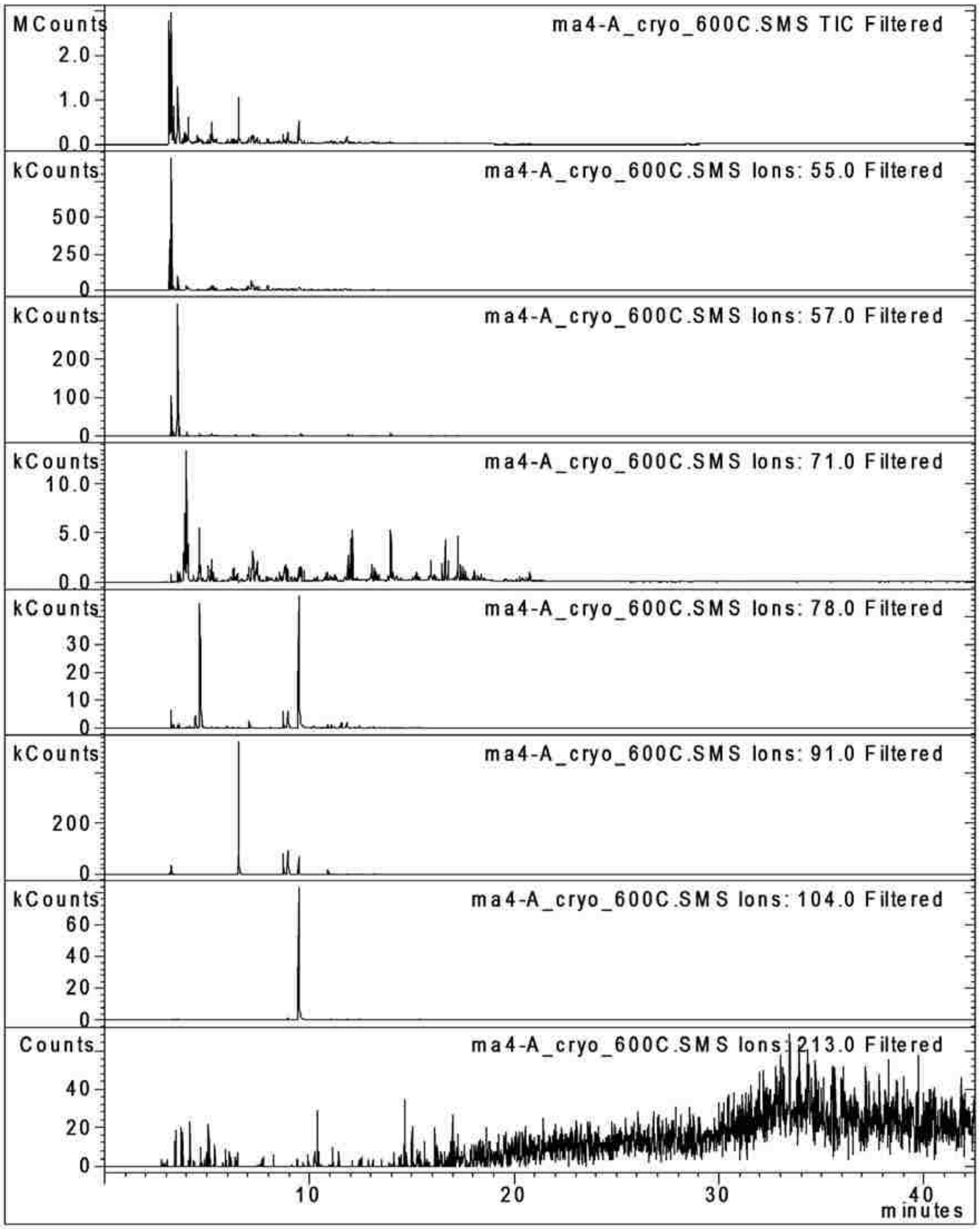

Sample mA4-Acetate aliquot. GC/MS spectra from Mormon Mesa geochronology sample mA4 (cryo analysis). The plots reveal relative contributions to the bulk chromatograph (top) from ion masses 55, 57, 71, 78, 91, 104, and 213.

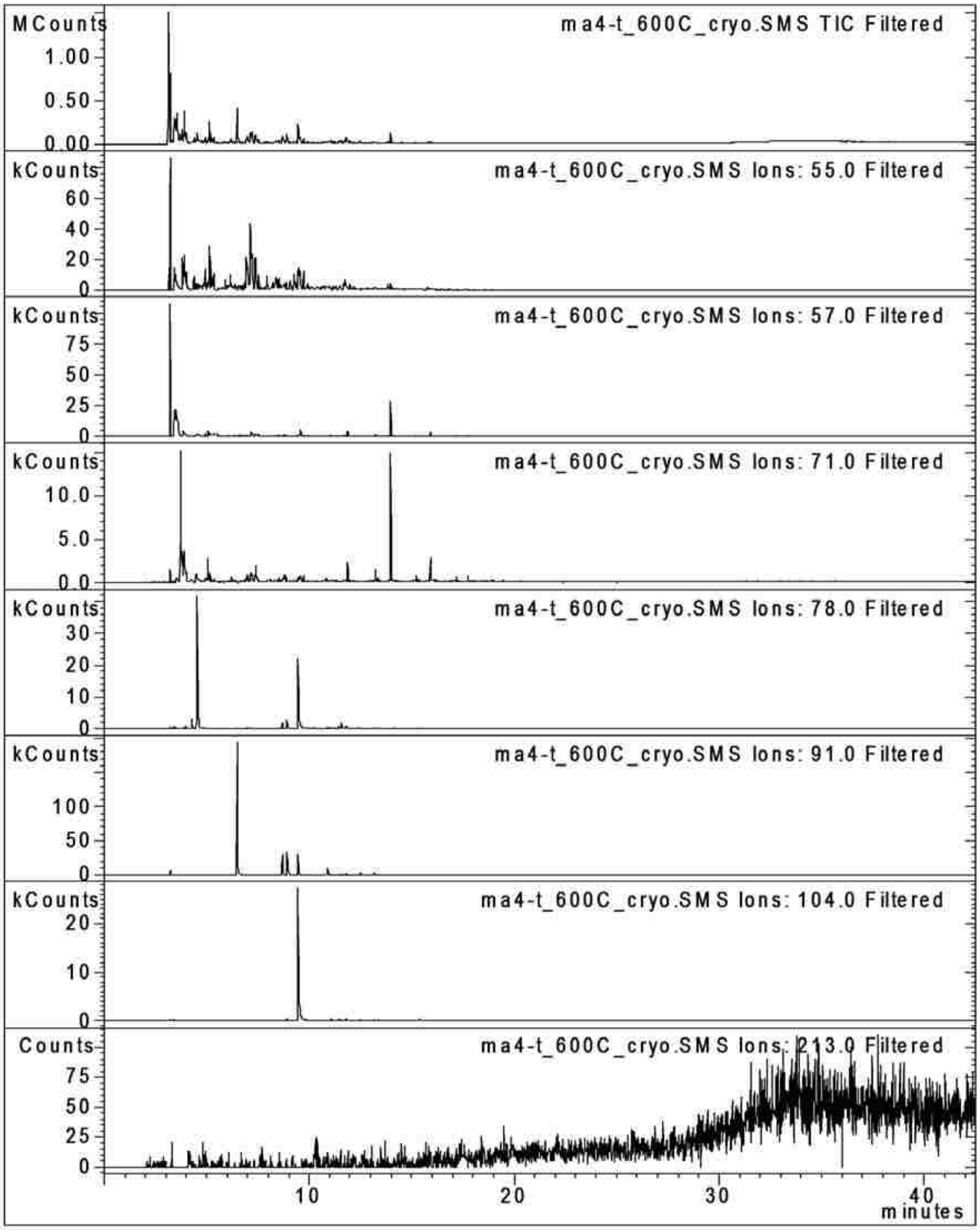

Sample mA4-Tiron aliquot. GC/MS spectra from Mormon Mesa geochronology sample mA4 (cryo analysis). The plots reveal relative contributions to the bulk chromatograph (top) from ion masses 55, 57, 71, 78, 91, 104, and 213.

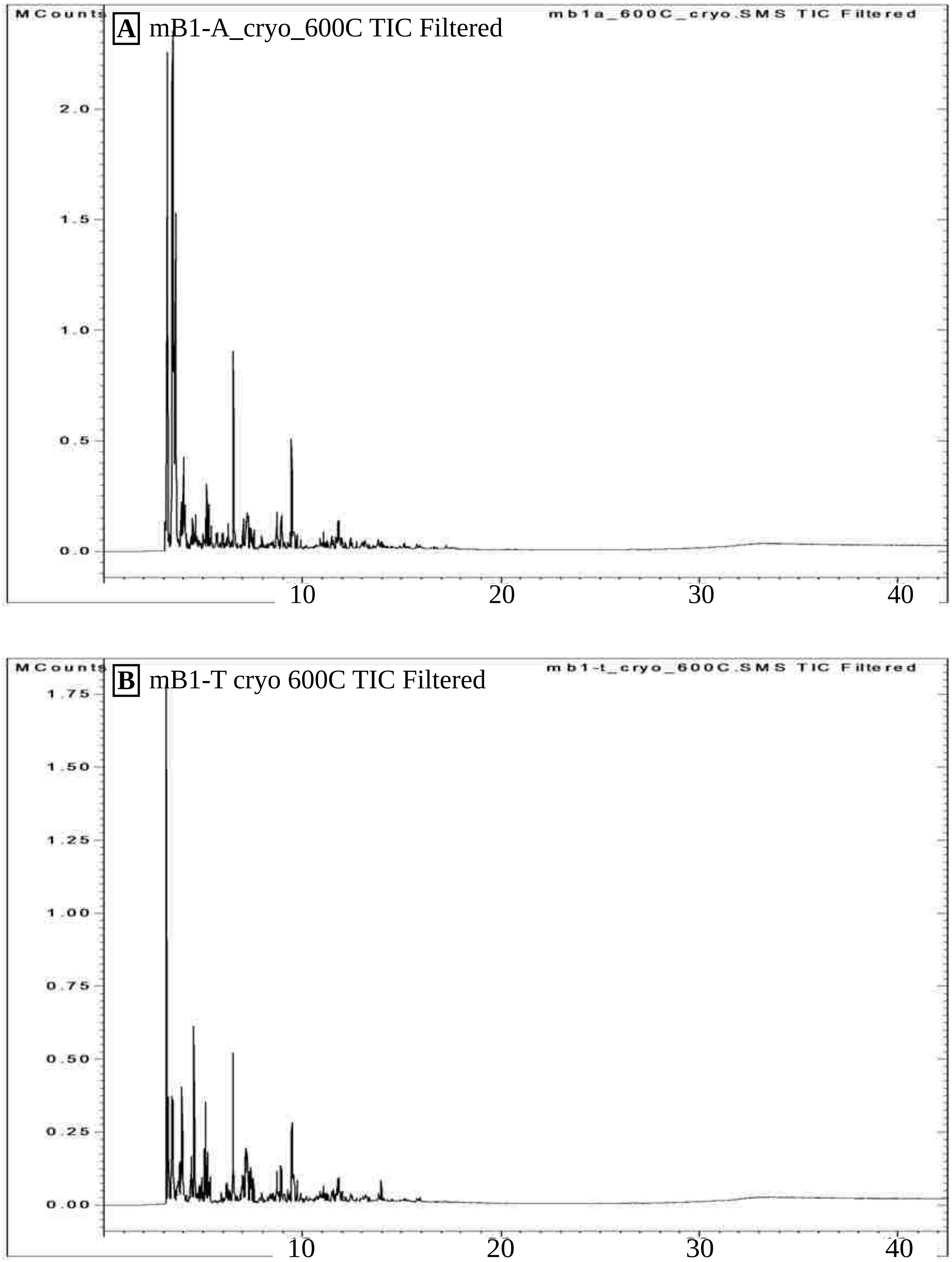

Sample mB1 - Acetate and Tiron aliquots. Bulk GC/MS chromatographs from (A) acetate aliquot and (B) tiron aliquot cryo analyses. No tmah analyses were conducted on this sample. Y-axis units are MCounts. X-axis units are minutes.

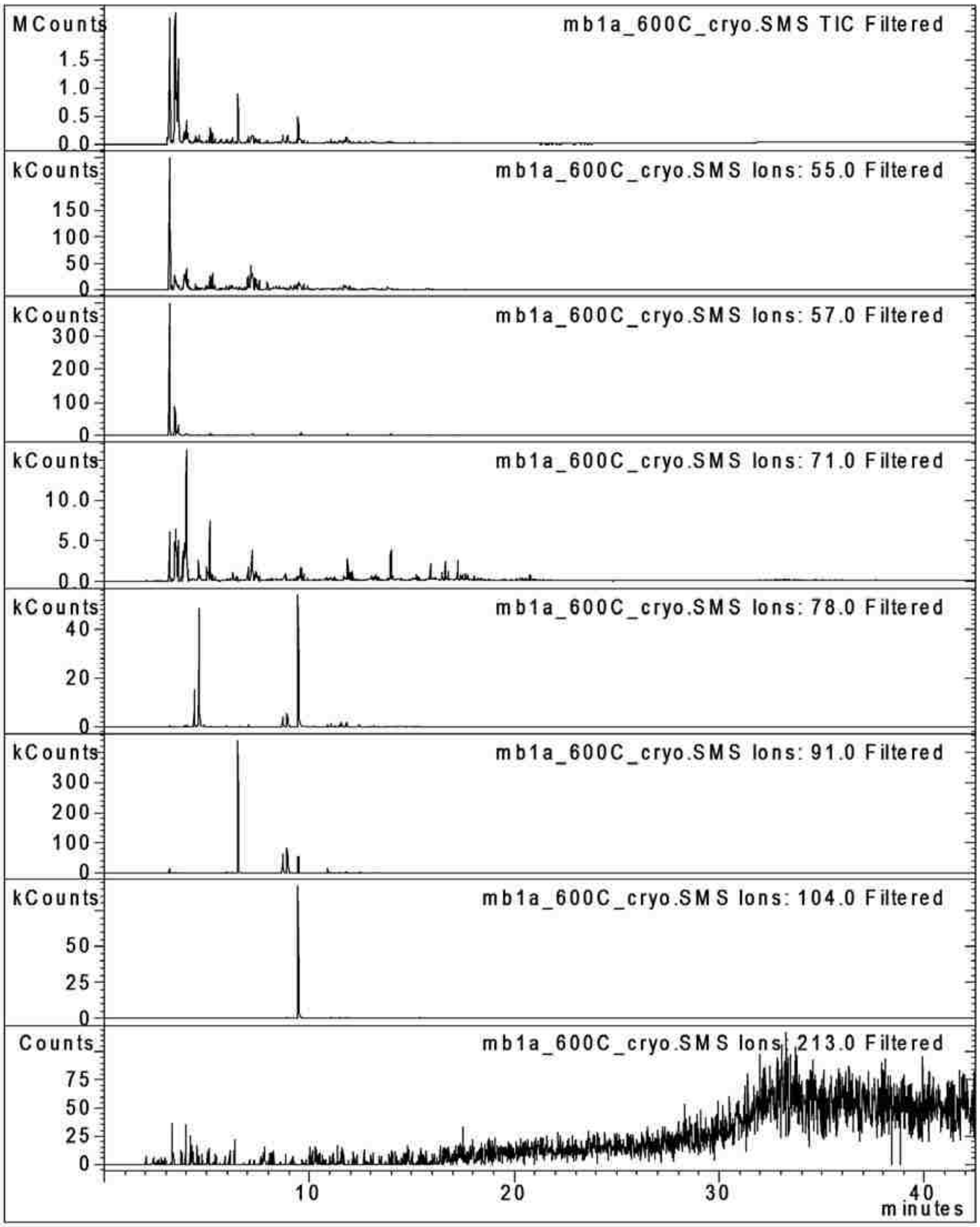

Sample mB1-Acetate aliquot. GC/MS spectra from Mormon Mesa geochronology sample mB1(cryo analysis). The plots reveal relative contributions to the bulk chromatograph (top) from ion masses 55, 57, 71, 78, 91, 104, and 213.

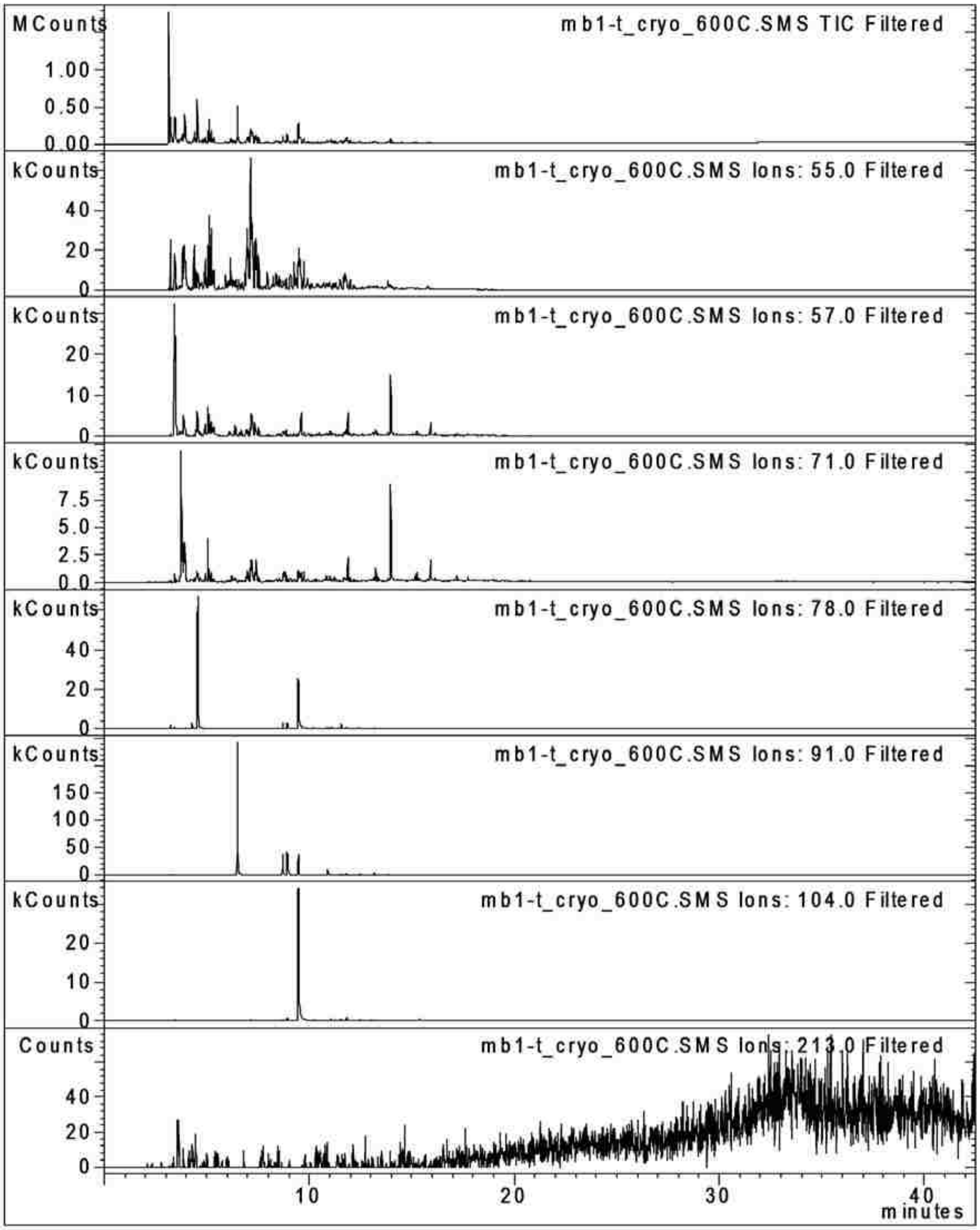

Sample mB1-Tiron aliquot. GC/MS spectra from Mormon Mesa geochronology sample mB1 (cryo analysis). The plots reveal relative contributions to the bulk chromatograph (top) from ion masses 55, 57, 71, 78, 91, 104, and 213.

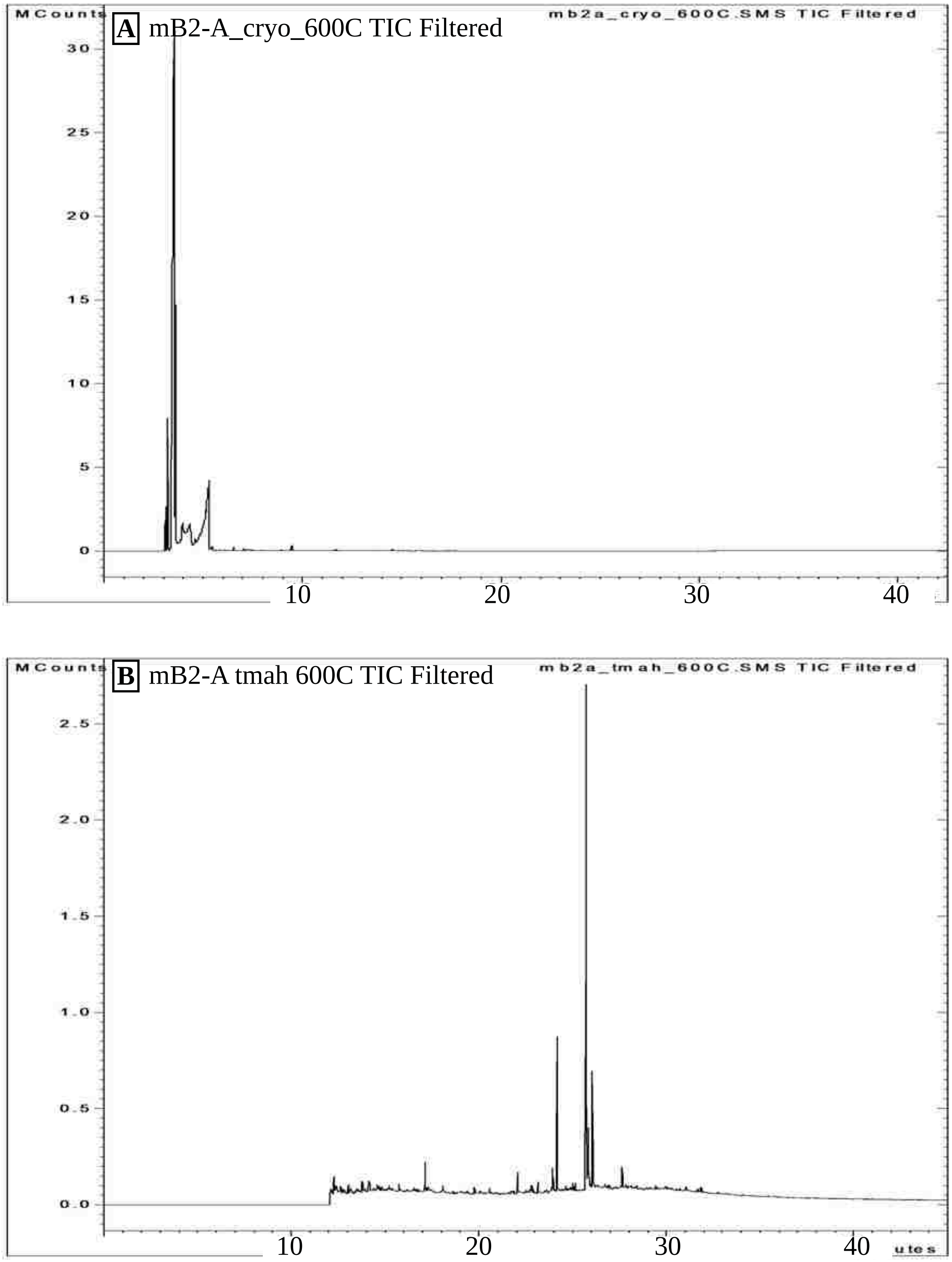

Sample mB2 - Acetate aliquot. Bulk GC/MS chromatographs from (A) cryo and (B) tmah analyses. Y-axis units are MCounts. X-axis units are minutes.

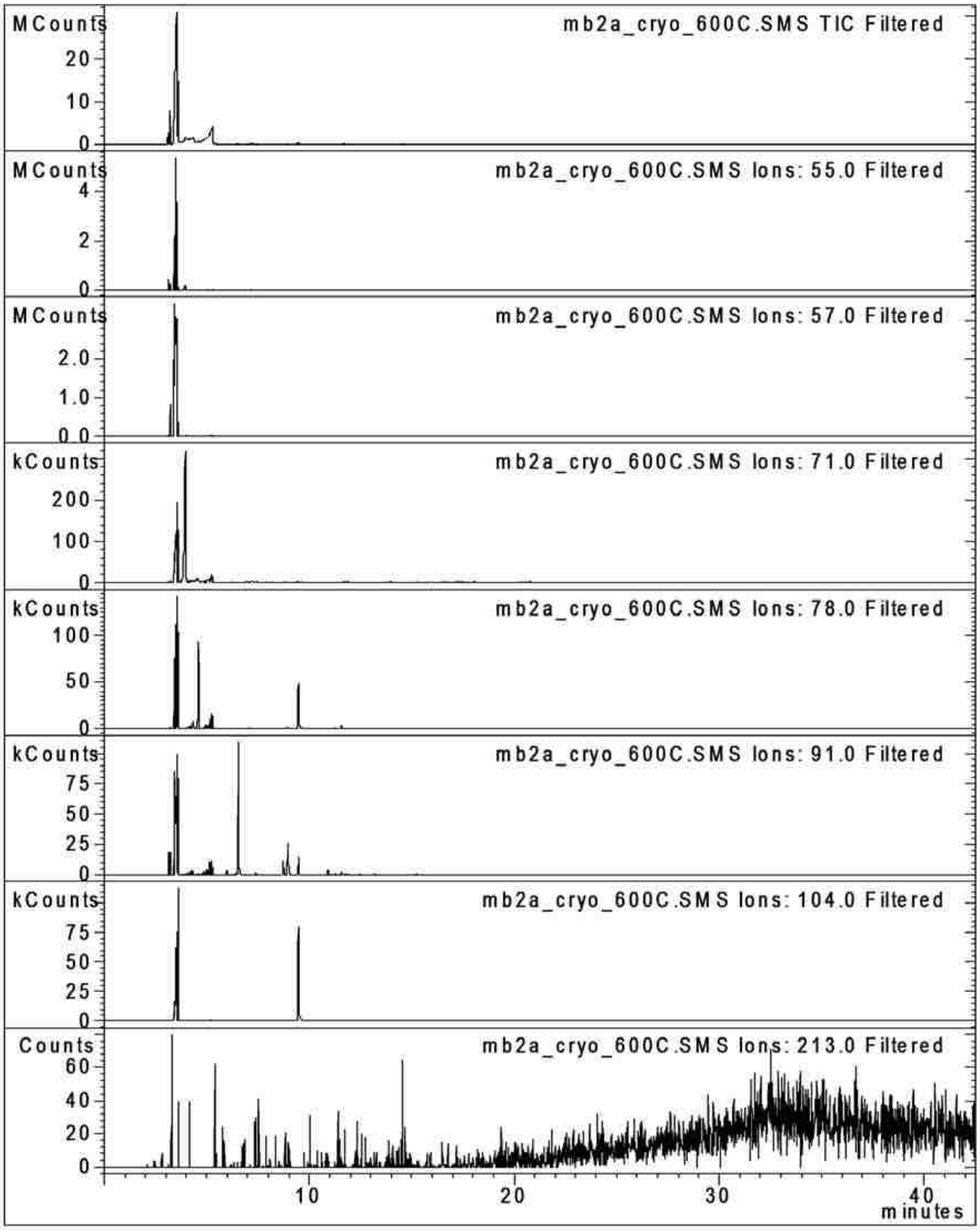

Sample mB2-Acetate aliquot. GC/MS spectra from Mormon Mesa geochronology sample mB2 (cryo analysis). The plots reveal relative contributions to the bulk chromatograph (top) from ion masses 55, 57, 71, 78, 91, 104, and 213.

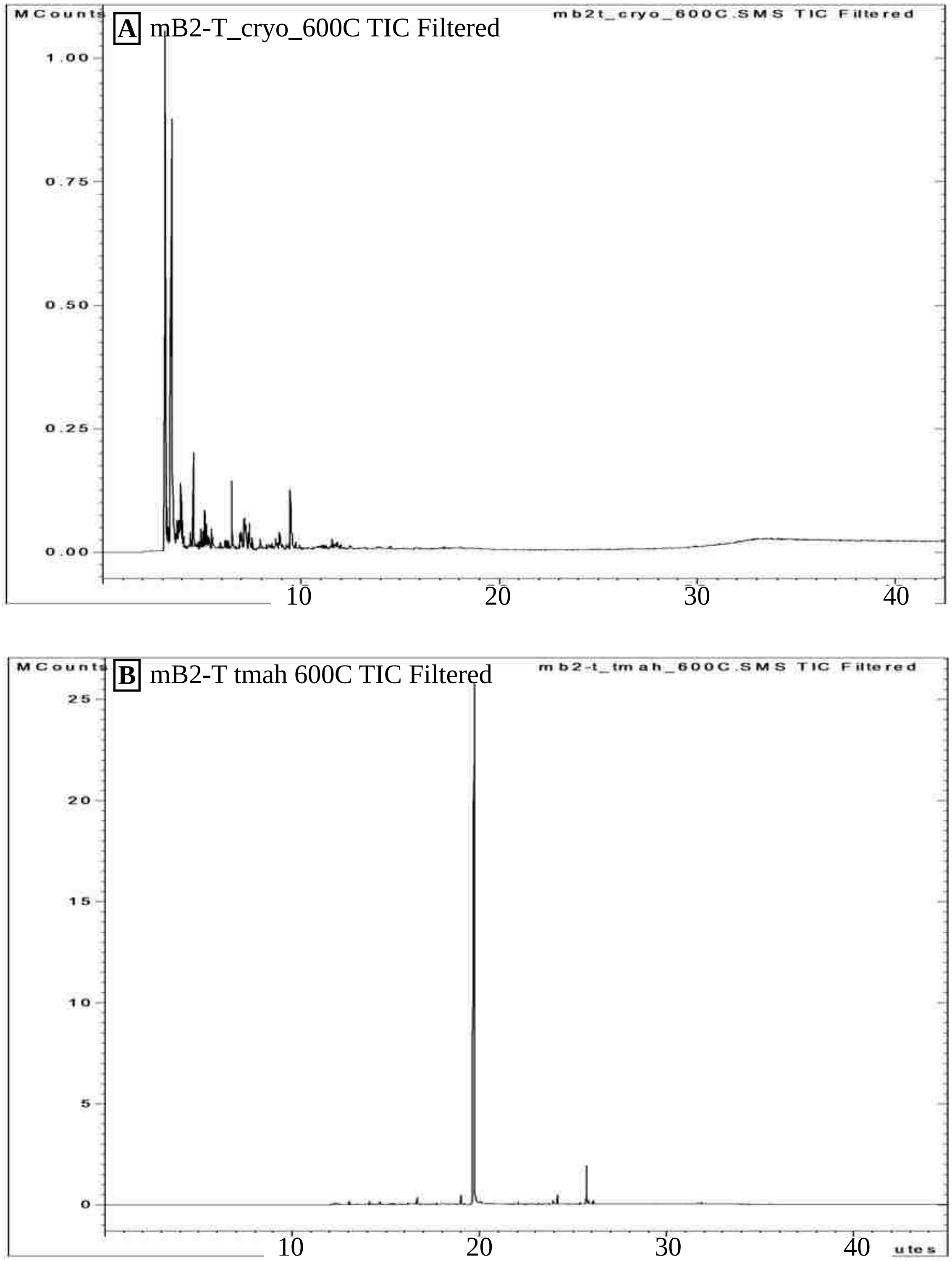

Sample mB2 - Tiron aliquot. Bulk GC/MS chromatographs from (A) cryo and (B) tmah analyses. Y-axis units are MCounts. X-axis units are minutes.

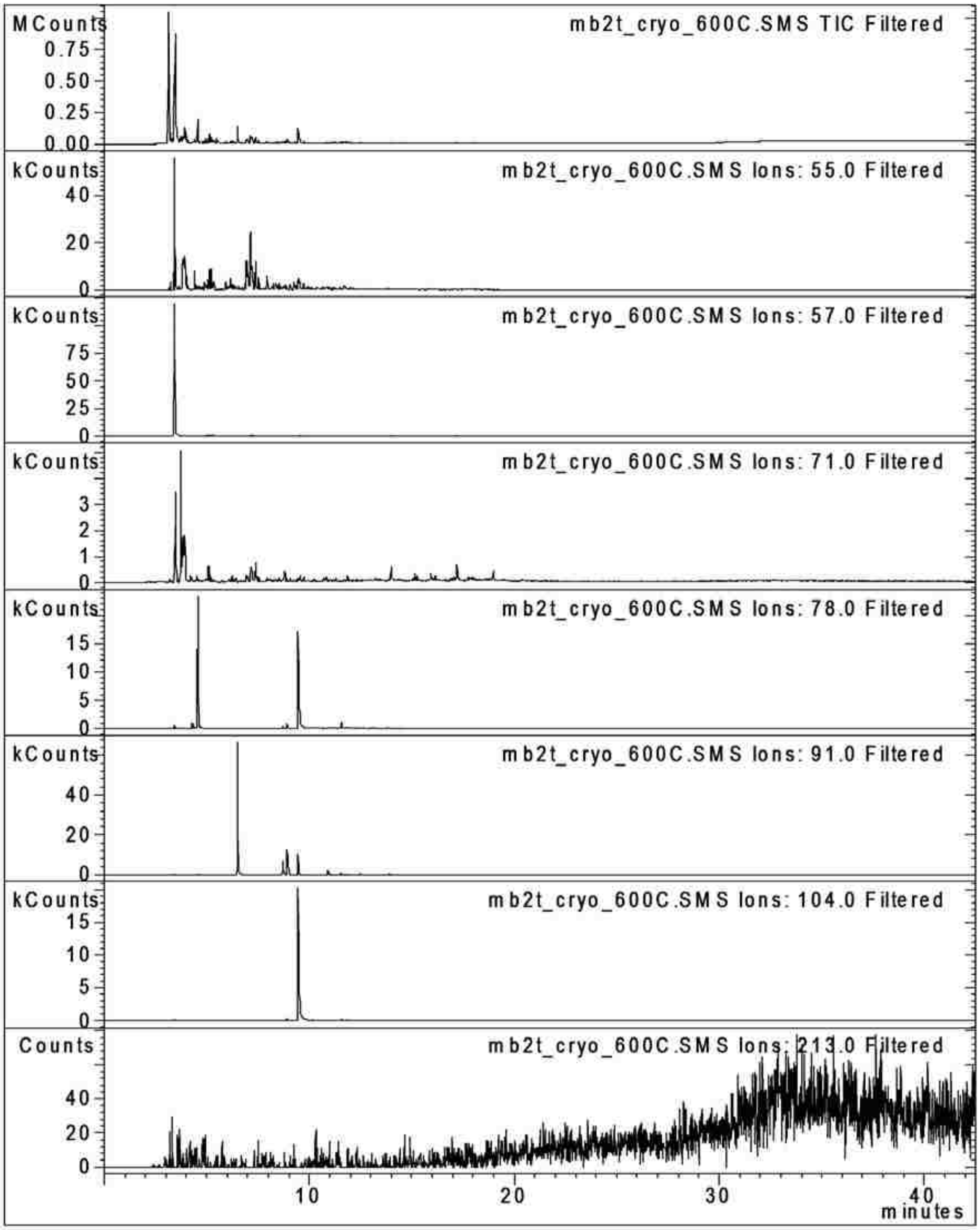

Sample mB2-Tiron aliquot. GC/MS spectra from Mormon Mesa geochronology sample mB2 (cryo analysis). The plots reveal relative contributions to the bulk chromatograph (top) from ion masses 55, 57, 71, 78, 91, 104, and 213.

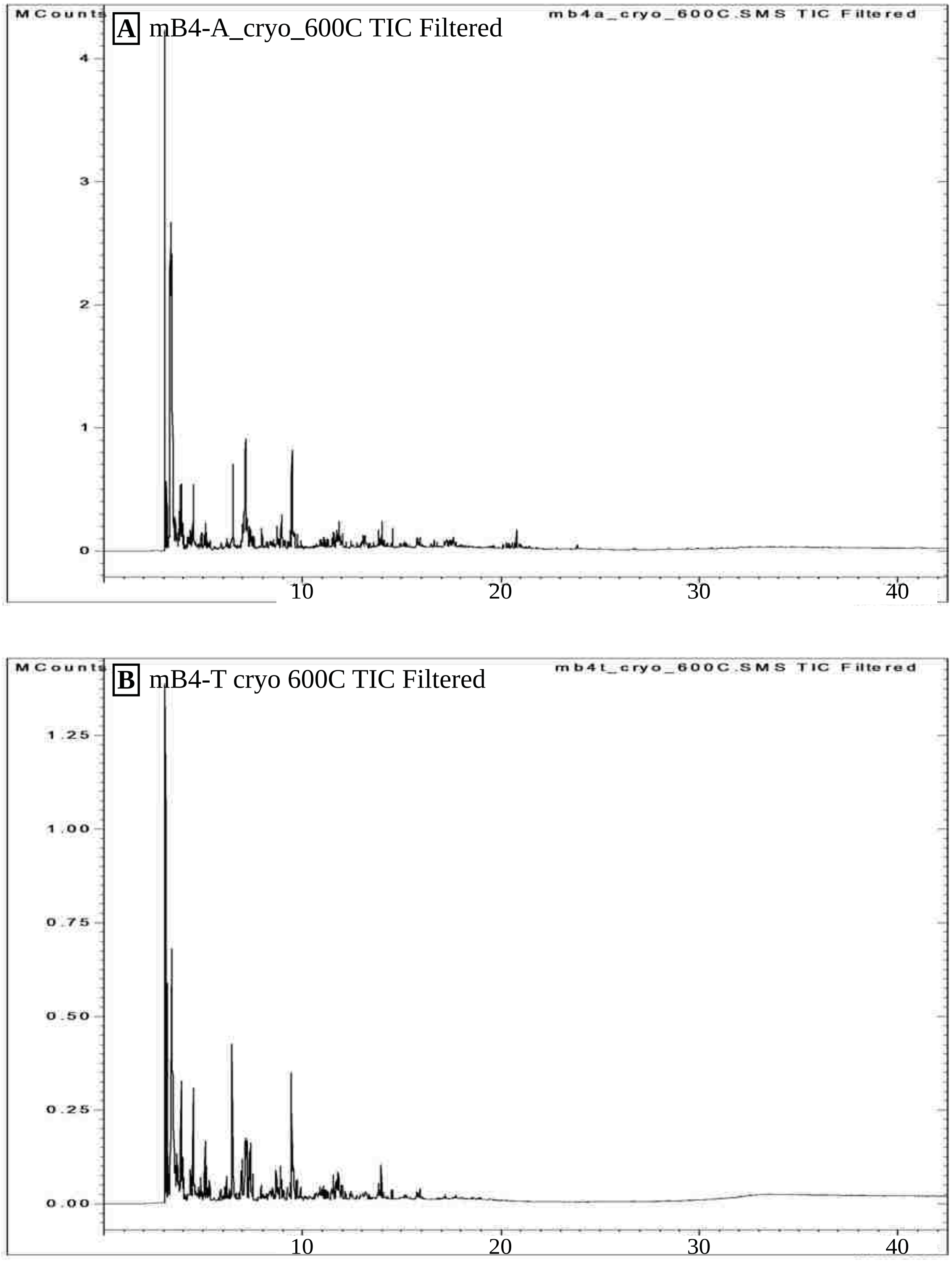

Sample mB4 - Acetate and Tiron aliquots. Bulk GC/MS chromatographs from (A) acetate aliquot and (B) tiron aliquot cryo analyses. No tmah analyses were conducted on this sample. Y-axis units are MCounts. X-axis units are minutes.

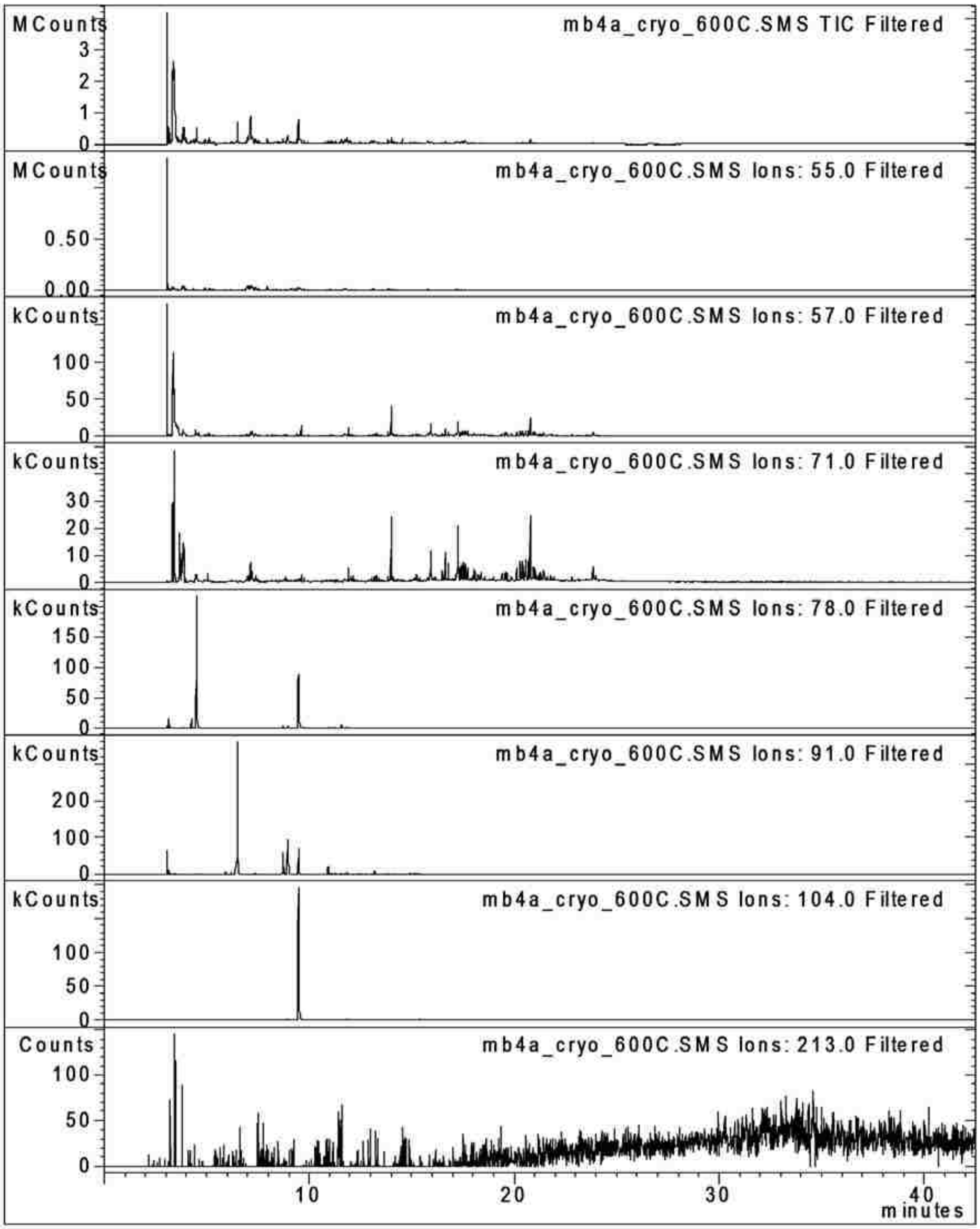

Sample mB4-Acetate aliquot. GC/MS spectra from Mormon Mesa geochronology sample mB4 (cryo analysis). The plots reveal relative contributions to the bulk chromatograph (top) from ion masses 55, 57, 71, 78, 91, 104, and 213.

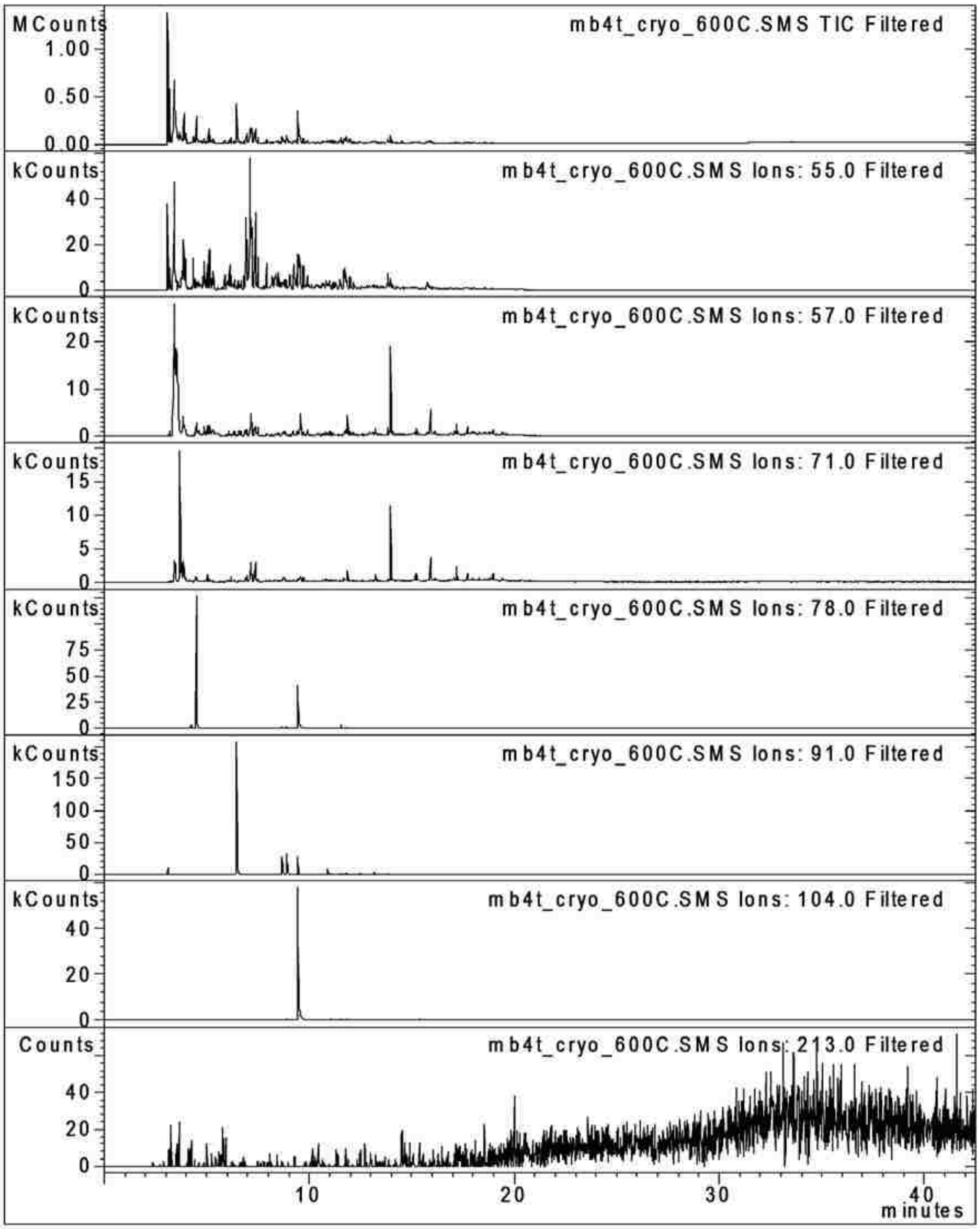

Sample mB4-Tiron aliquot. GC/MS spectra from Mormon Mesa geochronology sample mB4 (cryo analysis). The plots reveal relative contributions to the bulk chromatograph (top) from ion masses 55, 57, 71, 78, 91, 104, and 213.

APPENDIX 4.1

PHYLLOSILICATE XRD DATA

The following pages display the results of x-ray diffraction (XRD) analysis of the clay-sized particle fraction from four Clay Minerals Society Source Clays Repository reference standards (palygorskite, sepiolite, kaolinite, and montmorillonite) and 47 Mormon Mesa soil samples.

Abbreviations used are: B = barite, C = calcite and/or low magnesian calcite, Ch = chlorite, I = illite, K = kaolinite, P = palygorskite, Q = quartz, S = sepiolite, and Sm = smectite.

Treatments indicated for each sample or standard are K-saturation ("#K"), K-saturation with subsequent heating to 350°C for two hours ("#K350"), K-saturation with subsequent heating to 550°C for two hours, Mg-saturated ("#Mg"), and Mg-saturated slides heated under vacuum to 50°C in the presence of ethylene glycol ("#MgEG", or "#MgGly"). Profile and horizon locations for each sample are indicated below each XRD data set.

Maximum relative intensity peaks, or the most diagnostic peaks, for each of the minerals commonly seen in the Mormon Mesa samples are indicated when relevant, however, lower-intensity peaks are not labeled due to extensive overlap among the sub-100% relative intensity phyllosilicate peaks, and to preserve clarity of the XRD data. XRD interpretations made use of the full suite of diffraction peaks available for each mineral.

All data were interpreted using X'Pert Plus analytical software, and by making extensive comparisons between sample behavior, reference standard behavior, and published descriptions of typical phyllosilicate responses to K, Mg, and heat treatments (e.g., Dixon & Weed, 1989; Moore & Reynolds, 1997; Poppe et al., 2001 (see Chapter 3 reference section)). The data below were exported from X'Pert Plus file formats to black-and-white JPEG image files for compilation and printing. Peak labels were added in Adobe Illustrator as guidelines only, and are not exact.

Some of the most important treatment effects are noted here for the phyllosilicates, however, interpretations made in this study were not limited to these effects. The reader is referred to Dixon & Weed (1989), Moore & Reynolds (1997), Poppe et al. (2001), and other references for more detailed information on the topic.

Palygorskite is characterized by an especially strong peak at 1.04 to 1.05 nm, and after heating to 300 or 350°C produces a new peak at ~0.92 nm. This new peak decreases to 0.87 nm with additional heating (Dixon & Weed, 1989). Sepiolite is most easily characterized by an intense peak at 1.22 nm (Poppe et al., 2001). Slight expansion of palygorskite and sepiolite (at several d-spacings) was seen after ethylene glycol treatments in this study.

Kaolinite is characterized by 0.72 and 0.357 nm peaks when chlorite is absent (Dixon & Weed, 1989). Chlorite and kaolinite can be distinguished via the chlorite peak at 0.354 nm and the separate kaolinite peak at 0.357 nm, as well as the persistence of a 1.4 nm chlorite peak through heating to 550°C, which destroys kaolinite (Dixon & Weed, 1989). Chlorite and smectite were differentiated based on the shift of the ~1.4 nm smectite peak to ~1.7-1.8 nm with ethylene glycol treatment.

Significant illite compositions were confirmed based on the presence of a strong ~1.00 nm peak (in the presence of palygorskite, this peak typically forms a shoulder or spire adjacent to the 1.04 nm palygorskite peak), and the persistence of this peak through heating. Because palygorskite and sepiolite both generate new peaks across this region with heating ≥ 300°C, the presence of the illite shoulder in the base-line K treatment data, and close comparison of relative peak intensities between treatments were essential to detect illite present in small quantities.

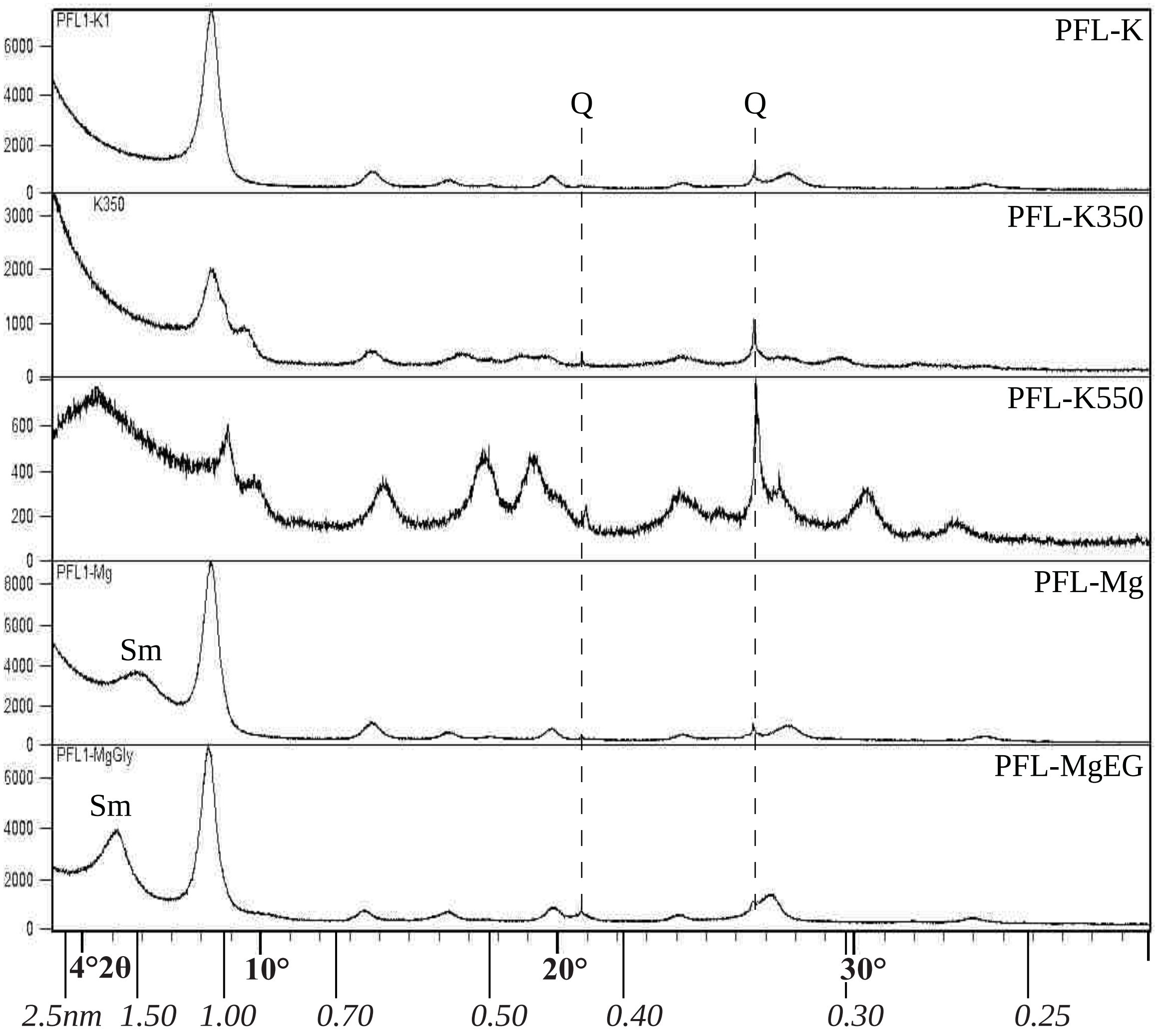

XRD spectra for palygorskite (attapulgite) reference standard PFL-1, palygorskite from Gadsden County, Florida (2007). This standard contains accessory smectite and clay-sized quartz.

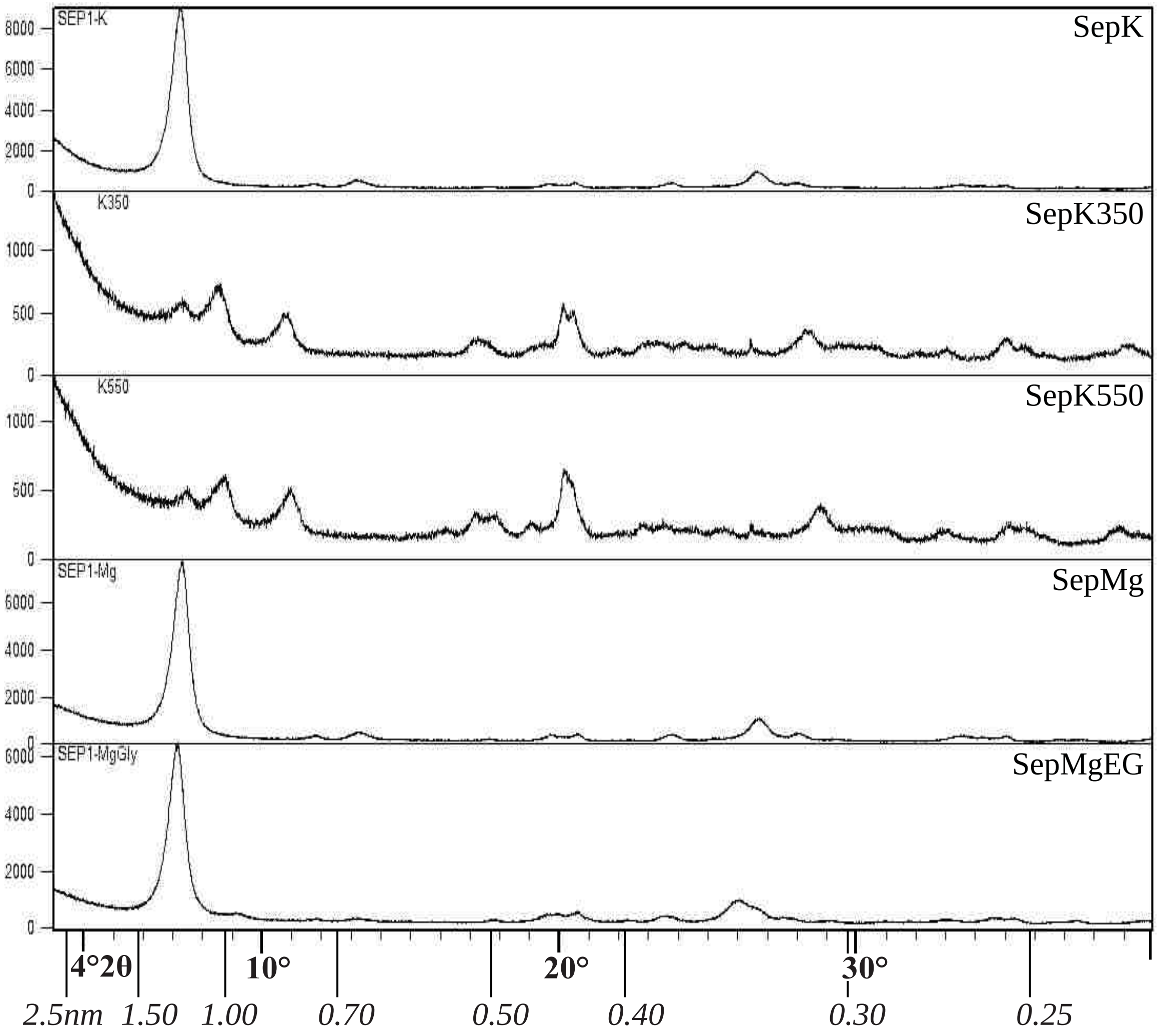

XRD spectra for sepiolite reference standard SepSp-1, sepiolite from Valdemore, Spain (2007).

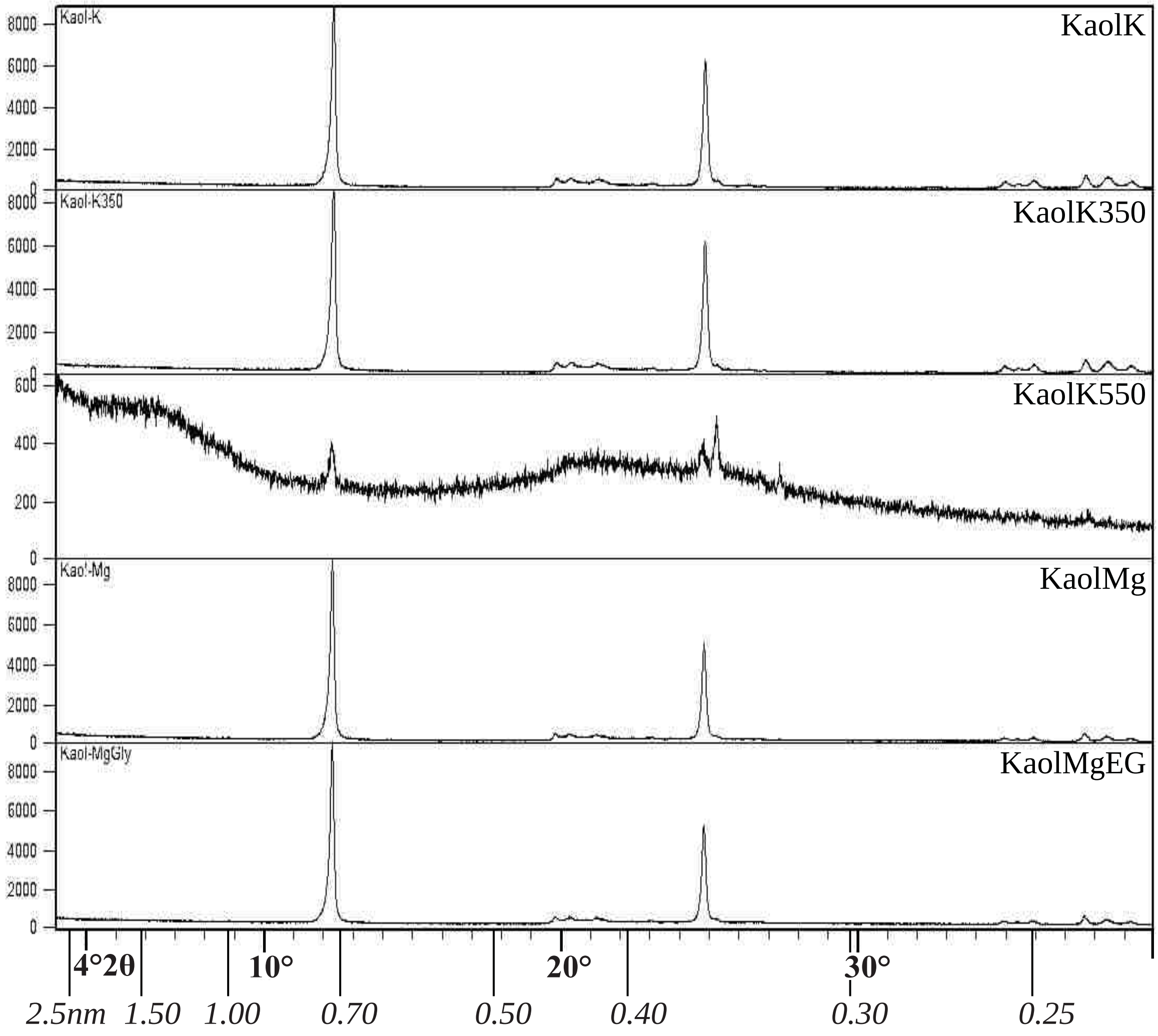

XRD spectra for Kaolinite reference standard KGa-1, well-crystallized kaolin from Washington County, GA (1986).

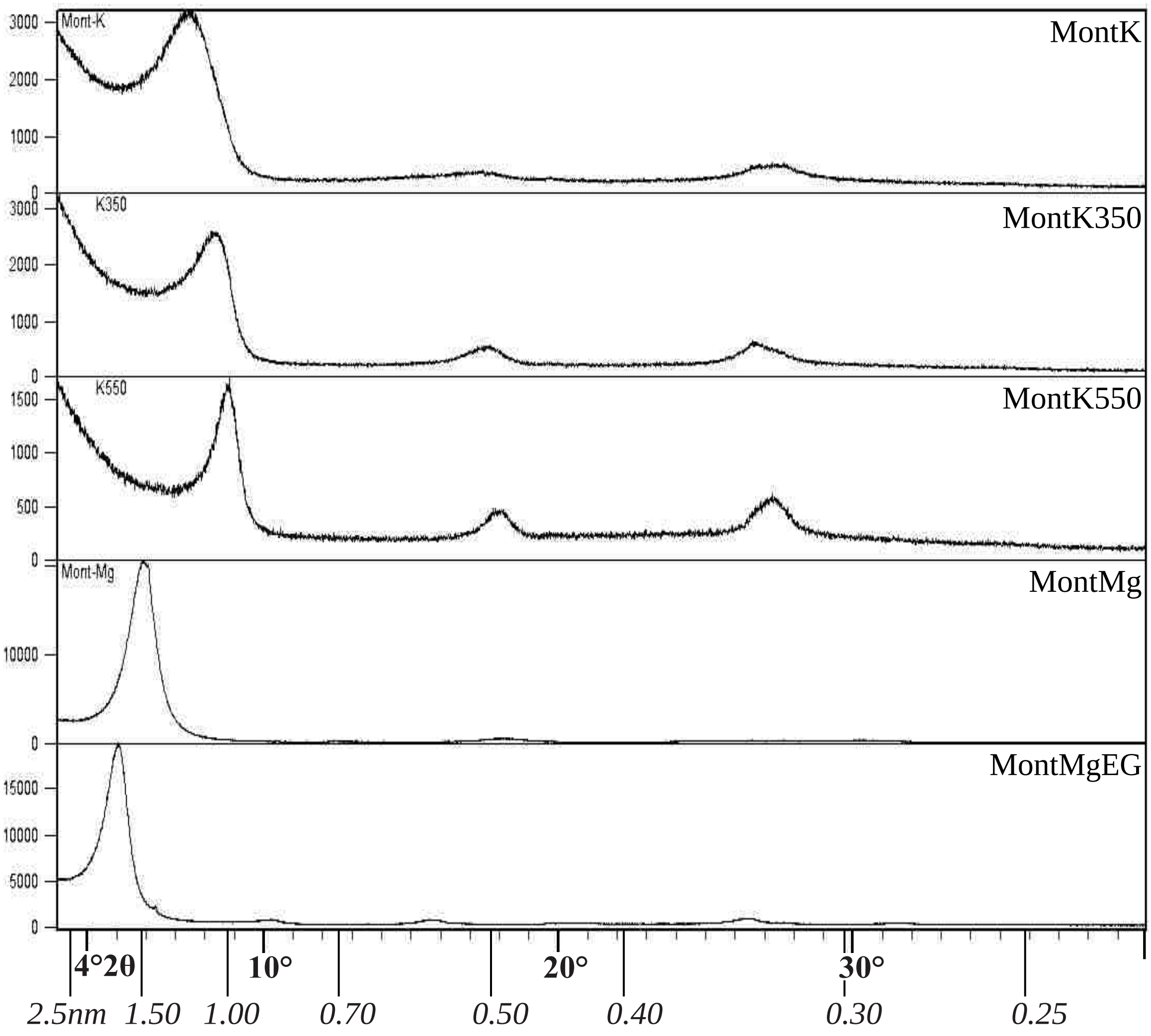

XRD spectra for smectite reference standard SCa-2, montmorillonite from San Diego County, CA (1986).

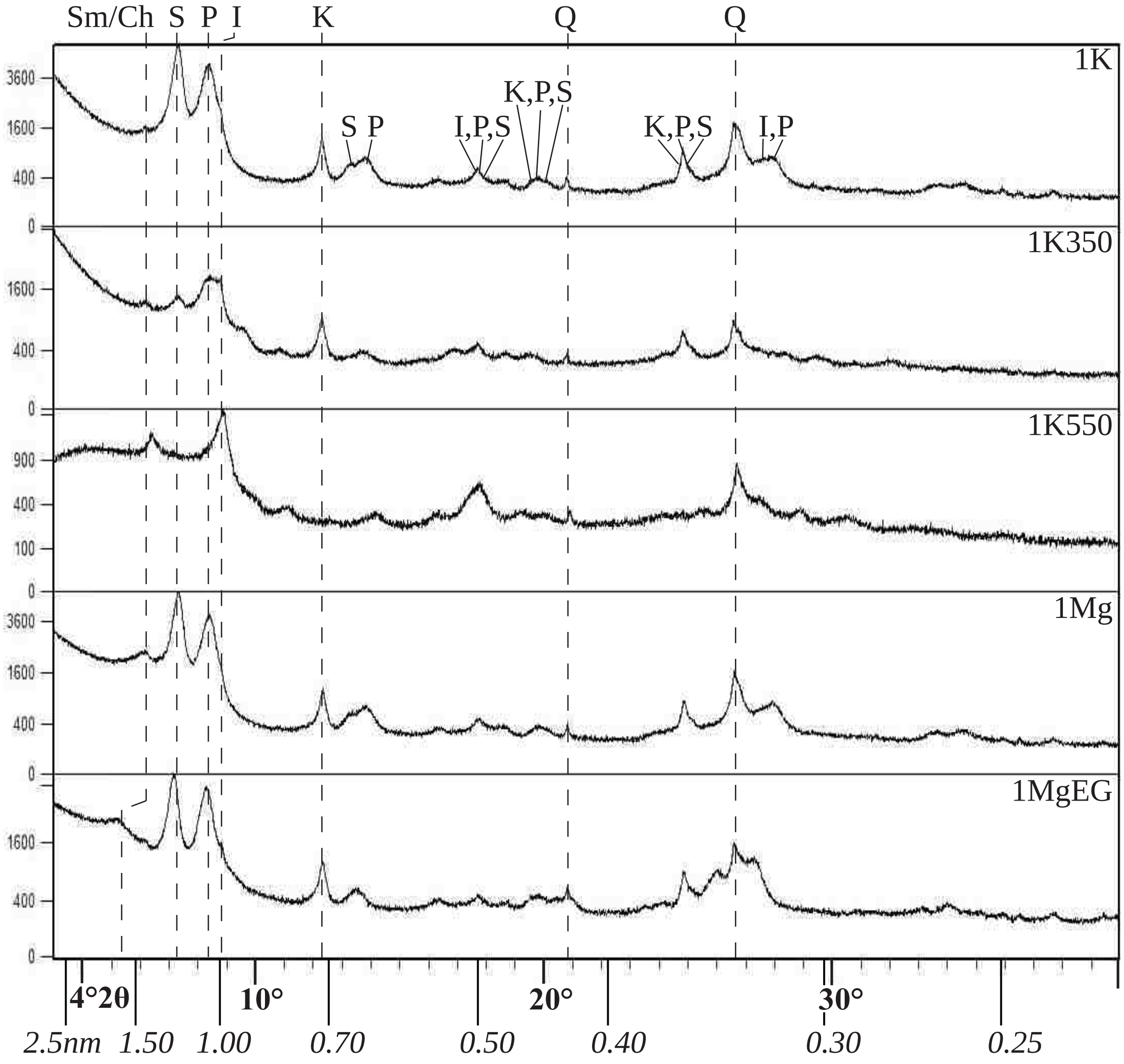

XRD spectra for Sample #1 (the < 2 mm fraction of the surficial rubble horizon of profile MM1-A). The sample contains, in order of decreasing relative abundance: sepiolite, palygorskite, kaolinite, quartz, illite, and minor amounts of chlorite/smectite.

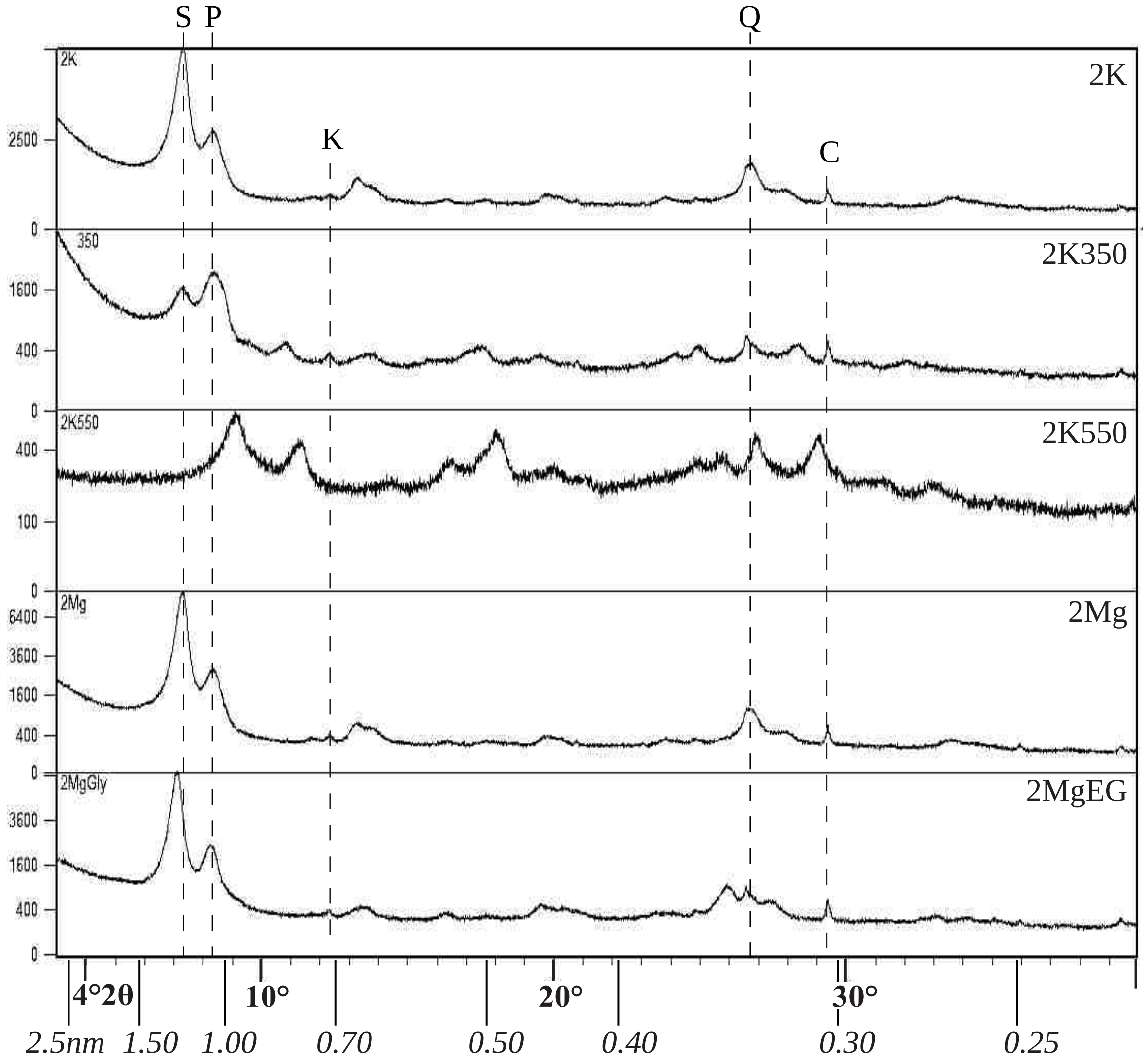

XRD spectra for Sample #2, profile MM1-A (clay-sized mineralogy of the > 2 mm fraction of the surficial rubble horizon of profile MM1-A). The sample contains, in order of decreasing relative abundance: sepiolite, palygorskite, quartz, calcite, and trace kaolinite.

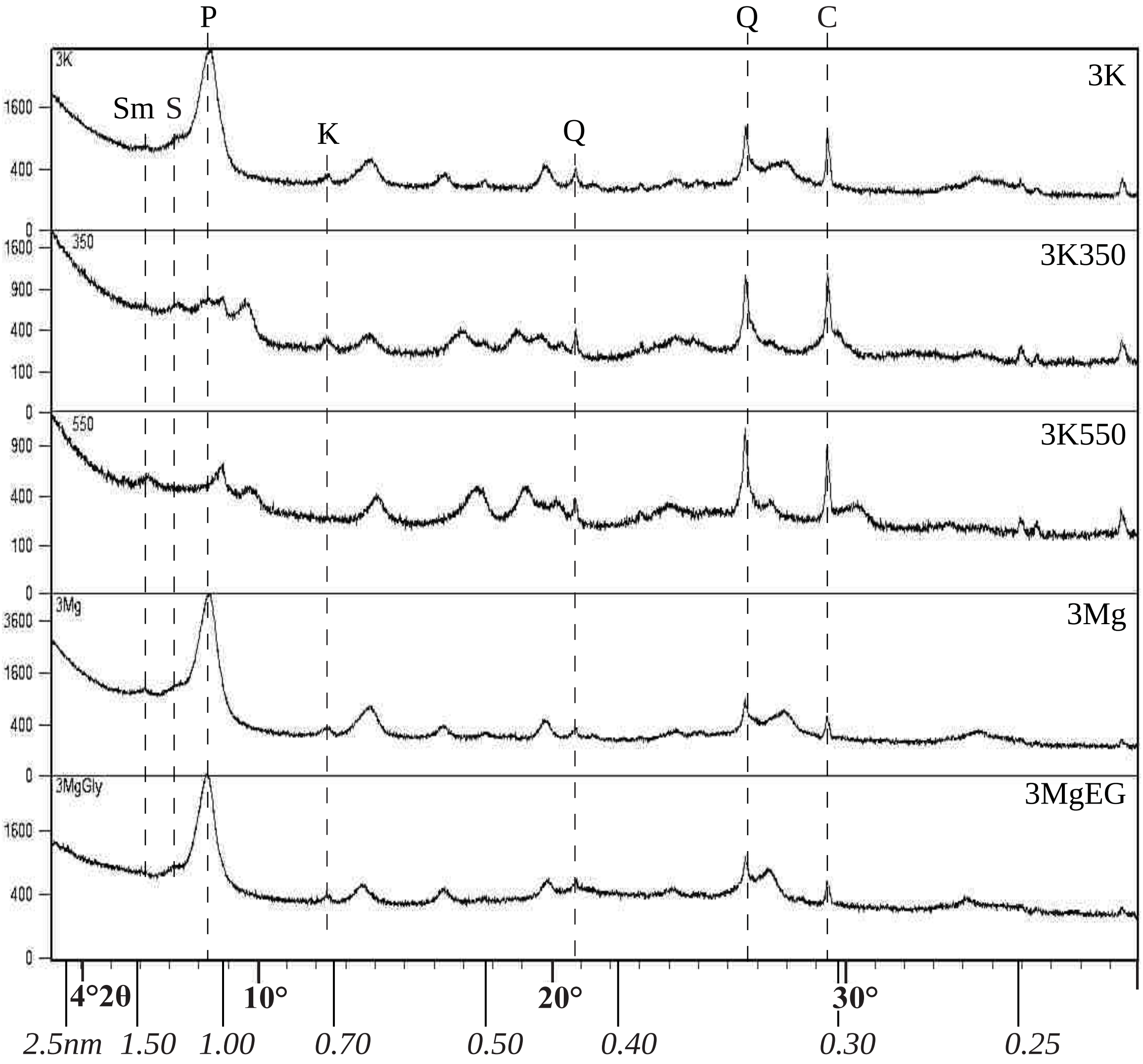

XRD spectra for Sample #3, profile MM1-A (upper Brecciated horizon). The sample contains, in order of decreasing relative abundance: palygorskite, quartz, calcite, sepiolite, kaolinite, and trace smectite.

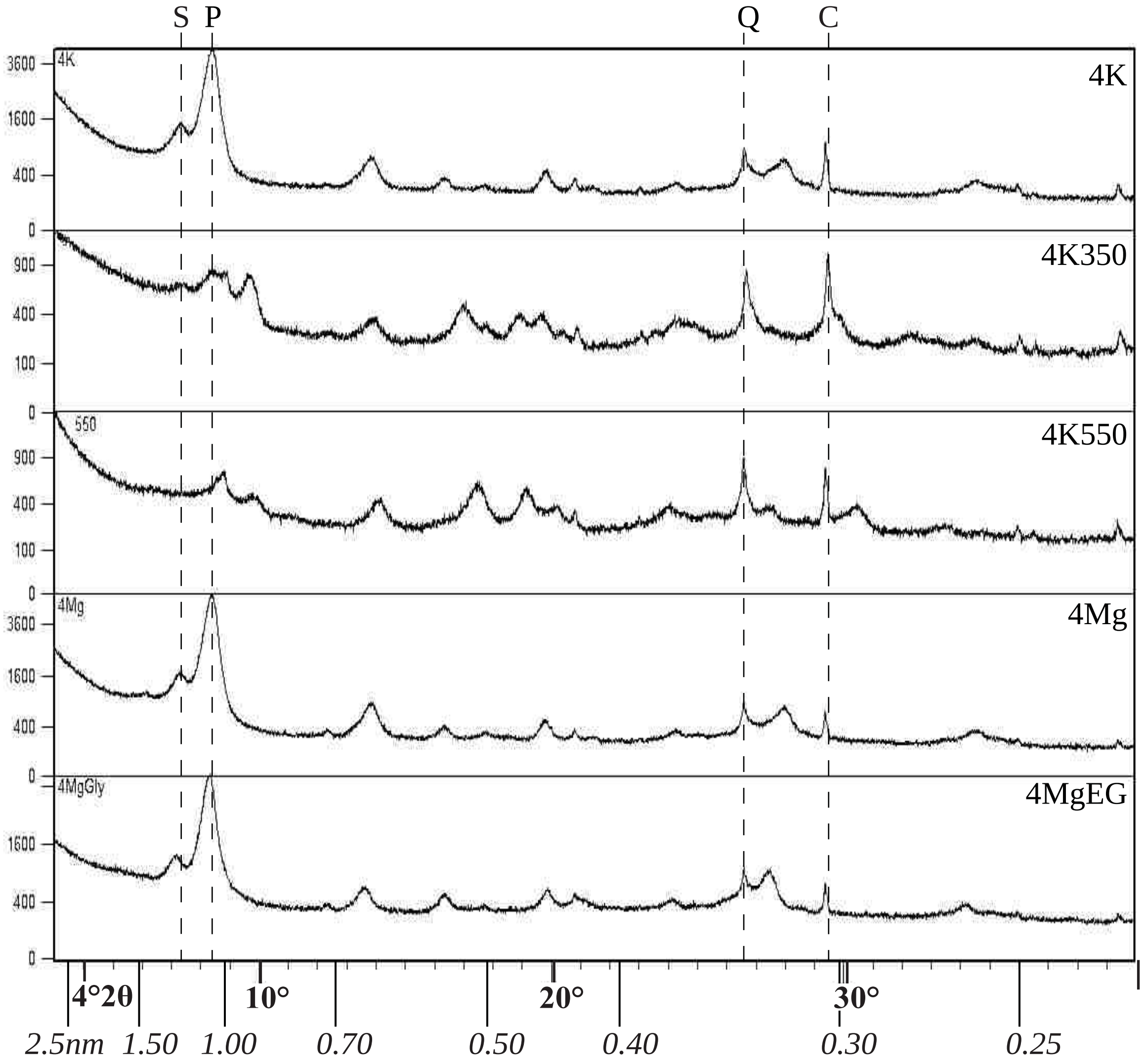

XRD spectra for Sample #4, profile MM1-A (middle Brecciated horizon). The sample contains, in order of decreasing relative abundance: palygorskite, quartz, calcite, sepiolite, and possible trace amounts of kaolinite.

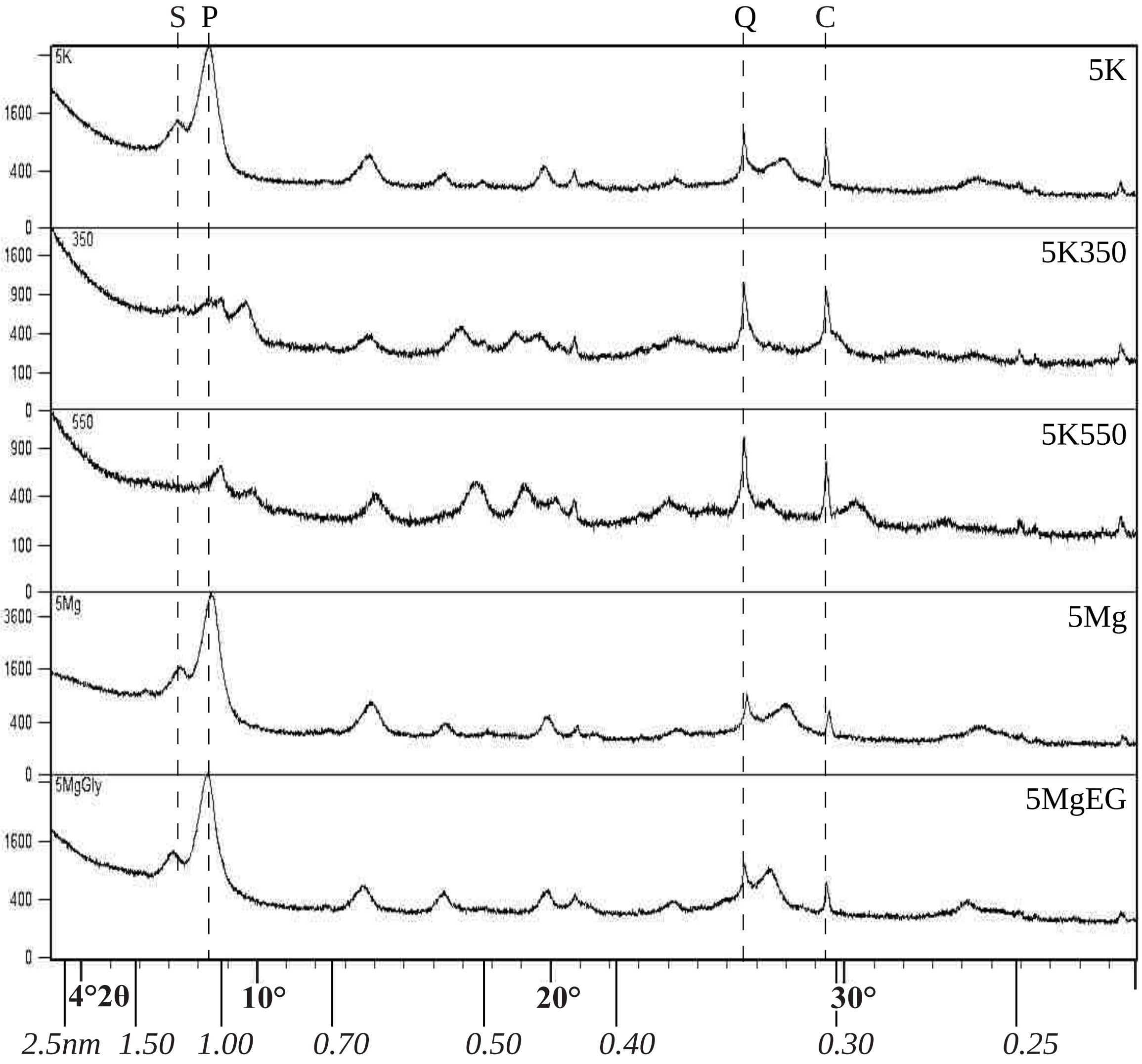

XRD spectra for Sample #5, profile MM1-A (basal Brecciated horizon). The sample contains, in order of decreasing relative abundance: palygorskite, quartz, calcite, and sepiolite. Trace illite is also present.

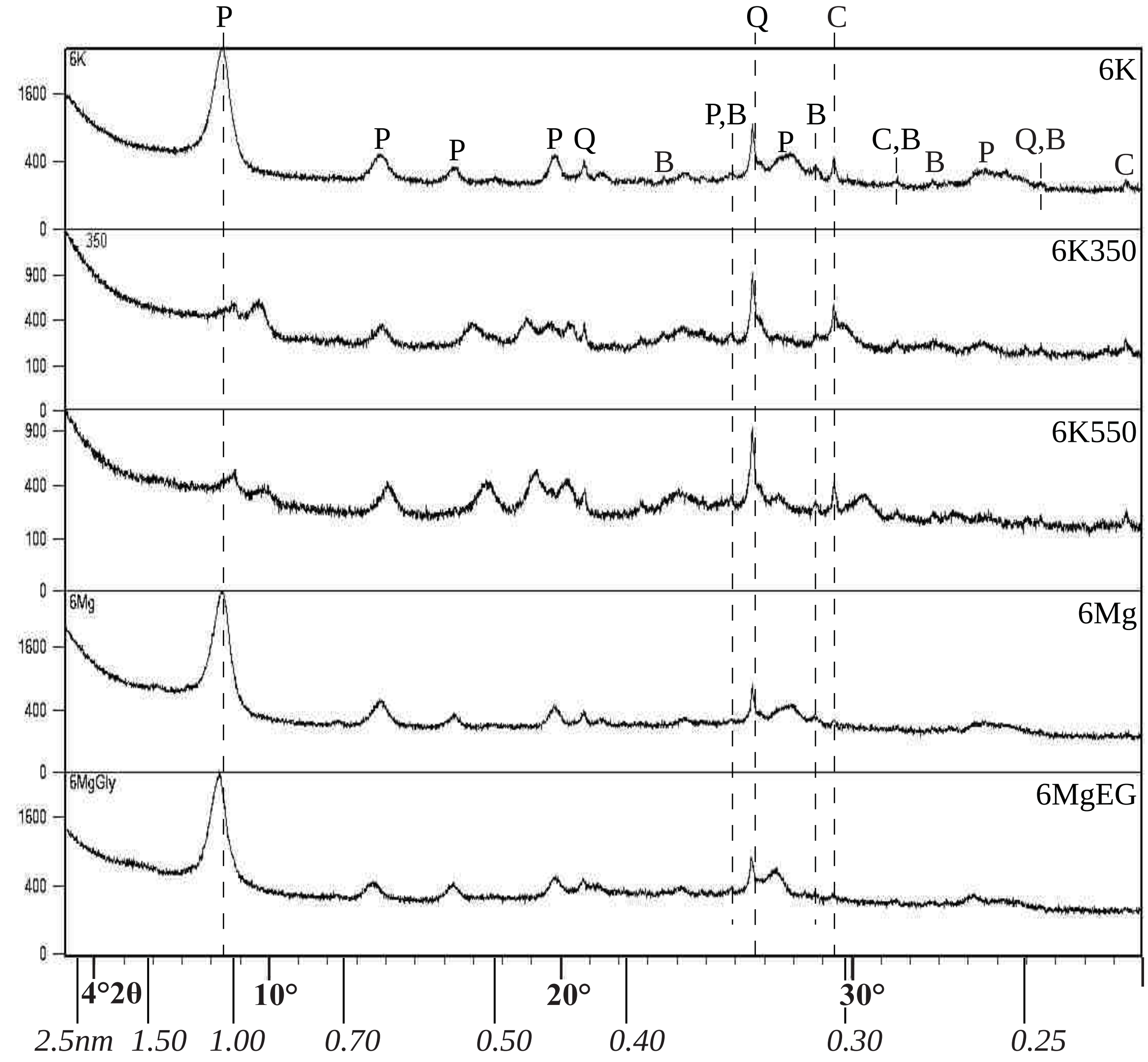

XRD spectra for Sample #6, profile MM1-A (upper Massive horizon). The sample contains, in order of decreasing relative abundance: palygorskite, quartz, calcite, and barite.

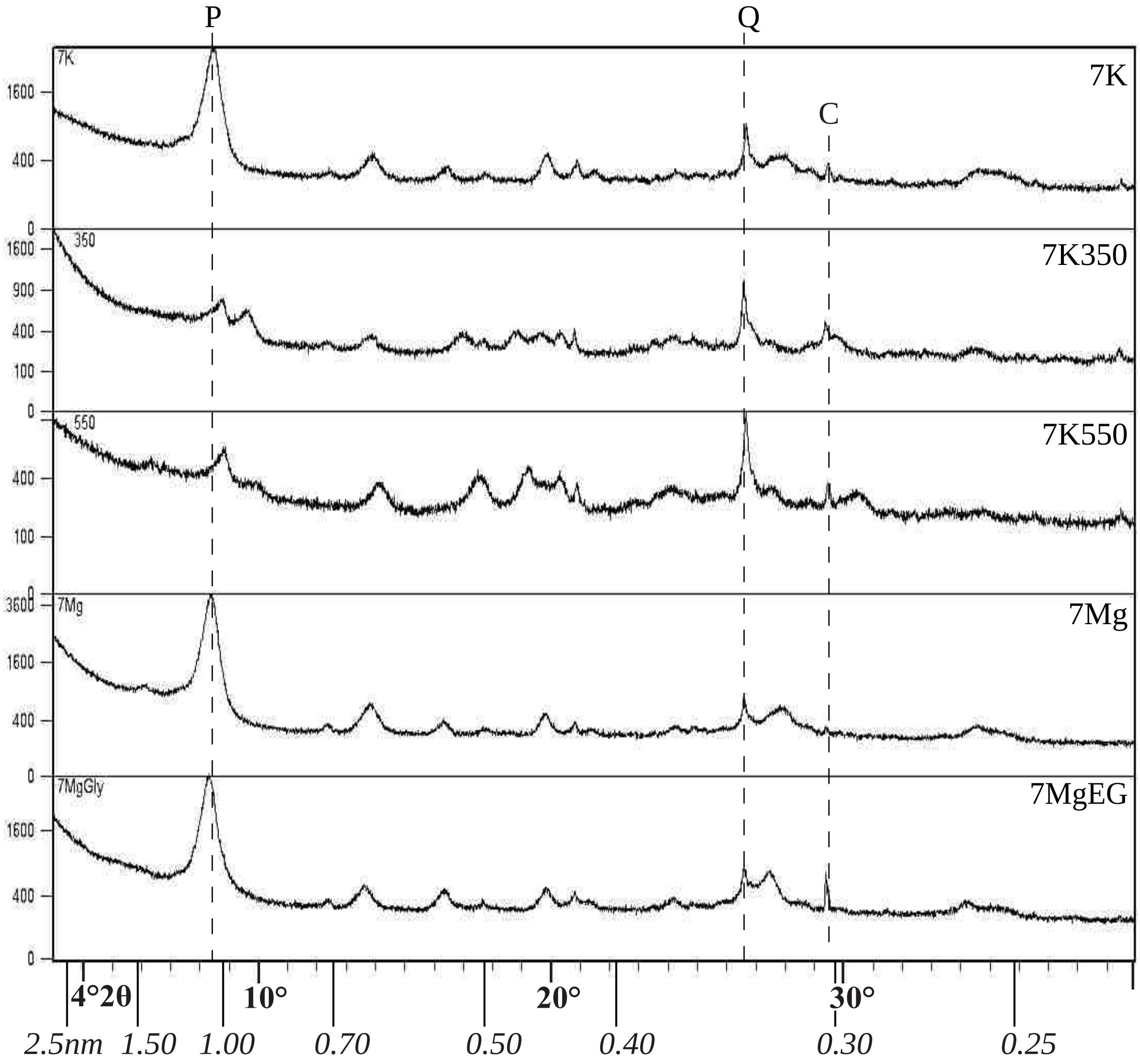

XRD spectra for Sample #7, profile MM1-A (middle Massive horizon). The sample contains, in order of decreasing relative abundance: palygorskite, quartz, and calcite.

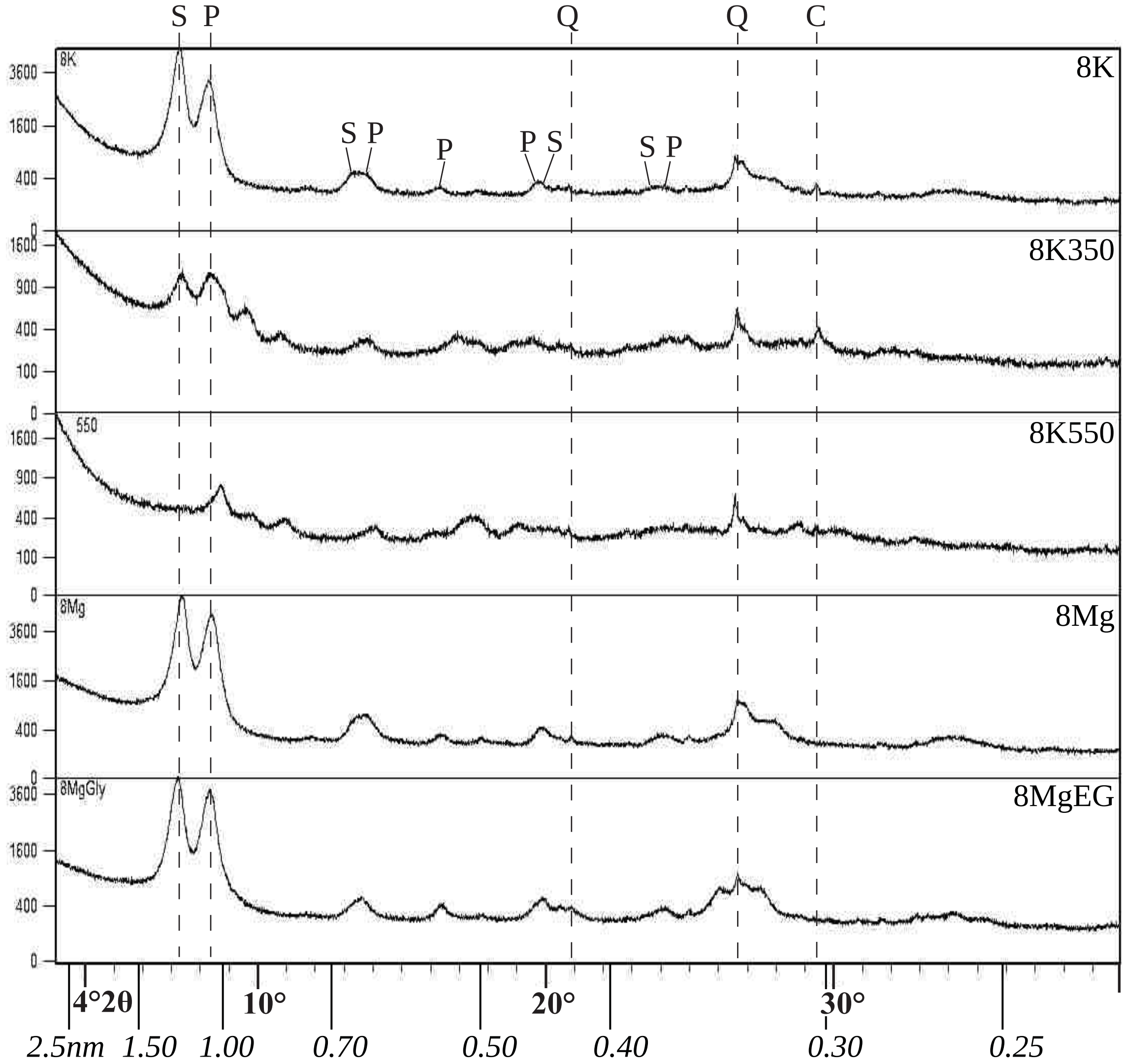

XRD spectra for Sample #8, profile MM1-A (basal Massive horizon). The sample contains, in order of decreasing relative abundance: sepiolite, palygorskite, quartz, and minor calcite.

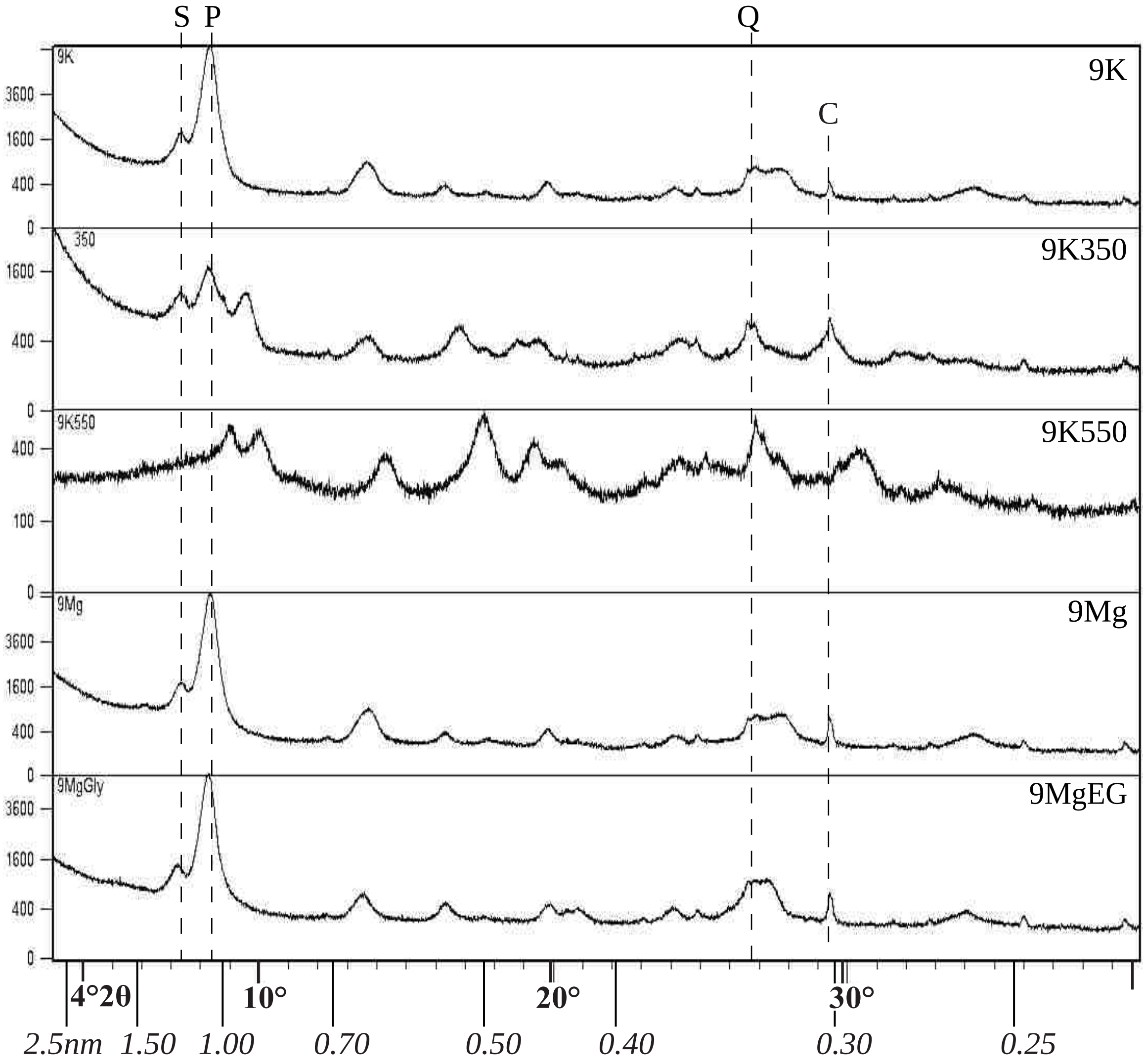

XRD spectra for Sample #9, profile MM1-A (upper Transitional horizon). The sample contains, in order of decreasing relative abundance: palygorskite, quartz, sepiolite, and calcite.

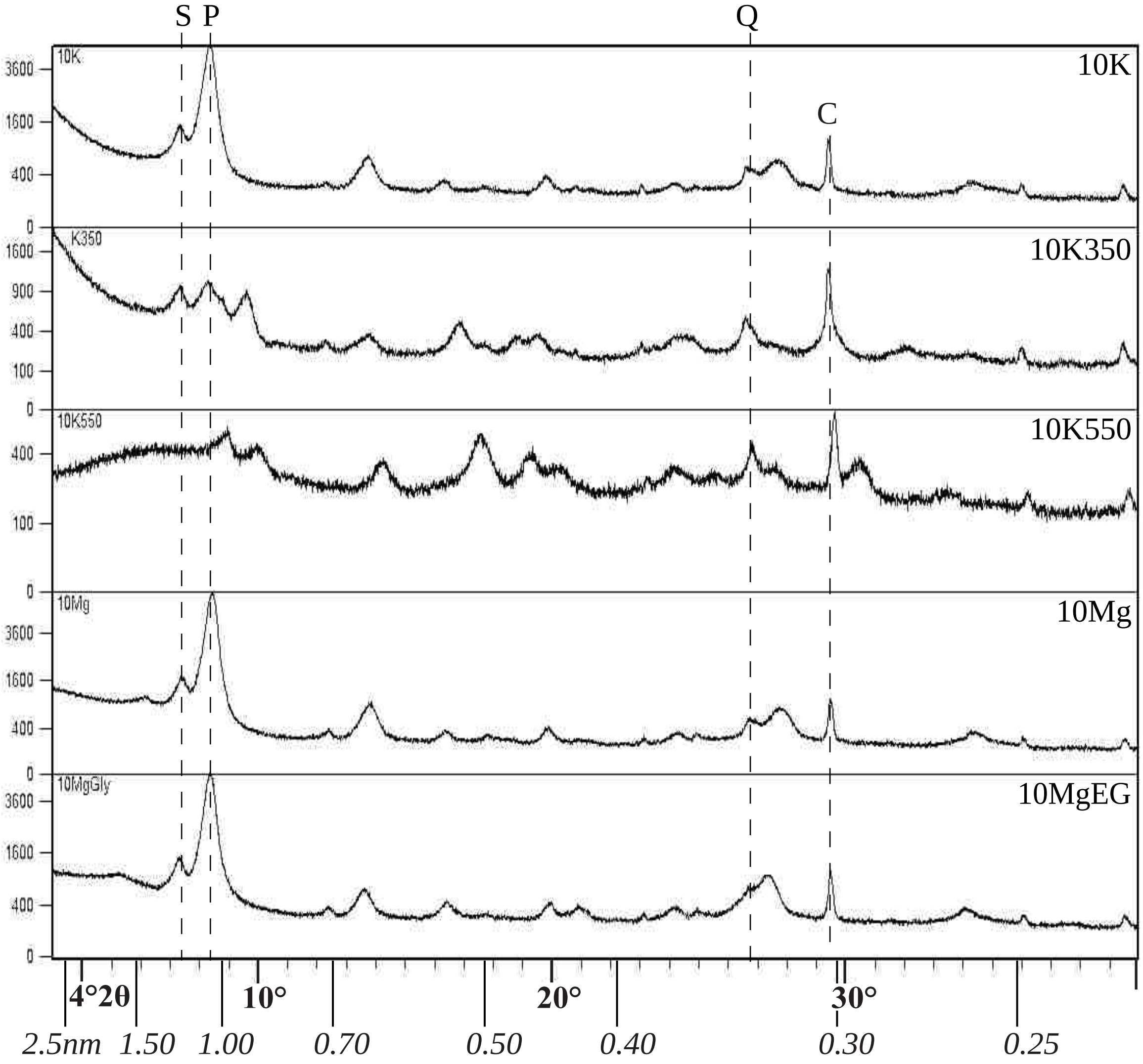

XRD spectra for Sample #10, profile MM1-A (middle Transitional horizon). The sample contains, in order of decreasing relative abundance: palygorskite, sepiolite, calcite, and quartz.

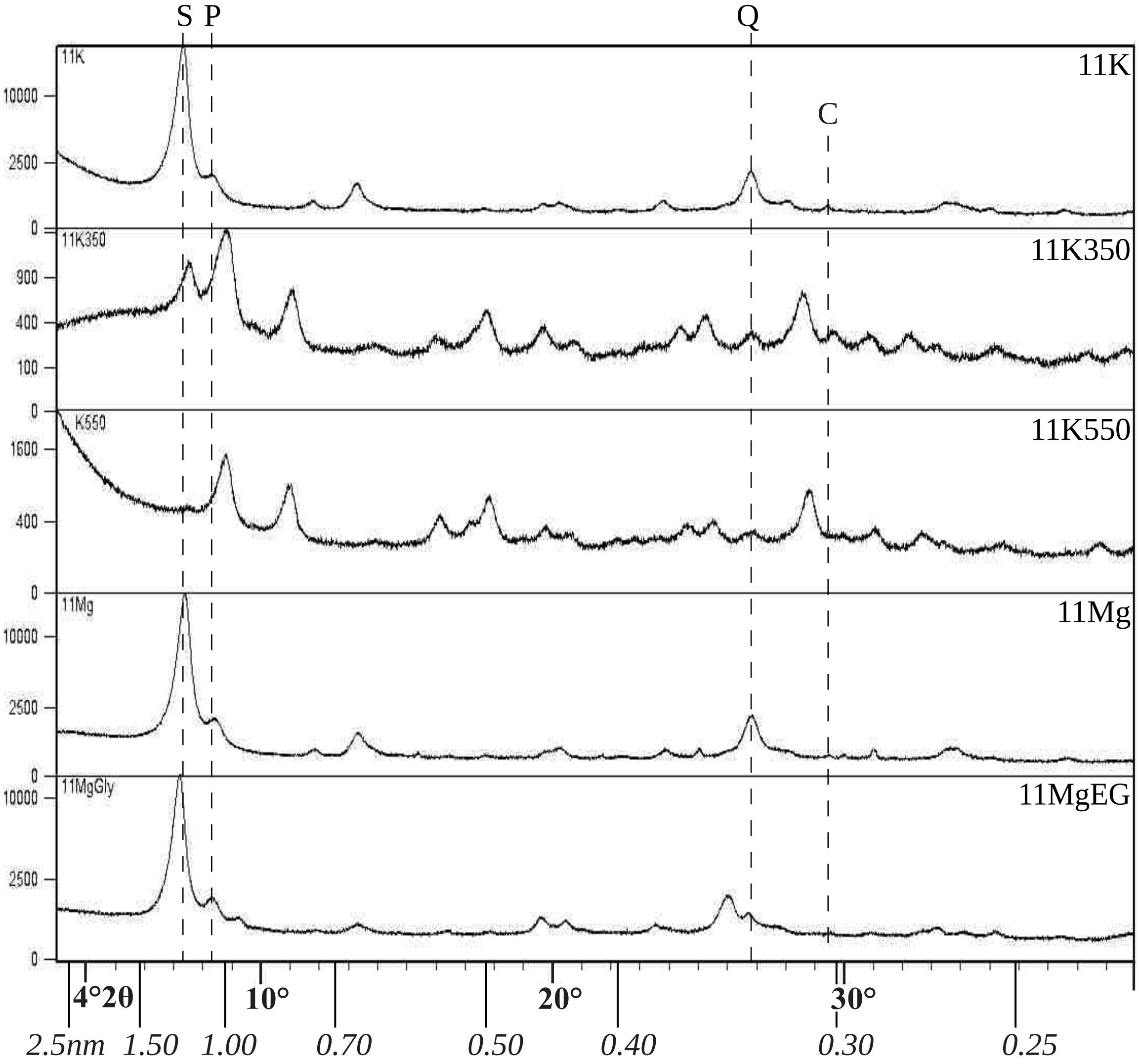

XRD spectra for Sample #11, profile MM1-A (basal Transitional horizon). The sample contains, in order of decreasing relative abundance: sepiolite, quartz, palygorskite, and calcite.

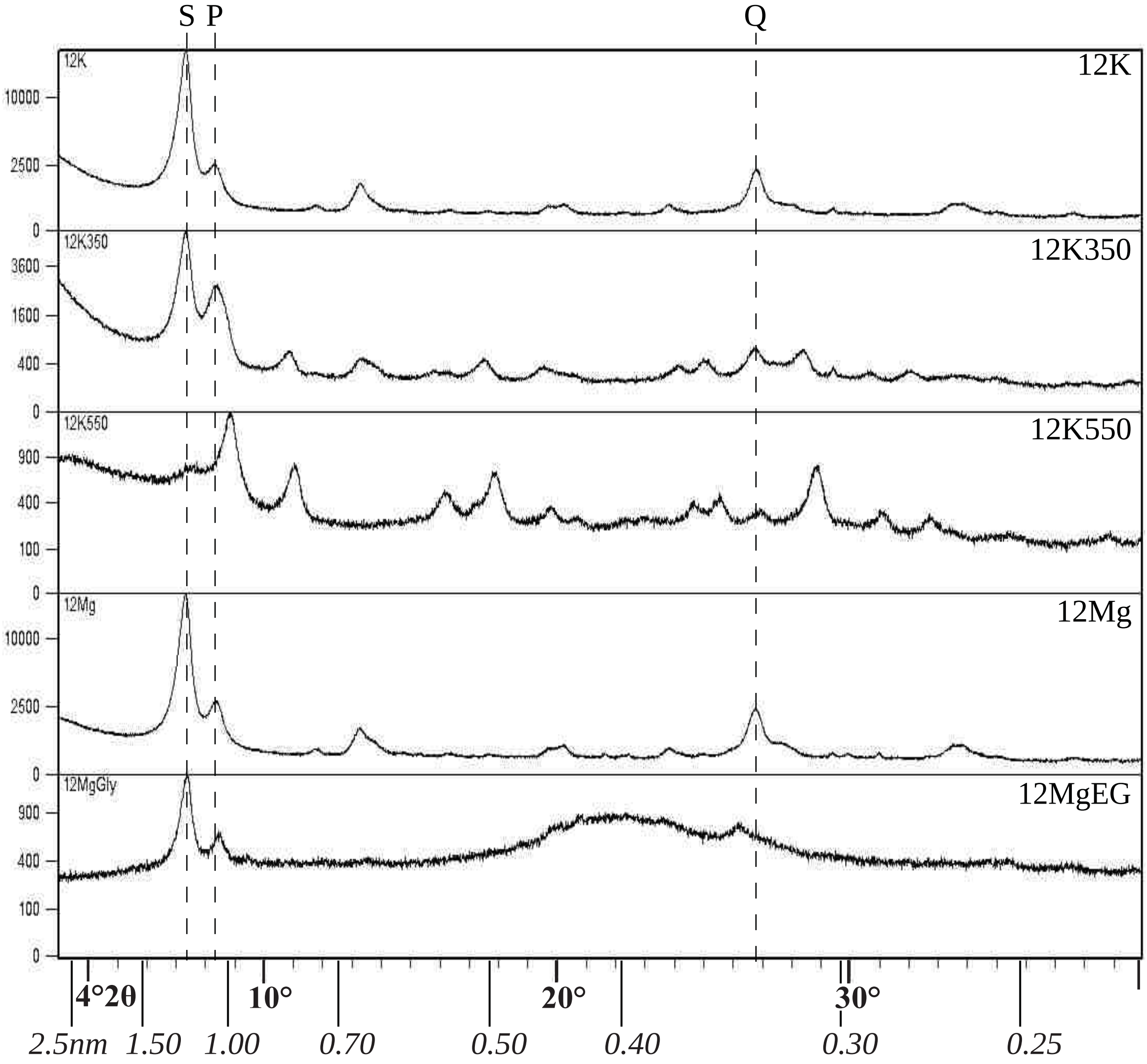

XRD spectra for Sample #12, profile MM1-A (upper Muddy Creek paleosol). The sample contains, in order of decreasing relative abundance: sepiolite, quartz, palygorskite, and trace calcite.

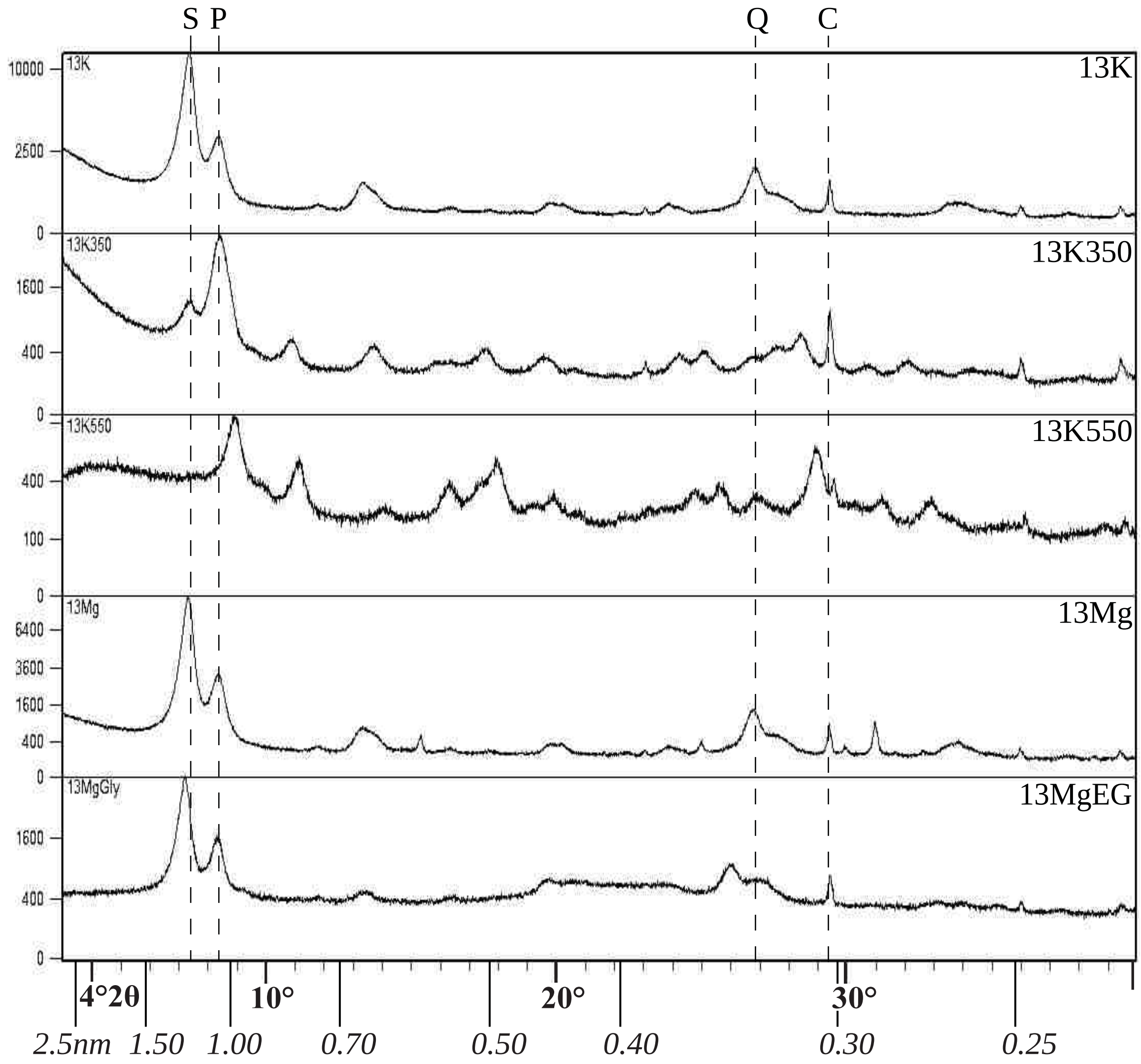

XRD spectra for Sample #13, profile MM1-A (middle Muddy Creek paleosol). The sample contains, in order of decreasing relative abundance: sepiolite, palygorskite, quartz, and calcite.

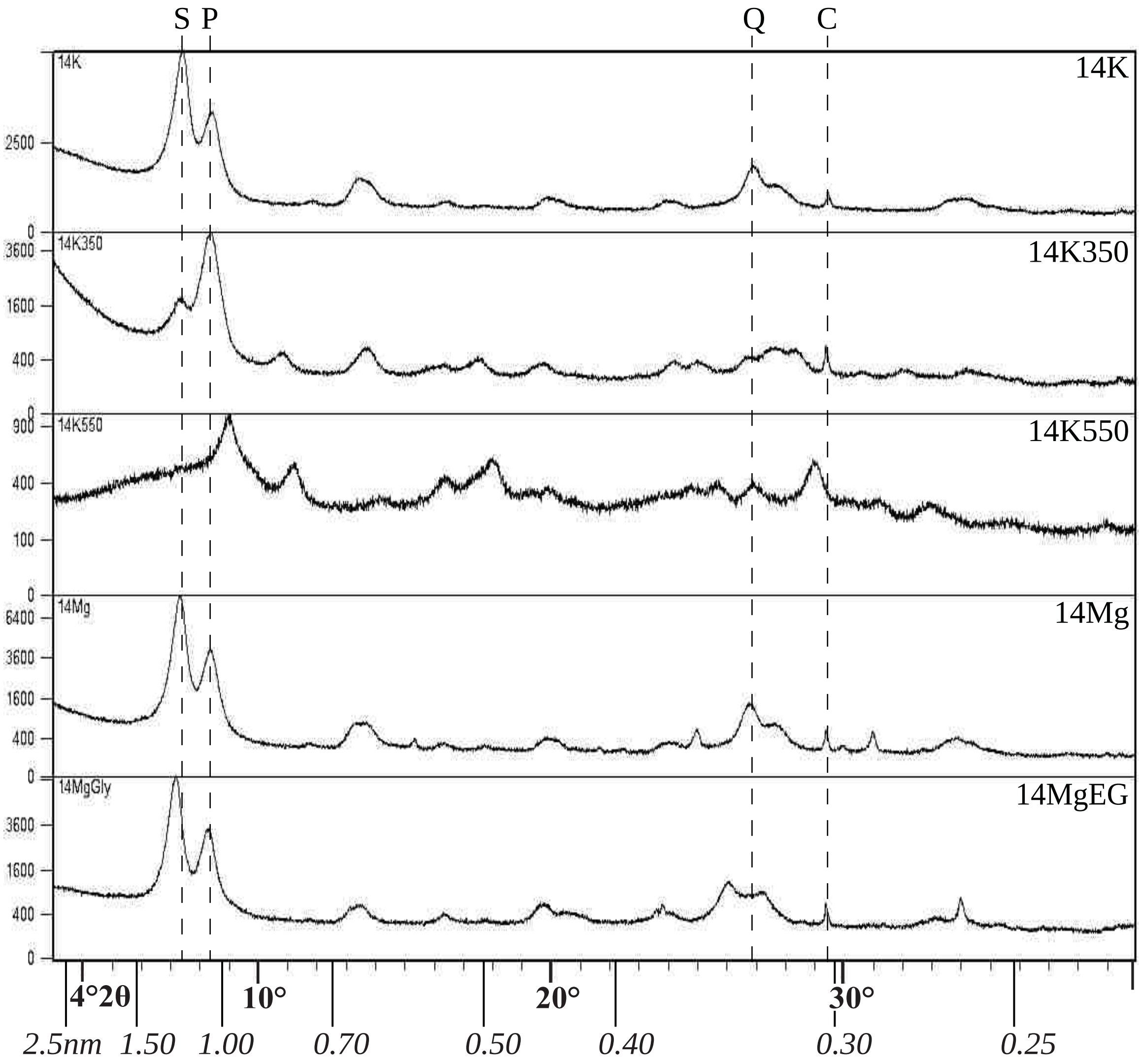

XRD spectra for Sample #14, profile MM1-A (basal Muddy Creek paleosol). The sample contains, in order of decreasing relative abundance: sepiolite, palygorskite, quartz, and calcite.

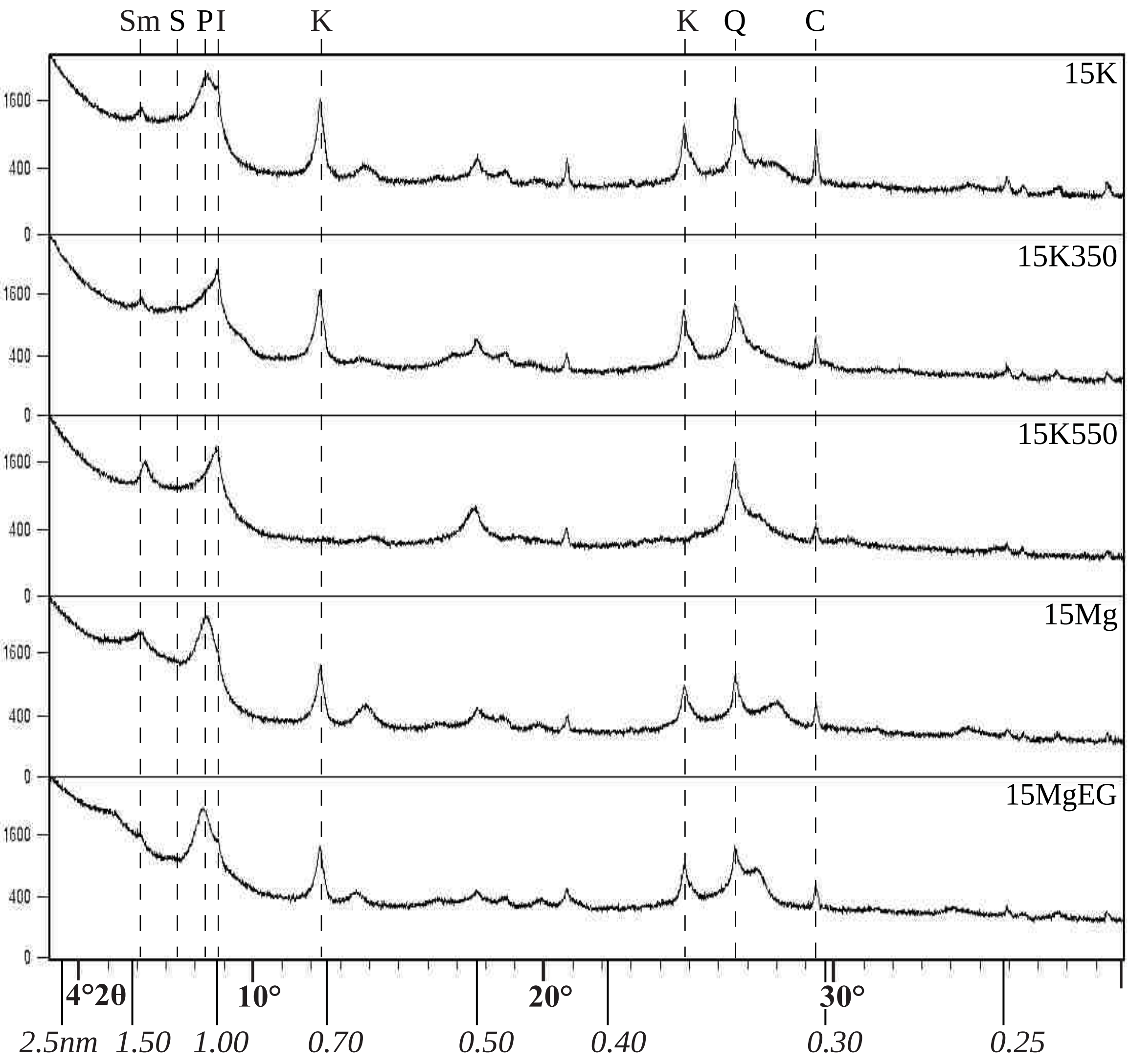

XRD spectra for Sample #15, profile MM1-B (< 2 mm fraction of the surficial rubble horizon). The sample contains, in order of decreasing relative abundance: kaolinite, quartz, palygorskite, illite, calcite, smectite, and trace sepiolite.

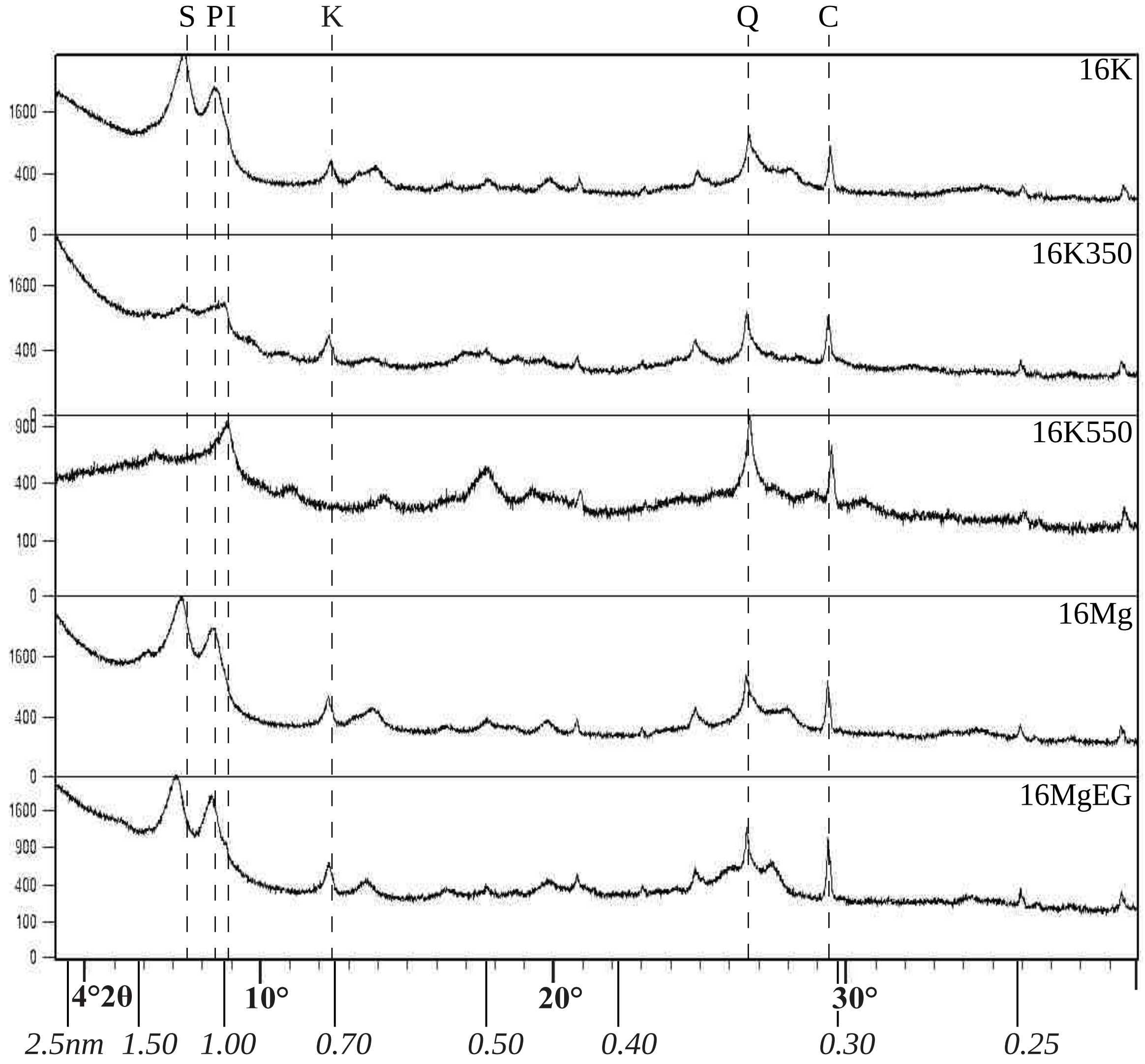

XRD spectra for Sample #16, profile MM1-B (> 2 mm fraction of the surficial rubble horizon). The sample contains, in order of decreasing relative abundance: sepiolite, palygorskite, quartz, calcite, kaolinite, illite, and trace smectite.

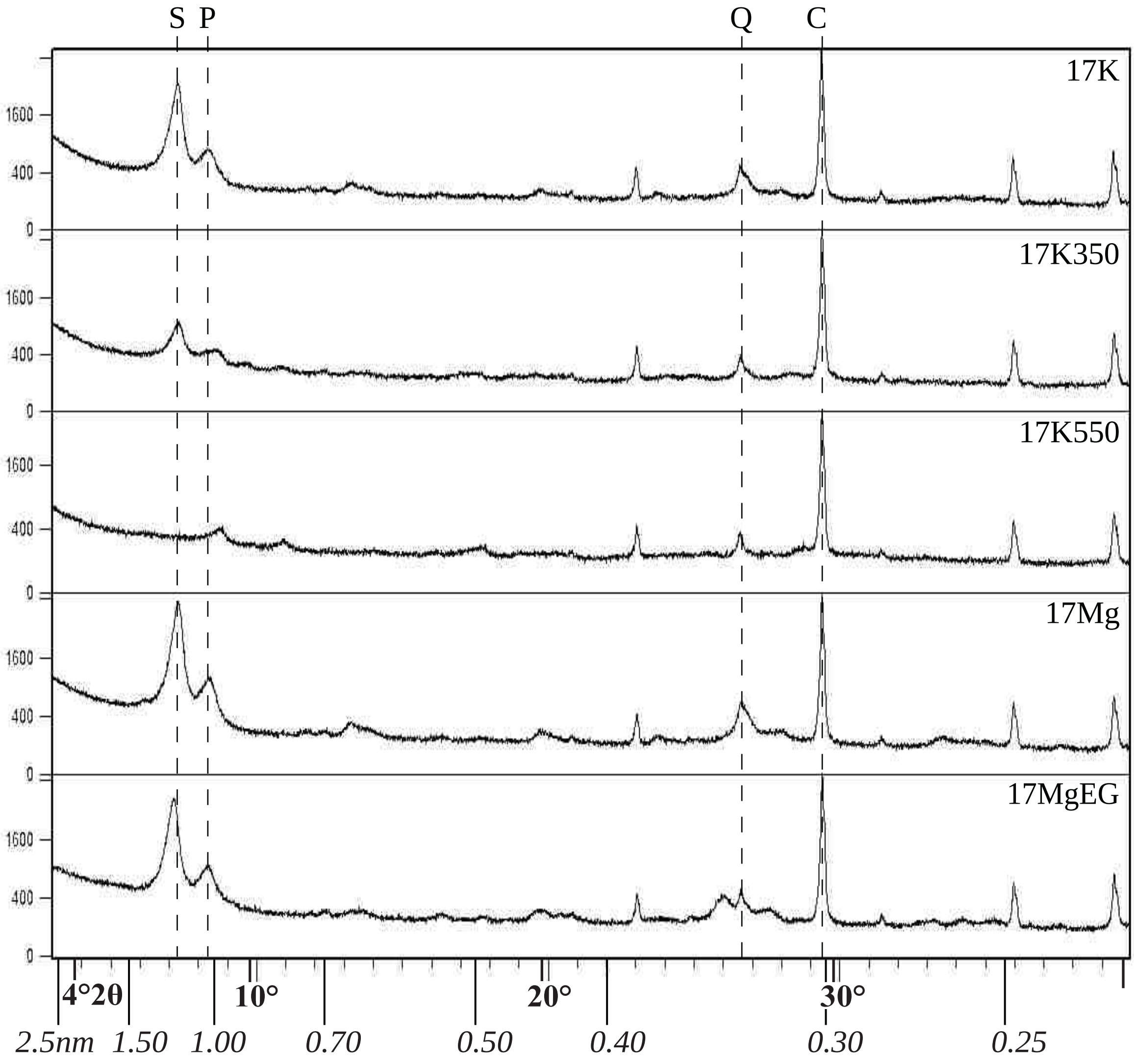

XRD spectra for Sample #17, profile MM1-B (upper Brecciated horizon). The sample contains, in order of decreasing relative abundance: calcite, sepiolite, palygorskite, and quartz.

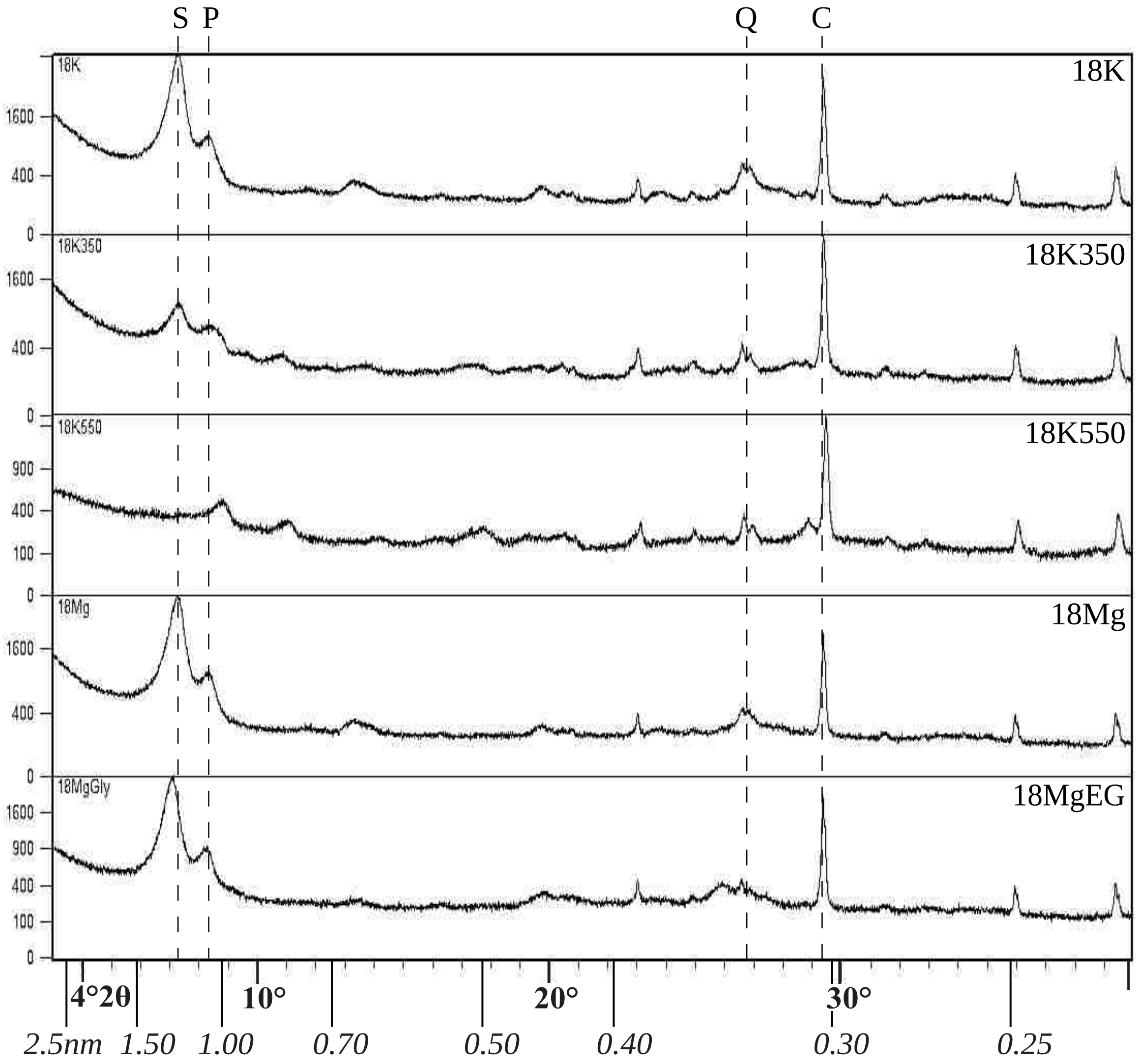

XRD spectra for Sample #18, profile MM1-B (middle Brecciated horizon). The sample contains, in order of decreasing relative abundance: calcite, sepiolite, palygorskite, and quartz.

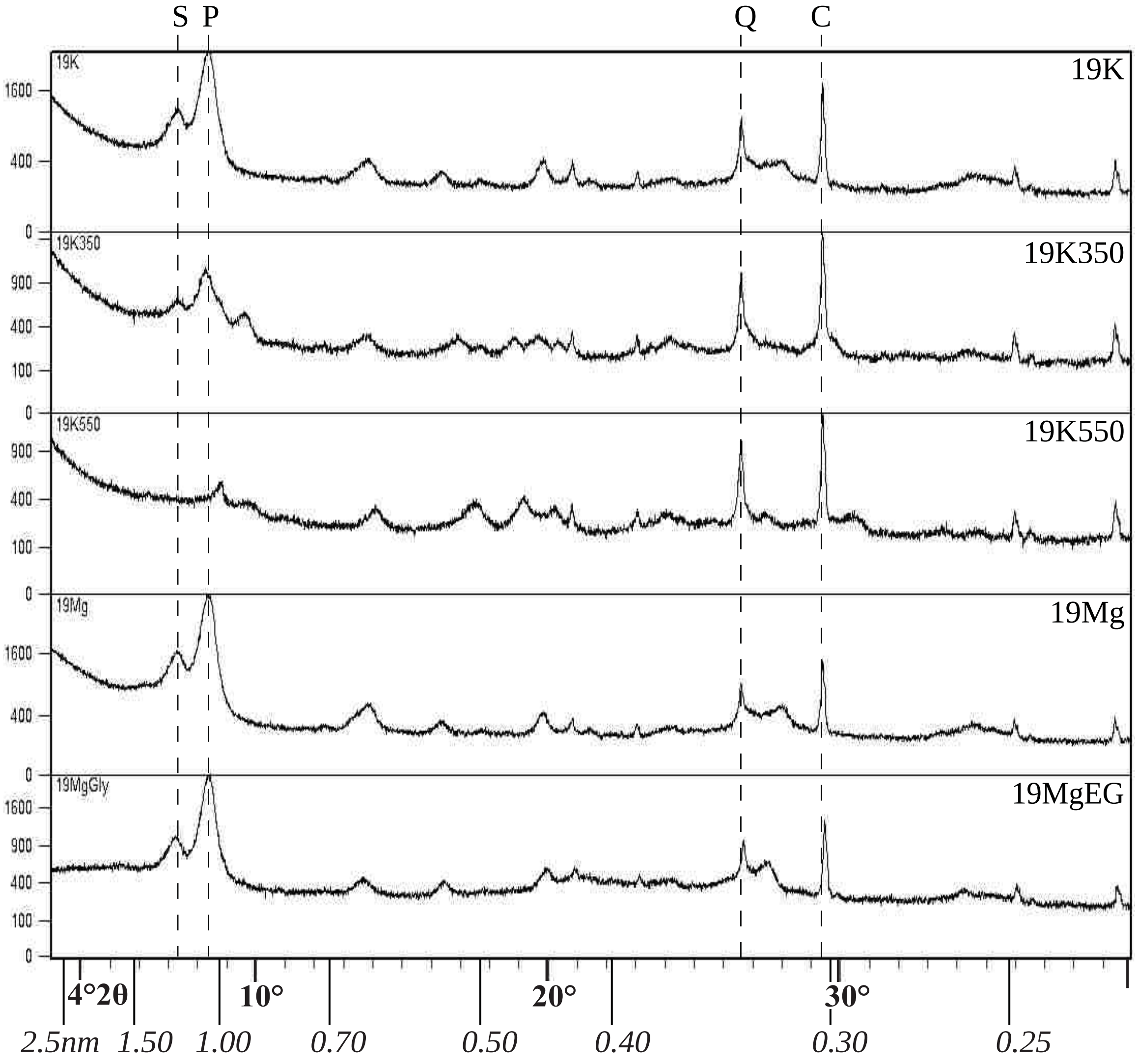

XRD spectra for Sample #19, profile MM1-B (basal Brecciated horizon). The sample contains, in order of decreasing relative abundance: palygorskite, calcite, quartz, and sepiolite.

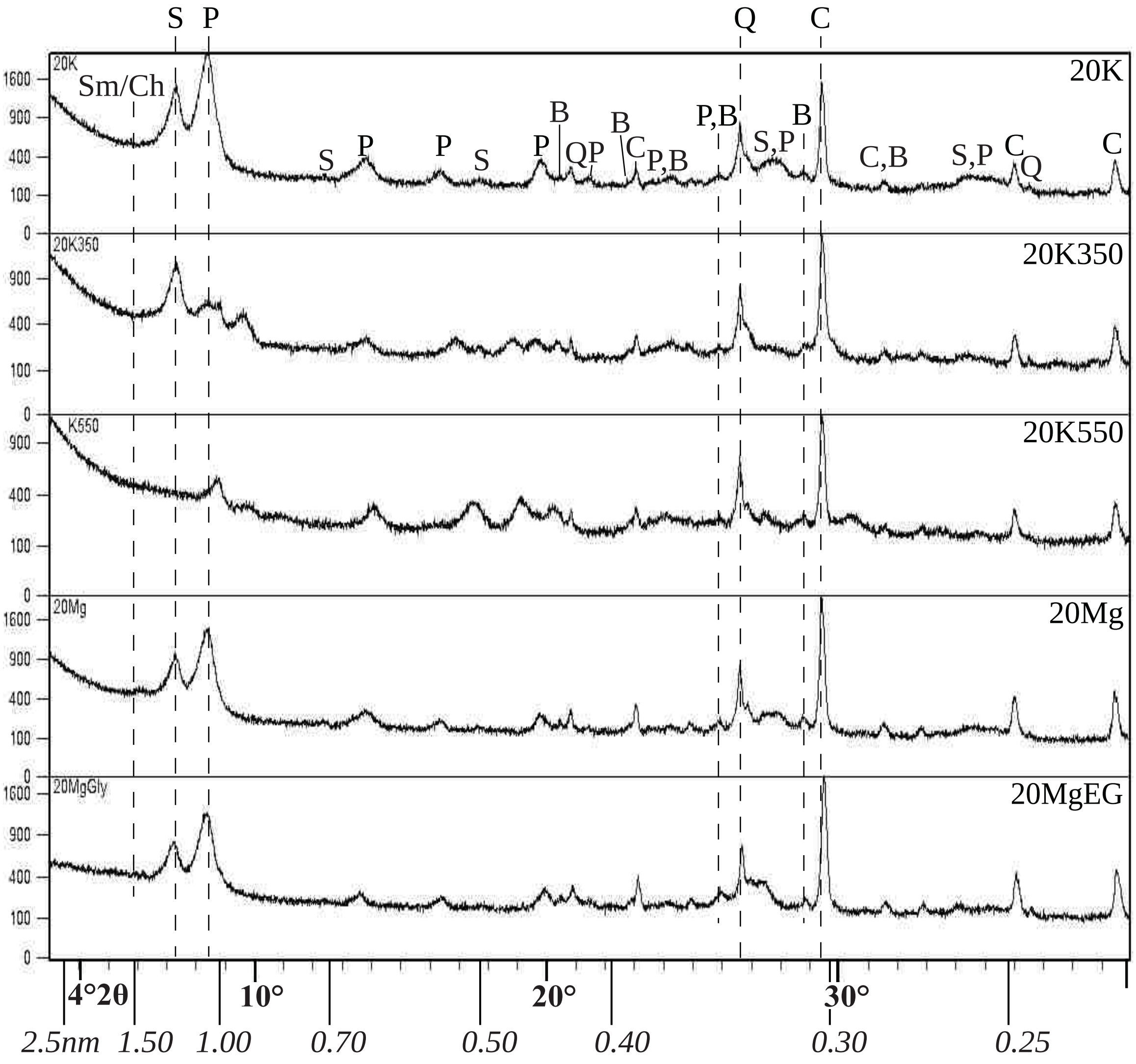

XRD spectra for Sample #20, profile MM1-B (upper Massive horizon). The sample contains, in order of decreasing relative abundance: palygorskite, sepiolite, calcite, quartz, and minor barite. Trace amounts of smectite or smectite-chlorite may be present.

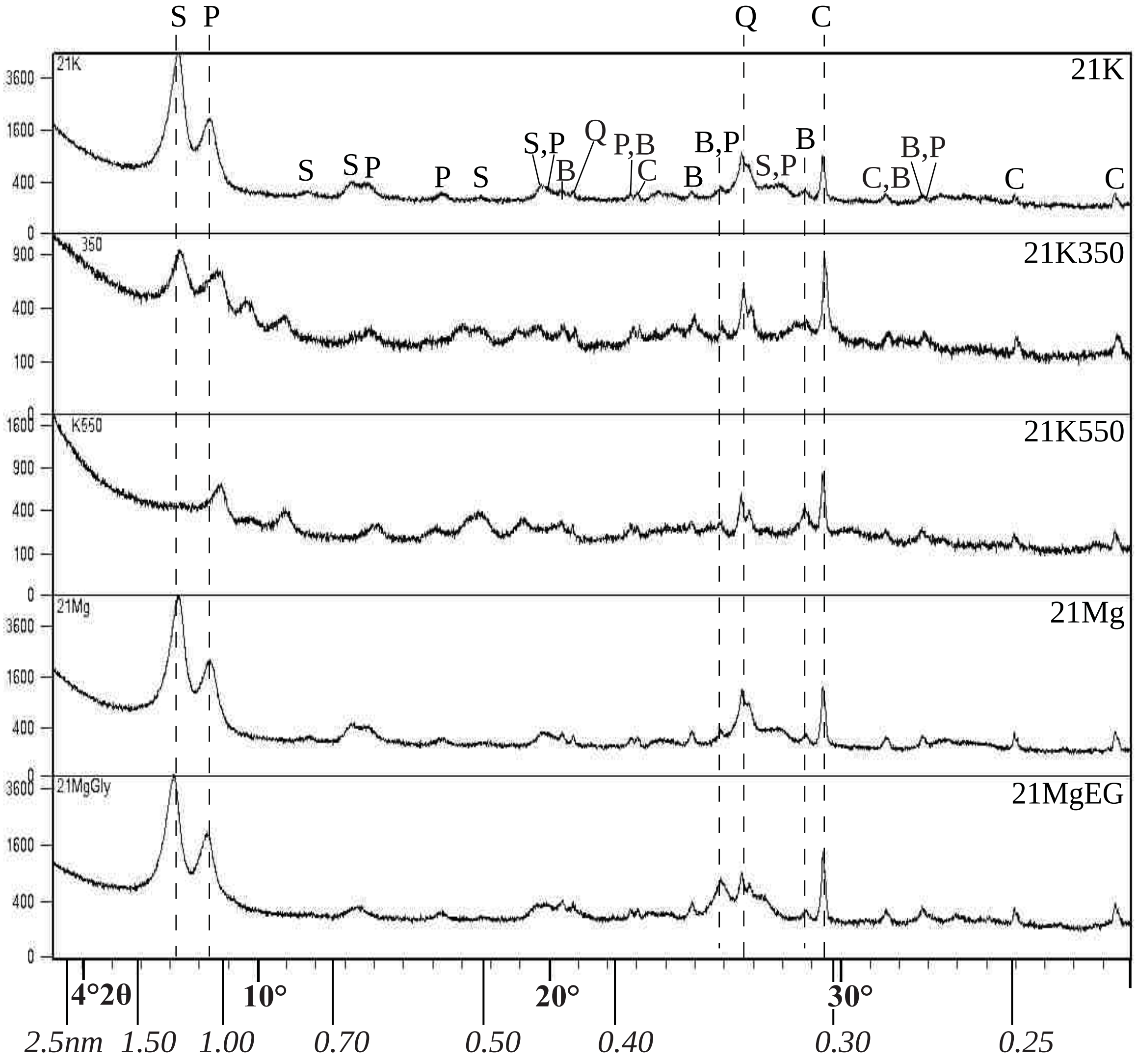

XRD spectra for Sample #21, profile MM1-B (basal Massive horizon). The sample contains, in order of decreasing relative abundance: sepiolite, palygorskite, equal calcite and quartz, and minor barite.

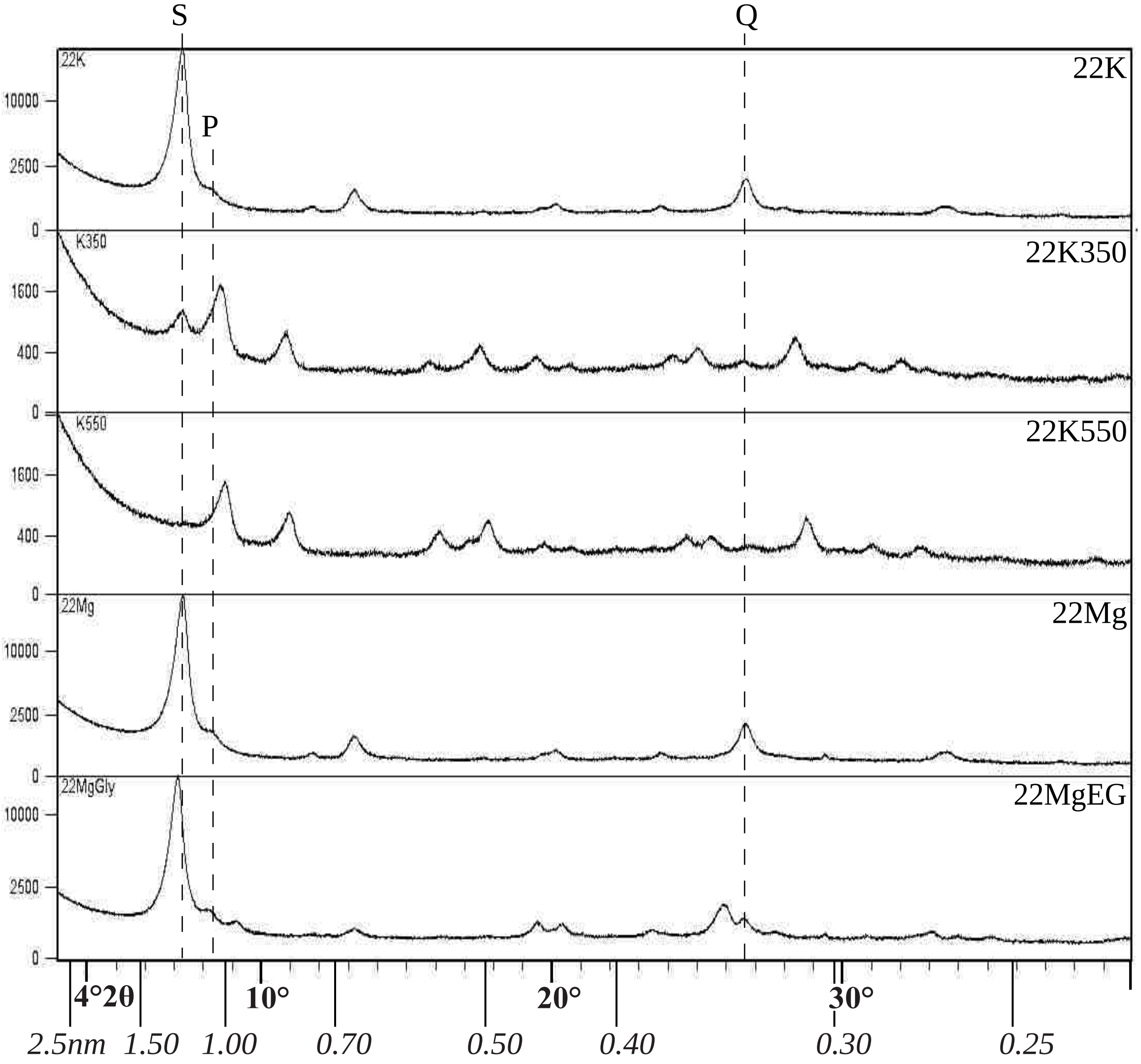

XRD spectra for Sample #22, profile MM1-B (upper Transitional horizon). The sample contains, in order of decreasing relative abundance: sepiolite, quartz, and minor palygorskite.

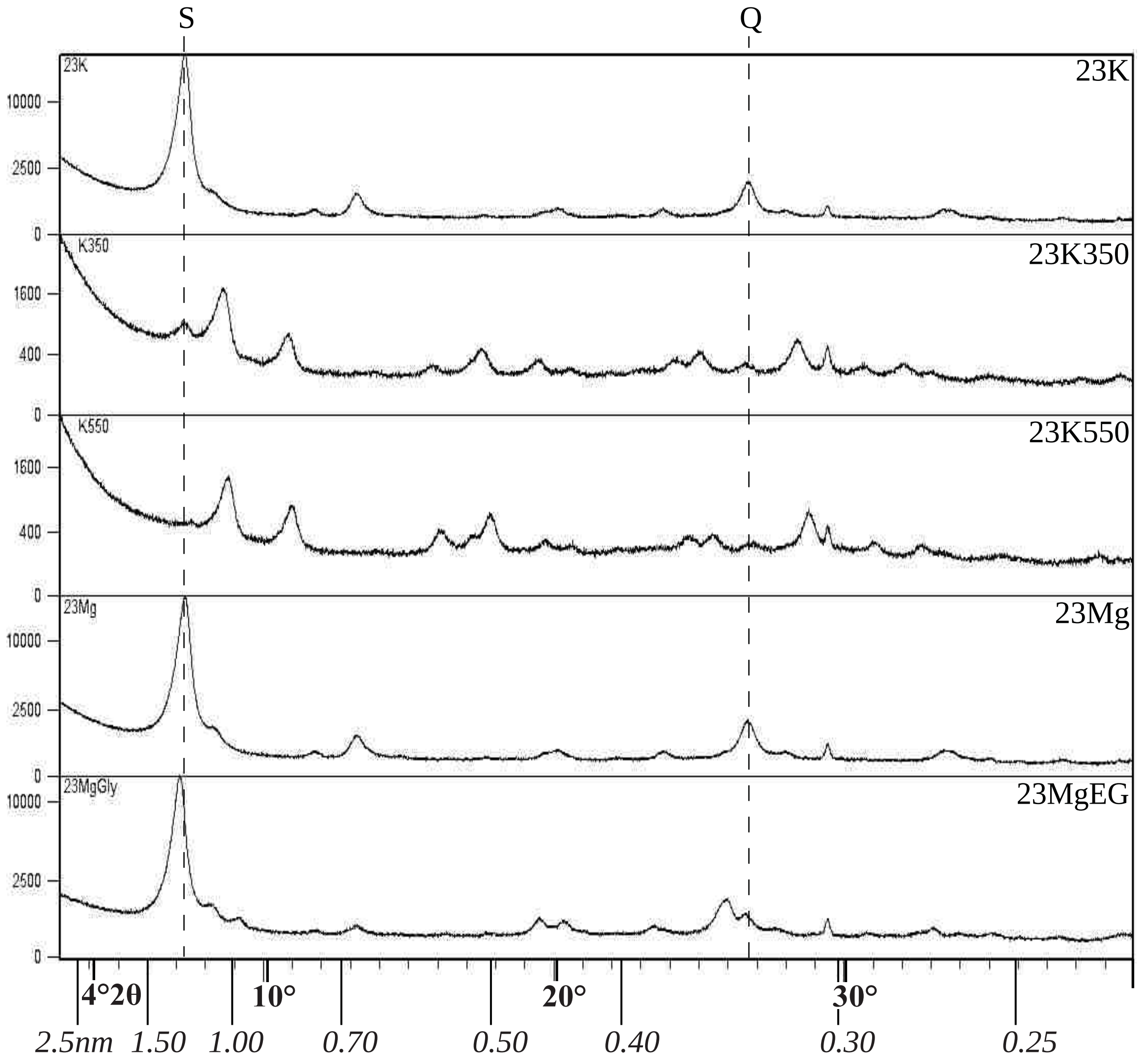

XRD spectra for Sample #23, profile MM1-B (middle Transitional horizon). The sample contains, in order of decreasing relative abundance: sepiolite, quartz, and trace palygorskite.

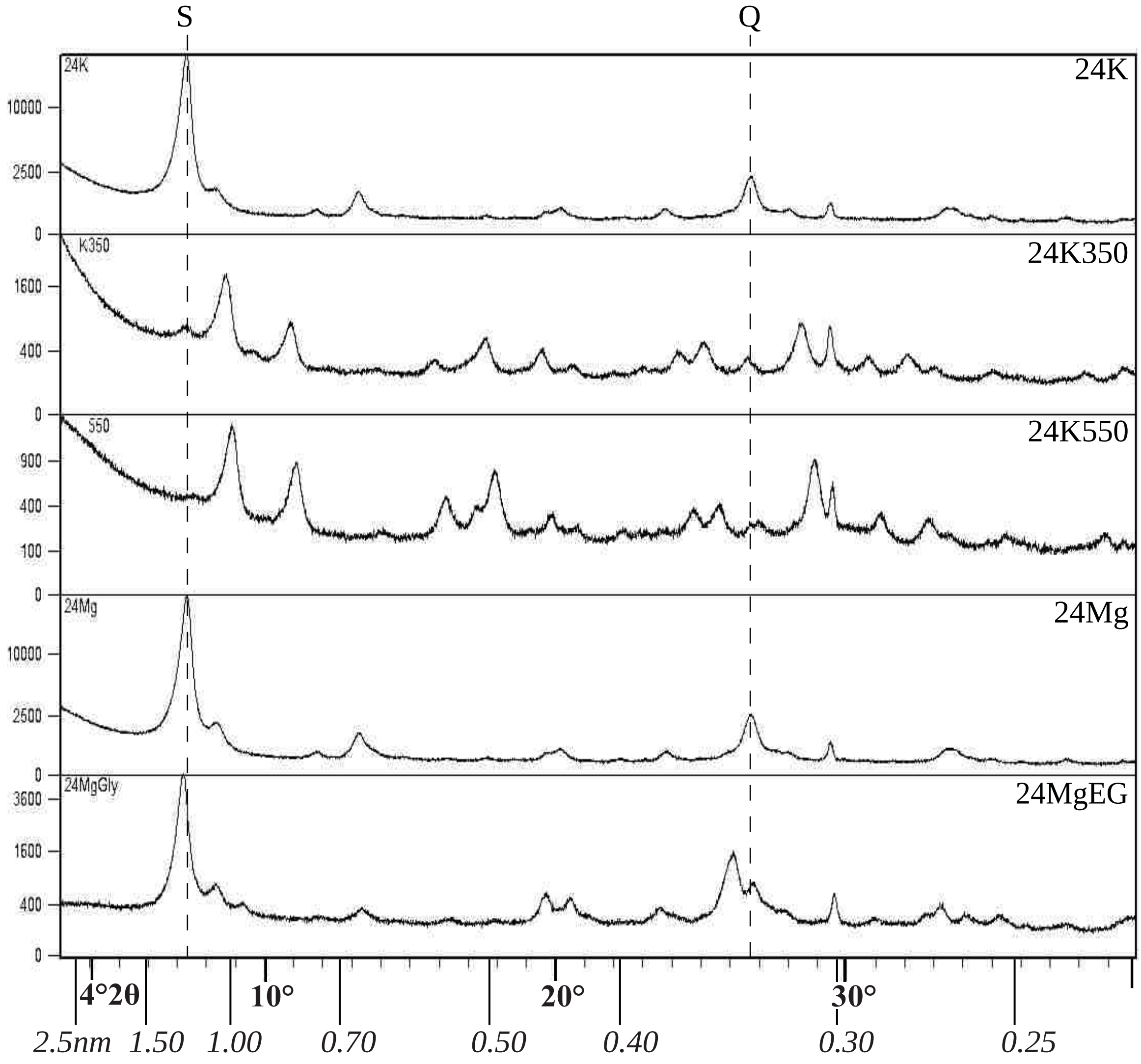

XRD spectra for Sample #24, profile MM1-B (basal Transitional horizon). The sample contains, in order of decreasing relative abundance: sepiolite, quartz, and minor palygorskite.

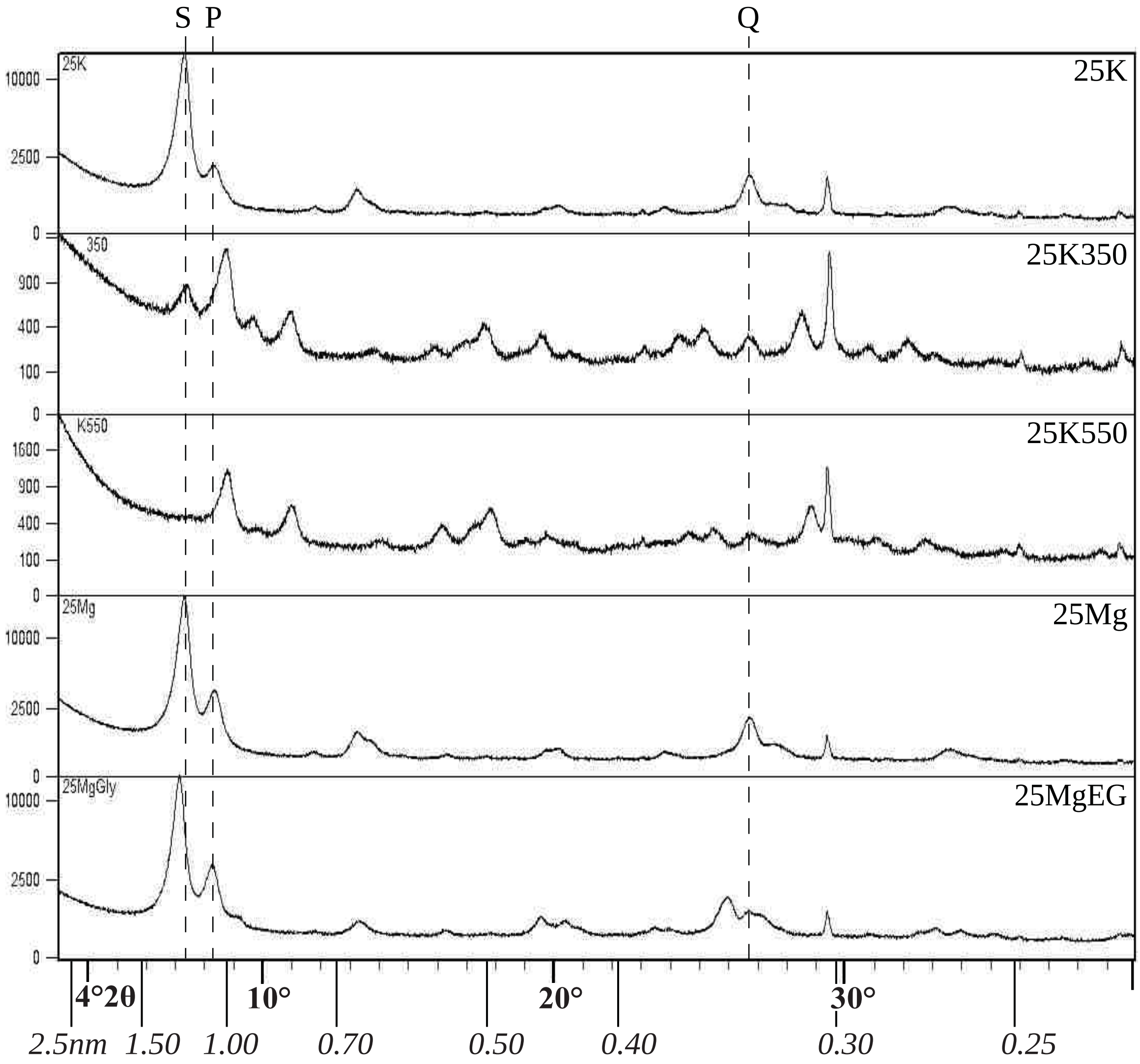

XRD spectra for Sample #25, profile MM1-B (upper Muddy Creek paleosol). The sample contains, in order of decreasing relative abundance: sepiolite, quartz, and palygorskite.

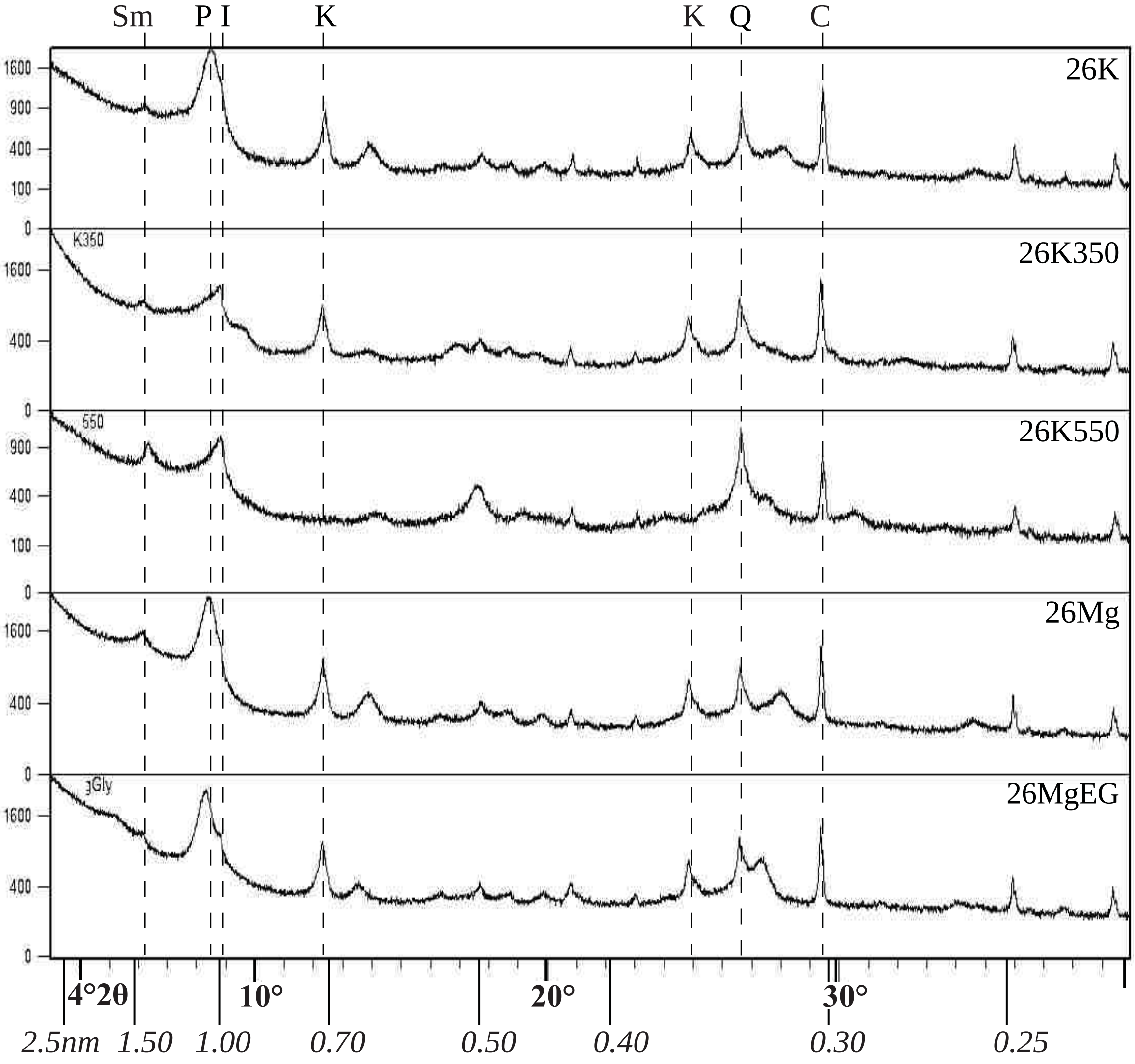

XRD spectra for Sample #26, profile MM1-C (< 2 mm fraction of the surficial rubble horizon). The sample contains, in order of decreasing relative abundance: palygorskite, kaolinite, calcite, quartz, illite, and smectite.

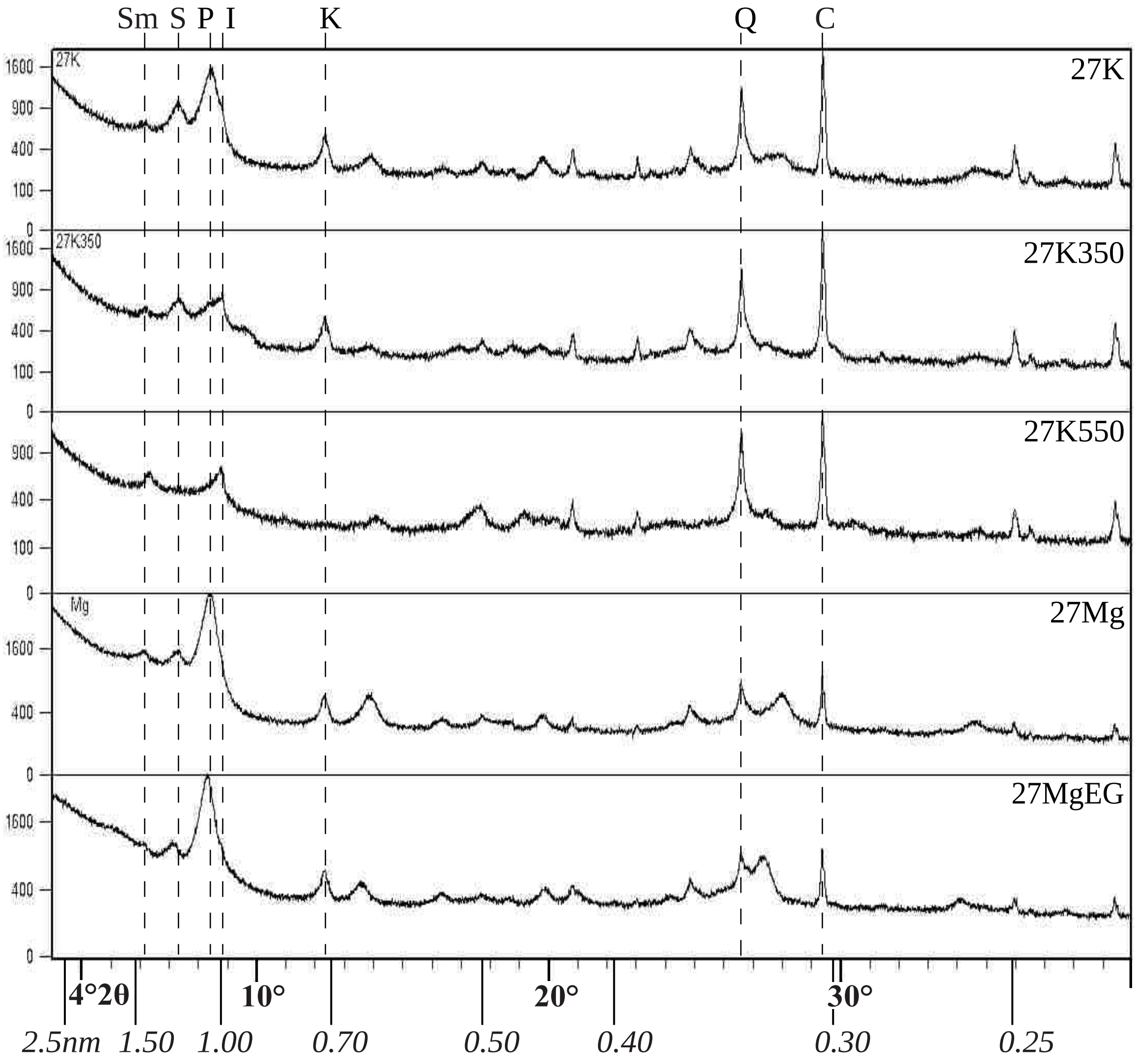

XRD spectra for Sample #27, profile MM1-C (> 2 mm fraction of the surficial rubble horizon). The sample contains, in order of decreasing relative abundance: calcite, quartz, palygorskite, sepiolite, kaolinite, minor illite, and minor smectite or smectite/chlorite.

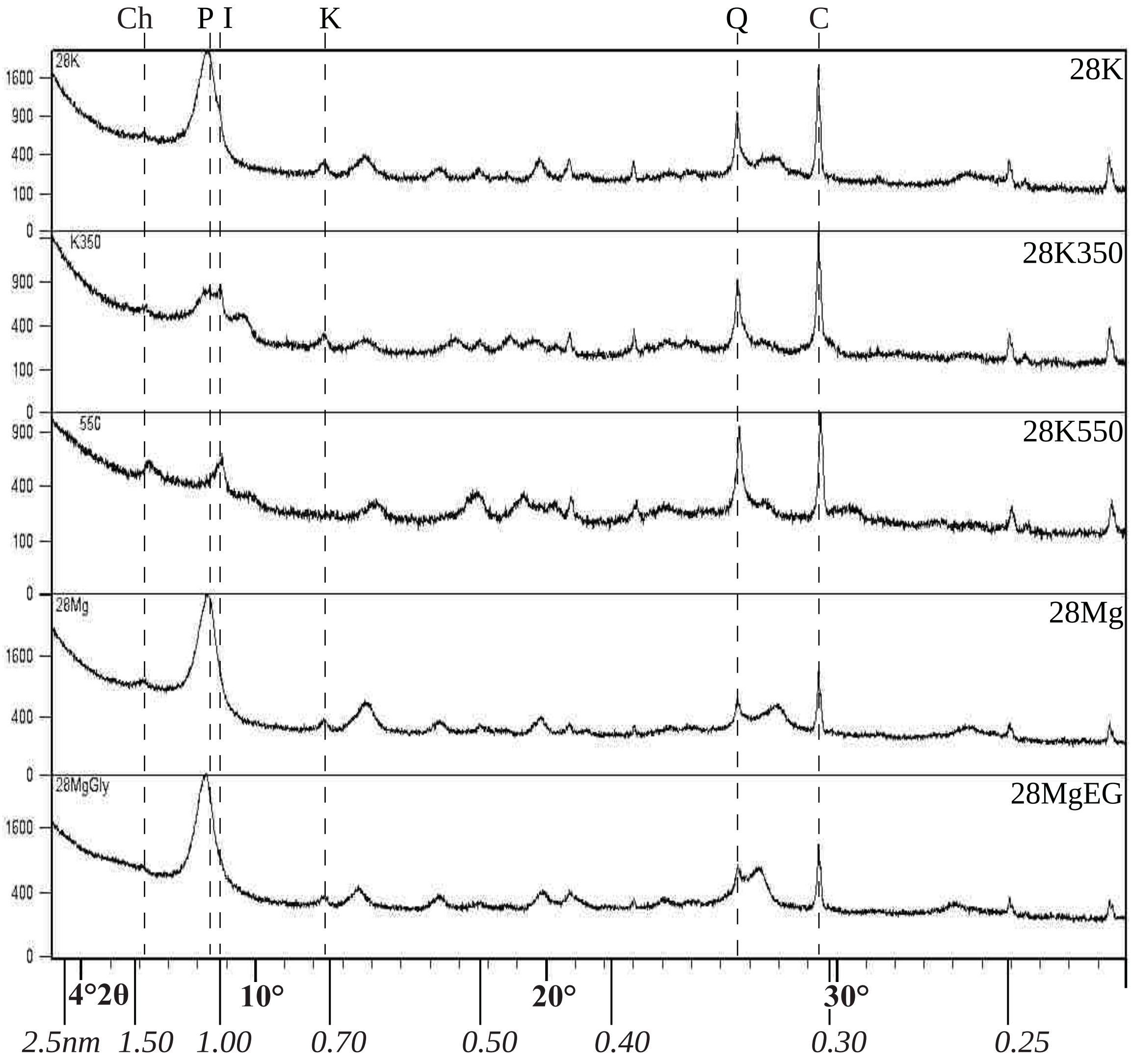

XRD spectra for Sample #28, profile MM1-C (upper Brecciated horizon). The sample contains, in order of decreasing relative abundance: palygorskite, calcite, quartz, illite, kaolinite and minor chlorite or chlorite/smectite.

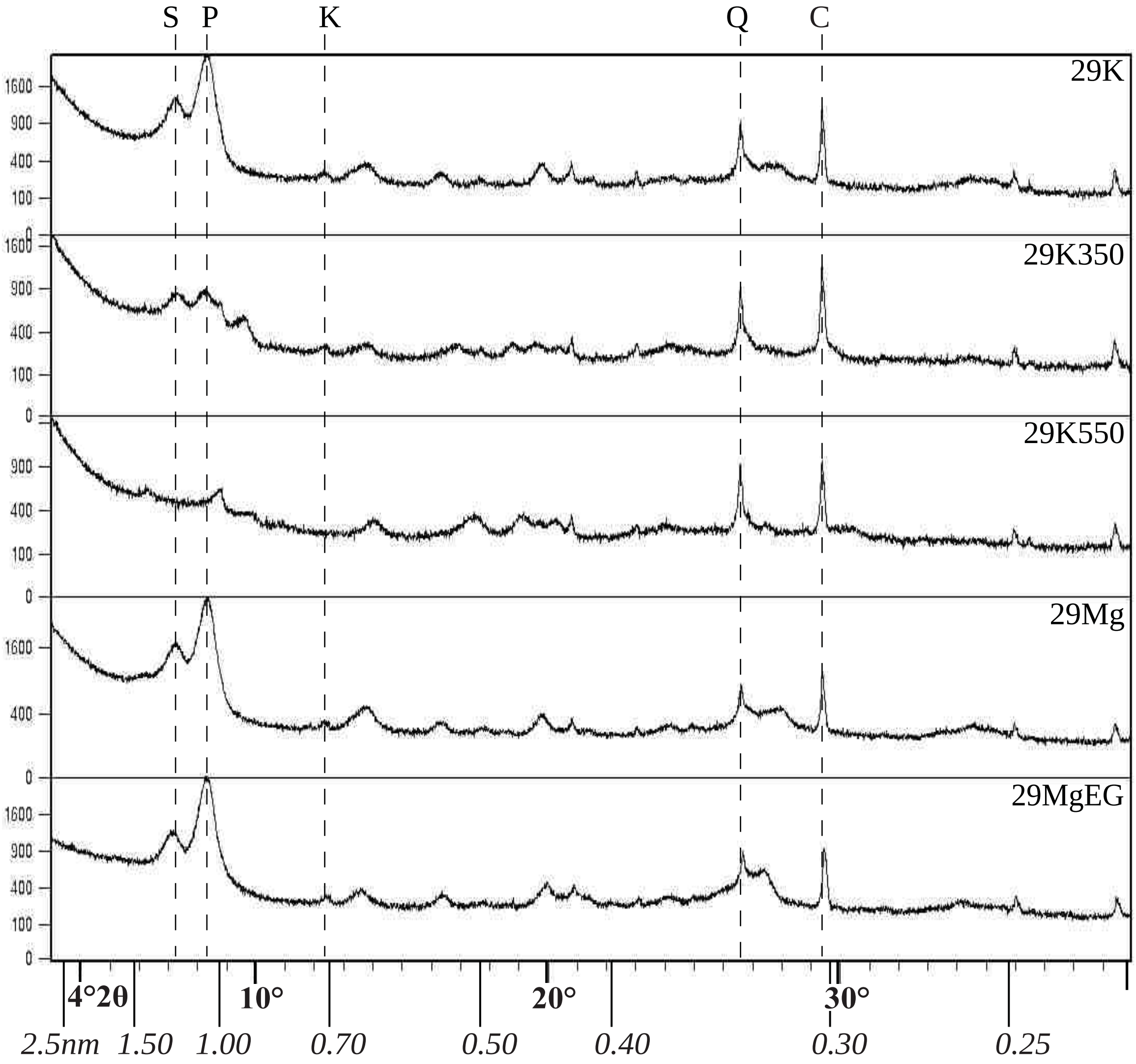

XRD spectra for Sample #29, profile MM1-C (middle Brecciated horizon). The sample contains, in order of decreasing relative abundance: palygorskite, calcite, quartz, sepiolite, and minor kaolinite and smectite.

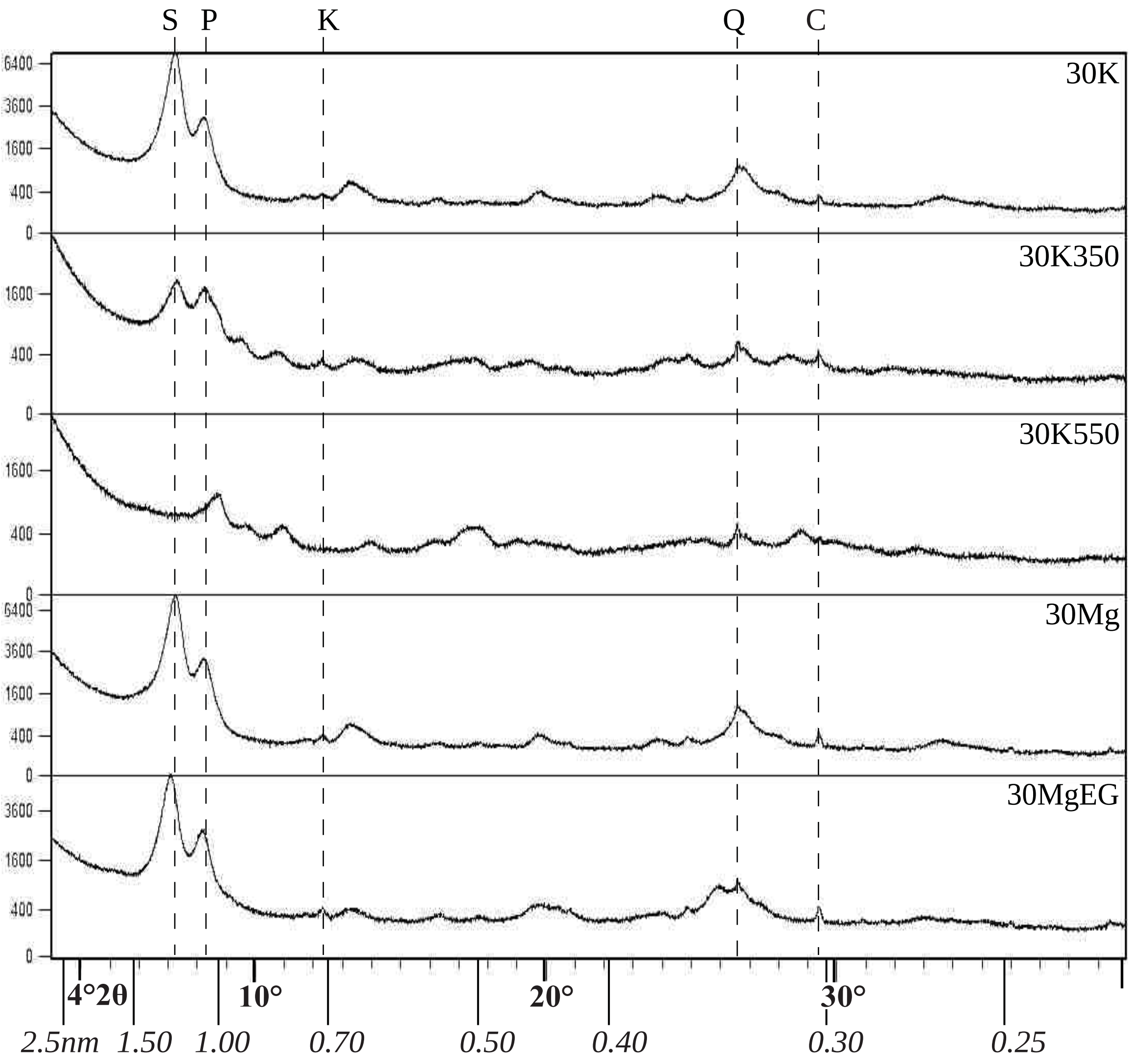

XRD spectra for Sample #30, profile MM1-C (basal Brecciated horizon). The sample contains, in order of decreasing relative abundance: sepiolite, palygorskite, quartz, calcite, and kaolinite.

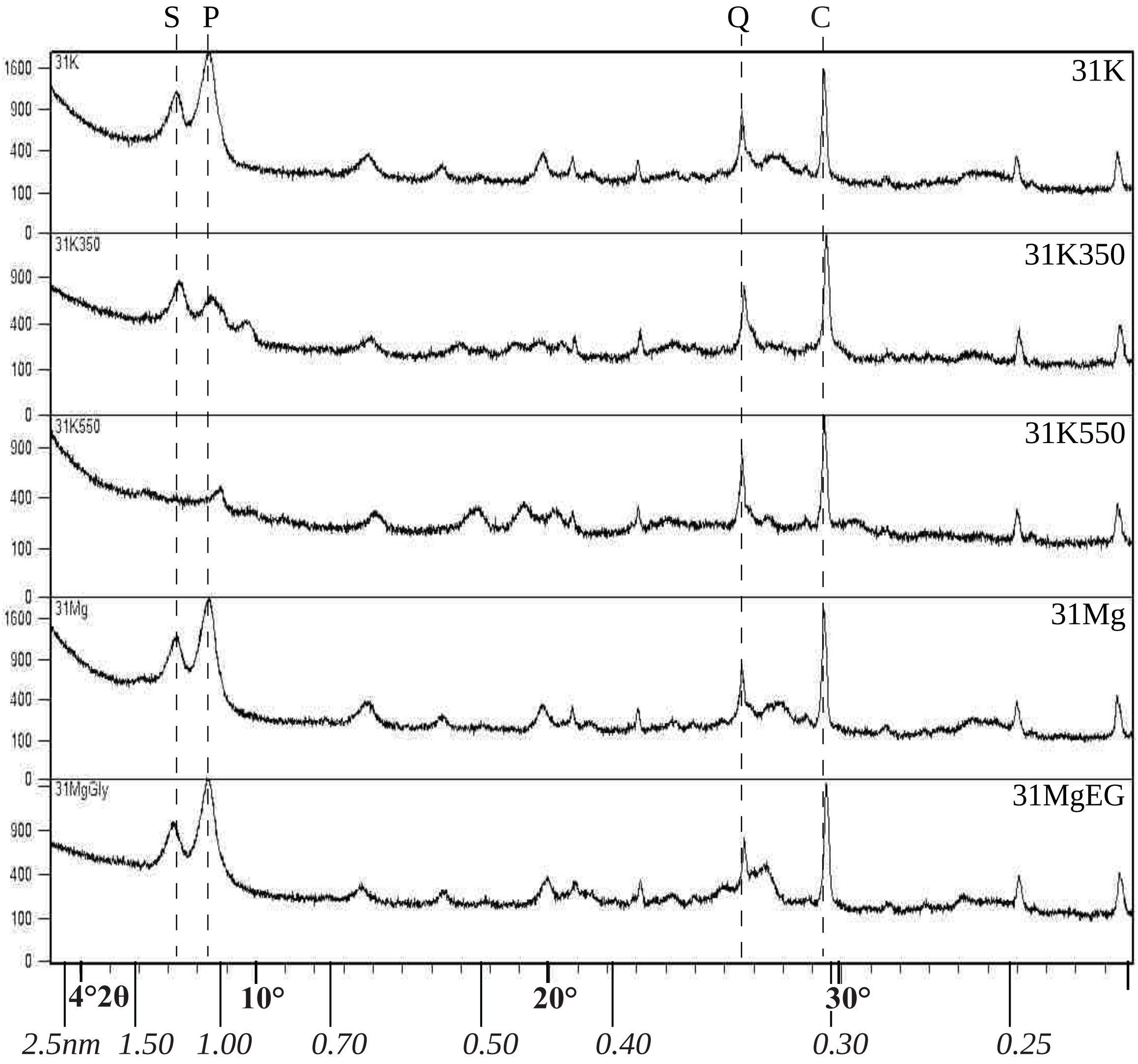

XRD spectra for Sample #31, profile MM1-C (upper Massive horizon). The sample contains, in order of decreasing relative abundance: palygorskite, calcite, quartz, sepiolite, and possible trace amounts of smectite.

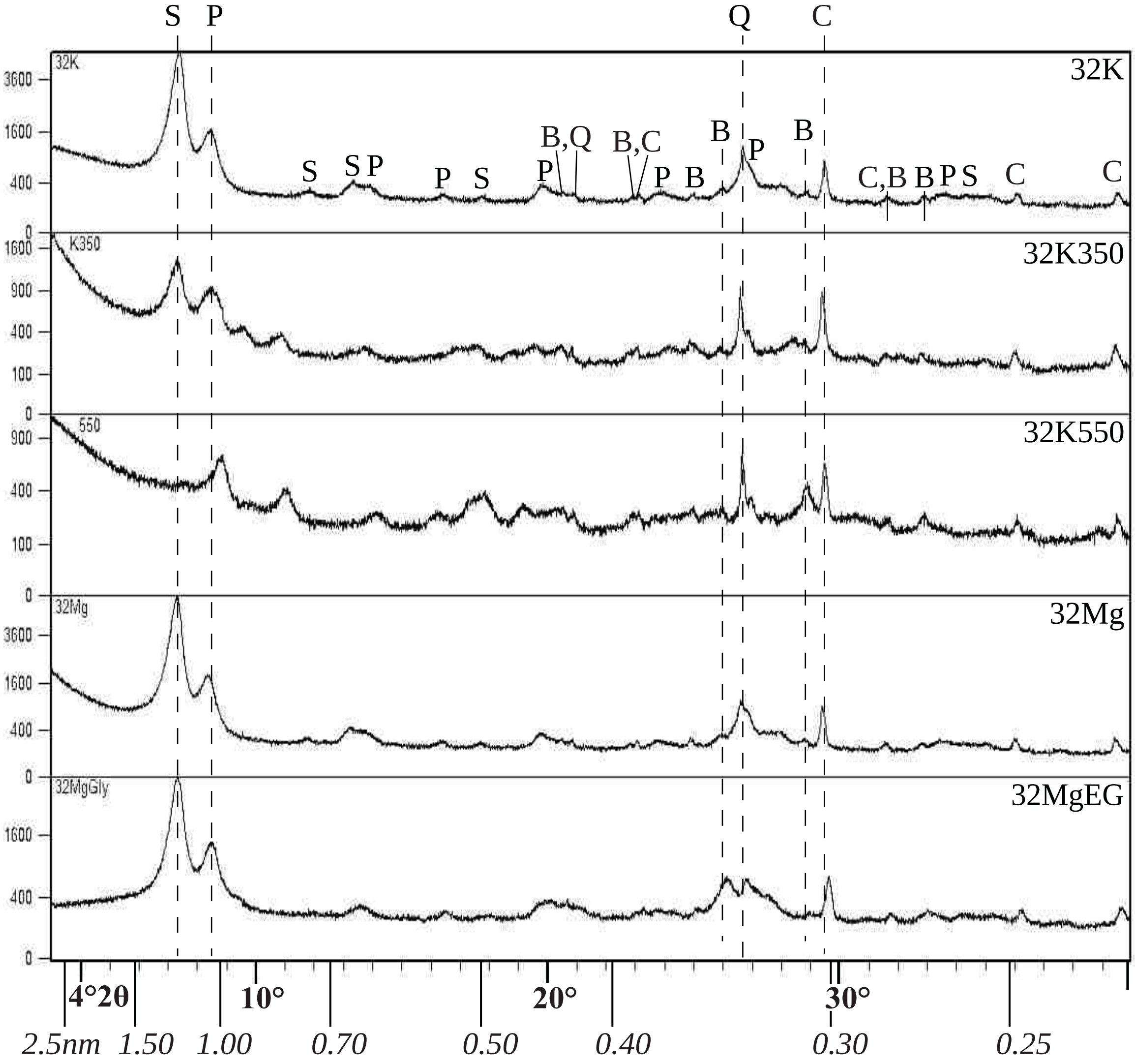

XRD spectra for Sample #32, profile MM1-C (middle Massive horizon). The sample contains, in order of decreasing relative abundance: sepiolite, palygorskite, quartz, calcite, and barite.

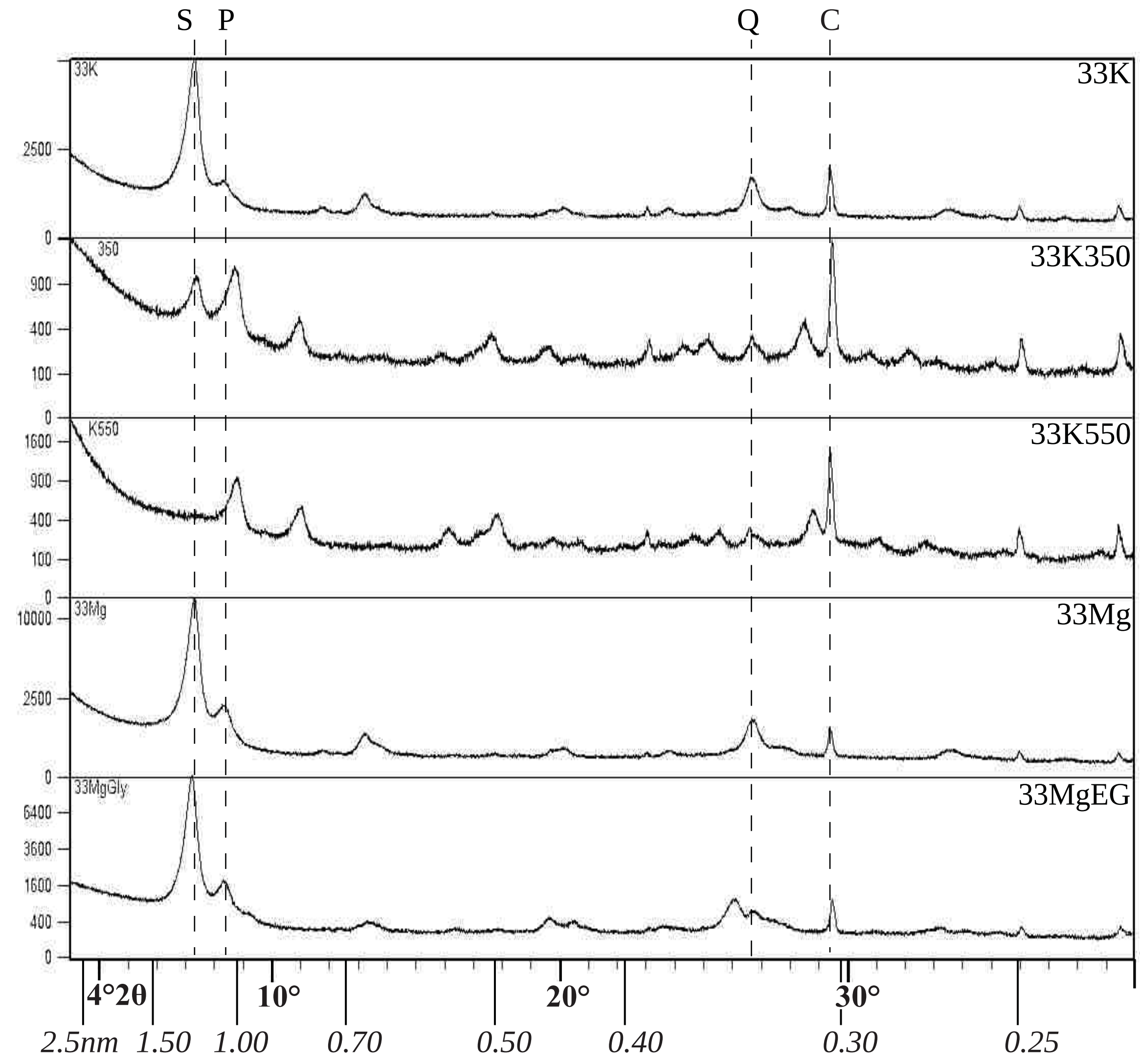

XRD spectra for Sample #33, profile MM1-C (basal Massive horizon). The sample contains, in order of decreasing relative abundance: sepiolite, calcite, quartz, and minor palygorskite.

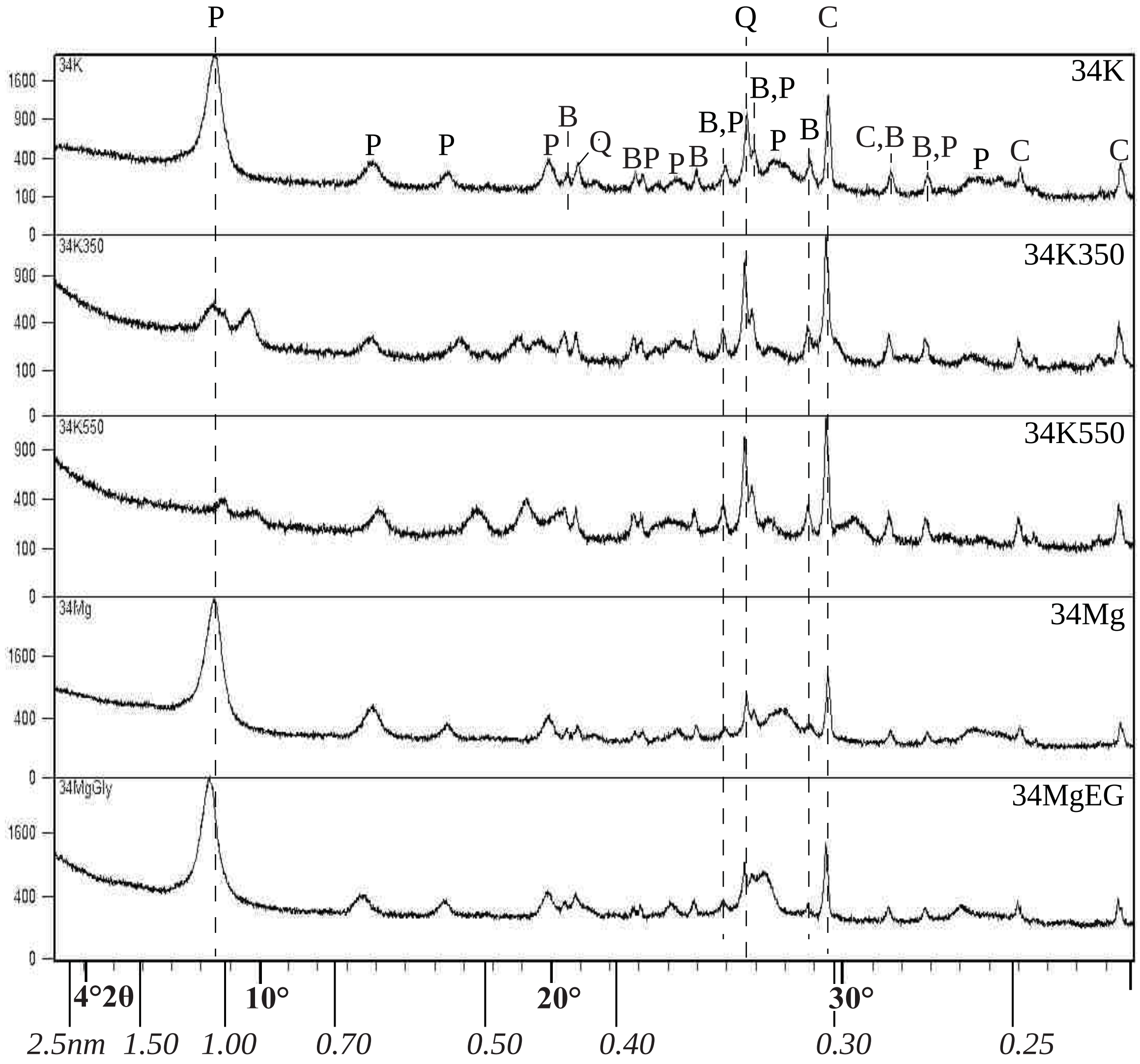

XRD spectra for Sample #34, profile MM1-C (middle Transitional horizon). The sample contains, in order of decreasing relative abundance: palygorskite, calcite, quartz, and barite.

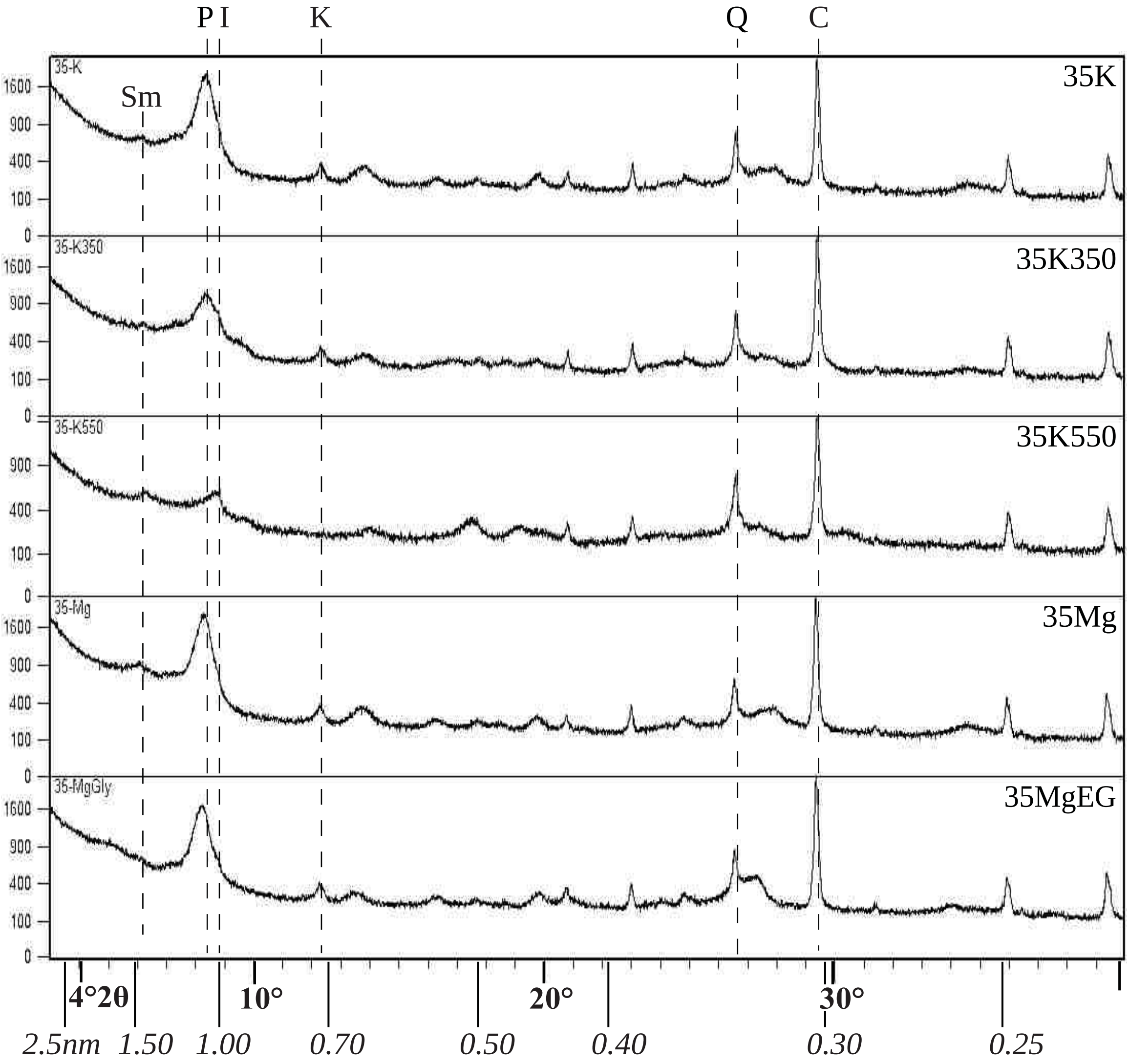

XRD spectra for Sample #35, profile MM2 (> 2mm fraction of the surface rubble horizon). The sample contains, in order of decreasing relative abundance: calcite, palygorskite, quartz, illite, kaolinite, and minor smectite or smectite/chlorite.

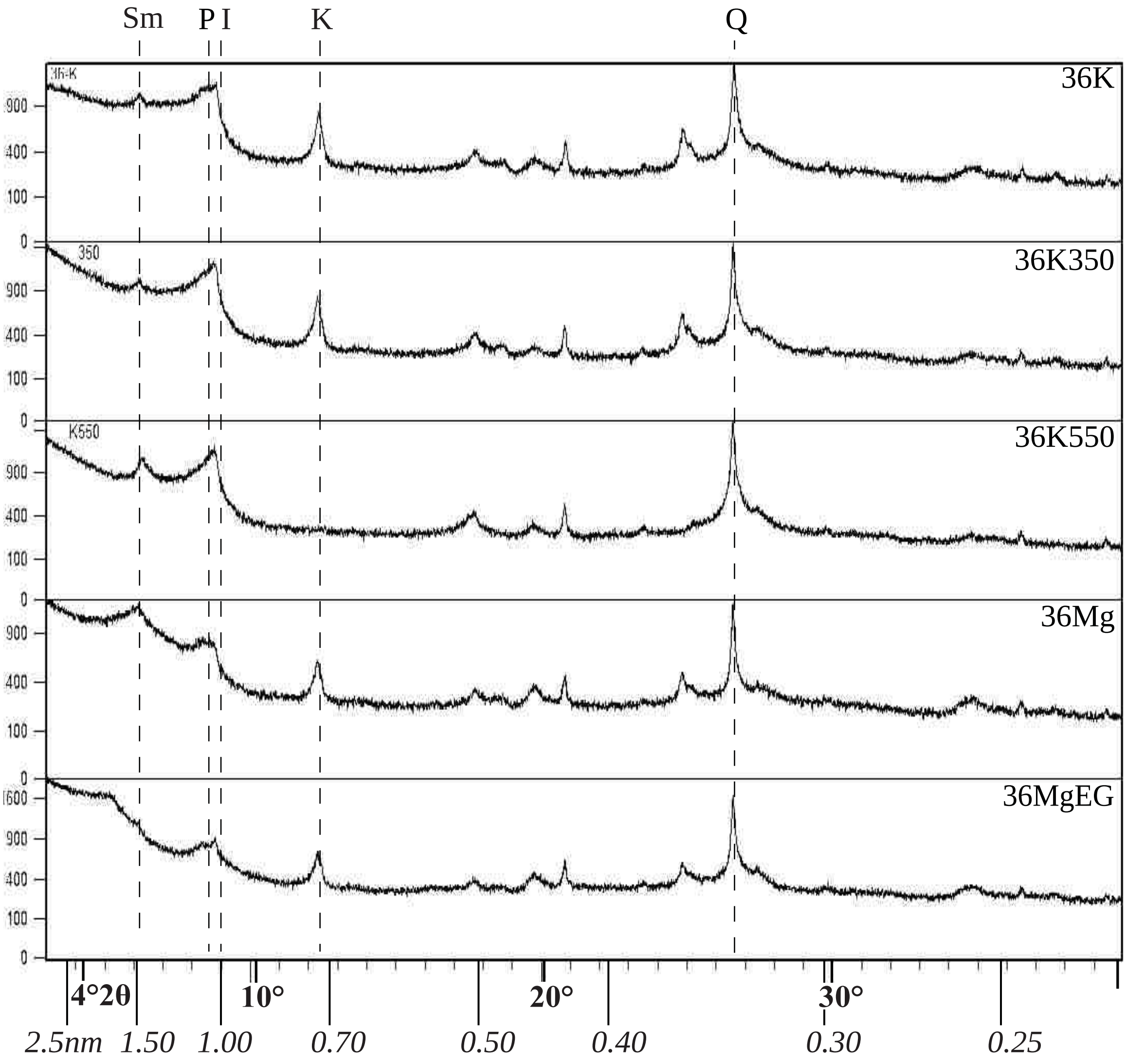

XRD spectra for Sample #36, profile MM2 (< 2mm fraction of the surface rubble horizon). The sample contains, in order of decreasing relative abundance: quartz, kaolinite, illite, palygorskite, and smectite.

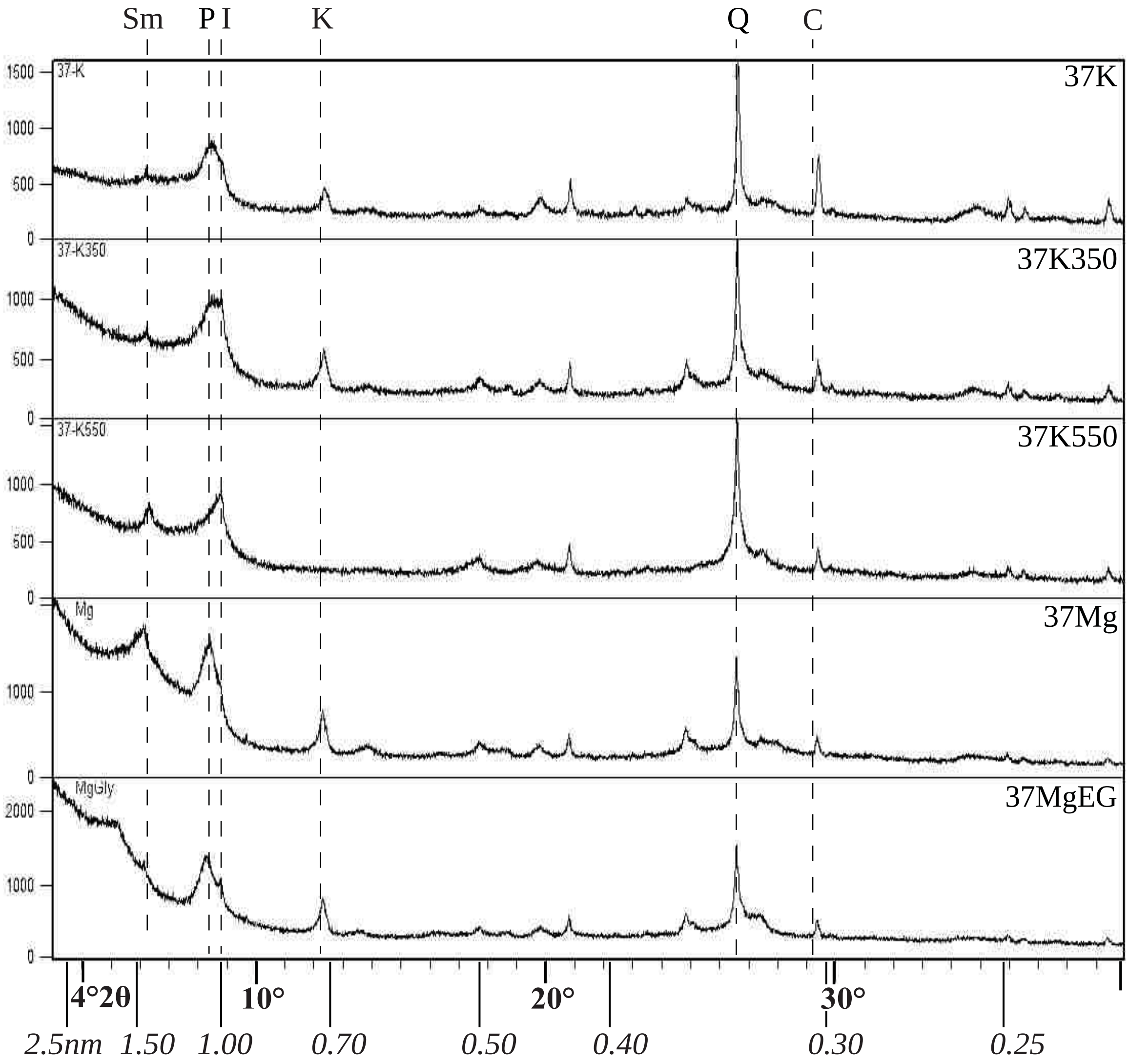

XRD spectra for Sample #37, profile MM2 (> 2 mm fraction of the surface rubble horizon). The sample contains, in order of decreasing relative abundance: quartz, calcite, palygorskite, kaolinite, illite, and smectite.

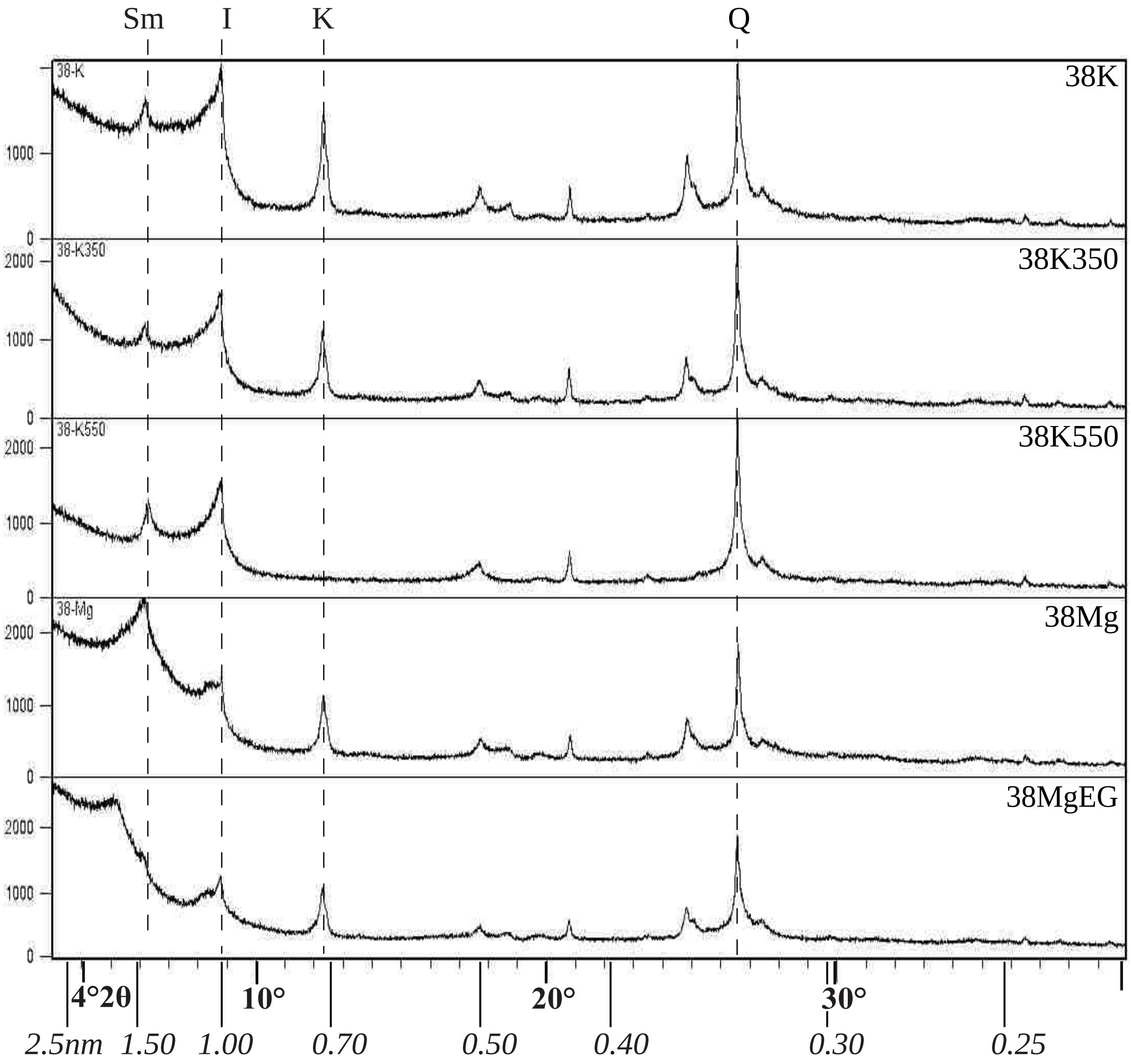

XRD spectra for Sample #38, profile MM2 (< 2 mm fraction of the surface rubble horizon). The sample contains, in order of decreasing relative abundance: quartz, kaolinite, illite, and smectite, with possible trace palygorskite.

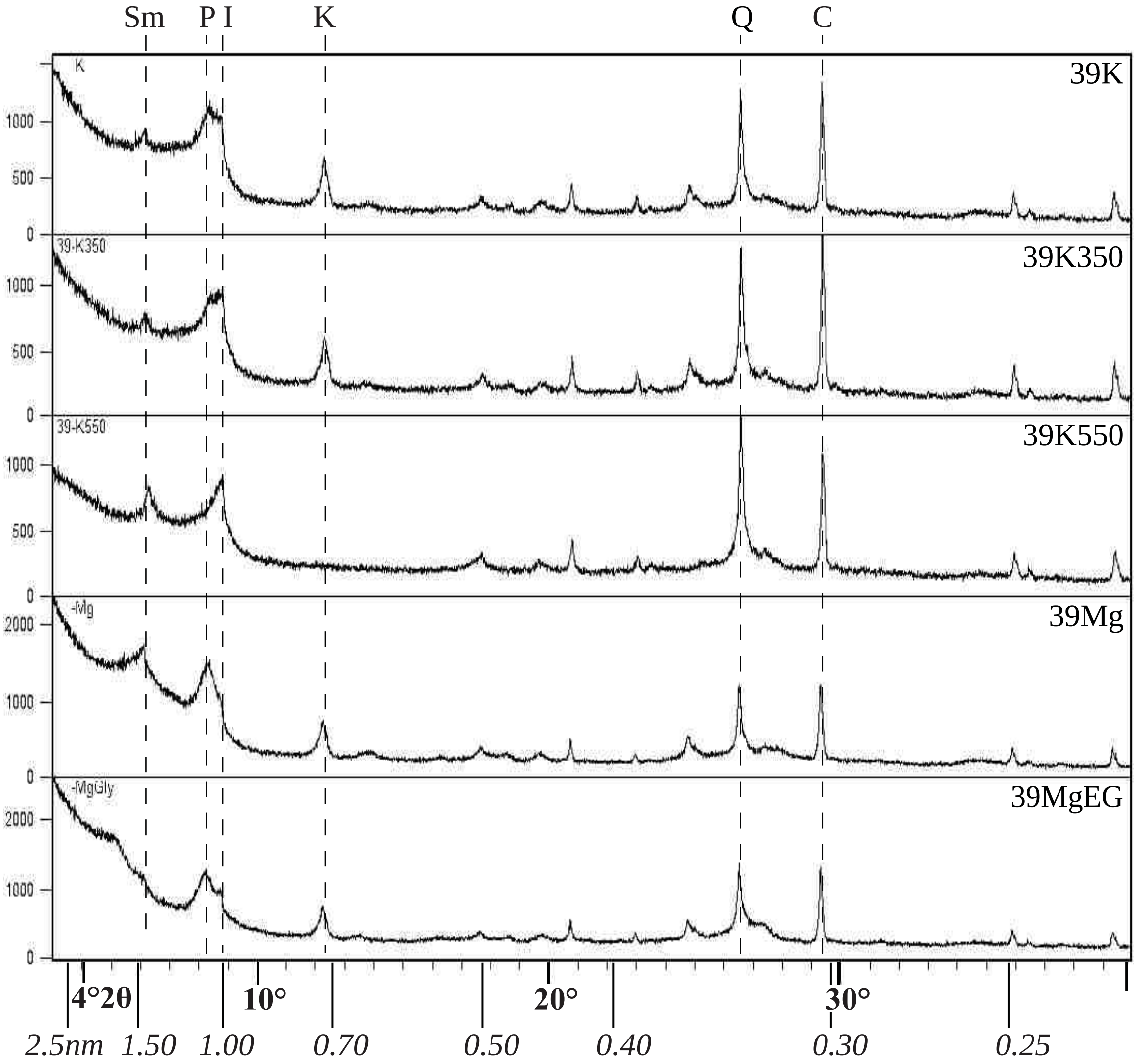

XRD spectra for Sample #39, profile MM2 (> 2 mm fraction of the surface rubble horizon). The sample contains, in order of decreasing relative abundance: calcite, quartz, kaolinite, palygorskite, smectite, and illite.

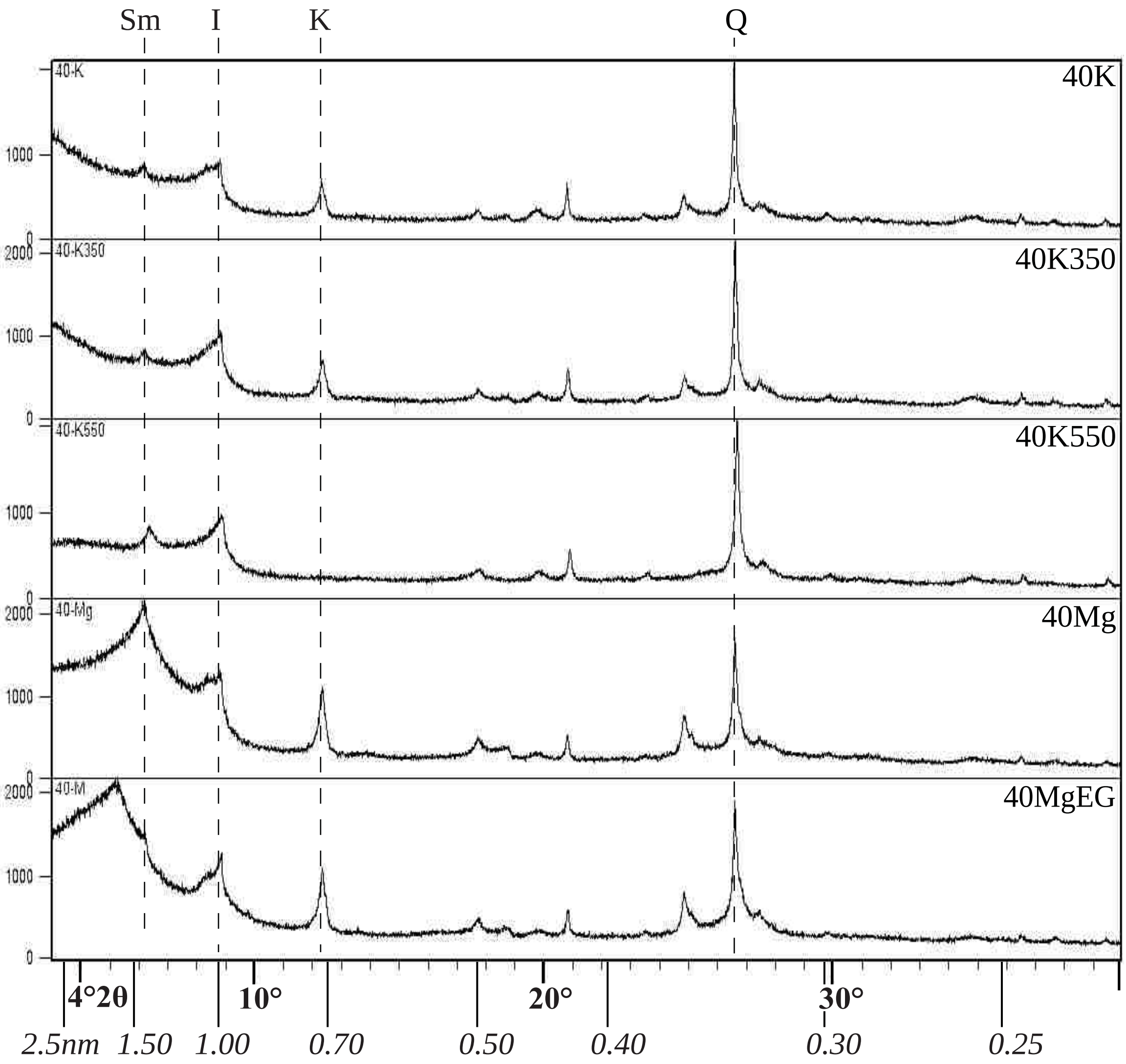

XRD spectra for Sample #40, profile MM2 (< 2 mm fraction of the surface rubble horizon). The sample contains, in order of decreasing relative abundance: quartz, smectite and kaolinite in comparable amounts, and illite.

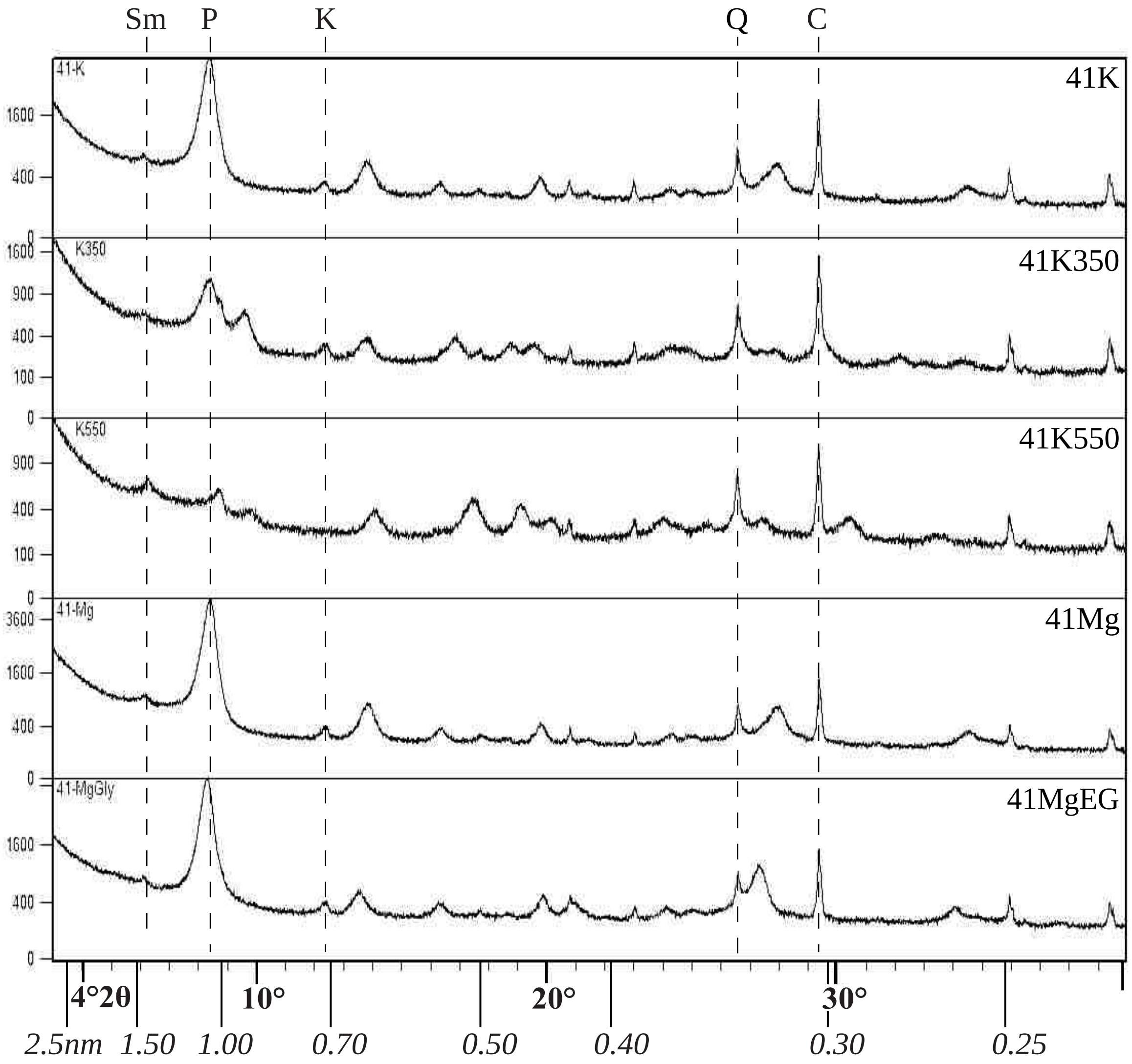

XRD spectra for Sample #41, profile MM2 (upper Brecciated horizon). The sample contains, in order of decreasing relative abundance: palygorskite, calcite, quartz, kaolinite, and minor chlorite or chlorite/smectite.

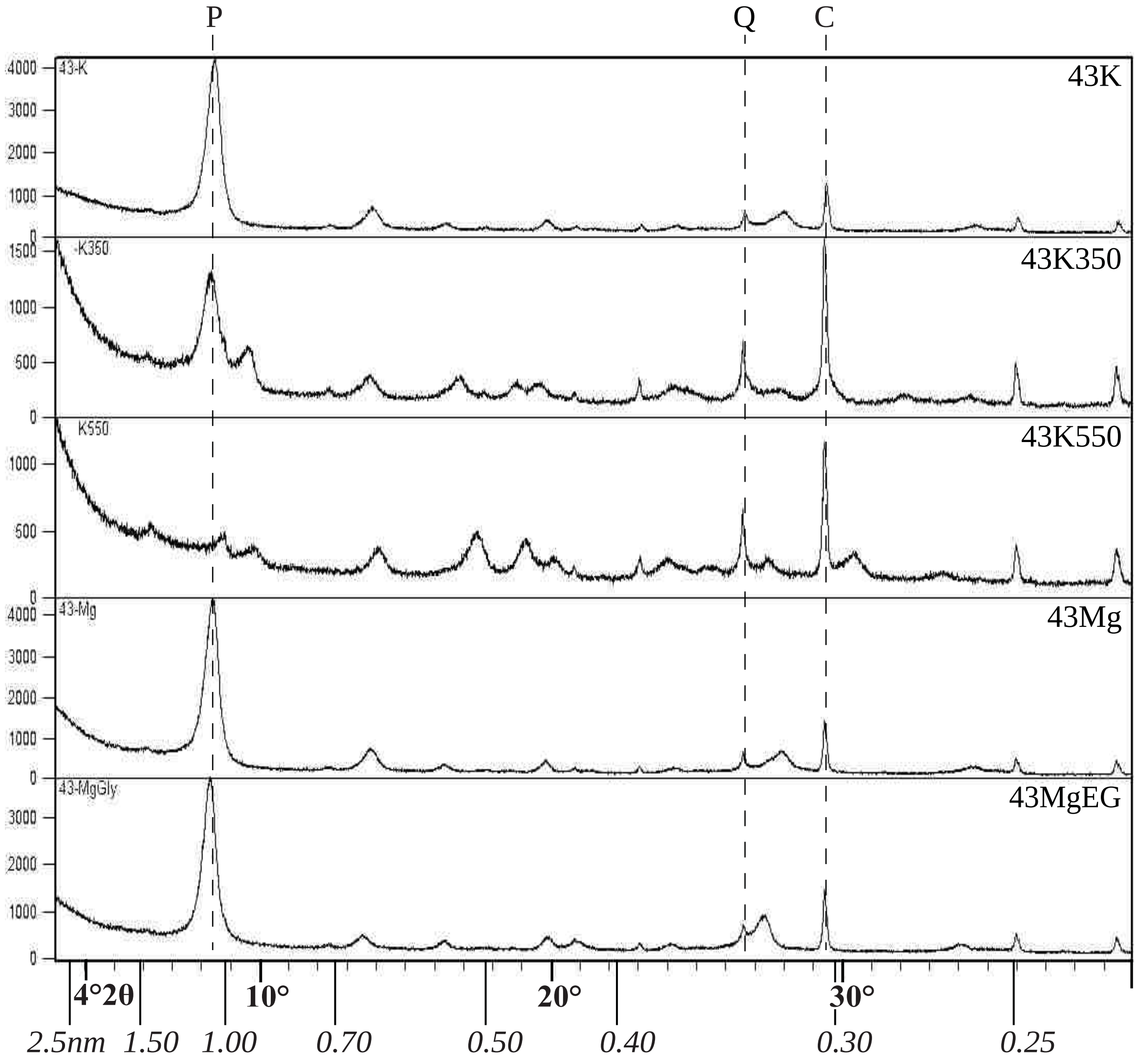

XRD spectra for Sample #43, profile MM2 (basal Brecciated horizon). The sample contains, in order of decreasing relative abundance: palygorskite, calcite, quartz, and trace chlorite or chlorite/smectite.

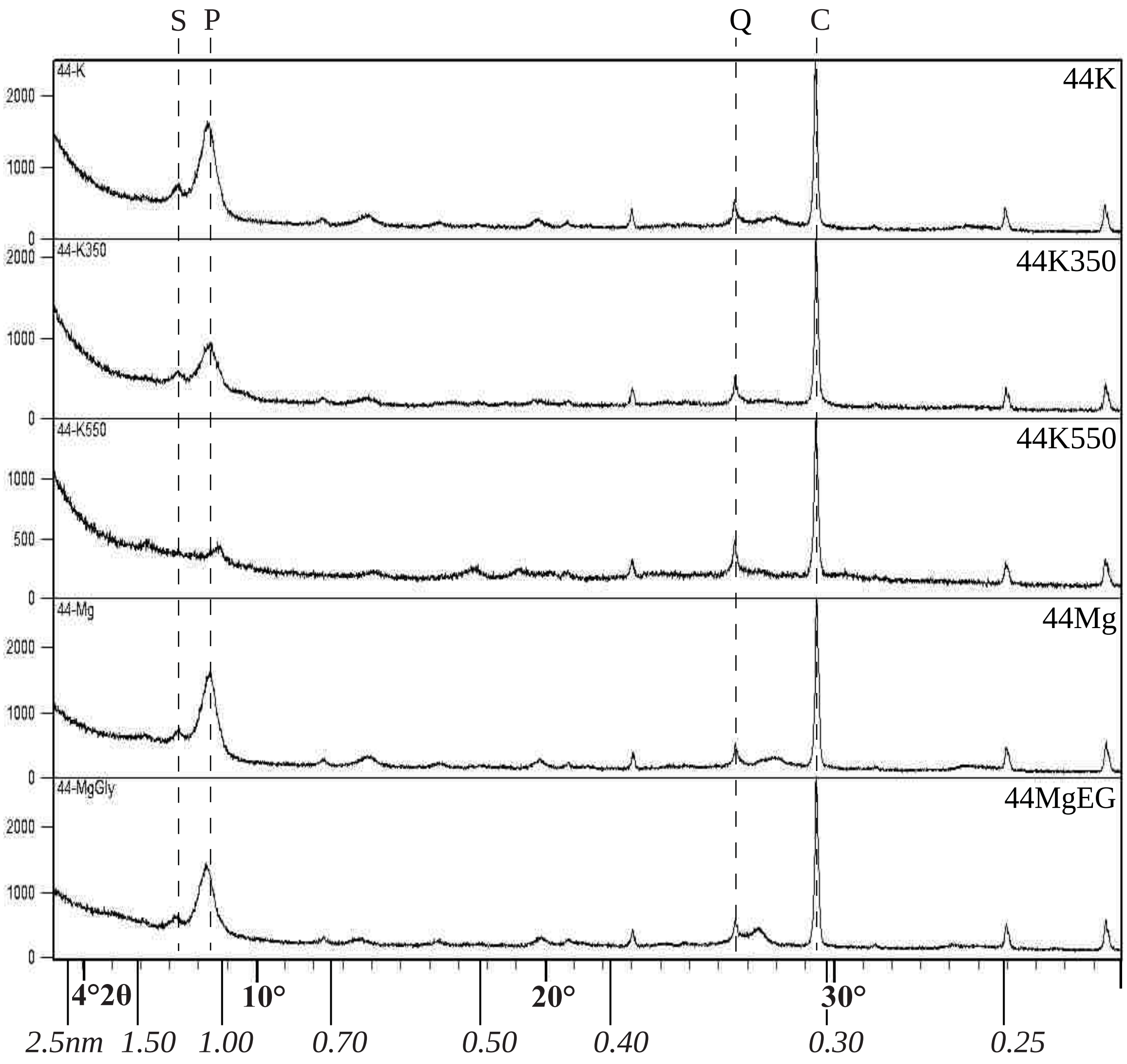

XRD spectra for Sample #44, profile MM2 (upper Massive horizon). The sample contains, in order of decreasing relative abundance: calcite, palygorskite, quartz, and sepiolite.

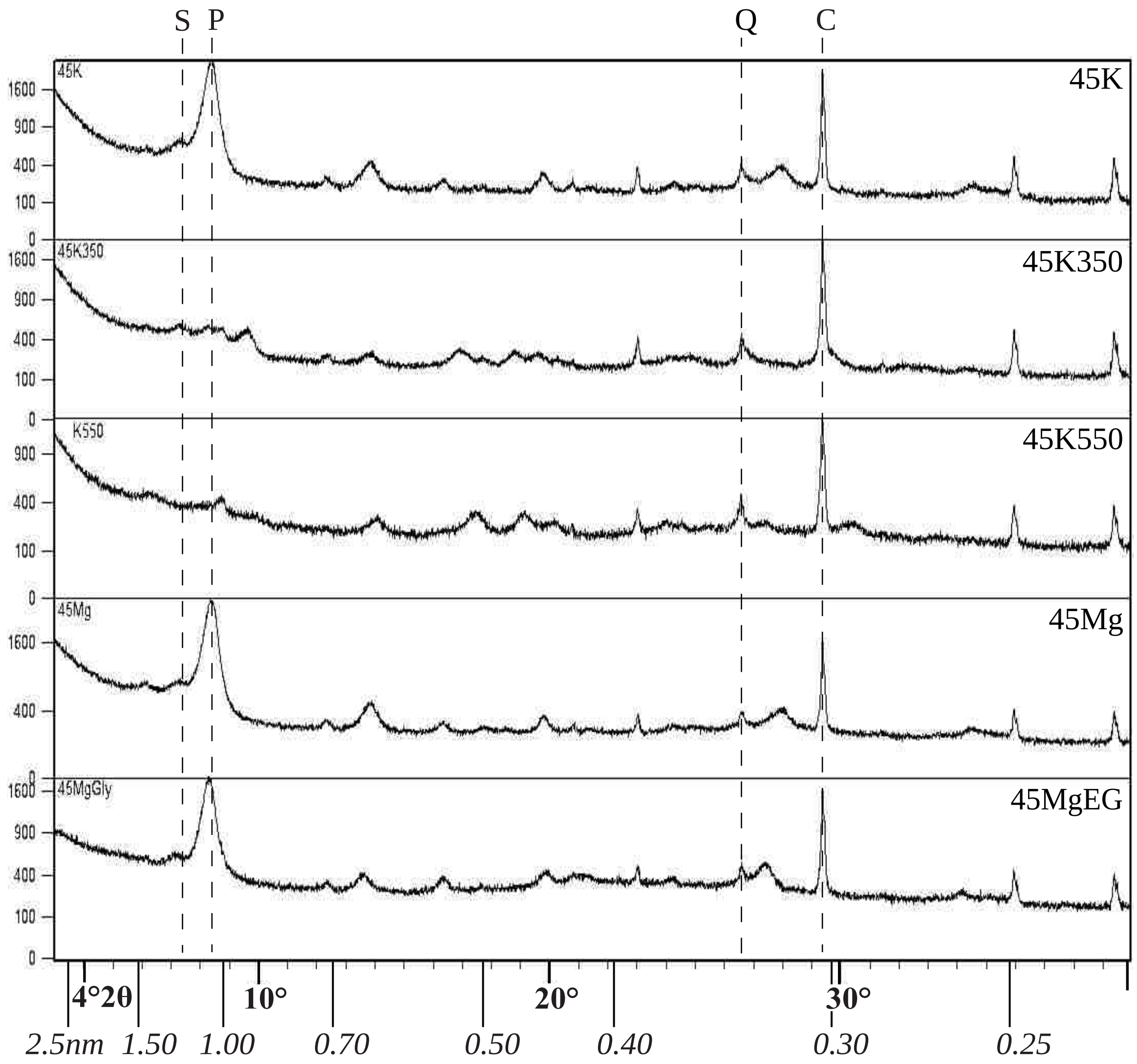

XRD spectra for Sample #45, profile MM2 (upper Massive horizon). The sample contains, in order of decreasing relative abundance: palygorskite, calcite, quartz, minor sepiolite, and possible trace smectite.

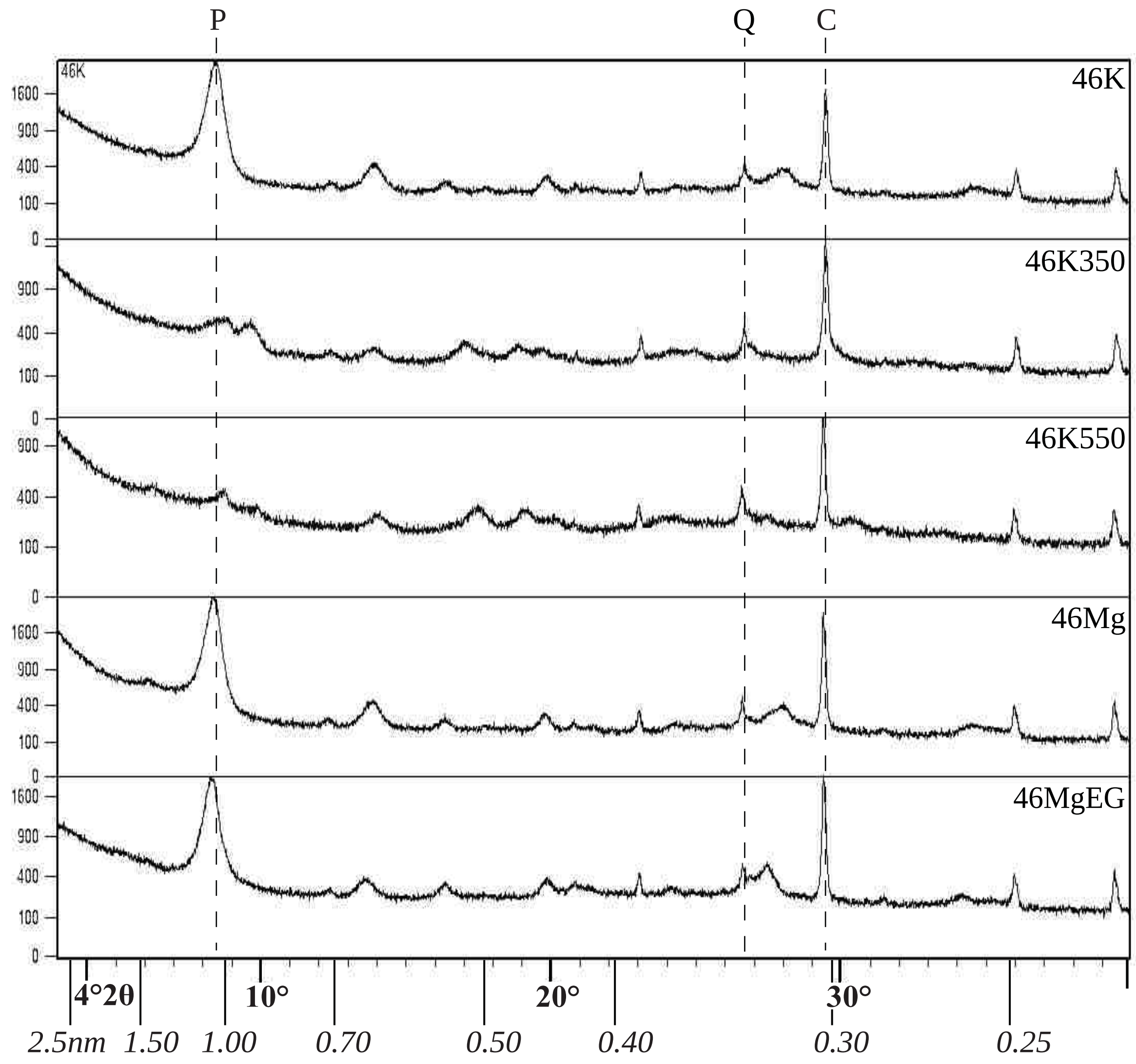

XRD spectra for Sample #46, profile MM2 (upper Massive horizon). The sample contains, in order of decreasing relative abundance: palygorskite, calcite, quartz, and trace smectite.

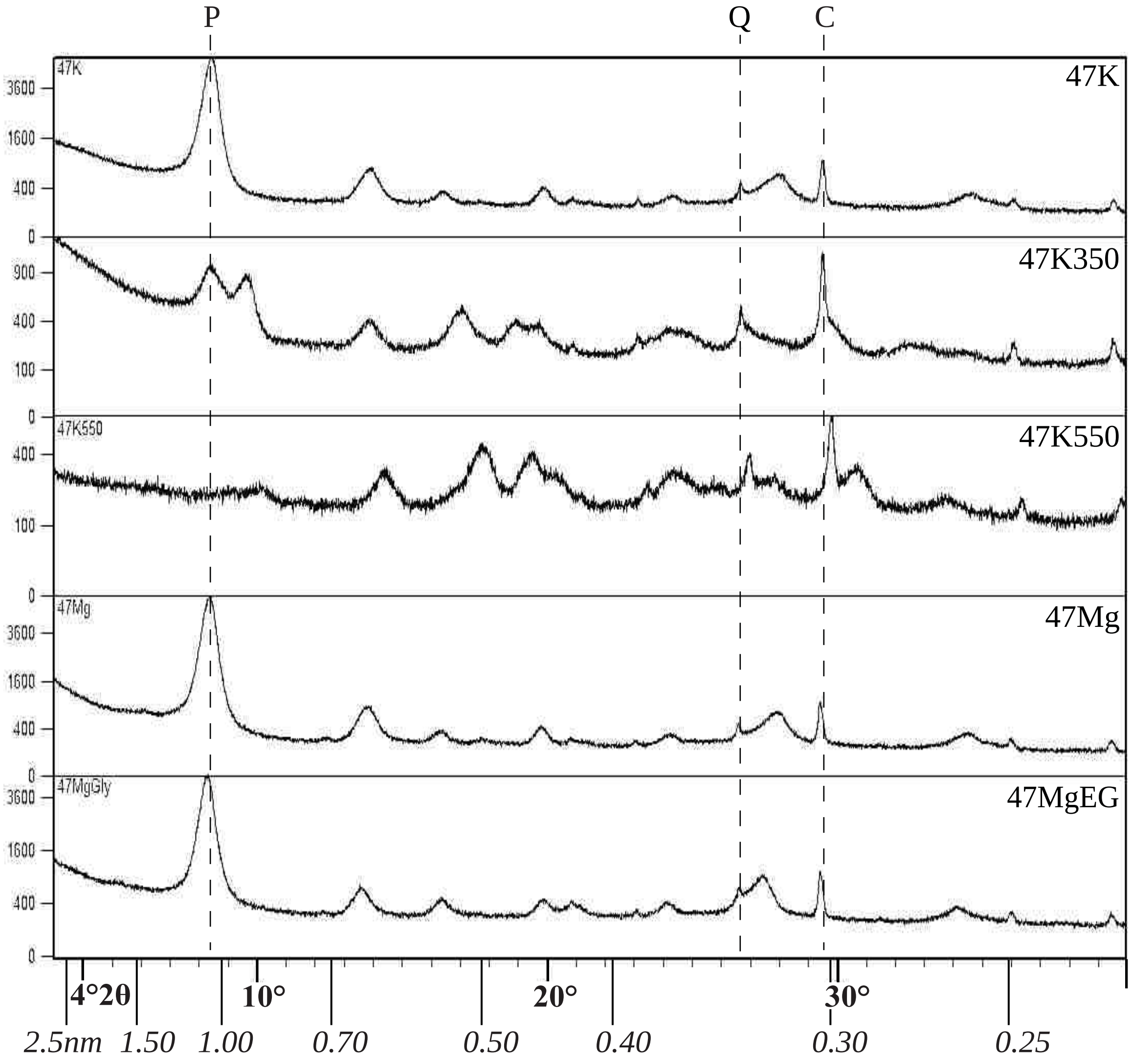

XRD spectra for Sample #47, profile MM2 (upper Transitional horizon). The sample contains, in order of decreasing relative abundance: palygorskite, calcite, and quartz.

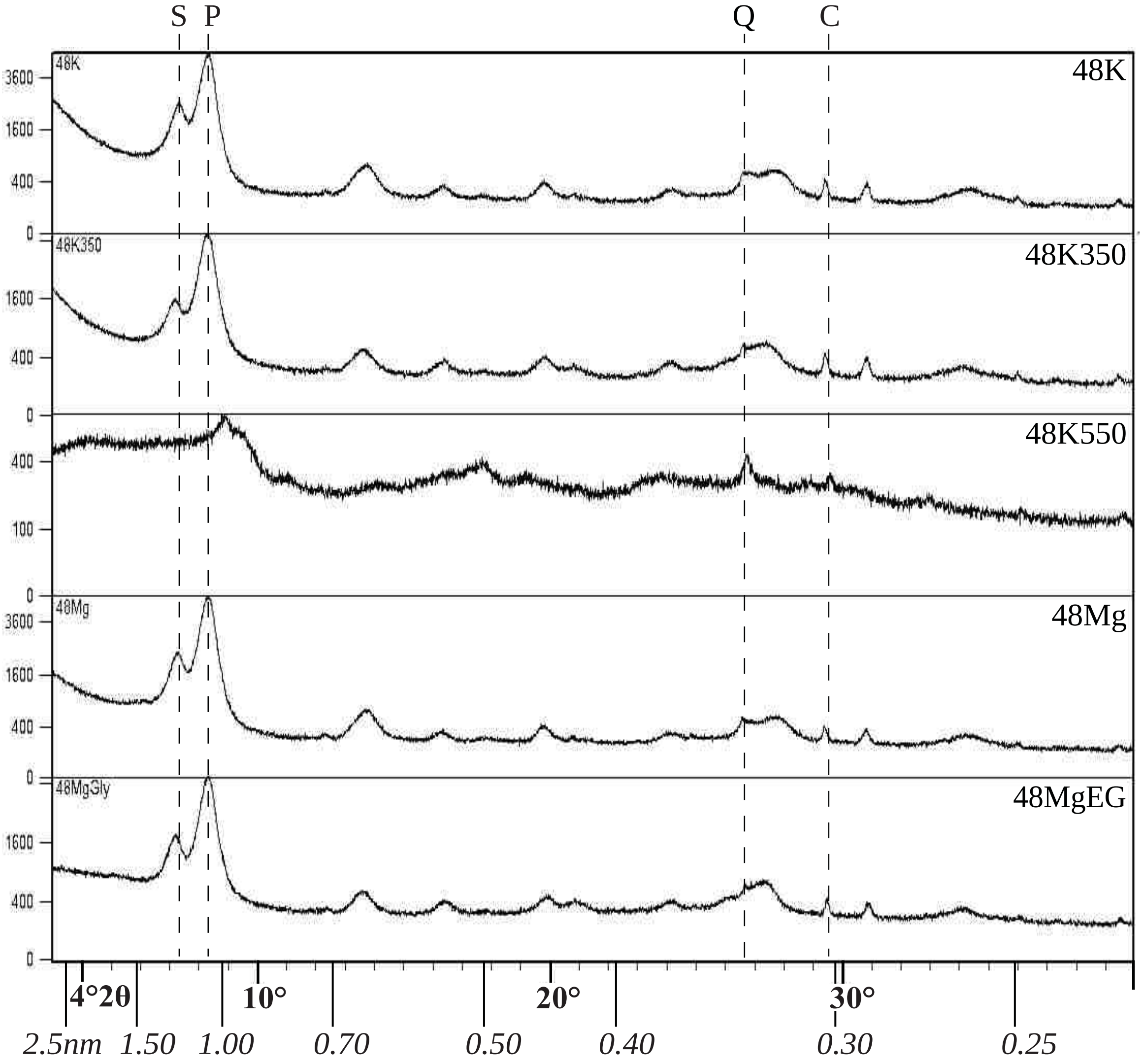

XRD spectra for Sample #48, profile MM2 (upper Transitional horizon). The sample contains, in order of decreasing relative abundance: palygorskite, sepiolite, quartz, and calcite.

APPENDIX 4.2

SOIL pH METHODS

Soil pH was determined on bulk, crushed samples using a 1:1 paste method after method 4C1a2a1 of Burt (2004).

Soil pH was determined in the laboratory with a Thermo Electron Corporation Orion 720A+ Advanced ISE/pH/mV/ORP meter and an Orion Ross Ultra combination pH electrode. The automatic temperature correction feature of the pH meter was also used.

Five grams of soil, crushed to pass a 2 mm sieve, were weighed into glass test tubes. Five milliliters of de-ionized water were added to each test tube and then the soil-water solutions were stirred and allowed to sit for one hour. Meanwhile, the pH meter was calibrated using standard buffer solutions of pH 4.00, 7.00, and 10.00 prepared from Tetrapek pHydrion tablets. After one hour, the pH of each soil sample was measured and recorded when pH stabilization was indicated by the meter. The electrode was rinsed with three successive immersions in beakers of deionized water before measuring the next sample.

APPENDIX 4.3

SOIL CHEMICAL DATA BY SAMPLE

Sample ID	Site	Profile	Horizon	Horizon Section	Depth Sampled (cm)	Depth Sampled (Mid)	pH	EC (uS)	$CaCO_3$%	Moisture (%)	Carbon* (%)	SO_4^{2-} S (mg/kg)	Cl^- (mg/kg)
1	MM1	A	Surface	Fine	0-20	10	8.43	69.36	46.8	2.91	1.35	4.45	5.64
2	MM1	A	Surface	Coarse	0-20	10	8.80	87.43	76.4	1.12	1.00	6.65	7.60
3	MM1	A	Brecciated	Top	40-50	45	8.97	99.61	85.4	0.38	0.69	13.0	4.56
4	MM1	A	Brecciated	Middle	50-60	55	8.99	81.95	76.4	0.63	0.92	26.8	25.3
5	MM1	A	Brecciated	Basal	65-80	75	8.91	130.0	77.0	0.53	0.80	16.9	4.70
6	MM1	A	Massive	Top	90-105	100	8.70	224.7	74.6	0.62	1.01	68.4	4.95
7	MM1	A	Massive	Middle	125-140	135	8.78	280.9	78.7	0.56	1.01	82.4	6.68
8	MM1	A	Massive	Basal	150-175	165	9.25	69.76	84.6	0.38	0.66	20.7	8.01
9	MM1	A	Transitional	Top	180-195	190	9.29	66.70	87.3	0.28	0.60	8.08	13.0
10	MM1	A	Transitional	Middle	265-280	275	9.29	74.85	85.3	0.25	0.53	5.48	4.22
11	MM1	A	Transitional	Basal	330-345	340	8.91	1531	75.5	1.76	1.09	10.3	36.1
12	MM1	A	MC Paleosol	Top	350-365	360	8.47	336.0	74.3	1.58	1.48	196	6016
13	MM1	A	MC Paleosol	Middle	400-410	405	8.54	187.0	48.5	2.28	1.46	77.8	963
14	MM1	A	MC Paleosol	Basal	470-480	475	8.63	208.7	46.0	1.56	1.15	65.5	60.6
15	MM1	B	Surface	Fine	0-30	15	8.78	103.4	21.4	3.69	1.37	3.64	9.33
16	MM1	B	Surface	Coarse	0-30	15	8.85	97.79	77.7	0.87	0.97	6.37	8.32
17	MM1	B	Brecciated	Top	50-70	60	8.97	123.7	86.3	0.54	0.88	23.4	10.6
18	MM1	B	Brecciated	Middle	100-120	110	8.86	486.9	81.7	1.14	1.43	76.5	158
19	MM1	B	Brecciated	Basal	130-150	140	8.84	1460	70.4	0.79	1.09	153	404
20	MM1	B	Massive	Top	175-220	200	8.92	289.5	77.5	0.40	0.82	114	9.11
21	MM1	B	Massive	Basal	220-240	230	9.10	464.8	74.0	0.48	0.85	60.5	48.5
22	MM1	B	Transitional	Top	270-280	275	8.42	4145	76.0	2.29	1.94	120	7426
23	MM1	B	Transitional	Middle	320-330	325	8.45	2344	69.8	3.49	2.03	165	6366
24	MM1	B	Transitional	Basal	350-370	360	8.28	2851	73.3	2.08	1.48	226	12470
25	MM1	B	MC Paleosol	Top	385-405	395	8.63	806.9	57.7	2.59	1.95	212	4664
26	MM1	C	Surface	Fine	0-15	10	8.60	99.04	28.4	1.43	1.38	2.83	41.1
27	MM1	C	Surface	Coarse	0-15	10	8.93	97.31	70.8	0.85	0.99	4.49	23.2
28	MM1	C	Brecciated	Top	30-45	40	8.80	232.0	76.4	0.71	1.22	32.6	8.43
29	MM1	C	Brecciated	Middle	55-70	65	8.72	421.7	73.9	0.65	1.10	59.8	18.6
30	MM1	C	Brecciated	Basal	85-100	95	8.90	134.2	75.1	1.38	1.35	33.0	32.7
31	MM1	C	Massive	Top	110-125	120	9.22	227.1	72.1	0.61	0.90	108	10.0

Sample ID	Site	Profile	Horizon	Horizon Section	Depth Sampled (cm)	Depth Sampled (Mid) (cm)	pH	EC (uS)	$CaCO_3$%	Moisture (%)	Carbon* (%)	SO_4^{2-} S (mg/kg)	Cl^- (mg/kg)
32	MM1	C	Massive	Middle	145-160	155	9.04	581.7	76.8	0.78	0.88	259	18.3
33	MM1	C	Massive	Basal	200-220	210	9.30	104.0	79.3	0.24	0.67	26.8	17.3
34	MM1	C	Transitional	Middle	305-320	310	8.83	362.8	71.1	1.43	1.22	137	1340
35	MM2		Surface	Coarse	0-15	10	9.20	95.88	82.4	0.29	0.89	8.97	16.1
36	MM2		Surface	Fine	0-15	10	8.93	85.97	14.8	1.50	1.09	5.90	3.98
37	MM2		Surface	Coarse	0-15	10	9.20	89.66	74.2	0.52	0.96	I.S.	I.S.
38	MM2		Surface	Fine	0-15	10	8.92	87.90	17.6	1.81	1.20	5.69	3.13
39	MM2		Surface	Coarse	0-15	10	9.10	86.59	71.8	0.51	0.83	I.S.	I.S.
40	MM2		Surface	Fine	0-15	10	9.03	86.54	14.5	1.77	0.87	5.39	2.14
41	MM2		Brecciated	Top	15-25*	20	9.09	255.8	67.2	0.41	1.04	44.4	142
42	MM2		Brecciated	Middle	20-30	25	8.84	730.5	80.4	0.51	1.03	30.2	107
43	MM2		Brecciated	Basal	30-40	35	9.10	165.7	79.5	0.45	0.92	28.3	36.4
44	MM2		Massive	Top	40-55	50	9.03	199.0	73.6	0.60	0.92	40.9	10.5
45	MM2		Massive	Top	40-55	50	8.85	210.5	77.8	0.71	1.36	21.9	7.26
46	MM2		Massive	Top	40-55	50	9.13	193.5	75.8	0.48	1.07	43.3	23.5
47	MM2		Transitional	Top	140-160	150	9.40	67.83	76.9	0.34	0.43	7.91	11.2
48	MM2		Transitional	Top	140-160	150	9.07	1011	62.5	0.73	1.08	105	645

"I.S." indicates insufficient sample mass remaining for analysis.

All samples were collected Feb 18, 2009

* Percent organic carbon was estimated using the difference in sample mass between (1) oven-drying at 105C for 12 hours and (2) after furnace-heating at 400C for 12 hours.

APPENDIX 4.4

SEM-EDS DATA

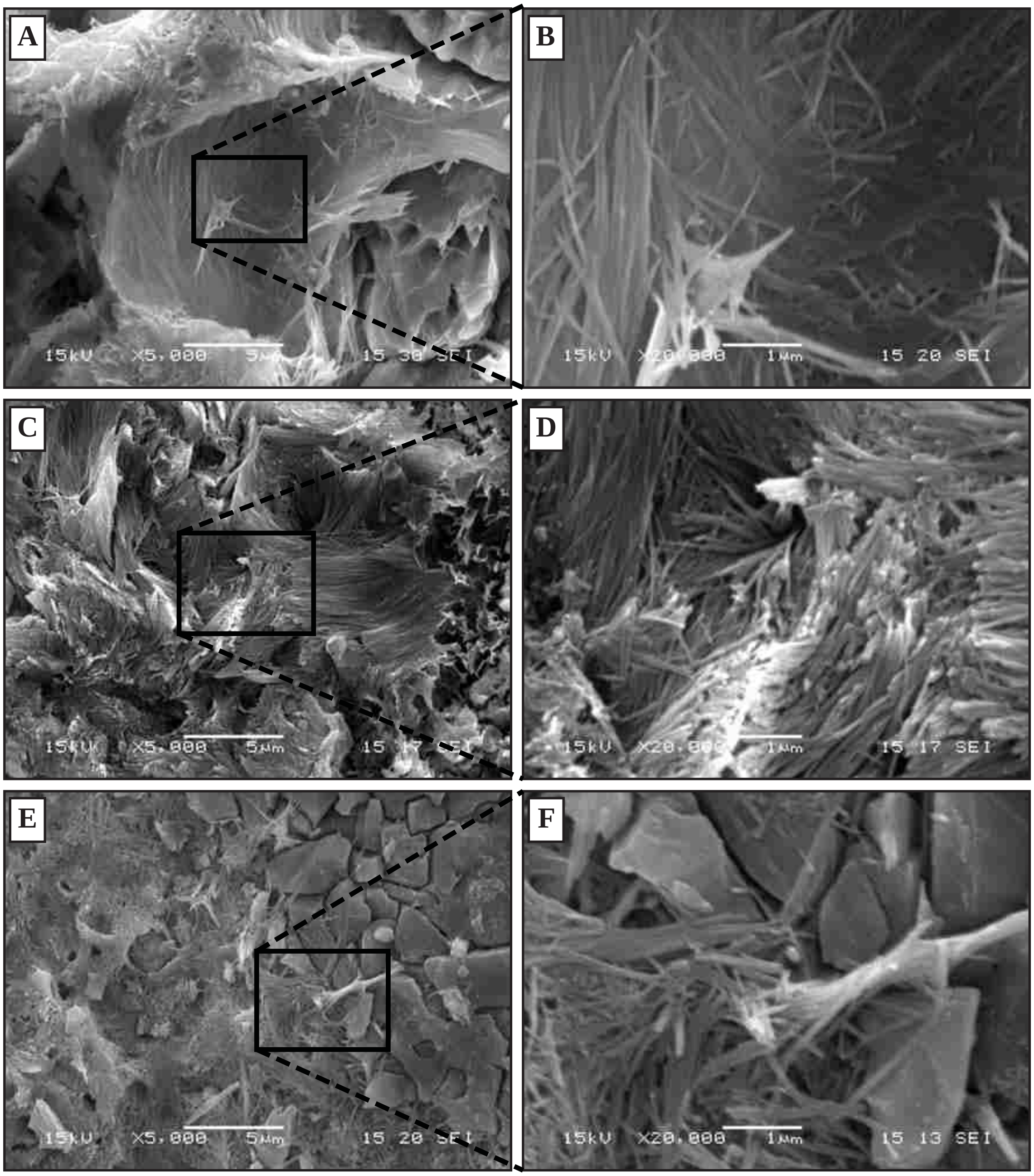

Palygorskite and/or sepiolite fibers are visible only at high magnification, and vary little in crystallite size or morphology within the massive horizon of Mormon Mesa's petrocalcic soil profile.

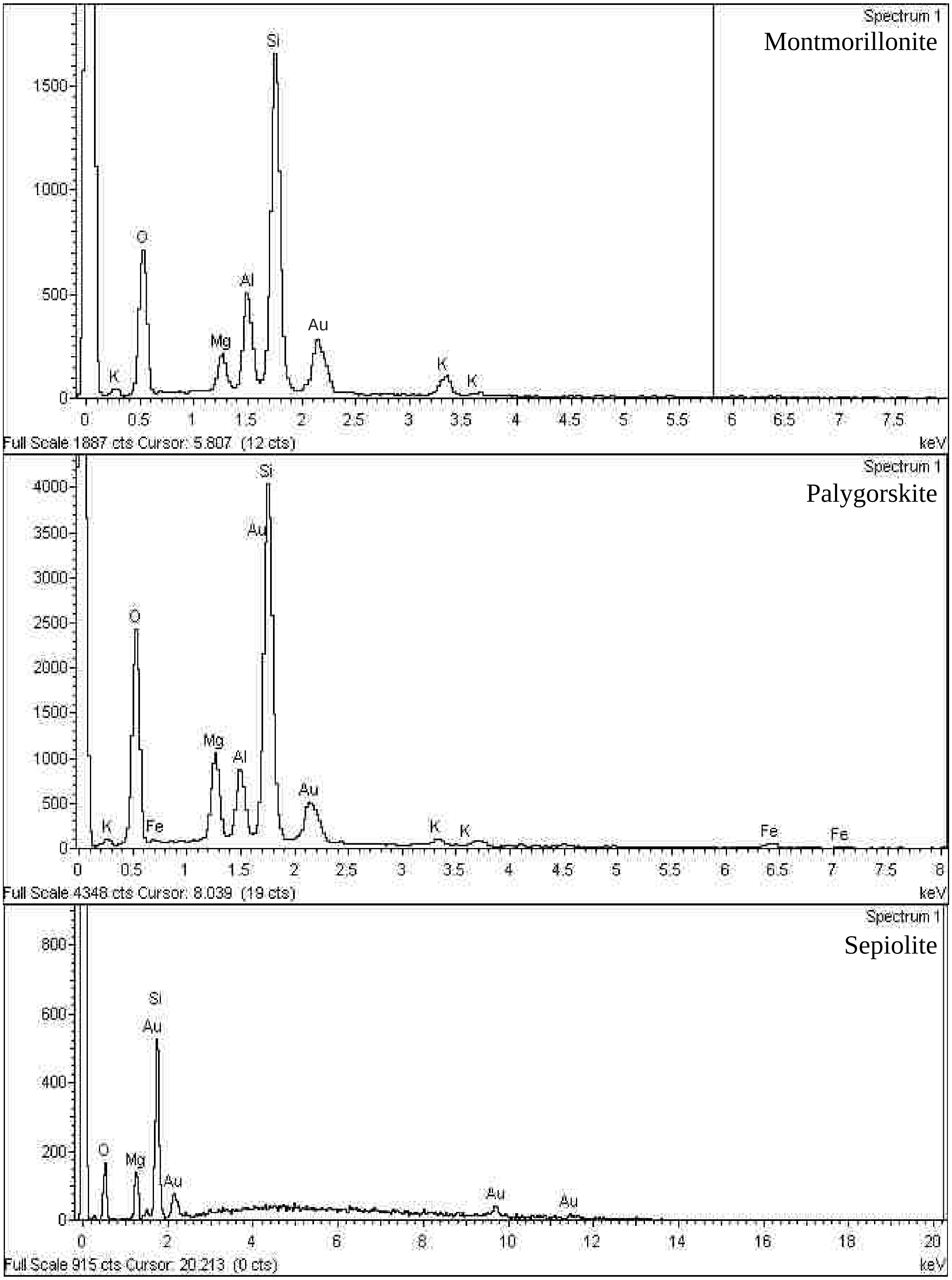

EDS spectra for: (A) Montmorillonite, (B) Palygorskite, and (C) Sepiolite reference standards purchased from the Clay Minerals Society Source Clays Repository. All samples bear K peaks as a result of pre-treatment for XRD analysis. Note variable Al and Mg contents.

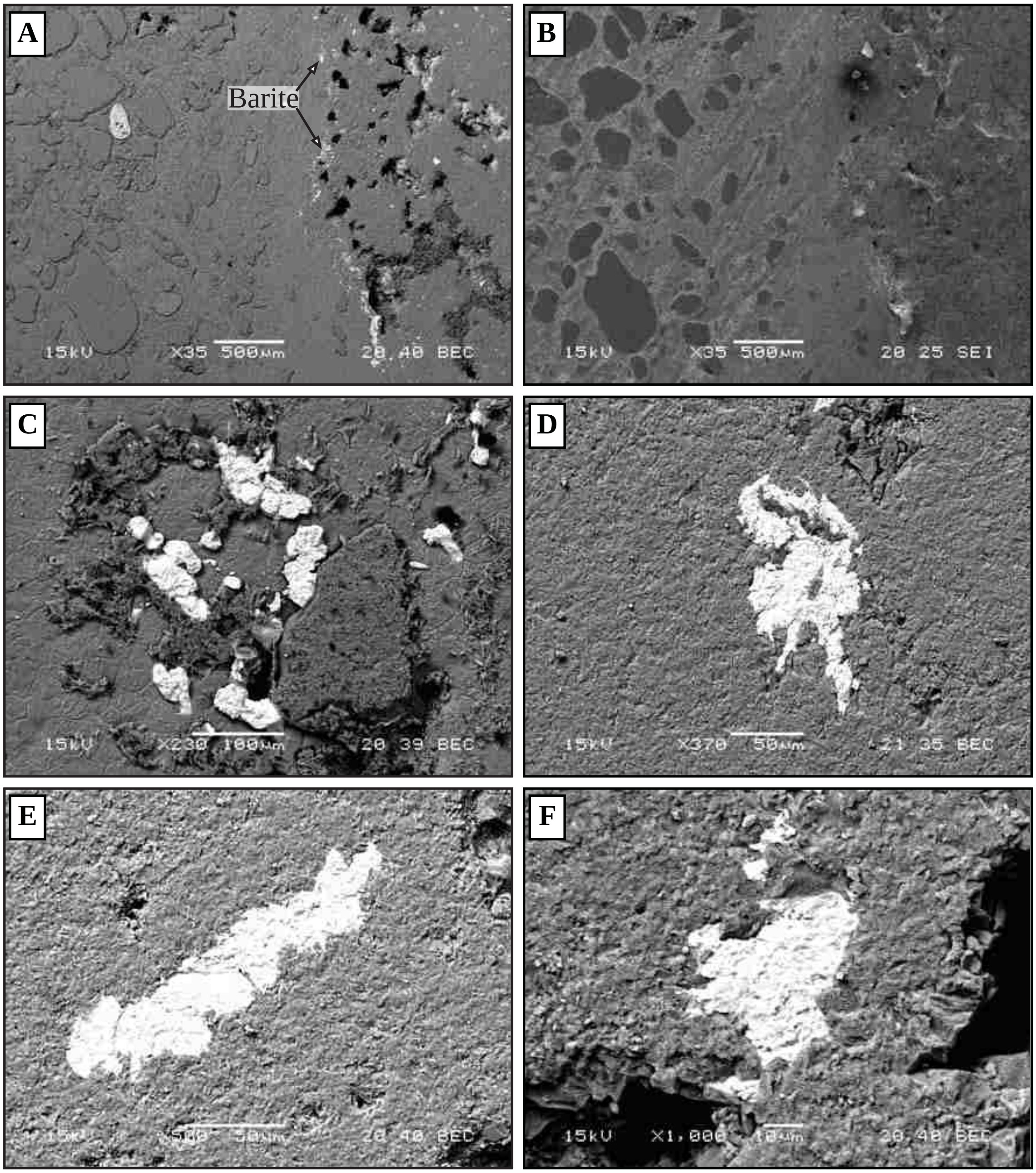

Pedogenic barite, appearing bright white in backscatter images, was found in the massive horizon of the Mormon Mesa petrocalcic soil. (A) Backscatter and (B) secondary electron images of pedogenic barite crystals precipitated along a laminar zone of porosity near the base of the massive horizon. (C) through (F) show poorly crystalline to anhedral masses of pedogenic barite surrounded by matrix carbonate and palygorskite or sepiolite clays. Up is to the right in images (A)-(C); the orientations of (D)-(F) are not known.

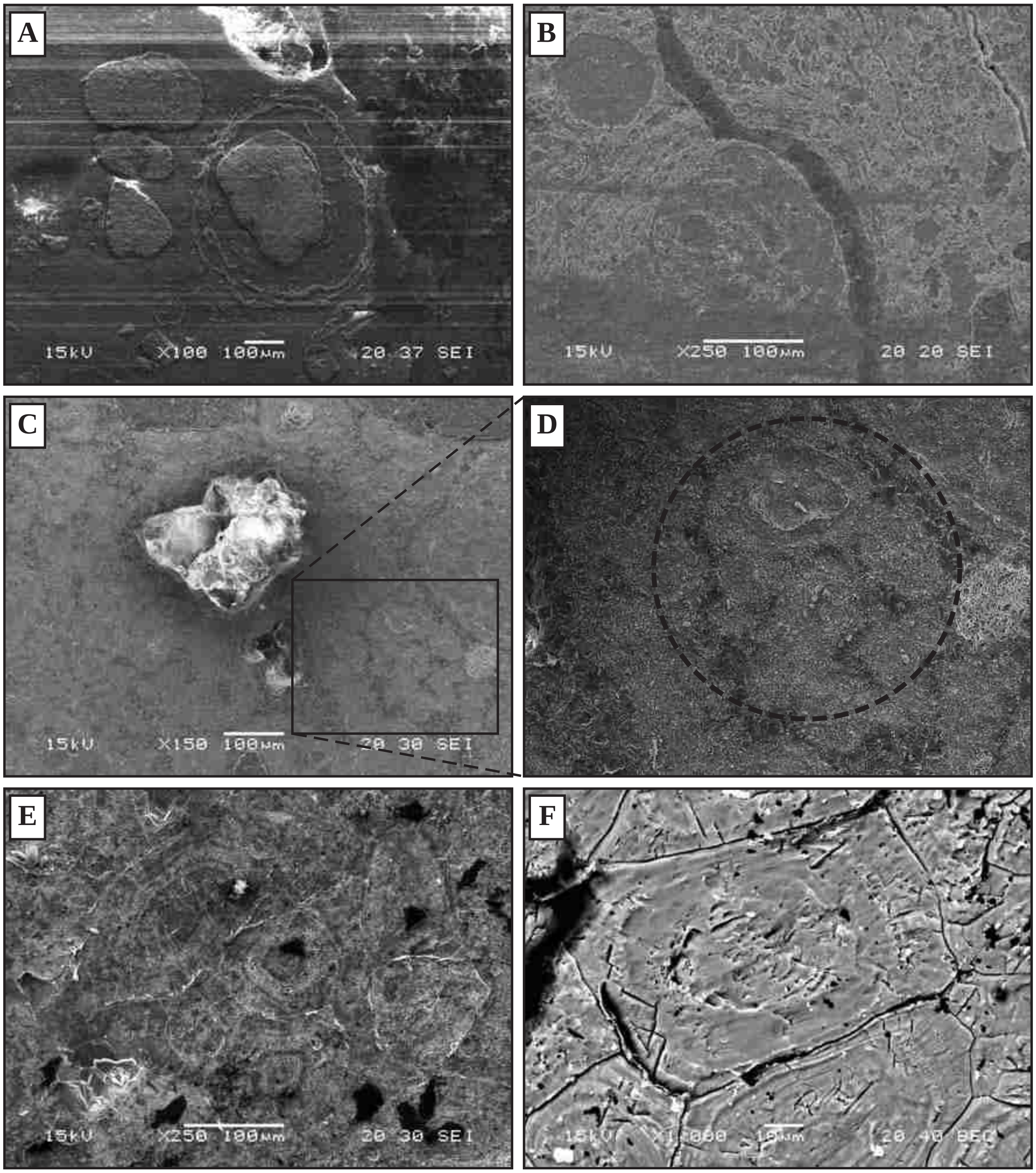

Pisolites, calcite growth structures, and mineral segregation patterns vary throughout the massive horizon. (A) Despite sample charging problems, fibrous clay is clearly visible ringing a quartz grain in this image. (B) Calcite has filled a fracture with curves paralleling the edge of a pisolitic feature in the massive horizon. (C) Coarser (darker) calcite crystals surround pore spaces and pisolitic structures, some of which (D) *may* have partly coalesced (circled). (E-F) Closely-abutting calcite and fibrous clay growth structures. Although infilling of root traces is a plausible explanation for some of the features in (E), the mechanism can not wholly account for the interlocking and/or rectangular shapes of many of the structures (F).

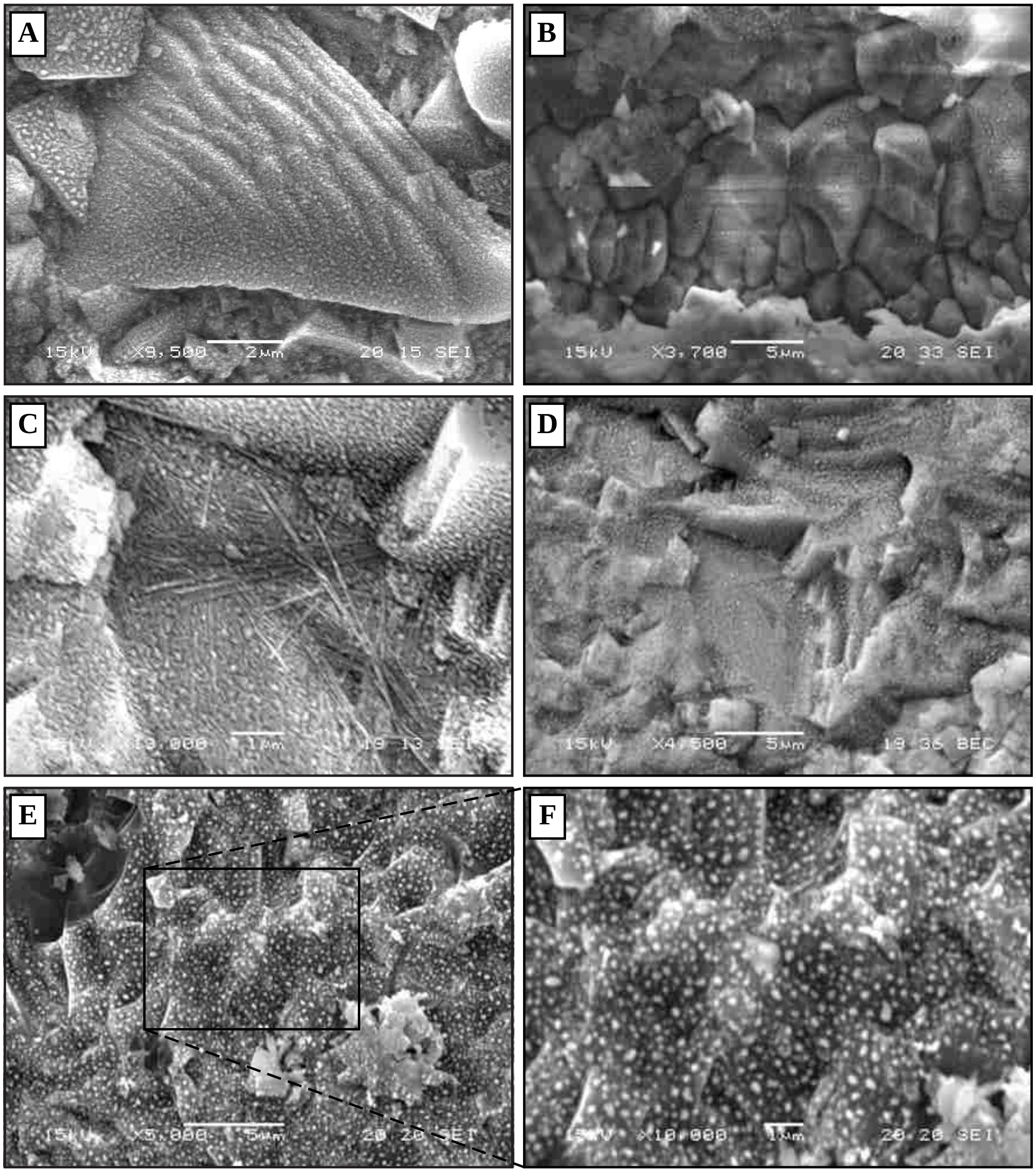

Unexplained nano-textures appeared in at least three thick-sections in this study. Because these irregular, dot-matrix or goosebump -like features appear on the surface of (A) quartz, (B) calcite, and also (C) fibrous clay phases in the affected samples, it is assumed that the texture is an artifact of acid-treatment or non-ideal sputter coating procedures. (D) The texture or coating is also apparent in backscatter mode. (E & F) The shape of individual "blebs" is variable, and they range in diameter from ~0.1 to 0.5 µm.

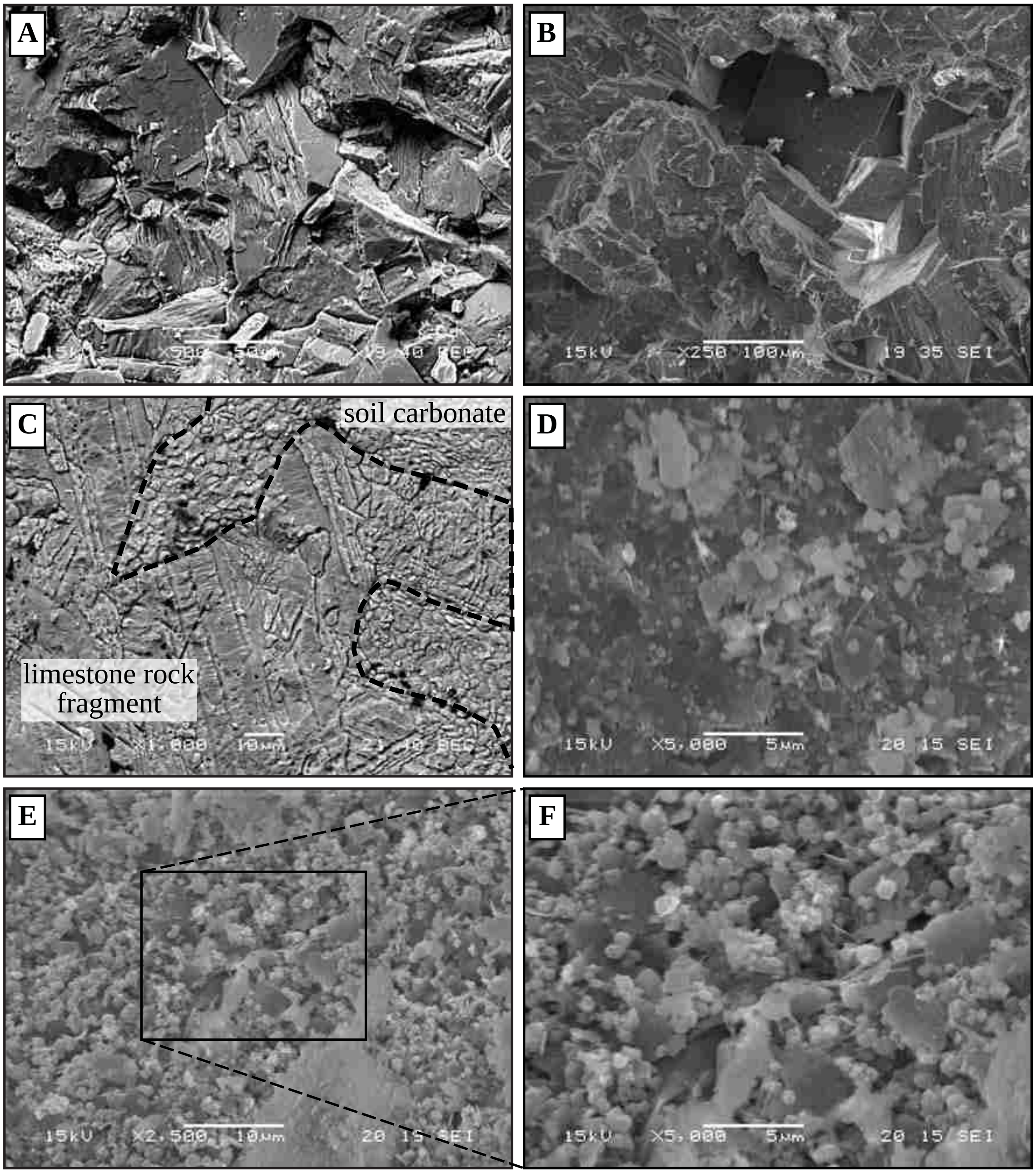

Limestone is characterized by (A & B) larger and distinctly rhombohedral calcite crystals as compared to pedogenic carbonate, as can be seen in this sample taken from the core of a limestone cobble found in a gravel bed (Muddy Creek Fm. sediments) underlying the Mormon Mesa petrocalcic horizon. (C): A limestone rock fragment engulfed by pedogenic carbonate in the massive horizon of Mormon Mesa. (D-F): Extracts of the clay-sized particle fraction of the limestone cobble in A&B after dissolution in NaOAc. Fine, fibrous crystallites, possibly consisting of palygorskite or sepiolite clays are seen in images of the extracted particles, however, the fibrous crystallites were too small for EDS analysis, and could also be acicular calcite.

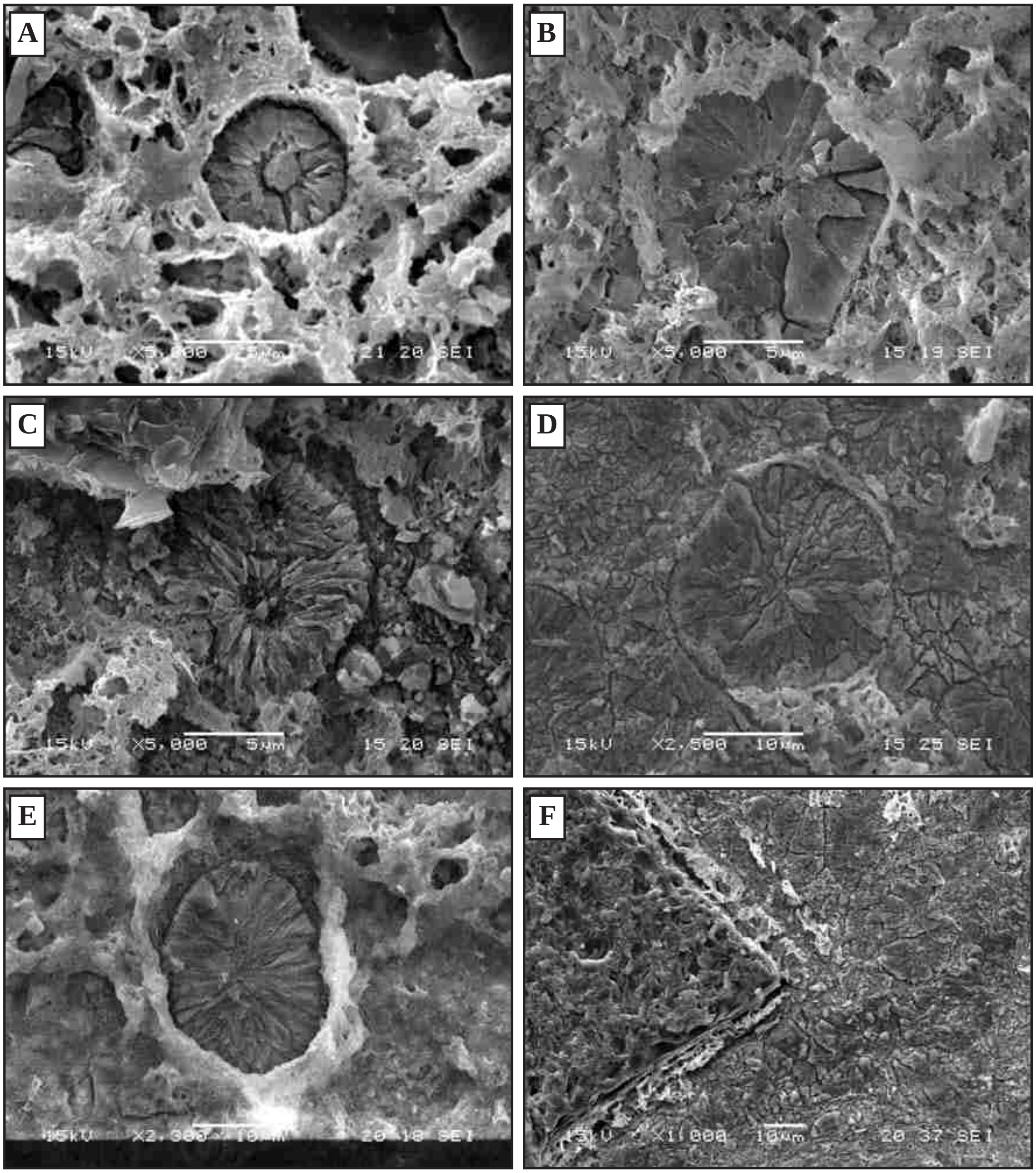

Microcodium structures (A-E) were identified in most of the Mormon Mesa massive horizon samples. In some instances, elongated morphologies were also seen, as in the matrix to the right of the quartz grain in (F).

VITA

Graduate College
University of Nevada, Las Vegas

Colin R. Robins

Degrees:

Bachelor of Arts, Geology and Spanish, 2001
Macalester College

Master of Science, Soil Science, 2004
Oregon State University

Special Honors and Awards:

Best graduate student oral presentation, UNLV Geosymposium, April 17, 2009
Jack and Fay Ross Fellowship, UNLV Department of Geoscience, 2007-2008
Induction, Phi Kappa Phi honor society, UNLV, 2008
Geological Society of America Graduate Student Research Grant, 2007
Wilford Gardner IUSS Congress Fellowship Grant Award – The National Academies, Policy and Global Affairs Division, Board on International Scientific Organization, 2006.
Summer Session Scholarship – Graduate College, UNLV, 2006
Bernada E. French Scholarship –Department of Geoscience, UNLV, 2006

Publications:

Robins, C.R., Buck, B.J., Williams, A.J., Morton, J.L., Howell, M.S., Yonovitz, M.L., and House, P.K., 2009. Comparison of flood hazard assessments on desert piedmonts and playas: A case study in Ivanpah Valley, Nevada. Geomorphology, 103 (4): 520-532.

Nicholl, M.J., Baron, A.G., Robins, C.R., Boxell, J., and Lin, Y. 2008. Using synthetic data and artificial wells to teach the construction and use of water level contour maps. Journal of Geoscience Education 56 (4): 317-323.

Abstracts and Presentations:

Robins, C.R., Buck, B.J., Spell, T., and Soukup, D., 2008. A Novel Approach to Arid Soil Dating: Extraction and ^{40}Ar*/^{39}Ar Geochronology of Pedogenic Sepiolite and Palygorskite. Abstracts with programs Houston, TX. 8 October 2008. Invited Abstract (National Science Foundation Poster Session).

Saldaña, S.C., Snelson, C.M., Taylor, W.J., Beachly, M., Cox, C.M., Davis, R., Stropky, M., Phillips, R., Robins, C., Cothrun, C., 2007. Preliminary Pseudo 3-D Imagery of the State Line Fault, Stewart Valley, Nevada Using Seismic Reflection Data. Trans. AGU, v. 88, no. 52, Fall Meet. Suppl., Abstract.

Williams, A., Buck, B.J., Merkler, D., House, P.K., Howell, M., Morton, J., Robins, C., Yonovitz, M., 2007. Alluvial fan flood hazard assessment: A comparison of FEMA, NRCS, and surficial geological maps in Ivanpah Valley, Nevada. Soil

Science Society of America Abstracts with Programs, Paper 1625. New Orleans, LA, Nov 4-8.

Robins, C.R., Buck, B.J., Merkler, D.J., Howell, M.S., Morton, J.L., Williams, A.J., Yonovitz, M.L., and House, P.K., 2007. Comparison of flood hazard assessments on alluvial fans using FEMA, NRCS, and surficial geologic maps: A case study in Ivanpah Valley, Nevada, Western Society of Soil Science Abstracts with Programs, Paper 227. Boise, ID, June 17-20.

Robins, C.R., Howell, M.S., Drohan, P.J., 2006. Assessing post-fire soil change: First-year results from a long-term monitoring project following ecosystem recovery in Mesa Verde National Park, CO USA. World Congress of Soil Science Abstracts with Programs, Paper 464 a. Philadelphia, PA, July 9-15.

Robins, C.R., Howell, M.S., Drohan, P.J., 2005. High intensity fire effects on mineralogy and pedogenesis of piñon-juniper woodland soils, Mesa Verde National Park, CO. Soil Science Society of America Abstracts with Programs, Paper 920. Salt Lake City, UT, Nov 5-9.

Dunn, R.K., Robins, C.R., and Miller, N.R., 2000. Late Quaternary alluvial deposits and landscape evolution of Sage Creek drainage basin, Badlands National Park, South Dakota. Geological Society of America Abstracts with Program, v. 32, no. 7, p. 25-26.

Reports:

Given, M., Boutin, A., Blankespoor, B., Corley, H., Digney, S., Gibson, E., Graham, A., Horowitz, M., Kassianidou, V., Knapp, A.B., Lufafa, A., McCartney, C., Noller, J., Robins, C., Slevin, S., Sollars, L., Tselios, T., and Jacobson, K.W., 2003. Troodos Archaeological and Environmental Survey Project: Report on the Fourth Season, July-August 2003.

Dissertation Title:

Phyllosilicate Mineralogy, $^{40}Ar/^{39}Ar$ Geochronology, and Genesis of Petrocalcic Soils in the Southwest U.S.A.

Dissertation Examination Committee:

Chairperson, Dr. Brenda J. Buck, Ph.D.
Committee Member, Dr. Matthew Lachniet, Ph.D.
Committee Member, Dr. Terry Spell, Ph.D.
Committee Member, Dr. Spencer Steinberg, Ph.D.
Graduate Faculty Representative, Dr. Lloyd Stark, Ph.D.